OXYGENATED FUEL STRATEGIES TO COMBAT AIR POLLUTION
A FEDERAL OVERVIEW

David J. Kortum and Meredith G. Miller
Field Operations and Support Division 6406J
U. S. Environmental Protection Agency
Washington, DC 20460

Keywords: oxygenate, pollution, MTBE

INTRODUCTION:
The use of oxygenate fuel additives in gasoline as a strategy to decrease dangerous ambient air levels of pollutants, especially carbon monoxide (CO), has recently expanded dramatically. Two especially significant programs to combat air pollution were required under the 1990 amendments to the Clean Air Act: the carbon monoxide oxygenated fuels program and the reformulated gasoline program. This paper explores the legislative and statutory history of oxygenate use in gasoline and oxygenate-based pollution abatement programs, program implementation problems and public reaction, health research on oxygenates and the resulting changes in ambient air quality for cities which have instituted programs.

STATUTORY BACKGROUND
Section 211(m) of the Clean Air Act as amended in 1990 (the Act or CAA) requires states with areas experiencing dangerous levels of carbon monoxide pollution to implement winter oxygenated gasoline programs no later than November 1, 1992. This mandate is applicable to 39 areas throughout the country, although just 36 began the program on November 1, 1992.

The oxygenated gasoline program requires gasoline in the specified control areas to contain an average of 2.7% oxygen by weight during that portion of the year in which the areas are prone to high ambient concentrations of CO, typically during the core winter months. The lengths of these control periods have been established by the EPA Administrator. The Act requires that the winter oxygenated gasoline program apply to all gasoline sold or dispensed in the larger of the Consolidated Metropolitan Statistical Area (CMSA) or the Metropolitan Statistical Area (MSA) in which the nonattainment area is located. (See Table 1 below for a complete list of the CMSAs and MSAs affected by this requirement and their control periods.)

Just a few states opted to allow averaging programs, including Pennsylvania and Ohio. Other states, such as Oregon and Washington, have adopted limited averaging scenarios, allowing individual companies to average their oxygen contents over the course of the season, but not allowing companies to sell and trade credits among themselves. The majority of the states adopted programs which did not allow for averaging, thus requiring that <u>each</u> gallon of gasoline contain no less than the minimum 2.7% oxygen by weight.

Table 1: Program Areas

November 1 - February 29

Hartford-New Britain-Middletown, CT CMSA
Seattle-Tacoma, WA CMSA
Philadelphia-Wilmington-Trenton, PA-NJ-DE-MD CMSA
Greensboro-Winston-Salem-High Point, NC MSA
Raleigh-Durham, NC MSA
El Paso, TX MSA
Denver-Boulder, CO CMSA
San Diego, CA MSA
Washington, DC-MD-VA MSA
Grant's Pass, OR
Baltimore, MD MSA
Medford, OR MSA
Missoula, MT
Klamath County, OR
Provo-Orem, UT MSA
Albuquerque, NM MSA
Colorado Springs, CO MSA
Fort Collins-Loveland, CO MSA
Portland-Vancouver, OR-WA CMSA

October 1 - April 30 New York-Northern New Jersey-Long Island, NY-NJ-CT CMSA

October 1 - January 31

Minneapolis-St. Paul, MN-WI MSA
Fresno, CA MSA
Reno, NV MSA
San Francisco-Oakland-San Jose, CA CMSA
Chico, CA MSA
Modesto, CA MSA
Sacramento, CA MSA
Stockton, CA MSA

October 1 - February 29

Las Vegas, NV MSA
Los Angeles-Anaheim-Riverside, CA CMSA
Phoenix, AZ MSA

September 1 - February 29 Spokane, WA MSA

Under authority set forth in another part of the Act, the Administrator promulgated labeling regulations for the sale of gasoline at retail gasoline stations in oxygenated gasoline control areas. Under the Agency's regulation, the gasoline pumps at retail stations in each control area must be labeled during the applicable control period with conspicuous labels. The labels must be clearly readable in order to provide the public with information that oxygenated gasoline is being dispensed.

Under section 211(k) of the Act, "reformulated gasoline" is required in certain ozone nonattainment areas beginning in 1995. Among other things reformulated gasoline requires at least 2.0 percent oxygen by weight throughout the year. Reformulated gasoline could represent as much as half of the gasoline utilized in the U.S. depending upon the number of states that decide to adopt the program. (Although some areas are required to adopt the program, other less severe ozone nonattainment areas can "opt into" the program.)

The program-generated demand, on a yearly basis, for oxygenates can be seen in Figure 1.

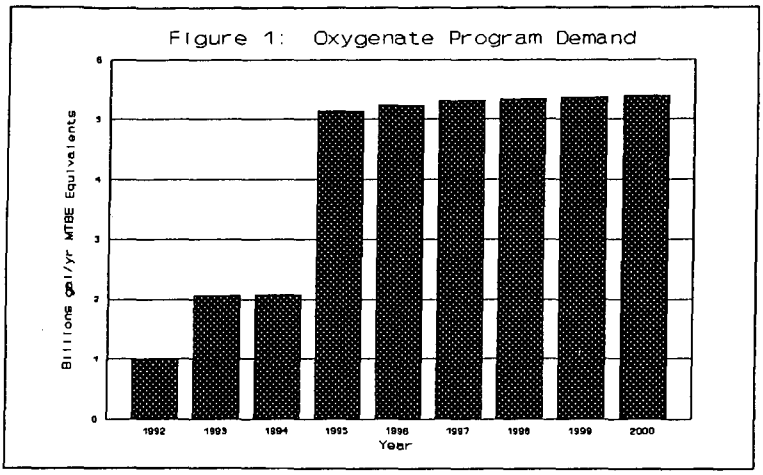

ENVIRONMENTAL BENEFITS OF OXYGENATED FUELS

Carbon monoxide (CO) is a colorless, odorless gas which can cause central nervous system effects such as a reduction in visual perception and manual dexterity, decreased exercise performance, and among individuals with chronic heart disease, a marked decrease in physical capacity and increase in chest pain. Motor vehicles are significant contributors to carbon monoxide emissions nationwide, adding approximately 75 percent to the CO inventory in major metropolitan areas. Millions of U.S. citizens are exposed to dangerous levels of this pollutant especially during the winter months.

One important strategy which an area may utilize to reduce CO emissions is the implementation of a cleaner-burning oxygenated gasoline program. For any given set of conditions, there is an optimum ratio of fuel to oxygen or air which provides the most efficient combustion. In cold weather when combustion tends to be less efficient, extra oxygen enhances combustion by offsetting fuel-rich operating conditions, especially during vehicle starting. If oxygen is added to the fuel in the form of oxygenates, a second source of oxygen becomes available (in addition to the primary source from the air). A gasoline blend containing 2.7 percent oxygen, by weight, will result in a 15% to 20% reduction in CO emissions, on a mile-for-mile basis, when compared to gasoline not containing oxygenates.

Oxygenates also cause decreases in unburned hydrocarbon exhaust emissions including certain toxic air pollutants such as benzene and 1,3-butadiene. Although oxygenates do increase aldehyde emissions, total toxic emissions decrease through oxygenate use.

WHAT OXYGENATES ARE USED?

Alcohols and ethers have been added to gasoline in various forms for over fifteen years, sometimes to enhance octane, sometimes simply as a fuel extender, and, more recently, to decrease emissions. Typically, although other oxygenates could be utilized (and have been in the past), fuel oxygen is added to gasoline in the form of ethanol, an alcohol, or methyl tertiary butyl ether (MTBE).[1] These oxygenates are used because they are the most economically viable in today's fuel market. Ethanol has been traditionally added to gasoline at 10 percent by volume, which adds approximately 3.5 percent oxygen to the fuel. However, in oxyfuel program areas, ethanol is often added at about 7.7 percent by volume to meet the program requirement of 2.7 percent oxygen. To reach the same oxygen level, MTBE is added at a level of approximately 15 percent by volume.

PROGRAM RESULTS

The previously stated 15 to 20 percent reduction in CO emissions is evidenced by what occurred last year in the cities which implemented an oxygenated fuels program. A preliminary study of exceedances of the National Ambient Air Quality Standard for carbon monoxide in these cities covering the winter months in the 1992-93 season during which an oxygenated fuels program was in place reveals a very telling picture. (See Figure 2.) For 21 areas which had not previously implemented oxygenated fuels programs, CO exceedances dropped by 95 percent when compared to the previous winter (1991-92). In California, where a program was implemented requiring slightly less total oxygen (2.0 percent oxygen instead of 2.7 percent - equivalent to about 11 percent MTBE instead of 15 percent), exceedances dropped by 80 percent. In areas with pre-existing programs, most of which required oxygen levels around 2.0 percent but, under the new program, increased to 2.7 percent, exceedances dropped by about 50 percent. Although normal year-to-year variations in meteorological conditions or patterns of vehicle use might have contributed to the decline in CO exceedances in some nonattainment areas, these aggregate national data suggest strongly that MTBE is having the kind of positive effect overall that was intended.

---

[1] Other oxygenates which can be used include tertiary amyl methyl ether (TAME) and ethyl tertiary butyl ether (ETBE), both of which have been used to a very small extent during the past season in some isolated cases. In the past certain blends of methanol and other alcohols have been used but these blends are not viable in today's market.

Figure 2

FIRST YEAR PROGRAM RESULTS

* Program compliance was excellent in first season.
* Comparison of data from this winter to data from last winter show an 80% reduction in CO exceedances.

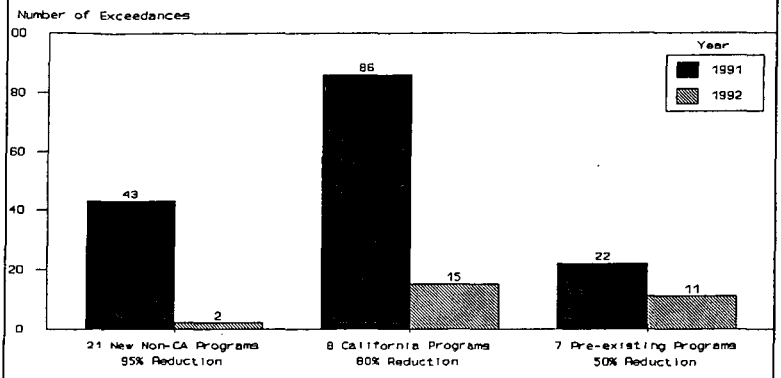

ote: California had 2.0% oxygen by weight program.

HEALTH ISSUES

Citizens in some areas of the country complained of acute health symptoms such as headache and nausea which they associated with use of MTBE in gasoline. There are a number of reasons why this reaction to MTBE-blended gasoline was unexpected. MTBE has been used in the U.S. as an octane enhancer since the late 1970's (at concentrations of 2-11%). Industry had tested many aspects of the fuel additive prior to 1992 and this research indicated no significant health concerns. Seven cities had, in fact, required wintertime use of oxygenated gasoline prior to 1992, most notably Denver which began its program in 1988, and experienced no problems similar to those in Alaska. Under the Clean Air Act oxygenated gasoline program, however, concentrations of MTBE must be generally higher than they were in Denver. (Denver required MTBE concentrations from 10-14.4%, while the Act requires 15%.)

The Environmental Protection Agency (EPA) took these concerns seriously and, in a very short time, organized a comprehensive strategy to investigate Alaska's complaints. In order to address the issue of health symptoms associated with acute exposures to

MTBE-blended gasoline, EPA outlined a six-month test program in January 1993. EPA coordinated almost $2 million worth of studies, working with the Centers for Disease Control and Prevention (CDC), the State of Alaska, industry groups represented by the American Petroleum Institute (API) and the Oxygenated Fuels Association (OFA), as well as other EPA and state offices.

The testing effort included animal studies, human clinical studies, epidemiological studies, exposure studies and automobile emissions studies and air and fuel sampling. In addition, ORD accelerated its review of existing research on chronic effects of MTBE. The results from these studies were presented at a workshop, sponsored by ORD, API and OFA, on July 26-28, 1993. The workshop enabled EPA and others to assess these health concerns before the start of the oxygenated gasoline season in 1993 in Alaska and elsewhere. EPA's assessment of the potential health risks associated with MTBE-oxygenated gasoline has been completed and indicates that MTBE appears to have very little acute health risk to healthy people under relatively temperate conditions. Hence, in terms of short-term acute health effects, these results seem to provide no basis to question continuing the overall MTBE oxyfuels program. This conclusion does not reflect that there may be a particularly sensitive subpopulation which may react to MTBE differently. However, results to date provide no firm evidence that such sensitive individuals exist or, if they do, how they might be identified. Further research on exposure to MTBE and the health effects of MTBE continues.

CONCLUSION:
Available data indicate that oxygenated fuels program implemented for pollution abatement have successfully decreased exceedences of the National Ambient Air Quality Standards for carbon monoxide pollution. Health research appears to indicate little health risk to healthy people under relatively temperate conditions.

SYMPOSIUM ON OXYGENATES AS FUEL ADDITIVES
AMERICAN CHEMICAL SOCIETY, FUEL DIVISION
SAN DIEGO NATIONAL MEETING
MARCH 13 -18, 1994

FUTURE FUEL DIVERSIFICATION WITH OXYGENATES

William J. Piel
ARCO Chemical Company
3801 West Chester Pike
Newtown Square, Pa 19073

Keywords: Emissions, Oxygenates, Fuels

INTRODUCTION

Fuel oxygenate blending in motor fuels first became commercialized in 1969 with the blending of t-butyl alcohol in gasoline. This first fuel alcohol was made by adding oxygen to isobutanes. Now most of this alcohol production is converted to isobutylene for methyl tertiary butyl ether (MTBE) production. MTBE blending was first commercialized in the U.S. in 1979 when the U.S. EPA granted a section 211F waiver request to blend it into unleaded gasoline. MTBE use grew during the 1980's as a high octane replacement for lead compounds in gasoline. Similarly, 10% ethanol blending was approved in 1978. With a government tax incentive for alcohols made from renewable sources, ethanol's use also grew as a non-petroleum gasoline extender in the mid-1980's.

Relative to mobile source emissions, the 1990 revision to the Clean Air Act (CAA) requires reductions of carbon monoxide (CO), volatile organic compounds (VOCs), and toxics from gasoline fueled vehicles. Reductions in nitrogen oxides (NOx) and greenhouse gases (such as carbon dioxide - CO2) were not required. The strategy in the CAA to decrease ground level ozone is by reducing VOC mass emissions by 15% in 1995 and 25% in 2000. The other attributing compound to ozone, NOx emissions, are only capped at the 1990 levels in the CAA. Based on the predictive models developed by the U.S. EPA and by the California Air Resource Board (CARB), it appears that the fuel reformulation will be able to achieve the year 2000 performance requirements targeted in the CAA.

Fuel oxygenates played a key role in both the Oxygenated Fuels and Reformulated Fuels outlined in the CAA. The next wave of environmental interest is to possibly modify motor fuels and/or motor vehicles for reductions in NOx emissions and greenhouse gases such as CO2. Fuel oxygenates can also play a significant role in such fuel modifications. To achieve the maximum emissions reduction potential, minor engine modifications may be required to take full advantage of the possible fuel property improvements.

FUEL OXYGENATES

Though MTBE and ethanol are the most commonly used oxygenates, there are many other potential fuel oxygenates that are being developed or investigated such as TAME (tertiary amyl methyl ether) and ETBE (ethyl tertiary butyl ethers)(Ref 1). The properties of these oxygenates and others are listed in Table 1. The most useful property of the oxygenates is their high octane. Outside of metal compounds, oxygenates are generally the only high octane alternative to aromatics in gasoline. The potential octane contribution of oxygenates are shown in Figure 1 as a function of the their oxygen contribution in gasoline.

While mixtures of alcohols are allowed up to 3.7 weight percent oxygen in gasoline under various EPA approved waivers, ethers are currently limited to 2.7 weight percent oxygen in gasoline. Under these limits, ethers can potentially add 3 to 4 octane numbers to the gasoline pool. If the oxygen limit for mixed ethers were raised to 3.7 percent, ethers could contribute 4 to 5 octane numbers ,and up to 20+ volume percent to gasoline. Their potentially large octane and volume contribution can play a significant role in replacing most of the aromatics in gasoline, and modifying future gasoline formulations for reductions in NOx and CO2 emissions as will be discussed later.

Besides their octane, a major advantage of ethers over aromatics is their relatively lower boiling temperatures. Since lead phasedown in gasoline, the increased use of aromatics in premium gasolines have lead to poor mid-range volatility and a degradation of cold engine driveability and performance(Ref 2). The automakers have been making an effort to limit this performance degradation by proposing a cap on a Driveability Index (DI) that is calculated from distillation temperatures of gasoline. Using their individual boiling temperatures, then DI differences between ethers and aromatics are illustrated in Figure 2. Though both provide octanes higher than a 100 (r+M)/2, the DI of most ethers are favorably lower while the high boiling temperatures of the aromatics contributed to higher DI for gasoline, particularly premium gasolines. The DI benefits of using ethers for octane is best illustrated by comparing the DI changes between the 1992 and 1993 winter DI averages for the oxygenated and non-oxygenated cities in the AAMA (American Automobile Manufacturers Association) gasoline surveys.

Gasoline Grade	DRIVEABILITY INDEX 1992	1993	DI CHANGE
Regular - Oxygenated	1112	1061	-53
Non-oxygenated	1071	1092	+21
Premium - Oxygenated	1154	1087	-67
Non-oxygenated	1153	1147	- 6

Though the non-oxygenated cities showed very little change in DI, the oxygenated cites (with predominately MTBE) showed very favorable decreases greater than 50 DI. Therefore, the use of ethers appears to provide an effective means for improving the mid-range volatility of the gasolines which should also benefit the 1990 CAA Reformulated Gasoline program.

EXHAUST NOx EMISSIONS

The work completed by AUTO/OIL established sulfur in gasoline as a major influence on tailpipe NOx because of its effect on the activity or efficiency of the catalytic convertors(Ref 3). However, the other fuel variables that effect NOx emissions were not quite as clear(Ref 4-5). Since NOx is a side reaction of combining oxygen and nitrogen during the combustion process, NOx in engine exhaust is expected to be a function of the peck temperatures during combustion. The dilemma is what fuel property changes have the most influence on the peak combustion temperatures. Earlier research by others had found the flame temperature and resulting NOx emissions of fuels to be most easily correlated with the hydrogen to carbon ratio (H/C) of the fuel (Ref 6-8) where high H/C has a lower flame temperature and therefore lower NOx thermal equilibriums.

This relationship can also be seem in some more recent work conducted with ARCO Chemical Europe in conjunction with BP Oil, and Volvo. ECE emission test were conducted with 11 different fuels of varying composition but relatively similar octanes in two 1991 non-cat cars with VOLVO engines (B-230 2.3 litres, 4 cylinders). The relative change in the NOx emissions compared to each fuel's hydrogen to fuel ratio in this study is shown in Figure 3. Also, three of the fuels contained oxygen, one from ethanol and two from MTBE. The data in Figure 3 suggest that the NOx emissions are strongly related to the fuels' hydrogen to carbon ratio independent of oxygen content in the fuel. This correlation to H/C ratio is consistent with the results reported in previously referenced studies.

However, in addition to the flame temperature of the fuel, the ultimate combustion temperature would also be expected to be a function of the octane of the fuel. Octane is a good indicator of the fuel's resistance to autoignite under the more severe operating conditions in the engine. Low octane fuel may autoignite early prior to optimum timing under severe engine conditions and thereby increase peak pressures and temperatures. Therefore, higher octane fuels would be expected to suppress autoignition and generate lower peak temperatures and lower NOx under severe engine operating conditions. The possible sensitivity of NOx to octane, particularly motor octane, of the fuel has been observed in some previous studies(Ref 9-10).

To test this theory that NOx production may be influenced by octane number independent of fuel composition, the octane of a reference fuel was artificially lowered by adding minute amounts of tertiary butyl hydro peroxide (TBHP), a very powerful pro-knock compound. FTP emission tests were conducted on two cars (1991 Dodge Spirit 2.5 liter/TBI and 1990 Ford Probe 2.2 liter/PFI) using the reference fuel (indolene) and the same fuel with two levels of peroxide. The average results for the two cars is as follows:

TBHP (ppm)	Fuel Octane MON	(R+M)/2	% NOx Changes
0	88.7	93.0	Base
420	87.2	91.4	+ 15%
1100	86.5	90.5	+ 14%

These results support the theory that octane number, independent of fuel composition, can also effect NOx emissions in the engine exhaust. Evidence of this octane effect has also been seen in Ethyl Corporation's work with MMT (methylcyclopentadienyl manganese tricarbonyl), a metal based octane additive. In the emission work to support a MMT waiver request, fuels containing 0.03125 grams of MMT per gallon increased the fuel's octane by approximately 0.8 octane numbers, but more importantly decreased NOx emissions(Ref 11).

A review of the emission results for AUTO/OIL's older car fleet shows similar fuel effects on the NOx emissions. Figure 4A shows the average NOx emissions relative to the fuels' H/C ratio. The AUTO/OIL's fuel matrix essentially falls into two groups: low H/C fuels and high H/C fuels. The NOx emissions from the high H/C fuels are approximately 12% lower than that from the low H/C fuels. The data also shows no oxygen effects since the emissions for the oxygenated fuels appear to be evenly dispersed among the non-oxygenated fuels. As Figure 4A shows, there also is more variance in the low H/C fuel group than the high H/C group. Much of this variance seems to be explained by the motor octane which varies as much as 5 octanes for the low H/C fuels as shown in Figure 4B. Though motor octane seems to explain some of the variance in the high H/C fuels as well, it is not as clear since the range of motor octane is only 2.5 numbers for this group.

The review of these studies suggest that much of the fuel effects on NOx emissions from gasoline vehicles can be explained by three main factors: the H/C ratio and the motor octane of the fuel as it effects peak combustion temperatures, and the fuel's sulfur content for its effect on the catalyst activity in the catalytic convertor. One other fuel quality for investigation is the ability of the fuel to warm-up the engine quicker (with higher DI), and thereby increase total NOx over an emissions test cycle. However, this might offset by the catalytic convertor also warming up quicker.

CARBON DIOXIDES EMISSIONS

Carbon dioxide (CO_2) from fuel combustion is considered to be a major source of greenhouse gases, and the current administration is dedicated to capping the year 2000 greenhouse gases at the same level as 1990. Though the stationary power sources may have the flexibility to switch from high fossil carbon fuels such as coal or heavy oils to low fossil carbon fuels such as natural gas or biomass fuels as a way to reduce CO_2, transportation fuels are not quite as flexibility. However, the CO_2 emissions associated with gasoline energy content is still related to the H/C ratio of the fuel components as shown in Figure 5. Aromatics represent the highest carbon content fuels and therefore the gasoline components with the highest CO_2 per unit of energy. Ethers, like paraffins, are gasoline components with the lowest CO_2 per unit of energy. Therefore, using ethers in place of aromatics for octane in gasoline may be an effective way to reduce fossil carbon dioxide emissions from gasoline by 4 to 5 percent. This CO_2 relationship to fuel H/C is consistent with the analysis reported by the AUTO/OIL analysis (Ref 12).

Raising the octane of gasoline presents another opportunity to significantly reduce CO_2 emissions from transportation fuels by allowing the automakers to raise the compression ratios of the engines of their new car models. Increasing the compression ratio would reduce fuel consumption by increasing the thermal efficiency of the engine's operation. The optimum octane for gasoline was last debated in industry about two decades ago when unleaded gasoline was about to be widely distributed in the marketplace (Ref 13-21). The conclusion from most of these studies was that the optimum octane for unleaded gasoline was around 91 to 92 (R+M)/2 octane even though the industry went with 87 (R+M)/2 as the standard octane for gasoline. The economic basis used in these studies was generally limited to comparing the cost of fuel savings versus the cost of raising the octane of gasoline. The environmental benefit of reducing CO_2 emissions was not considered in these studies at the time. If it had been included, it would have further supported the higher octane fuel / higher compression engine combination.

Figure 6 shows typical relationships to engine compression ratio which is derived from one of these studies (Ref 15). In the range of interest, Figure 6 shows that increasing the compression ratio by two numbers would increase fuel efficiency by approximately 10 percent but would also increase engine's octane requirement by approximately 6 octane numbers. This study suggest that each octane is potentially worth 1.8 % increase in fuel efficiency or fuel economy. This ratio between efficiency and octane seems to be approximately the same in most of these studies.

Some of these studies also attempted to address the issue on whether there was any increase in other emissions such as NOx or hydrocarbons(Ref 18-21). Their results suggested that there was little change in these emissions after re-optimizing other engine operating parameters such as timing and air to fuel mixtures. However, these studies did not evaluate any possible emission reduction benefits associated with also raising the fuel's octane for the higher compression ratio operation.

What these prior studies did not review in their analysis is any possible loss in driveability performance associated with higher fuel octane, particularly if high boiling aromatics should be the main source of the octane increases. As mentioned earlier, this is now a major concern of the automakers. Therefore, the source of increased octane would likely have to be from ethers which can potentially add five octane numbers to tha gasoline pool with out worsening the driveability index of the gasoline.

Another benefit of using ethers instead of aromatics for octane is their greater increase in combustion gas volumes. Higher H/C ratio fuels generate more moles or volumes of product gases per volume of combustion air that is consumed or drawn into the engine's cylinders. This higher volume of combustion gases increases combustion pressures even further for an added boost in engine efficiency and power. This comparison between ethers and aromatics is illustrated in Figure 7. In general, the ethers provide about 4 to 5 percent more gas volume than the aromatics during combustion.

Therefore, using oxygenates to further increase gasoline octane can potentially help reduce fossil based CO_2 emissions in two ways: one by reducing the carbon to energy ratio of the fuel, and second to allow the automakers to increase the fuel economy of cars by raising the engine compression ratio. Also,if oxygenates become a significant proportion of gasoline, it opens up an avenue to use more renewable carbon in gasoline since the alcohols in oxygenates can be made from renewable resources (Ref 22). This can further reduce the fossil based CO_2 emissions from transportation fuels.

SUMMARY
A review of the available data suggest there is still potential to reduce NOx emissions and the fossil fuel based CO2 emissions from mobile sources. Based on the review presented here, both of these emission reductions can be accomplished by increasing the hydrogen / carbon ratio of gasoline and also raising its octane number, particularly the motor octane. This would have been difficult to accomplish if the high carbon content aromatics were the only source of high octanes for gasoline blending. However, with the development of oxygenates as an octane enhancer, particularly ethers, both of these changes in gasoline can be done simultaneously and are technically feasible. Based on the reviews of past studies, both these changes in the fuel are probably economically and environmentally justifiable. Therefore, fuel oxygenates are not only capable of adding oxygen to gasoline to improve combustion, but they are also tools for increasing fuel H/C ratios as well as adding more octane for potentially better engine efficiencies in the future.

ABBREVIATIONS

DI - Driveability Index (1.5xT10 + 3.0xT50 + T90) degrees fahrenheit
ETBE - Ethyl tertiary butyl ether
IPTBE - Isopropyl butyl ether
MTBE - Methyl tertiary butyl ether
NOx - Nitrogen oxide compounds
MON - Motor octane number
RON - Research octane number
(R+M)/2 Average of RON and MON
H/C - Hydrogen to carbon atomic ratio
CO2 - Carbon dioxide

REFERENCES

1. Piel,WJ, "Expanding refinery technology leads to new ether potential", FUEL REFORMULATION, Vol 2 No.6 , Pgs 34-40, Nov/Dec 1992
2. Benson, JD,et.al.,"AUTO/OIL Air Quality Improvements Research Program An - Update of Research Results", presented at 1993 DEWITT Petrochemical Review Conference, March 1993
3. Benson, JD,et.al.,"Effects of Gasoline Sulfur Level on Mass Exhaust Emissions",SAE 912323
4. Benson, JD,et.al.,"Effects of Gasoline Composition and Properties on Vehicle Emissions: a Review of Prior Studies", SAE 912321
5. Benson, JD,et.al.,"The effects of Aromatics, MTBE, Olefins and T90 on Mass Exhaust Emissions from Current and Older Vehicles", SAE 912322
6. Ninomiya, JJ & Golovoy, A,"Effects of Air-Fuel Ratio on Composition of Hydrocarbons Exhaust from Isooctane ,Diisobutylene, Toluene and Toluene-n-Heptane Mixtures", SAE 690504
7. Carr,RC, et.al.,"The influence of fuel composition on emissions of carbon monoxide and oxides of nitrogen", SAE 700470
8. Harrington, JA & Shishu,RC,"A single cylinder engine study of the effects of fuel type, fuel stoichiometry, and hydrogen-to-carbon ratio on CO, NO and HC exhaust emissions", SAE 730476
9. **Present and Future Automotive Fuels**, by O. Hirao and R.F. Pefley, copywrit 1988 by John Wiley & Sons, Inc, pgs 101-106
10. Boekhaus, KL,et.al.,""reformulated Gasoline for California: EC-Premium Emission Control Gasoline", SAE 911628
11. Hollrah, DP, & Burns, AM,"MMT increases octane while reducing emissions", Oil & Gas Journal, Mar 11, 1991, pgs 86-90
12. Benson, JD, et.al., "Fuel composition effects on automotive fuel economy", SAE 930138
13. Editorial, "Air-quality control takes on a major role", Oil & Gas J., June 15, 1973, pgs 97-113
14. Wagner, TO, & Russum, LW,"Optimum octane number for unleaded gasoline", SAE 730552
15. Corner, ES, & Cunningham,AP, "Value of high octane number unleaded gasoline", ACS Los Angeles meeting, Mar 28 - Apr 2, 1971, D77-87
16. Hakala, NV, et.al. "The impact of product quality requirements on gasoline composition: past present, future", ACS New York Meeting, Aug 27 - Sept 1, 1972, B131-145
17. Lawrence, DK, et.al.,"Automotive fuels-refinery energy and economics", SAE 800225
18. Oberdorger, PE, "Compression ratio, emissions, octanes and fuel economy-an experimental study', 1972 API Proceedings, Div. of Refining, Vol 52, pg 936-953
19. Lee, RC, "Effects of composition ratio, mixture strength, spark timing, and coolant temperature upon exhaust emissions and power", SAE 710832
20. Felt, AE & Krause, SR, "Effects of compression ratio changes on exhaust emissions", SAE 710831
21. Baker, RE, et.al., "Selecting compression ratio for optimum fuel economy with emission constraints", SAE 770191
22. Piel, WJ, "Expanding Liquid Transportation Fuels Through Methanol, Higher Alcohols and Ethers", Proceedings of First Biomass Conference of the America's, Aug 30-Sept 2, 1993, Burlington, VT, Vol II, pgs 1116-1132

TABLE 1

TYPICAL PROPERTIES OF FUEL ALCOHOLS IN GASOLINE :

	Methanol (1) & Co-Solvent	Ethanol	Iso-Propanol	tert-Butanol	Iso-Butanol	tert-Amyl Alcohol
OCTANES: Blending (R&M)/2	108+	115	106	100	102	97
VAPOR PRESSURE: Neat RVP (100F)	4.6	2.3	1.8	1.7	0.6	0.7
Blending RVP (2)	31+	18	14	9	5	6
BOILING PT. (F)	148	173	180	181	226	216
DENSITY (LB/GAL)	6.63	6.61	6.57	6.59	6.71	6.79
ENERGY DENSITY: MBTU/Gal (LHV)	56.8	76.0	87.4	94.1	95.1	100.1
HEAT OF VAPOR.: MBTU/Gal @ NBP	3.14	2.39	1.90	1.55	1.67	1.58
OXYGEN CONTENT (WT.%)	50	34.8	26.7	21.6	21.6	18.2
SOLUBILITY IN WATER: (WT.%)	I	I	I	I	10.0	11.5

TYPICAL PROPERTIES OF FUEL ETHERS IN GASOLINE :

	MTBE	ETBE	DIPE	TAME	IPTBE	TAEE
OCTANES: Blending (R&M)/2	110	112	105	105	113	100
VAPOR PRESSURE: Neat RVP (100F)	7.8	4.0	4.9	2.5	2.5	1.2
Blending RVP	8	4	5	2.5	2.5	1
BOILING PT. (F)	131	161	155	187	188	214
DENSITY (LB/GAL)	6.19	6.20	6.1	6.41	6.30	6.39
ENERGY DENSITY: MBTU/Gal (LHV)	93.5	96.9	100	100.6	NA	NA
HEAT OF VAPOR.: MBTU/Gal @ NBP	0.86	0.83	0.9	0.90	NA	NA
OXYGEN CONTENT (WT.%)	18.2	15.7	15.7	15.7	13.8	13.8
SOLUBILITY IN WATER: (WT.%)	4.3	2.6	2.0	2.0	NA	NA

I - Infinite Solubility
NA - Not Available

(1) Typical for methanol waivered blends with cosolvents
(2) Blending RVP for 2.7% oxygen or higher in gasoline

FIGURE 1

Potential Octane Contribution of Oxygenates in Gasoline

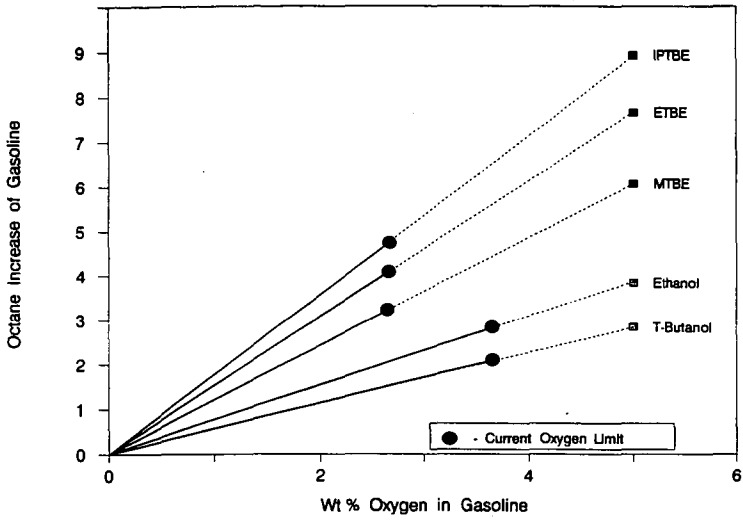

FIGURE 2

Driveability Index (DI) vs. Octane
for High Octane Blending Components

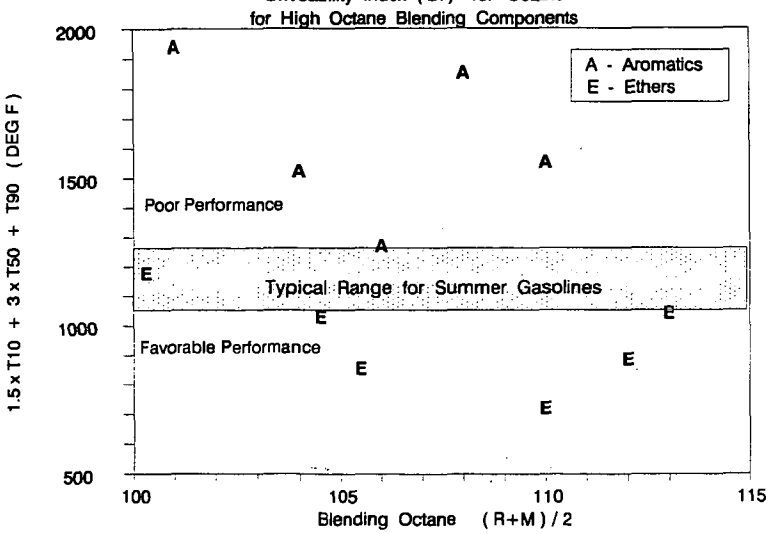

FIGURE 3

NOx Emissions Strongly Related To Fuel H/C Ratio

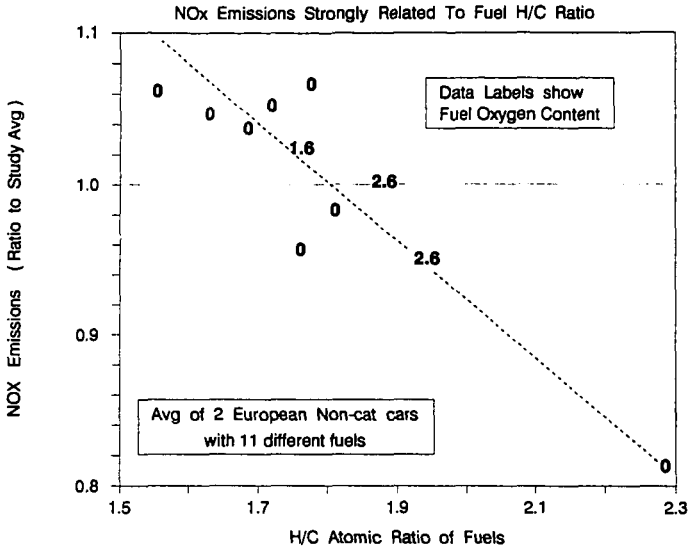

FIGURE 4A

NOx Emissions vs H / C Ratio of Fuel

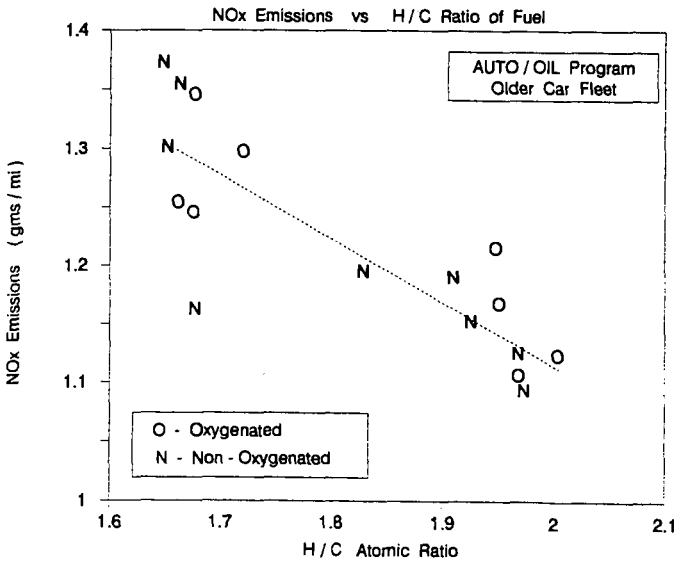

FIGURE 4B

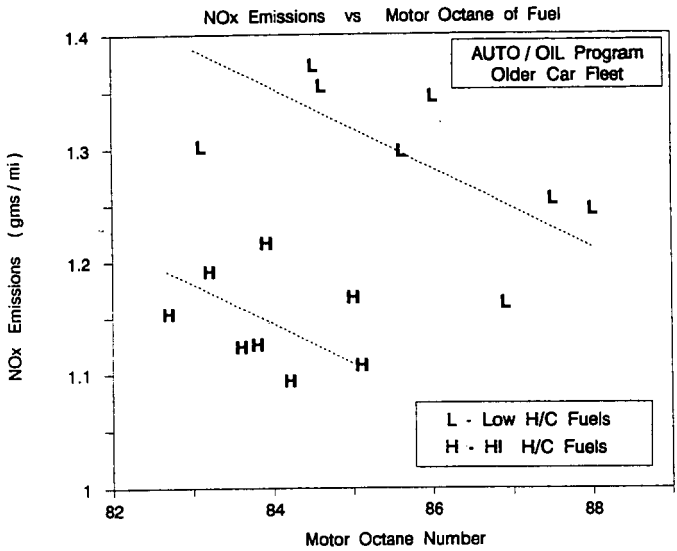

FIGURE 5

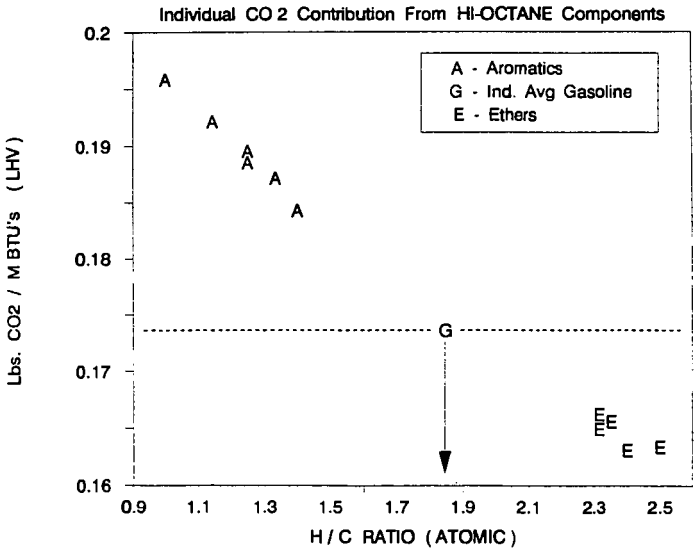

FIGURE 6

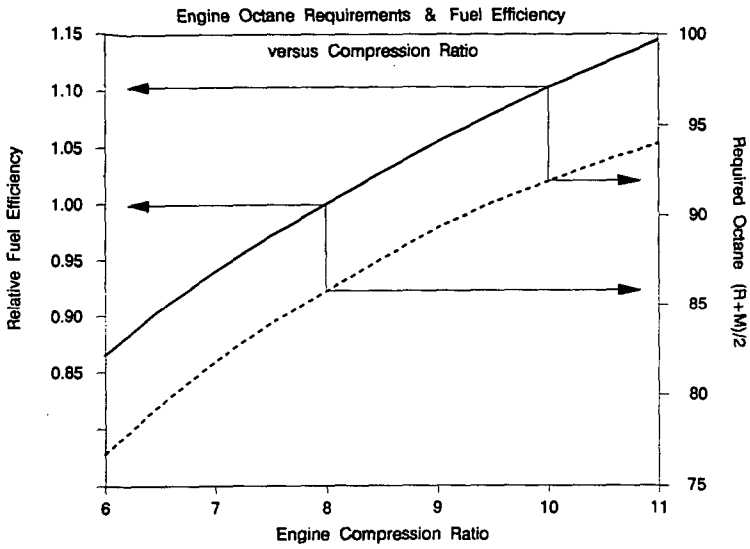

FIGURE 7

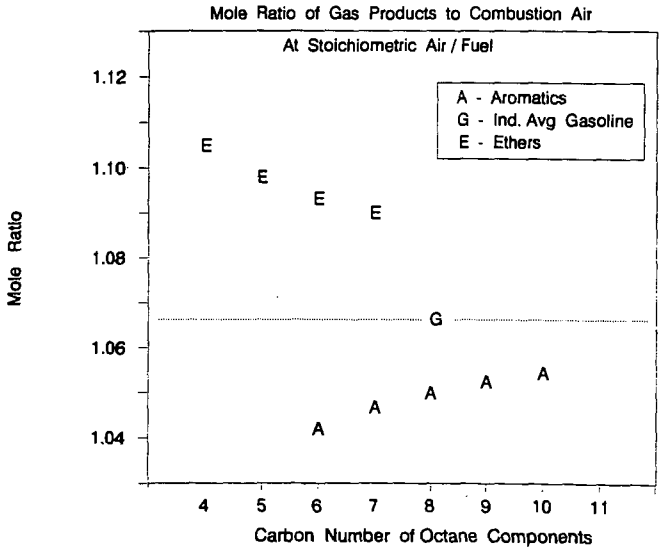

ALTERNATIVE FUEL USE IN COLORADO

Kim B. Livo
Dr. Jerry Gallagher
Martin W. Boyd
Air Pollution Control Division
Colorado Department of Health
4300 Cherry Creek Drive South
Denver, Colorado 80222

Abstract

The use of alternative fuels hold the promise of promoting energy diversity and reducing motor vehicle emissions. With the passage of the federal Clean Air Act Amendments of 1990, the National Energy Policy Act of 1992, and state initiatives such as from California, these fuels will have a far reaching influence on the fuels motor vehicle fleets operate on in the next century.

Many of the emission benefits of alternative fuels are dependent on the quality of the alternative fuel implementation, as well as the fuels themselves. To prevent degradation of motor vehicle emissions, the Colorado Department of Health has implemented alternative fuel retrofit system certification procedures. These, as well as EPA and California certification standards will allow present vehicles to have acceptable emissions, as well as future vehicles to meet required low emission standards.

Introduction

Transportation fuels have been at the heart of two major public policy issues facing the United States for the last several decades; pollution caused by motor vehicles, and the growing dependence on imported oil. Clean fuels, such as alternative fuels, are of increasing importance as a way to lower motor vehicle emissions. Diversification of transportation fuels is equally important, and will lessen or mediate future supply disruptions or price hikes which were saw in the oil shocks of the 1970s.

In Colorado, alternative fuel use has been growing dramatically since the start of the 1990s. Today there are more than 5000 vehicles capable of operating on alternative fuels. This growth is posing significant challenges to the fuels industry and fleet users. To support the expanding vehicle fleet, the fuels industry has been actively expanding the alternative fuel infrastructure. In turn, fleet users are being challenged to integrate and maintain new types of vehicles and fuels.

Background

Alternative fuel use in Colorado, and elsewhere, is been shaped largely by two significant pieces of federal legislation, the Clean Air Act Amendments of 1990 and the National Energy Policy Act of 1992. Developments in California are also effecting

alternative fueled motor vehicle use, as California "low emitting vehicle", "ultra low emitting vehicle" and "zero emitting vehicle" standards are driving the entire alternative fueled vehicle market

The Clean Fleet Fuels Program

The Clean Air Act Amendments of 1990 mandate the use of clean fuels for fleets, mainly as part of the Clean Fleet Fuels Program. This program is scheduled to begin in 1998 for public and private fleet of ten or more vehicles which are centrally refueled.

The Clean Fleets Fuels Program affects fleets in 21 ozone and one carbon monoxide non-attainment areas with populations of 250,000 or more based on the 1980 census. The program applies to automobiles and light and heavy duty trucks up to 26,000 pounds gross vehicle weight.

The Clean Fleet Fuels program is as the name suggests, a "clean" fuels program. It is a program which stresses air quality, rather than type of fuel, so is a performance, rather than alternative fueled, based program. To participate, a fuel/vehicle combination must meet the same standard as the California low emitting vehicle standard.

It is expected that alternative fuels will have an advantage in meeting the specific emission requirements of this program, but reformulated gasolines and clean diesel fuels may also participate. Any fuel, in combination with vehicle technology, which meets the standard is eligible for this program. This includes alternative fuels such as natural gas, propane, methanol, ethanol, and electricity, as well as clean gasolines and diesel fuels. Some types of vehicles will be exempted to this program. They include emergency and law enforcement vehicles, and vehicles which are garaged at home.

National Energy Policy Act of 1992

A second federal program expected to fuel the market for alternative fuels and fueled vehicles this decade and next, is the National Energy Policy Act of 1992. This act, unlike the Clean Fleet Fuels Program, is designed strictly to increase the use of alternative fuels and fueled vehicles. It mandates that certain fleets purchase alternative fueled vehicles.

The National Energy Policy starts in 1993 for the Federal fleet, and 1996 for State fleets and fuel provider fleets. Private and municipal fleets may have to participate also, as early as 1999, if the Secretary of Energy makes a determination that national alternative fuel usage goals require their inclusion to be met.

The National Energy Policy act affects all metropolitan areas in the United States with a population of over 250,000 people at the time of the 1980 census. It covers eligible fleets of fifty or more vehicles, with at least 20 or more in any one area. It affects vehicles with weights up to 8500 GVW. In addition, the covered vehicles must be capable of being centrally refueled.

Unlike the Clean Fleet Fuels Program, this program is an energy diversity program, so is not standards driven but rather alternative fuel driven. Alternative fuels which comply include, natural gas, propane, methanol, ethanol, and electricity.

Exempted vehicles for this program include, emergency and law enforcement vehicles, and vehicles garaged at home. At the discretion of the Sectary of Energy, the exemption for law enforcement vehicles may be waived.

State and Local Incentives

Colorado, because of air quality issues, as well as economic developmental reasons has encouraged the use of alternative fuels. In terms of air pollution, alternative fuels do hold the promise of reducing vehicle emissions which contribute to Colorado's winter-time carbon monoxide and PM-10 problems, and year round visibility concerns.

But showing promise does not necessarily lead to a solution. Mass emissions testing conducted by the Colorado Department of Health (CDH), has shown that not all alternative fueled vehicles are low emitting. As with traditional vehicles, good design and proper vehicle maintenance are needed to obtain and maintain appropriate vehicle emission levels. To assure that alternative fueled vehicles meet applicable emissions standards, the CDH regulates vehicle conversions through Air Quality Control Commission Regulation No. 14. Through this regulation, only CDH certified retrofit systems are allowed on vehicle conversions.

To encourage the use of alternative fueled vehicles, the state, and local municipalities, have adopted a number of incentive programs. One of the first programs established was a state fleet program which requires the state fleet manager to purchase or convert a number of vehicles to alternative fuels each year. Beginning in fiscal year 1991, the goal was 10% of all new vehicle purchases. This has been increased to 40% for the fiscal 1994 year.

The city of Denver has adopted a more pervasive ordinance, No. 330, administered by the City of Denver Health and Hospitals, requiring 10% of all fleet vehicles to be alternatively fueled for fleets of 30 of more vehicles. Diesel powered vehicles are excepted from conversion requirements, but are counted as part of that 30 or more vehicles.

Governor's Alternative Fuels Task Force

To encourage the use of alternative fuels, Colorado's governor, Governor Romer, established a Governor's Alternative Fuels Task Force. It was charged with the task of investigating ways of furthering the use of alternative fuels. This Task Force, composed of local state, county, and municipal officials, as well as citizens, met for over a year in determining the direction Colorado should take in meeting both clean air goals and economic development.

The principle recommendation of the Task Force was that Colorado implement a Clean Fleet Fuels Program as required by the Clean Air Act Amendments of 1990. Such a program should be implemented as soon as possible before the 1998 deadline. The task force also recommended an incentive program be developed to promote fuels such as CNG and propane which could reduce carbon monoxide emissions from appropriate vehicles. As a gas producing state, the use of fuels such as CNG and propane were also favored as a way of meet both clean air objectives, as well as economic development goals.

The recommendations of the Task force were given statutory authority through the passage of House Bill 1305.
House Bill 1305 authorized the Colorado Clean Vehicle Fleet Program, which will conform with the federal Clean Fleet Fuels Program mandated by Clean Air Act Title I, Part D and Title II, Part C , 1990.

The Colorado program will affect fleets with 10 or more vehicles in the Denver-Boulder CO non-attainment area. Colorado is the only state participating in the Clean Fleet Fuels Program strictly due to having a carbon monoxide non attainment area. Other states which have areas required to implement this program, and are in nonattainment for carbon monoxide, are also nonattainment for ozone.

By House Bill 1305, the Colorado Air Quality Control Commission was given the authority to promulgate rules and regulations for the implementation of this program. At the present time, the AQCC is preparing a regulation which will implement the program.

House Bill 1305 also authorizes the establishment of a mechanic certification program for vehicle conversions, and authorizes the establishment, but does not fund, an alternative fuels rebate program authorized to rebate up to half the cost of a vehicle conversion, or the alternative fueled vehicle premium on new vehicles. Such vehicles must demonstrate that reductions in carbon monoxide emissions, as well as for fine particulate matter, visibility pollutants will be achieved.

Other Activities

As in other states, there is also much activity being conducted through federally funded pilot programs, such as the Regional Transportation District operation of five large over the road methanol fueled transit buses, as well as large and smaller CNG powered buses. The U.S. Government Accounting Office is also in the process of obtaining a fleet of methanol flexible fueled automobiles. Coors brewing is operating an ethanol powered semi-truck tractor and a fleet of propane powered vans. Many other private and governmental fleets are also now operating CNG or propane powered vehicles.

The National Renewable Energy Lab is in the process of developing ways of lowering ethanol production costs. The Colorado School of Mines has established a heavy duty emissions laboratory, and Colorado State University has established a light duty emissions laboratory which are both measuring motor vehicle emissions from alternative fueled vehicles.

Conclusion

Presently almost all transportation fuels used are derived from oil. Increasingly that oil is imported. In 1990 it is estimated that close to half of all oil consumed in the United States was imported. With consumption increasing and production decreasing, it is expected that by the year 2010, approximately 70% of all oil consumed in the United States will be imported, if the measures in the National Policy Act are not implemented.

New federal clean fuel requirements will pose a significant challenge to states in the future. New alternative fuel infrastructures will have to be created. New motor vehicle designs will also be needed to utilize those fuels for maximum air quality and vehicle performance benefit. The potential is there to take advantage of the different characteristics of the new clean fuels to lower vehicle emissions as well as develop secure supplies of North American produced fuel.

OXYGENATED GASOLINE-THE CALIFORNIA EXPERIENCE

Dean C. Simeroth and Jose Gomez
California Air Resources Board
2020 L Street
P.O. Box 2815
Sacramento, CA 95812

KEYWORDS: Oxygenated Gasoline, California wintertime oxygenates regulations, gasoline oxygen content

ABSTRACT

The Air Resources Board (ARB) adopted regulations in December 1991, which require that gasoline contain 1.8 to 2.2 weight percent oxygen during specified months. The regulations were adopted in response to the Federal Clean Air Act Amendments of 1990. California's wintertime oxygenates program was implemented November 1, 1992. The use of oxygenated gasoline reduced ambient carbon monoxide concentrations by six to ten percent during the first implementation season. The wintertime oxygenates regulations sunset February 29, 1996. At that time, the wintertime oxygen content requirement becomes part of the Phase 2 reformulated gasoline regulations.

INTRODUCTION

This paper summarizes the California wintertime oxygenates regulations and discusses California's experience in implementing these regulations.

In response to the requirements of the federal Clean Air Act Amendments of 1990 (Act), the ARB adopted regulations in December 1991, which require that gasoline contain 1.8 to 2.2 weight percent oxygen during specified months. These regulations were implemented on November 1, 1992. Because California's regulations differ from the federal requirements, the ARB requested a partial waiver under section 211(m)(3) of the Act. The U.S. Environmental Protection Agency (U.S.EPA) is currently reviewing ARB's request for a waiver.

Based on our review of the program's first implementation season, the Board approved minor modifications to the regulations on September 9, 1993, which are intended to provide additional flexibility to those required to comply with the regulations, while not compromising the overall effectiveness of the program.

BACKGROUND

The Federal Requirements

The Act requires states with carbon monoxide (CO) nonattainment areas to implement oxygenated gasoline programs in these areas. In most cases, the states' programs must require that gasoline sold in the nonattainment areas have an oxygen content of at least 2.7 weight percent, during the specified months. The states are required to submit their oxygenated gasoline regulations as a revision to the State Implementation Plan (SIP). The U.S.EPA identified eight areas in California in which an oxygenated gasoline program is required, including: the Chico Metropolitan Statistical Area (MSA), the Sacramento MSA, the San Diego MSA, the Modesto MSA, the Fresno MSA, the Stockton MSA, the San Francisco-Oakland-San Jose Consolidated Metropolitan Statistical Area (CMSA), and the Los Angeles-Anaheim-Riverside CMSA. The EPA also specified the control period applicable in each of the affected areas[1]. The control periods are listed in Table 1.

ARB's Actions to Comply with the Act

In response to the requirements of section 211(m), the ARB promulgated oxygenated gasoline regulations following a hearing on December 12, 1991. The regulations were submitted as a revision to the SIP in October 1992. The wintertime oxygenates regulations sunset February 29, 1996, after which the year-round oxygen content requirements in the ARB's Phase 2 reformulated gasoline regulations will go into effect. Because over 70 percent of the gasoline used statewide is consumed in the U.S.EPA-designated areas, the Board made the wintertime oxygenates regulations applicable statewide. Additionally, the Board concluded that a statewide program simplifies enforcement and maximizes the CO emission reductions achieved in the nonattainment areas.

In setting the standards, the Board determined that while requiring the 2.7 weight percent oxygen content mandated by the Act would result in greater CO reductions it would also result in increased emissions of NO_x. An increase in NO_x emissions would interfere with efforts to attain the ambient air quality standards for particulate matter (PM_{10}), nitrogen dioxide (NO_2) and ozone. Therefore, the Board established a minimum and maximum oxygen content requirement at 1.8 and 2.2 weight percent, respectively.

The Board has requested that the U.S.EPA partially waive the minimum oxygen content requirement of 2.7 weight percent specified in the Act. Section 211(m)(3)(A) of the Act directs the U.S.EPA to waive the requirement for any area where the state demonstrates that the use of oxygenated gasoline would prevent or interfere with the area's attainment of an ambient air quality standard for any pollutant other than CO.

IMPACT OF OXYGENATED GASOLINE ON MOTOR VEHICLE EMISSIONS

Adding oxygen to gasoline affects the properties of gasoline in both performance and emissions. Generally, the oxygenates used today are ethanol and methyl tertiary butyl ether (MTBE). Over the past several years, there have been a number of test programs conducted to evaluate the impact of oxygen content on emissions. In the process of developing the wintertime oxygenates regulations, we evaluated all of the studies available to us at

the time and concluded that oxygen content in gasoline greater than 2.2 weight percent would increase NO_x emissions from motor vehicles[2,3,4]. In general, NO_x emissions increase as oxygen content increases.

Since the adoption of the wintertime oxygenates regulations and the Phase 2 reformulated gasoline regulations, we have been working to develop a predictive model to estimate emissions from alternative gasoline formulations that might be used in the vehicle fleet. As part of our waiver request to U.S.EPA, we used a draft version of the predictive model to evaluate the emissions characteristics of the most likely gasoline formulation that would be produced under the federal program[4]. This gasoline formualtion was developed as part of an analysis conducted by Turner Mason and Company for the Western States Petroleum Association. It should be noted that variations in the gasoline formulations actually produced will influence the actual impact on NO_x emissions. **Figure 1** shows the estimated impact on NO_x emissions for the different vehicle technology groups.

RATIONAL FOR LIMITING THE OXYGEN CONTENT OF GASOLINE

Emissions Inventory

Motor vehicle emissions are a major source of pollutant emissions, including CO, hydrocarbons (HC), and NO_x. HC and NO_x are precursors to ozone and PM_{10}. **Figure 2** shows that in 1987 emissions from on-road gasoline motor vehicles constituted about 57 percent of the total CO inventory, 35 percent of the VOC inventory, and 38 percent of the NO_x inventory. Gasoline vehicles accounted for about 36 percent of the PM_{10} precursors.

Air Quality in EPA-designated Areas

Both the ozone and PM_{10} standards are exceeded in all EPA-designated areas during some time in the control period. **Figure 3** shows the average number of days the state ozone standard was exceeded during the period of 1987 through 1990 for five air basins (which contain all of the U.S.EPA designated areas). **Figure 4** shows the average percent of PM_{10} observations exceeding the state standard. Because violations of the standards for CO, NO_2, ozone, and PM_{10} can occur simultaneously, it is critical that the efforts to reduce CO emissions don't increase emissions of the other pollutants.

As noted earlier, use of gasoline with oxygen content greater than 2.2 weight percent would result in larger CO reductions of CO emissions, but it would also increase NO_x emissions. Thus, it is critical to balance the need for CO reductions and the need to avoid NO_x increases. California's oxygenated gasoline regulations were designed to balance these competing effects.

ARB'S EXPERIENCE IMPLEMENTING THE OXYGENATED GASOLINE PROGRAM

Implementation Issues

During the first implementation period of the wintertime oxygenated gasoline program, staff became aware of various concerns regarding the application of the wintertime oxygenates regulations. After evaluation of the program, staff proposed several minor modifications to the regulations which were adopted by the Board on September 9, 1993[5]. The modifications include changing the control period applicable in the San Luis Obispo County, allowing the distribution of gasoline containing greater than 2.2 weight percent oxygen during the transition period, providing a one pound per square inch Reid vapor pressure exemption for ethanol blended gasoline produced during the calibration of blending equipment, and providing an exemption for small gasoline retailers that obtain their gasoline from areas outside California, if they meet specified conditions. These changes are intended to provide industry with additional flexibility in complying with the regulations, while maintaining the effectiveness of the regulations.

Air Quality Improvements During the 1992/93 Winter

Results of an analysis of CO, NO_x, and HC ambient air quality data collected at nine monitoring stations during the November 15, 1992 through Januarry 31, 1993 period indicates that concentrations of CO were significantly lower than past winters[6]. Although the 1992/93 winter had very favorable meteorology, we believe some of the reduction in CO concentrations are due to the use of oxygenated gasoline.

A linear regression analysis was done on the available data for the winter periods of 1985/86 through 1991/92 to characterize trends for the three periods 6 to 9 a.m., 6 to 9 p.m., and daily mean concentrations. The regression equations were used to compute the expected concentrations for CO, NO_x, and HC for the 1992/93 winter. The actual values for 1992/93 winter were divided by the expected values derived from the regression analysis.

The ratio of the 1992/93 actual concentrations to the expected concentrations were 72 percent for CO and 78 percent for NOx, respectively. The ratios of the NO_x concentrations were assumed to characterized the atmospheric dispersion during the winter 1992/93. Thus, the difference between the CO ratios and the NO_x ratios was attributed to the use of the oxygenated gasoline. The analysis indicates that the use of oxygenated gasoline accounted for about a six to 10 percent reduction in CO concentrations. **Figure 5** shows a summary of the ratios of actual to expected the concentrations of CO and NO_x.

CONCLUSIONS

California has successfully implemented its oxygenated gasoline regulations applicable in the winter months which has resulted in significant reductions of carbon monoxide emissions from motor vehicles. Although the regulations require a lower oxygen content than the minimum 2.7 weight percent specified in the Act, the regulations have been effective in reducing CO emissions. Minor modifications were made in September 1993 to address concerns raised during the first implementation season.

California's wintertime oxygenates regulations will help bring all CO nonattainment areas into compliance with the CO ambient air quality standards by the statutorily require deadlines. Additionally, the Phase 2 reformulated gasoline regulations which will become effective in March of 1996, will result in an additional CO reduction of about five percent.

REFERENCES

1. U.S. Environmental Protection Agency, *Supplemental Notice of Proposed Guidance on Establishment of Control Periods Under Section 211(m) of the Clean Air Act as Amended*, 57, FR 4408, February 5, 1992.
2. Air Resources Board, *California Phase 2 Reformulated Gasoline Specifications, Volume 2 Proposed Regulation for California Wintertime Oxygenates Program*, October 4, 1991.
3. Air Resources Board, *California Wintertime Oxygenates Program, Technical Support Document, Request for a Waiver of the Minimum Oxygen Content Requirements for Wintertime Gasoline, Pursuant to Federal Clean Air Act Section 211(m)(3)(A)*, October 1992.
4. Air Resources Board, *California Wintertime Oxygenates Program, Technical Support Document, Request for a Waiver of the Minimum Oxygen Content Requirements for Wintertime Gasoline, Pursuant to Federal Clean Air Act Section 211(m)(3)(A)*, Supplemental Submittal to U.S. EPA Docket No. A-93-13, June 17, 1993.
5. Air Resources Board, *Proposed Amendments to Regulations Regarding the Oxygen Content of Gasoline, and Regarding Exemptions from Motor Vehicle Fuels Requirements for Fuels Used in Test Programs*, July 23, 1993.

6. Dolislager, Leon J., Air Resources Board, *Did the Wintertime Oxygenated Fuels Program Reduce Carbon Monoxide Concentration in California?*, Presented at the Tenth International Symposium on Alcohol Fuels, November 7-10, 1993, Colorado Springs, CO.

Table 1		
EPA-Designated Areas	Control Period	
Chico MSA*	October 1	January 31
Sacramento MSA	October 1	January 31
San Diego MSA	November 1	February 29
Modesto MSA	October 1	January 31
Fresno MSA	October 1	January 31
Stockton MSA	October 1	January 31
San Francisco-Oakland-San Jose CMSA**	October 1	January 31
Los Angeles-Anaheim-Riverside CMSA	October 1	February 29

* Metropolitan statistical area

** Consolidated metropolitan statistical area

Figure 1

Results of ARB's Predictive Model for Gasoline Most Likely to be Produced Under 2.7 wt. % Program

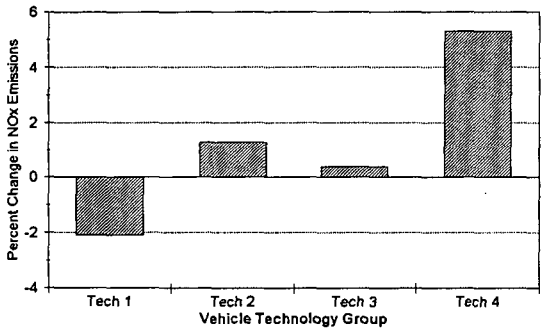

Figure 2

1987 Statewide Emissions Inventory

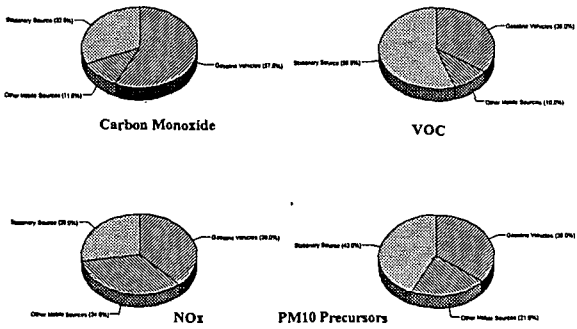

Figure 3

Avg. Number of Days Exceeding the *Ozone* State Standard

(1987 -1990 Data)

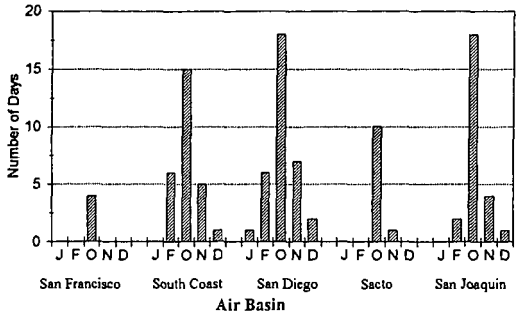

Figure 4

Avg. Percent of PM10 Observations Exceeding the 24-hr State Standard

(1987 - 1990 Data)

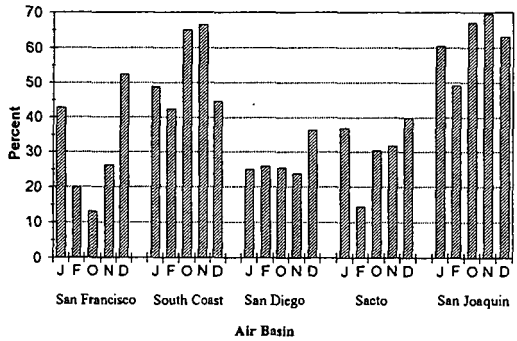

Figure 5

Ratios of Actual to Expected Concentrations

(winter 92/93)

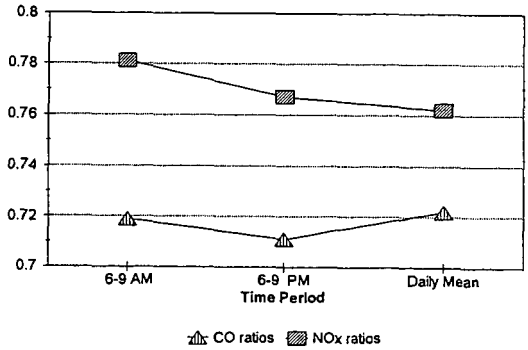

ENVIRONMENTAL AND ECONOMIC IMPLICATIONS OF OXYGENATED GASOLINE USE IN COLORADO: COLORADO'S OXYGENATED GASOLINE PROGRAM

Kim B. Livo
Dr. Jerry Gallagher
Air Pollution Control Division
Colorado Department of Health
4300 Cherry Creek Drive South
Denver, Colorado 80222

Abstract

Starting in the winter of 1987-1988, Colorado instituted an oxygenated gasoline program to control winter-time carbon monoxide emissions from motor vehicles. As a result of this and other air quality programs, as well as fleet turn over, the number of days exceeding the federal carbon monoxide standard has been reduce from 32 days in 1986 to 5 days in 1992.

The Colorado Department of Health estimates that for the winter of 1992-1993, carbon monoxide emissions from motor vehicles were reduced by 25% on a fleet wide basis. This reduction is credited with preventing a possible four additional high pollution days from occurring. The use of these gasolines increased the cost of gasoline in the Denver area by 3.5 cents per gallon.

Introduction

The Front Range area of Colorado is subject to numerous carbon monoxide (CO) high pollution episodes each winter. These are produced by the interaction of cold temperatures, temperature inversions, and carbon monoxide emissions from gasoline powered automobiles and trucks, as well as from residential wood burning and other sources. Of the total CO emissions, mobile sources contribute approximately 85%.

Elevated carbon monoxide concentrations occur on calm winter days, when temperature inversions develop which inhibit the dispersion of carbon monoxide produced from motor vehicle traffic and residential wood burning. Exceedances of the federal eight hour CO standard may result, especially in low laying, high traffic volume areas, such as downtown Denver.

As one of several strategies aimed at reducing motor vehicle CO emittions, the Colorado Department of Health (CDH) instituted an oxygenated gasoline program beginning in the winter of 1987-1988. Implementation of this program resulted from a comprehensive vehicle mass emissions test program conducted by the CDH in the 1980s.

Vehicle Mass Emissions Testing

Beginning with vehicle mass emissions testing in the late 1970s by the U.S. EPA, and soon after, by the Colorado Department of Health, it was noted that gasolines blended with alcohols, such as

ethanol and methanol, produced lower carbon monoxide emissions than non-blended gasolines (1,2). Later testing involving methyl tert-butyl ether (MTBE) blends produced similar results (3).

The test method used in this program is a mass-emissions test called the Federal Test Procedure (FTP). It is used by the U.S. EPA to certify emissions for new model light duty cars and trucks. In this test, a vehicle is placed on a dynamometer and is driven over a simulated driving cycle lasting 1372 seconds. Vehicle emissions are collected during this period, and the mass of these emissions are determined. The driving cycle involves both cold and hot vehicle starts, accelerations, decelerations, and steady cruise conditions, designed to simulate a typical urban commute.

Analyzing mass emissions results from these tests indicated that fuel oxygen content, rather than the particular oxygenate, was the most important parameter in producing carbon monoxide changes. In determining this effect, the CDH examined both linear and logarithmic relationships to correlate the mass emissions database (4). For the logarithmic models, both positive as well as negative curves could be fitted to the data, depending on the individual study analyzed. Because of the differences in curvatures, as well as because the linear model fit equally as well as the logarithmic models, a linear model has been adopted in describing the CO effect of using oxygenated gasolines. Table 1 describes the CDH carbon monoxide FTP mass emissions results using the linear model, averaged for oxygen content, and differentiated by vehicle emissions control technology class.

The U.S. EPA and other organizations have also conducted mass emission test programs which have corroborated and expanded upon the CDH mass emissions testing. In the latest study, the Auto/Oil Air Quality Improvement Research Program, fuel composition parameters, including oxygen content, have been varied to study emissions effects (5). Again, directionally, increasing oxygen content was found to reduce carbon monoxide emissions.

CO Vehicle Emission Reductions

In analyzing the CO vehicle emission reduction of oxygenated gasolines, the CDH relies on the U.S. EPA MOBILE vehicle emissions model. Employing this computer model, vehicle emissions from an area's motor vehicle fleet can be averaged and estimated. This model takes the CO emission reductions seen in the FTP mass emissions testing, and applies it across the entire motor vehicle fleet, and under different driving conditions. Inputs to the model include: vehicle age and distribution, speed, road type, time of day, and area type.

Utilizing the present MOBILE 5a emissions model, the CDH estimates that in the winter of 1992-1993, carbon monoxide exhaust emissions from motor vehicles, in the Front Range area, were reduced by 26.6% in October and November, and by 24.9% in January and February (6). Reductions in ambient CO concentrations are less, since mobile sources are not the sole source of CO emissions, and concentrations are dependent on the rates of production and dispersion.

Contributing to the effectiveness of the 1992-1993 program was the increased percentage of ethanol blended gasoline sold along the Front Range area. Ethanol blends made up 45% of the total gasoline sales of this winter, compared to 20% the winter before. When blended at the 10% vol. level, ethanol blends have a higher oxygen content than 15% MTBE blends (3.5% vs. 2.7% wt.). A higher oxygen content produces a greater average CO reduction. 15% vol. MTBE blends constituted the balance of the oxygenated gasoline sold.

During the winter of 1992-1993, the average oxygen content of the Front Range gasoline pool was 3.0% percent in November and December, dropping to 2.8% for January and February, when a new I.R.S. ruling took effect, permitted the blending of ethanol at a reduced level (7.8% vs. 10% vol.).

Air Quality

In terms of ambient air quality, there were five exceedances of the 9ppm eight-hour average national ambient air quality standard (NAAQS) for CO in the winter of 1992-1993. An additional four possible exceedances were prevented because of the use of oxygenated gasolines (6). Figure 1 documents the daily 8-hour maximum reading for the winter of 1992-1993. The lower clear bar represents monitored values. The solid dark bars represent estimated concentrations, if oxygenated gasolines were not used.

For the calendar year 1992, there were five days exceeding the NAAQS 8-hour average CO standard, a declined from 32 days in the calendar year of 1986. The continuing reduction in CO exceedances as shown in Figure 2, is due to a continuing decline in CO emissions due to fleet turn over, the use of oxygenated gasolines, vehicle inspection and maintenance programs, and no woodburning on high pollution days, as well as favorable weather conditions.

Costs

The Colorado Department of Health analyzed the costs associated with the 1992-1993 oxygenated gasoline program. The costs of base gasoline, oxygenates, transportation costs, as well as octane and butane credit savings were examined to determine oxygenated gasoline costs. These were then compared to the differential costs observed between oxygenated and non-oxygenated gasolines Denver RACK prices received from the Oil Price Information Service. Retail prices were also observed.

For the winter of 1992-1993, the average cost of gasoline increased by three and a half cents per gallon because of the Oxygenated Gasoline Program (6), a similar amount as for previous season's program. This cost represents increased refiner and blender costs due to oxygenate blending and does not take into account any changes in vehicle fuel economy.

While the average cost associated with blending oxygenates remained the same as the previous winter, the cost of gasoline blended with ethanol rose slightly. Average program costs remained similar to the 1991-1992 season however, because the

market share for ethanol blends increased, and ethanol blended gasoline costs remained below MTBE blended gasoline costs (2.75 cents/gal. vs 3.75 cents/gal.).

Supplies

This year over 360 million gallons of oxygenated gasoline were sold along the Front Range during the oxygenated gasoline program period (November 1, 1992 through February 28, 1993). Statewide, over 500 million gallons of gasoline (much of it oxygenated) was sold during this period.

Fuel Economy

Oxygenated gasolines have a small affect on fuel economy at high altitude. CDH fuel economy testing conducted during vehicle mass emission FTP testing, has shown on average, fuel economy reductions of up to 1.5% for some vehicle classes to slight increases of less than 1.0% for other motor vehicle classes.

Oxygenated gasolines lean the air to fuel ratio of a vehicle, increasing the engine's efficiency and in some older vehicles slightly improving fuel economy. Oxygenated gasolines have a slightly lower heating value though, which may decrease fuel economy in some vehicles, especially vehicles equipped with the latest oxygen sensors and feedback fuel injection. Altitude and the partial pressure at Denver (5280 feet) may also lessen fuel economy impacts of oxygenated gasolines. Table (2) gives CDH high altitude fuel economy test results for three types of emission control technologies, using 11% and 15% MTBE blends, and 10% ethanol blends.

Conclusions

Based on mass emissions testing, using the Federal Test Procedure, oxygenated gasoline have been demonstrated to decrease carbon monoxide emissions from gasoline powered motor vehicles. This decrease is related to oxygen content, and varies according to vehicle emission control technology class and vehicle operating modes. For the FTP, based on a linear oxygen effect, oxygenated gasolines decrease exhaust CO emissions by 4.83% to 6.45% for each one percent oxygen content, by weight, the gasoline contains.

Using the U.S. EPA MOBILE 5a motor vehicle emissions model, the CDH estimates that carbon monoxide emissions were reduced by 24.9 to 26.6% in the winter of 1992-1993. As a result of this and other air quality programs, as well as fleet turn over, the number of days exceeding the federal carbon monoxide standard has been reduce from 30 days in 1986 to 5 days in 1992. The use of these gasolines increased the cost of gasoline in the Denver area by 3.5 cents per gallon.

REFERENCES

1. Richardson, David, "Exhaust Emissions and Fuel Economy from Automobiles using Alcohol/Gasoline Blends under High Altitude Conditions", U.S. EPA, Office of Air, Noise, and Radiation, Oct. 1978.

2. Hollman, Ted, William Miron, "Effects of Ethanol-Blended Fuel on Motor Vehicles at High Altitude", Colorado Department of Health, Air Pollution Control Division, Mobile Sources Program, Sept. 1983.

3. Ragazzi, Ron, "The Effects of Two Different Oxygenated Fuels on Exhaust Emissions at High Altitude", Colorado Department of Health, Air Pollution Control Division, Mobile Sources Program, Jan. 1987.

4. Nelson, Ken, "The Effects of Fuel Oxygen on CO Emissions at High Altitudes",Colorado Department of Health, Air Pollution Control Division, Mobile Sources Program, May 1990.

5. Auto/Oil Air Quality Improvement Research Program (SP-920), Society of Automotive Engineers, Feb. 1992.

6. Livo, Kim, William Miron, "1993 Oxygenated Gasoline Program, Air Pollution Control Division Report to the Colorado Air Quality Control Commission", Colorado Department of Health, Air Pollution Control Division, Mobile Sources Program, April 15, 1993.

TABLE 1

CDH MASS EMISSIONS RESULTS

AVERAGE PERCENT CARBON MONOXIDE REDUCTION BY *VEHICLE EMISSION CONTROL TECHNOLOGY CLASS* AND OXYGEN CONCENTRATION

Vehicle Emissions Control Technology Group	2.0% Oxygen by wt. (11% MTBE)	2.7% Oxygen by wt. (15% MTBE, 7.8% ethanol)	3.5% Oxygen by wt. (10% ethanol 5% methanol)	1.0% Oxygen by wt.
Pre-Catalytic Converter	12.84%	17.33%	22.47%	6.42%
Two-way Oxidation Catalytic Converter Equipped	12.90%	17.4%	22.58%	6.45%
Three-way, Closed-loop, Catalytic Converter Equipped	9.66%	13.04%	16.91%	4.83%

Figure 1

Winter-time CO Concentrations
With and Without Oxygenated Gasoline

(8-HR DAILY MAX)

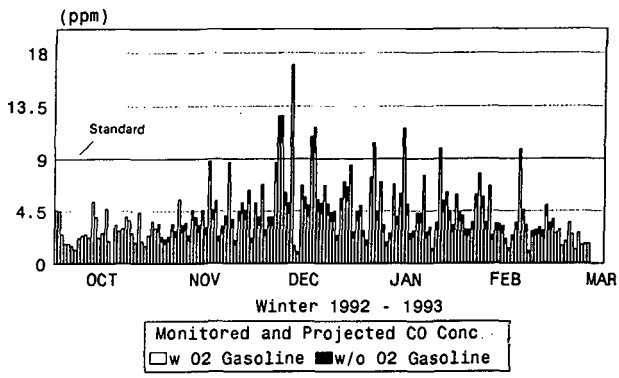

Figure 2

Colorado CO Exceedances

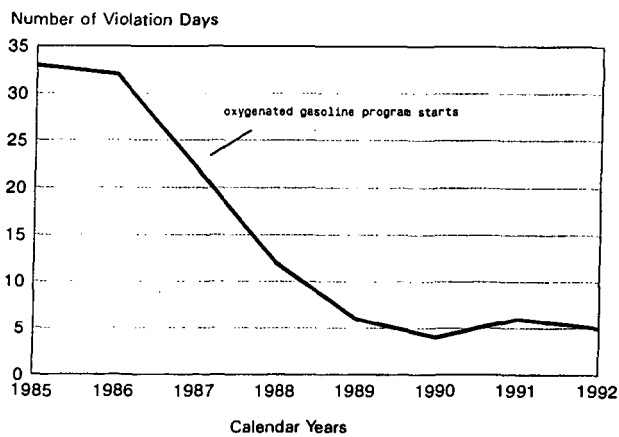

TABLE (2)

FUEL ECONOMY EFFECTS

VEHICLE TECHNOLOGY	CDH FTP Measured Fuel Economy Change		
	11% MTBE	15% MTBE	10% ethanol
Non-Catalyst	+0.82%	+0.21%	+0.11%
Catalyst	+0.84%	+0.18%	+0.33%
Closed Loop	+0.7%	-1.13%	-1.41%

WHY ARE ALCOHOL FUELS STILL ALTERNATE FUELS?

Reda M. Bata
Department of Mechanical and Aerospace Engineering
West Virginia University
Morgantown, WV 26506

Key Words: alternate, oxygenated, methanol, CNG

Abstract

The enthusiasm for using alcohols as alternate fuels in internal combustion engines (ICE) has been accelerating since the middle of 1970 and reached its peak by the middle of 1980. This was due to the serious effect of the exhaust emissions from automotive engines powered with oil-derived fuels coupled with a market rise in the cost of oil-derived fuels. Since then, the cost of oil has been decreasing and the need for alternate fuels has begun to slow down due to this economical reason. Alcohols are excellent fuels since they can be produced from renewable resources and their impact on health and the environment is limited. They are favorable for IC engines because of their high octane rating, burning velocities, and wider flammability limits. Experimental research and in-use applications showed drastic reduction in carbon monoxide (CO), particulate matter (PM), and moderate reduction in hydrocarbon (HC). Adverse effects on nitrogen (NO_x) and aldehyde (CHO) were also noticed.

Introduction

It is worth all of our efforts and dedications in order to become an energy-environment conscious nation. The attitude of increasing the stringent restrictions on pollutant emissions from automotive engines, the urgency for fuels derived from renewable sources, and the awareness of the expected rise in the price of oil-derived fuels in the future, have been the main motives of the 1990 Clean Air Act Amendments (CAAA) and the Energy Policy Act of 1992 (EPACT), Appendix A. Both acts are mandating the procurement of alternative fuel vehicles (AFV's) as well as imposing stringent exhaust gas emissions standards.

In the United States, the consumption of petroleum products exceeds the production rate of this strategic material. Meanwhile, the relaxation of the domestic companies to discover new oil fields because of the cheap surplus oil that is available in the international market, and the opposition from some environmentalists to explore new oil fields in the costal areas has been one of the major factors in creating the United States' negative balance of trade with other countries. Since new, revolutionary, non-traditional power plants are unexpected, and increasing demand is unavoidable as well, in the next few decades, the traditional IC engines will remain the prime power mover in our society. It took almost a century to develop the existing ICE, the oil refineries, and the distribution infrastructure. Huge investments have been dedicated for this business and they should be protected.

Alcohol fuels such as methanol (CH_3OH), ethanol (C_2H_5OH), iso-butanol (C_4H_9OH), methyl-tertiary-butyle-ether (MTBE), ethyle-tertiary-butyle-ether (ETBE), have proven to be excellent octane booster and blend with the traditional fuels, gasoline and diesel, and require minor engine modifications.

As stated in the National Energy Strategy in February, 1992, "The U.S. fleet of more than 185 million cars, buses, and trucks consume two-thirds of the oil used by the United States." In 1991, almost 50% of the oil consumed in our country was imported and it is expected that this percentage will increase up to 61% by the year 2010. The transportation system is consuming 63% of total U.S. oil consumption. The cost of damage to the environment caused by the exhaust gas emissions ranges from $11 billion to as high as $187 billion, (1). The

aforementioned scary statistics have led the U.S. Department of Energy's (DOE) Office of Transportation Technologies (OTT), through its Office of Alternative Fuels, to support innovative-cost-effective methods to produce and implement alternative fuels and achieve greater penetration into the marketplace. Details of the production plan is explained in Appendix B. Among the alternate fuels are reformulated gasoline (RFG) additives such as ethers (oxygenated fuel additives), methanol, and ethanol. Higher alcohols, such as iso-butanol, were not mentioned because of their higher cost of production and lack of political support when compared to methanol and ethanol.

The Rationale for Alternate Fuels

Two main reasons justify the use of alternate fuels; the finite unrenewable supply of crude oil, and protection of the environment from the increasing ozone (photochemical smog) as well as the greenhouse effect. Since crude oil is cheap and available, demand for the use of alternate fuels will be realized in the long-term strategy. Protecting the environment is the short-term demand as was proven by the debate associated with the Clean Air Act Amendment in 1990. Use of alternate fuels in association with the new engine technology has the potential to reduce the harmful pollutants that cause damage to the environment.

Why Alcohol Fuels

There is no miraculous, super fuel that will satisfy all the requirements of cost effectiveness, maximum thermal efficiency, and engine performance, and still remain clean enough to protect the environment. Every fuel has advantages and disadvantages, and selection of a particular fuel is a function of different parameters including the physical properties of the fuel as shown in Table 1 (3). If we start with the disadvantages of the alcohol fuels, they might be summarized as follows:

1. The economics of production. Unless the cost of alcohol production from renewable resources is made cost-effective, there will be no demand for it. These alcohols could be produced from biomass, coal, and natural gas.
2. Flame visibility of alcohol is difficult to be detected, which might be hazardous. The lack of visibility is due to the small number of carbon atoms present in the alcohol. Since there is very little carbon, there is no soot formation to give the flame color.
3. Cold startability problems. Due to their low vapor pressure, high latent heat of vaporization, and single boiling point, alcohols, especially ethanol, have difficulty meeting industry standards for starting in cold weather.

The last two of these disadvantages, however, can easily be solved. By the addition of a small amount of gasoline to the alcohol mixture, a more visible flame will be produced and the effect of cold weather on engine startablity can be brought well within the industry standards.

Although there are a few minor disadvantages to the use of alcohol fuels, the advantages more than outweigh its easily solvable problems. The advantages are as follows:

1. Methanol can be made out of organic material such as biomass and municipal waste. In the long-term, it could even be made out of coal. The United States has 25% of the worlds' supply of coal, which will be abundant for years to come.
2. Alcohol combustion produces higher combustion pressures inside the combustion chamber of the ICE due to the higher molal products to reactants ratio, compared to gasoline, which improves power output and thermal efficiency (2).
3. Alcohols have a higher average octane rating $\{(RON+MON)/2=104\}$ compared to gasoline. Increasing the compression ratio of the engine to 12:1 or higher increases power and fuel efficiency by 20% and 15% respectivily (3&4).
4. Alchols have better combustion characteristics and performance due to the increased volumetric efficiency of alcohol fuels, which is why methanol is a preferred racing fuel. Acceleration time decreases with power increase.
5. In case of fire, alcohols have higher visibility for escape-rescue, low asphyxiation, produce cool flame and low heat output which causes low burns, low smoke damage,

residue is easily washed away, and are extinguishable with water and more readily by powders and foams.

6. In case of leaks and spillages, alcohols are miscible in water and could be washed out with water for quick and easy removal. They are easily metabolized if absorbed by the ground.
7. Alcohol fuels have a lower evaporative emission. Not as many harmful by-products will be released into the atmosphere by using alcohol fuels.
8. Since the carbon content in alcohol fuels is very small, a negligable amount of soot is formed and released to the atmosphere when burned in the ICE.
9. Alcohol fuels are liquids, which make them accessible using the same means of transportation and handling infrastrucure of the conventional fuels with minor modifications.

Alternate Fuels and Environment

Deterioration in air quality is a vital issue that needs to be seriously monitored and limited. The transportation system is a major air pollution contributor due to the exhaust emissions such as carbon monoxide (CO), hydrocarbons (HC), nitrogen oxides (NO_x), carbon dioxide (CO_2), and particulate matter (PM). The transportation system is estimated, by the U. S. Enivironmental Protection Agency (EPA), to produce up to 44% of the total hydrocarbons emissions inventory in the U.S. The evaporative emissions share 31%, and the balance of 13% is from exhaust gas emissions. Production rate of exhaust gases differ from one place to another based on different parameters such as the geographic locations, altitude, weather conditions, traffic congestion, population, maintenance availability, etc. The greenhouse effect, which is caused by the production of carbon dioxide, has been suspected to cause the global warming and its adverse effect on the biological system. Ozone production is due to the chemical reaction between nitrogen oxides, hydrocarbons, and sunlight, which is known as photochemical smog. Los Angeles' polluted environment with photochemical smog is a good example, and is considered as one of the most non-attainment areas in the nation.

Implimentation of alternate fuels, in many pilot project over the nation, with dedicated and converted IC engines, has a positive effect on carbon monoxide and particulate matter reduction. Hydrocarbons emission, which is mainly "evaporative emission" is reduce when alcohol fuels are used. This trend is obvious in Table 2, which shows in-use emission measurements of regulated pollutants from jet A and neat methanol fuels, for similar vehicles and similar engines under transient test conditions. Hydrocarbons data do count the evaporative emissions which make up approximately 65% of the hydrocarbons emissions. In another study of carbon monoxide under steady-state conditions, wide open throttle (WOT), no load (NL), intermidiate load (IL), and full load (FL) are shown in Table 3. Four different fuels-20% by volume iso-butanol -gasoline blend (B20), 20% ethanol-gasoline blend (E20), ethanol-gasoline blend (20M), and base line gasoline (GAS)-were used. Carbon monoxide emissions from alcohol-gasoline blends were lower than that from gasoline, and M20 was the lowest.

Conclusions

Why are alcohol fuels still alternate fuels? Apparently, since production and use cost of conventional fuels (gasoline and diesel) are very cost-effective, nobody will use alcohol fuels except the Federal and State Governments because of the CAAA and EPACT through the AFV's programs. What about special fleets of companies, private sectors, and individuals ? We are not yet environment-concious users !

References

1. The National Renewable Energy Laboratory report prepared for the U.S. Department of Energy, DOE/CH 10093-157, DE 92016412, May 1993.
2. Nichols, R. J., "Applications of Alternatinve Fuels", SAE Paper 821573, 1982.
3. Sriram Popuri and Reda Bata, "A Performance Study of Iso-Butanol-, Methanol-, and Ethanol-Gasoline Blends Using A Single Cylinder Engine".
4. Nichols, R. J., et al, "Ford's Development of a Methanol fueled Escort", Proceedings of the International Alcohol Fuel Technology Symposium, Auckland, 1982, II, pp. 109-116.
5. Bata, R. M., Elrod, A. C., and Rice, R. W., "Emissions from I.C. Engines Fueled with

Alcohol-Gasoline Blends: A Literature Review", Published in the Engine Emissions Technology for lthe 1990's, ICE Division of the ASME, Vol. 4, October 1988, pp. 141-151.

Appendix A

Clean Air Act Amendments of 1990 (CAAA) -- The CAAA requires fleets in 22 urban regions to begin operating clean fuel vehicles (CFV's) by the end of the decade.. Beginning in 1998, 30 percent of new vehicle purchases by many fleets must be CFV's. This increases to 50 percent by 1999 and 70 percent by 2001. Stringent future emission standards are also established for cars, light-suty and heavy-duty trucks, and buses.

Energy Policy Act of 1992 (EPACT) -- EPACT establishes requirements for the purchase of AFV's in both public and private fleets. These requirements begin in 1993 for frderal fleets, 1996 for state and fuel supplier flets,and if necessary, in 1999 for private and municipal fleets. EPACT also provides economic and other incentives for fuel suppliers, original equipment manufactureres, and fleet owners.

Appendix B

Production of alcohol fuels on developing cost-effective biomass-to-fuel processes. The following strategy has been adopted by the DOE.

1. Establishing cost-effective techniques for growing the biomass resource.
2. Developing high-yield, low cost systems for converting biomass to fuels.
3. Demonstrating alternative fuels(including methanol, ethanol, and natural gas) in vehicle fleets across the United States.
4. Acquiring data on the performance of alternative-fueled vehicles from fleets across the U.S.

Selection and production of energy crops that have high-yield biomass feedstocks is a primary step in the biomass-to-fuel process. Energy crops that can be grown in short-rotation such as trees (2-8 years), grasses that can thrive in marginal conditions, and aquatic plants such as algae with high oil (lipid) content. Researchers and scientists are genetically manipulating trees and grasses to increase yield which would produce more alcohol in less time.

Table 1: Properties of Fuels

Characteristic	Gasoline	NO.1 Diesel fuel	Methanol	Ethanol	Iso-butanol	Gasohol
Chemistry	Mixture of Hydrocarbons	Mixture of Hydrocarbons				90% Unleaded Gasoline 10% Ethanol
Specific Gravity @ 60 F	0.72 - 0.75 *	0.82	0.79	0.79	0.81	0.73 - 0.76
Boiling Point o F o C	 85 - 437 30 - 225	 360 - 530 190 - 280	 149 65	 173 78.3	 227 108.1	 77 - 410 25 - 210
Net Heating Value (Mass) BTU/lb MJ/kg	 18,700 43.5	 18,500 43	 8,600 20.1	 11,600 27	 14,000 33	 18,000 41.9
Net Heating Value (Volume) BTU/gal MJ/l	 117,000 32	 126,000 35.3	 57,000 15.9	 76,000 21.3	 93,000 26	 112,900 30.9
Heat of Vaporization BTU/lb kJ/kg	 170 400	 250 600	 500 1,110	 390 900	 250 578.4	 200 465
Vapor Pressure @ 100 F psi kpa	 9 - 13 62 - 90	 0.05 0.34	 4.6 32	 2.5 17	 0.33 2.3	 8 - 16 55 - 110
Octane Number Research Motor	 91 - 100 82 - 92	 Not applicable	 112 91	 111 92	 113 94	Note 1
Cetane Number	Below 15	40 - 60	Below 15	Below 15	Below 15	Not applicable
Stoich. Air/Fuel Ratio	14.6	14.6	6.4	9	11.1	14
Vapor Flammability Limits	0.6 - 8	0.6 - 6.5	5.5 - 26	3.5 - 15	Note 2	Note 3
Appearance	Colorless to light amber color	Colorless to light amber color	Colorless	Colorless	Colorless, viscous	Colorless to light amber color
Vapor Toxicity	Moderate irritant	Moderate irritant	Toxic even in small doses	Toxic in only large doses	Moderate irritant	Moderate irritant

* For premium gasoline the range is 0.73 - 0.78 (0.75 is used in this study)

Note 1: May be the same as gasoline, or add 1.5 or 2 numbers depending on blending practice

Note 2: Values not available

Note 3: Values not published

Sources: SAE 820261, SAE 890434, Bosch Automotive Handbook

Table 2. Exhaust Gas Emissions For Jet A and Methanol 100

Vehicle	Fuel	CO	NOx	HC	PM
1	Jet A	37.8	32.3	2.41	0.72
2	M100	22.2	86.5	5.77	0.22
3	M100	18	19.5	6.95	0.1
4	M100	25	20.8	7.5	0.17

Table 3. Carbon Monoxide Emissions from Different Fuels

Fuels	1250 RPM (NL)	2200 RPM (IL)	2500 RPM (FL)
Gas	4.21	0.135	2.51
B 20	2.4	0.13	1.38
E 20	1.5	0.125	0.69
M 20	1.45	0.124	0.61

DECREASED BENZENE EVAPORATIVE EMISSIONS FROM AN OXYGENATED FUEL

C. H. Bobro, L. J. Karas, C. D. Leaseburge, and D. J. Skahan

ARCO Chemical Company
Research and Development
3801 West Chester Pike
Newtown Square, PA 19073-2387

Key Words: Ether Oxygenate, Oxygenated Gasoline, Benzene Emissions

ABSTRACT

A chromatographic head-space analysis was developed to determine the vapor phase concentrations of non-oxygenated and oxygenated fuels. The effect of ether oxygenates on benzene evaporative emissions was evaluated. A base fuel and three oxygenated fuels were prepared to contain 1 volume percent benzene at matched volatility levels. Head-space composition for each blend was measured, as a function of temperature, to determine the effects of oxygenates on benzene volatility. Results indicate MTBE (methyl *tert*-butyl ether), ETBE (ethyl *tert*-butyl ether), and TAME (*tert*-amyl methyl ether) each reduce benzene vapor phase concentrations. Benzene reductions averaged approximately 14 percent for fuels containing 2.7 weight percent oxygen. Reductions were temperature dependent, but not generally dependent upon type of ether oxygenate. Significant environmental benefits result from reducing benzene volatility and the resulting decrease in evaporative emissions. Benzene is classified by the EPA as a known human carcinogen. The 1990 Clean Air Act Amendments require reductions in gasoline benzene levels to reduce toxic emissions.

INTRODUCTION

The 1990 Clean Air Act Amendments require that gasoline sold in nine of the nation's most polluted cities be reformulated to produce less pollutant emissions. Beginning in 1995, reformulated gasoline will produce 15% less hydrocarbon emissions and regulated toxins. Hydrocarbon emissions are a key component to urban smog problems. Gasoline toxins reductions are an effective means of reducing human exposure risk to known and potential carcinogens. Benzene, a known human carcinogen contributes a significant fraction of the regulated emissions of toxins.

This paper examines the potential of ether oxygenates to reduce benzene evaporative emissions. The ether oxygenates under study include: MTBE (methyl-*tert*-butyl ether), ETBE (ethyl-*tert*-butyl ether), and TAME (*tert*-amyl methyl ether). An experimental program was developed to measure vapor phase hydrocarbon concentrations for both oxygenated and non-oxygenated synthetic fuels. Although a synthetic gasoline blend is used in this work, we believe conclusions based on the experimental data will successfully carry-over to actual reformulated gasoline(RFG).

EXPERIMENTAL

Fuel Composition

High purity oxygenates were used in all fuel compositions to minimize any impact that volatile impurities may have on altering head-space composition. Each ether oxygenate was freshly distilled immediately prior to use. Test hydrocarbons were purchased from Aldrich Chemical Company and were used without additional purification. The reported purity of our test oxygenates were > 99.99 % MTBE, 99.9% ETBE (without anti-oxidant), and 98% TAME.

Each batch of test fuel, typically 25 - 50 ml, was carefully blended so that the overall blending vapor pressure would be approximately 6.0 psi, assuming ideality. Total aromatic concentration in the blend is fixed at 20% toluene and 1% benzene to

simulate the RFG requirement of 1995. The three oxygenated fuels outlined in Table No. 1 were blended to contain 2.7 wt.% oxygen from the addition of either MTBE, ETBE, or TAME.

Table No. 1 Liquid Fuel Compositions

Fuel Oxygenate	Components	Composition (Vol.%)	Blending Vapor Pressure (Psi @ 100°F)
Base	Toluene Benzene 2,3-DMB	20.0 1.0 79.0	5.87
MTBE	Toluene Benzene 2,3-DMB MTBE	20.0 1.0 64.0 15.0	5.98
ETBE	Toluene Benzene 2,3-DMB 2,2-DMB ETBE	20.0 1.0 37.0 25.0 17.0	5.88
TAME	Toluene Benzene 2,3-DMB 2,2-DMB TAME	20.0 1.0 27.0 35.0 17.0	5.91

DMB = Dimethylbutane

Vapor Generation

A schematic diagram of the Micro Head-Space vapor generating apparatus is shown in Figure No. 1. Approximately 25 ml of fuel to be tested is place in a clean and dry 100 mL volumetric flask. The flask and contents are submersed in a temperature regulated water bath to insure accurate and uniform heat transfer. The volumetric flask is then fitted with a rubber septum through which is inserted a 1/8 inch stainless steel aerator line. This aerator is than attached to a metered ultra high purity helium delivery system. A metered amount of helium can be introduced into the head-space cavity, if necessary, to charge the sample loop. A thermocouple is inserted into the liquid through a second 1/8 inch Teflon® tube. Equilibrium head-space sample is carried through the sample port via diffusion. This fills the 0.3 mL sample loop contained in the Valco valve system. The entire system is place in a constant temperature oven to reach equilibrium. After the desired temperature has been reached in the liquid fuel sample, one hour is allowed to reach equilibrium before a head-space sample is taken for gas chromatographic analysis.

Vapor Analysis

Effluent head-space sample is helium flushed from the sample loop through a pre-heated (120°F) 1/16 inch stainless steel line to the injector port of a Varian 3700 Gas Chromatograph. Hydrocarbon and oxygenate analysis is performed on a Hewlett Packard PONA 50 meter x 0.2 mm x 0.5 micron fused silica capillary column. Typical vapor analysis is carried out under isothermal conditions at 140°F. All data is collected and integrated for analysis on a Fisons Multichrom data acquisition system. The GC analysis was done a minimum of three times at each temperature. An average of the area percents was then calculated for each component present in the vapor sample.

A gas sample calibration standard was prepared and analyzed in the following manner. A precisely weighted liquid sample of all components was transferred to an evacuated one-liter round bottom flask, fitted with a Teflon® lined serum cap. We have experimentally determined that a Teflon® lined serum cap is required to prevent the

irreversible absorption of aromatic components into rubber septum. The flask contents are allowed to equilibrate at atmospheric pressure with ambient air to give a vapor sample of known concentration. The mass at atmospheric pressure was well below the components dew point. An aliquot of this vapor sample is then charged directly to the sample loop which had been thermally equilibrated to the temperature of the initial head-space experiment and then analyzed. Area percents determined in each temperature study were then converted to vapor mole percent.

DISCUSSION

Head-space concentrations were predicted at 80, 100, and 120°F using UNIFAC-Flash Simulations[1] on all four test fuels with an ASPEN PLUS™ computer software package. These results are shown in Graph No. 1.

An examination of the computer generated data reveals that all three oxygenates suppress the volatility of benzene in the 80 - 120°F temperature range. A linear suppression is predicted over the 40°F range for each oxygenate. Overall benzene evaporative emissions are reduced an average of approximately 15% over the temperature range with MTBE. TAME yields a benzene reduction of approximately 13%. ETBE yields the lowest benzene suppression of approximately 10%. This data from the model strongly suggests that the amount of benzene suppression is **dependent** upon the type of ether oxygenate used with minor temperature effects.

An examination of the experimental benzene head-space concentration measurements obtained in our Micro head-space apparatus is outlined in Graph No. 2. These experimental results reveal that benzene suppression is **independent** of the type of ether oxygenate used and dependent upon the test temperature. This data supports the contention that reduced benzene evaporative emissions is a generic trait characteristic of all ether oxygenates. At a constant 2.7 wt.% oxygen content, benzene evaporative emissions were reduced an average of 14%, independent of the ether oxygenate structure. In general, there is a linear increase (approximately 8%) in the amount of benzene found in the head-space during a 40°F temperature increase. This trend is in line with our simplistic model of colligative polar solution interactions between ether oxygenates with aromatics which is manifested in lower benzene evaporative emissions. As the temperature is increased, solution molecules acquire sufficient kinetic energy which in turn increases volatility by weakening the colligative interaction.

CONCLUSIONS

Benzene evaporative emission reduction averaged approximately 14% for fuels containing 2.7 wt.% oxygen in the 80 - 120°F range

Reduced benzene evaporative emissions from an oxygenated fuel appear to be independent of the ether oxygenate molecular structure

LITERATURE CITED

1. A. Fredenslund, J. Gmehling, and P. Rasmussen, **Vapor-Liquid Equilibria Using UNIFAC, A Group Contribution Method**, Elsevier, Amsterdam, 1977.

Figure No. 1

Micro Head-Space Testing Apparatus

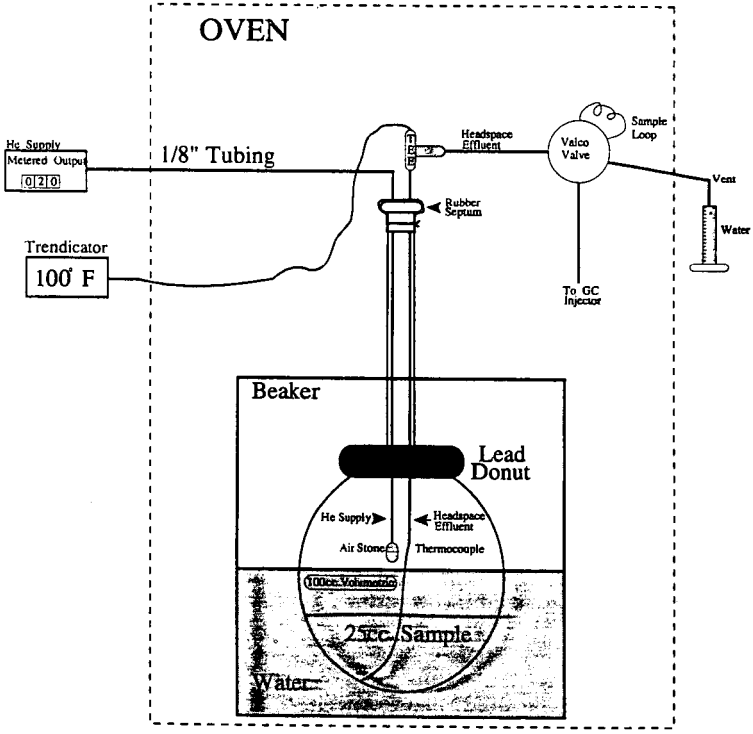

GRAPH No. 1

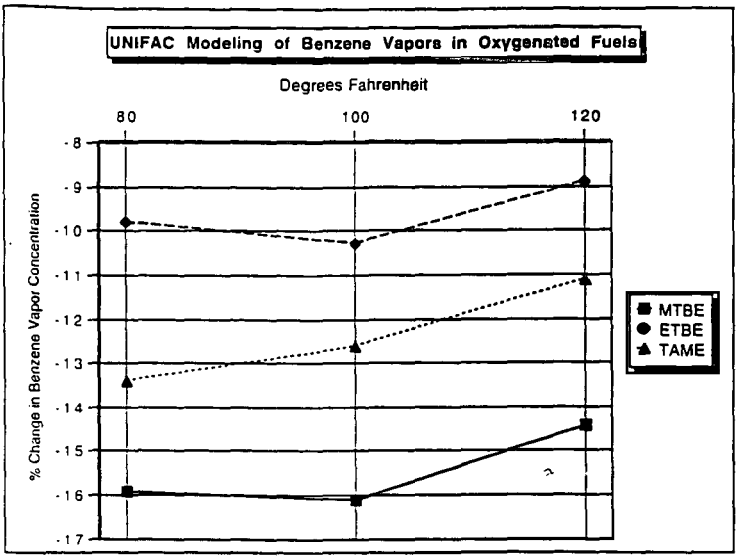

GRAPH No. 2

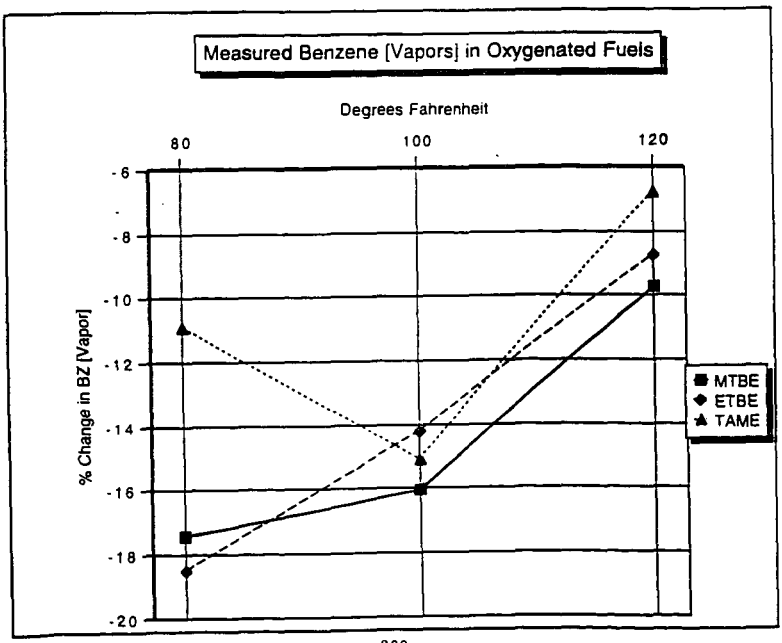

VAPOR PRESSURE INTERACTIONS OF ETHANOL WITH BUTANE AND PENTANE IN GASOLINE

Jimell Erwin
Southwest Research Institute
P.O. Drawer 28510
San Antonio, TX 78228

Keywords: Gasoline RVP, Ethanol Vapor Pressure Blending, Reformulated Gasoline

ABSTRACT

The utility of ethanol as a fuel component is hampered by the greater than linear contribution it makes to the vapor pressure of resulting fuel blends. Careful measurements were made to see whether RVP control *via* addition of pentane resulted in the same nonlinear vapor pressure effect as observed for the usual component used to control moreover vapor pressure, butane. Within the resolution of the pressure measurements, no difference was detected. The result was the same for RVP control with a mixture of butane and pentane.

INTRODUCTION

The Clean Air Act Ammendments of 1990 require the production of reformulated gasoline (RFG) for ozone non-attainment areas starting in 1995. Volatility of RFG is a concern because of two requirements of the law and associated regulations:

- RFG must contain at least 2.0 weight percent oxygen from alcohol or ether.
- Performance standards include reduction in both volatile organic compounds (VOC) and toxic emissions and must not increase nitrogen oxides.

These requirements attempt to drive alcohol concentration in opposite directions under some circumstances. Some oxygenates, including ethanol, increase volatility and in turn cause an increase in evaporative VOC emissions. The contribution of ethanol to volatility of gasoline blends is higher than would be expected based on the pure component vapor pressure of ethanol. Diluted in a predominantly hydrocarbon mixture as in gasoline, the ethanol loses the hydrogen bonding enjoyed by the OH- groups in the neat liquid and exhibits a nonlinear or *excess* vapor pressure.

In the last year, casual observations in various places refocused attention on the factors which affect vapor pressure of ethanol in gasoline blends. Specifically the differential of butane versus pentane RVP control in gasohol mixtures was of interest. The current work used careful measurements of RVP interactions of butane with ethanol or pentane with ethanol in unleaded gasoline to demonstrate ethanol's vapor pressure behavior.

PROCEDURES

A commercial gasoline (regular, summergrade purchased in San Antonio, Texas) was depentanized for use as the base stock in a test of RVP for several ethanol/gasoline mixtures. Depentanized gasoline was selected as the starting material to provide a full range of hydrocarbon types with which ethanol might interact to lower or raise the RVP of the blend. The experimental mixtures of base stock were made with butane alone, with pentane alone, or with butane and pentane to target RVP's (at standard 100°F) of 7 PSI and 8 PSI. These blends and the base gasoline were mixed with ethanol at 10 V%. This matrix is described in Table 1.

The work was done in a laboratory cold room (ambient temperature 35°F) with USP ethanol, reagent pentane, and commercial grade, normal butane. The cold lab was inherently dry, but no special precautions were taken to measure or control water content of the blends. The 8 RVP blends were made first and RVP was measured manually by ASTM D323. Later when the 7 RVP blends were made, both 7 and 8 RVP blends were measured by ASTM D5191 which is an automatic, instrumental method for RVP measurements using a Petrolab Grabner vapor pressure tester.

RESULTS

The results are conclusive, showing the differences in RVP highlighted in Figure 1. The bars represent RVP with and without ethanol, and for 8 RVP samples, the D323 and D5191 results were averaged. For every case studied, the ethanol produced an increase at 100°F (standard RVP temperature) around the average 1.13 PSI.

The behavior shown by the flat RVP difference line in the butane and pentane plots Figures 2 and 3, indicates that identity or concentration of the high volatility component(s) does not affect RVP (within the repeatability of the method, ±0.16 PSI). For measurements at 70°F and 130°F, the differences in vapor pressure are proportionately scaled as shown in Figures 4 and 5. The RVP differences cluster around 1.13 to 1.25 PSI at 100°F, the temperature at which the target blend compositions were calculated.

SUMMARY

No trend arising from identity of pressurizing agent (butane, pentane, or their blends) was observed in the vapor pressure increase arising from the 10 V% ethanol addition in the gasoline samples tested. The results for RVP difference with and without ethanol are as follows:

AVERAGE RVP INCREASE, PSI					
Base	Butane Blends		Pentane Blends		$C_4 + C_5$
Gasoline	7 RVP	8 RVP	7 RVP	8 RVP	8 RVP
1.14	1.20	1.15	1.25	1.10	0.94

ACKNOWLEDGEMENTS

The concept and funding for this work are from the U.S. Deaprtment of Energy, Alternative Fuels Utilization Program through the National Renewable Energy Laboratory, B.K. Bailey, Project Manager. The careful blending and vapor pressure measurements were made by R.M. Rainwater of the Fuels Technology Department at Southwest Research Institute.

TABLE 1. RVP Measurements: Ethanol + Base Gasoline
With or Without Butane or Pentane
RVP Estimates by ASTM D 5191
(Mini-Method gives RVPE ±0.12 PSI)

Description		Composition				Sample	Temperature		
		Basestock	Butane	Pentane	EtOH	ID	70°F	100°F	130°F
Depentanized Gasoline 1		100	--	--	--	Base 1	(1.28) *	(3.57) *	--
Simulated 8 RVP Gasoline	$C_4 + C_5$	74.65	4.79	20.55	0	Blend 2	4.99	8.82	14.39
	C_5	8.82	--	41.18	0	Blend 3	4.63	8.51	14.30
	C_4	90.74	9.26	--	0	Blend 4	5.03	8.67	13.58
8 RVP Samples * 10 V% ethanol	with base gasoline	90	--	--	10	Blend 5 Base + EtOH	2.04	4.57	8.85
	Blend 2	Blend 2 90V%			10	Blend 6	5.38	9.95	17.11
	Blend 3	Blend 3 90V%			10	Blend 7	5.29	10.11	17.84
	Blend 4	Blend 4 90V%			10	Blend 8	5.55	9.89	16.46
Depentanized Gasoline 2		100	--	--	--	Base 2	2.23	4.34	7.63
with 10 V% Ethanol		90	--	--	10	Base 2 + EtOH	2.65	5.62	10.37
Simulated 7 RVP	C_4	94.83 V%	5.17 V%	--	0	Blend 9	4.03	7.00	11.38
	C_5	68.55 V%	--	31.45	0	Blend 10	3.78	7.00	11.82
7 RVP Samples + 10 V% Ethanol	Blend 9	Blend 9 90.0 V%		--	10.0	Blend 11	4.33	8.18	14.11
	Blend 10	Blend 10 90.0 V%		--	10.0	Blend 12	4.22	8.25	14.67

* Calculated from Manual ASTM D 323

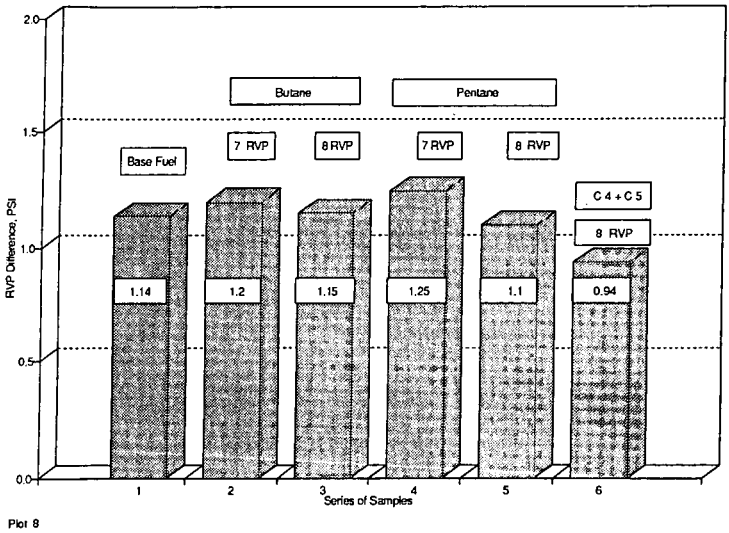

FIGURE I. RVP DIFFERENCES
Neat vs. Ethanol Blends

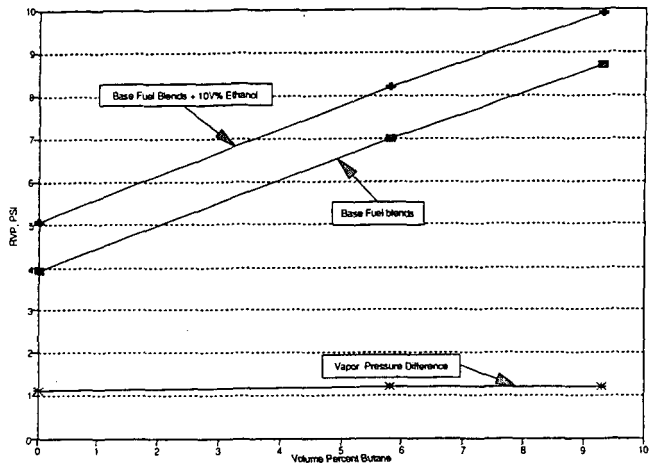

FIGURE 2. RVP VS. PERCENT BUTANE (100)

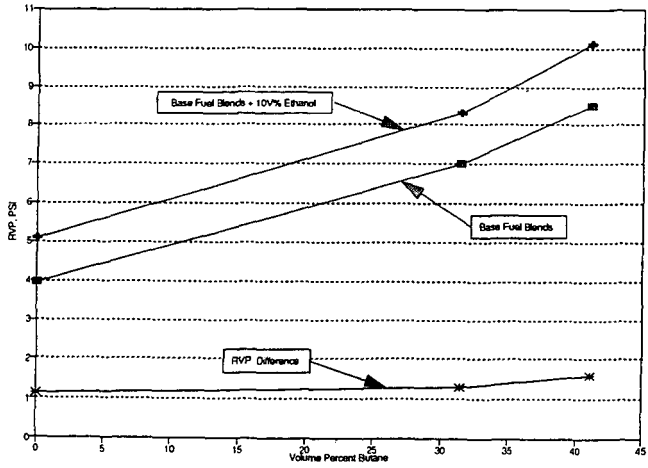

FIGURE 3. RVP VS. PERCENT PENTANE (100)

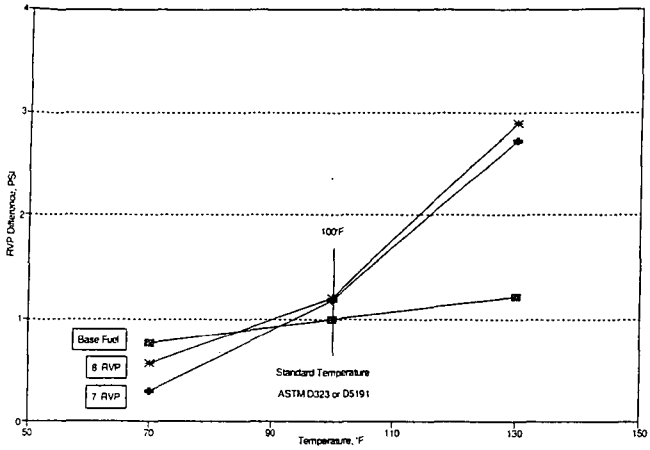

FIGURE 4. RVP DIFFERENCE VS. TEMPERATURE
Blends made with Butane

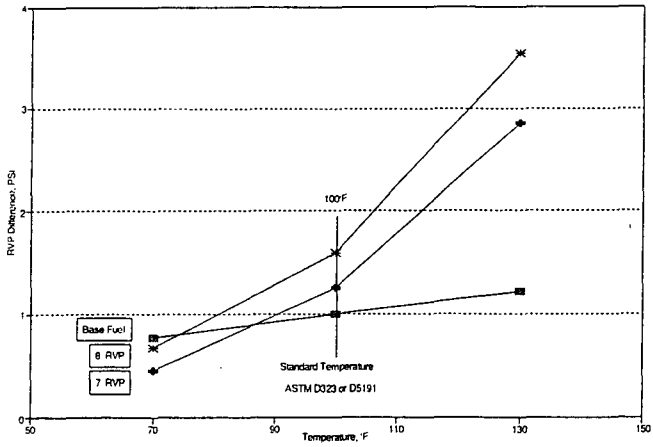

FIGURE 5. RVP DIFFERENCE VS. TEMPERATURE
Blends made with Pentane

LOW EMISSION OXYGENATED DIESEL FUEL

L. J. Karas, H. S. Kesling, Jr., F. J. Liotta, Jr., and M. K. Nandi,
ARCO Chemical Company, Research and Development,
3801 West Chester Pike
Newtown Square, PA 19073-2387

Keywords: Oxygenate, Diesel, Fuel, Emission Reduction

ABSTRACT

New diesel engines and fuels are required to meet stricter world-wide emission standards. Challenges include both lower particulate and NO_X emissions. MTBE, ETBE, and TAME utilization in gasoline results in emissions reductions. Similarly, oxygen containing additive use in diesel fuel applications gives substantial particulate emission reduction. In combination with diesel ignition improvement additives, a typical "on-road" 30% aromatic content oxygenated diesel fuel can give an emission profile similar to a 10% aromatic California reference diesel fuel. Oxygenate selection criterion and emission reductions in heavy duty engines are detailed for several commercial P-series glycol ethers and for a new ether oxygenate, di-t-butyl glycerol. A di-t-butyl glycerol product mixture is prepared by etherification of glycerol available as a by-product from commercial biodiesel manufacture. Various strategies for oxygenate use to enhance diesel fuel performance are discussed.

INTRODUCTION

The trend toward low emission diesel fuels is growing worldwide. In the United States, **Clean Air Act** legislation will mandate reduced particulates in 1994 and lower NO_X emissions in 1998. Emission reductions beyond these targets will require a combination of new engine technology, additives, and reformulated diesel fuels (1). The production of economically viable low emission diesel fuels will remain a substantial challenge into the years to come. Oxygenated diesel fuel may offer one possible solution.

Oxygenate utilization to produce "cleaner burning" diesel fuels has been known for over fifty years. Oxygenates are well known to reduce particulate emissions. Low molecular weight alcohols, such as methanol, ethanol, and t-butyl alcohol, have been reported to reduce emissions (2). Higher alcohols (3), carbonates (4), diethers (5), such as diglyme, and various glycol ethers (6) have also been reported. Particularly attractive are P-series glycol ethers which contain both an ether and a propylene glycol end-group.

This paper deals with oxygenate selection criterion and emission reductions in modern diesel engines. Various application strategies to reduce emissions and enhance diesel fuel performance are discussed.

OXYGENATE SELECTION

Key oxygen selection criterion include: cost, toxicity, environmental impact, fuel blending properties, and engine performance. Critical fuel blending properties, which were used to screen and identify viable oxygenate candidates, included: high oxygen content, diesel fuel solubility, flashpoint, viscosity, water solubility in the resultant fuel blend, oxygenate extractability from the fuel, and minimal impact on the natural diesel fuel cetane number.

The oxygenate should be soluble in diesel fuel from 1.0 to 5.0% to achieve maximum emissions reduction and improved engine performance. Above 5.0%, oxygenate cost per gallon of fuel treated is prohibitive. A number of high oxygen containing materials, such as ethylene and propylene carbonate, and most E - series glycol ethers, which

are based on ethylene glycol, were eliminated from consideration due to poor diesel fuel solubility. As aromatic content in future reformulated diesel fuels is reduced from 35% to 10 - 20%, oxygenate solubility in the less polar hydrocarbon fuels will become acute.

The oxygenated diesel fuel flashpoint needs to be over 52°C, as specified by ASTM D975, to reduce the transportation flammability risk. Many inexpensive ethers with high oxygen content, including MTBE, ETBE, TAME, and DIPE, were eliminated from consideration due to the low flashpoints of the resulting 1.0% oxygenated fuel blends. Fuel blends containing 1.0% or more of inexpensive dimethyl carbonate and diethyl carbonate, were also eliminated because the resulting blends had flashpoints lower than the target.

A key issue is how the additive behaves if the oxygenated blend becomes exposed to water. Both high degree of water solubility in the fuel blend and high degree of water extractability of the oxygenated additive from the fuel are unacceptable. Dimethyl and diethyl carbonate both have high water extractability from the fuel. Similarly, most fuel soluble E - series glycol ethers are easily extracted and are thus eliminated from consideration. P - series glycol ethers, generally, have acceptable partitioning characteristics.

Many intermediate molecular weight aliphatic, cycloaliphatic, and aryl alkyl alcohols meet the fuel blending selection criteria. Poly(ether) polyols based on propylene oxide or butylene oxide are viable oxygenate candidates. Methyl soyate, which is a form of biodiesel, meets selection criterion and was evaluated. Several commercial P - series glycol ethers and a new glycol ether oxygenate, di-t-butyl glycerol, are potentially inexpensive, and meet all the other selection criterion. Diglyme, which is associated with health risks, and too expensive to be economically viable, was also included in the test program so that benchmark comparisons can be made with previous studies. Various emission reduction strategies which utilize oxygenated diesel fuel are outlined in this paper.

OXYGENATED DIESEL APPLICATIONS

There are many opportunities to use an oxygenated diesel fuel for emission reduction. A standard 1993 E.P.A. certification D2 diesel fuel reformulated with oxygenate has the potential to reduce emissions from both pre-1991 engines, which are required to meet a 0.60 gram / brake horsepower - hour particulate target, and post-1991 heavy-duty diesel engines which must meet a 0.25 gram / brake horsepower - hour Clean Air Act particulate emissions target. In addition, oxygenated diesel fuel could has the potential to benefit 1994 and 1998 heavy-duty diesel engine emission performance.

To demonstrate operability in older engines, an E.P.A 13-mode emission test was conducted in a 1990 Cummins L-10 heavy-duty diesel engine. Results show a 39 cetane number diesel fuel containing 43% aromatics and 0.25% sulfur, when blended with 5.0% GE-C (commercial P - series glycol ether), have the potential to reduce particulates emission with little impact on NO_x. Similar results are expected in other older engines.

Most of the results reported in this paper focus on oxygenated diesel fuel performance in modern heavy-duty diesel engines. Emission testing was conducted in the prototype 1991 Detroit Diesel Series 60 CARB certification engine at Southwest Research Institute. Hot-start transient emissions, including hydrocarbons, carbon monoxide, NO_x, and particulate matter, were measured using the standard E.P.A. transient test cycle and are shown in Table 1. The reference fuel is a E.P.A. certification D2 diesel fuel with a 43 cetane number, 0.037 Wt.% sulfur, and a 31% aromatic content. Various oxygenates were blended into this reference fuel at concentrations from 1.0 to 5.0%. The cetane number of the oxygenated fuel blends were adjusted to 43 using ethyl hexyl nitrate.

Oxygenates significantly reduce hydrocarbon, carbon monoxide, and particulate

emissions, but give a sight increase in NO_X emissions. There is little or no increase in fuel consumption when an oxygenated diesel fuel is utilized. Results clearly demonstrate that reduced particulate matter emissions is a key benefit achieved through oxygenated diesel fuel use. In addition, 5.0% GE-C reduces unregulated aldehyde and ketone emissions by around 25%.

Not all oxygen containing additives are effective in reducing particulate emissions. 1-Phenyl ethanol and 1-cyclohexyl ethanol, for example, do not significantly reduce particulate emissions and methyl soyate is only marginally effective. Diethers, such as diglyme, and P - series glycol ethers; however, are very effective in reducing particulates. Based on a large amount of data, most of which could not be presented in a short paper, it can be concluded that particulate reduction is directly proportional to the ether oxygen content of the blended fuel. Results show GE-C at 1.0 wt.% oxygen gives around a 15% particulate emission reduction.

Table 1 Oxygenate Additive Effect On Hot-Start Transient Emissions
(Grams/Brake Horsepower - Hour)*

Additive; Conc. (Vol.%)	Oxygen Content (wt.%)	HC Ref. Fuel Cand Fuel	CO Ref. / Cand.	NO_X Ref. / Cand.	PM Ref. / Cand.
MBA; 5	0.78	0.425 (.029) 0.468 (.059)	1.852 (.043) 1.867 (.045)	4.155 (.032) 4.327 (.087)	0.180 (.006) 0.174 (.002)
Cyclohexyl Ethanol; 5	0.68	0.388 (.029) 0.466 (.017)	1.933 (.088) 1.994 (.015)	4.091 (.027) 4.181 (.063)	0.180 (.005) 0.177 (.008)
Methyl Soyate; 5	0.59	0.392 (.011) 0.319 (.066)	2.004 (.029) 1.843 (.127)	4.303 (.056) 4.331 (.097)	0.182 (.007) 0.174 (.006)
Diglyme; 5	2.05	0.421 (.036) 0.307 (.021)	1.939 (.082) 1.634 (.033)	4.231 (.086) 4.340 (.065)	0.174 (.007) 0.146 (.007)
Poly(ether) Polyol; 1	0.34	0.385 (.012) 0.305 (.037)	1.919 (.030) 1.676 (.009)	4.175 (.029) 4.213 (.065)	0.176 (.005) 0.166 (.003)
GE-C, 1	0.37	0.424 (.037) 0.395 (.025)	1.990 (.086) 1.920 (.116)	4.242 (.102) 4.239 (.034)	0.171 (.002) 0.163 (.008)
GE-C, 2	0.74	0.433 (.040) 0.407 (.035)	1.946 (.081) 1.866 (.020)	4.159 (.070) 4.166 (.103)	0.183 (.003) 0.159 (.010)
GE-C, 5	1.82	0.384 (.019) 0.291 (.008)	1.872 (.034) 1.568 (.021)	4.159 (.045) 4.235 (.042)	0.183 (.004) 0.154 (.003)

*** Emission testing was conducted in the prototype 1991 Detroit Diesel Series 60 CARB Certification engine at Southwest Research Institute. Hot-start transient emissions (hydrocarbons, carbon monoxide, NO_X, and particulate matter) were measured using the standard EPA transient test cycle and sampling techniques were based on 1992 Federal Test Procedures (FTP). The reference fuel is a standard EPA certification D2 diesel fuel with a 43 cetane number, 0.037 Wt.% sulfur, and 31% aromatic content. Oxygenates were blended into this reference diesel at the volume % indicated. Emissions are reported in Grams / Brake Horsepower - Hour. ( ) is one standard deviation. MBA is 1-phenyl ethanol. GE-C is a typical commercial P - series (propylene glycol based) glycol ether.**

Emission regulations are directed at reducing both particulate matter and NO_X emissions. Table 1 show ether oxygenates reduce particulates, but this particulate reduction is typically accompanied by a small increase in NO_X emissions. Increasing the oxygenated diesel fuel cetane number using chemical cetane improvers, such as ethylhexyl nitrate or di-t-butyl peroxide, has been shown to reduce NO_X emissions. Thus, the oxygenate / chemical cetane improver combination gives a diesel fuel with both lower particulate and NO_X emissions. Results outlined in Table 2 suggest this combination strategy provides an opportunity to prepare an oxygenated diesel fuel which will meet current California emission standards.

Table 2 **Oxygenated California Diesel Fuel***
(Grams / Brake Horsepower - Hour)

Fuel Type	Cetane No / Arom.(%)	HC	CO	NO_X	PM
EPA Base Ref.	43 31	0.433	1.979	4.17	0.174
Low Arom. Ref.	51 15	0.143	1.303	3.99 (3.98)	0.153 (0.159)
GE-C & Peroxide	53 31	0.153	1.225	4.04	0.160

*** Transient protocol and data analysis are identical to those described in Table 1. The glycol ether, GE-C, blend concentration is 2.0% and enough di-t-butyl peroxide was used to increase the diesel fuel cetane number of the GE-C & paroxide experiment by 10.0 units. Since a 10% aromatic CARB reference fuel could not be purchased, a 15% containing aromatic fuel was used as the CARB low aromatic reference fuel. The Coordinating Research Council's (CRC) VE-1 Model (7) waa used to correct emissions from the 15% aromatic fuel to CARB certification fuel properties on cetane, aromatic content, and sulfur. The number in ( ) is the adjusted emissions value. Considerable CRC data suggests the VE-1 Model is valid for this type of adjustment.**

Effective October 1, 1993 all diesel fuel used in California must have an emission footprint which is equivalent to a low sulfur - 10% aromatic containing CARB reference fuel. Southwest Research Institute's prototype 1991 Detroit Diesel Series 60 engine, which is utilized for the oxygenate study, is the CARB certification engine. The emissions from an oxygenated diesel fuel, which contains 2.0% glycol ether (GE-C) and enough di-t-butyl peroxide ignition improver to increase the cetane number by 10.0 units, are nearly identical to the "pseudo-CARB" low aromatic reference diesel fuel used in this study. These results predicts that a combination of an oxygenated diesel fuel and chemical cetane improver provides an opportunity to produce a California "alternative" oxygenated diesel fuel with a 31% aromatic content Which has an emission performance equivalent to a low sulfur - 10% aromatic CARB reference fuel.

Cost is a significant issue in the preparation of a California diesel fuel. Clearly, a 30% aromatic containing oxygenated diesel fuel, which uses commercially available, P - series glycol ethers, is more cost effective than using a low sulfur - 10% aromatic fuel. Refinery hydrogenation to reduce diesel fuel aromatic content to 10% is an expensive option. The strategy used by most refiners is to reformulate with a 20% aromatic base fuel using high levels of chemical cetane improver. The California Air Resources Board (CARB) indicate costs for qualified fuels of this type will increase the diesel fuel costs by five to eight cents per fuel gallon. The oxygenated diesel fuel cost currently fits into the upper part of this cost range. Less expensive oxygenates are needed to make an oxygenated California diesel fuel a viable option.

One "non-commercial" oxygenate, which has the potential for reduced cost, is di-t-butyl glycerol. A di-t-butyl glycerol product mixture is prepared by etherification of glycerol which is available as a by-product from commercial biodiesel manufacture. The envisioned strategy is to blend 5% of an 80:20 methyl soyate / di-t-butyl glycerol oxygenate mixture with conventional low sulfur D2 diesel to create an inexpensive oxygenated diesel fuel. The cost and availability of by-product glycerol is leveraging. Biodiesel is a commercial reality in Europe and would provide the best opportunity for implementation.

Coupled with new heavy-duty diesel direct injection engine technology, reformulated oxygenated diesel fuels offers a potential option for achieving the 1998 **Clean Air Act** target which mandates a NO_X reduction from 5.0 to 4.0 grams / brake horsepower - hour. The engine strategy for 1994 is to modify the engine design to give the 0.10 gram particulate target. Fortunately, NO_X, carbon monoxide, and hydrocarbon emissions are acceptable. In 1998 engines, an oxygenated diesel fuel, which reduced particulates by 15%, would allow the OEM's to tune less rigorously for particulates, thus providing more flexibility on the NO_X tuning.

There are numerous other opportunities to use oxygenates in specialty fuel applications where reduced emissions are of interest. For example, transit authority buses will use high quality low sulfur D1 or kerosene, particulate traps, and post-combustion catalysts to achieve a 0.07 gram particulate target for 1994. The downside for these specialty fuels is less power and higher fuel consumption. An oxygenated D2 diesel fuel has the potential to provide the same low emissions without increased fuel consumption. Other specialty fuel opportunities for an oxygenated fuel include: stationary powerplants, underground mining, marine diesel, locomotive diesel, and fuels for many smaller volume "off-road" applications.

CONCLUSIONS

Cleaner burning diesel fuels can be produced through the use of oxygenated additives. Carefully selected "commercially" available P -series glycol ethers, which have the desired characteristics, are effective in reducing hydrocarbon, carbon monoxide, and particulate matter emissions. The magnitude of the particulate emissions reduction is directly proportional to the "oxygen" content of the ether oxygenate containing fuel. A combination of a glycol ether oxygenate with a cetane improver results in further emission reductions, especially NO_X. One application strategy for the combination oxygenate / ignition improver diesel fuel formulation is a 30% aromatic containing oxygenated fuel which has the same emissions performance profile as the mandated low sulfur - 10% aromatic California diesel fuels.

ACKNOWLEDGEMENTS

The authors wish to express their appreciation to Mr. Dan M. Montalvo, Terry L. Ullman, Ms. Cynthia Chaffin, and Mr. Kent Spreen at Southwest Research Institute (SwRI) for their help with the emissions testing program. The authors also wish to thank Mr. Richard Englebach and Mr. Chris Green at ARCO Chemical Company for conducting the laboratory work on the oxygenated products associated with this paper.

LITERATURE CITED

(1) McCarthy, C. L., et. al, "Diesel Fuel Property Effects On Exhaust Emissions from Heavy Duty Diesel Engine That Meets 1994 Emission Requirements", SAE Paper 922267, October 1992.

McCarthy, C. L., et. al, Fuel Reformulation, March 1993, p. 34.

Cowley, L. T., et. al, "The Effect of Fuel Composition On Emissions From a Range of Heavy-Duty Diesel Engines", Coordinating European Council Paper CEC/93/EF03, May 1993.

(2) Ecklund, E. E., "State of-the-Art Report On the Use of Alcohols In Diesel Engines", SAE Paper 840118, 1984.

(3) Clerici, M. G., et. al., "Oxygenated Diesel Fuels Part - I", Presented At IX ISAF Meeting, Firenze (Italy), April 9 - 12, 1991.

Pecci, G. C., et. al, "Oxygenated Diesel Fuels Part - II", Presented At IX ISAF Meeting, Firenze (Italy), April 9 - 12, 1991.

(4) U.S. Patents 2,331,386; 4,378,973; 4,891,049; 4,904,279; and 5,004,480.

(5) Bennethum, J. E. ; Winsor, R. E.; "Toward Improved Diesel Fuel", SAE Paper 912325, 1991.

(6) Nikanjam, M., "Development of The First CARB Certified California Alternative Diesel Fuel", SAE Paper 930728, March 1993.

Liotta, F. J.; Montalvo, D. M., "The Effect of Oxygenated Fuels On Emissions

From a Modern Heavy-Duty Diesel Engine", SAE Paper 932734, October 1993.

(7) Ullman, T. L., et. al., "Study of Fuel Cetane Number and Aromatic Content Effects on Regulated Emissions From a Heavy-Duty Diesel Engine", CRC VE-1 Project Study, Southwest Research Institute, September 1990.

OXYGENATED MICROEMULSION DIESEL FUEL

H. S. Kesling, Jr., F. J. Liotta, Jr., and J. M. McFarland
ARCO Chemical Company, Research and Development
3801 West Chester Pike
Newtown Square, PA 19073-2387

Keywords: Oxygenate, Microemulsion, Diesel, Fuel

ABSTRACT

New low emission fuel technology is needed to meet stricter world-wide particulate and NO_X emission standards for both "on-road" and "off-road" fuel applications. The **Energy Policy Act of 1992** and the **1993 Executive Order 12844** establish clear national goals for the year 2000 and beyond which will reduce petroleum derived fuel use and provide greater utilization of alternate fuel vehicles. Technologies under evaluation include M85, E85, CNG/LPG, biodiesel esters, and electric vehicles. Microemulsion diesel fuel technology, which utilizes oxygenates to help compatibilize a biomass derived or hydrocarbon petroleum phase and water phase, offers strong potential as an alternate fuel option. Oxygenate selection criterion, microemulsion fuel formulation, and performance issues are discussed. Fuel formulations based on alcohol, glycol, ether, and glycol ether microemulsifying agents, which are readily available from world-scale propylene oxide / oxygenated coproduct technology, are described. Evaluation results suggest oxygenated microemulsion fuels are viable alternate fuel candidates.

INTRODUCTION

The trend toward low emission diesel fuels is growing worldwide. In the United States, **Clean Air Act** legislation will mandate reduced diesel particulates in 1994 and lower diesel NO_X emissions in 1998 (1). A combination of new engine technology, additives, and new low emission fuels will be required to achieve these targets. The **National Energy Policy Act of 1992** and **Executive Order 12844** of 1993 establish clear national goals for the year 2000 and beyond which will both reduce petroleum derived fuel use and ozone forming emissions. The **Clean Cities** program provides the framework for implementation which includes greater utilization of alternate fuel vehicles. In addition to "on-road" applications, there is considerable recent focus on "off-road" applications as a major source of particulate and NO_X emissions. A comprehensive E.P.A. report (2) describes our national problem. A NO_X emission inventory shows the magnitude of this problem in ozone nonattainment areas. Emissions from construction, agriculture, railroads, mining, marine, industrial stationary powerplants, airport services, and lawn and garden services all contribute to the global NO_X problem. New alternative fuel technologies under evaluation include: M85, E85, CNG, LPG, and biodiesel esters (3). Microemulsion diesel fuel technology also offers great potential for reducing emissions and dependency on oil (4).

DISCUSSION

Oxygenate Selection

Microemulsions are clear, stable, two-phase nanodispersions which readily form upon mixing water with an oil phase. Water-in-oil (w/o) microemulsions are comprised of a continuous non-polar hydrocarbon phase and a discontinuous aqueous phase. Because of the small droplet size (2 to 200 nanometers) of the discontinuous phase, these microemulsions appear to be clear, one-phase systems. Microemulsion diesel fuel technology uses a microemulsifier to compatibilize a diesel or biodiesel fuel and a water phase. The microemulsifier typically contains a surfactant and a compatibilizing agent (an oxygenate). The resulting microemulsion fuel, when utilized in conventional diesel engines, is "clean-burning", gives no power loss or increase in fuel consumption, and is thermal and shear stable in the fuel handling system.

The purpose of the oxygenate is to help solubilize the surfactant in the fuel, adjust the properties (i.e. viscosity) of the fuel, and possibly contribute to improving the ignition properties of the water-containing microemulsion fuel. Oxygenates in the microemulsifiers are also required to achieve inorganic salt tolerance, thermal and shear stability, and good shelf life. Oxygenates used as microemulsifying agents include C_{1-6} alcohols (5), benzyl alcohols (6), and glycols (7). Key issues are oxygenate cost, flammability, and impact on stability of the microemulsion fuel.

The oxygenates must be inexpensive to achieve economics which are competitive with specialty diesel fuels. Alcohols, such as methanol, ethanol, and t-butyl alcohol, are inexpensive and readily available. Although they all are effective in microemulsion fuel preparation, these alcohol microemulsifiers are flammable. Less volatile alcohols, such as 1-phenyl alcohol (MBA), eliminate the flash point issue, but the resulting microemulsions are more difficult to prepare and have narrower stability windows. Clearly, new candidates, which provide stability and less flammable microemulsion fuels, are desirable.

World-scale propylene oxide technology as practiced by ARCO Chemical Company produces t-butyl alcohol (TBA) and 1-phenylethanol (MBA) as primary coproducts. TBA is the precursor to isobutylene, MTBE, and ETBE and MBA is a styrene monomer precursor. Using these coproducts as building-blocks, several new oxygenates were developed which have application as microemulsifying agents.

Preparation

The microemulsions which have been formulated are water-in-oil microemulsions made up of four basic components: diesel fuel, surfactant, oxygenates, and water. The diesel fuel is a D-2 low sulfur fuel (< 0.5 wt% sulfur, 31% aromatics, 43 cetane number) which is commercially available. The surfactant for these formulations is the anionic long chain fatty acid Emersol 315. This linoleic/oleic/linolenic acid mixture has been neutralized (40% unless noted otherwise in Table I) with monoethanol amine (MEA). Oxygenates may be used alone or as combinations of several oxygenated compatibilizing agents. The microemulsifiers are formed by mixing the Emersol 315, MEA, and oxygenates.

The microemulsion fuels are mixed in the following order: diesel fuel, microemulsifier, water. After mixing the three components, the fuel mixture is shaken and allowed to settle. Any sign of phase separation, solid formation, or cloudy appearance over several weeks is a negative result. If a clear, single phase system is observed, the microemulsion is considered to have formed. Some of the microemulsion fuels prepared are listed in Table I.

Performance

As shown in Table I, the choice of oxygenate in the microemulsifier has a major influence on the stable formation of a microemulsion diesel fuel. Combinations of oxygenates can also improve the ability of the fuel to form stable microemulsions. Optimization of the fuels for surfactant concentration will also improve the formation potential. Although not specifically shown in these examples, it is expected that the character of the different oxygenated compatibilizing agents will change the surfactant requirement of the overall microemulsion fuel. This will allow optimization of the fuels for cost, water loading and performance. Among the performance issues of importance to microemulsion fuels are thermal stability, shear stability, flash point, storage stability, engine performance, and emissions.

TABLE I
Microemulsion Fuel Formulations†

Fuel #	ME‡	Wt% Oxygenate	Wt% Surfactant*	Stable Formation
1	A	34.1	65.9	+
2	B	34.1	65.9	+
3	C	34.1	65.9	+
4a	D1	34.1	65.9	+
4b	D2	34.1	65.9 (100%)	-
4c	D3	10.0	90.0 (27%)	-
5	E	34.1	65.9	+
6	F	33.9	66.1	-
7	G	33.9	66.1	+
10	J	34.0	66.0	+
11	K	33.8	66.2	-
12	L	34.2	65.8	-
13	M1	34.0	66.0	-
14	M2	33.8	66.2	+
15	N	34.0	66.0	-
16	O1	34.1	65.9	-
17	O2	34.6	65.4	+
18	P	34.6	65.4	-
19	R	34.4	65.6	+
20	E	34.1	65.9	+

† 71 / 19 / 10 vol% D-2 / ME / H_2O formulation except: Fuel 2: 75.5 / 14.5 / 10 vol% D-2 / ME / H_2O and Fuel 20: D-2 phase is 95% D-2, 5% of a 80/20 wt% mixture of biodiesel / Di-*t*-butyl glycerol (DTBG).

‡ ME is microemulsifier used in the particular formulation. Each letter designates a different oxygenate composition. Components of the various microemulsifiers will be discussed in the presentation.

*surfactant weight is total of fatty acid and MEA. MEA is added at 40 mol% (40% neutralization) unless noted differently by the number in parentheses

A microemulsion diesel fuel is generally expected to remain stable for several weeks in a temperature range between -10°C and 70°C. This range covers most extremes a fuel would face either in storage and delivery or in the heat of a modern diesel engine fuel delivery system. The fuel must also be stable to the shear forces present in the fuel delivery system within a diesel engine. Preliminary results show microemulsion diesel fuels containing oxygenates in the microemulsifier phase are thermally and shear stable. If the fuel can withstand these conditions in the engine and fuel system, the fuels can be used in current engine technology without major modifications. This makes microemulsion diesel fuel an immediate possibility as an alternative fuel.

Fuel flammability is a major concern. The flash point of the fuel must be above 52°C (126°F) in order to be transported via pipeline in the U.S. As well, the international flammability standard is 140°F. Depending on the oxygenates chosen, the flash point of the microemulsion fuel may be widely adjusted. This is best represented by the data shown in Table II. By using combinations of oxygenates, it is possible to optimize the microemulsion fuel for stability while providing a fuel that meets flammability standards. As an example, fuels 4a and 5 contain the same oxygenate, except in fuel 5 the oxygenate is in combination with another oxygenate. Fuel 5 is a more stable microemulsion fuel formulation compared to fuel 4a, yet still shows an acceptable flash point. Another benefit of microemulsion fuels containing a dispersed water phase is fire resistance. Studies have shown that a microemulsion diesel fuel can be self-extinguishing or will not burn in the presence of an open flame (6). The choice of oxygenate will have an influence of this property of a microemulsion diesel fuel.

TABLE II
MICROEMULSION FUEL FLASH POINTS

Fuel #	ME	Seta Flash Point (°F)
2	B	116
4a	D1	204
5	E	128
7	G	126
10	J	58
20	E	138

Long term stability is necessary to allow for tank storage of the fuel for extended periods of time, especially in some stationary applications. Several of the formulations have shown excellent long term stability, including some which are stable for over one year. Some of the stability data is shown in Table III.

TABLE III
LONG TERM STORAGE STABILITY
OF MICROEMULSION DIESEL FUELS

Fuel #	ME	Storage Stability
1	A	> 1 year
2	B	> 1 year
3	C	> 1 year
4a	D1	> 1 year
5	E	> 1 year
7	G	> 3 months
10	J	> 1 month
20	E	> 1 month

As previously mentioned, microemulsion diesel fuels can be used in current engine technology without major modifications to the engine. However, because of the water and surfactant concentrations in a microemulsion diesel fuel, some loss of ignition properties may be possible (4). The proper choice of oxygenate can reduce or eliminate this problem. As well, the aqueous phase of a microemulsion diesel fuel offers a way for the ignition properties of the fuel to be augmented with inexpensive cetane enhancers.

Regardless of these other performance issues, microemulsion fuels must reduce engine emissions to be a viable option as an alternative fuel. Microemulsion diesel fuels are known to reduce both NO_x and particulates significantly over standard diesel fuels (5). The NO_x reduction is believed to occur through the lowering of combustion temperatures. This is a result of the higher specific heat of the water and oxygenates in the microemulsion fuel. The microexplosion of the water in the discontinuous phase, more effectively vaporizing the fuel in the combustion chamber, is believed to lower the particulate emissions. Surfactant and oxygenate choice and concentrations have an effect on the size of the water micelles in the microemulsion fuel. Therefore, the selection of the proper oxygenated compatibilizer can improve the performance of the engine toward particulate emissions.

With these lower emissions, several new options are available as a result of the use of microemulsion fuels. First, in stationary applications, the lower NO_x emissions from microemulsion fueled sources may help offset other more costly and difficult NO_x emission reduction options. This will be especially beneficial when regional

attainment targets are enforced in the near future. Second, a decrease in NO_x and particulate emissions from a microemulsion fueled engine may allow flexibility to tune the engine to reduce other emissions as well.

CONCLUSIONS

With new emissions goals mandated by the Clean Air Act and other legislative mandates, alternatives to petroleum based fuels must be sought. Microemulsion diesel fuels are a cost-effective alternative fuel for both "on-road" and "off-road" applications. These fuels offer significantly reduced NO_x and particulate emissions compared to normal diesel fuel. Microemulsion fuels which contain low cost oxygenated compatibilizing agents offer a range of possible formulations for these fuels. These new formulations have widely tunable stabilities, flash points, and engine performance, depending on the oxygenates chosen. Microemulsion diesel fuels also work with the existing engine technology and do not require any changes to the engines or the fuel infrastructure.

Microemulsifier E offers strong possibilities as a component for microemulsion diesel fuels. This microemulsifier phase contains a combination of oxygenates that gives a fuel which meets many of the requirements for an acceptable alternative microemulsion diesel fuel.

ACKNOWLEDGEMENTS

The authors wish to thank Mr. Richard Englebach for conducting some of the laboratory work presented in this paper.

LITERATURE CITED

(1) McCarthy, C. L., et. al., "Diesel Fuel Property Effects On Exhaust Emissions From Heavy-Duty Diesel Engines That Meet 1994 Emission Requirements", SAE Paper 922267, October 1992.

McCarthy, C. L., et. al., Fuel Reformulation, March 1993, p. 34.

Cowley, L. T., et. al., "The Effect of Fuel Composition On Emissions From a Range of Heavy-Duty Diesel Engines", Coordinating European Council Paper, CEC/93/EF03, May 1993.

(2) E.P.A. 460/3-91-02, "Nonroad Engine and Vehicle Emission Study - Report", November 1991.

(3) SAE Publication SP-995, "Advanced Alternative Fuels Technology", October 1993.

(4) Griffith, W. L.; Compere, A. L., Oak Ridge National Laboratory Report, ORNL/TM-11248, "Correlating Microemulsion Fuel Composition, Structure, and Combustion Properties", 1989.

Griffith, W. L.; et. al., "High Alcohol Microemulsion Fuel Performance in a Diesel Engine", SAE Paper 902101, 1990.

(5) U.S. Patents 4,58,354; 4,568,355; 4,568,356; 4,744,796; and 5,104,418.

(6) U.S. Patent 4,770,670.

(7) European Patent Application, EP441002-B1, 1993

REFINERY FUEL OXYGENATES IN VIEW OF THE COMPLEX MODEL FOR REFORMULATED GASOLINE

by
C. D. Crawford and C. P. Haelsig
Fluor Daniel
3333 Michelson Drive
Irvine, California 92730

KEYWORDS: MTBE, TAME, ETBE

The final version of the Complex Model for reformulated gasoline (RFG) has now been issued with some surprising features that will significantly affect refinery fuel oxygenates planning. These include the following:

- The only oxygenates included in the model are MTBE, ETBE, TAME, and Ethanol.
- The Complex Model calculates that MTBE and TAME are significantly more effective for reduction of air toxics emissions than Ethanol and ETBE.
- The Complex Model calculates that MTBE and TAME typically produce about equal reduction in air toxics emissions at the same RFG oxygen content.

Although gasoline certification by the Complex Model is optional prior to 1998, after 1998 it will be mandatory for both reformulated and conventional gasolines. This paper considers refinery oxygenates production in view of these features of the Complex Model for RFG, basing the discussion on 2.0 weight percent oxygen content for RFG.

The Complex Model calculates that MTBE and TAME will be more effective in reducing calculated air toxics emissions than ETBE and Ethanol. Although MTBE can be purchased on the open market, MTBE production from the isobutylene contained in the FCC/Coker C4's cut is well-established practice, and can provide as much as 15 to 20 percent of the 2.0 weight percent reformulated gasoline oxygen content requirement for ozone non-attainment areas. Emerging high-olefin FCC catalyst technology can increase this contribution to approximately 25 percent or more.

TAME production from the isoamylenes contained in the FCC/Coker C5's cut is now commercial technology, with a number of plants onstream. Recently announced low-cost upstream C5 selective hydrogenation technology can reduce TAME production costs, making TAME a more economically attractive oxygenate than previously. Applying catalytic distillation for TAME production provides yield advantages, and can provide as much as 15 to 20 percent of the reformulated gasoline oxygen content requirement. Unreacted amylenes can flow to alkylation, or other uses. Developmental skeletal isomerization technology has been announced for C5 olefins, which could increase TAME yields to provide as much as 30 percent or more of the reformulated gasoline oxygen content requirement.

Overall, use of commercially proven technology for MTBE and TAME captive production currently can economically provide about 35 to 40 percent of refinery oxygenates blending requirements, based on FCC/Coker olefins sources. Since both MTBE and TAME are low-pressure processes conducted in mild steel equipment; existing equipment can be advantageously retrofitted to minimize plant investment.

Although the Complex Model shows less air toxics emissions reduction at a given RFG oxygen content, ETBE and Ethanol can play a role in certain RFG blends. It is possible with certain refinery configurations to meet mandated reductions in air toxics reduction using ETBE or Ethanol to furnish the 2.0 weight percent oxygen content requirement. For these refinery configurations, the primary driving force for oxygenates selection will be economics, since emissions targets can be met whichever oxygenate is used, provided the proper configuration is chosen.

High molecular weight developmental oxygenates such as DIPE, IPTBE, and TAEE offer potential advantages of high octane and low vapor pressure, plus extended captive production from propylene in the case of DIPE. However, these oxygenates are not

included in the current version of the Complex Model and special permits to blend them into fuels may be required where advantages for their use are anticipated.

Details of this paper, including Complex Model parametric studies and refinery configurations, will be presented at the national meeting. The attached figures are typical of those which will be included.

Figure 1
LOCATION OF NINE MAJOR COVERED OZONE NONATTAINMENT AREAS*
WHERE EPA RFG STANDARDS WILL BE MANDANTORY STARTING 1998*

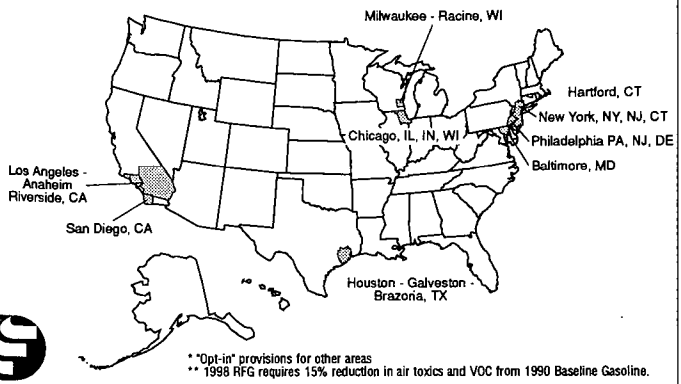

* "Opt-in" provisions for other areas
** 1998 RFG requires 15% reduction in air toxics and VOC from 1990 Baseline Gasoline.

Figure 2
IMPACT OF OXYGENATES SELECTION ON CALCULATED AIR TOXICS EMISSIONS
Final Complex Model

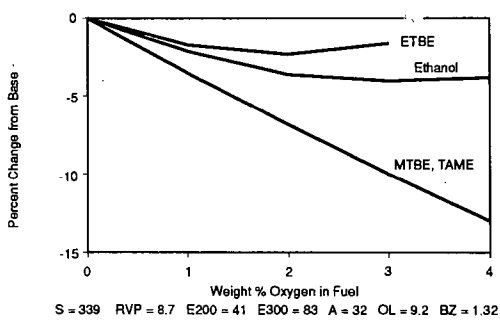

S = 339 RVP = 8.7 E200 = 41 E300 = 83 A = 32 OL = 9.2 BZ = 1.32

Figure 3
MTBE/TAME PRODUCTION FROM FCC C4+ LIGHT NAPHTHA

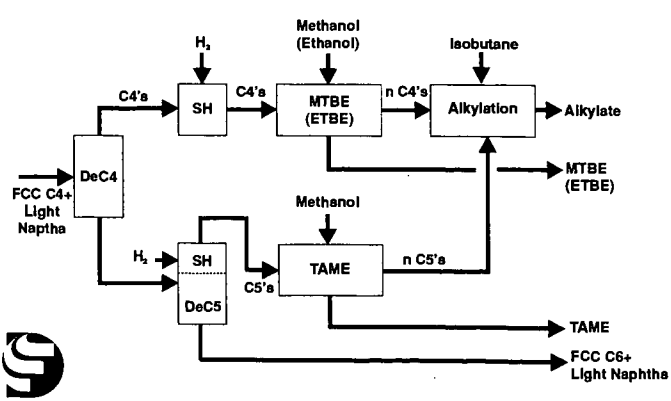

O:\DS\111\211\01626.CDR

WHICH OXYGENATE IS RIGHT FOR YOU?

Elaine J. Chang
Petrochemicals, Polymers, and Energy Center
SRI International
Menlo Park, California 94025

Keywords: oxygenates; reformulated gasoline; oxygenate economics

INTRODUCTION

Recent announcements of additional sources of oxygenates have generated considerable interest. Increasing demand for methyl tert-butyl ether (MTBE) worldwide, especially in the United States for oxygenated fuel and reformulated gasoline (RFG), provides the primary incentive for technologies that produce additional raw material (namely isobutene) and/or alternative oxygenate compounds. Normal butene isomerization and diisopropyl ether (DIPE) are two new processes introduced in 1992 to meet the oxygenate demand.

The U.S. Clean Air Act Amendments of 1990 (CAAA) have created a huge demand for capital. Between 1991 and 2000, the U.S. refining industry will need to make capital expenditures of about $37 billion (1990 dollars) to meet refinery regulatory requirements, and to manufacture reformulated gasoline and ultra-low sulfur diesel fuel.[1] To obtain financing, whether internally or from external sources, projects must provide sound economics and pose minimal technological risks. These concerns have prevented several large MTBE projects, involving both established and new technologies, from going forward.[2]

The introduction of normal butene isomerization and DIPE processes has generated a great deal of enthusiasm, but neither process had been licensed by the third quarter of 1993. Technology risk is a major barrier to obtaining financing inasmuch as lenders are unlikely to finance the first commercial application of any technology. Currently, Texas Olefins/Phillips Petroleum and Lyondell have demonstrated normal butene isomerization on a commercial scale in their plants. However, Mobil has not demonstrated the DIPE process beyond the pilot plant stage.

In this paper, we assess the technological aspects of normal butene isomerization and DIPE processes, and compare their economics with existing etherification processes.

DRIVING FORCES FOR USE OF OXYGENATES IN GASOLINE

Additives and improved refining processes have long been used to improve gasoline quality. Figure 1 shows how gasoline octane has been improved historically. To achieve widespread use, a new additive or process improvement must prove its economic worth. The addition of lead to increase gasoline octane was one of the most cost-effective methods, and its use was nearly universal until the detrimental environmental effects of lead became apparent.

The reasons for using oxygenates in gasoline have varied over time. Alcohols were added to commercial gasoline on an experimental basis as early as 1924. In response to the shortage of crude oil during the oil crises of 1973 and 1979, alcohols were promoted for use either as a substitute or a partial replacement for gasoline. Brazil developed the most significant program, which called for ethanol to be substituted for a large percentage of the gasoline consumed in that country. In the United States, a federally subsidized program was established to encourage the use of ethanol in gasoline nationwide. Although both the Brazilian and the U.S. ethanol programs are still active, the high cost associated with the use of ethanol constitutes a major disadvantage. Consequently, some form of monetary subsidy is required for acceptance of ethanol fuel.

During the mid-1980s, some U.S. gasoline marketers tried to introduce methanol into their gasoline. Both direct blending and cosolvent blending (methanol with tert butyl alcohol [TBA] to minimize phase separation) were tried. These blends were economically attractive because the cost of methanol was considerably lower than that of gasoline. However, compatibility and mechanical problems, together with limited availability of the cosolvent, prevented widespread acceptance of the use of methanol in gasoline.

Ethers, principally MTBE, became widely available in the early 1980s. They have gradually gained acceptance as gasoline blending agents because they offer high octane and excellent gasoline compatibility, and because they can be partially made from refinery by-product isobutene at a cost similar to the cost of producing toluene, whose octane quality is similar to MTBE in gasoline. Refiners originally began to

investigate the use of MTBE as an octane enhancer blended into gasoline at levels of 7 to 10%. Other ethers, such as ethyl tert-butyl ether (ETBE) and tert-amyl methyl ether (TAME), are newer products with gasoline blending properties somewhat similar to those of MTBE.

In the 1980s, the improved burning characteristics (more complete combustion) of MTBE-gasoline blends and their potential for reducing carbon monoxide and smog formation became recognized. Consequently, oxygenated fuel was adopted in the 1990 CAAA.

The CAAA requires the use of oxygenates in gasoline for environmental reasons. Most other countries will probably use oxygenates only for octane enhancement until the full environmental consequences of oxygenated and reformulated fuels are better understood.

EXISTING ROUTES FOR PRODUCING OXYGENATES

MTBE, produced by reacting isobutene with methanol, is the most widely used oxygenate. Isobutene, which is the critical raw material in meeting the demand for MTBE, is available from three commercial sources. By-product sources include mixed C_4 streams available from (1) catalytic cracking in refinery gasoline production, (2) steam cracking for ethylene production, and (3) TBA and propylene oxide (PO) production (dehydration of TBA, a coproduct with propylene oxide via the hydroperoxidation of isobutane). The rapid depletion of these traditional isobutene sources has led to the development of on-purpose isobutene production from field or mixed butanes. The dehydrogenation route to MTBE is a rapidly growing source of isobutene.

Figure 2 shows the world distribution of MTBE production by isobutene source. In the United States, dehydrogenation is now the major source for MTBE (40%), with fluidized catalytic cracker (FCC) and TBA/PO isobutene sources contributing about equal amounts (24% and 25%, respectively), and the remainder from steam cracking (11%). Dehydrogenation is also the major source of isobutene for regions rich in natural gas (e.g., Latin America, the Middle East). In contrast, ethylene cracking is a major source of isobutene in Europe and the Asia-Pacific region for MTBE productions. In these two regions, naphtha is the predominant feedstock in ethylene cracking with relatively high amounts of C_4 by-product, and FCC units are not as prevalent as in the United States.

Other ethers, such as TAME and ETBE, are based on similar technology as MTBE production. Potentially, TAME could be a large source of oxygenate in the United States. The use of ETBE faces two obstacles: (1) it competes with MTBE for isobutene, and (2) its economics depend in large part on government subsidies.

NEW ROUTES TO PRODUCE OXYGENATES

As we approach 1995, when reformulated gasoline regulations take effect in the United States, oxygenated gasoline and RFG will both become required by law, and MTBE supplies will tighten. Refiners may have no choice but to pay a premium above MTBE's octane value to obtain sufficient MTBE. As a result, many refiners are rushing to install their own oxygenate production capacity.

Isobutene is produced in refineries mainly in FCC units. In the United States, a shortage of refinery captive isobutene had kept MTBE plants' utilization rate low (i.e., 60% to 67% for 1988 through 1990).[3] To increase FCC isobutene production, higher FCC riser temperature or isobutene-selective catalysts can be used to raise the isobutene yield by 50-200%. Two drawbacks are the additional investment needed to debottleneck the FCC unit and reduced gasoline yield.

An alternative route is the isomerization of normal butene to isobutene. In addition, other oxygenates, which do not require isobutene as raw material, such as DIPE, can be considered.

Normal Butene Isomerization

Since March 1992, six companies—Lyondell, Phillips/Texas Olefins, Mobil, IFP, UOP, and Snamprogetti—have announced the development of one-step processes to isomerize normal butenes to isobutene. The 4-carbon monoolefins have 4 isomers: 1-butene, cis-2-butene, trans-2-butene, and isobutene. Isomerization of one of the butene isomers to increase the supply of another has long been practiced commercially. For example, refineries maximize the octane number of hydrofluoric acid alkylate by installing a butene isomerization unit (e.g., the Hydrisom process) upstream of the alkylation unit. The isomerization process converts 1-butene to 2-butene, the preferred HF alkylation feedstock.

Normal butene isomerization has been extensively researched, with a variety of catalysts developed to overcome some technological difficulties— low conversion (equilibrium-limited reactions), rapid catalyst deactivation, and undesirable side reactions such as disproportionation and polymerization. The mandates for oxygenated fuels have renewed interest in this process. As MTBE production exhausts the available supplies of isobutene from traditional sources, additional isobutene is being produced on-purpose from field butanes through isomerization to isobutane and dehydrogenation to isobutene. Dehydrogenation is a very capital-intensive, and thus expensive route to MTBE. Consequently, much interest has been generated by the announcement of a new route to produce isobutene by butenes isomerization.

Normal Butene Isomerization Thermodynamics

Butenes isomerization is equilibrium limited. The equilibrium composition changes only slowly with temperature. For normal butene isomerization to isobutene, the yield in a single pass is limited to between 40 and 50 mol% in the normal reaction temperature range of 350-550°C (662-932°F). The branched isomer is favored by lower temperatures, but a faster reaction rate is favored at higher temperatures.

When the carbon skeleton is rearranged, mixtures of butenes result. Skeletal isomerization involves C-C bond rupture and reformation. Once a carbonium ion is formed in the presence of a strong acid, several side reactions also take place (e.g., polymerization, isomerization, hydrogen transfer). Therefore, it is unlikely to achieve a clean product slate. The typical isobutene selectivity ranges between 85 and 90%.

Table 1 lists processes offered for licensing, and Table 2 summarizes reported yields. These processes differ in conversion, selectivity, cycle length, and catalyst regeneration methods.

Diisopropyl Ether

In March 1992, Mobil Research & Development Corporation announced the development of a new process to produce DIPE by direct hydration of propylene to isopropyl alcohol (IPA), followed by etherification using shape-selective zeolite catalysts. DIPE's high octane and low vapor pressure gasoline blending qualities make it an attractive oxygenate blending candidate for reformulated gasoline mandated by the CAAA. Table 3 compares the blending properties of DIPE with MTBE, ETBE, and TAME. Another claimed advantage of DIPE is that, unlike MTBE, ETBE, and TAME, it is a completely refinery-based oxygenate, with no outside alcohol supply required.

UOP also unveiled a DIPE process in 1993. Its process is probably based on Union Carbide's IPA process.

Catalytic hydration of propylene to produce IPA is an established technology. The reaction steps are:

$$\text{Propylene} + \text{Water} \rightarrow \text{Isopropyl Alcohol} \quad (1)$$

$$2\ \text{Isopropyl Alcohol} \rightarrow \text{Diisopropyl Ether} + \text{Water} \quad (2)$$

$$2\ \text{Propylene} + \text{Water} \rightarrow \text{Diisopropyl Ether} \quad (3)$$

The direct propylene hydration to IPA and DIPE is thermodynamically limited with IPA as the main product and DIPE as a by-product. The use of a strong acidic catalyst can achieve direct propylene hydration under the moderate temperatures and pressures favorable to propylene conversion. Pressure is an important parameter determining propylene conversion—higher pressures increase the propylene conversion per pass. The water/propylene ratio is used to control IPA and DIPE production. A high water/propylene ratio favors IPA production, and a low ratio favors DIPE formation. The presence of excess water inhibits oligomer formation. The reaction temperature is normally kept as low as possible to minimize polymerization.

Although the hydration of propylene to IPA and DIPE is a known technology, the product recovery scheme is more complex than other etherification processes. The reactor effluent contains a mixture of unreacted feed (propylene and water), products (DIPE and IPA), and by-products (oligomers which are mainly C_6 olefins). Separating these components requires multiple distillation and extraction operations because binary azeotropes form between water/IPA, IPA/DIPE, and DIPE/water, and together they form a ternary azeotrope. Consequently, many separation schemes have been developed in order to reduce process complexity and operating cost.

OXYGENATE ECONOMICS

Figure 3 summarizes oxygenate product values for MTBE, ETBE, TAME and DIPE, including 10% depreciation and 25% pretax rate of return on investment. All economics are based on U.S. Gulf Coast overnight construction in 1993.

MTBE Economics

The product values of MTBE, based on isobutene from refinery C_4s, steam cracker C_4s, TBA/PO, normal butene isomerization, and field butanes, are shown in Figure 3. The economics are developed for 2,400 b/d MTBE unit based on by-product isobutene, and 12,500 b/d MTBE plant from on-purpose isobutene—typical unit sizes for these applications. The value of isobutene is based on its value in alternative process uses. The major use for isobutene in refineries is alkylation feed. This comparison provides a picture of the current competitive situation.

From this comparison, we can conclude that MTBE production based on by-product isobutene sources is the least costly route. MTBE produced from isobutene derived from TBA/PO is the least expensive at an estimated product value of 70¢/gal. MTBE derived from steam cracking and FCC by-product isobutene has slightly higher product values of 74¢/gal and 78¢/gal, respectively. MTBE product values based on either an integrated normal butene isomerization unit or a dehydrogenation unit are of similar magnitude at $1.10/gal and $1.09/gal, respectively. These last two processes are considerably more costly than the traditional by-product isobutene sources. Integrating MTBE production with normal butene isomerization incurs higher raw material costs because normal butenes have a high alternative value as alkylation feedstock. Dehydrogenation technology uses less costly normal butanes as raw material, but is a highly capital-intensive process.

TAME Economics

TAME, a high octane, low vapor pressure oxygenate, is becoming the second fastest growing oxygenate behind MTBE. Under the forthcoming complex model for RFG, amylenes will probably be restricted in the gasoline pool because of their high Reid vapor pressure (RVP) and high atmospheric reactivity. Factors for TAME's rapid growth are:

1. It removes light olefins in gasoline, which may be limited in RFG because of the high ozone formation tendency.
2. It provides an additional source of oxygenate without competing for isobutene.
3. The alternative for light olefins removed is C_5 alkylation, which is less attractive [alkylation of C_5s increases acid consumption, and the slight octane improvement (90 versus 87 (R+M)/2), does not justify the additional processing cost].

Both as an oxygenate and as an octane enhancer, TAME's economics are attractive. TAME's product value is estimated to be 75¢/gal and 81¢/gal, based on isoamlyene value use as an alkylation unit feed and a gasoline blending component, respectively. The product value of TAME is competitive with that for MTBE if isoamylene is valued as the alkylation feedstock—the more likely scenario for the future.

ETBE Economics

Interest in ETBE has increased since the U.S. Treasury Department approved a 54¢/gal tax credit for ethanol used to produce ETBE. A similar tax credit is already allowed for ethanol used directly in gasoline blending. ETBE is preferred over ethanol as a blending component because it has a low vapor pressure (4 versus 19 psi). The tax credit extension makes production of ETBE more competitive with MTBE.

ETBE competitiveness hinges on the cost of ethanol. Currently, ETBE economics can be evaluated on the basis of three ethanol costs. Figure 3 illustrates that the product values of ETBE are estimated to be 83¢/gal for a 54¢/gal federal and state subsidy, $1.03/gal for a 20¢/gal state subsidy only, and $1.11/gal with no subsidy. ETBE is competitive with MTBE production from by-product derived isobutene only if ethanol continues to receive both federal and state subsidies. The subsidies make refinery operations dependent on government policy because the differential between methanol and grain-derived ethanol is unlikely to decrease substantially in the near future.

DIPE Economics

One of DIPE's main attractions is that it is a totally refinery-based oxygenate process. Although inexpensive water provides the source of oxygen for DIPE, propylene is a relatively high valued raw material. In addition to its value as fuel products (e.g., LPG or feed to an alkylation unit), purified polymer grade propylene is an important commodity in the basic petrochemical industry. We estimate 308,000 b/d of

propylene is produced by FCC units in the U.S. refineries. Of this quantity, 48% is used in motor fuel either as alkylate or as polymer gasoline, 45% is used as chemical feedstock, and 8% is used in liquefied petroleum gas (LPG).

Figure 3 shows that DIPE economics are sensitive to propylene feedstock cost. DIPE product value varies from 74¢/gal, $1.09/gal, and $1.11/gal for propylene valued as fuel, alkylate feedstock, and polymer grade product, respectively. Our valuations indicate that DIPE is not competitive with MTBE in the United States where propylene is unlikely to be valued as fuel.

CONCLUSION

Before November 1, 1992, MTBE was used mainly as an octane enhancer for gasoline. Historical MTBE prices have been consistent with its octane blending value. This relationship existed because refiners could always choose between using MTBE or changing their operations to increase the octane of their gasoline pools. MTBE's oxygen value is unclear at this time, even though the United States has already gone through one winter with mandatory oxygenated fuel. Stockpiling before the 1992-1993 winter season and low gasoline prices combined to cause the MTBE price to collapse. The average 1993 MTBE price—between 70¢/gal and 75¢/gal—is below its octane value.

Figure 4 shows the values of various gasoline blending components as a function of their octane number. The economic risks of MTBE (by-product derived isobutene) and TAME are somewhat reduced because they can always be blended into the gasoline pool at their octane value. However, a price premium for oxygen content is required to justify the building of MTBE plants based on either normal butene isomerization or dehydrogenation technologies, and DIPE. ETBE economics are precarious because the federal subsidy for ethanol will expire in 2002. The continuation of subsidies depends strongly on corn state lobbying and the U.S. budget deficit.

LITERATURE CITED

(1) *U.S. Petroleum Refining: Meeting Requirements For Cleaner Fuels And Refineries*, National Petroleum Council, August 1993.

(2) P.R. Wilkes, "MTBE Plant financing Requires Effective Risk Management," *Fuel Reformulation*, July/August 1992, pp. 19-23.

(3) "NPRA Reports on MTBE Utilization and Capacity; 22 U.S. Plants Report," *Hydrocarbon Processing*, July 1991, p. 33.

Table 1
NORMAL BUTENES ISOMERIZATION LICENSORS

Process Name	Developer	Licensor
Skeletal Isomerization	Lyondell	CDTech
SKIP	Phillips/Texas Olefins	Phillips
ISOFIN	BP and Mobil	Kellogg
Butesom	UOP	UOP
ISO-4	IFP	IFP
SISP-4	Snamprogetti	Snamprogetti

Table 2
NORMAL BUTENES ISOMERAZATION PROCESS CONDITIONS

	SKIP	Skeletal Isomerizatsion	ISOFIN	SISP-4	Equilibrium
Temperature, °C	480-550	370-440	350-430	450-490	350-520
Conversion, %	35	44	55-50	40-30	55-40
Selectivity, %	85-90	90	85-90	88-92	

Table 3 BLENDING PROPERTIES OF OXYGENATES						
	Ethers				Alcohols	
	MTBE	ETBE	TAME	DIPE	Methanol	Ethanol
Boiling point, °C	55.2	71.7	86.1	68	65	78
Density at 20°C, g/cm³	0.74	0.75	0.77	0.73	0.79	0.79
Molecular weight	88	102	102	102	32	46
Oxygen content, wt%	18.2	15.7	15.7	15.7	50	35
Heat of combustion, cal/g	8,940	9,440	9,408	9,100	5,423	7,094
Octanes						
Blending RON	118	119	112	110	126	129
Blending MON	102	103	99	97	101	101
Blending (R + M)/2	110	111	105.5	103	115	114
Blending RVP, psi	8	3.5	1	5.0	60	18
Maximum concentration, vol%	15	13	12	—	5	5

Figure 1
IMPROVEMENT IN GASOLINE OCTANE, 1910-1990

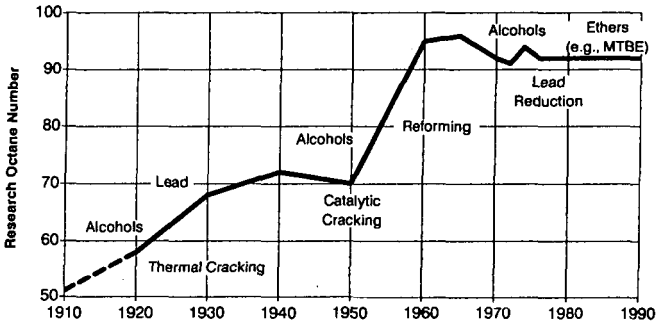

Figure 2
WORLDWIDE MTBE PRODUCTION BY ISOBUTENE SOURCE

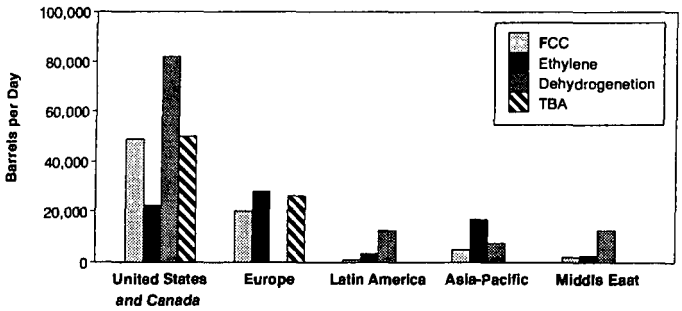

Figure 3

OXYGENATE PRODUCT VALUES: U.S. GULF COAST, 1993

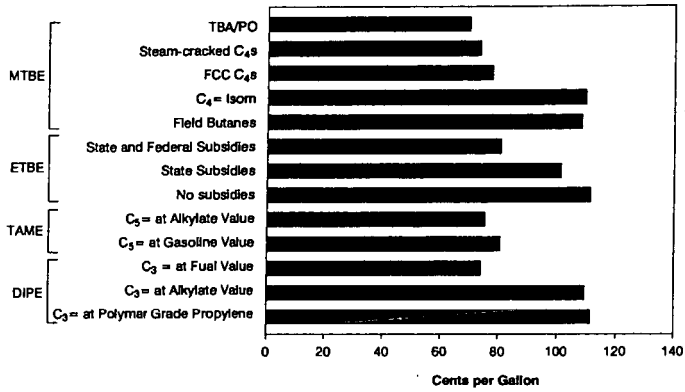

Figure 4

VALUE OF GASOLINE POOL COMPONENTS AS A FUNCTION OF OCTANE NUMBER, 1993

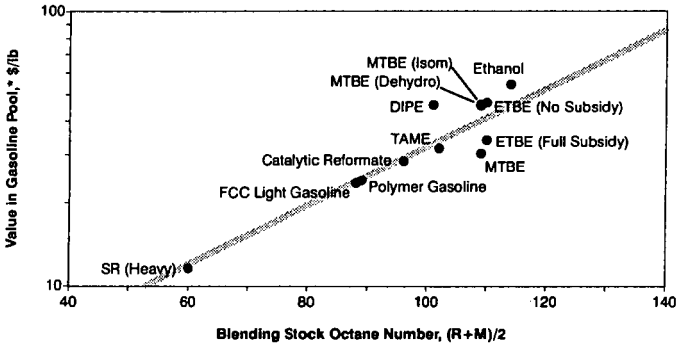

* Based on regular unleaded gasoline price of $23.10/barrel.

GASOLINE RANGE ETHER SYNTHESIS FROM LIGHT NAPHTHA PRODUCTS OF FLUID CATALYTIC CRACKING OF FISCHER-TROPSCH WAX.

W. J. Reagan
Amoco Oil Company
Naperville, Illinois 60566

Keywords: Fischer-Tropsch wax, Fluid Catalytic Cracking, Ether Synthesis.

The Fluid Catalytic Cracking of Fischer-Tropsch wax (C_{20}^{+} paraffins) produces two to four times the concentration of reactive iso-olefins (isobutylene, isoamylenes, isohexenes) than observed from conventional gas oil feedstocks. Methanol reacts with these olefins to form the corresponding tertiary alkyl methyl ethers: MTBE, TAME and MTHE's. These etherification reactions are mildly exothermic and equilibrium limited. The reaction temperature and the olefin molecular structure are important variables for maximum ether yields. The base naphtha research octane number increases by 2-4 numbers after the etherification reaction. The presence of hydrogen has a detrimental effect on ether yields because of hydrogenation of reactive olefins to paraffins. The catalytic cracking of Fischer-Tropsch wax provides a non-conventional source of olefins for ether synthesis that can supplement existing and dwindling petroleum supplies.

INTRODUCTION

Fischer-Tropsch (F-T) synthesis technology (1) produces liquid hydrocarbons from synthesis gas (hydrogen and carbon monoxide) derived from the gasification of coal or reforming of natural gas. The F-T liquid product consists of a broad range of normal paraffins (C_5-C_{50}+) and a small quantity of oxygenates and olefins. The distillate fraction, C_{12}-C_{18}, is an excellent quality fuel. The largest product fraction, C_{18}+, is primarily wax and is useless as a transportation fuel. These products are further treated by conventional petroleum processes, such as hydrotreating, reforming and catalytic cracking to produce conventional gasoline and distillate fuels. (2) Fluid catalytic cracking and hydrocracking studies have been reported by Mobil (3) and UOP. (4) Heavy wax (C_{20}+) fractions have also been treated with hydroisomerization and hydrocracking processes at Exxon. (5) Hydrodewaxing and catalytic cracking treatments of heavy wax from slurry F-T processing are also reported by Mobil. (6) In addition, pure component cracking studies (decanol, decanal) over the intermediate - pore zeolite HZSM-5 have been reported. (7) The catalytic cracking of F-T liquids was examined in some detail by Wojciechowski over large-pore faujasite (zeolite Y) and over HZSM-5 zeolite catalysts. (8,9) Governmental regulations, most recently in the Clean Air Act Amendments of November, 1990, have resulted in the phase-out of lead additives, lowering of the Reid vapor pressure of gasoline and in some geographical areas, the mandated use of oxygenates. Several types of ethers are now commercially produced and used as gasoline blending components. (10) Recent studies of methyl tertiary butyl ether (MTBE) and tertiary amyl methyl ether (TAME) suggest that these compounds may reduce automative carbon monoxide emissions, have high blending gasoline octane ratings, R+M/2, (MTBE-108, TAME-102) and have low Reid vapor pressure. These ethers are produced commercially by the etherification of the appropriate olefin by methanol (MTBE, isobutylene; TAME, isoamylenes). (11,12) There is less information in the open literature about the etherification reactions of C_6 olefins that are also present in significant quantities in fluid catalytic cracking product naphthas. The Etherol process (13) produces a mixed ether product from C_4-C_7 reactive iso-olefins in naphthas. One report (14) provides some information about the reaction of C_6 iso-olefins with methanol to produce the higher ethers, MTHE's, methyl tertiary hexyl ethers. MTBE has attracted the most attention in recent years. The growth rate for its production could reach 25% per year by 1995. (15,16) There is a growing need for alternative sources of olefins for ether syntheses as demand for these materials escalates beyond the capacity of conventional petroleum processes. There are no reported studies of the catalytic cracking processing of F-T liquids to produce C_3-C_8 olefins as feedstocks for the synthesis of gasoline range ethers.

EXPERIMENTAL.

The feedstock for this work is a sample of reactor wax from a commercial fixed bed F-T unit operated by Sasol, Limited. The analytical characterization of this feedstock is available in other studies.(4) The small scale (1 gram of feed, 3-5 grams of catalyst) catalytic cracking tests were performed on a Micro Activity Test unit (MAT) similar in design to the unit described in ASTM procedure, D3907-86. This test unit is equipped for detailed analyses of gas and liquid products and coke yields. The pilot plant tests were conducted in a circulating catalyst unit similar to a design described by ARCO. This unit operates with 2 to 3 kilograms of

catalyst and feed rates of 10-30 grams/minute. The ether synthesis experiments were carried out in a conventional high pressure micro-reactor. Three FCC catalysts, containing zeolite Y, zeolite Beta and zeolite HSZM-5 are the primary catalysts for the FCC studies. The Y zeolite catalyst is an Ultrastable Y faujasite (USY) zeolite catalyst taken from one of Amoco's commercial FCC units. The HZSM-5 catalyst is a commercial sample produced by Intercat Corp. The Beta sample was prepared in our laboratory by spray drying a commercially available Beta zeolite and a conventional silica-alumina matrix. Two commercial ion exchange resin catalysts, Rohm and Haas's Amberlyst 15 and Bayer's K 2634, were used in the ether synthesis runs.

RESULTS AND DISCUSSION.

A. Catalytic Cracking Tests.

Initial catalytic cracking runs with the small scale test system provide some insights into the catalytic cracking behavior of the wax feedstock. The initial choice of fluid catalytic cracking (FCC) catalyst and process conditions focuses on comparisons with conventional gas oil, the usual feedstock to commercial FCC units. At these conditions, (970°F reaction temperature, 3 catalyst to oil weight ratio), the wax feedstock readily converts (85%+ conversion) to high yields of C_4- gas (high in propylene and C_4 olefins) and naphtha (C_5-430°F). A summary of this comparison is presented in Table I. The conversion level is defined by convention as the sum of the products: naphtha, gas and coke. This high catalytic cracking conversion level for the wax feedstock agrees with the published Mobil data (3,6) on F-T wax cracking. In addition, historical pure component hydrocarbon cracking studies (17) suggest that long chain paraffins crack at much greater rates than the shorter chain paraffins. The low coke yield of the wax feedstock will be an important parameter when commercial heat balanced operations are evaluated. The relatively low octane number of the wax product naphtha results from the higher concentrations of low octane number paraffins compared to the gasoline from the more aromatic gas oil feedstocks. The octane numbers in the Table I are estimated results from detailed naphtha analyses by gas chromatography and correlations with octane engine tests. The target of these studies is to optimize the yields of branched olefin intermediates (isobutylene and isoamylenes) for ether synthesis. Three FCC catalysts, containing zeolite Y, zeolite Beta, and zeolite HZSM-5, were tested for wax conversion and product selectivity as a series of blends with an inert solid. Table II presents the detailed product distributions for the three catalysts at a similar conversion level of about 83%. Both the Beta and HZSM-5 catalysts produce much higher yields of the desirable olefins. However, this occurs at the expense of naphtha product. In addition, the HZSM-5 catalyst produces very high yields of propylene. These screening test results show that FCC catalyst variations can provide for widely different product distributions.

B. Pilot Plant Catalytic Cracking Tests.

Some initial wax catalytic cracking screening tests on the pilot plant unit are presented in Table III. The high conversions of the wax feedstock in the pilot plant agree with the small scale test results. The Beta zeolite catalyst converts a greater fraction of the wax feedstock to light olefins, including propylene, isobutylene and isoamylenes, than the Y zeolite catalyst. The higher olefin yields are offset by a significantly lower naphtha yield for the Beta zeolite catalyst compared to the standard Y zeolite catalyst. The test results for the HZSM-5 catalyst mixture are similar to the Beta zeolite. High yields of the target light olefins are produced but the naphtha yield is much lower than the Y zeolite catalyst. This trade-off of light olefin and naphtha yields can be adjusted by the amount of the HZSM-5 additive. The total liquid products from several pilot plant catalytic cracking runs were combined and distilled (ASTM Method D-2892) to produce light naphtha (<200°F) fractions for the etherification studies.

C. Ether Synthesis.

Since the reaction of isobutylene and methanol to form MTBE is well known, this study will focus on the production of TAME and MTHE ethers from the light naphtha products of the pilot plant wax cracking studies. A small, fixed bed unit was used for these etherification studies. The initial test runs involve the reaction of 2-Methyl-2-butene with methanol to produce TAME. Table IV shows the comparison of TAME yields (conversion of isoamylene to TAME: moles TAME out/moles isoamylene in*100). The test conditions are: variable temperatures, 200 PSIG unit pressure, 0.66 WHSV (olefin) and 1.2 mole ratio of methanol/olefin. The catalyst for these runs is Amberlyst 15, a commercial etherification catalyst The reaction temperature is a major factor in this etherification reaction. The sharp

rise in TAME yield at 150°F and the decline at 200°F suggests that equilibrium limitations exist at these temperatures and reaction conditions. The maximum yields of ethers will occur at these equilibrium conditions. Table V presents the detailed composition of the light naphtha samples from the pilot plant wax catalytic cracking runs. The iso-olefin contents of the samples, feeds "B" and "C", are higher from the pilot plant wax catalytic cracking runs than the light naphtha sample, feed "A". This is due to the use of high olefin selective FCC catalysts, Beta and HZSM-5, in the pilot plant runs, Nos. 940-01,02 and 941-01. The same Y zeolite catalyst was used in the runs for feed "A" and "C" . The high iso-olefin content of feed "C" results from the lower conversion level. The reactive isoamylenes, 2-Methyl-2-butene and 2-Methyl-1-butene for TAME synthesis and the reactive C_6 iso-olefins, 2-Methyl-1-pentene, 2-Methyl-2-pentene, 2,3-Dimethyl-1-butene, and cis and trans 3-Methyl-2-pentene for MTHE synthesis are the important components. This light naphtha, feed "A" sample and methanol are the feedstock for a series of etherification runs at the same process conditions for the 2-Methyl-2-butene/methanol tests. Due to the limited availability of the naphtha, only two reaction temperatures are available. A summary of the conversion of the various C_5 and C_6 iso-olefins to their respective methyl ethers, Table VI, shows that reaction temperature is a major factor in the etherification reaction. The decrease in conversion with the increase in the carbon number of the iso-olefin agrees with other literature etherification studies. (18,20) The reaction products from these runs have a significant yellow color, especially at the higher reaction temperature of 150°F. This color is not present for the pure component 2-Methyl butene-2 tests. It is likely that polymerization of olefins to C_{10}+ hydrocarbon "color bodies" is responsible for the colored product. The color of the ether product could be a significant product quality issue. Table VII presents the results of the etherification runs with the "B" and "C" light naphthas at 150°F. In these runs, both Amberlyst 15 and another commercial etherification catalyst, Bayer's K2634 are under study. The Bayer catalyst contains a noble metal in addition to the strong acid functionality. The noble metal is available for olefin isomerization and diolefin saturation, in the presence of hydrogen. The nominal reaction conditions from the previous set of runs, 200 PSIG, 2.9 grams of catalyst, methanol 1.37 g/hr, naphtha, 5.5 g/hr are the same except that only one reaction temperature, 150°F, is available. The iso-olefin conversion results are similar for both catalysts and the three feedstocks, in the absence of hydrogen gas in the reactor. The calculated research octane values for the products of these etherification runs are 2-4 numbers higher than the starting light naphtha feedstocks, Table VIII. As expected, this octane increase depends to some extent upon the concentrations of the ethers in the product. Blending octane numbers for the mixed ether light naphtha fractions are also shown in Table VIII. There is a fair agreement with the calculated (by GC) octane numbers. When hydrogen gas is present, Run No. 034-1, Table VIII, there is a major loss of iso-olefin conversion. These reaction conditions result in the hydrogenation of both reactive iso-olefins and linear olefins. This is an undesirable result since both the production of ethers and the octane number of the product decreases significantly. The run with added hydrogen gas, 034-1, has a lower research octane rating (79.5) than the feedstock (84.6) or the run with no added hydrogen, 034-3, (85.8). This octane loss is due to the conversion of high octane value olefins to low octane value paraffins. There is a significant improvement in the color of the etherification products in the presence of hydrogen gas.

These etherification runs clearly demonstrate that the light naphtha fractions from the catalytic cracking of Fischer-Tropsch wax are excellent ether synthesis feedstocks.

ACKNOWLEDGEMENT.

This work was supported by the U. S. Department of Energy, Pittsburgh Energy Technology Center, Pittsburgh, Pennsylvania under Contract No. DE-AC22-91PC90057. D. Kovach and R. Brown performed the experimental work. J. Newbury provided the GC naphtha analyses.

REFERENCES

1. Anderson, R. B. The Fischer-Tropsch Synthesis; Academic (New York), 1984.
2. Stuart, J. S., et al. Oil & Gas Journal, August 31, 1981, 62.
3. Kuo, J. C. W., et al. 1988 AIChE Annual Meeting (Washington, DC, 11/17/88, Preprint No. 61D); 1984 AIChE Annual Meeting (Anaheim, California, Preprint No. 11D); Department of Energy, Final Report, October, 1985, DOE/PC/60019-9A.
4. Shah, P. P., et al. "F-T Wax Characterization and Upgrading"; Final Report, Department of Energy, June 6, 1988, DOE/PC/80017-T1.
5. Exxon R&E Company, U.S. 4,832,819, May 23,1989.

6. Mobil Oil Company, U.S. 4,684,756, August 4, 1987.
7. Riley, M.; Anthony, R. G. J. Cat., 103, 87-94, 1987.
8. Abbot, J.; Wojciechowski, B. W. Ind. Eng. Chem. Prod. Res. Dev.1985,24, 501-507.
9. Kobolakis, I.; Wojciechowski, B. W. Can. J. Chem. Eng., 63, April 1985, 269-277.
10. Piel, W. J. Energy Progress, 8, No. 4, 201, 1988; Oil & Gas J., December 4, 1989, 40.
11. Reychler, A. Bull. Soc. Chim. Belg.; 21, 71 (1907).
12. Ancillotti, F., et al., J. Catalysis; 46, 49-57 (1977).
13. Halsig, C. P., et al., NPRA, 1986 Annual Meeting, Paper AM-86-94.
14. Krause, A. O. I., et al., 8th Int. Cong. Catal., 5, 553, 1984.
15. Oil & Gas J., January 27,1992, 21.
16. Oil & Gas J., November 30,1992, 48.
17. Corma, A.; Wojclechowski, B. W. Catal. Rev.-Sci. Eng., 27(1), 29-150, 1985

TABLE I

INITIAL COMPARISONS OF FISCHER-TROPSCH WAX CRACKING AND CONVENTIONAL GAS OIL FEEDSTOCKS

MAT Test Results: 970°F, 3 C/O, Equilibrium Catalyst
Product Distribution and Product Properties

	Gas Oil	Wax
Conversion, wt%	61.6	88.1
Products, wt%:		
C_2^-	2.6	1.8
$C_3 + C_4$	11.6	31.4
C_5	6.9	15.9
C_6 - 430°F	36.2	36.8
430°F+	38.4	11.9
Coke	4.3	2.2
Isobutylene	1.3	4.5
Isoamylenes	2.3	5.8
Nephtha, RON	90.4	85.8
MON	79.8	77.6

TABLE II

MAT TEST RESULTS--CATALYST COMPARISONS AT 880°F

Catalyst Type	Zeolite T	Zeolite Beta	Zeolite HZSM-5
Run No.	031	042	055
Conversion, Wt%	83.0	83.3	83.8
Product Yields, Wt%:			
C_1	0.6	0.6	1.5
C_2^-	7.4	8.9	17.5
$C_2^=$	0.8	0.9	2.7
C_4^-	13.2	17.7	27.4
$C_4^=$	3.7	3.6	3.6
C_5^-	11.7	13.5	13.9
$C_5^=$	3.6	2.2	2.0
C_6-430°F	41.7	35.8	15.3
430°F+	17.0	16.8	16.2
Coke	0.3	0.2	0.1
Isobutylene	5.8	9.4	12.3
Isoamylenes	7.7	9.2	9.8
C_6-430°F	57.0	51.4	31.1
RON	85.2	84.4	84.4
MON	76.2	74.6	76.0

TABLE III

PILOT PLANT RUNS

RUN NO.	939-05	940-2	941-1
Reaction Temp., °F	879	910	965
C/O Ratio	2.25	3.35	2.84
WHSV (hr^{-1})	42.2	61.5	54.61
Catalyst	Steamed eq. USY	Steamed Beta	Steamed eq. USY (75%)/HZSM-5(25%)
Conversion, wt%	85.0	96.5	89.0
Product Yields, wt%:			
C_2^-	0.51	0.66	1.22
C_2=	6.28	13.68	16.03
C_3	0.90	1.81	2.47
iC_4	3.40	7.66	3.40
nC_4	0.99	2.09	1.92
iC_4=	6.75	12.99	12.95
tC_4=	3.19	5.44	5.33
cC_4=	2.31	3.98	3.76
iC_5	3.35	3.73	2.16
nC_5	0.96	1.51	1.40
Total C_4=	10.54	10.24	12.47
C_5-430°F	46.08	31.53	24.81
430°F+	14.06	3.67	11.60
Coke	0.68	1.00	0.47

TABLE IV

TAME PRODUCTION

Methanol/2-Methyl-2-butene feedstock

Reaction Temperature, °F	TAME YIELD*
125	50
150	80
200	59

*TAME YIELD = moles TAME out/moles isoamylenes in * 100.

TABLE V

HYDROCARBON COMPOSITION OF 200°F NAPHTHAS

Feed ID:	92-0490-01A Feed A*	93-0024-01A Feed B	93-0024-01C Feed C
Pilot Plant Run Nos.	939-01, + 02 eq. USY catalyst conversion = 93.6%	940-01, 02 941-01 Beta/HZSM-5 catalyst Conversions = 90,96%	939-04 eq. USY catalyst conversion = 83%
Total Paraffins wt%	6.69	8.44	4.32
Total Iso-paraffins wt%	42.71	17.64	22.88
Total Aromatics wt%	1.74	2.62	0.35
Total Naphthenes wt%	3.96	5.55	3.16
Total Olefins wt%	44.51	64.47	68.6
Reactive iso-olefins wt%			
C5's			
2-methyl-1-butene	1.25	2.15	1.76
2-methyl-2-butene	4.26	5.67	5.64
C6's			
2,3-dimethylbutene	0.8	0.73	0.97
2-methyl-1-pentene	2.35	2.49	3.02
2-methyl-2-pentene	4.01	5.27	5.46
3-methyl-trans-2-pentene	2.49	3.13	3.29
3-methyl-vis-2-pentene	3.98	5.48	5.35

TABLE VI

REACTIVE ISO-OLEFINS CONVERSION TO ETHERS
Reaction Temperature (Averages of Three Weight Balance Tests)

Feed A		
Iso-olefin Component	125°F	150°F
	wt%	wt%
C5		
2-Methyl-1-butene	85.4	89.9
2-Methyl-2-butene	29.9	65.5
C6		
2,3 Dimethyl-1-butene	56.5	83.4
2-Methyl-1-pentene	65.9	87.5
2-Methyl-2-pentene	20.7	48.6
3-Methyl-cis-2-pentene	21.7	38.6
3-Methyl-trans-2-pentene	20.8	29.8

TABLE VII

REACTIVE ISO-OLEFINS CONVERSION TO ETHERS

	Feed A	Feed B			Feed C	
200°F- Naphtha	92-049-01A	92-0024-01A			93-0024-01C	
Reaction Temp, °F	150	150	150	150	150	150
Catalyst	Amberlyst 15	Amberlyst 15	K2634	K2634	K2634	K2634
			No H2	H2	H2	No H2
iso-olefin component						
C5's						
2-Methyl-1-butene	89.9	90.2	87.1	77.2	78.1	87.7
2-Methyl-2-butane	65.5	62.2	66.2	42.9	38.2	61.2
C6's						
2,3,Dimethyl-1-butene	83.4	---	---	---	---	---
2-Methyl-1-pentene	87.5	85.5	84.1	72.2	78.6	86.9
2-Methyl-2-pentene	48.6	56.1	62.7	44.2	31.5	51.5
3-Methyl-Cis-2-pentene	38.6	31.0	43.4	23.8	7.3	25.8
3-Methyl-trans-2-pentene	29.8	32.2	43.7	25.9	20.7	33.3

TABLE VIII

LIGHT NAPAHTA ETHERIFICATION RUNS HYDROCARBON COMPOSITION OF FEED AND PRODUCTS

Run No.	Reaction Temp	Catalyst	Research Octane Number*	Blending Research Octane Number
Feed A				
92-0490-01A	---	---	80.92	66.9
15586-024-2	125°F	Amberlyst 15	80.09	77.9
15586-024-6	150°F	Amberlyst 15	83.76	79.9
15586-024-8	150°F	Amberlyst 15	83.88	--
Feed B				
93-0024-01A	---	---	83.12	83.9
15586-031-2	150°F	Amberlyst 15	87.43	87.9
05586-033-1	150°F	Bayer K2634	87.48	85.9
15586-033-3	150°F	Bayer K2634	85.78	84.9
Feed C				
93-0024-01C	---	---	84.56	95.9
15586-034-1	150°F	Bayer H2 K2634	79.47	88.9
15586-034-3	150°F	Kayer no H2 K2634	85.78	95.9

*Calculated

TABLE VIII

LIGHT NAPAHTA ETHERIFICATION RUNS HYDROCARBON COMPOSITION OF FEED AND PRODUCTS
(Continued)

Run No.	Paraffins	Iso-paraffins	Aromatics	Naphthenes	Olefins	Oxygenates	Unknowns
Feed A							
92-0490-01A	6.689	42.712	1.736	3.956	44.507	0.071	0.33
15586-024-2	7.804	40.230	1.985	4.474	33.762	11.406	0.34
15586-024-6	6.463	40.429	2.247	4.576	29.671	16.294	0.32
15586-024-8	6.337	40.466	2.263	4.586	29.58	16.436	0.33
Feed B							
93-0024-01A	8.437	17.637	2.623	5.549	64.472	0.17	1.11
15586-031-2	7.417	17.989	3.687	6.424	41.847	21.815	0.821
05586-033-1	7.381	17.340	3.691	6.583	41.716	22.445	0.844
15586-033-3	8.205	17.668	3.62	6.512	45.889	17.277	0.83
Feed C							
93-0024-01C	4.315	22.881	0.353	3.161	68.651	0.15	0.49
15586-034-1	14.535	24.733	2.405	5.436	35.369	17.382	0.19
15586-034-3	5.921	22.489	1.977	4.497	43.51	21.192	0.415

*Calculated

SYNTHESIS OF OXYGENATES FROM H_2/CO SYNTHESIS GAS AND USE AS FUEL ADDITIVES

Richard G. Herman, Kamil Klier, Owen C. Feeley, and Marie A. Johansson
Zettlemoyer Center for Surface Studies and Department of Chemistry,
7 Asa Drive, Lehigh University, Bethlehem, PA 18015.

Keywords: Oxygenates, Synthesis Gas, Ethers, MTBE, Alcohols

ABSTRACT

Alternative processes for synthesizing fuel-grade oxygenates are centered on conversion of synthesis gas into C_1-C_8 alcohols and ethers. Over Cs/Cu/ZnO-based catalysts, mixtures of methanol/ isobutanol are predominantly formed. It has been found that these alcohols can be directly coupled over certain strong acid organic-based catalysts to form unsymmetric C_5 ethers, mainly the kinetically favored methyl isobutyl ether (MIBE) with some of the thermodynamically favored methyl tertiarybutyl ether (MTBE), the symmetric ethers of dimethylether (DME) and diisobutylether (DIBE), or selectively dehydrated to form isobutene over sulfated zirconia. Based on these reactions, a 2-stage, dual catalyst configuration can be utilized to give MTBE as the dominant ether product. The octane numbers and cetane ratings of the oxygenates have been determined and are compared, e.g. adding 10 vol% MIBE and MTBE to 82.3 MON gasoline altered the MON of the gasoline by -1.5 and +1.4 units, respectively, and MIBE has a high cetane number of 53, compared to 42 for typical U.S. diesel fuel.

INTRODUCTION

Beginning in the 1970s, environmental concerns led to a phasing out of lead in gasoline, and recent legislative requirements are inducing the lowering of aromatics and light (high vapor pressure) hydrocarbons in reformulated gasoline. To maintain the required octane level of gasoline and to provide environmental benefits, oxygenate additions, either as alcohols or ethers, to gasoline have been steadily increasing. At the present time, the preferred oxygenate is methyl tertiarybutyl ether (MTBE) because it compensates for the loss in octane number caused by a reduction in aromatics, reduces the vapor pressure of the gasoline fuel, and provides some reduction in vehicle tailpipe hydrocarbon and carbon monoxide emissions [1]. Currently, MTBE is manufactured from methanol and isobutene *via* a liquid phase synthesis over acid resin catalysts, as represented by Equation 1, where isobutene is usually obtained as a side product from petroleum refinery FCC units [2-4]. Although older FCC units can produce 8 wt% C_4 products in their output [5], the typical FCC refinery product slate now contains 1.4 wt% C_4 compounds [6], and improved processes utilizing catalytic additives such as improved ZSM-5 tend to decrease the yield of C_3 and C_4 olefins in the light ends further still [7]. Thermal cracking of the isobutane in the light ends can also be carried out to obtain isobutene [6]. Although cracking processes are being modified to yield more C_4 as a by-product, the availability of refinery supplied isobutene is limited.

$$(CH_3)_2C{=}CH_2 + CH_3OH \rightarrow (CH_3)_3C\text{-}O\text{-}CH_3 \qquad 1)$$

Alternative feedstocks and processes not directly dependent on isobutene for the synthesis of oxygenates are highly desirable, and new catalysts and catalytic processes are being investigated and developed. One of the alternative processes that have been developed for the synthesis of pure isobutene is the endothermic dehydration of tertiary butanol [8]. Another possible source of isobutene for ether synthesis is dehydration of isobutanol, represented by Equation 2, that is produced from synthesis gas. An overall scheme of using coal as the initial resource involves gasification of the coal to synthesis gas, purification (and water gas shifting if necessary) of the synthesis gas, higher alcohol synthesis, and direct synthesis of ethers from the alcohols. Both the

alcohols and ethers can be used as fuels and fuel additives as desired. Methanol and isobutanol are the predominant products formed from H_2/CO synthesis gas over alkali-promoted Cu/ZnO-based catalysts [9-14], as well as over non-copper-containing high temperature alkali-promoted alcohol synthesis catalysts [15,16]. Since the two alcohols are produced together, direct coupling of these two alcohols to produce fuel-grade ethers is also of interest. It has been shown [17,18] that over acid resin catalysts, the dominant reaction is direct coupling that results in the formation of methyl isobutyl ether (MIBE), Equation 3. However, if a selective catalyst were found for converting isobutanol to isobutene (even as a transient intermediate) with subsequent reaction with methanol (Reaction 2 followed by Reaction 1), a desirable route to high octane MTBE from natural gas or coal-derived synthesis gas would be provided [19]. Such a process would alleviate isobutene dependence on petroleum feedstocks.

$$(CH_3)_2CHCH_2OH \rightarrow (CH_3)_2C{=}CH_2 + H_2O \qquad 2)$$
$$(CH_3)_2CHCH_2OH + CH_3OH \rightarrow (CH_3)_2CHCH_2\text{-}O\text{-}CH_3 + H_2O \qquad 3)$$

EXPERIMENTAL

A variety of organic resin catalysts and inorganic oxide and zeolite catalysts have been probed for alcohol conversion reactions [20,21], and the catalysts investigated in the current study consisted of Amberlyst-15 (used as received) and sulfated zirconia. The sulfate-modified zirconia (SO_4^{2-}/ZrO_2) was prepared as described by Hino and Arata [22]. Zirconyl chloride octahydrate ($ZrOCl_2 \cdot 8H_2O$) was added to aqueous ammonia to precipitate high surface area $Zr(OH)_4$ that was washed and then dried at 100°C overnight. The dried $Zr(OH)_4$, e.g. weighing ≈10 g, was placed on a folded filter paper, and 150 ml of 1 N H_2SO_4 was poured through it. The wet powder was dried at 110°C overnight and then calcined in air at 620°C for 3 hr. The BET surface area of this catalyst was found to be 60 m^2/g and the sulfur content was 0.84% by weight.

The catalysts were tested for ether synthesis from binary methanol/isobutanol (2-methyl-1-propanol) reactant mixtures in the vapor phase in a downflow stainless steel bench-scale reactor system that is automated so that testing can be carried out under continuous operation at designed experimental conditions. A schematic of the reaction system was shown previously [19]. Typically, N_2/He gas was utilized as the carrier/inlet gas, and the alcohol mixture was added at the top of the reactor *via* a high pressure Gilson pump or an ISCO piston pump provided by Air Products and Chemicals, Inc. The conversion and product composition was monitored by continual sampling, e.g. 0.5 hr, of the exit stream by GC analysis using in-line, heated, automated Valco sampling valves and by collection of the liquid product for analyses by GC, NMR, and GC/MS.

The dedicated Hewlett-Packard Model 5890 Series II gas chromatograph (GC) with a capillary column (25 m x 0.32 mm ID wall coated open tube (WCOT) with a chemically bound 5.0 μm thick methyl silicon coating) is interfaced and controlled by a PC data station using chromatographic software (Chrom Perfect) from Justice Innovations, Inc. At the same time, the GC is interfaced with a Hewlett-Packard Model 3396 Series II recorder/integrator, which can also produce a hardcopy of each chromatogram and listing of the associated integrated peak areas.

All of the catalytic tests reported here were carried out a 1 atm. According to our standard procedure, the catalysts were diluted with 0.5 or 3 mm Pyrex beads to a total volume of 20 ml. The catalyst bed was centered in the stainless steel reactor between two glasswool plugs. The remainder of the reactor volume was filled with 3 mm Pyrex beads that served to preheat and mix the entering gas, as well as minimizing dead volume in the reactor. The charged reactor was brought to the reaction temperature in a flow of approximately 80% He and 20% N_2. When the temperature was stabilized, the equimolar alcohol mixture was pumped into the reactor at the preset flow. The reaction was carried out at each temperature for at least 3-6 hr. Steady state conversions of methanol and isobutanol were usually obtained within the first 1-2 hr time-on-stream.

RESULTS AND DISCUSSION

Direct Coupling or Dehydration of Alcohols Over Amberlyst-15 and SO_4^{2-}/ZrO_2. Thermodynamic calculations of the direct coupling of methanol and isobutanol indicate that low temperatures, i.e. 50-90°C, are necessary to achieve favorable selectivity to desired products, especially MTBE and MIBE [18,19]. The upper temperature of 90°C was chosen for this study in order to maximize conversion. Low pressure, i.e. 1 atm, is utilized in these reactions in light of the findings of Nunan et al. [17,18] that indicated lower pressures favored greater isobutene formation, the precursor of MTBE. The alcohol partial pressure was chosen such that no condensation would occur within the reaction system, and this was determined empirically under reaction conditions. A summary of the experimental conditions used with the Amberlyst-15 catalyst is given below:

Catalyst weight	5.00 g (dry)	MeOH flow rate	1.72 mol/kg cat/hr
Reaction temperature	90°C	i-BuOH flow rate	1.72 mol/kg cat/hr
Total Pressure	1 atm	He + N_2 flow rate	16 mol/kg cat/hr.

The space time yields (STY) of the products are given in Table 1. It is seen that the molar yields of DME, butenes, and MIBE were comparable, while only 0.5% of each reactant was converted to MTBE. The entry "Butenes" includes iso-, *trans*-2-, and *cis*-2-butene with isobutene predominating (greater than 85% of the butene content)..

The sulfate-modified zirconia catalyst (5 g) was tested under the same conditions employed with Amberlyst-15, but higher temperatures were also utilized. At 90°C, only MIBE was detected, but the yield was very low. However, at higher temperature isobutanol was selectively dehydrated to butenes in the presence of methanol. Indeed, at 175°C, the SO_4^{2-}/ZrO_2 showed 95% conversion with over 80% selectivity to butenes, principally isobutene (Table 1). At the latter temperature, small amounts of C-8 and C-12 products (0.5 mol%) were observed. Non-sulfated zirconia was found to be totally inactive for the dehydration of either methanol or isobutanol over the temperature interval tested (90-175°C).

Dehydration of Isobutanol Only Over the SO_4^{2-}/ZrO_2 Catalyst. The activity and selectivity of dehydrating isobutanol over SO_4^{2-}/ZrO_2 in the absence of methanol was investigated. The SO_4^{2-}/ZrO_2 catalyst (5 g) calcined to 620°C was centered in the reactor as described previously. The reaction conditions utilized included the temperatures of 125, 135, 150, 175, 200, and 225°C and isobutanol feed rates of 1.69-20.28 mol/kg catalyst/hr while maintaining the He + N_2 flow = 18.78 mol/kg catalyst/hr. The isobutanol space velocity of 1.69 mol/kg cat/hr was used in an initial temperature dependence study from 125 to 175°C. At 175°C, 85% of the isobutanol was converted to butenes. Comparison to the first entry row in Table 1 indicates that absence of the methanol reactant produced only a small increase in isobutanol conversion.

At the temperature of 200°C, the isobutanol flow rate was raised sequentially to 6.76, 13.52, and 20.28 mol/kg cat/hr. A final test was performed at 225°C using 20.28 mol isobutanol/kg cat/hr. Testing was carried out for several hours at each point of temperature and space velocity. The only major products observed with the on-line GC analysis were isobutene, *trans*-2-butene, and *cis*-2-butene. Trace amounts of octenes and C_8 ethers were seen. At higher reaction temperatures, small amounts of methanol and other products believed to be cracking products of isobutanol were seen as was seen for isobutanol only dehydration over H-mordenite. The yields of the major products under these conditions are presented in Table 1. It can be seen that the predominant product was isobutene in each case. The highest productivity of isobutene of 11.35 mol/(kg cat. × hr) was obtained at 225°C and a flow rate of 20.28 mol isobutanol/kg cat/hr). The selectivity of isobutene among the butenes at this high productivity was 79% (12.2 mol% *trans*-2-butane and 8.7 mol% *cis*-2-butene). This production of isobutene corresponds to 1.1 kg isobutene/kg cat/hr, and therefore the dehydration of isobutanol over SO_4^{2-}/ZrO_2 is a fast reaction at this temperature.

Dual Reactor Synthesis of MTBE. The concept of this experiment was to selectively dehydrate isobutanol in the reactant alcohol mixture to isobutene over one catalyst and then to couple the isobutene with methanol to form MTBE over a second catalyst. In this dual bed experiment at ambient pressure, the first catalyst bed contained 5 g of SO_4^{2-}/ZrO_2, calcined to 620°C, while the second bed contained 0.5 g of Amberlyst-15. The reactant gas flow of the methanol/isobutanol = 1/1 mixture was 1.72 mol/kg cat/hr of each alcohol with a carrier gas flow of 17.2 mol/kg cat/hr of N_2 and He. The first bed was maintained at 175°C to effect the selective dehydration of isobutanol to isobutene, while the second bed consisting of the resin catalyst was kept at 90°C for the MTBE synthesis reaction. A short line of copper tubing connected the two beds and served as a heat exchanger. The space time yields of the products are given in Table 1.

In this experiment, the conversions of isobutanol and methanol corresponded to ≈77 mol% and ≈20 mol%, respectively. This productivity of MTBE is more than an order of magnitude higher than that obtained by the direct coupling of methanol and isobutanol over the Amberlyst-15 resin at 90°C. The butenes consisted of 0.90, 0.09, and 0.08 mol/kg cat/hr of isobutene, *trans*-and *cis*-2-butene, respectively. In addition, 0.03 mol *tert*-butanol/kg cat/hr was also observed. It was observed that lowering the second bed temperature to *ca.* 40°C (non-steady state conditions) increased the yield of MTBE to ≈0.35 mol/kg cat/hr, which principally reflected the enhanced reaction of methanol with the isobutene that is favored by lower reaction temperatures. Indeed, the decrease in the yields of "butenes" was due solely to a lower amount of isobutene (≈0.70 mol/kg cat/hr) in the product mixture, while the *trans*- and *cis*-2-butene yields remained constant.

This experiment under unoptimized conditions shows that it is feasible to considerably increase the yield of MTBE formed from alcohols *via* a 2-step process, although the yield obtained under these conditions was limited by the low pressure and high temperature employed, as well as the small amount of Amberlyst-15 used as the second catalyst bed. In these experiments, water was not separated from the product stream between the beds.

Fuel Characteristics of Oxygenates. Determination of the octane numbers of MIBE and MTBE was performed by AMOCO Oil Company. The standard ASTM methods D-2699 and D-2700 were used for Research Octane Number and Motor Octane Number, respectively. Cetane determinations were carried out at the Southwest Research Institute. Octane number were determined for MIBE, MTBE, and a 50/50 by volume mixture of MIBE and MTBE. MTBE was obtained from Aldrich, while the MIBE was synthesized in-house by the Williamson ether synthesis as described previously [19]. For the purpose of octane number determination, this product was distilled under nitrogen to yield a >96% purity of MIBE, as determined by gas chromatography. The major impurity was isobutanol. The peroxide level of the ether samples was <20 ppm and was considered to be acceptable for all three samples.

The results obtained by AMOCO Oil Co. are summarized in Table 2. It can be seen that MTBE increased the research octane number by 2.8 units and the motor octane number by 1.4 units, which is in good agreement with values obtained by Spindelbalker and Schmidt [23]. MIBE, on the other hand, decreased both the research octane number and motor octane number by 3.2 and 1.5 units. The gasoline/ether mixture containing both MIBE and MTBE (5 vol% of each) had the same values as the base unleaded regular gasoline. In this case, an appreciable amount of oxygen was added to the ULR gasoline without altering its octane rating.

The blending octane numbers were calculated according to the following equation: Blending Research Number = RON (component A) × (percent component A) + RON (component B) × (percent component B). Table 3 lists the blending numbers for MIBE and MTBE. MTBE and MIBE are structurally not very different, but it is clear from the results presented above that MTBE is superior to MIBE for octane enhancing purposes. Comparisons of the blending octane and cetane numbers of oxygenates are given in Table 4. In this table, ETBE = ethyltertiary-

butylether, IPTBE = isopropyltertiarybutylether, DIPE = diisopropylether, and TAME = tertiary-amylmethylether. Changes (Δ) in RON and MON were determined at 10 vol% levels of the oxygenates in gasoline. It is clear that MIBE has a poor octane number but a high cetane number.

ACKNOWLEDGEMENT

This research was supported in part by the U.S. Department of Energy (Pittsburgh Energy Technology Center), principally under Contract No. DE-AC22-90PC90044.

REFERENCES

1. "*Critical Technologies: The Role of Chemistry and Chemical Engineering*," National Research Council, National Academy Press, Washington, D.C., pp 22-23 (1992).
2. Chase, J. D. and Galvez, B. B., *Hydrocarbon Process.*, 60(3), 89 (1981).
3. Chase, J. D., in "*Catalytic Conversions of Synthesis Gas and Alcohols to Chemicals*," ed. by R. G. Herman, Plenum Press, New York, 307 (1984).
4. *Hydrocarbon Process.*, 68(11), 96 (1989); and Satterfield, C. N., "*Heterogeneous Catalysis in Industrial Practice*," 2nd Ed., McGraw-Hill, Inc., New York, 260 (1991).
5. Haggin, J., *Chem. Eng. News*, 67(23), 31 (1989).
6. Monfils, J. L., Barendregt, S., Kapur, S. K., and Woerde, H. M., *Hydrocarbon Process.*, 71(2), 47 (1992).
7. Krishna, A. S., Hsieh, C. R., English, A. R., Pecoraro, T. A., and Kuehler, C. W., *Hydrocarbon Process.*, 70(11), 59 (1991).
8. Abraham, O. C. and Prescott, G. F., *Hydrocarbon Process.*, 71(2), 51 (1992).
9. Klier, K., Herman, R. G., and Young, C.-W., *Preprints, Div. Fuel Chem., ACS*, 29(5), 273 (1984).
10. Klier, K., Herman, R. G., Nunan, J. G., Smith, K. J., Bogdan, C. E., Young, C.-W., and Santiesteban, J. G., in "*Methane Conversion*," ed. by D. M. Bibby, C. D. Chang, R. F. Howe, and S. Yurchak, Elsevier, Amsterdam, 109 (1988).
11. Nunan, J. G., Bogdan, C. E., Klier, K., Smith, K. J., Young, C.-W., and Herman, R. G., *J. Catal.*, 116, 195 (1989).
12. Nunan, J. G., Herman, R. G., and Klier, K., *J. Catal.*, 116, 222 (1989).
13. Herman, R. G., in "*New Trends in CO Activation*," ed. by L. Guczi, Elsevier, Amsterdam, 265 (1991).
14. Herman, R. G., Klier, K., Young, C.-W., Nunan, J. G., Feeley, O. C., and Johansson, M. A., *Proc. 9th Intern. Pittsburgh Coal Conference*, 409 (1992).
15. Tronconi, E., Ferlazzo, N., Forzatti, P., and Pasquon, I., *Ind. Eng. Chem. Res.*, 26, 2122 (1987).
16. Tronconi, E., Lietti, L., Forzatti, P., and Pasquon, I., *Appl. Catal.*, 47, 317 (1989).
17. Nunan, J. G., Klier, K., and Herman, R. G., *J. Chem. Soc., Chem. Commun.*, 676 (1985).
18. Nunan, J. G., Klier, K., and Herman, R. G., *J. Catal.*, 139, 406 (1993).
19. Klier, K., Herman, R. G., Bastian, R. D., DeTavernier, S., Johansson, M., Kieke, M., and Feeley, O. C., in "*Proc. Liquefaction Contractors' Review Meeting*"-September 1991, U.S. DOE-PETC, Pittsburgh, PA, ed. by G. J. Stiegel and R. D. Srivastava, 20-49 (1991).
20. Klier, K., Herman, R. G., Johansson, M. A., and Feeley, O. C., *Preprints, Div. Fuel Chem., ACS*, 37(1), 236 (1992).
21. Feeley, O. C., Johansson, M. A., Herman, R. G., and Klier, K., *Preprints, Div. Fuel Chem., ACS*, 37(4), 1817 (1992).
22. Hino, M. and Atara, K., *J. Chem. Soc., Chem. Commun.*, 851 (1980).
23. Spindelbalker, C. and Schmidt, A., *Erdoel, Erdgas, Kohle*, 102, 469 (1986).

TABLE 1. Product yields (mol/kg cat/hr) over the single bed and dual bed catalysts from methanol = isobutanol = 1.72 mol/kg cat/hr reactants and from isobutanol only at different flow rates at 1 atm at the temperatures utilized in this study.

	$T_{Reaction}$	DME	Butenes	MIBE	MTBE	C8 Ether
SO_4^{2-}/ZrO_2	175°C	0.10	1.29	0.05	0.01	trace
Amberlyst-15	90°C	0.04	0.04	0.05	0.01	0.01
Dual Reactor[a]	1. 175°C 2. 90°C	0.06	1.07	0.06	0.16	trace[b]
	2. 40°C	0.06	0.87	0.06	0.35	trace[b]
$(SO_4^{2-}/ZrO_2)^c$	175°C	------	1.44	------	------	trace[b]
$(SO_4^{2-}/ZrO_2)^d$	200°C	------	4.45	------	------	trace[b]
$(SO_4^{2-}/ZrO_2)^e$	200°C	------	6.80	------	------	trace[b]
$(SO_4^{2-}/ZrO_2)^f$	200°C	------	7.75	------	------	trace[b]
$(SO_4^{2-}/ZrO_2)^f$	225°C	------	14.37	------	------	trace[b]

[a]The catalyst in Reactor 1 was ZrO_2/SO_4^{2-} and in Reactor 2 was Amberlyst-15.
[b]Plus trace of octenes.
[c]The reactant consisted of isobutanol only with a flow rate of 1.69 mol/kg cat/hr.
[d]The reactant consisted of isobutanol only with a flow rate of 6.86 mol/kg cat/hr.
[e]The reactant consisted of isobutanol only with a flow rate of 13.5 mol/kg cat/hr.
[f]The reactant consisted of isobutanol only with a flow rate of 20.3 mol/kg cat/hr.

TABLE 2. Octane numbers of the ether/gasoline fuel mixtures.

Sample	Research Octane Number	Motor Octane Number	Peroxide (ppm)
Unleaded Regular Gasoline (ULR)	92.1	82.3	-
10% MTBE in ULR	94.9	83.7	14
10% (MTBE/MIBE) in ULR	92.0	82.4	6
10% MIBE in ULR	88.8	80.8	17

TABLE 3. Blending research octane number (BRON) and blending motor octane number (BMON) of MTBE and MIBE in unleaded regular gasoline.

Sample	BRON	BMON
MTBE in ULR	120.1	96.3
MIBE in ULR	60.8	67.0

TABLE 4. Selected properties of hydrocarbon fuels and oxygenated additives.

Oxygenate (or Fuel)	Blending Octane Number (R+M)/2	Cetane No.	ΔRON[a]	ΔMON[a]
MIBE	64	53[b]	-3.3[c] -1.9[d]	-1.5[c] -3.0[d]
MTBE	108 109[e], 110[f], 108[g]	< 10	+2.8[c] +3.4[d]	+1.4[c] +2.8[d]
ETBE	110[e], 112[f]		+2.1[d]	+2.2[d]
IPTBE	100.5[e], 113[f]			
DIPE	104.5[e], 105[f]			
TAME	104.5[e], 105[f]			
Methanol	116[e], 108[f]	3		
Ethanol	113[e], 115[f]	8		
i-Propanol	108.5[e], 106[f]			
1-Butanol	87[e]	25	+1.0[d]	+0.6[d]
i-Butanol	102[f]	13	+3.1[d]	+2.1[d]
t-Butanol	101[e], 100[f]		+1.9[d]	+2.0[d]
Butane	94[g]			
Gasoline	--------		------	------
Diesel Fuel	--------	> 42	------	------

[a]Determined at the level of 10 vol% of additive in gasoline.
[b]Determined by the Southwest Research Institute with a sample submitted by us; J. Erwin, private communication.
[c]Determined by AMOCO Oil Co. with samples submitted by us using an unleaded gasoline baving RON = 92.1 and MON = 82.3; W. J. Reagan, private communication.
[d]From Reference 23 using an unleaded gasoline having RON = 82.4 and MON = 76.6.
[e]From G. H. Unzelman, *Oil & Gas J.*, 33 (April 10, 1989).
[f]From W. J. Piel, "*Proc. First Biomass Conf. of the Americas*," Burlington, VT (1993).
[g]From W. J. Piel, *Energy Prog.*, 8(4), 201 (1988).

The Mechanism of Higher Oxygenate Synthesis over Supported Rh Catalysts

Steven S. C. Chuang, Raja Krishnamurthy, Mark A. Brundage, Michael W. Balakos
Department of Chemical Engineering,
The University of Akron,
Akron, Ohio 44325-3906

Keywords: Rhodium, Higher oxygenates, Infrared spectroscopy

Extensive mechanistic studies have shown that higher oxygenates are formed from the insertion of CO into adsorbed alkyl species that is generated from CO dissociation and partial hydrogenation. The reduced Rh surface is known to be responsible for the formation of alkyl species. However, little is known about the nature of the active sites for CO insertion on various promoted Rh catalysts that are active for higher oxygenate synthesis. *In situ* infrared spectroscopy reveals linear CO on the single reduced Rh site as the most active adsorbed CO species for CO insertion on Rh/SiO_2 and Cu-, Ag-, Ce, and Mn-promoted Rh/SiO_2 catalysts. Tilted CO exhibiting a band below 1700 cm^{-1} is identified as a spectator that does not participate in CO insertion. Increasing reaction pressure causes an increase in the residence time of alkyl intermediate allowing CO insertion to occur. The selectivity toward higher oxygenates can be improved by increasing the relative concentration of linear CO sites and by increasing reaction pressure.

INTRODUCTION

The catalytic synthesis of oxygenates from synthesis gas, i.e., CO/H_2, is an important route to the production of clean fuels and chemical feedstocks from indirect coal liquefaction (1-12). There are a considerable number of experimental studies on the mechanism of higher oxygenate synthesis on Rh/SiO_2 and Cs-Cu-ZnO catalysts. Mechanistic study on Cs-Cu-ZnO reveals that Cs promotes β addition between surface species resulting in an increase in selectivity toward 1-propanol and 2-methyl-1-propanol, the principal higher alcohol products (6,7). The Cs-Cu-ZnO catalyst is more active and selective toward methanol than higher alcohols (7). Promoted Rh catalysts have been found to exhibit selectivity up to 75% for the formation of C_{2+} oxygenates in the conditions ranging from 0.07 MPa to 10 MPa and 473-573 K (13). Although the reaction pathway and the nature of active sites for higher oxygenate formation on Rh/SiO_2 catalysts have been identified (13-16), the effect of promoter and support on the nature of active sites remains unclear.

At present, there is no satisfactory single step synthesis that permits economic production of higher oxygenates (17). An in-depth understanding of the mechanism is a key step toward rational design of selective catalysts for higher oxygenate synthesis and the development of a more selective route to higher oxygenates.

This paper reports the use of *in situ* infrared (IR) spectroscopy to investigate the nature of CO insertion sites and the residence time of intermediates involved for CO insertion on Cu-, Ag-, Ce-, and Mn- promoted Rh/SiO_2 catalysts. *In situ* characterization of reaction intermediates is essential for the development of a fundamental understanding of catalytic processes (18-20). *In situ* infrared spectroscopy has been one of the most important tools for studying the nature and structure of adsorbed species and its coverage on supported catalysts under reaction conditions (16,21-26). The structure of adsorbed species is closely related to the nature of the sites.

Investigation of the nature and reactivity of adsorbed species will provide information on the activity of sites to which the adsorbed species bonds.

EXPERIMENTAL

A 0.5 wt% Rh/SiO_2 was prepared by impregnation of SiO_2 (Strem, 350 m^2/gm) with an aqueous solution of rhodium chloride. Cu-Rh/SiO_2 catalyst with 3 wt% Rh loading was prepared by coimpregnation of aqueous solutions of copper and rhodium nitrates with Cu to Rh molar ratio of 1.0. Ag-Rh/SiO_2 with Rh loading of 3 wt% was prepared by the coimpregnation of aqueous solutions of silver and rhodium nitrates with Ag to Rh molar ratio of 1.0 . A Ce-Rh/SiO_2 catalyst with 5 wt% Rh loading and Ce to Rh molar ratio of 0.74 was prepared by coimpregnating the silica support with a mixture of rhodium chloride and cerium nitrate solutions. Mn-Rh/SiO_2 catalyst with 4 wt% Rh loading and Mn to Rh molar ratio of 0.1 was prepared by sequential impregnation of manganese nitrate and rhodium chloride solutions. The ratio of solution to the support material used was 1 ml to 1 gm. After impregnation the catalyst samples were dried in air at 303 K and then reduced in flowing hydrogen at 673 K for 16 hr. The reduced catalysts were pressed into a self-supporting disk and then placed in the IR cell for *in situ* studies.

CO adsorption and the reaction of preadsorbed CO with C_2H_4 and H_2 were carried out in an infrared (IR) reactor cell. The IR cell can be operated at temperatures up to 723 K and at a pressure of 6.0 MPa (16). Infrared spectra were measured by a FTIR spectrometer with a DTGS detector at a resolution of 4 cm^{-1}. CO adsorption was conducted by exposing the catalyst to 0.1 MPa of CO at 303 K. Gaseous CO was removed by flowing helium. The infrared spectra of adsorbed CO were recorded at 0.1 MPa of CO or He. The reactivity of the adsorbed CO for CO insertion was investigated by introducing C_2H_4/H_2 (molar ratio of C_2H_4:H_2 = 1:1) to the adsorbed CO in the IR cell that served as a batch reactor. The infrared spectra of adsorbed CO and intermediates during the reaction were measured as a function of reaction time.

RESULTS AND DISCUSSION

It has been proposed that the formation of C_{2+} oxygenates over Rh-based and IFP catalysts involves the insertion of CO into adsorbed C_nH_x that is produced from CO dissociation and hydrogenation as shown in Fig. 1 (12-16,27-29). Higher alcohols such as ethanol can be produced from either the hydrogenation of acetaldehyde or direct hydrogenation of acyl species. A high selectivity (up to 75% carbon efficiency) has been achieved on promoted Rh catalysts at 573 K and 10 MPa (3,29). The selectivity can be compared to the maximum selectivity of 25% for C_2 products predicted by Anderson-Schulz-Flory distribution (29). The reaction pathway in Fig 1. also suggests that CH_4 and C_{2+} oxygenates are produced from the same C_1 precursor, i.e., CH_x. Thus, it has been suggested that C_{2+} oxygenates should be viewed as C_1 compounds in Anderson-Schulz-Flory distribution that could, in principle, be produced with 100% selectivity (29). However, high hydrogenation activity of Rh catalyst and thermodynamically favorable formation of CH_4 usually lead to a substantial yield of CH_4. The challenge is how to suppress hydrogenation and enhance CO insertion in higher oxygenate synthesis.

The nature of active sites for CO hydrogenation has been a subject of extensive studies (13-16,27-29). It is generally agreed that CH_x is formed from CO dissociation followed by hydrogenation on the reduced Rh sites. However, the number of surface atoms (i.e., the size of ensemble) required for CO dissociation remains unclear.

Much controversy has existed on the nature of the active site for CO insertion on Rh catalysts for more than a decade (16). Since CO insertion is a key step toward the formation of

higher oxygenates, clarification of CO insertion sites is essential for the development of a comprehensive mechanism for C_2 oxygenates synthesis. Recently, we have employed ethylene hydroformylation as a probe reaction to determine the nature of active sites for CO insertion on the Rh catalysts. In ethylene hydroformylation, ethylene is hydrogenated to adsorbed ethyl species that may undergo CO insertion leading to the formation of propionaldehyde; adsorbed ethyl species can also be hydrogenated to ethane as shown in Fig. 2 (16,27). CO insertion into adsorbed ethyl species is analogous to CO insertion into CH_x species. Investigation of CO insertion into adsorbed ethyl species produced from C_2H_4 and H_2 provides direct information for elucidation of CO insertion sites without the complication resulting from CO dissociation and hydrogenation.

Our previous study on the reactivity of adsorbed CO on a reduced 3 wt% Rh/SiO_2 reveals that the linear CO adsorbed on a single Rh site is involved in CO insertion leading to the formation of propionaldehyde (16). Bridged CO and gem-dicarbonyl CO exhibit little reactivity towards CO insertion. Similar studies were conducted on the oxidized Rh/SiO_2 catalysts and showed that single Rh^+ sites are more active for CO insertion than the single Rh^0 sites (16). However, Rh^+ sites are not able to withstand the reducing atmosphere of CO/H_2 above 393 K.

The high activity of linear CO sites and the lack of activity of bridged CO sites has led to preparation of supported Rh catalysts containing primarily linear CO sites. Adsorbed sulfur blocked the bridged CO sites, increasing the concentration of linear CO sites resulting in an increase in CO insertion selectivity and activity. Low-loading supported Rh catalyst contains highly dispersed Rh crystallite. Highly dispersed Rh which contains primarily single Rh sites may chemisorb linear CO. In contrast, CO adsorption on the 0.5 wt% Rh/SiO_2 produced bands at 2027 and 2004 cm^{-1} that can be assigned to weakly adsorbed $Rh(CO)_4$ as shown in Fig. 3 (30). The intensity of the bands decreased in flowing helium suggesting that the species was weakly adsorbed. The exposure of this adsorbed CO to ethylene and hydrogen did not result in any reaction at 303 K. CO adsorption at 323 K also produced weakly adsorbed $Rh(CO)_4$ bands at 2027 and 2004 cm^{-1} similar to those observed at 303 K. Exposure of adsorbed CO to ethylene and hydrogen at 323 K produced a propionaldehyde band at 1708 cm^{-1} after approximately 20 min of reaction. An increase in the amount of propionaldehyde formed is shown by the increase in the intensity of the adsorbed band with time as observed in Fig. 3. An increase in the hydrocarbon band near 2983 cm^{-1} is also observed with reaction time. The simultaneous formation of propionaldehyde and ethane indicates that CO insertion into adsorbed ethyl species competes with ethylene hydrogenation.

CO adsorption on a $Cu\text{-}Rh/SiO_2$ catalyst produced a linear CO band at 2058 cm^{-1}, a bridged CO band at 1875 cm^{-1}, and gem-dicarbonyl bands at 2091 and 2027 cm^{-1}as shown in Fig. 4. A band at 2127 cm^{-1} assigned to CO adsorbed on Cu is also observed. Reaction of C_2H_4 and H_2 with adsorbed CO on $Cu\text{-}Rh/SiO_2$ catalyst shows the formation of propionaldehyde 1 min after addition of the reactants. A decrease in the bands at 2127 cm^{-1} and 2058 cm^{-1} and the formation of propionaldehyde indicates that the linear CO on Rh and CO adsorbed on Cu participate in CO insertion into the adsorbed ethylene. The rate of propionaldehyde formation is much faster on the $Cu\text{-}Rh/SiO_2$ catalyst in comparison to the highly dispersed Rh/SiO_2 catalyst. A decrease in intensity was observed in the gem-dicarbonyl bands after approximately 10 min of reaction with the simultaneous formation of ethane at 2983 cm^{-1} and a small amount of CO_2 at 2341 cm^{-1}. Thus, the addition of Cu appears to increase the rate of CO insertion as indicated by the higher rate of formation of propionaldehyde on the $Cu\text{-}Rh/SiO_2$ catalyst as compared to the dispersed Rh/SiO_2 catalyst.

CO adsorption on $Ce\text{-}Rh/SiO_2$ produced linear CO band at 2048 cm^{-1}, bridged CO band at 1857 cm^{-1}, gem-dicarbonyl bands at 2090 and 2027 cm^{-1}, and a tilted CO at 1766 cm^{-1}. CO

adsorption on Mn-Rh/SiO_2 produced linear CO band at 2040 cm^{-1}, bridged CO at 1835 cm^{-1}, weakly adsorbed gem-dicarbonyl band at 2090 cm^{-1}, and a tilted CO band at 1670 cm^{-1}. CO adsorption on Ag-Rh/SiO_2 produced linear CO band at 2072 cm^{-1}, a weak bridged CO band at 1879 cm^{-1}, and gem-dicarbonyl bands at 2095 and 2030 cm^{-1}.

The linear CO was found to be active for CO insertion. There is no obvious correlation between the wavenumber of linear CO and its CO insertion reactivity The tilted CO that has been suggested to be highly active for CO insertion is in fact a spectator that does not participate in the reaction.

In conclusion, linear CO site is active for CO insertion. The selectivity toward higher oxygenates can be improved by increasing the relative concentration of linear CO sites and increasing reaction pressure.

REFERENCES

1. Ellgen, P. C., Bartley, W. J., Bhasin, M. M., and Wilson, T. P., Adv. Chem. Ser., 178, 147 (1979).
2. Yoneda, Y., Progress in C1 Chemistry in Japan, (Research Association for C_1 Chemistry, Eds.) Elsevier, New York-Tokyo, 1989.
3. Anderson, R. B., Fischer Tropsch and Related Synthesis. Academic Press, New York, 1983.
4. Klier, K., Adv. Catal., 31, 243 (1982).
5. Sachtler, W. M. H., Proceedings of 8th International Congress on Catalysis, Vol. 1, p. 151 (1984).
6. Nunan, J. G., Bogdan, C. E., Klier, K., Smith, K. J., Young, C. Y., and Herman, R. G., J. Catal., 116, 195 (1989).
7. Nunan, J. G., Herman, R. G., and Klier, K., J. Catal., 116, 222 (1989).
8. Murchison, C. B., Conway, M. M., Stevens, R. R., Quarderer, G. J., Proceedings of 9th International Congress on Catalysis, Vol. 2, p. 626 (1988).
9. Cochran, G. A., Eur. Patent Appl. 841029325, 1984.
10. Courty, P., Forestiere, A., Kawata, N., Ohno, T., Raimbault, C., and Yoshimoto, M., in "Industrial Chemicals via C_1 Processes." ACS Symposium Series No. 328, p 42, Washington, D. C., 1985.
11. Courty, P., Durand, D., Freund, E., and Sugier, A., J. Mol. Catal., 17, 241 (1982).
12. Pan, W. X., Cao, R., and Griffin, G. L., J. Catal., 114, 447 (1988).
13. Ichikawa, M., Chemtech., 674 (1982).
14. Chuang, S. C., Tian, Y. H., and Goodwin, J. G., Jr., J. Catal., 96, 449 (1985).
15. Bell, A. T., Catal. Rev. Sci. Eng., 23, 203 (1981).
16. Chuang, S. S. C., and Pien, S. I., J. Catal., 135, 618 (1992).
17. "Coal Liquefaction: A Research Needs Assessment Executive Summary," DE-AC01-87ER30110, A report prepared for the U. S. Department of Energy, 1989.
18. Delgass, W. N., Haller, G. L., Kellerman, R., and Lunsford, J. H., "Spectroscopy in Heterogeneous Catalysis," Academic Press, New York, 1979.
19. Rabo, J. A., in "Proceedings of the 10th International Congress on Catalysis," Part A, p. 1, Akademiai Kiado, Budapest, 1993.
20. Tamaru, K., "Dynamic Relaxation Methods in Heterogeneous Catalysis", in Catalysis: Science and Technology, vol. 9, J. R. Anderson and M. Boudart (eds.), p. 87, Springer-Verlag, Berlin-Heidelberg-New York, 1991.
21. Yates, J. T. Jr., and Madey, T. E., Eds. "Vibrational Spectroscopy of Molecules on Surfaces," Plenum Press, New York, 1987.

22. Hicks, R. F., Kellner, C. S., Savotsky, B. J., Hecker, W. C., and Bell, A. T., J. Catal., 71, 216 (1981).
23. Li, Y. E., and Gonzalez, R. D., Catal. Lett., 1, 229 (1988).
24. Moser, W. R., Cnossen, J. E., Wang, A. W., and Krouse, S. A., J. Catal., 95, 21 (1985).
25. Chuang, S. S. C., and Pien, S. I., J. Mol. Catal., 55, 12 (1989).
26. King, D. L., J. Catal., 61, 77 (1980).
27. Sachtler, W. M. H., and Ichikawa, M., J. Phys. Chem. 90, 4752 (1986).
28. Biloen, P., and Sachtler, W. M. H., Adv. Catal. 30, 165 (1981).
29. van den Berg, F. G. A., Ph. D. Thesis. University of Leiden. The Netherlands, 1984.
30. Hanlan, L. A., and Ozin, G. A., J. Amer. Chem. Soc., 96, 6324 (1974).

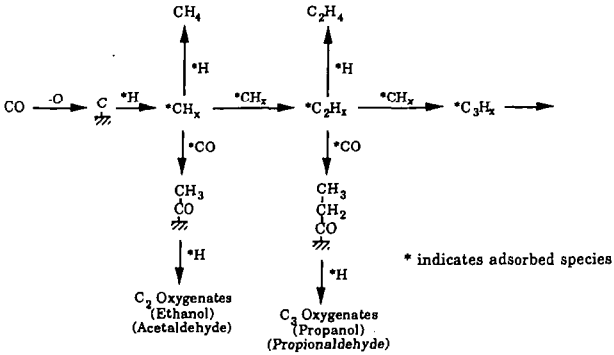

Figure 1. Reaction pathway for higher oxygenates synthesis on Rh- and IFP-based catalysts.

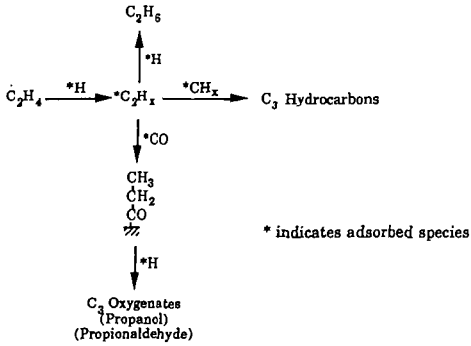

Figure 2. Reaction pathway for ethylene hydroformylation.

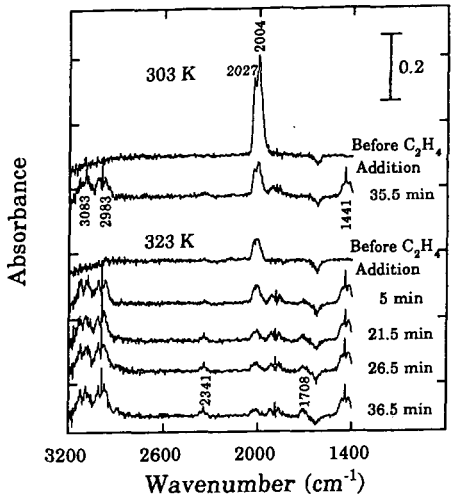

Figure 3. C_2H_4/H_2 addition to CO (ads.) on 0.5% Rh/SiO_2

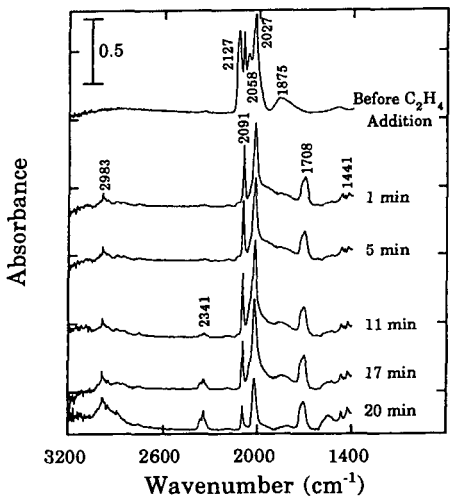

Figure 4. C_2H_4/H_2 addition to CO (ads.) on Cu-Rh(1:1)/SiO_2

OXYGENATES FROM SYNTHESIS GAS

Wolfgang Falter and Willi Keim
Institut fur Technische Chemie
RWTH Aachen
Worringerweg 1
52074 Aachen, Germany

Keywords: Oxygenates, Synthesis Gas, Isobutanol

The direct synthesis of oxygenates starting from synthesis gas is feasible by homogeneous and heterogeneous catalysis. Homogeneous Rh and Ru based catalysts yielding methyl formate and alcohols will be presented. Interestingly, modified heterogeneous catalysts based on "Isobutyl Oel" catalysis, practized in Germany (BRD) up to 1952 and in the former DDR until recently, yield isobutanol in addition to methanol. These "Isobutyl Oel" catalysts are obtained by adding a base such as Li < Na < K < Cs to a $Zn-Cr_2O_3$ methanol catalyst. Isobutanol is obtained in up to 15% yield. J. Seibring [1] synthesized, with a $ZrO_2-In_2O_3-CuO-ZnO-K_2O$ catalyst, isobutanol in yields up to 22%. G. Kolle-Gorgen [2] produced with a $ZrO_2-MnO_2-Pd-K_2O$ catalyst isobutanol in yields up to 30%.

Our best catalyst a Zr-Zn-Mn-Li-Pd catalyst produced isobotanol up to 60% at a rate of 740g isobutanol per liter catalyst and hour. The reaction conditions with T = 715K, p = 25 MPA, GHSV = 20,000 h^{-1} are rather severe. With changing pressure the selectivity to isobutanol changes. There is a significant temperature impact, which is evident from Fig. 1

Whereas at 625K about 72% methanol is formed, this portion decreases to 6% at 725K. In parallel, the isobutanol portion in the liquid product increases from 4% to 625K to 45% at 715K. The catalyst is quite stable over a run of about 720 hours. In catalyst preparation, the pH of the precipitation is critical. Fig. 2 outlines best values for isobutanol rest and around pH-values. Finally Fig. 3 exhibits a typical selectivity pattern obtained in various runs.

1. J. Seibring. *Thesis RWTH* Aachen 1985.

2. G. Kolle-Gorgen, *Thesis RWTH* Aachen 1985.

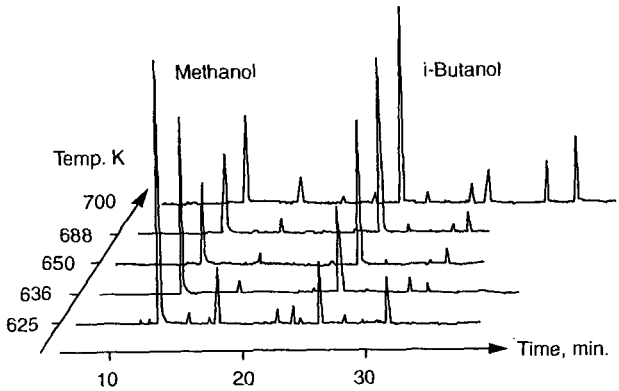

Figure 1. Temperature dependence i-BuOH selectivity (Zr-Zn-Mn-Li-Pd catalyst, 10 MPa, GHSV 10,000 h^{-1})

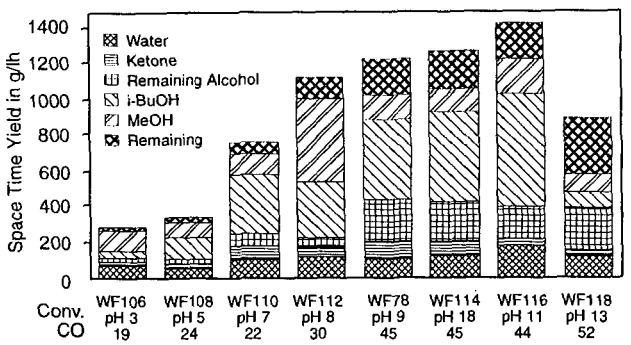

Figure 2. Impact of pH-value on catalyst preparation Zr-Zn-Mn-K-Pd, T = 700 K,p = 25 MPA, GHSV = 20,000 h^{-1}

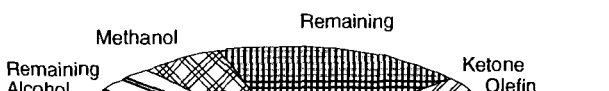

Figure 3. Product selectivity Zr-Zn-Mn-Li-Pd catalyst T = 715 K, p = 25 MPA, GHSV = 20,000 h^{-1}

DIMETHYL CARBONATE PRODUCTION FOR FUEL ADDITIVES

Y.Okada, T.Kondo, S.Asaoka
R&D Center, Chiyoda Corporation
3 - 13 Moriya-cho Kanagawa-ku Yokohama 221, Japan

Key wards : Dimethyl carbonate, Octane enhancing oxygenates, Zeolite catalysts

INTRODUCTION

Dimethyl carbonate is very attractive as for use as an oxygenate for fuel additives. A feasible method of mass production at a low cost is needed for producing dimethyl carbonate for fuel additives.

The transesterification process is one of the dimethyl carbonate production processes[1]. In this process, ethylene carbonate with methanol is transesterificated to dimethyl carbonate.

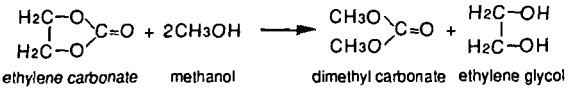

In the transesterification process, ethylene glycol is co-generated with dimethyl carbonate. The ethylene glycol is considered to correspond economically with the conventional product from hydration of ethylene oxide, because the quality of the ethylene glycol produced by transesterification is equal to the quality of the conventional product and the demand for ethylene glycol is growing year by year. Therefore, development of the dimethyl carbonate process through the transesterification is indicated.

Oxidative carbonylation processes in both the liquid-phase and vapor-phase are known as the other dimethyl carbonate processes. Liquid-phase oxidative carbonylation is the oxidation of carbon monoxide with oxygen in methanol in the presence of copper chloride[2]. A catalyst is used in a slurry mixture. In the vapor-phase oxidative carbonylation, the reaction of carbon monoxide and methyl nitrite by the oxidation of methanol and nitric oxide in the presence of both palladium chloride and copper chloride is used[3]. These processes are based on oxidation due to the presence of both oxygen and chloride.

Transesterification is a mild reaction with small exotherm, and is carried out in the liquid phase without toxic chemicals and corrosiveness. These features will be the merit of scale up with a low fixed capital.

We started transesterification process development for dimethyl carbonate production from the above considerations. Zeolites were studied as catalysts for this transesterification, due to their properties of resistance to heat and organic solvents. Zeolite catalysts can be used in fixed bed reactors without a catalyst separation unit. Chiyoda has developed processes using zeolites, for example, the Z-forming process to produce BTX from light hydrocarbons, the 2,6-DIPN production process using zeolite adsorbent, etc.

EXPERIMENTAL

Catalysts

Almost all of the popular industrial zeolites, for example the A, X, Y, L, Mordenite, ZSM-5 type, etc., were used in the catalysts screening. Several types of zeolites with adjusted cation species were screened next. Those catalysts were provided to reaction tests after calcination.

Test units

Reaction tests were performed in batch reactors and fixed bed reactors. Stainless steel was used for the reactors. Fixed-bed flow reactors were operated automatically under good material balance and well controlled of catalysts bed temperature.

RESULTS

The catalysts screening were performed from the points of activity, selectivity and sustainability. The reaction condition, the regenerating method, etc., were studied in order to develop the process for dimethyl carbonate production through transesterification. We will discuss some results of the catalysts screening and catalytic performance tests. The details of catalysts design will be discussed in the future.

Catalysts screening

Various structure types of zeolites were examined during the first step of the catalysts screening based on activity, selectivity and sustainability. The influence of the cation species of zeolite on catalytic ability was studied next in several types of zeolites. A part of the results for the catalysts screening of commercially available zeolites is as follows.

Zeolite types

Na form zeolites with Al_2O_3/SiO_2 molar ratios varying from 0.04 to 0.5 were used.

The activity is varied according to the types of zeolites as shown in Fig.1. it is considered that the order of activity depends on Al_2O_3/SiO_2 which represents the quantity of active site of the zeolites. Zeolite A with the largest Al_2O_3/SiO_2 ratio of 0.5 shows the highest activity, and ZSM-5 with the small Al_2O_3/SiO_2 of 0.04 has a very low activity. It seems that the activity depends on the quantity of active sites of the zeolites. Zeolite A has the most active sites, because the maximum value of Al_2O_3/SiO_2 in the zeolites is at 0.5. After that, the catalysts with the same Al_2O_3/SiO_2 of different structures were examined.

Cation species

The influence of the cation species including proton on catalytic ability was studied for several types of zeolites. We will discuss a part of the results for commercially available zeolites having different cation species.

The H form zeolites shows no activity. Fig.2 shows a comparison of the activity with 3 A(KA), 4 A(NaA) and 5 A(CaA) zeolites which have same Al_2O_3/SiO_2. The 3 A (KA) zeolite shows the highest activity. The order of the activity in zeolites A is as follows; 3 A>4 A>5 A. As for A type of zeolites which have the same crystalline structure, the activity depends on the cation species.

Several types of K form zeolites were studied. Fig.3 gives a comparison of the activity of the industrially popular 3 A and L types of the zeolites, and the activity of the K form X type which is in adjusted cation species. The order of the activity for these zeolite types is A > X > L. The activity depends on the Al_2O_3/SiO_2 and here zeolite A also shows the highest activity of the K form zeolites.

From the results of catalysts screening, the activity of the zeolite catalysts depends on the Al_2O_3/SiO_2 which represents the quantity of active sites, and the activity level of the site depends on the cation species.

Catalytic performance tests

Catalytic performance tests were achieved in order to study the zeolite catalysts for use in fixed bed reactors. The content of the cation species, the temperature for calcination, the material for binder, etc., were studied in addition to the catalysts screening.

Table 1 shows an example of catalytic performance tests. A 46% of one pass dimethyl carbonate yield was obtained at 120 (℃) and 10 (kg/cm^2).

CONCLUSION

The catalytic activity of zeolites for the production of dimethyl carbonate for use an oxygenate for fuel additives was studied.

We studied the activity of some of the industrially popular zeolites by the catalysts screening based on activity, selectivity and sustainability. We found that the order of zeolite catalyst activity depends on the Al_2O_3/SiO_2 which represents the quantity of active sites. Zeolite A with a maximum value of Al_2O_3/SiO_2 at 0.5 in the various zeolite types shows the highest activity.

The influence of the cation species of the zeolites was studied using several types of zeolites. The order of the activity for industrially popular zeolites A is; 3A (KA) > 4A (NaA) > 5A (CaA). It is believed that the activity level of the site depends on the cation species. In the case of zeolite A, the order of activity for cation species is as follows; $K^+ > Na^+ > Ca^{2+}$.

Catalytic performance tests were achieved to study zeolite catalysts for use in fixed bed reactors. A 46% of one pass dimethyl carbonate yield was obtained at 120 (℃) and 10 (kg/cm^2). Zeolite catalysts can be used in fixed bed reactors with significant properties of resistance to heat and organic solvents in comparison with ion exchange resin. The zeolite catalysts for dimethyl carbonate production by transesterification were prepared using commercially available zeolites by a simple ion exchange treatment.

REFERENCES

1) John F.Knifton et al, J.of Molecular Catalysis, vol.67, 389-399 (1991)
2) Ugo Romano et al., Ind. Eng. Chem. Prod. Dev., vol.19, 396-403 (1980)
3) EP 425197 (1990)

Table 1 Fixed- bed flow reaction test

Temp. (℃)	Press. (kg/cm^2)	DMC Yield (%)
120	10	46

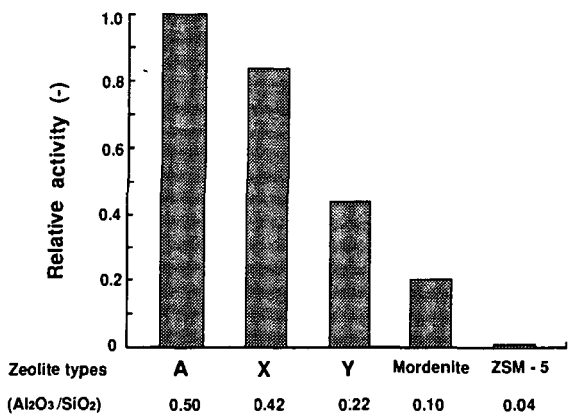

Fig.1 Activity of various types of zeolites

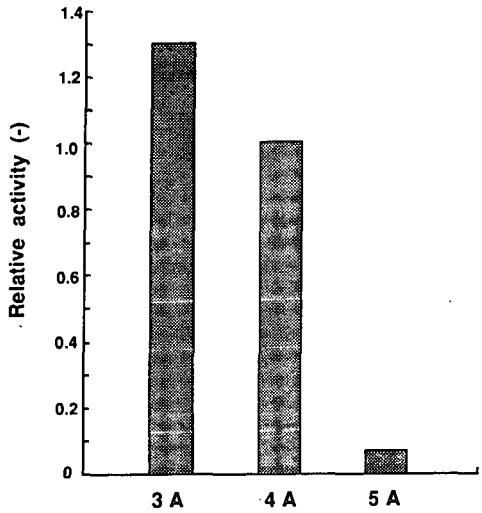

Fig.2 Activity of A type zeolites

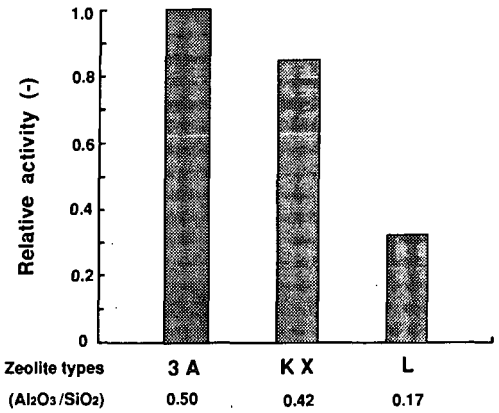

Fig.3 Activity of K form zeolites

DEMONSTRATION OF MICRONIZED COAL REBURNING FOR NO_2 CONTROL ON A 175 MW UNIT

Thomas F. Butler
Tennessee Valley Authority (TVA)

John C. Welling
Fuller Company

James U. Watts
Department of Energy (DOE)

Dale T. Bradshaw
Tennessee Valley Authority (TVA)

ABSTRACT

The Tennessee Valley Authority (TVA) has been selected for the Department of Energy's (DOE's) Clean Coal Technology IV program to demonstrate micronized coal reburn technology for control of nitrogen oxide (NO_x) emissions on a 175 MWe wall-fired steam generator at its Shawnee Fossil Plant. As the technology of the MicroFuel Department of Fuller Power Corporation makes this demonstration feasible, TVA has selected them as the prime contractor for the project and partner in the commercialization of this technology. This retrofit demonstration is expected to decrease NO_x emissions by 50 to 60 percent. Up to 30 percent of the total fuel fired in the furnace will be micronized coal injected in the upper furnace creating a fuel-rich reburn zone. Overfire air will be injected at high velocity for good furnace gas mixing above the reburn zone to insure complete combustion. Shawnee Station is representative of a large portion of boilers in TVA's and the nation's utility operating base. Micronized coal reburn technology compares favorably with other NO_x control technologies and yet offers additional performance benefits. This paper will focus on micronized coal reburn technology and the plans for a full-scale demonstration at Shawnee.

INTRODUCTION

According to recent industry studies, 44 percent of the nation's coal-fired plants will have seen their 30th birthday by the turn of the century. Older fossil plants typically have the following operating characteristics, and many of these conditions lead to high NO_x production:

- high excess air,
- deteriorating coal fineness,
- poor control of secondary air,
- mill capacity limited from coal switching,
- poor turn-down ratio, and
- cyclic duty operation.

TVA has a high boiler population that falls into this category, yet demand upon this existing fossil generating capacity continues. Therefore, TVA has investigated methods of reducing NO_x while improving overall boiler performance.

A substantial database has been developed in the reduction of nitrogen oxides (NO_x) by various combustion modifications both here and abroad. Accurate control of coal particle fineness and air fuel ratios are essential ingredients in their success. The purpose of this project is to demonstrate the effectiveness of micronized coal (80 percent less than 325 mesh) combined with an advanced coal reburning technology.

Up to 30 percent of the total fuel fired in the furnace will be micronized coal. This fuel will be injected into the upper region of the furnace, creating a fuel-rich zone at a stoichiometry of 0.8 to 0.9. Overfire air will be injected at high velocity for good furnace gas mixing above the reburn zone, insuring an oxidizing zone for an overall furnace stoichiometry of 1.15 (excess air of 15 percent). Micronized coal reburn technology reduces NO_x emissions with minimal furnace modifications and enhances boiler performance with the improved burning characteristics of micronized coal (Figure 1).

The addition of the reburn fuel into the furnace solves several problems concurrently. Units that are mill limited now have sufficient fuel capacity to restore their lost capacity. Restoration of lost capacity, as a benefit to NO_x reduction, becomes a very economical source of power generation. Reburn burners can also serve as low-load burners, and units can achieve a turndown of 8:1 without consuming expensive auxiliary fuels. The combination of micronized coal reburn fuel and better pulverizer performance will increase unit performance by increasing carbon burnout.

Micronized coal reburn technology can be applied to cyclone-fired, wall-fired and tangentially-fired pulverized coal units. The overfire air system can also be easily adapted to incorporate in-furnace sorbent injection for SO_2 control.

A baseline test profile of the furnace, along with furnace flow and computer modeling, will be conducted prior to the design and installation of the MicroMill™ systems and micronized coal injector/burners. An extensive test program will document performance during a three-year operational period.

DOE CLEAN COAL TECHNOLOGY DEMONSTRATION PROGRAM

The Clean Coal Technology Demonstration (CCT) program is a multibillion-dollar national commitment, cost shared by the government and the private sector to demonstrate economic and environmentally sound methods for using our nation's most abundant energy resource, coal. The program will foster the energy-

efficient use of the nation's vast coal resource base. The program will contribute significantly to the long-term energy security of the United States, further the nation's objectives for a cleaner environment and improve its competitive standing in the international energy market.

The objective of the CCT is to demonstrate a new generation of innovative coal utilization processes in a series of "showcase" facilities built across the country. The program takes the most promising of the advanced coal-based technologies and, over the next decade, moves them into the commercial marketplace through demonstration. These demonstrations are on a scale large enough to generate all the data for design, construction and operation that are necessary for the private sector to judge their commercial potential and make informed, confident decisions on commercial readiness.

DOE selected TVA's micronized coal reburning at Shawnee as one of the nine projects to be demonstrated under Round IV of CCT. Since NO_x and SO_2 have been designated by the 1990 Clean Air Act Amendments passed by the U.S. Congress as precursors of acid rain precipitation, controlling NO_x has presented challenging problems in achieving a low-cost retrofit control system. To date, there have been several methods used to reduce NO_x; however, each has some disadvantages. Low NO_x burners have been fairly successful but may not provide sufficient reduction by themselves. Gas reburning also has been successful, but it requires a steady supply of gas at a reasonable cost. Coal reburning shows promise in providing a NO_x control system which can be readily retrofitted and operated at low cost. Coal reburning does not require external modifications to the flue gas duct system nor does it require major modifications to the boiler or a separate type of reburn fuel. In fact, coal reburning may help some power producers who have had to derate their unit due to coal switching that was implemented to meet SO_2 reduction requirements.

Site

Site Description. The host site will be one of Units 1-9 at TVA's Shawnee Fossil Plant which was built to help meet the huge electric power requirements of a nearby DOE facility. Construction began in January 1951 and was completed in 1956.

Units 1-9 are 175 MWe (gross) front wall-fired, dry-bottom furnaces burning East Appalachian low-sulfur coal. The plant was originally designed to burn high-sulfur coal; but in the 1970s, the plant was modified to burn low-sulfur coal in order to meet an emission limit of 1.2 lbs. $SO_2/10^6$ Btu of heat input without the use of any sulfur dioxide control technology. Each unit has been equipped with a baghouse to control particulate emissions. Flue gas from each unit discharges to one of two 800-foot stacks, also constructed in the 1970s. The nine existing pulverized coal units are representative of a large number of wall-fired units in the industry which will be required to reduce NO_x emissions in response to the 1990 Clean Air Act Amendments.

Coal Acquisition

TVA has contracts in place to supply Shawnee with low-sulfur bituminous coals from Kentucky and West Virginia. These coals will be used as the primary fuels for the project. TVA has conducted test burns of western coals such as Powder River Basin (PRB) at a number of sites, including Shawnee, since the late 1970s. PRB coal will be obtained for testing during this demonstration.

REBURN CONCEPT

Concept Operation

Micronized coal reburning for NO_x control will operate in the same manner as natural gas reburning on coal-fired boilers. In effect, the entire furnace operates as a low NO_x burner. The existing burners shall be operated at a lower than normal stoichiometric ratio, with special attention being applied to fuel/air control. Microfine coal with a surface area of 31 m^2/gm is fired substoichiometrically in a reburn zone above the top row of the existing burners. Oxidation of high-surface-area micronized coal consumes oxygen very rapidly, converting NO_x to molecular nitrogen. NO_x conversion requires a residence time of 0.5 to 0.6 seconds. Above the reburn zone, high velocity overfire air will uniformly mix with the substoichiometric furnace gas to complete combustion, giving a total excess air ratio of 1.15. This concept should reduce NO_x emissions 50 to 60 percent from current levels of 0.82 to 0.95 $lbs/10^6$Btu to an emission level of 0.33 to 0.48 $lbs/10^6$Btu.

The proposed project will demonstrate the effectiveness of reducing nitrogen oxide emissions with an advanced coal reburning technology utilizing micronized coal. This technology can be applied in new as well as existing pulverized coal-fired furnaces. The coal used in reburning can be the same coal as used in the main fuel burners. A schematic of this system is shown in Figure 1. In addition, this reburn technology can be combined with various sulfur dioxide (SO_2) control technologies such as fuel switching, dry sorbent injection or other postcombustion technologies.

The addition of MicroMill systems will increase total heat input and will allow classifier settings on existing pulverizers to be adjusted for improved fineness, relating directly to combustion efficiency and lower Loss on Ignition (LOI). Stoichiometry in the lower furnace is maintained at 1.05 (5.0 percent excess air) to assure an oxidizing zone and minimize slagging and corrosion. The stoichiometry at burner level 5, the reburn level, is 0.8 to 0.9; and with the addition of overfire air at level 6, the furnace will have an existing stoichiometry of 1.15 (15 percent excess air), compared to the current operating condition of 1.21 (21 percent excess air). Thus, the micronized coal reburn system not only reduces NO_x emissions but also improves boiler efficiency and increases boiler capacity.

Process Advantages

Reburning is a recognized, effective technology for controlling NO_x emissions in a pulverized coal-fired boiler; however, most of the reburning activity to date has been with natural gas or oil as the reburn fuel. The following advantages of micronized coal reburning for NO_x control compare favorably with other NO_x control technologies.

- Disadvantages of natural gas and oil. Both natural gas and oil have been demonstrated to be effective reburning fuels; however, they are subject to one or more of the following disadvantages:

- availability, especially in winter,
- unstable/escalating fuel cost,
- operational problems firing dual fuels, and
- reduced boiler efficiency due to hydrogen in fuel.

- Micronized coal as reburn fuel, even with the additional coal handling and micronization cost, is a cost effective alternative to gas and oil due to the substantially lower fuel cost and elimination of problems associated with gas and oil.
- Flexibility: The technology is flexible enough to combine with other NO_x control technologies and reduce NO_x emissions to required lower levels.
- Site specific benefits:
  - reduced energy replacement costs due to improved ability to operate at a rated load, even with wet coals and/or equipment problems (mills, feeders),
  - reduced capacity costs due to increased power generation,
  - increased fuel flexibility allowing use of lower quality coals while mitigating deratings caused by fuel handling limitations,
  - the ability to operate existing pulverizers at reduced throughput without loss in unit capacity will improve coal fineness and possibly reduce unburned combustible in ash, thus increasing value of the ash as a marketable commodity,
  - improved turndown and stability at low loads without firing supplemental fuels and maintaining superheater outlet temperatures at low loads, and
  - knowledge gained from this demonstration can be used to scale up the micronized coal reburn technology for installation on TVA's Allen Fossil Plant (330 MWe cyclone fired).

NO_x Control Strategy

A majority of the 300,000 MWe generated by coal-fired utility units will be impacted by the 1990 Clean Air Act Amendments requiring reduction of NO_x emissions. It is unlikely that one NO_x control method will meet the needs of this diverse boiler population. NO_x control strategies fall into two major categories: combustion modification and postcombustion technologies.

Combustion modification includes low NO_x burners, reburning and fuel air staging. The postcombustion options are Selective Noncatalytic Reduction (SNCR) using reagents such as ammonia or urea and Selective Catalytic Reduction (SCR) using both reagent injections and catalysts.

In selecting a NO_x control strategy for a given unit, utility engineers must weigh many factors including the type of unit, operating requirements and unit design ratings versus current operating capabilities. Most utilities will probably select some form of combustion modification as their preferred NO_x control methods. Many utilities, already familiar with pulverized coal burners and burner management systems, will elect to install low NO_x burners as the method of controlling the combustion process.

There is, however, a large population of utility boilers for which reburning is an attractive option. Wet bottom furnaces such as cyclones and some wall-fired furnaces that operate in a slagging mode are obvious choices for reburning, and the addition of a micronized coal reburn system can be utilized in such diverse applications as start-up, low-load operation and restoring lost capacity. In addition, units that operate at very low loads for long periods of time, units that are relegated to cyclic duty and units that have pulverizer load limitations resulting from fuel switching are all very good candidates for micronized coal reburning as a primary NO_x control method.

SUPPORTING ACTIVITIES

While the micronized coal reburn system is in a state of technical readiness for full-scale demonstration, there will be several supporting activities to insure a high degree of success for the demonstration. Among these activities are furnace cold-flow and computer modeling. The modeling will be conducted in the first phase and will provide even further evidence of adequacy, availability, suitability and quality of the data and analysis to support the full-scale demonstration.

Diagnostic tests will be conducted to determine temperature and velocity patterns in the furnace, supplementing similar previous tests in another unit at the plant with different burner registers. Boiler performance tests will also be conducted providing flue gas flow rate, gas composition and unburned combustibles. These tests will be used to initiate preliminary design of the reburn injector/burners and overfire air nozzles. A cold-flow model will be built to simulate the existing burner windbox assembly, burners and air registers as well as the furnace flow regime, including the lower and upper furnace past the furnace nose and into the convection section. This flow model will permit determination of the number and location of both the reburn injector/burners and overfire air nozzles. With the cold-flow model existing windbox, burner and furnace flow patterns can be observed. In addition, the model will provide an easy, convenient method to vary the number and location of the reburn injector/burners, overfire air windbox and nozzles to assure dispersion and mixing of the micronized coal in the reburn zone and the overfire air in the burnout zone. The cold-flow model will also be available during Phase 3 of the test program in the event any fine tuning of the reburn system is required. The computer modeling of the furnace will provide not only screening for the cold-flow model but also predict reburn system performance on the furnace and boiler as well as the effect of heat release and mixing in the reburn zone.

Once the flow and mixing characteristics have been determined from the modeling activities, the reburn injector/reburner will be selected or designed. The design will accommodate the unit's flow characteristics while achieving local mixing of the micronized coal-air stream from the injector to achieve combustion at a prescribed fuel-rich condition (0.8 stoichiometry) for reburn operation and at normal fuel-lean conditions for start-up and low-load boiler operation.

MICRONIZED COAL TECHNOLOGY

Technology Description

The technology described in this paper is a combination of a technology that produces micro-fine coal reliably and economically with a known NO_x control technology (fuel reburning). When micronized coal is fired at a stoichiometry of 0.8 to 1.2, devolatilization and carbon conversion occur rapidly.

Micronized coal is defined as a coal ground so the 80 percent of the coal particles are 43 microns or smaller. The MicroFuel® system, consisting of the MicroMill and an external classifier, micronizes coal to a particle range of 10 to 20 microns.

The combined surface area of just one gram of micronized coal particles is 31 square meters, contrasted to a surface area of 2.5 square meters per gram for standard-grind pulverized coal.

The MicroMill system is a patented centrifugal-pneumatic mill with the replaceable rotating impeller as the only moving part. Size reduction is accomplished by the particles themselves striking against one another as they whirl in a tornado-like column of air inside the MicroMill. Centrifugal force retains material in the cone and Rotational Impact Zone (RIZ) as the particles reduce in size prior to being conveyed by the air stream entering the center of the rotating impeller. Figure 2 is a sectional view of the MicroMill, and Figure 3 is a cutaway view of the MF-3018 MicroMill.

Material entering the impeller is swept out of the MicroMill to the classifier, which separates particles by size. Micronized coal particles below 43 microns are discharged directly to the burners, and larger particles are returned to the MicroMill for further size reduction. Figure 4 is a dimensional elevation of a complete MicroMill system.

The net result of micronized coal as a reburn fuel is a uniform compact combustion envelope allowing for complete combustion of the coal/air mixture in a smaller volume than conventional pulverized coal. Heat rate, heat flux, carbon loss and NO_x formation are all impacted by coal fineness.

ENVIRONMENTAL ASPECTS

With the exception of significant reductions in NO_x emission, the environmental impact of the proposed project is inconsequential.

Shawnee currently burns low-sulfur Appalachian coal (1.195 lb. $SO_x/10^6$Btu). Lower-sulfur western coal (0.35 lb. $SO_x/10^6$Btu) will be burned briefly as part of the demonstration. During that period, SO_x emissions will be further reduced. The use of eastern low-sulfur coals with reduced grindability has made the existing pulverizers marginal. Equipment problems or wet coal will result in further derating of the unit. The introduction of micronized coal reburning as an additional fuel will allow Shawnee to overcome mill limitations and operate at somewhat higher capacity factors.

No significant changes in the emissions of greenhouse gases or air toxics are projected. A minor increase in emissions of CO and hydrocarbons may occur at times during the demonstration as parametric testing may occasionally result in slightly less than complete combustion. However, existing pollution control equipment should be able to maintain emission levels within regulatory limits. Emissions monitoring will be performed to insure continued compliance.

No new waste products will be generated by the micronized coal reburn process, as no reagents are utilized. Existing requirements for fly ash and bottom ash disposal are expected to remain constant. Current water usage by the unit averages 3.1 million gallons per day for ash sluicing, and no change is projected for the demonstration. Average fly ash particle size will decrease slightly, but existing baghouses will efficiently collect fly ash.

PREOPERATIONAL AND OPERATIONAL TESTING

Preoperational testing will be conducted to include baseline data acquisition and characterization of existing and newly designed components. Parametric testing will document the effect of the following reburn system variables:

- primary burner zone stoichiometry,
- reburn zone stoichiometry,
- final (burnout zone) stoichiometry,
- reburn zone momentum,
- micronized coal consumption in the reburn zone,
- reburn fuel particle size,
- load,
- coal composition reliability, and
- boiler load response.

All Continuous Emission Monitor (CEM) and boiler operation signals which can be efficiently monitored in real time will be directly stored on disk. The database will permit ready and efficient reduction and analysis of the data, both during execution of the program and during final analysis and evaluation. Information from the long-term test will permit evaluation of system efficiency and reliability under actual operating conditions. Also, the extended operating period will provide data for projecting economic impacts.

CONCLUSIONS

TVA has a strong history of leadership in the development of new and emerging technologies and the performance of successful R&D programs. TVA believes that this nitrogen oxide emission control technology shows promising benefit to its own system, as well as the utility industry in general, since it is taking a leadership position in sponsoring a micronized coal reburn demonstration.

The combination of micronized coal supplying up to 30 percent of the total furnace requirements and reburning for NO_x control will provide flexibility for

significant environmental improvement without adding higher operating costs or furnace performance deratings normally associated with environmental controls.

By meeting the objectives of this important coal reburning project, coal will be shown to be its own best friend in controlling NO_x emissions and providing economical power to the public well into the future.

This report was prepared by Fuller Power Corporation pursuant to a cooperative agreement funded by the U.S. Department of Energy and TVA; and neither the Tennessee Valley Authority or any of its subcontractors or the U.S. Department of Energy, or any person acting on behalf of either:

- makes any warranty or representation, express or implied, with respect to the accuracy, completeness, or usefulness of the information contained in this report, or that the use of any information, apparatus, method, or process disclosed in this report may not infringe on the privately-owned rights; or

- assumes any liabilities with respect to the use of, or for damages resulting from the use of, any information, apparatus, method or process disclosed in this report.

Reference herein to any specific commercial product, process, or service by trade name, trademark, manufacturer, or otherwise, does not necessarily constitute or imply its endorsement, recommendation, or favoring by the U.S. Department of Energy. The views and opinions of the authors expressed herein do not necessarily state or reflect those of the U.S. Department of Energy.

The American Society of Mechanical Engineers shall not be responsible for statements or opinions advanced in this paper. This paper, number 93-JPGC-FACT-10, was presented at the Joint ASME/IEEE Power Generation Conference in Kansas City, Kansas, October 17-22, 1993.

ATTACHMENT A

Reburn Technology for Boiler NO_x Control by R.W. Borio of Combustion Engineering Inc., R.E. Hall of U.S. Environmental Protection Agency, R.A. Lott of Gas Research Institute, A. Kokkinos of Electric Power Research Institute, and S. Durrani of Ohio Edison, presented at the 6th Annual Coal Preparation, Utilization and Environmental Control Contractors Conference.

An Evaluation of Natural Gas Cofiring for Emissions Control on a Coal-Fired Boiler by P.K. Vitta, S.M. Wilson, M.T. Newton, M.D. Conner of Southern Company Services, Inc., presented at the ASME International Joint Power Generation Conference, 1990.

Preliminary Study of the Effects of Natural Gas Co-Firing on Coal Particle Combustion by A.R. Schroeder, D.A. Thompson, H. Krier, J.E. Peters and R.O. Buckius of the Department of Mechanical and Industrial Engineering, University of Illinois.

Results of Combustion Modification for the Reduction of NO_x Emission by K.R.G. Hein and G. Jager of RWE Energie AG, Germany, presented at the Joint ASME/IEEE Joint Power Generation Conference, 1990.

New Steam Generators with Low NO_x Pulverized-Coal Firing by K. Straub and F. Thelen, of Steag AG, Germany, presented at the Joint ASME/IEEE Power Generation Conference, 1990.

Review of Research Activities on Pulverized Coal Firing Systems by F. Adrian of L&C Steinmuller GmbH, West Germany, presented at the Joint ASME/IEEE Power Generation Conference, 1990.

Pilot Scale Process Evaluation of Reburning for In-Furnace NO_x Reduction by J.M. McCarthy, B.J. Overmoe, S.L. Chen, W.R. Seeker and D.W. Pershing of Energy and Environmental Research Corporation, Irvine, California, presented at the Joint ASME/IEEE Power Generation Conference, 1990.

Micronized Coal Technology: Process & Potential Applications by Allen C. Wiley of MicroFuel Corporation, Ely, Iowa, presented at the 4th Annual Pittsburgh Coal Conference, 1987.

Micronized Coal for Boiler Upgrade/Retrofit. Duke Power Coal Start-up Tests by A. C. Wiley of MicroFuel Corporation, T. Rogers and M. Beam of Duke Power Company, and L. Berry of Peabody Engineering Company, presented at Gen-Upgrade 90.

Micronized Coal for Boiler Upgrade/Retrofit. Duke Power Coal Start-up Tests, Update and Results by A.C. Wiley of MicroFuel Corporation, T. Rogers and M. Beam of Duke Power Company, and L. Berry of Peabody Engineering Company, presented at Power Gen Conference, 1990.

Technical and Economic Feasibility for the Application of Micronized Coal as a Replacement for Number 2 Oil for Start-up and Low-Load Operation at Illinois Power Havana #6 Cycling Unit by F. Rosenberger of Illinois Power Company, C.J. Guilfoyle of Sargent & Lundy, and W. O. Parker, Jr. of MicroFuel Corporation, presented at American Power Conference, 1991.

Bench and Pilot Scale Process Evaluation of Reburning for In-Furnace NO_x Reduction by S.L. Chen, J.M. McCarthy, W.D. Clark, M.P. Heap, W.R. Seekez, D.W. Pershing, Twenty-First Symposium (International) on Combustion, The Combustion Institute, 1986, p. 1159-1169.

Process for the Disposal of Nitrogen Oxide by R.D. Reed of John Zink Company, U.S. Patent 1,274,637,1969.

Fourteenth Symposium (International) on Combustion, p. 897, by J.O. Wendt, C.V. Sternling and M.A. Matovich, The Combustion Institute, 1973.

Sixth Symposium (International) on Combustion, p. 154, by A.L. Myerson, F.R. Taylor and B. Faunce, The Combustion Institute, 1957.

Development of Mitsubishi "MACT" In-Furnace NO_x Removal Process by Y. Takahashi, et al., presented at U.S.-Japan NO_x Information Exchange, Tokyo, Japan, May 1981.

Evaluation of In-Furnace NO_x Reduction by S. Miyamae, H. Ikebe and K. Makino, proceedings of the 1985 Joint Symposium on Stationary Combustion NO_x Control, 1986.

Three-Stage Pulverized Coal Combustion System for In-Furnace NO_x Reduction by N. Okigami, Y. Sekiguchi, Y. Miura, K. Sasaki and B. Tamaru, proceedings of the 1985 Joint Symposium on Stationary Combustion NO_x Control, 1986.

Three Stage Combustion (Reburning) on a Full Scale Operating Boiler in the USSR by R.C. LaFlesh, R.D. Lewis and D.K. Anderson of Combustion Engineering, Robert E. Hall of US EPA, and V.R. Kotler of All Union Heat Engineering Institute (VTI), Moscow, USSR, presented at the Joint EPA/EPRI Symposium on Stationary Combustion NO_x Control, 1991.

Comparisons of Micronized Coal, Pulverized Coal and No. 6 Oil for Gas/Oil Utility and Industrial Boiler Firing by E.T. Robinson of Advanced Fuels Technology Company, Oliver G. Briggs, Jr. of Riley Stoker Corporation, and Robert Bessette of IES, presented at the American Power Conference, 1988.

Reburn Technology for NO_x Control on a Cyclone-Fired Boiler by R.C. Booth of Energy Systems Associates, R.E. Hall of US EPA, R.A. Lott of GRI, A. Kokkinos of EPRI, D.F. Gyorke of DOE-PETC, S. Durrani of Ohio Edison, H.J. Johnson of OCDO, J.J. Kienle of East Ohio Gas; R.W. Borio, R.D. Lewis, M.B. Keough of ABB Combustion Engineering, presented at the Joint EPA/EPRI Symposium on Stationary Combustion NO_x Control, 1991.

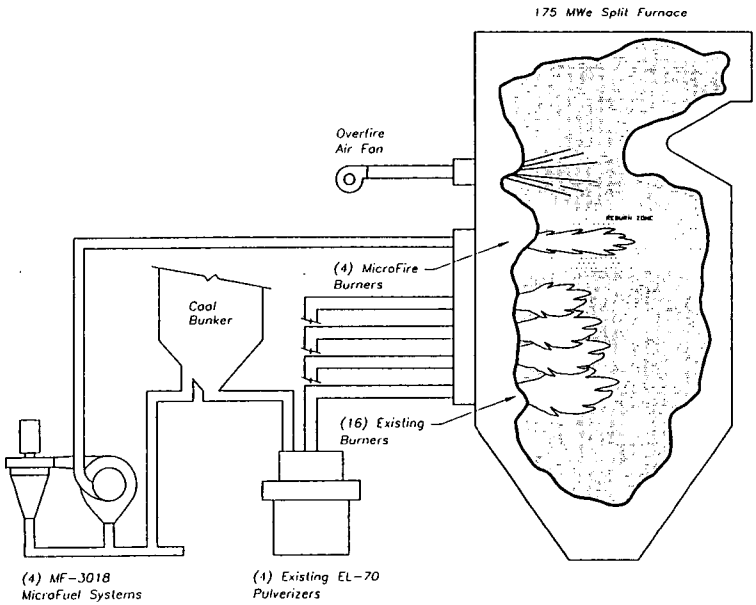

Tennessee Valley Authority		
DWG. No. 25-0001		
D.O.E. PON DE-PS01-91FE62271		
TVA Shawnee Station Unit 6 Micronized Coal Reburn Demonstration NOx Control-175 MW Wall Fired Unit Concept Diagram		
Date	04/24/91	DLS

Figure 1

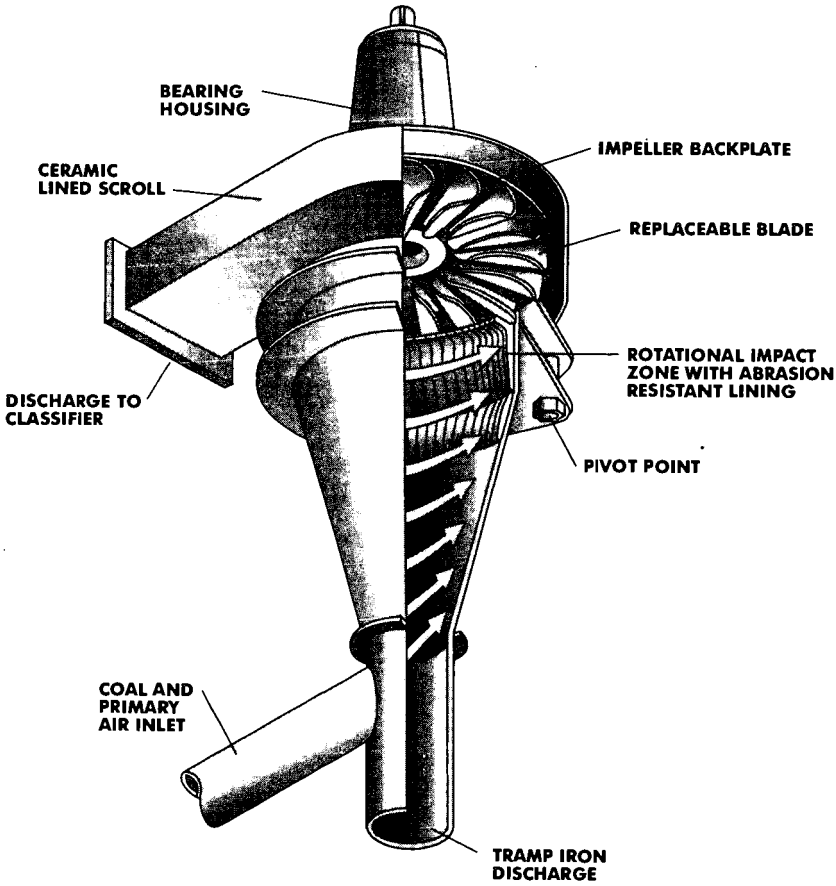
BEARING HOUSING
CERAMIC LINED SCROLL
IMPELLER BACKPLATE
REPLACEABLE BLADE
ROTATIONAL IMPACT ZONE WITH ABRASION RESISTANT LINING
DISCHARGE TO CLASSIFIER
PIVOT POINT
COAL AND PRIMARY AIR INLET
TRAMP IRON DISCHARGE

Figure 2

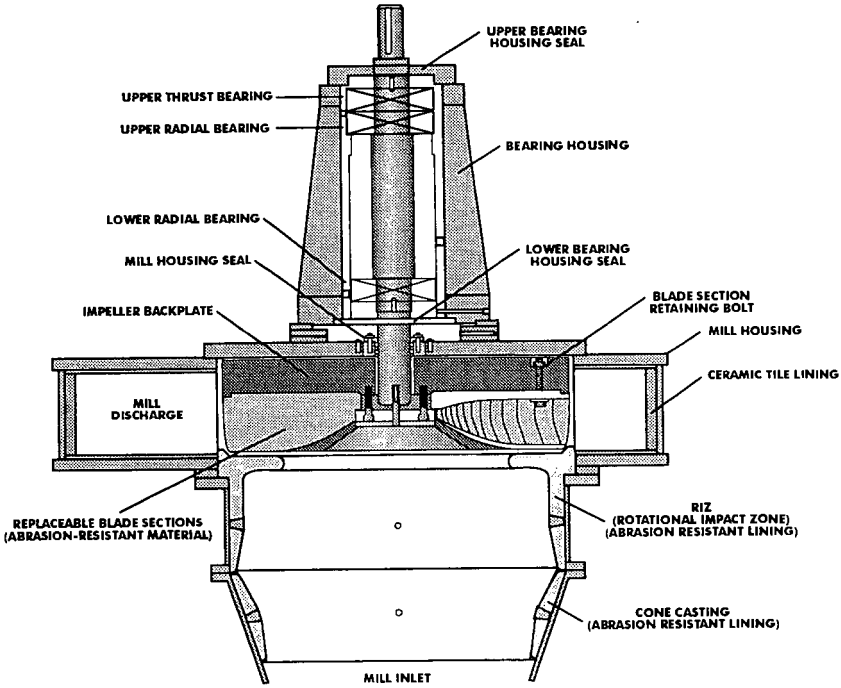
UPPER BEARING HOUSING SEAL
UPPER THRUST BEARING
UPPER RADIAL BEARING
BEARING HOUSING
LOWER RADIAL BEARING
MILL HOUSING SEAL
LOWER BEARING HOUSING SEAL
IMPELLER BACKPLATE
BLADE SECTION RETAINING BOLT
MILL HOUSING
CERAMIC TILE LINING
MILL DISCHARGE
REPLACEABLE BLADE SECTIONS (ABRASION-RESISTANT MATERIAL)
RIZ (ROTATIONAL IMPACT ZONE) (ABRASION RESISTANT LINING)
CONE CASTING (ABRASION RESISTANT LINING)
MILL INLET

Figure 3

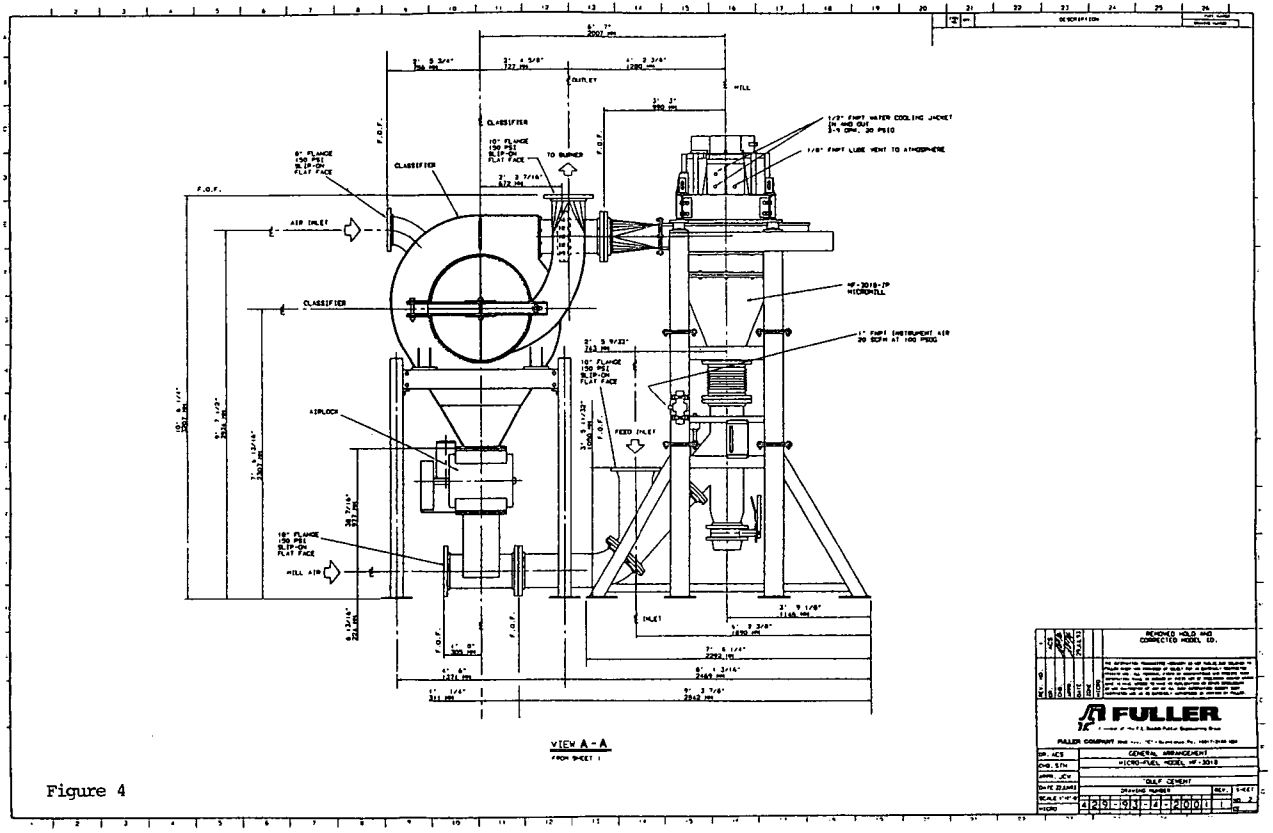

CLASSIFIER
AIR INLET
AIRLOCK
MILL AIR
FEED INLET
INLET
OUTLET
MILL
TO BURNER
F.O.F.
VIEW A-A
FROM SHEET 1
FULLER
GENERAL ARRANGEMENT
MICRO-FUEL MODEL MF-3018

Figure 4

OPERATING EXPERIENCE WITH THE INTEGRATED DRY NO_x/SO_2 EMISSIONS CONTROL SYSTEM

R. A. Smith, L. J. Muzio, G. H. Shiomoto
Fossil Energy Research Corp.
23342C South Pointe, Laguna Hills, CA 92653

T. G. Hunt
Public Service Company of Colorado
5900 East 39th Ave., Denver, CO 80207

Keywords: NO_x Removal, SO_2 Removal, Low-NO_x Burners

INTRODUCTION

This paper presents the results to date from the Public Service Company of Colorado (PSCC), U. S. Department of Energy (DOE), and Electric Power Research Institute (EPRI), sponsored Integrated Dry NO_x/SO_2 Emissions Control System project. This DOE Clean Coal Technology III demonstration project is being conducted at PSCC's Arapahoe Generating Station Unit 4, located in Denver, Colorado. The Integrated Dry NO_x/SO_2 Emissions Control System consists of five major control technologies that are combined to form an integrated system to control both NO_x and SO_2 emissions. NO_x reduction is obtained through the use of low-NO_x burners, overfire air, and urea-based Selective Non-Catalytic Reduction (SNCR), while dry sorbent injection using either sodium- or calcium-based reagents with humidification is used to control SO_2 emissions. The project goal is to provide up to a 70% reduction of both NO_x and SO_2 emissions. The combustion modifications were expected to reduce NO_x by 50% with the expectation that the SNCR system would provide the remaining 20% reduction. Dry Sorbent Injection was expected to provide 50% removal of the SO_2 emissions while using calcium-based reagents. As sodium is much more reactive than calcium, it was expected to provide SO_2 removals of up to 70%.

UNIT DESCRIPTION

Arapahoe Unit 4 is a 100 MWe down-fired boiler which was built in the early 1950's, and was designed to burn Colorado lignite or natural gas. Currently, the main fuel source is a Colorado low-sulfur (0.4%) bituminous coal. The original firing configuration consisted of 12 intertube burners located on the roof of the furnace. Each burner consisted of a rectangular coal/primary air duct which was split into 20 separate nozzles that injected the coal/air mixture evenly across the furnace roof. Secondary air was injected around each of the individual coal nozzles, and there were no provisions to control the rate of fuel and secondary air mixing. Baseline NO_x levels for this boiler ranged from approximately 780 to 840 ppmc (ppm, dry corrected to 3% O_2), depending on load. Arapahoe Unit 4 uses a fabric filter dust collector for particulate control.

SYSTEM DESCRIPTION

Babcock & Wilcox (B&W) provided the low-NO_x burners and overfire air system for the Arapahoe Unit 4 project. B&W's DRB-XCL® (Dual Register Burner - aXially Controlled Low-NO_x) burner had been successfully used to reduce NO_x emissions in wall-fired boilers, but had never been used in a vertically-fired furnace. The burner features dual spin vane registers which allow control of the swirl imparted to the secondary air in both the inner and outer regions of the flame. These registers provide a great amount of control over the rate of combustion, and thus the amount of NO_x formed. The burners also feature a sliding air damper which allows the total secondary air flow to be controlled independently of the spin vane setting. In many older burner designs, a single register is used to control both the total secondary air flow and the rate of air/fuel mixing.

While low-NO_x burners alone have proven to be effective for reducing NO_x, combustion staging can further reduce NO_x emissions. Overfire air delays combustion by redirecting a portion of the secondary air to a region downstream of the main combustion zone. Three B&W Dual-Zone NO_x ports were added to each side of the furnace approximately 20 feet below the boiler roof. A numerical modeling study was performed by B&W in order to determine the optimum size and location for the ports. As a result, the NO_x ports were not spaced symmetrically across the furnace side walls. The ports were also designed to inject up to 25% of the total secondary air through the furnace sidewalls. The dual-zone NO_x

ports separate the overfire air into two regions. The outer zone features adjustable spin vane registers which disperse air in the region near the wall. The center zone produces an air jet with sufficient momentum to penetrate deep into the furnace. The two-stage injection provides faster mixing and more equal distribution of overfire air into the furnace.

NOELL, Inc. designed and supplied the urea-based SNCR system for the Arapahoe Unit 4 project. The disadvantage of urea injection, as with any SNCR chemical, is that the process operates over a very narrow temperature window. If the temperature is too high, the urea can be converted to NO_x. If the temperature is too low, NO_x removal efficiencies are reduced, and the emissions of unreacted chemical (ammonia slip) increases. The system at Arapahoe Unit 4 uses NOELL's proprietary dual-fluid injection nozzles to distribute the chemical uniformly into the boiler. A centrifugal compressor is used to supply a large volume of medium pressure air to the injection nozzles to help atomize the solution and rapidly mix the chemical with the flue gas. Two levels of injection nozzles were installed in order to provide the capability to follow the optimum temperature window as its location within the boiler changed with load. A cold-flow modeling study and detailed furnace exit gas temperature measurements were performed in order to determine the optimum location of the two injection levels.

Prior to the installation of the low-NO_x combustion system, a short test program was conducted to assess the performance of the urea-based SNCR system with the original burners. Early tests at the cooler Level 2 injection location showed the region to be too cold for urea injection, even at full load. Subsequent temperature measurements revealed that the furnace exit gas temperatures were significantly lower (on the order of 150 to 200°F) than those measured previously. Although the reason for the decrease in temperature could not be conclusively identified, it required that the remainder of the test effort be focused on the hotter Level 1 injection location. During the Level 1 tests, it was found that NO_x reductions at low load were somewhat less than expected. Recent full-scale SNCR tests[1] have shown that aqueous ammonia (NH_4OH) can provide increased system performance compared to that for urea in certain temperature ranges. A short term test using aqueous ammonia achieved greater NO_x reduction than urea at low load. These results made it desirable to investigate NH_4OH injection in more detail during the SNCR tests scheduled after the low-NO_x combustion system retrofit. However, due to safety concerns, it was preferable to store urea rather than NH_4OH on-site. To this end, NOELL, Inc. designed and installed a system that allows on-line catalytic conversion of urea into ammonia compounds.

A combination of dry technologies is used at Arapahoe Unit 4 to reduce SO_2 emissions. PSCC designed and installed a dry sorbent injection system that can inject either calcium- or sodium-based reagents into the flue gas upstream of the fabric filter. The reagent is fed through a volumetric feeder into a pneumatic conveying system, and then into a pulverizer where the size of the material can be reduced to approximately 90% through 400 U.S. Standard mesh. The material is then injected evenly into the duct at a point approximately 100 feet upstream of the fabric filter. A bypass can also be installed to convey the calcium-based reagents into the flue gas upstream of the economizer in a region where the temperature is approximately 1000°F.

While significant SO_2 reductions can be achieved with sodium-based reagents, calcium hydroxide is less reactive. In order to improve SO_2 removals with calcium hydroxide, a humidification system was installed in the duct upstream of the fabric filter. The system was designed by B&W and consists of 84 I-jet humidification nozzles which can inject up to 80 gpm of water into the flue gas stream. The system was designed to achieve a 20°F approach to saturation at full load conditions.

RESULTS

Fossil Energy Research Corporation is conducting all testing of the Integrated Dry NO_x/SO_2 Emissions Control System. Currently, the individual testing of the low-NO_x burners, overfire air, urea injection, calcium duct injection, and calcium economizer injection has been completed. Sodium duct injection testing has started and will continue through January 1994. Testing of the complete

integrated system will continue through mid-1994 with up to four weeks of testing on a high sulfur (2.5%) coal. Although all data have not been reviewed, some preliminary results of the individual technologies comprising the Integrated Dry NO_x/SO_2 Emissions Control System will be presented.

COMBUSTION MODIFICATIONS. Figure 1 shows the original baseline NO_x emissions compared to the post-combustion retrofit emissions, both with and without the SNCR system in operation. The combination of low-NO_x burners and overfire air alone resulted in NO_x reductions varying from 63 to 69% across the load range. The post-retrofit results shown in the figure are for the maximum staging (i.e., maximum overfire air) configuration. In this configuration, approximately 25% of the secondary air is introduced through the NO_x ports at full load. It was not possible to reduce the overfire air flow to zero as the ports are located in a very hot section of the furnace and, therefore, require a minimum amount of air flow to assure adequate cooling. These NO_x port cooling requirements limited the minimum overfire air flow to approximately 15% of the total secondary air at full load. Tests at the minimum overfire condition indicate that the low-NO_x burners are responsible for the majority of the NO_x reduction over the range of overfire air flow rates tested, as the removals increase only 10% as overfire air is increased from 15 to 25% at full load. At 80 MWe, where the overfire air flow can be reduced to 8% of the secondary air before NO_x port temperatures become a concern, the increase in NO_x reduction was only 8% as the overfire air was increased from 8 to 25%. However, it must be noted that it was not possible to totally separate the effects of the low-NO_x burners and overfire air system, since the overfire air flow could not be reduced to zero.

Flyash unburned carbon levels measured after the retrofit were unchanged from the baseline levels, and did not appear to be greatly affected by the amount of overfire air. CO emissions were also comparable to the baseline levels with maximum overfire air, and tended to increase as overfire air flow was reduced to the minimum values. This was not expected, as low-NO_x combustion retrofits have been known to result in increases in flyash unburned carbon levels and CO emissions. It is hypothesized that this behavior is due to the penetration and mixing of the overfire air in this down-fired configuration. It is also possible that the lack of an effect on flyash unburned carbon is partially due to the reactive nature of the Western coal utilized by the Arapahoe station. This reactivity allows flexibility in operation of the low-NO_x burners and overfire air system without resulting in increases in unburned carbon levels. However, as mentioned above, CO emissions were found to be sensitive to changes in combustion system operating parameters.

SELECTIVE NON-CATALYTIC REDUCTION. Figure 1 also shows the NO_x emissions attainable when operating the SNCR system at urea injection rates which limit NH_3 slip at the fabric filter inlet to 10 ppm. The NO_x removals (measured relative to the 240 to 280 ppmc post-retrofit levels) range from 7 to 45% over the load range of 60 to 110 MWe, respectively. The temperature-sensitive nature of the urea injection process and the limitation of only a single usable injection level is apparent in that the NO_x removals for a fixed NH_3 slip level are much lower at the reduced loads where the flue gas temperature is also reduced. The reduction in NO_x emissions due to the combined affects of the low-NO_x combustion system retrofit and SNCR range from 66 to 82% over the load range of 60 to 100 MWe.

While urea injection allowed reasonable levels of NO_x removal at higher loads, it was not very effective at reduced loads. A third set of temperature measurements revealed that the low-NO_x combustion system retrofit resulted in another decrease in furnace exit gas temperatures (this one on the order of 180 to 240°F). In an effort to increase low-load removal, the urea injection system was modified with an on-line ammonia conversion system. This system converts urea to liquid ammonia compounds immediately before injection into the boiler. As ammonia reacts faster than urea and in a lower temperature window, it was expected to provide higher NO_x removal at lower loads. The results (Figure 2) showed that, when injected into the same location in the Arapahoe Unit 4 boiler, converted urea provided higher NO_x removals than urea when compared on an equal ammonia slip basis. However, the increased NO_x removals with converted urea required higher chemical injection rates (ranging from 67 to 133% higher than those for urea injection

at the same load). Therefore, at loads of 80 MWe and greater, urea was the most efficient of the two chemicals.

In addition to creating unwanted ammonia emissions, SNCR can increase nitrous oxide (N_2O) emissions. N_2O emissions with converted urea were lower than those for urea. For converted urea, the fraction of NO reduced which was converted to N_2O ranged from 3 to 8%, depending on load for a stoichiometric (N/NO) ratio of 1.0. With urea, the conversion ranged from 29 to 35% at a similar chemical injection rate. The N_2O conversion with urea injection was much higher than that seen before the low-NO_x combustion system retrofit (11 to 16% at a N/NO ratio of 1.0). It is likely that the increase is due to the reduction of the flue gas temperatures in the injection region seen after the retrofit.

DRY SORBENT INJECTION WITH CALCIUM HYDROXIDE ($Ca(OH)_2$). Testing of the dry sorbent injection system with $Ca(OH)_2$ consisted of two phases: duct injection with humidification and economizer injection without humidification. All testing to date has been with a low-sulfur coal and baseline SO_2 emissions in the range of 400 ppmc.

The results of the duct injection tests with humidification at a stoichiometric (Ca/S) ratio of 2.0 are shown in Figure 3. The maximum SO_2 removal of 44% was obtained during a short-term test with the humidification system operating at a 20°F approach to saturation. Immediately after this test, problems developed with the dry flyash transport system, and it is suspected that the low approach temperature operation contributed to the problem. More recently,problems with increased pressure drop across the fabric filter, and deposit build up on the bags occurred after operating the humidification system at a 30°F approach temperature. Currently, studies are still ongoing to determine if these problems were due to steady state operation at the 30°F approach temperature or transient conditions during load changes. At this higher approach temperature, SO_2 removal is reduced to a range of 26 to 36% at a Ca/S ratio of 2.0.

SO_2 removals with $Ca(OH)_2$ injection at the economizer have been much lower than expected. At a Ca/S ratio of 2.0 without humidification, SO_2 removals ranged from 5 to 8%. It was found that distribution of the sorbent with the original injection nozzles was very poor, and only approximately one-third of the flue gas was being treated. Improved nozzles which increased the distribution to approximately two-thirds of the flue gas were installed on one side of the boiler. With the improved distribution, SO_2 removals increased to only 10 to 12% at a Ca/S ratio of 2.0.

DRY SORBENT INJECTION WITH SODIUM SESQUICARBONATE. Testing of the dry sorbent injection system with sodium sesquicarbonate ($NaHCO_3 \cdot Na_2CO_3 \cdot 2H_2O$) has just recently begun, and only minimal data is available at this time. Figure 4 shows the SO_2 removals as a function of the stoichiometric injection rate (Na_2/S ratio) over the range of 0 to 1.5. At a Na_2/S ratio of 1.4, SO_2 removals of 53 to 63% have been achieved to date. It has been further documented during short-term tests that SO_2 removals in excess of 70% can be achieved at Na_2/S ratios slightly above 2.0. One byproduct of the dry sodium based SO_2 removal process is the oxidation of NO to NO_2. This can lead to plume coloration and visibility problems. For instance, NO_2 levels have been seen to increase by 6 to 13 ppm (from a baseline level of 1 to 2 ppm) while injecting sodium sesquicarbonate at Arapahoe Unit 4. One potential synergistic benefit of the Integrated Dry NO_x/SO_2 Emission Control System will be the suppression of the NO to NO_2 oxidation with sodium injection by the NH_3 slip from the SNCR system. These benefits will be documented during future testing of the entire integrated system.

CONCLUSIONS

The Integrated Dry NO_x/SO_2 Emissions Control System has been in operation for over one and one-half years and preliminary conclusions are as follows:

- NO_x reduction during baseloaded operation of the unit with the low-NO_x burners and overfire air ranges from 63 to 69% with no increase in flyash unburned carbon levels or CO emissions.

- Low-NO_x burners provided the majority of the NO_x reduction, while the overfire air system supplied approximately 8 to 10% additional NO_x reduction over the range of overfire air flow rates tested.

- Urea injection allows an additional 7 to 45% NO_x removal with an ammonia slip of 10 ppm at the fabric filter inlet. This increases total system NO_x reduction to 82% at full load, significantly exceeding the project goal of 70%.

- Higher NO_x reduction is possible using ammonia compounds as the SNCR chemical, but significantly higher stoichiometric ratios are required at loads of 80 MWe and above. However, it must be noted that the performance of the SNCR system with urea was limited by a large unexpected decrease in furnace exit gas temperature at this particular installation and, therefore, any comparison of the performance of ammonia compounds to that for urea must take this into account.

- N_2O generation is a potential concern with urea injection, but was greatly reduced when ammonia compounds were injected.

- The maximum SO_2 removal attained during short-term tests with calcium hydroxide injection and duct humidification was 44%.

- Preliminary results indicate SO_2 removals with sodium sesquicarbonate injection in excess of 60%.

DISCLAIMER
This report was prepared pursuant to a Cooperative Agreement partially funded by the U.S. Department of Energy, and neither Public Service Company of Colorado, any of its subcontractors, the U.S. Department of Energy, nor any person acting on behalf of either:

(a) Makes any warranty or representation, express or implied, with respect to the accuracy, completeness, or usefulness of the information contained in this report, or that the use of any information, apparatus, method or process disclosed in this report may not infringe privately-owned rights; or

(b) Assumes any liabilities with respect to the use of, or for damages resulting from the use of, any information, apparatus, method or process disclosed in this report.

Reference herein to any specific commercial product, process, or service by trade name, trademark, manufacturer, or otherwise, does not necessarily constitute or imply its endorsement, recommendation, or favoring by the U.S. Department of Energy. The views and opinions of authors expressed herein do not necessarily state or reflect those of the U.S. Department of Energy.

REFERENCES
Teixeira, D. P., et al., "Selective Non-Catalytic Reduction (SNCR) Field Evaluation in Utility Natural Gas-fired Boilers," GRI92-0083, March 1992.

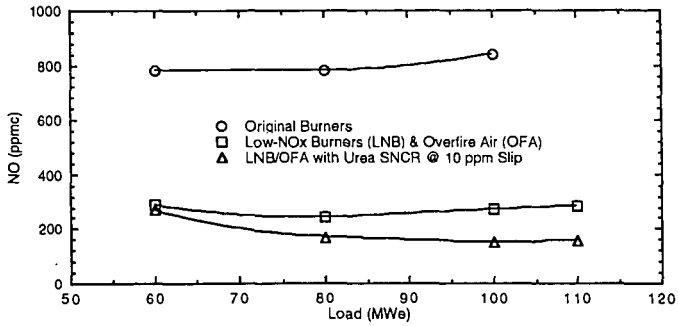

Figure 1. Pre-and Post-Retrofit NO_x Emissions

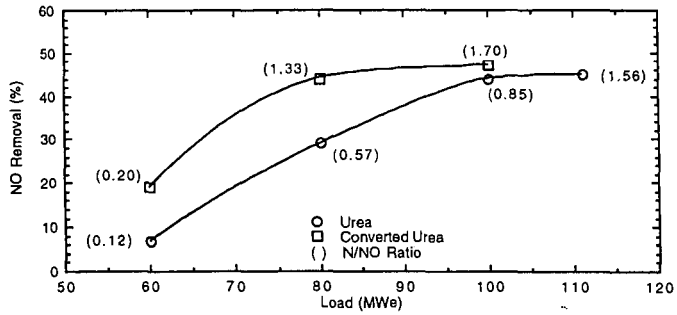

Figure 2. NO_x Removals for Urea and Converted Urea Injection at a Fixed NH_3 Slip Level of 10 ppm

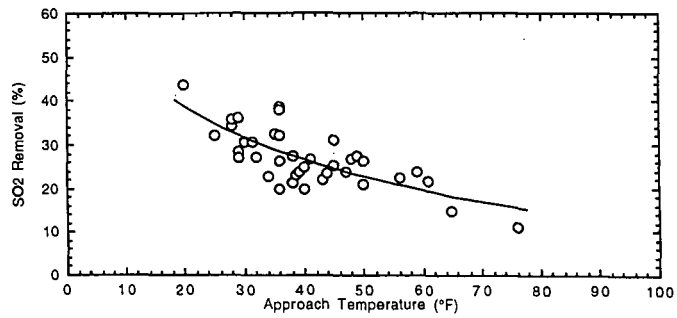

Figure 3. SO_2 Removals with Calcium Hydroxide for Duct Injection with Humidification (Ca/S = 2.0)

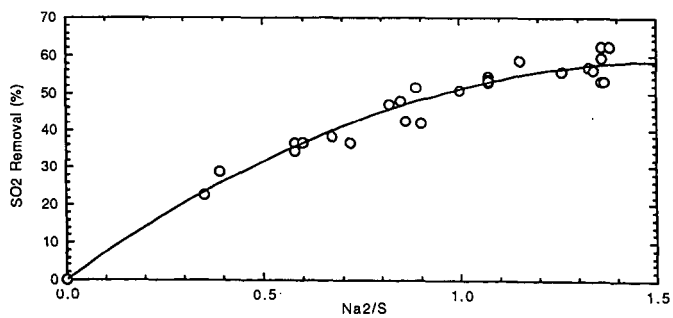

Figure 4. SO_2 Removals with Sodium Sesquicarbonate for Duct Injection without Humidification

GAS REBURNING AND INTEGRATED NO_x AND SO_2 CONTROL: READY FOR COMMERCIAL INSTALLATIONS

B.A. Folsom, R. Payne, and R. Lyon
Energy and Environmental Research Corporation (EER)
Irvine, California 92718

Keywords: Emission Control, NO_x, SO_2

INTRODUCTION

Gas Reburning (GR) is a retrofit NO_x control technology for boilers and furnaces. This paper presents recent field test results from demonstrations of GR and integrated NO_x and SO_2 control technologies on three coal fired utility boilers: tangential, wall and cyclone fired. GR was integrated with Sorbent Injection for enhanced SO_2 on two units and with Low NO_x Burners for enhanced NO_x control on one unit. Recent test results are presented from all three sites. An economic analysis compares costs for GR and integrated technologies with competing conventional technologies.

GAS REBURNING AND INTEGRATED TECHNOLOGIES

GR is a NO_x control technology where NO_x emissions are reduced by reactions with hydrocarbon fragments produced from natural gas (1). Figure 1 shows the application of GR to a front wall fired boiler.

In contrast to conventional firing systems which have a single combustion stage, GR is a three zone process. In the primary zone, the normal boiler fuel (coal, oil, or gas) is fired through conventional (or low NO_x) burners under low excess air conditions. The firing rate is reduced by 15-20% to accommodate the natural gas. This reduces combustion intensity and NO_x emissions.

In the reburning zone, natural gas is injected to produce a slightly fuel rich zone (nominally 90 percent theoretical air). The natural gas, principally methane (CH_4), breaks down to produce hydrocarbon fragments (CH and CH_2). The hydrocarbon fragments react with the NO_x produced in the primary combustion zone to reduce it to atmospheric nitrogen (N_2).

The gases exiting the Reburning Zone contain considerable carbon monoxide (CO) as well as unburned hydrocarbons. These are consumed in the burnout zone by injection of additional combustion air (overfire air), completing the heat release.

Since GR does not require modifications to the main firing system, it is compatible with all types of firing systems. Demonstrations are currently being conducted on tangential, wall and cyclone fired systems. Applications on stokers are also feasible.

By itself, GR can achieve NO_x control of 60-70% and SO_2 control proportional to the gas firing (typically 15-20%). NO_x and SO_2 control can be increased by integrating GR with other control technologies. Examples include:

- <u>Low NO_x Burners (LNB)</u> NO_x control increases to about 75%. GR-LNB is being demonstrated on a wall fired unit (2).

- <u>Selective Non-Catalytic Reduction (SNCR)</u> The integration of SNCR with GR is termed Advanced Gas Reburning (AGR). The GR system is tuned to optimize the conditions for SNCR improving agent utilization, increasing NO_x control to about 85%, and eliminating NH_3 slip. AGR has been tested at pilot scale (3).

- <u>Methanol Injection</u> A small amount of methanol injected into the back pass of the boiler converts NO to NO_2 which can be removed in a wet scrubber. The integration of Methanol Injection with AGR, CombiNO_x, increases NO_x control to the 90-95% range. CombiNO_x has been tested at pilot scale (3).

- <u>Sorbent Injection (SI)</u> A calcium based sorbent can be injected in several ways to boost SO_2 control. GR integrated with furnace sorbent injection (GR-SI) can increase SO_2 control to about 50% with conventional sorbents and to over 80% with advanced sorbents, such as

PromiSORB. GR-SI is being demonstrated on tangential and cyclone fired units (4).

- SO_2 Scrubber Since the GR modifications affect only the boiler, GR is fully compatible with all types of post combustion emission controls such as SO_2 Scrubbers.

Figure 2 shows the ranges of NO_x and SO_2 control achievable with these integrated technologies in comparison to conventional technologies without GR (Low NO_x Burners, SNCR, SCR and SO_2 Scrubber).

DATA FROM THREE FULL SCALE DEMONSTRATIONS

EER is demonstrating GR and integrated technologies on three utility boilers in two DOE Clean Coal Technology Projects as shown in Table 1. The host sites are all utility boilers and include the three major firing configurations: tangential, wall and cyclone fired. They cover a capacity range from 33 to 158 MW, a factor of nearly 5/1. As part of the design process, EER projected (and published) performance goals. NO_x control of over 60% was projected for each of the units.

At all three units the emission control equipment has been installed and tested extensively. The NO_x control goals have been achieved. Testing has been completed at the Hennepin tangentially fired unit and Illinois Power, the host utility, has elected to retain the equipment. Testing is still in progress at the other three units.

Figure 3 shows how NO_x decreases as the gas injection rate increases for all three units. It should be noted that the wall fired unit is equipped with low NO_x burners and the zero gas point corresponds to emissions from the low NO_x burners. At the Hennepin tangentially fired unit, additional tests were conducted with the unit operating on 100% gas and utilizing the GR system. As shown in figure 3, NO_x emissions were reduced to 0.05 lb/10^6 Btu. All three demonstrations include long term testing where the emission control systems are operated by plant personnel. The tests have been completed at Hennepin; NO_x averaged 0.245 lb/10^6 Btu, a 67.3% reduction.

ECONOMICS

The capital cost of GR is highly site specific. For a typical installation on a large unit (300-500 MW), the capital cost is typically in the range of 15-30 $/KW for a easy and difficult retrofits, respectively.

The operating cost for gas reburning is almost entirely related to the differential cost between the gas and the base fuel. No additional operators are required and maintenance is minimal. For coal fired units, gas generally costs more than coal and the differential cost is the largest cost component. For gas fired the fuel cost impact is zero and operating costs are near zero.

In evaluating GR operating costs it is important to account for several benefits of GR other than NO_x control. These include:

1. SO_2 Reduction in proportion to the fraction of gas fired. The value of the SO_2 reduction will depend on the utility's alternatives for SO_2 control and the SO_2 allowance market price.

2. Reduced Ash Disposal in proportion to the gas firing percentage.

3. Reduced Maintenance and Improved Availability Reducing the amount of coal and ash passing through the power plant components reduces coal and ash related maintenance. Availability via gas use to replace coal during mill outages.

The total cost of emission control can be calculated by adding the capital and operating cost components via the Electric Power Research Institute (EPRI) Technology Assessment Guide (TAG) procedure. An EPRI TAG analysis was conducted for GR and integrated technologies along with conventional emission control technologies including low NO_x burners, SNCR and SCR. Figures 4 and 5 show the results for coal and gas fired units, respectively. The coal fired

analysis was based on a baseline NO_x level of 1.0 lb/10^6 Btu and a gas to coal cost differential of 1.00 \$/10^6 Btu. SO_2 credits were evaluated at 300 \$/ton for coals with 1.2 and 6.0 lb/10^6 Btu SO_2 emission potential. As shown in figure 4, the cost effectiveness of the GR technologies is comparable to low NO_x burners and SNCR but GR achieves substantially higher NO_x control. For high levels of NO_x control, where SCR is the only commercially available competing technology, GR-LNB and AGR are much more cost effective.

The gas fired analysis utilized baseline NO_x levels of 0.3 and 0.5 lb/10^6 Btu. The results shown in figure 5 are generally similar to the coal fired case except that: (1) the overall costs are higher due to the lower initial NO_x level and no SO_2 credit, and (2) the GR costs have dropped relative to the LNB and SNCR costs since there is no cost differential associated with the gas injected into the reburning zone.

CONCLUSIONS

EER has designed, installed and tested GR systems on three utility boilers covering a 5/1 capacity range and involving all three major firing configurations (tangential, wall and cyclone). In all cases the NO_x control goals were achieved or exceeded with no operational problems. GR can be installed as a stand alone technology to achieve NO_x control in the range of 60%. Higher levels of NO_x and/or SO_2 control can be achieved by integrating other synergistic controls. Costs for GR technologies are generally competitive with other technologies which can achieve comparable levels of NO_x control.

EER has been working on GR technologies for over 12 years. The results from these three Clean Coal Technology demonstrations have provided EER with the design and performance data base necessary to apply GR in the commercial market place. Accordingly, EER is now offering GR and integrated technologies with commercial guarantees for industrial and utility Clean Air Act compliance applications.

ACKNOWLEDGEMENT

The reported work was conducted as part of the DOE Clean Coal Technology Program. The GR-Sorbent Injection demonstrations at Illinois Power's Hennepin Station and City Water, Light and Power's Lakeside Station were cofunded by DOE, the Gas Research Institute, and the State of Illinois. The GR-Low NO_x Burner demonstration at Public Service Company of Colorado's Cherokee Station was cofunded by the Gas Research Institute, Public Service Company of Colorado, Colorado Interstate Gas, the Electric Power Research Institute, and Energy and Environmental Research Corporation.

The authors wish to thank the personnel at each organization and especially the power plant staff for their direct involvement in the projects.

REFERENCES

1. B.A. Folsom, C.C. Hong, T.M. Sommer and J.M. Pratapas, "Reducing Stack Emissions by Gas Firing in Coal-Designed Boilers -- Field Evaluation Results," 1993 Joint Symposium on Stationary Combustion Nox Control, Miami Beach, Florida (May 24-27, 1993).

2. A. Sanyal, T.M. Sommer, C.C. Hong, B.A. Folsom and R. Payne, "Low NO_x Burners and Gas Reburning -- An Integrated Advanced NO_x Reduction Technology," The Institute of Energy/International Symposium on Combustion and Emission Control, University of Wales, College of Cardiff, U.K. (September 21-22, 1993).

3. J.N. Pont, "Results from a Modeling and Experimental Evaluation of the CombiNO_x Process," presented at the 1993 American Chemical Society Meeting, Denver, Colorado.

4. D. Rodriguez, C. Gomez, R. Payne and P. Maly, "Demonstration of Promoted Dry Sorbent Injection in a 75 MWe Tangentially-Fired Utility Furnace," EPRI/EPA/DOE 1993 SO2 Control Symposium, Boston, Massachusetts, August 24-27, 1993.

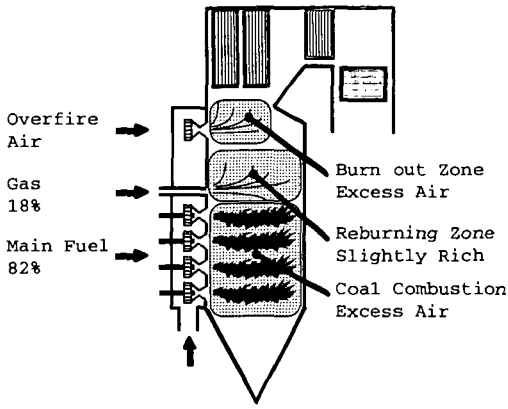

Figure 1. Gas Reburning on a Wall Fired Boiler

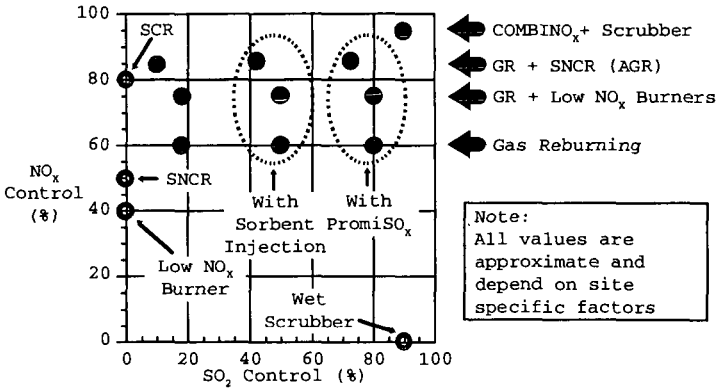

Figure 2. NO_x and SO_2 Control Comparison

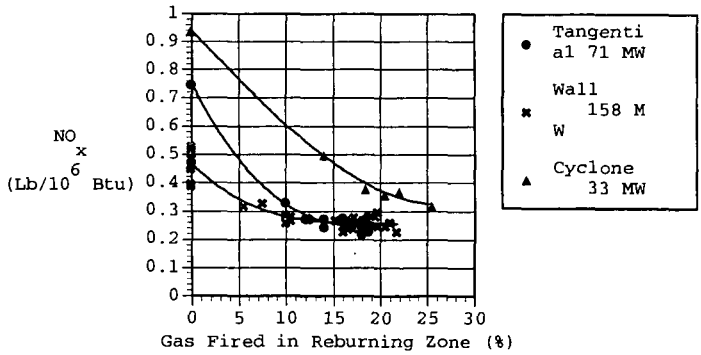

Figure 3. Gas Reburning Data from Three Demonstrations

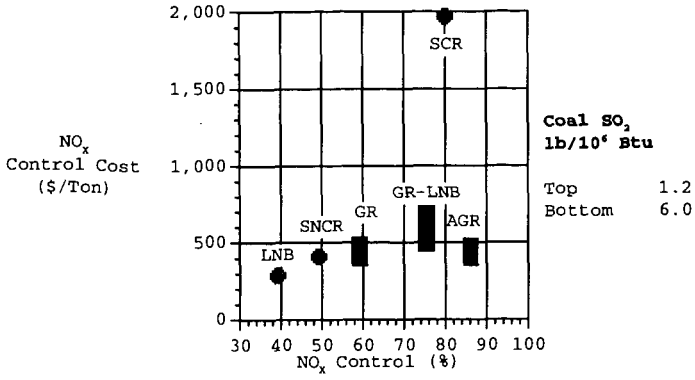

Figure 4. Gas Reburning Economics for Coal Fired Boiler

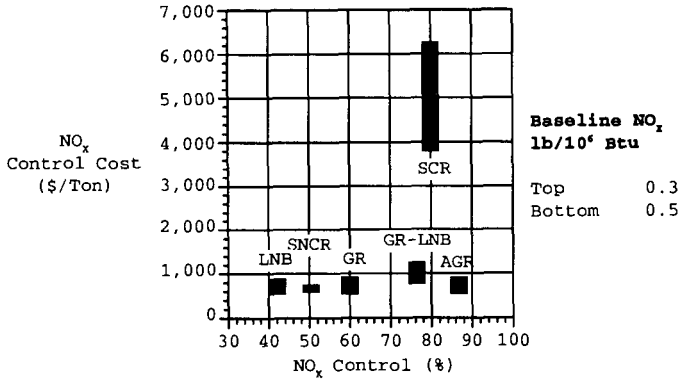

Figure 5. Gas Reburning Economics for Gas Fired Boiler

Table 1. Three Demonstrations

CCT	TECH.	UNIT	CAP MW net	FIRING CONFIG	Status	FUNDING
1	Gas Reburning	Illinois Power Hennepin 1	71	Corner	Comp. 1 Year Test	$37,000,000 DOE GRI Illinois ENR
	Sorbent Injection	CWLP Lakeside 7	33	Cyclone	1 Yr. Test in Pro	
3	Gas Reburning Low NOX Burners	P.S. Colorado Cherokee 3	158	Wall	Para. Comp. 1 Year Test in Pro	$16,000,000 DOE GRI PS Colorado CIG EPRI EER

LIFAC SORBENT INJECTION : AN ALTERNATIVE SO_2 CONTROL STRATEGY

James Hervol
Christopher Keating
ICF Kaiser Engineers, Inc.
Four Gateway Center
Pittsburgh, Pennsylvania 15222

Juhani Viiala
Tampella Power Corp.
2300 Windy Ridge Parkway
Atlanta, Georgia 30067

Keywords : SO_2 Control, Sorbent Injection, Clean Coal Demonstration

Introduction

The Clean Coal Technology Program (CCT) has been recognized in the National Energy Strategy as a major initiative whereby coal will be able to reach its full potential as a source of energy for the nation and the international marketplace. Attainment of this goal depends upon the development of highly efficient, environmentally sound, competitive coal utilization technologies responsive to diverse energy markets and varied consumer needs. The CCT Program is an effort jointly funded by government and industry whereby the most promising of the advanced coal-based technologies are being moved into the marketplace through demonstration. The CCT Program is being implemented through a total of five competitive solicitations. This paper discusses the LIFAC sorbent injection technology which was selected in the third round of CCT solicitations.

LIFAC North America, a joint venture partnership of ICF Kaiser Engineers, Inc. and Tampella Power Corporation of Finland, will demonstrate the LIFAC flue gas desulfurization technology developed by Tampella. This technology provides sulfur dioxide emission control for powerplants, especially existing facilities with tight space limitations. Sulfur dioxide emissions are expected to be reduced by up to 85% by using limestone as a sorbent. The limestone is injected into the upper regions of a furnace, where calcining to lime and partial absorption of SO_2 occur. Subsequently, the combustion gas is passed through a unique piece of equipment known as the activation reactor. This is a vertical elongation of the ductwork between the air preheater and ESP where the combustion gas is humidified and SO_2 absorption is completed. The LIFAC technology will be demonstrated at Whitewater Valley Unit No. 2, a 60-MWe coal-fired powerplant owned and operated by Richmond Power and Light (RP&L) and located in Richmond, Indiana. The Whitewater plant consumes high-sulfur coals with sulfur contents ranging from 2.0 - 2.9 percent.

The project, co-funded by LIFAC North America and DOE, is being conducted with the participation of Richmond Power and Light, the State of Indiana, the Electric Power Research Institute, and the Black Beauty Coal Company. The project has a total cost of 21.4 million dollars and a duration of 48 months from the preliminary design phase through the testing program.

The sponsors of this project believe that LIFAC has the potential to be a new and important SO_2 control option for U.S. utilities subject to the Clean Air Act's acid rain regulations. To be considered as a commercially feasible option in this particular emissions control market, LIFAC must demonstrate a high SO_2 removal rate while remaining competitive with other options on a cost per ton of SO_2 removed basis. To this end, the sponsors of this project have designed the demonstration with the following goals in mind:

- Sustained High SO_2 Removal Rate - Incorporated into the test plan are several periods of long term testing which are intended to demonstrate LIFAC's SO_2 removal and reliability characteristics under normal operating conditions.

- Cost - LIFAC must compete with both low capital cost, low SO_2 removal rate options such as sorbent injection and high capital cost, high SO_2 removal rate options such as wet scrubbing. This project will demonstrate LIFAC's competitiveness on a cost per ton of SO_2 removed basis with these currently available alternatives.

- Retrofit Adaptability - The host site chosen required a retrofit with tight construction conditions that will prove LIFAC's ability to be installed where other technologies might not be possible. Construction was also to demonstrate LIFAC's ability to be built and brought on-line with zero plant down time other than scheduled outages.

- System Compatibility - A major concern of utilities is the degree of compatibility of SO_2 removal systems with their existing operations. This demonstration will show LIFAC's minimal impact on the host site's boiler and associated subsystems.

LIFAC Process History and Description
In 1983, Finland enacted acid rain legislation which applied limits on SO_2 emissions sufficient to require that flue gas desulfurization systems have the capability to remove about 80 percent of the sulfur dioxide in the flue gas. Tampella Power, therefore, began developing an alternative, economical sorbent injection system. Initially, development first involved laboratory and pilot plant tests, then full-scale tests of sorbent injection of limestone. Subsequent research and development by Tampella led to the addition of a humidification section after the furnace which became known as the LIFAC process.

In 1986, the first large full scale test was performed at Imatran Voima's Inkoo powerplant using a 70 megawatt side-stream from a 250 megawatt boiler. A 76 percent SO_2 removal rate with 1.5% sulfur coal was reached. A second LIFAC activation reactor was constructed to handle an additional 125 megawatt side-stream. This newer reactor is achieving removal rates of 75 to 80 percent while using Ca/S molar ratios of between 2 and 2.5 to 1. Also, in 1988 the first tests with high-sulfur U.S. coals were run at the Neste Kulloo Laboratory. A Pittsburgh No. 8 Seam coal containing 3 percent sulfur was tested and an SO_2 removal rate of 77 percent was achieved at a Ca/S molar ratio of 2 to 1.

LIFAC Process Description
The LIFAC system combines conventional limestone injection into the upper furnace region with a post-furnace humidification reactor located between the air preheater and the ESP. The process produces a dry, stable waste product that is removed from both the bottom of the bumidification reactor and the ESP.

Finely pulverized limestone is pneumatically conveyed and injected into the upper region of the boiler where temperatures are approximately 1800 to 2200 degrees Fahrenheit. At these temperatures the limestone ($CaCO_3$) calcines to form lime (CaO) which readily reacts with the SO_2 to form calcium sulfate ($CaSO_4$). All of the sulfur trioxide (SO_3) reacts with the CaO to form $CaSO_4$.

Approximately 25 percent of the sulfur dioxide removal occurs in the boiler with the remaining 75 percent and the unreacted lime passing through the air preheater to the humidification reactor. There the flue gas is sprayed with water that allows the unreacted lime to hydrate to $Ca(OH)_2$ which more readily reacts with the sulfur dioxide and forms $CaSO_3$. A combination of the proper water droplet size and residence time allows for effective hydration of the lime and complete water evaporation to create a dry reactor bottom product.

After exiting the humidification reactor, the flue gas is reheated before entering the ESP. The humidification and lower gas temperature enhance the efficiency of the ESP. Seventy-five percent of the LIFAC-produced spent sorbent and fly ash is collected by the ESP with the other 25 percent collected by the humidification reactor. Both the reactor and ESP ash may be recycled to a point ahead of the reactor to improve sorbent utilization and to improve the SO_2 removal efficiency of the system to the range of 75 to 85 percent. A schematic of the LIFAC process is shown in Figure 1 along with the typical sampling locations used during the demonstration.

Process Advantages
LIFAC is similar to other current sorbent injection technologies but has unique advantages with its use of a patented vertical humidification reactor. And while LIFAC's sulfur dioxide removal efficiency is not as high as traditional wet flue gas desulfurization systems, its cost and simplicity of design, construction and operation offer other advantages over these alternative systems. In particular the advantages of the LIFAC system are:

- High SO_2 removal rates - Currently available sorbent injection systems have been unable to sustain high SO_2 removal rates with any consistency. LIFAC has proven in

the past and intends to demonstrate during this project the ability to achieve and sustain high SO_2 removal rates of 75 to 85 percent over long operating periods.

- By-products - Wet lime and limestone scrubbing systems create a wet byproduct ash that must be further treated before disposal. LIFAC produces a dry solid waste ash containing calcium sulfide, calcium sulfate and fly ash. This waste is easily disposed of under U.S. regulatory requirements, may be recycled to increase LIFAC's efficiency and may have commercial applications in the cement industry.

- Compatibility and Adaptability - LIFAC has minimal impact on the host's site and systems, primarily the boiler, ESP and ID fan. In addition, LIFAC requires little space and few utilities and therefore is easily installed even in small or cramped powerplant sites.

Construction and Systems Integration
Construction of the LIFAC system has occurred in two phases over a period of one and a half years. The first phase of construction was completed during a routine plant outage in March, 1991. The period was utilized to install tie-ins to the host site's existing systems.

Ductwork and three dampers were installed between the air preheater and ESP to allow flue gas flow to the LIFAC activation reactor. Tie-ins were also made to the powerplant's high-pressure steam, condensate and river-water supplies. The high-pressure steam is required to reheat the flue gas exiting the LIFAC reactor and the water is needed for flue gas humidification inside the reactor. Injection ports were also installed in the boiler walls about 10 feet above the nose elevation.

The second phase of construction began in the Fall of 1991 with the driving of reactor piling and the installation of underground conduit runs. Work continued through to the Summer of 1992 with no need for plant downtime other than normally scheduled outages. During this time the limestone storage area was completed and the injection system was installed on Unit #2. The activation reactor was constructed and then tested with both cold air during a scheduled Unit #2 outage and hot flue gas during a low electricity demand period. Other powerplant tie-ins such as the steam and condensate system were also tested during low demand periods in the evening or on weekends.

Schedule
The current schedule for the LIFAC demonstration program extends over a four year period from the beginning of preliminary design in August 1990 through the testing program to be completed in early August 1994. However, preliminary test results are now available.

Currently the demonstration project is on schedule. All construction work was completed at the beginning of August 1992. Equipment check-out was performed in July and August and the first limestone delivery was received in early September. Initial tests with limestone injection into the boiler along with post-furnace humidification were conducted in October to December 1992. The project team was prepared to conduct the test plan beginning in early 1993.

Test Plan
The test plan for the LIFAC demonstration is composed of five distinct phases, each with its own objective. The first of these phases, which has already been completed, consisted of the initial baseline testing portion of the project. Measurements were taken to characterize the operation of the host's boiler and associated subsystems prior to the use of the LIFAC system.

The second, or parametric, phase of testing is currently underway and will be performed to determine the best combination of LIFAC process variables for SO_2 removal. The variables being studied include the limestone injection nozzles' angle and location, the Ca/S molar ratio, the need for supplemental injection air at the boiler, the water droplet size and injection nozzle arrangement in the reactor, the ash recycling ratio and the approach to saturation temperature of the flue gas exiting the activation reactor. The best combination of these variables will be chosen at the conclusion of this phase and used for the remainder of the test program.

Optimization tests will be conducted to examine the effects of different coal and limestone feeds on the SO_2 capture rate. Coals with sulfur contents as high as 3.3 percent will be tested to determine LIFAC's compatibility with high sulfur U.S. coals. Limestones with different compositions will also be tested to determine the LIFAC system's adaptability to local sorbent sources.

Long term testing will also be performed to demonstrate LIFAC's performance under commercial conditions. The LIFAC system will be in operation 24 hours per day for several weeks using the powerplant's baseline coal, high calcium limestone and the optimum combination of process variables.

The final phase of testing is composed of the post-LIFAC tests. The baseline tests will be repeated to gather information on the condition of the boiler and its associated subsystems. Comparisons will be made to the original baseline data to identify any changes either caused by the LIFAC system or independent of its operation.

Preliminary Results

Parametric testing was initiated at 60 MW to assess the broad impacts of limestone injection, flue gas humidification, and sorbent recycle. Figure 1 shows average reductions achieved throughout the LIFAC process. About 22 percent SO_2 reduction is achieved in the boiler. This is increased to about 52 percent with humidification, and further raised to 75 percent with the use of sorbent recycle from the ESP ash hoppers. These tests were conducted with a fine grind limestone (80% minus 325 mesh) with a Ca content above 90 percent. A Ca/S molar ratio of 2.0 was held near constant and a 4 to 5° Fahrenheit approach to saturation was maintained in the activation reactor.

Figure 2 shows the impacts of varying the Ca/S molar ratio. The majority of the tests have been conducted at 2.0, but the trends are as expected. The higher the Ca/S ratio, the higher the SO_2 reduction. Results show, however, that SO_2 reductions of 75 to 85 percent are possible when spent sorbent is recycled and a 3 to 5° Fahrenheit approach to saturation temperature is maintained.

Figure 3 shows the impact of recycling spent sorbent under various boiler loads. The Ca/S molar ratio was maintained at about 2.0 and the level of humidification is high (4 to 5° Fahrenheit above saturation). Generally, there is an 18 to 25 percentage point increase in SO_2 reduction as a result of sorbent recycle. With recycle, total SO_2 reductions ranged from 75 to 85 percent depending on boiler load.

At this point it has been shown at RP&L and other LIFAC installations that the system can be installed and operated without affecting normal powerplant operations. It will also be shown that the system can economically reduce SO_2 emissions when compared with other flue gas desulfurization technologies.

References

1. Ball, M.E. and Enwald, T., "LIFAC Demonstration at Poplar River", *GLOBE-92, Product and Technology Demonstration Seminars,* March 1992.

2. DOE Contract No. DE-FC22-90PC90548, "*LIFAC Demonstration at Richmond Power and Light White Water Valley Unit #2*", March 1992.

3. Rose, J., Hervol, J., Viiala, J., Koskinen, J., Patel, J. and Huffman, I., "*LIFAC Flue Gas Desulfurization*", March 1992.

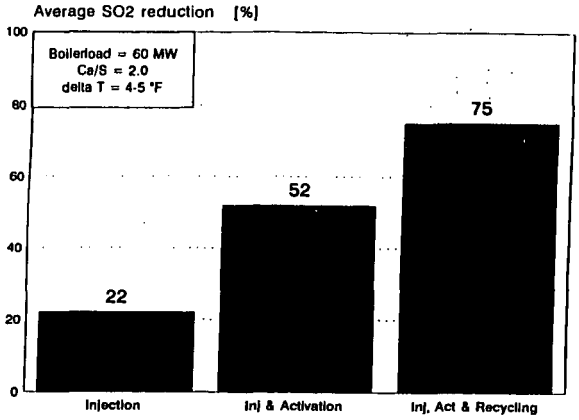

Figure 1. PARAMETRIC EFFECTS

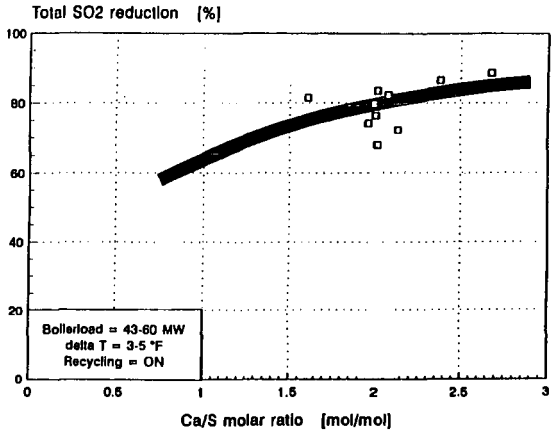

Figure 2. SO_2 REDUCTION vs. Ca/S MOLAR RATIO

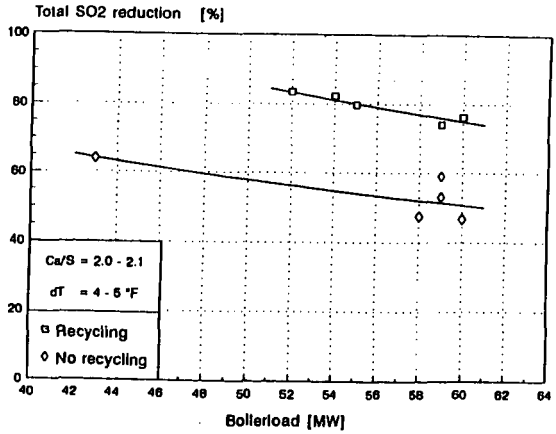

Figure 3. SO_2 REDUCTION vs. BOILER LOAD

COMPLIANCE BENEFITS OF POWDER RIVER BASIN COAL AND COAL REBURNING

G. J. Maringo, Babcock & Wilcox, Barberton, Ohio
A. S. Yagiela, Babcock & Wilcox, Barberton, Ohio
R.J. Newell, Wisconsin Power & Light, Madison, Wisconsin

ABSTRACT

Cyclone-fired boilers are typically high emitters of NO_x, simply as a result of cyclone furnace design requirements. Babcock & Wilcox (B&W) developed the cyclone furnace originally to burn lower grade coals, high in ash and sulfur contents, with unremarkable heating values. To combust the lower grade fuels, the cyclone furnace develops very strong turbulence and extremely fast mixing of fuel and combustion air. A major portion of ash is thrown to the walls where it melts and runs out of the furnace through a slag tap. Large coal particles are trapped in this slag layer allowing complete carbon burn out to be achieved. In this way, the majority of ash and large coal particles are kept out of the main boiler. The resulting high combustion temperatures are conducive to NO_x formation. Typically, NO_x emissions range from about 0.80 to 1.8 lbs/10^6 Btu, with SO_2 emissions entirely a function for the fuel.

Standard low NO_x burner combustion technologies are not applicable for cyclone-equipped boiler operation. The emerging reburning technology offers cyclone boiler owners a promising alternative to expensive flue gas cleanup techniques for NO_x emission reduction. Reburning involves the injection of a supplemental fuel (natural gas, oil or coal) into the main furnace to produce locally reducing conditions which convert NO_x produced in the main combustion zone to molecular nitrogen, thereby reducing overall NO_x emissions.

B&W has obtained encouraging results from engineering feasibility studies,[1] pilot-scale proof of concept testing,[2] and a U.S. Department of Energy Clean Coal II project to demonstrate the cyclone coal reburning technology on a full size utility boiler. The host site for the demonstration was Wisconsin Power & Light's (WP&L) 110 MW_e Nelson Dewey Station. It was at Nelson Dewey that the benefits of fuel switching to a Powder River Basin (PRB) coal as an SO_2 compliance strategy with coal reburning for NO_x emissions reduction became apparent.

The addition of a reburn system capable of providing up to 30% additional fuel input to the furnace means that a utility could switch to lower Btu compliance coal and minimize or eliminate a derate. This paper describes the emissions and impact on boiler operations of coal switching and reburning on Nelson Dewey Unit No. 2.

INTRODUCTION

The Clean Air Act Amendments of 1990 pose significant challenges to electric utilities to reduce both SO_2 and NO_x emissions. The Act mandates an approximate 3.5 million ton/yr reduction in SO_2 emissions from 111 selected existing utility boilers by January 1, 1995. An additional 5.3 million ton/yr reduction is also mandated to occur by January 1, 2000 in order to reach a long term SO_2 emissions cap of 8.9 million ton/yr. Titles I and IV of the Act mandate NO_x reduction from stationary sources. Title IV (acid rain) requires the use of low NO_x burner technology and Title I (ozone non-attainment) requires reasonable, available control technology (RACT) to reduce NO_x. The impact on utilities is that by the year 2000, more than 200,000 MW_e must be retrofitted with low NO_x systems.

The limitations imposed by the Act are particularly challenging, especially for NO_x emissions from cyclone-fired boilers. The Coal Reburning for Cyclone Boiler NO_x Control Demonstration at WP&L was selected under Round II of the U.S. Department of Energy's Innovative Clean Coal Technology Program to address NO_x reduction in cyclone-fired boilers. As an addendum to this demonstration, testing was performed on a Western subbituminous PRB coal. Reburn NO_x reduction performance on the Western coal was very encouraging. The use of reburn to minimize or eliminate a unit derate as a result of fuel switching was also demonstrated. Consequently, cyclone reburn can be viewed as a NO_x reduction alternative which compliments and enhances a coal switching strategy used to comply with SO_2 regulations.

WP&L's involvement in this project was undertaken for several reasons. The State of Wisconsin enacted acid rain legislation in 1986, which will be fully implemented in 1993. The state law requires significant reduction of SO_2 emissions and the study of potential reduction of NO_x emissions. To meet SO_2 emission levels at the Nelson Dewey station, WP&L has switched from a medium sulfur bituminous to a low sulfur Western subbituminous coal. In addition, to investigate the potential of reducing NO_x emissions at Nelson Dewey Unit No. 2, WP&L retrofitted the coal reburning technology.

BACKGROUND

Compliance with SO_2 limits will require a utility to exercise a combination of options. These include post combustion flue gas desulfurization (wet scrubbers, dry scrubbers, etc.), repowering with fluidized beds or other technology, acquiring of additional allowances from over compliance at other plants in the utility's system, purchasing additional allowances from other utilities, and fuel switching. Of the 111 named sites more than 64% elected to switch fuels to meet SO_2 compliance.

NO_x is produced at high temperatures by oxidation of nitrogen from combustion air (thermal NO_x) and nitrogen in the fuel (fuel NO_x). Formation of NO_x is reduced by depressing combustion zone temperatures and by delaying the admission of sufficient oxygen to complete combustion. Compliance with NO_x limits for the majority of boilers will require use of an internally-staged low NO_x burner, and optional air staging with overfire air ports.

Reducing NO_x emissions from cyclone-fired boilers presents a different challenge. Typical delayed combustion techniques are not applicable to cyclones because they rely on developing an oxygen deficient or reducing atmosphere to hamper NO_x formation. A reducing condition in the confines of a cyclone barrel is unacceptable due to the potential for tube corrosion and severe maintenance problems. Generally, cyclone fuels are typically high in sulfur content which combined with high temperature in a reducing zone concrete major corrosion problems. Cyclone operation must occur under excess oxygen conditions. High temperatures and severe turbulence within the cyclone barrel attribute to the high NO_x levels typically observed from cyclone boilers. The 26,000 MW_e of generating capacity that cyclones represent is about 15% of pre-New Source Performance Standards (NSPS) coal-fired generating capacity, but contribute 21% of NO_x emitted by pre-NSPS coal-fired units.

Reburn Technology Definition

To address the special needs of the cyclone boiler population with respect to NO_x reduction, B&W developed the coal reburning technology. Reburning is a process by which NO_x normally produced in the cyclone is reduced (decomposed to molecular nitrogen) in the main furnace by injection of a secondary fuel with a very limited amount of combustion air. The secondary (or reburning) fuel creates an oxygen-deficient (reducing) region where hydrocarbon radicals produced under sub-stoichiometric conditions compete for available oxygen. Any NO_x in the reburning zone, by virtue of the thermodynamics of the process, is reduced to elemental N_2 while the oxygen is used to continue combustion of hydrocarbon radicles. This process accomplishes the NO_x decomposition. Because reburning occurs while the cyclone operates in a normal oxidizing condition, its effects on cyclone performance can be minimized.

The reburning process employs multiple combustion zones in the furnace, defined as the main combustion, reburn and burnout zones (Fig. 1). The main combustion zone is operated at a stoichiometry of 1.1 (10% excess air) and combusts the majority of the fuel input (70 to 80% heat input). The balance of fuel (20 to 30%) is introduced above the main combustion zone (cyclones) in the reburn zone through reburning burners. These burners are operated in a similar fashion to a standard wall-fired burner except that they are fired at extremely low stoichiometries. The combustion gases from the reburn burners mix with combustion products from the cyclones to obtain a furnace reburning zone stoichiometry in the range of 0.85 to 0.95 which is needed to achieve maximum NO_x reduction. A sufficient furnace residence time within the reburn zone is required for flue gas mixing and NO_x reduction kinetics to occur.

The balance of the required combustion air (totaling 15 to 20% excess air at the economizer outlet) is introduced through overfire air ports. As with the reburn zone, a satisfactory residence time within this burnout zone is required for complete combustion. The added capability to supply fuel to the furnace through the reburn burners is critical to maintaining full load operation while using a lower Btu value PRB fuel.

Reburn Equipment Optimization for PRB Fuels

In a fuel switching scenario, cyclone furnaces typically experience a 20 to 30% derate due to the volume limited nature of a cyclone furnace in addition to boiler performance. To maintain the original nameplate capacity, an additional 20 to 30% fuel volume is required to compensate for the lower heating value of the PRB coal (8500 Btu/lb versus 11,500 Btu/lb). This increase will not be tolerated by a cyclone furnace and major operational problems will result (high carbon carryover, reduced temperatures in the cyclone and difficult slag removal). To help eliminate this problem, the coal reburning system offers a means to increase fuel volume flow to the boiler.

The coal reburn system includes a pulverizer sized for 20 to 30% of the total fuel input to the boiler. When firing PRB coal, the cyclones continue to operate within design rating (ton/h and heat input) while the pulverizer provides the additional 20 to 30% of the heat input required through the reburn burners to approach full load on compliance coal. In this way, the coal reburn system can reduce or eliminate, on a site specific basis, the derate accompanying a fuel switch to PRB fuel as an SO_2 compliance strategy. The avoided cost of a unit derate can justify the price of a reburn system and at the same time allow the utility to achieve NO_x and SO_2 compliance goals.

BASELINE OPERATION

Boiler Description

Nelson Dewey Unit No. 2, shown in Fig. 2, is a B&W radiant boiler. The design rate is 100 MW_e but the current maximum continuous rating (MCR) is 110 MW_e. The boiler is fired with three cyclone furnaces located horizontally on the front wall with clockwise swirl. Hot combustion gases exit the cyclones at temperatures above 3000F. A target wall in the boiler directs the cyclone flow downward toward the floor of the boiler. The gas then turns upward and passes through slag screen tubes where it enters the main furnace. The lower furnace and slag screen are refractory-lined to keep the slag in a molten state.

The primary demonstration coal for cyclone reburn was Illinois Basin (Lamar) bituminous coal. The majority of the testing was done on this fuel to reflect the large cyclone utility contingent which fires higher Btu, high sulfur bituminous coal. Following the bituminous coal testing, subbituminous PRB coal tests were performed to evaluate the effect of coal switching on reburn operation. This work was important to Wisconsin Power & Light, since switching to the PRB coal for SO_2 compliance was to be implemented by January 1, 1993, within WP&L's system.

Baseline NO_x/CO Emissions

Baseline NO_x emissions tend to be 10 to 15% lower than those produced with bituminous coal when firing a cyclone boiler with subbituminous coal. The high moisture, low fixed carbon/volatile matter ratio and low fuel nitrogen content are factors which tend to suppress NO_x formation. Fig. 3 shows that this trend was observed at Nelson Dewey over the boiler's load range (8 to 10% reduced NO_x emissions).

The higher NO_x level at 38 MW_e with Lamar firing is due to single cyclone operation. The higher localized temperatures achieved in firing the single cyclone at a higher capacity results in higher NO_x levels. Also, the cooling air flow to the idle cyclones increases combustion gas oxygen content which is conducive to NO_x formulation. Although no baseline data at this load was available during PRB firing, the same trend is expected.

CO emission levels during baseline operation were low while firing either of the two coals. Generally speaking, the CO levels were slightly lower with PRB coal versus Lamar (30 to 45 ppm versus 60 to 70 ppm over the load range).

Baseline Boiler Operation with PRB Coal

In addition to the 20 to 30% derate often necessary when switching to higher moisture and lower heating value Western fuels, other related factors must be addressed. These include fouling/slagging problems, higher furnace exit gas temperatures (FEGT), exceeding convection pass metal alarm temperatures, increased attemperater spray flows, furnace overpressure alarms, and higher opacity. Based upon the testing at Nelson Dewey, the maximum load achievable during day to day operation firing PRB coal was about 108 to 110 MW_e without the reburn system in operation. WP&L's main load limitations were cyclone maximum loading and furnace overpressure alarms. With the reburn system operating, the unit was able to achieve 118 MW_e while burning PRB coal,

equal to maximum load firing Lamar coal.

It should be emphasized that to address some of the problems characteristic of PRB coal, WP&L had already installed numerous furnace wall sootblowers (air and water blowers available). This was the result of proactive Western fuel firing testing. Also, the cyclone vortex burners were fired by minimizing primary air flow to improve the combustion process within the cyclone barrel. Because of the upgrades and testing experience which WP&L compiled, minimal (if any) problems with fouling/slagging, convection pass metal temperatures, spray flow limitations and opacity levels were encountered during this test project.

Baseline Percent Efficiency Loss Due to Unburned Carbon

Baseline percent efficiency loss due to unburned carbon (UBCL) versus boiler steam flow (load) is shown in Fig. 4. Both Lamar bituminous and PRB results are shown. Over the load range, UBCL for PRB coal was lower, particularly at low loads where reduced cyclone temperatures deteriorated combustion performance. With the higher volatile matter content of the PRB coal, these problems were offset at low load. For PRB coal, UBCL ranged from 0% to full load to about 0.3% at very low load. This is not considered a significant impact to overall boiler performance.

Baseline Furnace Exit Gas Temperature

Baseline FEGTs were slightly higher during PRB coal firing as compared to the Lamar testing. Fig. 5 shows increases in temperature of about 35, 90 and 10F at full, medium and low loads, respectively. With reburn operation, FEGT's at full load with Lamar coal were reduced by about 150F. FEGT depression with the PRB coal at full load was less, at about 50F. The difference is thought to be due to the reflective nature of PRB ash deposits in the furnace which reduce heat absorption in the furnace. Overall, FEGT with PRB coal and reburn in operation is very close to that of the bituminous coal baseline, offsetting the normally expected FEGT increase with PRB coal. These temperatures are based upon on-line boiler performance model calculations and confirmed via actual in-furnace temperature measurements.

REBURNING OPERATION

Reburning Test Parameters

Numerous variables are associated with the reburn system and a test matrix was established to determine optimized operation. The subsequent sections discuss the information collected throughout the parametric evaluations of PRB coal. Complete information on Lamar coal as well as test parameters and ranges tested have been presented in earlier papers.[3]

Reburning NO_x/CO Emission Levels

Reburn zone stoichiometry is the most critical factor in changing NO_x emission levels during coal reburning operation. The reburn zone stoichiometry can be varied by altering air flow quantities (oxygen availability) to the reburn burners, by changing the percent of reburn heat input, the gas recirculation flow rate, or the cyclone stoichiometry.

Fig. 6 shows economizer outlet NO_x and CO emissions corrected to 3% O_2 while firing PRB coal. A 50% NO_x reduction was achieved at a reburn zone stoichiometry of about 0.91. As presented in earlier papers[3], the 50% NO_x reduction point for Lamar bituminous coal was achieved at a reburn zone stoichiometry of about 0.89, a more aggressive reducing atmosphere. The data of Fig. 6 also show that the lowest reburn stoichiometry, 0.85, achieved 62.9% NO_x reduction. The CO emission levels increased from 45 ppm at baseline to 92 ppm with reburn operation.

It is apparent that reburning is more effective with PRB coal since a less aggressive reburn zone stoichiometry than that used for bituminous coal achieved 50% NO_x reduction. This infers that either less reburn fuel heat input or higher reburn burner stoichiometries could be used to obtain a given NO_x reduction with PRB coal.

Comparisons between the PRB and the Lamar coal tests for load versus NO_x emissions are shown in Fig. 7. PRB operation achieved lower overall NO_x emission levels and these levels are consistent across the load range. Two factors contribute to the lower NO_x emissions. First, the baseline NO_x levels are approximately 10% less with PRB fuel because of inherent fuel characteristics. Secondly, a higher percentage reduction is realized during reburn operation. This is probably due to the higher fuel volatile content

and increased formation of hydrocarbon radicals in the substoichiometric region of the furnace. A change in overall mixing is also a possible explanation. An important observation from Fig. 7 is that NO_x emissions could be maintained at a constant level over the 110 to 41 MW_e load range during the PRB testing. The higher volatile content made possible more stable reburn burner flame characteristics at lower loads with lower air rates, than were necessary for flame stability with bituminous coal at low load. This allowed lower reburn zone stoichiometries at low load with corresponding improved NO_x reduction.

The direct comparison between the Lamar and PRB coal tests are shown in Tables 1 and 2. This direct comparison is based upon operating the reburn system under similar conditions (e.g., same reburn percentage heat input and reburn zone stoichiometries). Optimizing PRB operation further improved overall NO_x emission levels as shown in the Tables.

Increasing load above 110 MW_e while firing PRB resulted in higher NO_x emissions. At 118 MW_e, the resultant NO_x level was 275 ppm (0.37 lb/10^6 Btu). This increase in NO_x level was due to the fact that a lower percentage of reburn heat input could be supplied as a result of reburn feeder limitations. Also, no baseline NO_x emission levels were obtained at this higher load because the boiler could not accommodate it while firing PRB.

Reburning General Boiler Operation

Even though the project testing program is complete, WP&L continues to operate the reburn system. To compensate for the lower heating value of PRB fuel (8500 Btu/lb), WP&L operates the cyclones within design capacity, and uses the reburn system for an additional 30% coal flow. With this strategy, reburn operation minimized or eliminated the derate impact when switching fuels while accomplishing the primary objective of reducing NO_x emissions. WP&L's typical pre-retrofit low load was about 30 MW_e and without reburn in operation this level was not affected after the retrofit. Due to reburn flame stability issues and the fact that the cyclones have to maintain a minimum firing rate, the low load condition was increased to 37 MW_e with reburn in service. Although not ideal, the resultant boiler turndown was 66% with reburn in operation, exceeding the project's goal of 50% turndown.

Table 3 summarizes the remaining general results observed throughout coal reburn operation while firing both of the tested fuels.

CONCLUSION

The addition of a reburning system, in combination with a switch to Western subbituminous coal may provide utilities with the optimum strategy for both NO_x and SO_2 compliance in cyclone-fired boilers. Switching to lower sulfur content coal will lower SO_2 emissions to Phase I compliance levels, and the addition of the reburning system may negate the 20 to 30% capacity derate normally associated with such a switch. In addition, NO_x emissions are lowered with reburn in operation. The avoided cost of derating a unit could easily justify the price of a reburn system and at the same time allow the utility to achieve NO_x and SO_2 compliance.

Acknowledgements

The authors extend their appreciation to the following people for their help in the management and performance of this study:

- J. M. Campbell, Plant Manager - Nelson Dewey Station
- S. Gebhart, Power Plant Engineer - WP&L
- R. W. Corbett, Technical Project Manager - U. S. Department of Energy

References

1. G. J. Maringo, *et al.*, "Feasibility of Reburning for Cyclone Boiler NO_x Control," EPA/EPRI Joint Symposium on Stationary Combustion NO_x Control, New Orleans, Louisiana, March 23-27, 1987.
2. H. Farzan, *et al.*, "Pilot Evaluation of Reburning Cyclone Boiler NO_x Control, "EPA/EPRI Joint Symposium on Stationary Combustion NO_x Control, San Francisco, California, March 6-9, 1989.
3. A.S. Yagiela, *et al.*, "Results of Babcock & Wilcox's Clean Coal Technology Combustion Modification Projects: Coal Reburning for Cyclone Boiler NO_x Control and Low NO_x Cell™ Burner Demonstrations," 2nd Clean Coal Technology Conference, Atlanta, Georgia, September 7-9, 1993.

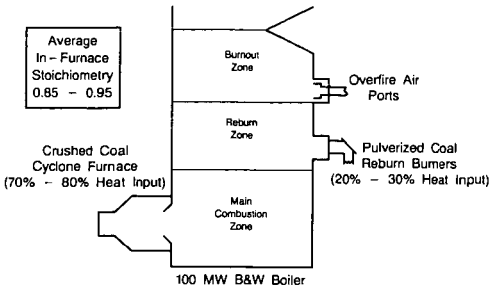

Fig. 1 Cyclone reburn combustion zones.

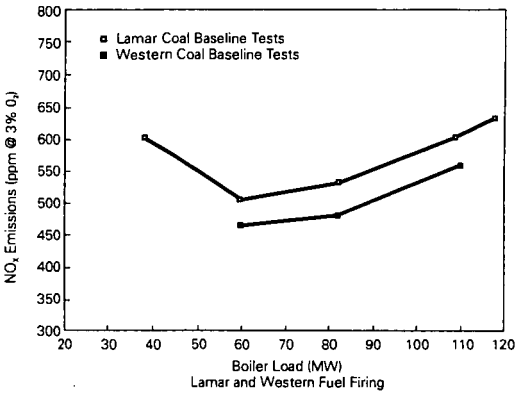

Fig. 2 Wisconsin Power & Light Company Nelson Dewey Station Unit No. 2.

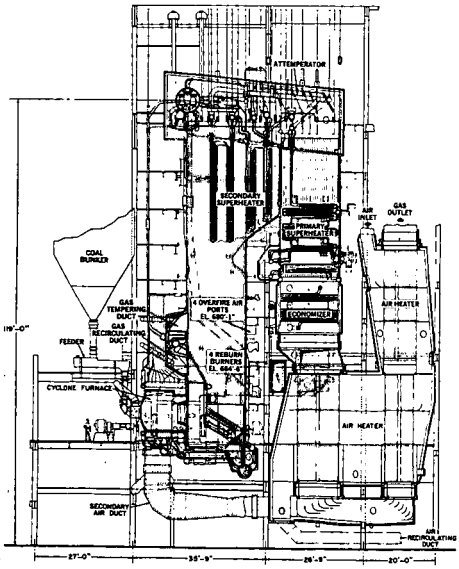

Fig. 3 Baseline NO_x emissions versus load at Nelson Dewey Unit No. 2.

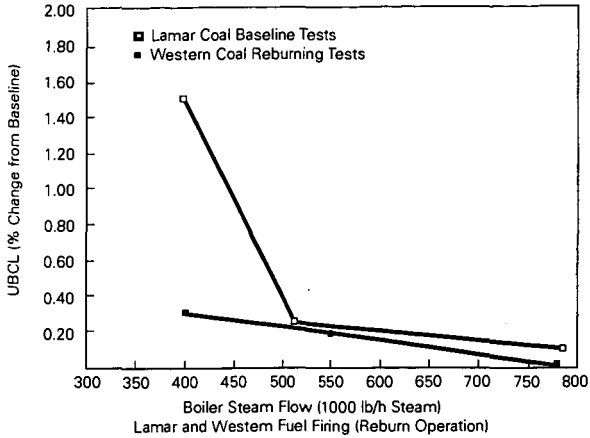

Fig. 4 Unburned carbon (UBCL) efficiency loss (percent change from base) versus load.

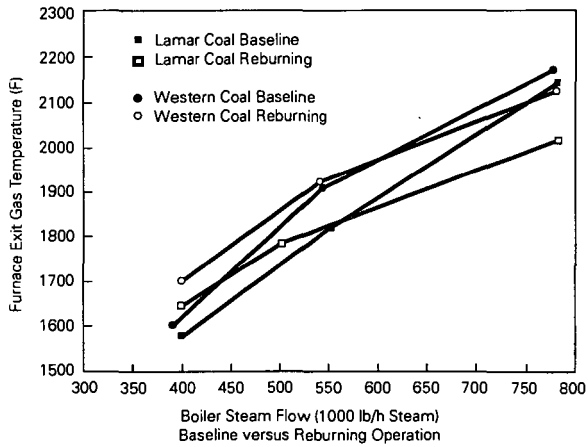

Fig. 5 Furnace exit gas temperature versus load.

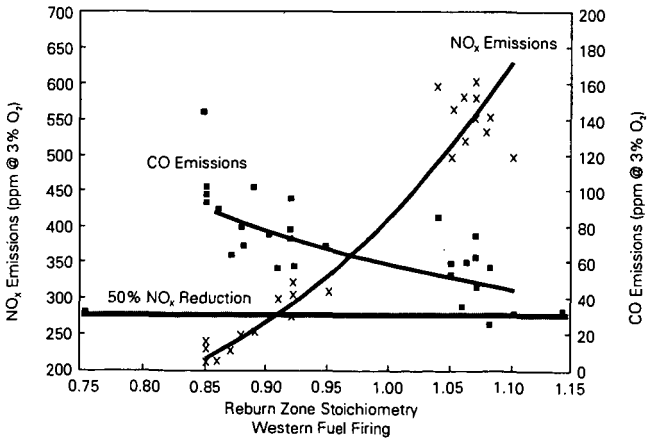

Fig. 6 NO_x and CO emissions versus reburn zone stoichiometry with PRB coal.

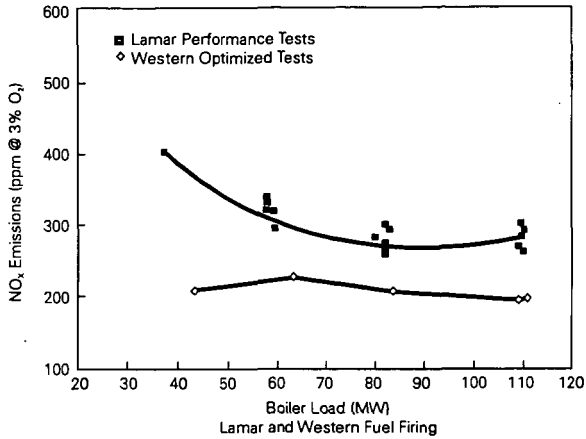

Fig. 7 NO_x emissions at different loads.

Table 1

Reburn NO_x Emissions, ppm at 3% O_2* versus Load					
Load MW_e	Baseline Lamar, ppm	Reburn Lamar, ppm	Baseline PRB, ppm	Reburn PRB, ppm	Optimized Reburn PRB, ppm
110	615	290	560	234	208
82	540	285	480	234	215
60	510	325	465	232	220

* 735 ppm = 1 lb/10^6 Btu NO_x

Table 2

Reburn NO_x Emissions as a Percent Reduction from Baseline versus Load			
Load, MW_e	Lamar Coal	Reburn PRB Coal	Optimized Reburn, PRB Coal
110	52%	58%	62%
82	47%	51%	55%
60	36%	50%	53%

Table 3

Coal Reburning Effects on General Boiler Operation			
Parameter	Anticipated Results	Actual Lamar Results	Actual PRB Results
Slagging/fouling	No change	No change	No change
Header/tube temperatures	25 to 50F higher	No increase from base	No increase from base
SSH and RH spray flows	30% higher	75% lower	25% lower
Opacity	5 to 10% higher	No increase from base	No increase from base
Furnace corrosion	No change	No change	No change
UBCL (full to low load)	Would increase	0.1 to 1.5%	0.0 to 0.3%
FEGT at full load	Would increase	Decrease 100 to 150F	Decrease 25 to 50F

LEGAL NOTICE
The Babcock & Wilcox Company (B&W) pursuant to a cooperative agreement partially funded by the U.S. Department of Energy (DOE) and a grant agreement with IDENR for the DOE and IDENR and neither B&W, DOE, IDENR, nor Southern Illinois University at Carbondale, nor any person acting on their behalf:

a. Makes any warranty or representation, express or implied, with respect to the accuracy, completeness, or usefulness of the information contained in this paper, or that the use of any information, apparatus, method, or process disclosed in this paper may not infringe private-owned rights; nor

b. Assumes any liabilities with respect to the use of, or for damages resulting from the use of, any information, apparatus, method, or process disclosed in this paper.

Reference herein to any specific commercial product, process, or service by tradename, trademark, manufacture, or otherwise, does not necessarily constitute or imply its endorsement, recommendation, or favoring by DOE. The views and opinions of the authors expressed herein do not necessarily state or reflect those of DOE.

EFFECT OF BUBBLE GENERATING DEVICES ON RECOVERY OF CLEAN COAL FROM REFUSE USING COLUMN FLOTATION

B.K. Parekh and J.G. Groppo
Center for Applied Energy Research
University of Kentucky
3572 Iron Works Pike
Lexington, KY 40511

Keywords: Flotation, beneficiation, clean coal, refuse

ABSTRACT

Column flotation testing was conducted on the flotation feed slurry obtained from a preparation plant located in the southern Illinois coal basin using three different bubble generating devices, static sparger, gas saver and foam jet. Each of these devices were tested with three different types of frother and various column operating variables to provide maximum combustible recovery, minimum product ash and maximum pyrite rejection. Alcohol frothers were most effective for use with the static sparger, somewhat less effective for the foam jet and ineffective for the gas saver. Glycol frothers were effective for all three bubble generating systems, providing high combustible recovery (>90 percent), low clean coal ash (4-6 percent ash) and high pyrite rejection (70-80 percent).

INTRODUCTION

Cleaning of fine coal to a very low mineral matter content would have a significant impact on the marketability of high sulfur coals. Most coal preparation plants discard the fine (-28 mesh) coal due to currently available inefficient and uneconomical conventional flotation processes. These fine size refuse slurries are excellent feedstocks for producing low ash, low pyritic sulfur clean coal because the major amount of impurities are liberated.

The column flotation technique has received attention for its ability to provide clean coal containing low mineral matter at high combustible recovery. Yoon,[1] Yang[2] and Christophersen[3] have reported success in removal of high amounts of mineral matter from various fine coals. Parekh et al.[4,5] have reported that using their 'Ken-Flote' column, up to 95 percent of pyritic sulfur was rejected from the Upper Freeport coal at 90 percent combustible recovery.

EXPERIMENTAL PROCEDURES

Samples of the froth flotation feed were collected from the Kerr-McGee Galatia preparation plant in plastic 55-gallon drums. Representative samples of the slurry were analyzed for percent solids, size distribution and proximate analysis. Baseline flotation tests were conducted using a Denver Model D-12 laboratory flotation machine to determine optimum reagent dosages.

For the column flotation studies, a 5 cm (2-inch) ID, 6 m (20-ft.) tall 'Ken-Flote' column was used (Figure 1). A description of the column has been reported elsewhere.[4,5] Figure 2 shows schematics of the three different types of bubble generating devices tested in this slurry. The static sparger was mounted inside the column and required only the addition of air at 0.276 KPa (40 psig). The gas saver was mounted externally and a mixture of air and reagentized water was forced through it. The 'foam jet' was mounted internally, and a mixture of air and reagentized water was forced through a porous metal plug to generate air bubbles.

The three different types of frothers used in the study and their suppliers were:
MIBC: Straight chain alcohol (Shell Oil Co.)
AF76: Mixed alcohols (American Cyanamid Co.)
M150: Glycol-based (Betz Chemical Co.)

RESULTS AND DISCUSSION

The particle size and ash analyses of the Galatia flotation feed are summarized in Table 1. The slurry contained 3.5 percent solids with an average particle size of 21.4 microns and had 41.72% ash.

Baseline flotation data obtained using the Denver flotation machine identified optimum fuel oil dosage to be 0.67 Kg/t (1.5 lb/t), while frother dosage was determined to be 0.33 Kg/t (0.75 lb/t) for each of the three frothers tested. With these dosages, combustible recovery ranged from 82 to 87 percent for the three frothers while the clean coal ash content ranged from 12.2 to 15.6 percent.

Column Flotation Tests

The column operating parameters that were varied were washwater rate, airflow rate and the type of bubble generating system used. Tables 2, 3 and 4 summarize the best results obtained for each of the frothers tested. These results were derived from a number of tests conducted using statistical design experiments.

The results obtained using MIBC and the three bubble generating devices are summarized in Table 2. The static sparger provided 91.4 percent combustible recovery, 5.97 percent clean coal ash and 66.8 percent pyrite rejection when 0.2 L/min washwater and 1.0 L/min airflow were used. Pyrite rejection improved to 76.3 percent when the foam jet was used for bubble generation, however, combustible recovery decreased to 88.4 percent while clean coal ash improved to 5.10 percent ash. MIBC was not suitable for use with the gas saver (64.9 percent combustible recovery and 3.66 percent clean coal ash).

Results obtained with AF76 are summarized in Table 3. When the static sparger was used with 1 L/min airflow and 0.6 L/min washwater, combustible recovery was 89.9 percent with 5.25 clean coal ash and 75.8 percent pyrite rejection. The foam jet provided slightly higher combustible recovery (91.3 percent) with similar clean coal ash (5.20 percent ash) and pyrite rejection (75.5 percent). Optimum airflow requirement for the foam jet with AF76 was 3 L/min while optimum washwater was 0.2 L/min. As with MIBC, AF76 was not a suitable frother for use with the gas saver providing only 47.2 percent combustible recovery.

All the bubble generating devices provided excellent flotation results with M150 frother as shown in Table 4. The static sparger provided 88.6 percent combustible recovery, 6.21 percent clean coal ash and 64.8 percent pyrite rejection. With the gas saver, combustible recovery improved to 91.0 percent, clean coal ash was reduced to 5.68 percent and pyrite rejection improved to 72.5 percent. The best results were obtained with the foam jet which provided 90.1 percent combustible recovery, 4.80 percent ash in the clean coal and 76.9 percent pyrite rejection.

CONCLUSIONS

Based on the experimental data presented, it can be concluded for the Galatia flotation feed that:

- Column flotation provided lower ash (4 to 8%) clean coal product at 90 percent combustible recovery with the three frothers used.
- Column flotation also rejected 50-80 percent pyrite depending on the column operating parameters and the type of frother used. The best results were obtained with the foam jet and M150 frother combination, where 77 percent pyrite rejection was achieved while maintaining 90 percent combustible recovery.
- M150 was an effective frother for all the three bubble generating systems tested, providing high (>90 percent) combustible recovery and low (4-6 percent) clean coal ash content.

ACKNOWLEDGEMENTS

This work was sponsored by the Illinois Department of Energy and Natural Resources through its Coal Development Board and Center for Research on Sulfur in Coal, and the U.S. DOE. The authors would like to acknowledge guidance provided by Dr. Dan Banerjee, Project Monitor, CRSC.

REFERENCES

1. Yoon, R.H. et al., 1990, "Recent Advances in Fine Coal Flotation, Advances in Coal and Mineral Processing Using Flotation, S. Chander and R.R. Klimpel (Eds.), AIME, pp. 211-218.
2. Yang, D.C., 1990, "Packed Bubble Column Flotation of Fine Coal," Coal Preparation, Vol. 8, pp. 19-48.

3. Christophersen, J.A., and A.J. Jonaitis, 1990, "Diester Flotaire Column Flotation Cell - Plant Experience," Advances in Coal and Mineral Processing Using Flotation, S. Chander and R.R. Klimpel (Eds.), AIME, pp. 113-119.
4. Parekh, B.K., A.E. Bland, J.G. Groppo and J. Yingling, 1990, "A Parametric Study of Column Flotation for Fine Coal Cleaning," Coal Preparation, Vol. 8, pp. 49-60
5. Parekh, B.K., A.E. Bland, and W.F. Stotts, 1988, "Advanced Froth Flotation Cell Design: 'Ken-Flote' Column Performance on Ultrafine Coal," submitted to U.S. DOE, Pittsburgh, PA.

Table 1. Analysis of Kerr-McGee Galatia Flotation Feed

SIZE FRACTION (Mesh)	WEIGHT PERCENT	PERCENT ASH	ASH DISTRIBUTION (Percent)
+200	15.2	7.00	2.5
-200+325	9.4	13.10	2.9
-325+500	8.4	17.45	3.5
-500	67.0	56.66	91.1
Calc Feed	100.0	(41.72)	100.0

Table 2. Optimum Results Obtained with Column Flotation of the Galatia Slurry Using MIBC Frother

BUBBLE GENARATOR	AIRFLOW (lpm)	WASHWATER (lpm)	COMBUSTIBLE RECOVERY %	CLEAN COAL ASH %	PYRITE REJECTION %
SPARGER	1.0	0.2	91.4	5.97	66.8
GAS SAVER	2.0	0.2	64.9	3.66	ND
FOAM JET	1.0	0.2	88.4	5.10	76.3

Table 3. Optimum Results Obtained with Column Flotation of the Galatia Slurry Using AF76 Frother

BUBBLE GENARATOR	AIRFLOW (lpm)	WASHWATER (lpm)	COMBUSTIBLE RECOVERY %	CLEAN COAL ASH %	PYRITE REJECTION %
SPARGER	1.0	0.6	89.9	5.25	75.8
GAS SAVER	2.0	0.2	47.2	3.32	ND
FOAM JET	3.0	0.2	91.3	5.20	75.5

Table 4. Optimum Results Obtained with Column Flotation of the Galatia Slurry Using M150 frother

BUBBLE GENARATOR	AIRFLOW (lpm)	WASHWATER (lpm)	COMBUSTIBLE RECOVERY %	CLEAN COAL ASH %	PYRITE REJECTION %
SPARGER	1.0	0.2	88.8	6.21	64.8
GAS SAVER	1.0	0.2	91.0	5.68	72.5
FOAM JET	2.0	0.4	90.0	4.80	78.9

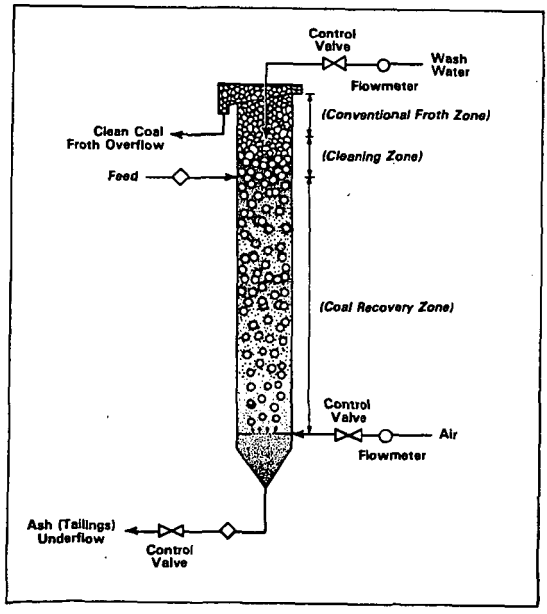

Figure 1. Line Diagram of the 'Ken-Flote' Column Flotation Cell.

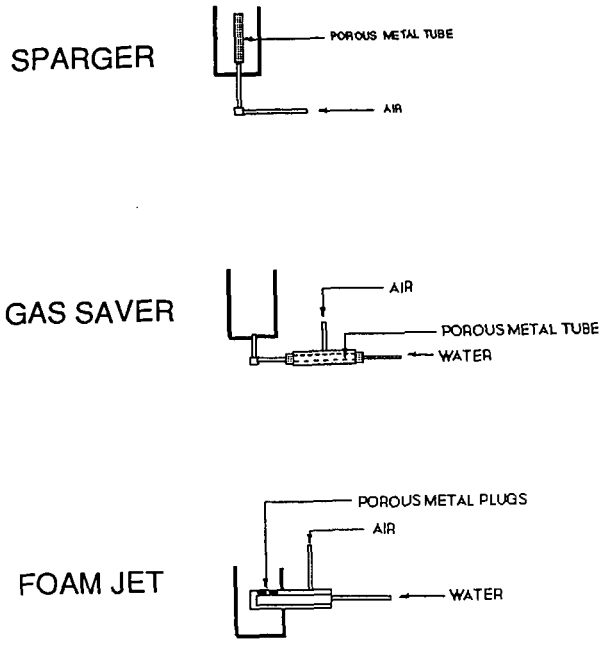

Figure 2. Diagrams of the Three Bubble-Generating Devices Utilized in Column Flotation Testing.

DEEP CLEANING OF A hvA BITUMINOUS COAL USING A POLYETHYLENE OXIDE/POLYPROPYLENE OXIDE BLOCK CO-POLYMER

H. Polat, M. Polat and S. Chander
Mineral Processing Section
Penn State University
University Park, PA 16802

Keywords: Bituminous Coal, Flotation, Block Co-polymer

ABSTRACT

Deep cleaning of a hvA bituminous coal using flotation process was investigated in this study. A -1/4 inch raw coal containing about 35% ash was subjected to initial flotation tests at nominal feed sizes of -600 μm and -212 μm. In both cases a clean coal product of 13% ash with a combustible matter recovery of about 80% was obtained. Since the ash content was much too high for deep cleaning, a second sample which was the product of a conventional coal preparation plant was used in subsequent studies. It contained about 7% ash. The material was wet ground to nominal feed sizes of -600 μm, -212 μm and -65 μm, respectively, and floated using n-dodecane as collector. The reduction in ash was marginal for the -600 μm and -212 μm coals. However, a clean coal product of 3.9 % ash could be obtained with a high yield using -65 μm feed. The product quality was further improved by introducing a mild oil agglomeration stage prior to flotation and by using an ethylene oxide/propylene oxide block copolymer as an additive. The ash content of the clean coal so obtained was 2.5% with a combustible matter recovery of about 76%.

INTRODUCTION

A super clean coal is considered to be of practical importance in many industrial applications such as liquefaction, coal/water slurries, etc. Liberation of combustible matter from ash forming minerals by size reduction is a necessary step in deep cleaning. In some cases fine grinding to particle sizes less than 100 μm might be required to achieve a satisfactory liberation. With decrease in particle size, the effectiveness of conventional coal cleaning methods mainly involving gravity diminishes. The coal recovery decreases, selectivity becomes poor, and medium recovery becomes a problem. Coal flotation is one of the most promising method for cleaning material at fine sizes. Use of an oily collector and other reagents is often necessary to enhance the hydrophobicity of coal and to promote its flotation. When oil is used alone it might also increase the hydrophobicity of the ash minerals and result in a decrease in the selectivity of the flotation process. It is generally recognized that selectivity of coal flotation does not improve below particle sizes of 100 μm (Crawford, 1936; Davis, 1948; Miller, 1964; Raleigh and Aplan, 1991). Two methods might be used to improve efficiency of separation: I. Decrease floatability of ash forming minerals by the use of dispersants and depressants. II. Increase the floatability of coal by reagents that make coal more hydrophobic. Method I was been demonstrated by Yancey and Taylor, 1935; Zimmerman, 1948; Miller, 1964; Choudhry and Aplan, 1990; Aplan, 1989; Perry and Aplan, 1985, 1988; Arnold and Aplan, 1989.

In this study, Method II was employed to increase the efficiency of coal cleaning by flotation. An ethylene oxide/propylene oxide (PEO/PPO) block co-polymer was used as a reagent to increase the hydrophobicity of flotation in the presence of oily collector. Utilization of a mild oil agglomeration stage prior to flotation was also investigated to further promote the ash rejection.

EXPERIMENTAL PROCEDURE

Flotation

A Wemco Model 71260-01 flotation machine was used in the flotation experiments. The stirrer speed was kept constant at 1000 rpm. The solids concentration in the flotation feed was 10% by weight. The flotation pulp was conditioned for 3 minutes to disperse the coal. Dodecane was added in required amounts as the oily collector and the pulp was conditioned for additional 3 minutes. The desired quantity of surfactant was added as an aqueous solution. After conditioning with the surfactant and dodecane, 0.5 kg/T methyl isobutyl carbinol (MIBC) was added as the frother. The slurry was further conditioned for 2 more minutes prior to introduction of air into the cell. The froth was removed at preset time-intervals for a total of 8 minutes. The natural pH of the pulp was 8.0 and no pH adjustments were made throughout the experiments. The flotation products were filtered, dried, weighed and analyzed to determine their ash content.

To prepare the flotation feed, a rod mill was used to wet grind the sample from 1/4 inches to the nominal feed sizes of -600 μm and -212 μm. To prepare the -65 μm feed, a Bleuler mill was employed. The grinding time was determined through prior grinding tests.

Mild Oil Agglomeration

A mild oil agglomeration of the coal slurry prior to flotation was performed in an attempt to further decrease the ash content. For this purpose, dodecane and a solution of block co-polymeric surfactant was emulsified in a blender for 3 minutes. A coal slurry of 400 ml (1% solid) was added into this solution and blending was continued for 3 more minutes to produce loose agglomerates of coal particles. The slurry was than transferred into the flotation cell and flotation experiments were carried out by addition of frother only.

MATERIALS

Coal Samples

The run-of-mine and clean coal samples were obtained from Emerald Mine in Pittsburgh, PA. The coal was a hvA bituminous sample of Pittsburgh seam. The ash and sulfur contents are given in Table 1.

Surfactants

Two different polymeric surfactants from BASF Cooperation were used in this study to enhance the rejection of ash minerals from coal. These were water soluble and added to the pulp as an aqueous solution. The number of hydrophobic and hydrophilic groups and other properties are given in Table 2. The molecular structure of this type of surfactants is given in Figure 1. Dodecane from Aldrich Chemical Company was used as the oily collector. The frother used in this study was methyl isobutyl carbinol (MIBC) obtained from Shell.

RESULTS AND DISCUSSIONS

Flotation of Raw Coal

Initial flotation studies were performed using a raw coal containing 35% ash from Emerald Mine, Pittsburgh at nominal feed sizes of -600 μm and -212 μm using dodecane as the collector. The results are presented in Figure 2. The decrease in ash was not satisfactory for both the -600 μm and -212 μm feed materials. A clean coal product of about 12 to 13% ash with a combustible recovery of about 80% was obtained. This observation was in agreement with other studies where no improvement in the product quality was observed with decreasing feed size (Crawford, 1936; Davis, 1948; Miller, 1964, Raleigh and Aplan, 1991). It is possible that even though grinding to a smaller sizes increased liberation, the problems associated with flotation of fine particles increased. Further cleaning of this sample was not attempted. Instead a clean coal sample from a processing plant with 7.0% ash was used.

Flotation of Precleaned Coal

Flotation studies in the presence of dodecane

The second sample tested in this study was a pre-cleaned hvA bituminous coal which was obtained from a conventional coal preparation plant and had an ash content of 7.0%. Similar to the raw coal sample, flotation studies were conducted at various feed sizes in the presence of dodecane as collector. The results of flotation studies are given in Figure 3. As one can see, the reduction in ash was minimal for the -600 μm and -212 μm feed materials. However, a clean coal product of about 3.9 % ash could be obtained with a combustible matter recovery of 75% for the -65 μm feed after 2 minutes of flotation. These results show that an increase in selectivity is possible with improved liberation. In order to further decrease the ash content of the sample two surfactants were employed for the -65 μm feed material.

Flotation Studies in the Presence of Dodecane and Block Co-polymers Surfactants

Aliquots of aqueous solutions of the PEO/PPO block co-polymers (BC3 & BC7) and the collector were added simultaneously to the flotation cell. The results are given in Figure 4 for the two polymeric surfactants. For comparison, the flotation data for dodecane alone is also included. It can be seen that the presence of the polymeric surfactants substantially enhanced the ash rejection. A clean coal with an ash content of 2.9% and a combustible matter recovery of 75% could be obtained in the presence of BC3 after 2 minutes of flotation. The corresponding ash was 3.1% for BC7. The amount of ash rejection was found to be a function of both surfactant type and concentration.

Flotation Studies Preceded by a Mild Oil Agglomeration Stage

In this series of tests, the coal slurry was agitated in a blender to produce loose agglomerates of coal particles. The surfactant, BC7, concentration was same as in previous tests. The agglomerated mass was floated and the results are presented in Figure 4. It can be seen that the product quality improved substantially. A clean coal product of 2.5% could be obtained with a recovery of 75%. A more significant advantage of the pre-agglomeration stage was a substantial increase in rate of flotation. To quantify this effect flotation rates were obtained by plotting flotation yield as a function of flotation time and the data were fitted to a first order model with a rectangular distribution of floatabilities (Huber-Panu et al., 1976; Klimpel, 1980). The mathematical form of this model is given by:

$$R_{(t)}=R_{\infty}\{1-[(1-e^{-kt})/kt]\}$$

where $R_{(t)}$ is the recovery at time t, R_{∞} is the ultimate recovery and k is a rate constant. The parameters estimated by the model are given in Table 3. The mean residual square (MRS) errors were somewhat high but the use of alternate models, namely, classical first order, first order with sinusoidal and normal distributions of floatabilities (a summary of these models is given by Miller et al., 1993) gave even higher fitting errors. It can be seen that the ultimate recovery is somewhat similar (around 100%) for all the cases. The flotation rate is between 2 and 3.5 min^{-1} for the test where flotation was employed only. Use of a mild agglomeration stage significantly accelerated the kinetics of flotation. The flotation rate obtained for this case was 10.66 min^{-1}. It is interesting to note that this increase in the rate of flotation was also accompanied with a decrease in the ash content, showing the effectiveness of the agglomeration stage.

CONCLUSIONS

Flotation processing of a hvA bituminous coal was investigated for coals ground to several feed sizes. To improve the influence of PEO/PPO block co-polymers, the selectivity of separation was studied. Based on these tests, the following conclusions were made:

- For the raw coal sample, no improvement in the ash rejection was observed with decrease in feed size. An ash content of 12 to 13% with a combustible matter recovery of about 80% was obtained.
- In case of clean coal, the reduction in ash was marginal for the -600 μm and 212 μm coals. However, for the -65 μm feed a clean coal product of 3.9% ash was obtained with a high yield.
- The clean coal quality was improved further by addition of block co-polymers. The ash content of clean coal so obtained was 2.9% for BC3 and 3.1% for BC7 with a combustible matter recovery of about 75%.
- When a mild oil agglomeration was used prior to flotation the clean coal quality improved further. The clean coal ash content so obtained was 2.5% with a combustible matter recovery of about 76%. In addition, the use of the agglomeration stage resulted in a significant increase in the rate of flotation.

ACKNOWLEDGEMENTS

The authors acknowledge the support from the Mineral Processing Section, The Pennsylvania State University and DOE Cooperative Agreement No: DE-FC22-92PC92162. Receipt of reagent samples from BASF Corporation and Shell Oil Company is also acknowledged.

REFERENCES

Aplan, F. F., 1989, Coal Flotation-The Promise and the Problems, Advances in Coal and Mineral Processing Using Flotation, S. Chander and R.R Klimpel, eds., Littleton, CO, SME-AIME, pp. 95-104.

Arnold, B. J. and Aplan, F. F., 1989, The Use of Pyrite Depressants to Reduce the Sulfur Content of Upper Freeport Seam Coal, Proceedings of Processing and Utilization of High Sulfur Coals, III, R. Markuszewski and T. D. Wheelock, eds., Ames, IA, Elsevier, Amsterdam, pp. 171-185.

Choudhry, V. and Aplan, F. F., 1990, The Depression of Pyrite During Coal Flotation, Manuscript submitted to Minerals & Metallurgical Processing.

Crawford, J. T., 1936, Importance of Pulp Density, Particle Size and Feed regulation in Flotation of Coal, Transactions, AIME, Vol. 119, pp. 150-162.

Davis, D. H., 1948, Froth Flotation of Minus 48 Mesh Bituminous Coal Slurries, Transactions, AIME, Vol. 177, pp. 320-337.

Huber-Panu, I., Ene-Danalache, E. and Cojocariu, D. G., 1976, Mathematical Models of Batch and Continuous Flotation, Flotation-A.M. Gaudin Memorial volume, ed. M.C. Fuerstenau, New york, NY: AIME, pp. 675-724.

Klimpel, R. R., 1980, Selection of Chemical Reagents for Flotation, Mineral Processing Plant Design, 2nd Edition, A. L. Mular and R. B. Bhappu, eds., AIME, New York, New York, Chapter 45, pp. 907-934.

Miller, F. G., 1964, Reduction of Sulfur in Minus 28 Mesh Bituminous Coal, Transactions, AIME, Vol. 229, pp. 7-15.

Miller, B. G. et al., 1993, The Development of Coal-Based Technologies for Department of Defence Facilities, DOE Interim Report for Project DE-FC22-92PC92162, 110 pp.

Perry, R. W. and Aplan, F. F., 1985, Polysaccharides and Xanthated Polysaccharides as Pyrite Depressants During Coal Flotation, Proceedings of the International Conference on Processing and Utilization of High Sulfur Coals, Attia, Y.A., ed., Elsevier, Amsterdam, pp. 367-393.

Perry, R. W. and Aplan, F. F., 1988, Adsorption of Polysaccharides and Related Compounds onto Coal and Their Effect on the Flotation of Coal and Pyrite, Separation Science and Technology, Vol. 23, pp. 2097-2112.

Raleigh, Jr. C.E. and Aplan, F.F., 1991, Effect of Feed Particle Size and Reagents on Coal-Mineral Matter Selectivity During the Flotation of Bituminous Coals, Minerals & Metallurgical Processing, Vol. 290, pp. 82-90.

Yancey, H. F. and Taylor, J. A., 1935, Froth Flotation of Coal: Sulfur and Ash Reduction, US Bureau of Mines, R.I. 2363.

Zimmerman, R. E., 1948, Flotation of Bituminous Coal, Transactions, AIME, Vol. 177, pp. 338-355.

Table 1. A summary of the coal samples used in the study.

Coal samples	Ash (%)	Sulfur (%)
Pittsburgh (Clean coal)	7.0	1.32
Pittsburgh (Raw coal)	35.0	1.85

Table 2. Selected properties of the surfactants used in this study.

Surfactant	Code	Number of hydrophobic groups (PPO)	Number of hydrophilic groups (PEO)	M.W.	HLB*	Surface tension, dyne/cm
Ethylene oxide/ propylene oxide block co-polymer	BC3	30	26	2650	11	43.0
	BC7	56	60	5900	13	33.0

* *Hydrophile-lipophile balance.*

Table 3. The ultimate yields, flotation rates and mean residuals for fitting the first order kinetics equation with rectangular distribution of floatabilities.

	Dodecane (0.07 kg/T)	BC3 (0.1 g/T)	BC7 (20 g/T)	Aggl. & Flotation
R_∞	100.0	99.4	94.3	100.0
k	3.45	2.34	1.97	10.66
MRS*	3.14	8.97	25.56	17.80

* *Mean residual square*

Figure 1. Structural formula of PEO/PPO block co-polymers used in this study.

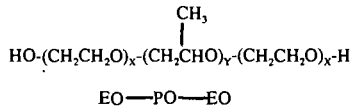

X = Number of moles of ethylene oxide
Y = Number of moles of propylene oxide

Figure 2. Combustible matter-ash recovery curves for the run-of-mine sample of Pittsburgh seam coal.

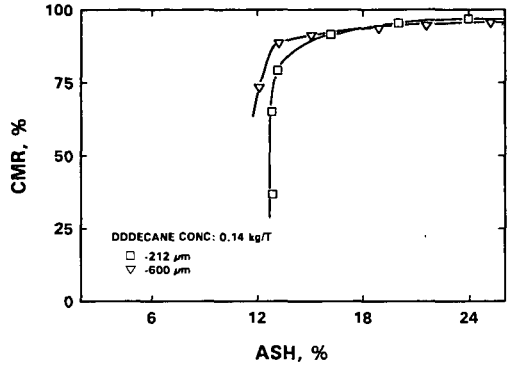

Figure 3. Combustible matter-ash recovery curves for the pre-cleaned sample of Pittsburgh seam coal.

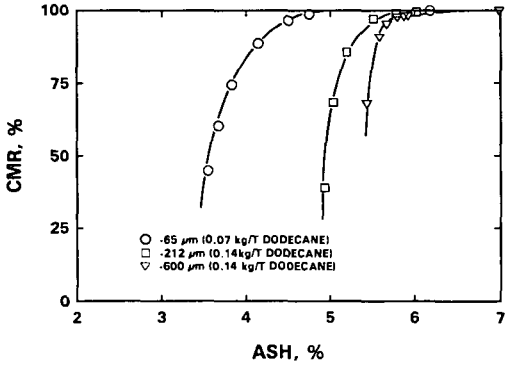

Figure 4. Effect of PEO/PPO block co-polymers on the combustible matter recovery and ash content.

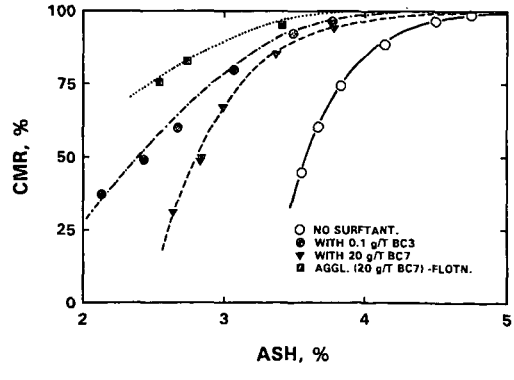

EFFECT OF CHEMICAL TREATMENTS ON BENEFICIATION OF LOW RANK COALS

M. Polat*, S. Chander* and D. C. Cronauer**
* Mineral Processing Section
Penn State University
University Park , PA 16802

** Amoco Oil Company
Research and Development Department
PO Box 3011
Naperville, IL 60566

Keywords: Lignite, flotation, sulfurous acid treatment

ABSTRACT

Cleaning of low rank coals is desirable for preparation of feed stock for liquefaction of coal. In this investigation, the effect of chemical pretreatment on the beneficiation of low rank coals was studied. In the first phase of the research, a lignite sample from Texas with an ash content of 12.9% was pretreated with sulfurous acid prior to separation. Treated coal was subjected to flotation or Liquid-Liquid Extraction (LLE) for further cleaning. A final clean coal product of 4.4% ash was obtained with a combustible matter recovery of about 95%. In the second phase, a chemically treated low rank coal sample with 3.3% ash was further cleaned using a mild agglomeration stage prior to flotation. When a non-ionic, block co-polymer surfactant was used with the oily collector, a clean coal product of 1.85% ash could be obtained with a combustible matter recovery of over 85%.

INTRODUCTION

It is well known that lignites are very difficult to clean from the mineral matter using conventional flotation due to their poor floatability. According to Sun (1954) the floatability index of lignites was 12 taking Ceylon Graphite with an index of 100 as standard. The average floatability index for hvA bituminous coals was 94 on the same scale. The poor floatability was also confirmed by Aplan (1976, 1980 and 1988) who observed that the measured contact angle using captive bubble method was zero for lignites. Use of an oily collector alone does not improve the floatability due to low adsorption of oil on lignites (Sun, 1954; Gayle et al, 1965). This is most probably due to high oxygen content of lignites and the abundance of surface functional groups (Fuerstenau et al, 1983; Gutierrez-Rodriguez and Aplan, 1984 and Schobert, 1990). It was reported that the average oxygen content of lignites could be as high as 30%, carboxylic groups constituting about half this amount (Quast and Readett, 1987). Another important consequence of the presence of the surface functional groups is that these groups act as ion exchange sites for cations such as Na, Ca, Mg and K, and may result in the accumulation of carbonaceous ash. In general 90 - 100% of the Na, 75 -90% of the Mg, 50 - 75% of the Ca and 35 - 50% of the K in low rank coals may be accumulated by the ion exchange process (Schobert, 1990). These cations which are bonded to the organic portion of the coal as inherent ash are practically impossible to clean using conventional separation techniques.

Chemical treatment of lignites prior to separation may be beneficial due to dissolution of these ion exchange cations, resulting a direct decrease in the ash content. Different types of pretreatment have been suggested in the literature. Mochida et al showed that pretreatment of lignites using HCl improved their conversion during coal liquefaction (1983). Cronauer et al utilized sulfurous acid to chemically clean the lignites (1991). The authors suggested that sulphurous acid converts carboxylic salts to free carboxylic acids through the following reaction:

$$(R\text{-}COO)_2Ca + 2H_2SO_3 \longrightarrow 2R\text{-}COOH + Ca(HSO_3)_2$$

It was pointed out that sulfurous acid was cheap, less corrosive and easily recoverable. In addition to dissolving the cations from the coals structure, the dissolution process may change the floatability of lignite due to its effect on the surface functional groups.

Objective of this study was to investigate deep cleaning of lignites using a combination of chemical dissolution and physico-chemical separation methods. The study was conducted in two parts. In the first part a raw lignite sample was subjected to chemical treatment using sulfurous acid under a variety of conditions. The treated sample was then further cleaned using Liquid-Liquid Extraction (LLE) method using heptane as the carrier liquid. In the second part a pretreated lignite sample was subjected to cleaning using flotation or mild oil agglomeration followed by flotation, MOAF. A block co-polymer surfactant was also used in this part of the study to improve ash rejection.

EXPERIMENTAL

Material

The raw lignite sample used in the first part of the study was obtained from Amoco Company, Naperville, IL and originated from Martin Lake, Texas. The sample had an ash content of 12.9% and was less than 6.35 mm in particle size. A semi-quantitative spectroscopic analysis on the ashed lignite showed that the ash material contained about 10% Ca, 5% Mg and 1% Na. The Si content was around 2%. The sample was ground to a feed size of -150 μm to be used in the flotation and LLE studies.

The coal sample used in second part of the study had been pretreated by the Amoco Oil Company with sulfurous acid and had an ash content of about 3.3% . It is referred as Sample No. 2 and had a narrow size distribution of 212x1650 μm. It was wet ground to various feed sizes for the flotation or mild oil agglomeration-flotation studies.

A polypropylene/polyethylene block co-polymer surfactant was used to enhance the ash rejection during flotation or mild oil agglomeration-flotation studies. This surfactant was previously shown to be very selective in the flotation of a low rank coal (Chander et al, 1993). It was added to the system in an oil-dispersed form. The chemical structure of the surfactant is given in Figure 1.

Methods

Liquid-Liquid Extraction

The process of Liquid-Liquid Extraction (LLE) involves selective transfer of hydrophobic particles of organic matter from aqueous phase to an emulsion phase. This process is especially useful at fine sizes (Hsu and Chander, 1988). The tests were conducted in a baffled, 500 ml vessel of standard geometry (Holland and Chapman, 1966). The vessel was slightly tapered at the bottom to allow for easy removal of the separated phases. The total solution volume in a given test was 400 ml. The slurry contained 1% solids by weight and 15% heptane as the organic phase. Following initial conditioning to wet and disperse the lignite, the desired reagents were added and the slurry was conditioned 10 more minutes. Heptane was added and the stirring was continued for preset periods of time at a selected stirrer speed. Finally, the emulsion phase containing the coal particles was allowed to separate out from the aqueous phase containing the mineral matter. Both phases were removed from the bottom of the vessel, filtered, dried and analyzed. Practically all the heptane was recovered from the emulsion phase during the filtering step.

Flotation

A Wemco model 21260-01 flotation machine equipped with a 1 liter cell was used in the flotation experiments. The impeller speed was kept constant at 1000 rpm in all the flotation tests. The solid concentration was kept constant at 5% when flotation was used alone. For the tests where a mild oil agglomeration step was utilized prior to flotation, the solid concentration in the flotation cell was determined by the amount of solids in the agglomeration stage. The slurry was preconditioned for 3 minutes before any reagent addition. Dodecane and methylisobutylcarbinol (MIBC) were used as the oily collector and frother, respectively. The experiments were carried out at the natural pH of the slurry which was mostly on the acidic side due to prior acid treatment. The flotation products were dried, weighed and analyzed.

Mild Oil Agglomeration Flotation

A limited number of tests were performed in which a mild agglomeration stage was combined with flotation. This process is referred to as MOAF in this article. In this procedure the conditions were chosen such that the coal particles were agglomerated in a high shear environment to produce loose agglomerates of about one millimeter in diameter. For this purpose dodecane or dodecane-block co-polymer surfactant solution was emulsified in a blender for three minutes. A coal slurry of 400 ml of varying solids content was added into this solution and the blending was continued for 3 more minutes. This procedure produced loose agglomerates of the coal particles. The slurry containing the agglomerates was transferred into the flotation cell and flotation tests were carried out by addition of frother only. In some cases, dodecane-surfactant mixture was added directly to the coal slurry prior to any blending procedure.

RESULTS AND DISCUSSIONS

Studies with the Raw Texas Lignite Sample

Pretreatment with Sulfurous Acid

A 6.0% aqueous solution of SO_2, sulfurous acid (H_2SO_3), was utilized to dissolve the cations from the coal structure. The experiments were conducted at different acid concentrations and temperatures using a nominal -150 μm feed material. An optimum decrease in the ash content was observed at an acid concentration of 1.0% at 50°C. Under these conditions the ash content of the lignite sample decreased from 12.9% down to about 6.5% with a combustible matter recovery of almost 100%. A semi-quantitative spectrographic analysis conducted on the as-received and H_2SO_3 treated samples showed that there was approximately a ten-fold decrease in the Ca, Mg and Na contents of the lignite sample, supporting the reverse extraction of the cations from the carboxylate structure. The fact that the Na content also decreased substantially is an important result since sodium is known to cause slagging problems in combustion.

Both the as-received and the chemically treated samples were subjected to zeta potential measurements in order to determine the effect of chemical treatment on the electrokinetic behavior. A Lazer Zee Meter from Pen Kem Inc., New York, was used for this purpose. It was observed that the point of zero charge of the as-received sample was around a pH of 2.4. This was in a good agreement with the data in the literature (Arnold and Aplan, 1989). The point of zero charge decreased with increasing concentration of H_2SO_3 and found to be around a pH of 1.8 for an acid concentration of 6.0%.

In order to determine the effect of the acid treatment on the floatability of the lignite sample contact angle measurements were conducted using a method first described by Wei et al (1992). In this method a particle was gently placed at the air-water interface and the cross sectional areas of both parts of the particle above and below the interface were measured with a microscope coupled to an image analyzer. The ratio of these areas are related to the contact angle. To prepare the sample for the contact angle measurements a sufficient amount of lignite sample was screened to obtain a narrow size fraction of 600x850 μm. Half of this sample was treated with distilled water whereas the other half was treated with 1.0% sulfurous acid. The samples were dried in a vacuum oven at room temperature. Measurements conducted on about 150 particles for each sample showed that the mean advancing contact angle increased from 62 degrees for the untreated coal to 72 degrees for the H_2SO_3 treated coal. This apparent increase in the contact angle suggests that the sulphurous acid treatment results in an increase in the hydrophobicity of the lignite sample.

Flotation

Flotation experiments were carried out using both the untreated, 12.9% ash, and the H_2SO_3 treated, 6.5% ash, samples. The feed size of the both samples was -150 μm. The concentration of dodecane and MIBC were 20 kg/T and 0.8 kg per ton of coal, respectively. The flotation tests were carried out at the natural pH values of 6.3 for the raw sample and 4.4 for the H_2SO_3 treated sample. A quartz depressant, Na_2SiO_4, was also used in the flotation tests. It was observed that the untreated sample could not be beneficiated using flotation. The ash content of the product was 12.6% after 8 minutes of flotation with a coal recovery of 50.4 in the presence of 0.4 kg of Na_2SiO_4 per ton of coal. The flotation response of the treated sample was also not very promising. The ash content of the clean coal product was about 5.5% when the coal recovery was 95%. The high coal recovery obtained in the case of the treated sample was in agreement with the observation stated in the preceding section that acid treatment should enhance the floatability of the lignite sample. Since no satisfactory results were obtained using flotation, LLE method was employed in subsequent tests.

Liquid-Liquid Extraction

In this series of tests, heptane was emulsified with lignite slurry in a standard vessel. The lignite particles were extracted in the hydrocarbon to form an emulsion phase. Upon completing the transfer of coal particles from aqueous phase into the emulsified heptane phase, the mixing was stopped and the phases were allowed to separate. The emulsion containing the coal particles was separated from the aqueous phase which contained the mineral matter. The LLE experiments were carried out under a variety of test conditions with the sulfurous acid treated lignite sample which contained 6.5% The variables tested included pH, stirrer speed, mixing time and depressant type and concentration. The best ash rejection was obtained at the natural pH value of the sample and at a stirrer speed of 1800 rpm. The subsequent testing was carried out under these conditions. The result of the mixing time experiments are given in Table 1. It can be seen that the ash content of the product does not vary appreciably whereas the combustible matter recovery steadily increases

with increasing mixing time.

Sodium silicate and sodium dicarbonate were used as depressants at different concentrations to increase the efficiency of separation. In the case of Na_2SiO_4 a clean coal product of 4.6% ash with a combustible matter recovery of 94% was obtained at a Na_2SiO_4 concentration of 0.13 kg per ton of coal. The results obtained with $Na_2Cr_2O_7.2H_2O$ were slightly better. A clean coal product of 4.4% ash was obtained with a combustible matter recovery of 95% at a $Na_2Cr_2O_7.2H_2O$ concentration of 0.25 kg per ton of coal.

Studies with the H_2SO_3 Treated No. 2 Sample

The sample was processed using conventional flotation or mild oil agglomeration flotation, MOAF in order to further reduce the ash content. The quality of separation was increased in both cases when a block co-polymer surfactant was added into the oily collector. The results of these studies are given in the following paragraphs.

Flotation

The sulfurous acid treated sample was ground to a nominal feed size of -150 μm and floated at a natural pH of 2.9. A clean coal product of 2.2% ash was obtained with a combustible matter recovery of 70% when the concentration of the oily collector was 4.0 kg per ton of coal. The ash content did not change with an increase in the oil concentration up to 40 kg per ton of coal. However, the combustible matter recovery slightly increased to 74%. When 0.8 kg of a block co-polymer surfactant was added into 4.0 kg of oil per ton of coal, the combustible matter recovery increased to 87% and the ash content of the clean coal was 2.2%. The ash content of the pretreated coal sample could not be reduced to less than 2.0% when additional flotation studies were performed. Hence, a mild oil agglomeration stage was used prior to flotation step.

Mild Oil Agglomeration Flotation

Initial MOAF tests were carried out to determine the best particle size for ash rejection. The concentration of the oily collector and the surfactant were 250 kg and 8 kg per ton of coal, respectively. Three different feed sizes of -150 μm, -60 μm and -38 μm were tested in these experiments. The results are given in Table 2. It was observed that a clean coal product of 2.0% ash could be obtained with a combustible matter recovery of 85% when the nominal feed size was -38 μm. Neither the ash nor the coal recovery was better for the other two feed sizes. Hence, subsequent studies were carried out using a feed size of -38 μm. In the next set of MOAF tests, sodium hexametaphosphate (calgon) was added into the coal slurry to promote dispersion of the coal particles. The collector and the surfactant concentrations were kept the same as before. Calgon concentrations of 0.02 kg, 0.1 kg, 0.5 kg and 2.0 kg per ton of coal were tested. The results of these tests are given in Table 3. It can be seen that addition of the dispersant improved the separation appreciably. A clean coal product of 1.94% ash could be obtained with a coal recovery of 92% when 0.5 kg of calgon per ton of coal was added. In order to determine the effect of the block co-polymer surfactant, the concentration of the surfactant was varied keeping the oil concentration constant at 250 kg per ton of coal. The amount of surfactant used was 0, 2, 8, 8 and 25 kg per ton of coal, respectively. The results are given in Table 4. It was observed that increasing the amount of the surfactant in the system decreased the ash content while increasing the combustible matter recovery. The surfactant amount of 25 kg per ton of coal resulted in a better product. In another set of experiments the oil to surfactant ratio was kept constant at 10. The oil amounts in these tests were 125, 250 and 500 kg per ton of coal. The ash contents and the combustible matter recoveries for these tests are given in Table 5.

In the above tests the emulsification of oil-surfactant solution was carried out in the presence of the coal slurry. A different set of experiments was conducted where the oil-surfactant solution was emulsified for 3 minutes prior to the addition of the coal slurry in order to reduce the amount of surfactant and oil used in the process. The coal slurry was added to this emulsified phase and the agglomeration was initiated. The experiments were carried out using the same oil to surfactant ratio of 48. The oil amounts employed in this set were 48, 96 and 192 kg per ton of coal. The results of these experiments are given in Table 6. It was seen that pre-emulsification decreased the amount of surfactant required for separation. A clean coal product of 1.85% ash could be obtained with a coal recovery of 85% using 192 kg of oily collector with 2 kg of surfactant per ton of coal.

CONCLUSIONS

Deep cleaning of lignite samples was investigated using a combination of chemical dissolution and physico-chemical separation methods. Sulfurous acid, H_2SO_3, was utilized in the dissolution studies. The treated samples were subjected to liquid-liquid extraction, flotation and mild agglomeration-flotation separations to further decrease the ash content.

The findings of this study can be summarized as follows:

1. In the absence of sulfurous acid treatment, lignite could not be beneficiated.

2. Sulfurous acid leaching was very effective in removing salts of Ca, Mg and Na. A clean coal sample of 6.5% ash was obtained from a raw lignite sample with 12.9% ash using a 1.0% solution of sulfurous acid.

3. The acid treatment rendered the low rank coal more hydrophobic most probably due to some chemical changes at the surface during the dissolution of the cations from the carboxylate structure.

4. A clean coal product of 4.4% ash was obtained with 95% combustible matter recovery from a 12.9% ash lignite sample by a combination of sulfurous acid treatment and LLE separation.

5. For a second sample prepared by Amoco Oil Company, the ash content of sulfurous acid treated coal was reduced from 3.3% to 1.85% with a combustible matter recovery of 85%, using the mild oil agglomeration-flotation method.

6. Even though large amount of hydrocarbon was used to obtain the clean coal products of desirable quality, it was possible to recover and recycle most of it.

ACKNOWLEDGEMENTS

The authors acknowledge the support from the Department of Energy, under contract number DE-AC22-91PC91051.

REFERENCES

Aplan, F. F. (1976), "Coal Flotation", A. M. Gaudin Memorial International Flotation Symposium, Ed. by M. C. Fuerstaneau, pp. 1235-1264.

Aplan, F. F. (1980), "Estimating the Floatability of Western Coal", Gold, Silver, Uranium and Coal, Geology, Mining, Extraction and Environment, Ed. by M. C. Fuerstaneau and B. R. Palmer, New York, pp. 380-398.

Aplan, F. F. (1988), "How the Nature of Coal Influences Its Cleaning", Industrial Practice of Fine Coal Cleaning, Ed. by R. R. Klimpel and P. T. Luckie, SME Littleton, CO, pp. 99-111.

Arnold, B. J. and Aplan, F. F. (1989), "The Hydrophobicity of Coal Macerals", Fuel, Vol. 68, pp. 651-658.

Chander, S., Polat, H. and Mohal, B. (1993), "Flotation and Wettability of a Low Rank Coal in the Presence of Surfactants", Preprint 93-64, SME Annual Meeting in Reno, Nevada.

Cronauer, D., Joseph, T.J., Davis, A., Glick, D. and Luckie, P.T. (1992), "The Beneficiation of Martin Lake Texas Lignite", Fuel, Vol. 71, pp. 65-73.

Fuerstaneau, D. W., Rosenbaum, J. M. and Laskowski, J. (1983), "Effect of Surface Functional Groups in the Floatability of Coal", Colloids and Surfaces, Vol. 8, pp. 153-174.

Gayle, J. B., Eddy, W. H. and Shotts, R. O. (1965), "Laboratory Investigation of the Effect of Oxidation on Coal Flotation", Report of Investigations 6620, US Bureau of Mines.

Gutierrez-Rodriguez, J. A. and Aplan, F. F. (1984), "The Effect Oxygen on the Hydrophobicity and Floatability of Coal", Colloids and Surfaces, Vol. 12, pp. 27-51.

Holland, F. A. and Chapman, F. S. (1966), Liquid Mixing and Processing in Stirred Tanks, Reinhold Publishing, New York.

Hsu, T. C. and Chander, S. (1988), "Interfacial and Colloidal Effects in Liquid-Liquid Separation of Ultrafine Coal", Interfacial Phenomena in Biotechnology and Materials Processing, Ed. by Y. A. Attia, B. M. Moudgil and S. Chander, Elsevier Science Publishers B. V., Amsterdam, pp. 399-411.

Mochida, I., Moriguchi, Y. and Shimomara, T. (1983), Fuel, Vol. 62, p. 471.

Quast, K. B. and Readett, D. J. (1987), "The Surface Chemistry of Low Rank Coals", Advances in Colloid and Interface Science, Vol. 27, pp. 169-187.

Schobert, H. H. (1990), The Chemistry of Hydrocarbon Fuels, Butterworths, Boston.

Sun, S. C. (1954), "Hypothesis for Different Floatabilities of Coals, Carbons and Hydrocarbon Minerals", Transactions of AIME, Vol. 199, PP. 67-75.

Wei, D., Chander, S. and Hogg, R. (1992), "Distribution of Wettability of Coal", Coal Preparation, Vol. 10, pp. 37-45.

Woodburn, E. T., Robbins, D. J. and Flynn, S. A. (1983), "The Demineralization of a Weathered Coal by Froth Flotation", Powder Technology, Vol. 35, pp. 1-15.

Table 1. Results of the LLE tests as a function of mixing time.

Mixing Time (minutes)	Ash (%)	CMR (%)
5	4.63	93
10	4.80	95
20	4.69	96
40	4.90	97
80	4.78	98

Table 2. Results of the MOAF tests as a function of feed size.

Feed size	Ash (%)	CMR (%)
-150 μm	2.40	69
-60 μm	2.40	63
-38 μm	2.02	85

Table 3. Results of the MOAF tests as a function of calgon concentration.

Concentration	Ash (%)	CMR (%)
0.00 kg/T	2.02	85
0.02 kg/T	1.97	93
0.10 kg/T	2.03	88
0.5 kg/T	1.94	92
2.0 kg/T	1.97	92

Table 4. Results of the MOAF tests as a function of surfactant concentration.

Surfactant Concentration	Ash (%)	CMR (%)
0 kg/T	2.23	82
2 kg/T	2.25	82
8 kg/T	2.02	85
25 kg/T	1.96	88

Table 5. Results of the MOAF tests as a function of collector concentration at a fixed collector to surfactant ratio of 10.

Collector Concentration	Ash (%)	CMR (%)
125 kg/T	2.49	75
250 kg/T	1.96	88
500 kg/T	1.99	91

Table 6. Results of the MOAF tests as a function of collector concentration at a fixed collector to surfactant ratio of 48*.

Collector Concentration	Ash (%)	CMR (%)
48 kg/T	2.18	58
96 kg/T	1.95	72
192 kg/T	1.85	85

* *Reagents were Pre-emulsified in a blender before addition of coal slurry.*

Figure 1. Structural formula of PPO/PEO block co-polymer used in this study

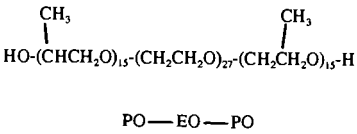

ENZYMATIC CONVERSION OF COAL IN NONAQUEOUS MEDIA

Alexander M. Blinkovsky and Jonathan S. Dordick
Department of Chemical and Biochemical Engineering, University of Iowa,
Iowa City, IA 52242

Keywords: coal depolymerization; peroxidases; aqueous-organic media for biocatalysis.

ABSTRACT.
Two different peroxidases--from horseradish roots and soybean hulls--were studied as potential biocatalysts for modification of coal in aqueous-organic media. Both enzymes were found to cause polymerization of Mequininza lignite in a mixture (1:1 v/v) of DMF and acetate buffer (pH 5). At pH 2.2, incubation of the lignite with soybean peroxidase in 50% DMF resulted in both polymerization and depolymerization.

INTRODUCTION

It has been demonstrated earlier that both isolated enzymes[1,2] and intact microorganisms[3-5] can selectively modify coal. However, coal bioprocessing has not been highly successful. One of the most difficult problems that remains is the lack of sufficient enzyme-coal interactions that are necessary for substantial depolymerization and solubilization. The insolubility of coal in water severely limits the extents of either microbial or enzymatic degradation. Any truly effective coal depolymerization process, therefore, must take place in a non-aqueous medium that can solubilize at least some fractions of the coal. The use of enzymes in nonaqueous solvents[6,7] has now become common place and numerous enzymes and conditions have been studied in organic media. Specifically, peroxidases are known to be highly active in nonaqueous media, with turnover numbers often enhanced in organic solvents over that in water[8]. Several peroxidases (e.g., chloroperoxidase, lactoperoxidase, and horseradish peroxidase)[1,2] display activity on the oxidation of coal-related compounds including lignin[9]. In the present work, our efforts have focused on study of two different peroxidases as potential biocatalysts for modification of coal structure and for depolymerization of coal in aqueous-organic media. We have evaluated also multi-enzyme systems from whole cells of bacteria in respect of oxidation of a coal model compound.

MATERIALS AND METHODS

Mequininza lignite (from Spain) was used as a substrate. The lignite was not subjected to any treatment except for thorough grinding. Horseradish peroxidase (EC 1.11.1.7) type II was obtained from Sigma Chemical Co (St. Louis, MO). Peroxidase from soybean hulls (EC 1.11.1.7) was obtained from Enzymol, International (Columbus, OH). The enzymes were used without additional purification. Before incubation with the enzymes, the lignite was fractionated on lipophilic Sephadex LH-60. Gel permeation column chromatography on lipophilic Sephadex LH-60 is traditionally used as a tool to separate molecules of different molecular weight in a non-aqueous medium as well as to determine the molecular weight distribution. Intermolecular associations of coal polymers with the resin, and to each other, were eliminated by employing DMF supplemented with 0.1 M LiCl. The range of molecular weights which can be separated by this technique is 500 - 60000 D.

In a typical experiment, 7.5 mg of the soluble coal fraction was dissolved in 1 ml of pure DMF and 0.8 ml of the aqueous buffer (containing 1 mg of enzyme) was added. The reaction was initiated upon pumping 0.2 mL of hydrogen peroxide into the vial over a period of two minutes. The final concentration of hydrogen peroxide was 0.66-0.8 mM. A control reaction which included all reagents, except enzyme, was initiated concurrently. The incubation mixtures were shaken at 100 rpm at 30°C for 24 h during which time 0.1 mL aliquots were taken. Before analysis of the molecular weight distribution, the samples of the lignite after incubation with peroxidases were dried in vacuum at 45°C and redissolved in 0.1 mL of pure DMF. Supernatant was loaded onto a glass column (24 x 1 cm) packed with Sephadex and eluted at a flow rate 0.1 mL/min. The column was calibrated with polystyrenes with molecular weights of 2, 4, 15, and 50 kD. Fractions (1 mL) were measured via absorbance at 280 nm.

Dibenzothiophene and byphenyl were used as coal model substrates to study oxidation by whole cells of *Beijerinckia* and by the *Beijerinckia* enzyme system in aqueous-organic media. Cells were grown via the method of Laborde and Gibson[10], harvested and lyophilized. The freeze-dried cells were ground then to a fine powder. NADH was added to the incubation mixture as a cofactor of the oxygenase system for the disrupted cells. In a typical experiment, wet whole cells of *Beijerinckia* (0.3-0.4 g)were incubated with saturated concentrations of the substrates in 10 mL of phosphate buffer (0.05 M, pH 7.2) containing 0.1% of pyruvate and 1-20% (v/v) of organic solvents. In the case of the lyophilized cells (fine dry powder), incubation was carried out in acetate-phosphate buffer at pH 5.0-7.5 containing up to 50% of an organic solvent at a concentration of cells and NADH of 4 mg mL^{-1} and 1 mM, respectively. Periodically, aliquots of the reaction mixtures were withdrawn, dried in vacuum at 40°C, redissolved in pure acetonitrile, and analyzed with a Waters μBondapak C_{18} column (3.9 x 300 mm). The mobil phase consisted of an acetonitrile-water mixture; the flow rate was 1 mL min^{-1}. Absorbance peaks were monitored at 230 nm.

RESULTS AND DISCUSSION

Proxidase-Catalyzed Polymerization of Lignite

It was previously shown[9] that horseradish peroxidase (HRP) is active in dioxane-water and DMF-water solutions in the one-electron oxidation of phenolic units of kraft lignin, a relatively inert polymeric compound. Horseradish peroxidase suspended in dioxane was also reported[1] to cause the limited solubilization and depolymerization of leonardite, a low rank coal.
In our prelimenary investigation we found that peroxidase from soybean hulls (SBP) possesses a much higher oxidative potential in comparison to horseradich peroxidase. Oxidative cleavage of natural coal --Mequininza lignite-- has been attempted using both peroxidases. This lignite represents a highly oxidized, non-bituminous coal.

The lignite powder is poorly soluble in tetrahydrofuran (THF) and dioxane (less than 1% w/w from total amount) and insoluble in water. Both THF and dioxane solubilize only low molecular weight fractions with molecular weight less than 2 kD (data not shown). DMF has been found to dissolve ca. 25% of coal. The solution in DMF contains a broad range of molecular weights as it is seen from Fig. 1, with some coal polymers soluble at molecular weights > 50 kD.
The DMF-soluble coal was fractionated on the GPC column and fraction number 11 (4 kD) was collected for further experimentation. At this molecular weight, both polymerization and depolymerization of the coal fraction can be monitored.

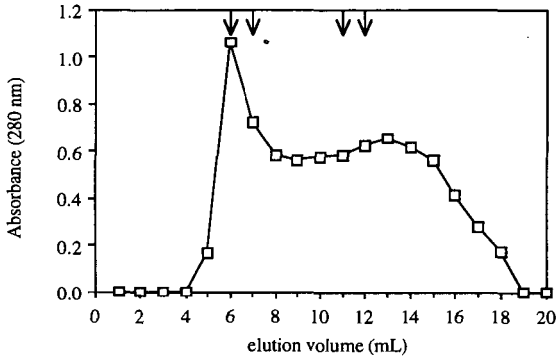

Fig. 1. Gel permeation chromatography of Mequininza lignite fractions soluble in DMF. Arrows indicate molecular weight markers: from left to right, 50, 15, 4, and 2 kD.

Lignite modification reactions were studied using HRP and SBP catalysis with this intermediate molecular weight fraction in 50% DMF at pH 5 (50 mM acetate buffer). In both cases, the incubations resulted in turbid solutions. Control reactions which included water insted of hydrogen peroxide did not lead to formation of turbudity. Sediments were not completely soluble in pure DMF. Figures 2 and 3 depict changes in the molecular weight profile of the lignite fraction for HRP and SBP as catalysts. In both cases, following 24 h, clear polymerization was observed. The highest soluble polymeric products had molecular weights > 50 kD. The DMF-insoluble fractions appear to consist of high molecular weight polymers produced during peroxidase catalyzed oxidative cleavage of coal structure. No evidence of depolymerization was detected. These findings are in accordance with previous literature obsrvations[1,10] that peroxidases are excellent catalysts to oxidize phenolic polymers such as lignins and coals, particularly in the presence of organic solvents.

Oxidative Power of Soybean Peroxidase -- Depolymerization of Coal in Aqueous DMF Solutions

In related research, we have studied the oxidative ability of SBP. The enzyme is highly active and stable under acidic conditions. At low values of pH, it has been observed that SBP is capable of oxidizing veratryl alcohol (personal communication of J. P. McEldoon). The catalytic activity of SBP on veratryl alcohol was strongly dependent on the pH and the presence of calcium ions. It was found that the pH optimum of veratryl alcohol oxidation is ca. 2.15 with very little oxidation above pH 3. Furthermore, the enzyme is strongly stabilized by $CaCl_2$ concentrations of up to 0.1 M. Evidently, the low pH results in a significant increase in the oxidation potential of SBP and enables a compound such as veratryl alcohol to be oxidized. Given the high oxidation potential of SBP at low pH, it occured to us that this enzyme is acting more as a lignin peroxidase than a typical plant peroxidase. In that regard, we proceeded to re-investigate the action of SBP on DMF-soluble lignite at pH 2.2. Figure 4 shows that both polymerization and depolymerization occured after 24 h incubation of fraction 11 of the lignite with SBP in 50% DMF, 0.1 M tartrate buffer, pH 2.2 containing 0.1 M $CaCl_2$. Approximately 10% of the initial lignin precipitated out of the enzyme reaction, indicating that some very high molecular weight material was produced. In the absence of enzyme, no coal modification took place.

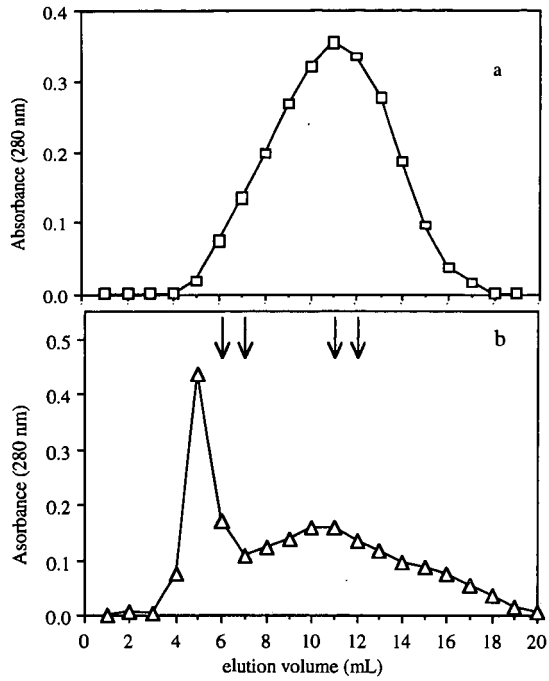

Fig. 2. Gel permeation chromatography of Mequininza lignite fraction No 11 (MW 4 kD) before incubation with horseradish peroxidase (a) and after 24 h incubation at pH 5 in 50% DMF (b).

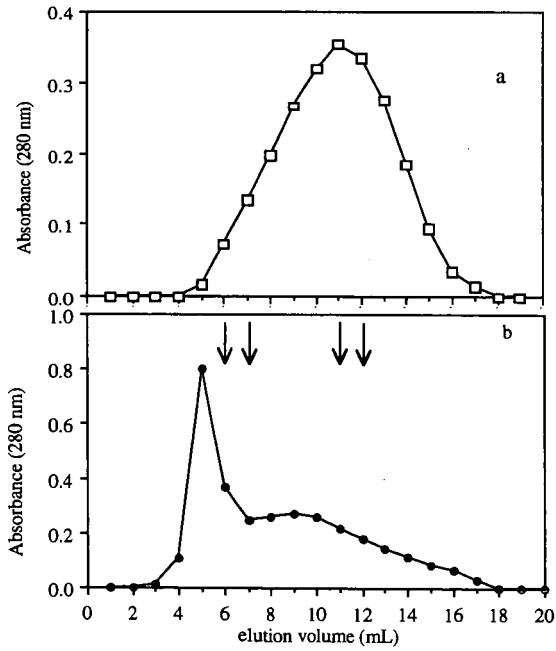

Fig. 2. Gel permeation chromatography of Mequininza lignite fraction No 11 (MW 4 kD) before incubation with soybean peroxidase (a) and after 24 h incubation at pH 5 in 50% DMF (b).

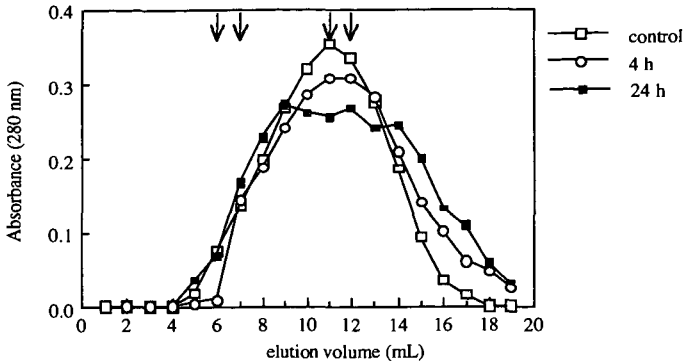

Fig. 4. Gel permeation chromatography of Mequininza lignite fraction No 11 (MW 4 kD) before incubation with soybean peroxidase and after incubation at pH 2.2 (0.1 M tartrate buffer, 0.1 M $CaCl_2$) in 50% DMF.

We reasoned that a relatively low molecular weight fraction of lignite was more susceptible to polymerixation than depolymerization. To test this hypothesis, we examined the action of SBP in 50% DMF (pH 2.2) with a higher molecular weight fraction of DMF-soluble lignite. Figure 5 shows that the high molecular weight fraction (ca. 50 kD) was unaffected in the absence of the enzyme, yet was obviously depolymerized in the presence of SBP.

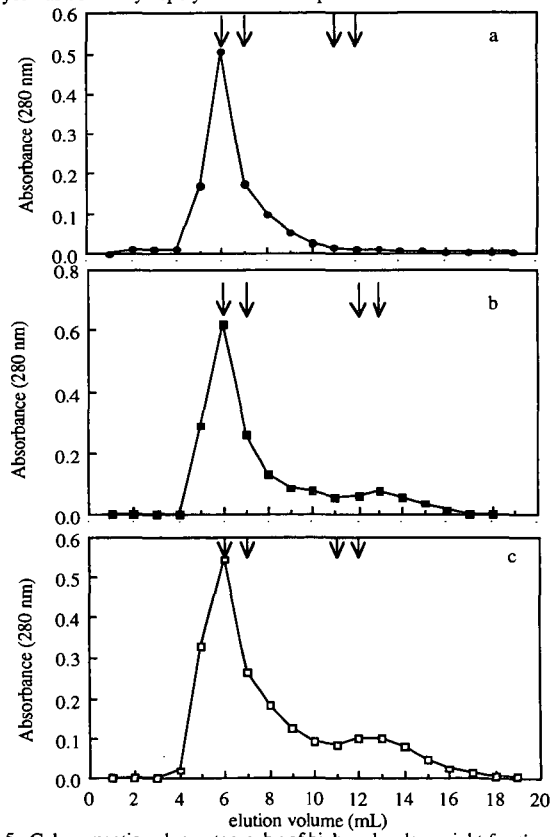

Fig. 5. Gel permeation chromatography of high molecular weight fraction No 6 (MW 50 kD) of Mequininza lignite before incubation (a) with soybean peroxidase and after 4 h (b) and 24 h (c) incubation at pH 2.2 (0.1 M tartrate buffer, 0.1 M $CaCl_2$) in 50% DMF.

Activity of Oxygenase Enzymes on Coal Model Compounds

The unique specificities and reactivitites of oxygenase enzymes in organic solvents can be exploited for biocatalytic transformation of coal. Mono- and dioxygenases from bacteria consist of a three-enzyme system comprised of an iron-sulfur hydroxylase/oxygenase, a ferridoxin electron transfer protein, and an NAD(P)H reductase. The reaction mechanism of this multienzyme system remains poorly characterized and the use of the isolated enzyme system has been poorly successful. Nevertherless, several promising biotransformations have been performed on coal-related compounds using whole cells. For example, Laborde and Gibson demonstrated[10] that fermentation of dibenzothiophene (DBT) with *Beijerinckia* B8/36 resulted in the accumulation of 1,2-dihydroxy-1,2-dihydrodibenzothiophene and dibenzothiophene-5-oxide in the cell culture. Further reatment of the first product by the *Beijerinckia* sp. led to the accumulation of 1,2-dihydroxydibenzothiophene. We have initially evaluated the catalytic activity of the *Beijerinckia* enzyme system in aqueous-organic media. The whole cells were unable to grow in the solvents, yet retained intrinsic enzyme activity. Conversions (ca. 25%) of both biphenyl and DBT were observed in the media containig up to 50% of DMF or dioxane. Moreover, several unidentified products that were not detected after fermentation of biphenyl and DBT with *Beijerinckia* sp.in aqueous media were found in aqueous-organic mixture. It was also found that the *Beijerinckia* enzyme system from the lyophilized cells is active in non-aqueous media in the presence of NADH. Cofactor regeneration system comprising horse liver alcohol dehydrogenase and ethanol was applied to provide long term activity of the oxygenase system from a fine powder of the freeze-dried cells of *Beijerinckia* sp.in non-aqueous media. Improvement of the ability of the *Beijerinckia* oxygenase enzyme system to catalyse coal model compounds degradation in aqueous-organic media is the subject of continuing investigations.

REFERENCES

1. Scott, C.D., Woodward, C.A., Thompson, J.E., and Blankinship, S.L. *Appl. Biochem. Biotechnol..*, 1990, **24/25**, 799.
2. Dordick, J.S., Ryu, K., and McEldoon, J.P. *Resources, Conservation and Recycling,* 1991, **5**, 195.
3. Cohen, N.S. and Gabriele, P.D. *Appl. Environ. Microbiol.*, 1982, **44**, 23.
4. Scott, C.D., Strandberg, G.W., and Lewis, S.N. *Biotechnol. Prog.*, 1986, **2**, 131.
5. Pyne, J.W. Jr., Stewart, D.L., Fredrickson, J., and Wilson, B.W. *Appl. Environ. Microbiol.*, 1987, **53**, 2844.
6. Dordick, J.S. *Enzyme Microb. Technol.*, **1989**, *11*, 194.
7. Klibanov, A.M. *Acc. Chem. Res.*, 1990, **23**, 114.
8. Ryu, K., and Dordick, J.S. *J. Am. Chem. Soc.*, 1989, **111**, 8026.
9. Blinkovsky, A.M.and Dordick, J.S. *J. Polym. Sci.: Part A: Polym. Chem.*, 1993, **31**, 1839.
10. Laborde, A.L. and Gibson, D.T. *Appl. Environ. Microbiol.*, 1977, **34**, 783.
11. Popp, J.L., Kirk, T.K., and Dordick, J.S. *Enzyme Microb. Technol.*, 1991, **13**, 964.

MOLTEN CAUSTIC LEACHING AT LOW CAUSTIC/COAL RATIOS

Fred W. Steffgen, Benjamin R. Turner, and Dale A. Chatfield
PCR Technologies
10373 Roselle Street - Suite K
San Diego, CA 92121

KEWORDS: Molten caustic leaching, coal desulfurization, sulfide coal interaction

INTRODUCTION

Molten caustic leaching (MCL) of coal has been studied under a variety of conditions, many of which studies have been conducted using a large excess of liquid caustic (3:1 caustic/coal or higher) so that, with stirring, coal is suspended in it. This provides a uniform temperature throughout the mixture and is preferred for chemical research. Some development studies have made use of lower ratios of caustic, such as TRW's 20 lb/hr kiln work by Meyers[1,2], and the studies of Chriswell and Markuszewski at Ames Laboratory[3] and by Kusakabe in Japan[4]. In the Japanese work, Illinois #6 coal was impregnated with mixed KOH and NaOH (52:48 parts by weight) from an aqueous solution to give 51 wt% caustic on the dry coal which after MCL treating, 2 hr at 375°C, produced a coal having only 0.50 wt% total sulfur. Less caustic should help in reducing the cost of an MCL process. Moreover, at high ratios much more caustic is present than necessary to form salts of sulfur and mineral matter in coal. We have calculated that to form the sodium salts of the sulfur and mineral matter present in an 8% ash, 4.2% sulfur, Pittsburgh #8 coal would take about 0.15 parts of sodium hydroxide for one part of dry coal. This does not take into account carbonate formation nor cleavage of carbon-oxygen bonds which also can occur.

The work at Ames National Laboratories has shown that a 2.0:1 ratio can be very effective for desulfurization but that lower ratios tend to give less conversion of sulfur. This group has also demonstrated improved conversion can be obtained by heating in two stages, first to an intermediate temperature, e.g., 250° for an hour, followed by a second-stage, rapidly increasing the temperature to 390°C and immediately cooling, to give desulfurization equivalent to two hours at 390°C. A recent paper reported by Akhtar and Chriswell[5] reveals that treating Illinois #6 coal in boiling water for one hour, makes the coal more reactive in a subsequent MCL treating step. TRW's work demonstrated production of low sulfur coal in continuous flow MCL using standard process equipment, such as, a kiln reactor, filters, and centrifuges made from caustic- and acid-resistant materials. Most of their tests were conducted above 2.0:1 ratio. They have also found a means of counter-current water washing that does not require the usual acidification step[2].

Because the use of less caustic could offer cost advantages, PCR Technologies prepared a Small Business Innovation Research (SBIR) proposal for studying MCL at low caustic/coal ratios which resulted in a grant awarded by the US Department of Energy[6]. The objectives of this work have been to examine MCL under conditions that could be used for commercial chemical coal cleaning. This has meant using reasonably low levels of acid water and caustic. Tests have been made using coal from three different seams: western Kentucky #9, Illinois #6, and a low- and a high-sulfur Pittsburgh #8. Semiannual reports issued from the grant have shown that significant amounts of desulfurization and demineralization occur at ratios of 0.5:1 to 2:1 but, at most conditions used, desulfurization was not sufficient to meet New Source Performance Standards (NSPS) for the year 2000. NSPS will require certain coal burning facilities to emit no more than 1.2 lbs SO_2/MMBtu by the year 2000. We have found some single-step sets of conditions at 0.75 ratio with which KY #9 coal and a low-sulfur Pgh #8 coal did meet the 1995 NSPS goal of 2.5 lbs SO_2/MMBtu. However, using 2:1 caustic/coal ratio, the 1.2 lbs SO_2/MMBtu level was met with the same two coals. Sulfur removal attained at low ratios in single-step and in two-step MCL tests are compared and experiments showing how the desulfurization level appears to be limited by the presence of sulfide are addressed in this paper.

EXPERIMENTAL

Most of the experiments described were conducted in an annealed stainless steel, 1-3/8" I.D. pipe reactor containing a 4-3/4" stirrer

blade having a width nearly the diameter of the pipe. During tests, the stirrer was rotated by an induction motor at 5.5 rpm and the reactor held at an angle of 30° from horizontal. Nitrogen gas was passed slowly through the reactor, at atmospheric pressure, while heating the reactor in a hinged furnace. A thermowell passed through a bottom closure and acted as a bearing for the bottom of the stirrer shaft which allowed the MCL reaction temperature to be monitored.

Most often, test conditions were randomized to avoid any sequence or time bias. In a typical test, 18g of 14 mesh x 0 coal and an amount of NaOH beads (20-40 mesh) to give the desired caustic/coal ratio were poured into the reactor and the top screwed in place. The furnace was heated rapidly while the reaction mixture was stirred constantly. Reaction temperatures of 350° to 430°C were reached in about 65 to 85 minutes respectively. The reaction period time was begun as the internal temperature reached 3°C below test temperature and ended when the temperature dropped 3°C below that value. Usually internal temperatures were held within +/-3°C of this value. Cooling was begun in anticipation of the end of the reaction period by turning off the heat, opening the split-hinged furnace, and turning a fan on. The cool-down was about twice as fast as heat-up time. The initial gallon-size samples of high- and low-sulfur Pgh #8 and western KY #9 coals were received from TRW and are coals TRW used in their integrated kiln test program. The IL #6 coal, IBC-101, was received from the Illinois State Geological Survey. A second, larger sample of high-sulfur Pgh #8 coal was obtained through Tra-Det Inc., Wheeling WV. Sodium hydroxide beads (20 x 40 mesh) were used as the source of caustic for these MCL tests. In a few tests, sulfide was added to a caustic/coal mixture, in which case the sulfur source was either Fisher 21.2% aqueous ammonium sulfide solution (9.97 wt% sulfur) or Aldrich 98% sodium sulfide nonahydrate, ACS reagent.

A few larger scale runs were made using a Parr Instrument Co. 6-liter stainless steel stirred reactor so that a partially or completely desulfurized product could be made from 400 to 2000g of the coal. Reactants, including some water, were loaded into the reactor and pressure tested using nitrogen. Tests were conducted either at a fixed pressure, e.g., 400 psig, using a back-pressure regulator with slow flow of nitrogen through the regulator or the reactor was sealed containing at least 30 psig (nitrogen) and allowed to attain whatever pressure occurred at run conditions. For depyriting runs at 250°C, water vapor pressure accounted for most of the pressure observed. Products from the Parr reactor were used as feed for second-stage, atmospheric pressure tests in the pipe reactor.

Products were generally worked up by digesting the cooled mixture of caustic/coal in an amount of hot water equal to four times the weight of coal, filtering the coal and rinsing with up to two weights of hot water. The coal was acidified while dispersed in 2 to 4 weights of water by adding dilute HCl until a pH of 1.2 was maintained for five minutes. (Sulfuric acid would likely be used commercially.) The slurry was then heated to 90+°C for 20 minutes with stirring. The hot slurry was filtered and rinsed with two weights of hot water. Moist coal samples were dried at 105° to 110°C.

Coal analyses were conducted by Standard Laboratories, Inc., Cresson, PA. Alkaline wash filtrates were titrated at PCR Technologies to determine total alkalinity (to pH 4.0) and free NaOH (to pH 8.35) in the presence of excess $BaCl_2$.

RESULTS AND DISCUSSION

High-sulfur Pgh #8 coal was found to be the most resistant to MCL of the three coal seams selected for our study and was chosen for our initial experiments. Over eighty tests were made with this coal in Phase I and II of our grant. A low-sulfur Pgh #8 was also tested in six runs, twenty-one tests were made with IL #6 coal, and over fifty tests with western KY #9 coal. Data (in some cases averages of duplicate runs) for tests at both 0.75:1 and 2:1 caustic/coal ratios are shown in Table 1. Our goal was to obtain a low-sulfur product that would emit 1.2 lbs SO_2/MMBtu or less on combustion. Even a cursory scan of Table 1 shows that few tests actually achieved this goal and then only from low-sulfur Pgh #8 and KY #9 coals treated at 2.0:1 caustic/coal ratio and temperatures of 390°C or higher.

In MCL treating, pyritic sulfur is much more reactive than organic sulfur and can be removed at a temperature about 100°C lower than is necessary for desulfurizing organic sulfur structures in coal. Thus, effective MCL treating becomes a matter of removing of organic sulfur in the quest for acceptable NSPS coal product. The problem, at first glance might seem to be due to the slow desulfurization reaction rate of organic sulfur in coal. However, longer reaction time often had little effect on desulfurization with these coals. This was more noticeable for those tests using 0.75:1 caustic/coal than 2:1. This could be caused by some organic sulfur structures in coal being more resistant to reaction than others, by steric hindrance of some sulfur moieties, by parts of the solid coal not being in contact with the caustic, by the caustic reacting with coal constituents that used up the caustic, or by a reversible reaction in which a concentration of by-product builds up and prevents further desulfurization at that temperature. Except for high-sulfur Pgh #8, tests at 2:1 ratio definitely caused more desulfurization than did those at 0.75:1. Product from 0.75 ratio runs were obviously wetted and formed solid masses on cooling. Therefore, lower conversion levels should not be due to impervious coal or steric hindrance since higher ratios of caustic/coal increased sulfur removal. Titrations of the water wash filtrates from tests showed that some weak acid salts were formed, but 32 to 80 wt% of free NaOH was still available for tests at 0.75:1 and 55 to 81 wt% at 2:1 ratio. There was ample unreacted caustic remaining to continue the desulfurization reaction. Poor reactivity could best be attributed to more resistant sulfur bonds after the facile carbon-sulfur bonds had reacted or to some form of reversible reaction.

Therefore, an investigation into sulfide as a possible by-product that could interfere with coal desulfurization by a reversible or retrograde reaction was begun. Pyrite in MCL reaction forms sulfide and can quickly build up in the caustic before organic sulfur begins to react. This sulfide concentration effect would be much greater with low ratio tests. Therefore, the first attempt to test whether sulfide in the caustic can reduce the desulfurization of coal was to remove the pyrite from KY#9 coal in a mild MCL reaction and then treat that product in a second-step MCL treat. Both reactions were made with 0.75:1 ratio caustic/coal; the first step was run at 320°C for 50 minutes and the second step at 390°C for only two minutes. Table 2 compares the results with other tests made for various reaction times at 390°C. The first step or "pretreat" test removed 88% of the pyritic sulfur and also about 12% of the organic sulfur. The second step test removed 50% of the remaining organic sulfur and nearly met NSPS year 2000 criteria. For comparison at the same temperature, a 2-minute test removed 34% of organic sulfur and the best level attained, at 50 minutes, removed only 40%. In another approach to investigate the influence of sulfide, hydrogen sulfide was added to a 2:1 ratio of caustic and coal in an amount equivalent to 4-times the weight of total sulfur in KY #9 coal. The H_2S gas was generated from a weighed amount of $(NH_4)_2S$ solution and carried by nitrogen flow into the reactor while holding the MCL reactor charge at 170° to 180°C. Immediately thereafter, the MCL test was run at 390°C. The result was that, although pyrite was effectively removed from the coal, the organic sulfur content remained essentially unchanged. The presence of this much sulfide in the caustic clearly prevented desulfurization of organic sulfur. A hypothesis that MCL desulfurization can be severely affected by the concentration of sulfide in caustic began to unfold.

Another coal, the low-sulfur Pgh #8, was used for a second series of tests to see if it was similarly sensitive to a change in sulfide concentration. Table 3 repeats a few test results of Table 1 for comparison with 2-step MCL treating. In the "pretreat" step, coal was depyrited in the 6-liter reactor using 0.5:1 caustic/coal and enough water to give a 38% solution of the NaOH. Depyriting was conducted for 25 minutes at 250°C and produced a very low pyrite coal with an organic sulfur content elevated about 25% to 1.26 wt%. This depyrited, low-sulfur coal was then used in second-step MCL reactions in the small reactor. Tests were made at 0.25, 0.50, and 0.75 ratios for 25 and 100 minute tests at 390°C. With as little as 0.25 ratio, the NSPS 2000 sulfur dioxide limit was almost achieved and the higher ratio tests were well below the NSPS limit by 25 to 65 %. Two-step MCL treating was necessary to produce NSPS compliance coal when using 0.75 and lower ratios, but it is apparent that there are coals of

moderate to low sulfur content which would respond well to MCL treating at low ratios.

The original high-sulfur Pgh #8 coal was depleted in laboratory tests and a large, fresh sample was needed for larger-scale tests. The original sample had a combined sulfate and pyrite content indicating it had contained 1.57 wt% pyritic sulfur, when fresh, and 2.76 wt% organic sulfur. Our second high-sulfur Pgh #8 sample, obtained from the same mine by Tra-Det, Inc., contained 1.95 wt% pyritic sulfur, 0.05 wt% sulfate sulfur, and 2.45 wt% organic sulfur. In Table 4, data showing a comparison of MCL tests at 2.00:1 ratio for the two coal samples are presented. The Tra-Det sample was somewhat less resistant to treating and met the 1995 NSPS but not that for 2000. Shown next are two-step results from depyriting high-sulfur Pgh #8 coal in the 6-liter reactor and the use of this product in second-step MCL tests. The depyriting was conducted using a 0.62 ratio for 25 minutes at 250°C, during which the reactor was maintained at a pressure of 400 psig. Pyrite conversion was 95% and organic sulfur content increased about 20% when loss of mineral matter, volatiles and pyrite were considered. Using the depyrited, high organic sulfur product as a coal feed, second-step, 25-minute MCL tests were made at 0.25, 0.75 and 2.00 ratios and 390o to 430°C reaction temperatures with interesting results. The 0.25:1 ratio test desulfurized 36% of the organic sulfur but still had more than twice the SO_2/MMBtu level desired. However, desulfurization with 0.75:1 ratio at 410° and 430°C produced compliance coal product and the 2.00:1 ratio tests, as would be expected, gave even lower sulfur levels at 390°, 410° and 430°C. Two-step, low-ratio treating offers promise for achieving NSPS compliance product even from a high-sulfur coal.

In another experiment, excellent chemical cleaning of Pgh #8 was obtained using a very high ratio, 5.00:1, for 25 minutes at 400°C. However, the following test shows that sulfur removal is reversible when treated in the presence of NaOH and sulfide as in a MCL test. The clean coal contained only 0.73 wt% total sulfur, of which 0.69 wt% was organic. This clean coal was mixed with both NaOH (1.67:1) and Na_2S (0.50:1) and treated for 25 minutes at 390°C. The amount of Na_2S added provided 3.69 g S^{--}, several times the total sulfur content of untreated Pgh #8 feed coal and demonstrates that sulfide can cause a higher sulfur product to form. The result was that organic sulfur in the sulfided MCL product increased to 1.42 wt%, about twice the amount of organic sulfur in the cleaned coal. The previously clean coal, 0.97 lbs SO_2/MMBtu, now would produce 2.03 lbs SO_2/MMBtu on combustion.

If sulfide concentration builds-up sufficiently, a retrograde sulfurizing reaction can occur that will limit or possibly slowly increase the organic sulfur content in coal. Whether the same type of organic sulfur compounds form as are desulfurized has not been determined. Studies of the reactions of organosulfur compounds thought to represent structures in coal[7,8], such as thiophene, benzothiophene or dibenzothiophene have not been approached as reversible reactions. Often desulfurized products were obtained that also lacked an oxygen. Once that has happened, it is less likely a reaction to incorporate sulfur in a hydrocarbon would occur than it would be to have an exchange between phenolic oxygen and thiophenolic sulfur in the presence of molten caustic. We suspect that the latter type reactions are at play and that some of the phenolics may come from hydrolysis of furan structures in coal.

With coals containing less than 6 wt% sulfur, it is not likely that sulfide could build-up to a high concentration at high ratios so the reverse reaction might not be noticed. However, at low caustic/coal ratios, especially when the coal contains over 2 wt% total sulfur, a desulfurization limitation may occur well before NSPS criteria are reached.

We believe that MCL desulfurization of coal is sensitive to the molar concentration of sulfide ion in the caustic solution. If the molar concentration is low enough, desulfurization can proceed rapidly and only a few minutes, not hours, of MCL reaction time is necessary at temperatures above 370°C. If the sulfide concentration is high, desulfurization cannot proceed regardless if the time or temperature would otherwise be practical for MCL treating. For coals having much pyrite, a low temperature depyriting step followed by a MCL reaction

to remove the requisite amount of residual organic sulfur can achieve compliance coal quality. By considering carefully the amount of sulfur to be removed and the reactivity of the coal, low ratios of caustic/coal could in many instances be used in place of much larger amounts of caustic.

SUMMARY

Conditions have been presented showing MCL desulfurization of coals from three coal seams at low caustic/coal ratios. Ratios at 2.00:1 were successfully used in single-step MCL reactions for treating of a 2 wt% sulfur Pgh #8 coal and a 3.4 wt% sulfur western KY #9 coal to achieve NSPS 2000 compliance product, 1.2 lbs SO_2/MMBtu. Coals having over 4 wt% sulfur were not successfully treated under the same conditions, but a 4.4 wt% sulfur Pgh #8 coal in a two-step reaction at 0.75:1 ratio of caustic/coal did achieve this goal. Several examples of two-step treating have been presented in which the first step is a lower temperature reaction to remove pyrite.

Experiments have demonstrated that desulfurization is sensitive to the presence of sulfide in caustic during MCL treating. Reducing sulfide concentration by depyriting a coal before MCL treating can allow the second-stage MCL treat to be effective even at quite low caustic/coal ratios. Introduction of sulfide into the MCL caustic, can retard desulfurization or at higher levels actually increase sulfur content. The increase is measured as organic sulfur.

ACKNOWLEDGEMENT
We gratefully acknowledge financial support for this study by the Department of Energy, Office of Energy Research for the SBIR grant, DE-FG03-90ER80957.

We thank The TRW company for providing us with samples of high-sulfur and low-sulfur Pgh #8 and western KY #9 coals they used in their kiln studies for DOE contract DE-AC22-86PC91257.

Finally we thank John Spotts and Robert Pawlak for conducting a number of the MCL reactions reported.

DISCLAIMER
References to any specific commercial process, product or service is to facilitate understanding and is not meant to imply endorsement or favoring by PCR Technologies or the US Department of Energy.

REFERENCES

1 Molten-Caustic Leaching (Gravimelt) System Integration Project, Final Report, Contract No. DE-AC22-86PC91257
2 Nowak, M. and Meyers, R., Molten-Caustic Leaching (MCL) Process Integration in Processing and Utilization of High-Sulfur Coals V, B.K. Parekh and J.G. Groppo, eds., Elsevier, Amsterdam, 1993
3 Markuszewski, R., Chriswell, C., Norton, G., and Jewell, D., Improvements in Chemical Coal Cleaning, DOE Contract No. W-7405-Eng-82, Quarterly Report for January/March 1991
4 Kusakabe, K., Orita, M., Kato, K., Morooka, S. Kato, Y and Kusunoki, K., Fuel 1989, Vol 68, p 396
5 Akhtar, S. and Chriswell, C., Hydrothermal Pretreatment of Coal before Molten Caustic Leaching in Processing and Utilization of High-Sulfur Coals V, B.K. Parekh and J.G. Groppo, eds., Elsevier, Amsterdam, 1993
6 Steffgen, F. and Chatfield D., Chemical Coal Cleaning At Low Caustic/Coal Ratios, DOE SBIR Grant No. DE-FG03-90ER80957 to Pacific Creative Research, SemiannualReports No. 1, 2, and 3
7 Utz, B., Friedman, S., Soboczenski, S. Molten Hydroxide Coal Desulfurization Using Model Systems in Fossil Fuel Utilization, Am. Chem. Soc., Washington, D.C., 1986, pp 51-61
8 Nowak, M., Utz, B., Fauth, D., and Friedman, S., Fused Salt Reactions of Organosulfur Compounds, Am. Chem. Soc. Div. Fuel Chem. Preprint 1987, 32 (4), 46-52

Table 1
SMALL REACTOR MCL DESULFURIZATION EXPERIMENTS
SINGLE-STEP REACTIONS

----Run Conditions------			--Analyses, mf basis--			---Sulfur Forms, mf----		
NaOH/Coal	Temp.	Time	Sulfur	Ht Value	SO2	Pyritic	Sulfate	Organic
Ratio	C	min	wt%	Btu/lb	lbs/MMBtu	wt%	wt%	wt%
A: High-Sulfur Pgh#8 Coal			4.33	12521	6.91	1.07	0.50	2.76
0.75	370	50	1.89	13535	2.79	0.14	0.32	1.43
0.75	390	150	1.87	14221	2.63	0.02	0.05	1.80
0.75	410	50	2.16	13973	3.09	0.05	0.07	2.04
0.75	430	25	1.92	13205	2.91	0.06	0.31	1.55
0.75	430	100	1.73	13699	2.52	0.07	0.13	1.52
0.75	470	50	1.25	13081	1.91	0.18	0.29	0.79
2.00	350	50	2.65	14157	3.74	0.05	0.06	2.54
2.00	370	50	2.43	14156	3.43	0.05	0.08	2.30
2.00	390	50	2.43	14013	3.47	0.07	0.11	2.26
2.00	390	150	2.06	13980	2.94	0.04	0.20	1.82
2.00	410	50	2.43	13569	3.57	0.04	0.25	2.14
2.00	430	25	2.20	13572	3.24	0.06	0.20	1.93
2.00	430	50	2.54	13184	3.85	0.05	0.35	2.14
B: Low-Sulfur Pgh#8 Coal			2.03	13844	2.93	1.02	0.01	1.01
0.75	390	50	1.07	14082	1.52	0.11	0.03	0.93
0.75	430	*2	1.09	14201	1.53	0.08	0.04	0.97
0.75	430	25	1.03	13900	1.48	0.05	0.05	0.93
2.00	390	50	0.62	14464	0.86	0.04	0.01	0.57
2.00	430	*2	0.53	14446	0.73	0.03	0.00	0.49
2.00	430	25	0.26	14101	0.37	0.02	0.01	0.23
C: IL#6 Coal			4.35	12485	6.97	0.90	0.11	3.34
0.75	350	50	2.77	13500	4.10	0.16	0.10	2.50
0.75	370	50	1.99	13120	3.03	0.10	0.18	1.71
0.75	390	*5	1.82	13935	2.61	0.09	0.05	1.68
0.75	390	50	1.63	13336	2.44	0.06	0.16	1.41
0.75	390	*100	1.71	13711	2.49	0.07	0.06	1.58
0.75	410	50	1.64	13004	2.52	0.04	0.27	1.33
0.75	430	50	1.50	13150	2.28	0.07	0.24	1.19
2.00	350	50	2.87	13764	4.17	0.10	0.05	2.72
2.00	370	50	1.71	13618	2.51	0.03	0.09	1.59
2.00	390	50	1.93	13517	2.85	0.05	0.09	1.79
2.00	410	50	1.00	13308	1.50	0.01	0.21	0.78
2.00	430	50	1.43	13254	2.16	0.07	0.25	1.11
D: W.KY#9 Coal			3.39	12730	5.32	0.90	0.50	2.00
0.75	370	2	1.87	14071	2.66	0.24	0.02	1.62
0.75	390	2	1.48	14055	2.10	0.12	0.04	1.33
0.75	390	25	1.36	13416	2.02	0.06	0.09	1.21
0.75	390	100	1.40	13697	2.04	0.07	0.07	1.26
0.75	410	2	1.42	13975	2.03	0.11	0.04	1.27
0.75	430	2	1.38	13773	2.00	0.08	0.06	1.25
2.00	370	2	1.49	14138	2.11	0.10	0.02	1.38
2.00	390	2	1.09	14216	1.53	0.05	0.02	1.02
2.00	390	100	0.43	12561	0.68	0.04	0.08	0.31
2.00	410	2	0.74	14175	1.04	0.04	0.03	0.67
2.00	430	2	0.64	13803	0.92	0.06	0.07	0.52
2.00	430	25	0.65	13396	0.96	0.04	0.14	0.47

* Coal pretreated 50 minutes at 320C.

TABLE 2
MCL EXPERIMENTS WITH KENTUCKY #9 COAL
EFFECTS OF REMOVING OR ADDING SULFIDE

-----Run Conditions-----			--Analyses, mf basis--			---Sulfur Forms, mf---		
NaOH/Coal	Temp.	Time	Sulfur	Ht Value	SO2	Pyritic	Sulfate	Organic
Ratio	C	min	wt%	Btu/lb	lbs/MMBtu	wt%	wt%	wt%
			3.39	12730	5.32	0.90	0.50	2.00
Single-Step Tests								
0.75	390	2	1.48	14055	2.10	0.12	0.04	1.33
0.75	390	25	1.36	13408	2.02	0.06	0.09	1.21
0.75	390	100	1.40	13697	2:04	0.07	0.07	1.26
Two-Step Test: Step 1 - Removing Sulfide (Mostly Pyrite)								
0.75	320	50	1.91	14190	2.69	0.11	0.04	1.76
Two-Step Test: Step 2 - MCL Treat of Depyrited Coal								
0.75	390	2	0.94	14376	1.31	0.03	0.02	0.89
Single-Step Tests								
2.00	390	2	1.09	14216	1.53	0.05	0.02	1.02
2.00	390	100	0.43	12561	0.68	0.04	0.08	0.31
Single-Step Test - Adding Sulfide to Untreated Coal								
**2.00	390	25	2.14	13853	3.09	0.04	0.11	1.99

** H2S added at 170/180C to give 5.89g Na2S, leaving 29.96g NaOH;
Resulting in 1.66:1 NaOH/coal and 0.33:1 Na2S/coal.

TABLE 3
MCL EXPERIMENTS WITH LOW-SULFUR PITTSBURGH #8 COAL
EFFECTS OF REMOVING OR ADDING SULFIDE

-----Run Conditions-----			--Analyses, mf basis--			---Sulfur Forms, mf---		
NaOH/Coal	Temp.	Time	Sulfur	Ht Value	SO2	Pyritic	Sulfate	Organic
Ratio	C	min	wt%	Btu/lb	lbs/MMBtu	wt%	wt%	wt%
Low-Sulfur Pgh #8			2.03	13844	2.93	1.02	0.01	1.01
Single-Step Tests								
0.75	390	50	1.07	14082	1.52	0.11	0.03	0.93
0.75	430	2	1.09	14201	1.53	0.08	0.04	0.97
0.75	430	25	1.03	13900	1.48	0.05	0.05	0.93
2.00	390	50	0.62	14464	0.86	0.04	0.01	0.57
Two-Step Tests: Step 1 - Removing Sulfide (Pyrite)								
0.50	250	25	1.38	14389	1.92	0.08	0.04	1.26
Two-Step Tests: Step 2 - MCL Treat of Depyrited Coal								
0.25	390	25	0.91	14418	1.26	0.04	0.02	0.86
0.50	390	25	0.59	13234	0.89	0.02	0.03	0.54
0.75	390	25	0.60	14525	0.83	0.02	0.07	0.52
0.75	390	100	0.28	13304	0.42	0.01	0.03	0.24

TABLE 4
MCL EXPERIMENTS WITH HIGH-SULFUR PITTSBURGH #8 COAL
EFFECTS OF REMOVING OR ADDING SULFIDE

-----Run Conditions-----			--Analyses, mf basis--			---Sulfur Forms, mf---		
NaOH/Coal	Temp.	Time	Sulfur	Ht Value	SO2	Pyritic	Sulfate	Organic
Ratio	C	min	wt%	Btu/lb	lbs/MMBtu	wt%	wt%	wt%
TRW Sample			4.33	12521	6.91	1.07	0.50	2.76
Tra-Det Sample			4.45	13326	6.67	1.95	0.05	2.45
Single-Step Tests - Comparing Two Pgh #8 Samples								
TRW@ 2.00	390	50	2.43	14013	3.47	0.07	0.11	2.26
T-D@ 2.00	390	25	1.83	14391	2.54	0.05	0.05	1.73
TRW@ 2.00	430	25	2.20	13572	3.24	0.06	0.20	1.93
T-D@ 2.00	430	20	1.39	13842	2.01	0.05	0.08	1.26
Tra-Det Sample Used for All Tests Below								
Two-Step Tests: Step 1 - Removing Sulfide (Pyrite)								
0.62	250	25	3.33	13413	4.96	0.09	0.09	3.17
Two-Step Tests: Step 2 - MCL Treat of Depyrited Coal								
0.25	390	25	2.16	14257	3.03	0.03	0.11	2.02
0.75	390	25	1.34	12844	2.08	0.05	0.13	1.16
0.75	410	25	0.79	14028	1.13	0.02	0.10	0.67
0.75	430	25	0.63	13867	0.91	0.03	0.06	0.54
2.00	390	25	0.65	14312	0.91	0.01	0.11	0.54
2.00	410	25	0.34	14109	0.48	0.02	0.08	0.23
2.00	430	25	0.38	13746	0.55	0.04	0.08	0.27
Single-Step Test: High Ratio MCL Treat								
*5.00	400	25	0.73	15066	0.97	0.02	0.01	0.69
Single-Step Test - Adding Sulfide to MCL Cleaned Coal (*)								
1.67	390	25	1.51	14884	2.03	0.03	0.06	1.42
0.50 Na2S								

DESIGN OF MULTI-STAGE LIQUEFACTION PROCESS FOR COMPLETE COAL CONVERSION AND EXTENSIVE UPGRADING

Isao Mochida, Kinya Sakanishi, Masahiro Kishino, Katsuyuki Honda
Institute of Advanced Material Study, Kyushu University,
Kasuga, Fukuoka 816, JAPAN

Keywords: Multi-stage liquefaction, Coal pretreatment, Hydrogen donor, Catalytic upgrading

INTRODUCTION

Increasing coal consumption to meet the increasing demand of energy in the world should minimize the effects on the environment on the earth. The highest efficiency of energy use and the deepest reduction of pollutants such as SOx, NOx and solid waste are the key technologies to solve the problems of climate change, acid rain and environmental contamination urgently to prepare their rapid growth. Thus, clean coal technologies are most expected to be developed. The ultimate cleaning of coal can be achieved only after the complete conversion of coal into fluid form by removing completely the pollutant sources of S, N and minerals since they are bound intimately to the organic parts.

The liquefaction has been proved to provide the whole products to be completely free from pollutants and very handy for clean uses. The problems still remain in the low efficiency and high cost. Hence, the authors set up the targets of the current liquefaction technology.[1)]

1. Complete conversion of coal organics into fluid fuels, leaving only minerals to be fully separated in forms free from contaminants.
2. Catalyst recovery from minerals to recycle it and reduce the amount of solid wastes.

To achieve the targets, authors are examining;

1. Coal pretreatment to enhance its reactivity throuth removal of minerals and oxgen functional groups as well as reagent impregnation.[2,3)] The problems of scale and sludge are expected to be moderated.[4)]
2. Design of hydrogen donor and dissolving solvents[5,6)]
3. Rapid heating and short contact time at a fairly high temperature for the hydrogen transferring liquefaction[7,8)]
4. Design of recoverable catalysts of high activity[9)]

The suppression of preasphaltene formation by controlling retrogressive reactions during the liquefaction, or its activaton and digestion if it is produced, and the modification of less reactive components including some of inert macerals are the key objectives in our current study.

EXPERIMENTAL

An Australian subbituminous (Wandoan) coal, its liquefaction residue(WD-LR) in a 1 t/d process support unit at 450℃ under 17 MPa H_2 pressure, and an Australian brown(Morwell) coal were ground to pass 250 μm screen and dried in vacuo for 10 hr at 100℃. Their elemental analyses are summarized in Table 1.

The ground coal was mixed with 10 vol% alcohol / 0.01 N or 1 N HCl, stirred for prescribed times under reflux or at room temperature, filtered, washed with water, and dried at 100℃ for 10hr.

Synthetic FeS_2 and commercially available KF-842(Ni-Mo/Al_2O_3) catalysts were presulfided at 360℃ for 6 hr before their use.

1,2,3,10b-tetrahydrofluoranthene(4HFL) was chosen as a liquefaction solvent because of reasons why it has high dissolving activity when dehydrogenated, high boiling point and thermal stability, and four donorable hydrogens in a molecule. 4HFL was prepared from fluoranthene by hydrogenation at 250℃ under 15 MPa using the sulfided NiMo catalyst,[7,8)] followed by vacuum distillation and recrystallization procedure for its purifications.

Liquefaction was carried out in an autoclave (50ml volume). The ground coal (3.0g), the

solvent (4.5g) and catalyst (0.09g) were transferred to the autoclave. The products remaining in the autoclave were extracted with THF, benzene and hexane.The hexane soluble (HS), hexane insoluble but benzene soluble (HI-BS), benzene insoluble but THF soluble (BI-THFS), and THF insoluble (THFI) substances were defined as oil, asphaltene, preasphaltene, and residue, respectively. A small amount (<5%) of solvent derived products, which remained in the HI-BS fraction, was corrected by g.c. analysis. The gas yield was calculated by the difference between the initial (dry ash free base) and recovered residual weights. Thus, the weight loss during the experiment was included in the gas yield.

The first step in two-step liquefaction was carried out in a tube bomb of 20 ml capacity (the heating rate: ca.250℃/min) or autoclave of 50 ml capacity (ca.8℃/min). The coal (3 g) and the solvent (3 or 4.5 g) were transferred into the reactor, which was then pressurized with nitrogen to 1 MPa at room temperature after replacing the air with nitrogen. The tube bomb was then immersed in a molten tin bath at the prescribed temperature and agitated axially. The same procedure was applied to the autoclave liquefaction except for much slower heating rate in an electric furnace.

RESULTS

Effects of Deashing Pretreatment on the Liquefaction of Wandoan coal

Products distributions in the non-catalytic hydrogen-transferring liquefaction of Wandoan and its deashed coals are illustrated in Figure 1. 4HFL solvent of three times weight to the coal was very effective to liquefy the non-treated coal into 38% oil and 34% asphaltene by the reaction at 420 ℃-30 min under 2 MPa N_2 pressure, leaving 18% preasphaltene and 6% residue. The deashing with 1 N HCl / 10% methanol at 60℃ increased very much the oil yield upto 49% with decreased yields of asphaltene, preasphaltene, and residue. Especially, the reductions of asphaltene and residue yields are remarkable by deashing. These results suggest that the deashing pretreatment can accelerate the conversions of THFI residue containing some of inert macerals to soluble fractions, since the coal carries ca. 20 % of total unreactive macerals, as well as those of pre-asphaltene and asphaltene to oil.[10,11]

Figure 2 illustrates the products distributions in the catalytic liquefaction of Wandoan and its deashed coals at 450℃ with FeS_2 catalyst under 15 MPa H_2 pressure. The liquefaction at 450℃ -60 min and 4HFL/coal ratio of 1.5 converted 90% of the coal into soluble products with major products of 48% oil and 38% gas, leaving 9% of THFI residue. The deashing pretreatment at room temperature, regardless of the acid concentration, reduced the residue to 5%, although the enhanced yield of gas led to no increase of oil yield. It is noted that the deashing pretreatment even under much milder conditions with dilute acids can activate the coal, reducing the heavy liquefaction products probably by suppressing their retrogressive reactions.

Figure 3 illustrates the two-stage liquefaction of Wandoan and its deashed coals under reaction conditions of 450℃-7 min at the first step without catalyst and 400℃-20 min under 10 MPa H_2 pressure at the second step with FeS_2 catalyst. The deashing pretreatment at 60℃ with 10% methanol/1 N HCl decreased the gas yield very much with 70% oil yield by the mixed solvent of 75% 4HFL / 25% pyrene at the solvent/coal ratio of 1.5, although the yields of heavy products were larger than those of the non-treated coal probably due to shortage of transferable hydrogens at the solvent/coal ratio of 1.5. Highly active catalysts for direct hydrocracking of asphaltene and pre-asphaltene and/or rehydrogenating dehydrogenated solvents are to be designed for furhter increase of distillate yield at the low solvent/ coal ratio of 1.5 under lower hydrogen pressure of 10 MPa.

Influences of Deashing on the Liquefaction of Morwell coal

Effects of deashing time under reflux and at room temperature on the non-catalytic hydrogen-transfer liquefaction of Morwell coal are illustrated in Figures 4 and 5, respectively. The deashing under reflux for 24 hr gave inferior product distributions compared to those of the same treatment but for shorter treatment times, indicating that some retrogressive reactions should take place during the deashing under reflux. On the other hand, the deashing at room temperature for 24 hr provided

much better product distributions, giving 40% of oil yield and ca. 60% of oil+asphaltene yield.

Figure 6 shows the product distribution in the two-step liquefaction of deashed Morwell coal which was pretreated in 10% methanol/1 N HCl under reflux and at room temperature for 24 hr. The pretreatment at room temperature gave higher oil yield ca.50% with less preasphaltene yield of 2% than those given by the deashing under reflux conditions. Thus, the complete conversion to oil and asphaltene, which can be fed to the second upgrading stage, can be achievable by the multi-stage liquefaction scheme.

Catalytic Upgrading of Wandoan liquefaction distillation residue(WD-LR)

Figure 7 shows products distributions in the catalytic upgrading of WD-CR produced in the 1t/d process support unit of NEDOL process. The WD-CR consists of 27% HS, 44% HI-BS, 11% BI-THFS, and 18% THFI. The single-stage hydrotreatment at 380℃-40 min with FeS_2 catalyst increased HS yield to 54%. The two-stage hydrotreatment, where the first stage was non-catalytic hydrogen transfer at 4HFL/CR of 1.5 at 450℃-7 min without catalyst followed by the second stage at 400℃-20 min with FeS_2 catalyst, further increased the HS yield to 71% with decreasing yields of BI-THFS and THFI to 2 and 3 %, respectively. However, a large amount (24 %) of HI-BS (asphaltene) still remained even after the two-stage hydrotreatment, indicating that the asphaltene fraction should suffer some retrogressive reactions during the PSU liquefaction process because of higher reaction temperature and/or excessive heating during the vacuum distillation of liquefaction products. Hence, multi-stage approaches are suggested to be designed to suppress the retrogressive reactions for the complete conversion of organic fractions into oil, because the refractory products are very difficult to be upgraded even in the catalytic process.

DISCUSSIONS

Current research on the coal macromolecules emphesizes their linearity in terms of their covalent bonds in their chain concerned, suggesting their high solubility in potential. The three dimensional networks of the macromolecules are principally formed by the non-covalent bridges through their chains to determine the properties and reactivity such as solubility and recombination of the thermally fissioned bonds as the solid or highly viscous state of the coal. Hence, the liberation of any non-covalent bridges prior to or duing the liquefaction is expected to enhance the solubility of macromolucles and suppress the retrogressive reaction of produced radical species, favoring the progress of liquefaction. Such non-covalent bridges can be found in the asphaltene and preasphaltene which are substantially polymeric, carrying still a number of polar functional groups.

The resons why the inert macerals are inert in the pyrolytic and liquefaction processes appear multi-fold. Many fusinites are believed to be like char, where a large condensed-aromatic planes have stacked in amorphous manners as if it had been carbonized. However, some of the inertinites consist of organic macromolecular chains strongly bound each other just like some thermosetting polymers such as cellulose. The latter structure can be liberated to be reactive by deshing treatment.

The present study revealed that acid washing to remove cationic ions enhanced the liquefaction to reduce the organic residue. By the acid of solvent of hydrogen donor and dissolving ability, no THF insoluble organic residue is left after the liquefaction of some coals, especially for Australian brown coals.[1] The present study revealed that the deashing pretreatments can accelerate the depolymerization of Wandoan subbituminous coal, converting it almost completely to THF soluble fraction even though it has a large amount of inert macerals.[12] Such pretreatments significantly reduced the amount from coals which carry a significant amount of inert macerals. Some of inert macerals are activated to be liquefied by the treatment. The acid treatment is also effective to activate asphaltene and preasphaltene by removing trace amount of cationic ions. Such all results indicate major roles of cationic bridges in the coal macromolucles which are one of the major obstacles for their smooth depolymerization.

Other pretreatments such as preheattreatment[13] and impregnation of polar reagent[14] are

also effective, although their significance is not fully proved. Althouh more effective conditions or procedures should be explored, the principles to liberate macromolecular assembles appear correct. The intermolecular bridges are postulated as hydrogen bonds, cationic bridges, charge transferring polar bonds, and π - π stacking. Such bridges except for the last one in the high ranking coals are based on the polar groups. Hence, any procedures to remove polar groups and to loosen their non- covalent interactions can be effective. The recombination reactions should be carefully avoided when the polar groups are intended to be removed. The conditions should be carefully controlled.

Selection of solvent in terms of hydrogen donor and dissolving ability as well as optimization of liquefaction conditions in terms of heating rate, temperature and time are carefully designed[15], since the progressive and retrogressive reactions always take place competitively and consecutively in the coal liquefaction. The change of solvent according to the reaction progress should be also taken into account. The optimum conditions for the catalysis under high hydrogen pressure may differ from those of non-catalytic thermal process.[16] Hence, the multi-stages are very reasonable to set up the optimum conditions from the respective stages. Although we have not yet reached to clarify the optimum conditions, we have achieved the highest yields of oil and asphaltene with least amount of organic residue.

The present authors have proposed twe types of recoverable catalysts for the coal liquefaction.[1] They are separable by their stable ferromagnetism under coal liquefaction conditions and by floating ability to the boundary layer of two solvents. Preliminary results may promise their recovery and catalytic activities. The deashing pretreatment facilitate the recovery and regeneration of the catalyst for its repeated uses.[17] Further development is now in progress.

REFERENCES

1) Mochida,I., Sakanishi,K., Sakata,R., Honda,K., Umezawa,T., Energy & Fuels in press.
2) Mochida,I., Yufu,A., Sakanishi,K., Korai,Y., Fuel, 1988, 67, 114.
3) Larsen,J.W., Pan,C.-S., Shawver,S., Energy & Fuels, 1989, 3, 557.
4) Sakanishi,K., Honda,K., Mochida,I., Okuma,O., Proc.Pittsburgh Coal Conf., 1993, 198.
5) Mochida,I., Takayama,A., Sakata,R., Sakanishi,K., Energy & Fuels, 1990, 4, 81.
6) Sakata,R., Takayama,A., Sakanishi,K., Mochida,I., Energy & Fuels, 1990, 4, 585.
7) Mochida,I., Otani,K., Korai,Y., Fuel, 1985, 64, 906.
8) Mochida,I., Kawamoto,N., Kishino,M., Otani,K., Korai,Y., Fuel, 1986, 65, 81.
9) Mochida,I., Sakanishi,K., Kishino,M., Honda,K., Umezawa,T., Yoon,S.H., ACS Div. Fuel Chem., 1993(Denver), 38(1), 93.
10) Mochida,I., Kishino,M., Korai,Y., Sakanishi,K., J.Fuel Soc.Jpn., 1986, 65, 828.
11) Mochida,I., Yufu,A., Sakanishi,K., Zhao,X.Z., Okuma,O., Hirano,T., J. Fuel Soc. Jpn., 1989, 68, 244.
12) Mochida,I.,Kishino,M.,Sakanishi,K.,Korai,Y.,Takahashi,R., Energy & Fuels, 1987, 1, 343.
13) Mochida,I.,Yufu,A.,Sakanishi,K.,Korai,Y.,Shimohara,T., J.Fuel Soc.Jpn., 1986, 65, 1020.
14) Korai,Y., Torinari,Y., Mochida,I., Cokes-circular Jpn., 1992, 41(4), 232.
15) Mochida,I., Sakanishi,K., Korai,Y., Fujitsu,H., Fuel Process. Technol., 1986, 14, 113.
16) Sakata,R., Sakanishi,K., Mochida,I., Proc. Int. Conf. Coal Sci., 1991, 707.
17) Sakanishi,K., Honda,K., Sakata,R., Mochida,I., 5th Australian Coal Sci., 1992, 97.

Table 1 Elemental Analyses of Coals and Liquefaction Residue

	Wt % (d.a.f. basis)				Ash
	C	H	N	(O+S)diff.	(Wt %)
Wandoan coal	76.3	6.1	1.1	16.5	7.9
Deashed Wandoan coal	76.2	6.2	1.0	16.6	7.0
Wandoan-PSU residue	85.8	5.6	1.5	7.1	29.4
Morwell coal	66.7	4.9	0.6	27.8	2.3
Deashed Morwell coal	63.4	5.0	0.6	31.0	1.7

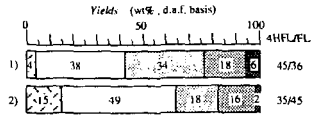

Figure 1 Effect of deashing on the hydrogen-transfer liquefaction yield from Wandoan coal

: Gas , : Oil , : Asphaltene , : Preasphaltene , : THFI

1): non-treated Wandoan coal,
2): Deashed Wandoan coal under reflux in10vol%MeOH/1 N HCl for 24hr
(liquefaction conditions 4HFL/coal =9.0/3.0(g), 20 atm N_2 ,420℃-30min)

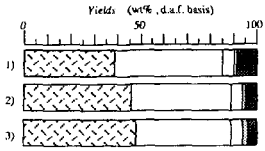

Figure 2 Effect of deashing on the catalytic liquefaction yield from Wandoan coal

: Gas , : Oil , : Asphaltene , : Preasphaltene , : THFI

coal pretreatment conditions;
1) non-treated Wandoan coal
2) 1N-HCl/10vol%EtOH / room temperature / 6hr
3) 0.01N-HCl/10vol%EtOH / room temperature / 6hr
liquefaction conditions (catalytic liquefaction);
4HFL/coal/FeS_2 catalyst =4.5/3.0/0.09(g),
H_2 reaction pressure=15 MPa, 450℃-60 min

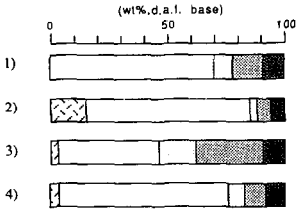

Figure 3 Influence of deashing on the two-stage liquefaction of Wandoan coal
(4HFL/Pyeren/Coal = 3.4/1.1/3.0 g)
Gas, Oil, Asp. , Preas. , THFI
1),2): non-treated coal,
3),4): deashed coal under reflux in 10% MeOH/1 N HCl
1) Non-catalytic first stage at 450℃-7 min
2) Catalytic second stage at 400℃-20 min
3) Non-catalytic first stage at 450℃-7 min
4) Catalytic second stage at 400℃-20 min

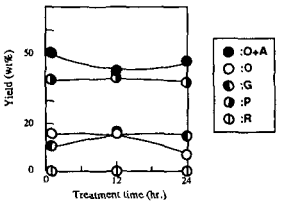

Figure 4 Effect of deashing time under reflux on the liquefaction yield from Morwell coal
(Deashing treatment ; under reflux in 10% MeOH/1N HCl)
(430℃-2min., 4HFL/coal=1.5/1, no catalyst, 20 atm N_2, tube bomb)

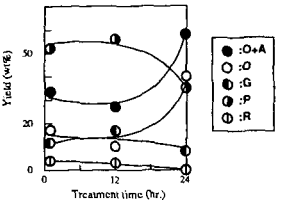

Figure 5 Effect of deashing time at room temperature on the liquefaction yield from Morwell coal
(Deashing treatment ; at room temperature, 10% MeOH/1N HCl)
(430℃-2min., 4HFL/coal=1.5/1, no catalyst, 20 atm N_2, tube bomb)

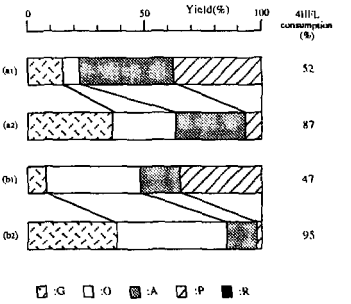

Figure 6 Two-stage liquefaction of deashed Morwell coal

(a1),(b1) First-stage Non-catalytic Hydrogen-transferred Morwell Coal in the Two-stage Hydrotreatment (430℃-2min, 20 atm N_2, tube bomb and molten tin bath, rapid heating)
4HFL/coal=4.5g/ 3.0g
(a2) ,(b2) Second-stage Catalytic Hydrotreated Morwell Coal in the Two-stage Hydro-treatment (380℃-20 min, 50 cc autoclave, slow heating)

(a1),(a2) Deashing treatment ; under reflux , 24hr, 10% MeOH/1N HCl
(b1),(b2) Deashing treatment ; room temp., 24hr, 10% MeOH/1N HCl

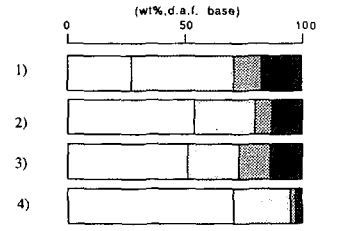

Figure 7 Single- and two-stage hydrotreatments of Wandoan liquefaction residue(WD-LR)

Oil, Asphaltene, Preasphaltene, THFI

1) WD-LR as received
2) Single-stage hydrotreatment at 380℃-40 min(autoclave) under 10 MPa H_2 with FeS_2 and 75% 4HFL/25% pyrene at solvent/WD-LR of 1.5
3,4): Two-stage hydrotreatment;
3) Non-catalytic first-stage hydrotreatment at 450℃-7 min(rapid heating) under 2 MPa N_2 with 75% 4HFL/25% pyrene at solvent/WD-LR of 1.5
4) Catalytic second-stage hydrotreatment at 400℃-20 min(autoclave) under 10 MPa H_2 with FeS_2

CHANGES IN ORGANIC SULFUR COMPOUNDS IN COAL MACERALS DURING LIQUEFACTION

Randall E. Winans
Chemistry Division, Argonne National Laboratory
Argonne, IL 60439

J. T. Joseph and R. B. Fisher
Amoco Oil Company Research and Development
Naperville, IL 60566

Keywords: Coal macerals, liquefaction, sulfur types

INTRODUCTION

Environmentally sound use of coal for energy production involves effective sulfur removal from the feed coal and/or coal-derived products. Physical cleaning of coal is effective in removing substantial quantities of inorganic sulfur compounds such a pyrite. However, removal of organic sulfur by physical means has not been extremely successful. It is likely that only chemical methods will be useful in substantial removal of organic sulfur. A thorough knowledge of the chemistry of organic sulfur in coal will be valuable in attempts to remove organic sulfur from coal or its liquefaction or pyrolysis products by chemical methods. Since different coal macerals have different liquefaction reactivities, the analysis of sulfur functionalities on separated macerals is deemed to be more meaningful than studying the whole coal. Liquefaction behavior[1] and organic sulfur speciation of the macerals separated from Lewiston-Stockton coal (Argonne Premium Coal Sample bank, APCS-7) by XPS, XANES, and HRMS has been previously described[2]. This paper describes the preliminary speciation of sulfur compounds in the asphaltene fraction of the liquefaction products from these macerals.

EXPERIMENTAL

Separation of liptinite, vitrinite, and inertinite macerals from APCS 7 coal was achieved by density a gradient centrifugation methods[3]. The liquefaction of the macerals was performed in tubing bomb reactors under hydrogen pressure and in the presence of tetralin as a donor solvent. The details of maceral separation and liquefaction procedures have been published earlier[1]. The liquefaction products were successively extracted with hexane, toluene, and tetrahydrofuran (THF). The hexane soluble fraction together with light gases was called oils+gases, hexane insoluble-toluene soluble fraction was called asphaltenes, and toluene insoluble-THF soluble fractions was called preasphaltenes. Desorption chemicals ionization (DCI) and desorption electron impact (DEI) mass spectral analyses of the asphaltene and preasphaltene fractions were carried out on a three sector high resolution Kratos MS 50 Mass Spectrometer, operating at 10,000 to 40,000 resolving power[2]. The oil fraction was not analyzed because of the presence of large quantities of tetralin and its reaction products.

RESULTS AND DISCUSSION

Table 1 Maceral Characteristics and Product Yields

			Per 100 Carbons				Wt. % maf		
Maceral	% C (maf)	% Ash	H	N	S	O	Oil	Asphaltene	Preasph.
Liptinite	81.7	--	110	1	0.5	8.9	20	54	13
Vitrinite	80.2	0.9	78	1.7	0.3	12	7	33	22
Inertinite	85.4	2.4	46	1.3	0.7	7.5	0	13	12

Selected information on these maceral samples and liquefaction yields are shown in Table 1. It is apparent that the sulfur content of these samples is typical of a bituminous coal, with an intermediate value. As has been seen observed in other samples, the liptinite is slightly richer in sulfur than the vitrinite. However, the difference may be much larger for the organic sulfur. The demineralization does not remove the pyrite which probably accounts for some of the 0.9% ash in the sample. The inertinite probably contains even more pyrite. Most of the sulfur in these macerals was derived from peptides in the original plant material and is not of secondary origin such as found in high sulfur coals.

The distribution of sulfur compounds determined by DEIHRMS for the unreacted macerals is shown in Figure 1. Although only a fraction of the organic sulfur compounds are volatilized by pyrolysis, in a comparison with two direct techniques the ratio of aliphatic to aromatic sulfur compounds agree within experimental error[2]. This result suggests that the species observed are representative of the whole maceral. The average size of the molecules is observed by DEIHRMS is 300-350 which, based on the heteroatom content, would suggest that an average molecule will have more than one heteroatom. This is statistically more significant for the less abundant heteroatom such as sulfur. The results shown in Figure 1 match this hypothesis. It is interesting to note the relatively large abundance of compounds containing both nitrogen and sulfur. This may be related to the hypothesized origin of sulfur compounds from peptides which are rich in nitrogen. Also, the abundant yield of the combination with oxygen would result from this type of input of organic materials. Overall, the abundance of aromatic sulfur species increases in the order liptinite < vitrinite < inertinite which also follows inversely the liquefaction reactivity.

The sulfur results for HRMS of the asphaltene fractions are shown in Figure 2. Several general trends can be noted. Aliphatic sulfur compounds are in very low abundance while larger polycyclic aromatic sulfur compounds are in significant abundance. What is striking is the dominance of molecules containing two sulfur atoms. These species are similar across all three maceral groups as is demonstrated in Figure 3. Because of this similarity, we feel that they are the result of secondary reactions possibly between H_2S and the solvent tetralin. Possible disulfide structures for the hydrogen deficiency of 9 is shown below(I and II). These species are currently be investigated using tandem MS which will provide structural information. Another commonality between the three macerals is found for S+O for a hydrogen deficiency of 14. A likely possible structure is the combination of a thiophene and furan(III).

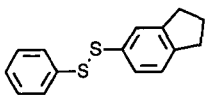

I

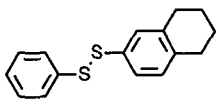

II

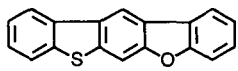

III

If the results for the ashpaltene is adjusted for the yields, one can directly compare products with the starting material. This has been done for the liptinite and the results are shown in Figure 4. For the single sulfur compounds the aliphatics are gone and large polycyclic aromatics were formed. However, the overall abundance decreased. The total yields of two sulfur compounds were very similar but there was a different mix of molecules with the same general trend observed for the single sulfur. The S+O species shifted to more polycyclic aromatics in the products. Compounds with both N and S must be very reactive under these liquefaction conditions since they are gone in the products.

SUMMARY

Several general trends were observed in the reactivity patterns of sulfur compounds in macerals. Sulfur is reduced in the asphaltene fraction compared to the initial maceral. Aliphatics are removed and polycyclic aromatic compounds are both stable and probably formed under these conditions. Molecules containing two sulfur atoms are formed. The preasphaltenes are now being analyzed by DEIHRMS.

ACKNOWLEDGEMENT

This work was performed under the auspices of the Office of Basic Energy Sciences, Division of Chemical Sciences, U.S. Department of Energy, under contract number W-31-109-ENG-38.

REFERENCES

1. Joseph, J. T.; Fisher, R. B.; Masin, C. A. ; Dyrkacz, G. R.; Bloomquist, C. A.; Winans, R. E. *Energy Fuels*, **1991**, *5(5)*, 724-729.
2. Winans, R. E.; Melnikov, P. E.; Dyrkacz, G. R.; Bloomquist, C.A.; Gorbaty, M. L.; George, G. N. *Am. Chem. Soc., Div. Fuel Chem. Prepr.*, **1993**, *38(2)*, 375-378.
3. Dyrkacz, G. R.; Bloomquist, C. A., *Am. Chem. Soc., Fuel Chem. Prepr.*, **1988**, *33(3)*, 128-135.

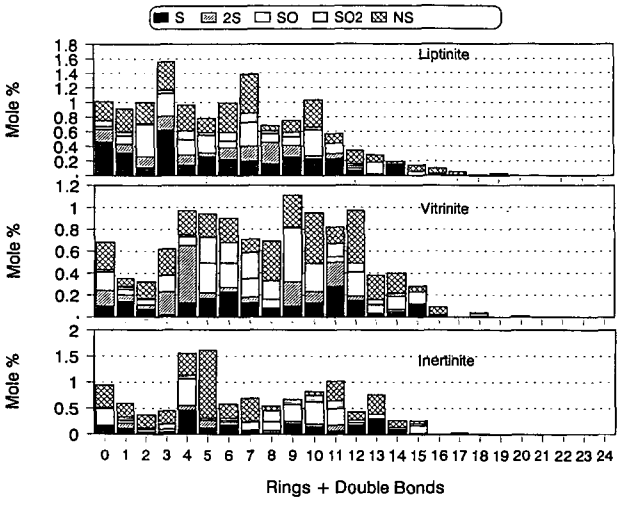

Figure 1. Distribution of sulfur containing molecules from DEIHRMS of the unreacted macerals.

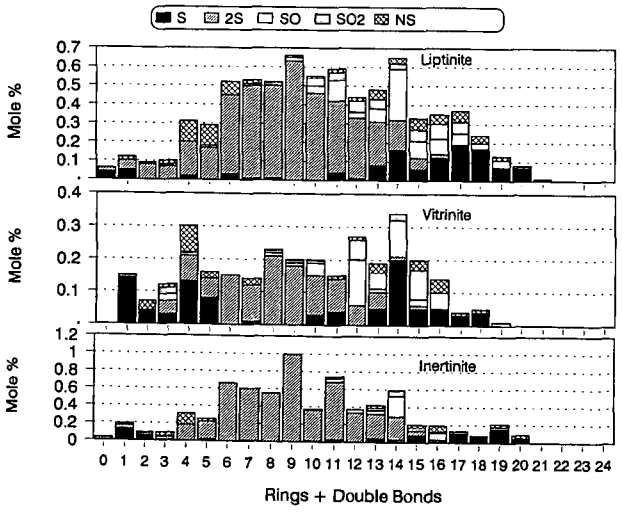

Figure 2. Distribution of sulfur containing molecules from HRMS analysis of the asphaltene products of the liquefaction of the macerals.

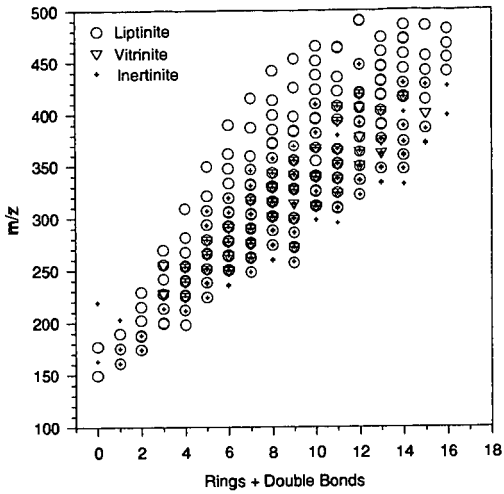

Figure 3. Occurrence of molecules which contain two sulfur atoms in the asphaltene products.

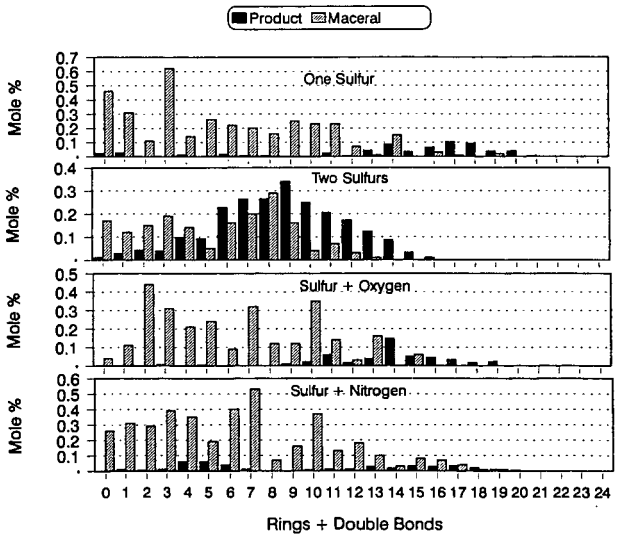

Figure 4. Comparison of sulfur types from the whole maceral and from the asphaltene product of the liptinite. Raw product data were multiplied by 0.54, which is the yield for asphaltene.

CHEMICAL DESULFURIZATION OF COAL: PARTITIONING SULFUR TO GAS AS H_2S

John M. Stencel, James K. Neathery, and Jidong Yang
Center for Applied Energy Research
University of Kentucky
Lexington, KY 40511

Keywords: Coal desulfurization, gasification, phosphoric acid

INTRODUCTION

The yields and characterisitics of products from mild temperature gasification or pyrolysis of coal have been evaluated extensively in fundamental and process development efforts. At 500°C, the following has been presented as representing the sulfur product distribution from US bituminous coals (1,2):

$$\text{Total sulfur in gas} = 0.31 \times S_{coal}$$
$$\text{Total sulfur in tar} = 0.06 \times S_{coal}$$
$$\text{Total sulfur in solid} = 0.61 \times S_{coal}.$$

This type of distribution is affected by factors such as coal type, sulfur content and form, particle size, heating rates, temperature of pyrolysis, reactor and process design, and the type of reactants to which the coal is subjected. For example, increasing the pyrolysis residence time usually decreases the sulfur content in the char and increases the tar and gas yields and their sulfur content.

As indicated above, and in other mild temperature gasification studies of low-to-high sulfur coals at temperatures between 400-825°C (3-5), the coal sulfur was distributed nonselectively to all products. As a consequence, the upgrading required to meet environmental regulations has to be applied to more diverse products than the coal from which the products were derived. The severity of such upgrading, and the severity to which coal has to be treated to release all of its sulfur, depends on the chemical form of the sulfur. Recent analytical efforts have begun to define these sulfur forms in coal, the most refractory organic species of which are thiophenic in nature (6,7).

In the current study, the mild temperature pyrolysis of Illinois basin coals mixed with phosphoric acid under continuous-feed, bench-scale fluidized bed conditions at 500°C is reported. The extent of sulfur removal and its partitioning to gas as H_2S are discussed in relation to its chemical form in the coal. Swelling characteristics of coal/acid mixtures are also discussed relative to operation of the fluidized bed reactor.

EXPERIMENTAL

The two coal samples (labelled as VA and VB) were obtained from the Illinois Basin Coal Sample Program and were both from the Springfield seam (Indiana V), but were sampled at different locations in the seam and at different times. Their composition is presented in Table 1.

The coals were admixed with 50% strength, reagent grade phosphoric acid to attain coal:acid weight ratios of 1.0:0.65 and 1.0:0.96 or with water to produce a coal-only sample having a coal:acid ratio of 1.0:0. These mixtures were dried at 200°C in a nitrogen purged furnace then vacuum dried at the same temperature. The dried samples were stored in sealed containers subsequent to purging with argon until they were treated in a bench-scale reactor.

A schematic of the fluidized bed reactor system is presented in Figure 1. The reactor had a 7.6 cm diameter and was 100 cm in height. Dried coals were loaded into a pressurized hopper located on a precision screw feeder. Coal was dropped from the screw outlet of the feeder into a eductor line which led to the bottom of the gasifier. Gasification tests were as long as four hours in duration with average coal feeds of 0.1-0.3 kg/h.

Nitrogen, nitrogen/air or nitrogen/steam were used as the fluidizing gas during pyrolysis. These gases were pre-heated in a furnace upstream from the fluid bed. Heat traced lines were used to maintain constant temperatures throughout the reactor and its associated output streams. Chars were collected in the down-leg of a cyclone and in an underbed collection flask. A three-stage condensate collection system was used, with the first stage at 140°C, the second stage at 15°C, and the third stage at 0°C.

Subsequent to pyrolysis and before analysis, the chars were hot water filtered to remove excess phosphorus. For these experiments, a stainless steel, 1.4 l pressure filter (Model KST, Lars Lande Manufacturing, Inc.) was insulated and connected to an in-line water heater, a flow meter and a pump.

RESULTS AND DISCUSSION

Product yields for the two coals were repeatable and similar. On a maf basis, and calculated from (weight feed - weight product)/weight feed, the char yields were near 65% for either 1.0:0.96 or 1.0:0.65 parent coal:acid ratios, and between 70-80% for the same acid ratios when treating physically cleaned coals. These numbers are to be compared with char yields near 60% for coals without added phosphoric acid. The tar yields varied between 0.5-1.5% for coal:acid feeds and near 5% for coal-only feeds. Increasing the phosphoric acid concentration decreased significantly the tar yields.

The duration of the pyrolysis tests using coal-only feeds was slightly greater than one hour, whereas for coal:phosphoric acid feeds the test durations were greater than 2.5 hours. This difference was solely a consequence of difficulties in operating the fluidized bed reactor. For coal-only, agglomeration of the coal in the bubbling bed caused defluidization and bed blockage, and accumulation of tar at the air-side outlet of the cyclone caused pressure increases within the pyrolysis zone and, eventually, bed blockage. Relative to the swelling character of the feed coal, the free swelling index (FSI) was 3.4 whereas the FSI of a 1.0:0.96 mixture was less than one. Previous work examined the effects of HCl on the swelling character of coals (8,9); the present data indicate that phosphoric acid also greatly affects coal thermoplastic properities.

Data presented in Table 1 show the composition of chars produced from the two coals with and without phosphoric acid. Approximately 20% of the sulfur originally in the coals remained in the chars after the 500°C fluidized bed testing of coal:acid mixtures, whereas nearly 70% of the sulfur remained in the char after pyrolysis of coal-only samples. About 90% of the sulfur remaining in the char produced from coal:acid mixtures was organic in nature. The sulfur in the tars accounted for less than 1% of the total amount of sulfur originally in the coals, whereas over 75% of the coal sulfur was selectively partitioned to the gas phase as H_2S.

Char yields were greater for the coal:acid ratio of 1.0:0.65 than for the 1.0:0.96 ratio, and sulfur removal was increased with increasing acid concentration. This behavior may be a result of competition between alkylating and polymerization functions of phosphoric acid, in combination with the influence of creating char porosity during gasification. For example, the BET N_2 surface area of the char from VA was 445 m^2/g when using the 1.0:0.96 coal:acid ratio whereas it was 177 m^2/g when using the 1.0:0.65 ratio. The extent to which sulfur can be removed from coal during hydropyrolysis has been attributed, in part, to the development of porosity (8). In addition, an increased rate of heating during gasification or pyrolysis influences the softening, swelling and shrinking properties of the coals, and changes significantly the porosity of the char. However, phosphoric acid treatment does not increase the concentration of oxygen in the chars relative to that in the coals.

The amount of sulfur removed from coal:acid mixtures was significantly greater than the amount of sulfur removed from coal-only feeds. The extent to which sulfur was removed is similar to that observed in fixed-bed testing using coal:phosphoric acid mixtures (10), although in the current case the mean residence time of the coal within the reactor was on the order of minutes rather than hours.

Practically total elimination of the pyritic sulfur occurred for all coal:acid mixture feeds. It was also observed that this elimination could be facilitated at temperatures as low as 200°C - i.e. during the initial drying/evacuation before fluidized bed treatment at 500°C. Hence, phosphoric acid decreases the temperature at which pyrite decomposition is initiated. In comparison to the sulfur distribution shown above, which is typical of that obtained during mild temperature gasification, the pyrolysis of coal:phosphoric acid under the same conditions produced the following distribution:

Total sulfur in gas ~ 0.80 S_{coal}
Total sulfur in tar ~ 0.01 S_{coal}
Total sulfur in char < 0.20 S_{coal}.

The form of the sulfur which remained in the Indiana V chars is not known. However, the chemical form of sulfur species in Indiana V coal has been investigated by XANES spectroscopy (11). Even though this XANES-investigated sample was oxidized, about 16% of its sulfur could be identified as a thiophenic species. Such a value is in close agreement with the amount of sulfur remaining in the chars from coal:acid mixtures. Hence, the sulfur in the chars may be predominantly thiophenic species.

Phosphorus remaining in the char after pyrolysis can be removed by hydrolysis since there is reversibility between orthophosphoric acid (H_3PO_4) and the pyrophosphoric form ($H_2P_2O_7$) and more polymeric metaphosphate forms. Such removal and the sulfur partitioning suggests a coal utilization scheme as depicted in Figure 2. It would produce valuable elemental sulfur or sulfuric acid from the gas phase H_2S, minimize byproducts formation, and integrate with advanced topping combustor cycles.

ACKNOWLEDGEMENTS

The authors gratefully acknowledge the assistance of Dr. Jack Groppo, Chris Yates and Allen Howard. This work was supported by the Center for Applied Energy Research and the Illinois Clean Coal Institute.

REFERENCES

1) Khan, M. R., ACS Reprint, Div. Fuel Chem., Vol. 33, No 1, pp 253-264 (1988)
2) Khan, M.R., Fuel, 68, 1439(1989).
3) Khan, M.R., Fuel, 68, 1522(1989).
4) Alvin, M.A., Archer, D.H., and Ahmed, M.M., EPRI AP-5005 (Project 2051-2), final report January 1987.
5) Stephenson, M.D., Williams, A.D., Ellis, S.L., Sprague, J.A. and Clauson, G.L., 2nd Intn'l Conf. on Processing and Util. of High Sulfur Coal, (Elsevier Sci. Publ. Co., 1987) pp. 192-201.
6) Gorbaty, M.L., George, G.N., and Keleman, S.R., Fuel, 69, 945(1990).
7) Calkins, W.H., ACS reprints, Div of Fuel Chem. Vol 30 (1985).
8) Lu, G.Q., and Do, D.D., Fuel Proc. Technol. 28, 247(1991)
9) Lee, C.W. and Jenkins, R.G., Energy & Fuels, 3, 703(1989).
10) Derbyshire, F.J., Jagtoyen, M., McEnaney, B., Rimmer, S.M., Stencel, J.M., Thwaites, M.W., Proc. ICCS Conf.,9/16-20/91, Newcastle, England, Butterworth-Heinemann, pp. 480-483.
11) Huffman, G.P., Vaidya, S.A., Shah, N., and Huggins, F.E., Preprints, ACS Div. Fuel Chem., 37,1094(1992).

Table 1. Composition of Indiana V coals (sample A and B) and chars produced during 500°C, fluidized bed pyrolysis.

ANALYSIS(%)	COALS VA	COALS VB	1.0:0.96 RATIO* CHAR A	1.0:0.96 RATIO* CHAR B	COAL-ONLY CHAR B'
Moisture	6.16	5.48	1.88	4.88	3.84
Ash	7.14	8.65	23.61	21.25	10.54
Vol. Mat.	38.37	40.09	22.45	21.54	20.93
Fixed C.	48.30	45.80	52.01	52.22	64.70
Carbon	69.29	67.87	66.77	66.78	74.28
Hydrogen	5.49	5.46	1.86	2.52	3.10
Nitrogen	1.47	1.42	1.61	1.36	1.70
Sulfur	3.45	3.95	0.81	0.95	2.64
Pyritic S	1.50	1.40	0.13	0.18	-
Organic S	1.95	2.51	0.66	0.70	-
Sulfatic S	0.01	0.04	0.02	0.04	-

*1.0:0.96 = Coal:Acid Ratio (see text).

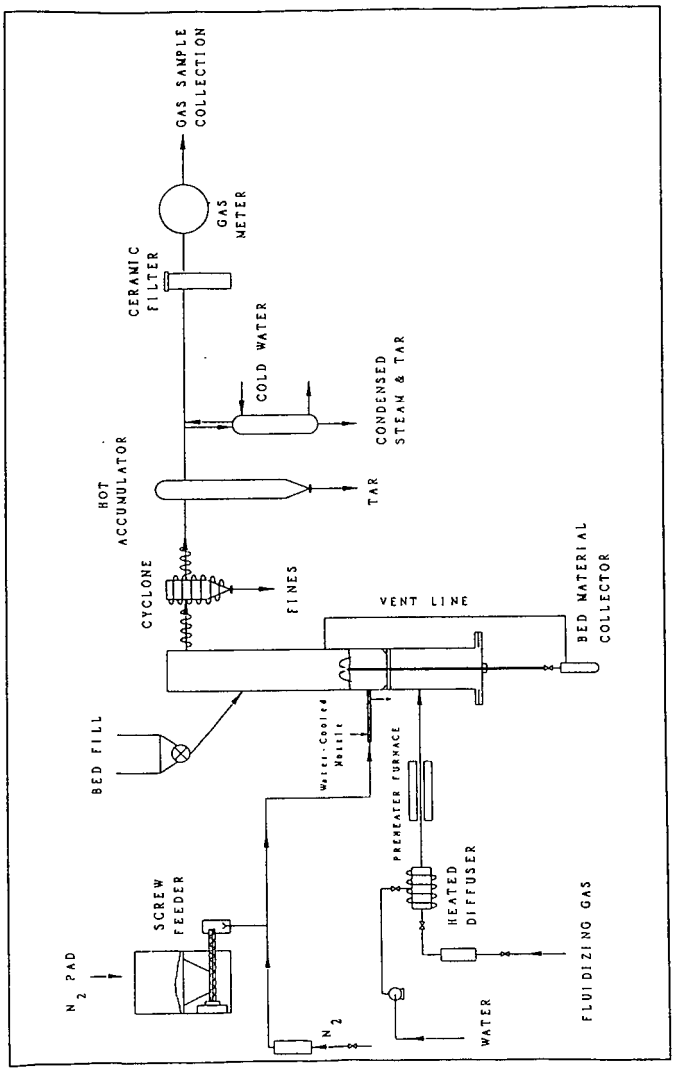

Figure 1. Experimental system used to pyrolyze coal and coal:phosphoric acid mixtures under fluidized conditions.

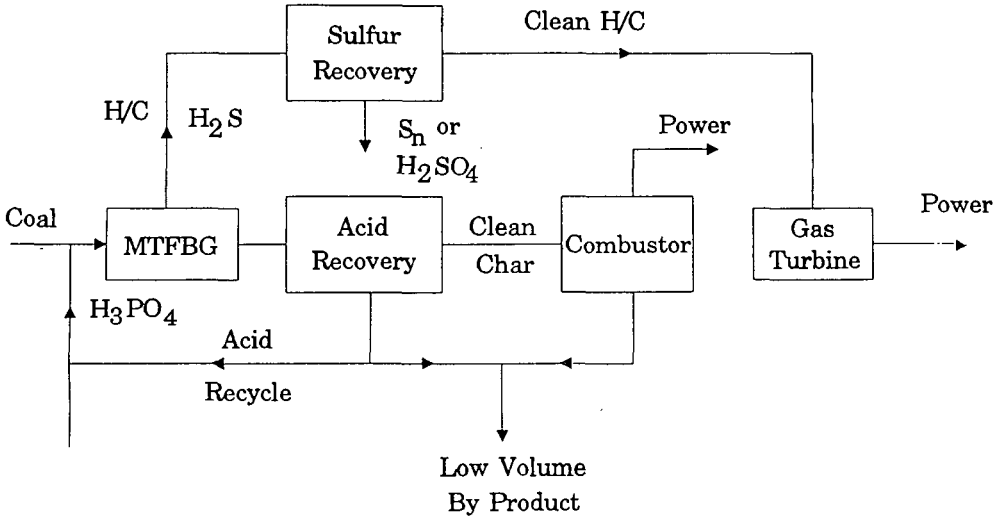

Figure 2. Proposed process using coal:phosphoric acid mixtures.

The Effects of Pre-Oxidation of Cellulose on the Properties of Chars for Methane Storage

Fraser J. Norton, Gordon D. Love and Peter J. Hall
Department of Pure and Applied Chemistry
University of Strathclyde,
295 Cathedral Street Glasgow G1 1XL
SCOTLAND

Key words: Cellulose oxidation, methane storage, porosity formation.

Introduction

In the present economic climate and with ecological awareness at a high, the need for cheaper more environmentally friendly fuels has never been greater [1]. Natural gas is an abundant and relatively clean burning fuel. It is conventionally stored at high pressures for transportation and for use as an alternative vehicle fuel, (Compressed Natural Gas (CNG) pressure is 3000psi). Adsorbed Natural Gas (ANG) systems, which involve adsorption of gas onto porous media, (operating pressure, 500psi), have emerged as a viable alternative to CNG for use as a storage system for natural gas as a vehicle fuel. The methane is stored in the micropores (<20Å) of the adsorbent where the physical forces are such that the methane is at a higher density than that of liquid methane. Weaker forces in the meso (20-200Å) and macro-pores (>200Å) mean that compressed gas at 500psi only is stored in them. Since a finite volume (i.e. storage vessel) of adsorbent can be utilised, it is important that the adsorbent not only possesess high levels of microporosity, but that it is also of a high enough density. Activated Carbons contain high levels of microporosity and can be produced with satisfactorally high densities to be good adsorbents for methane storage. However, the process of creating an activated carbon generally involves gasification of the char with CO_2, O_2 or H_2O in order to increase the overall surface area. This treatment tends to widen the porosity and thus produce higher levels of meso- and macro-pores. By paying more attention to the precursor and the effects of altering its structure on the carbon produced, it may be possible to produce a more uniform microporosity. It was therefore decided to take pure cellulose and change its structure through air oxidation, observing any changes in the porosity of the resultant carbon produced.

Cellulose can be viewed as a linear condensation polymer consisting of D-anhydroglucopyranose units linked by β-1,4-glycosidic bonds [2]. The structure observed for the fully extended cellulose polymer is that of a flat ribbon with laterally protruding hydroxyl groups able to form both inter- and intra-molecular hydrogen bonds. Well-ordered areas of the cellulose structure contain hydrogen bonding between adjacent hydroxyl groups and the disordered areas show water bridging between adjacent chains [3]. The physical structure of cellulose has been studied using a variety of techniques including Differential Scanning Calorimetry (DSC). The difficulty in finding a first order phase transition in cellulose at a temperature lower than that of decomposition, (~500K) has been noted by Hatakeyama *et al* [4].

There has long been interest shown in the partial oxidation of cellulose by chemical means through the use of different reagents, mainly as a means of preventing damage to the cellulose structure during processes such as textile fibre and wood pulp bleaching [2]. However, utilisation of the product formed from physical oxidation through simple heating in an oxygen or air atmosphere of cellulose seems to have been somewhat neglected as a research field, probably because of its degrading effects on the cellulose

polymer. The oxidation of alkali cellulose by gaseous oxygen in order to reduce the degree of polymerisation of wood pulp for viscose rayon production has been the major application of this type of oxidation process, with a controlled degradation of the polymer being desirable.

Cellulose derivatives in the form of biomass are the most common source materials for the production of active carbons. A wide variety of cellulose derivatives varying from coal, lignite, peat, wood through to agricultural waste products are used commercially [5]. The range of activation conditions and methods is equally wide using lower temperature chemical activation [6], higher temperature steam or CO_2 activation [5], or a combination of both. The production of active carbons generally involves pyrolysis of cellulose bases in a highly oxidizing environment with the result that the pyrolysis is performed on oxidized cellulose.

The objective of the present paper is to investigate the effects of pre-oxidation of pure cellulose on the nature of chars produced by pyrolysis in N_2. This is achieved by characterization of the fresh and oxidized cellulose by a variety of common polymer analytical techniques, solid state NMR, (DSC) and elemental analysis. Mass losses during pyrolysis of the fresh and oxidized cellulose was monitored by thermogravimetric analysis (TGA). Characterization of the resulting chars was by nitrogen adsorption at 77K and BET analysis to yield surface area.

Experimental

Cellulose powder (20 micron) was obtained from the Aldrich Chemical company and used as supplied. Oxidation was performed at 473K for varying time in a forced circulation oven in air. Pyrolysis was performed in a tube furnace in a flowing nitrogen atmosphere. The carrier flow rate was 1 $lmin^{-1}$ and the sample size ~5g.

DSC was performed on a Mettler DSC 30 system. Temperature calibration was by the melting points of Indium, Lead and Zinc standards. Temperatures are accurate to ±0.5K. Enthalpy calibration was by integrating the melting endotherm of an Indium standard supplied by Mettler. It was estimated that enthalpies were accurate to ±0.05 J/g. Standard aluminium pans were used with two pin holes to allow evaporation of water and the removal of pyrolysis products. The sample size was 10mg. The polymer was spread in a monolayer over the base of the aluminium pans to maximize heat transfer to the cellulose. The procedure was as follows. The samples were dried *in situ* at 373K for 30 mins and then quenched to the starting temperature of 300K. DSC was then performed at 10K/min to a temperature of 523K using a nitrogen carrier. The samples were again quenched to 300K and DSC performed at 10K/min to 523K. The cycling procedure was repeated a further three times to identify only reversible phase changes in the samples.

25 MHz ^{13}C solid state nmr spectra of oxidised cellulose samples were obtained using a Bruker MSL100 spectrometer equipped with a 7-mm double-bearing probe for cross polarisation (CP) and magic angle spinning (MAS). The samples were spun at a speed of 5kHz, which is sufficient to reduce the side-band intensities to below 5% of those of the central aromatic bands in coals [7]. Typically four thousand scans were accumulated with high-power ^{1}H decoupling in CP experiments employing a contact time of 2ms and a recycle delay of 1.5s. Dipolar dephasing was carried out on one sample to estimate the fraction of non-protonated aromatic carbon present after oxidation. Delays of between 0-200μs were introduced immediately before acquisition during

which the ^1H decoupler was switched off. Those carbons bound to hydrogen are rapidly dephased while non-protonated and rotationally mobile (methyl) carbon dephase more slowly. The attenuation of the non-protonated aromatic carbon signal with increasing dephasing time follows a single exponential law. Thus by plotting ln(aromatic signal area) versus dephasing time and extrapolating the best line fit through data in the region 60-200μs to time zero, one can obtain an estimate of the fraction of non-protonated aromatic carbon. All FIDs were processed using exponential line broadening factors of 20Hz prior to Fourier transformation.

TGA was measured in a Stanton Redcroft TG750. A heating rate of 10 K/min was used and an air carrier. The typical sample size for TGA was ~10mg.

Surface area determinations were made from N_2 adsorption at 77K with a BET analysis. Samples were outgassed in situ to 10^{-4} Torr at a temperature of 398K for at least 12 hours before the adsorption was determined volumetrically in a Micromeretics Accusorb 2100E machine.

Results and Discussion

Chemical Composition Variation

Table 1 shows the ultimate analyses of the cellulose following the oxidation procedure described above. The O/C ratio decreases rapidly from 24 hours to 75 hours of oxidation and then shows a slight increase up to 456 hours. The initial decrease in oxygen content can be attributed to dehydration and, at the later stages of oxidation, loss of CO and CO2 on de-polymerisation of the cellulose. The slight increase in oxygen content from 75 hours to 456 hours is thought to be due to oxygen chemisorption by the cellulose. The H/C ratio decreases with an initial fast rate from 24 hours up to 75 hours of oxidation followed by a slower rate of H loss with time of oxidation and appears to be approaching some limiting value. Solid State ^{13}C NMR measurements were made to investigate the chemical changes on oxidation further. Figure 1 shows the NMR measurements on the oxidized cellulose samples. The aromatic/aliphatic ratios were determined by integrating the aromatic and aliphatic peaks which are indicated in Figure 1. The observed peaks were comparable to the accepted allocation of signals for cellulose [8]. The unoxidized cellulose showed no significant aromatic functionality, which is consistent with the accepted structure of cellulose [2]. However, even relatively mild oxidation was sufficient to produce a small aromatic content. This was corroborated by a colour change from white in the unoxidized cellulose to light brown in the 24 hour oxidized sample. The variation of the aromatic/aliphatic ratio with time of oxidation is shown in Figure 2. Initially, the ratio decreased slightly from a value of 0.152 for 24 hour oxidation to 0.106 following 50.5 hours of oxidation. The aromatic/aliphatic ratio then displayed a monotonic increase with time of oxidation up to 456 hours.

The decrease in H/C values may be associated with initial dehydration, (the O/C ratio decreased concurrently with H/C), accompanied by increasing aromaticity combined with the onset of cross-linking and more dehydration as the extent of oxidation increases. The variation of chemical composition based on C 100 together with the NMR data enables reasonable chemical structures to be constructed.

Figure 2 shows that the initial decrease in H/C ratio can not wholely be explained by simpley an increase in aromaticity. In fact the loss of hydrogen at this stage appears predominantly to be associated with an increase in crosslinkage of the cellulose

combined with dehydration.

The initial decrease in overall aromaticity of the oxidised samples up to 50.5 hours can be explained by the observed competitive generation of non-cellulose related aliphatics (at ~35ppm and 190ppm) in addition to the created aromatics (at~128,162ppm). An early indication of possible carbon crosslinking taking place is seen after 24 hours of oxidation (Figure 1a) when the C-6 signal (at ~70ppm) disappears. By 75 hours of oxidation, the cellulose structure has been completely altered (Figure 1b) and the cellulose peaks at have disappeared. The spectra at this stage consists of large aliphatic signals at 40ppm, due to alkyl groups, and 80ppm, due to ether groups, with a smaller aliphatic carbonyl signal at ~190ppm and aromatic peaks at 128ppm and 162ppm. The newly generated aromatic peaks at 128 and 162ppm dominate the NMR plots after 165 hours oxidation, with the new aliphatics at 40ppm and 80ppm taking a secondary role. The main aromatic peak centered at 128ppm corresponds to protonated and non-protonated aromatics (possibly bridgeheads for crosslinking), and the smaller peak at 162ppm corresponds to phenolic aromatics.

The general picture of changes on oxidation therefore appears to be an initial dehydration, occurring first at cellulose position C-6, with carbonyl production and generation of crosslinks with some aromatic production. This is followed by significant aromatic production with crosslinking by a mixture of short aliphatic groups and ether linkages.

Differential Scanning Calorimetry

The DSC plot, (Figure 3), for fresh cellulose shows a broad endotherm on run 1 from 330-400K due to the evaporation of water which was present on the surface of the polymer. After this water has been removed it can be seen that there is an endotherm indicative of a reversible second order phase transition probably due to a glass to rubber transition in the region 370-380K, which was obscured by the large evaporation endotherm. It has previously been observed by Hatakeyama *et al* [4] that dry cellulose exhibits no phase transition at a temperature below that of decomposition. This disagreement could arise from the fact that our own DSC sensor is somewhat more sensitive than that of Hatakeyama. Figure 4 shows the intensities of the glass transitions for the oxidised cellulose samples. The intensities of the Tg's are defined conventionally. It was noted that the Tg intensities decrease with increasing extent of oxidation. This may be due to an increase in cross-linking and density in the polymer which will make the structure considerably more rigid.

Oxidation and Carbonization

Table 2 shows the weight losses following oxidation and carbonization of the cellulose. The initial weight loss on oxidation up to 75 hours is extensive, with the loss from 75 hours to 456 hours being a lot smaller. The decomposition of cellulose in an oxygen atmosphere is well documented [9]. Initial weight loss is principally due to dehydration of water hydrogen bonded to the structure followed by dehydration of the actual cellulose structure, decarboxylation and general decomposition and depolymerisation of the cellulose. The weight loss after 75 hours being due mainly to hydrogen loss as the structure aromatises with some loss of CO and CO_2. The carbon yields shown in Table 2 are the percentage of carbon in the original cellulose that remains in the char. The theoretical maximum carbon yield, if all of the carbon in the cellulose were converted into carbon in the char, is 68%. the char yield obtained for the untreated cellulose on carbonisation at 1173K using a heating rate of 10K/min of 18.4% is comparable to that quoted by Brunner and Roberts [10]. Increasing the extent of

oxidation decreases the overall carbon yield as more of the initial carbon in the cellulose structure is burnt away to form CO and CO_2 during the oxidation stage before carbonisation.

Thermogravimetric Analysis

Figure 5 shows the TGA plots for the oxidised cellulose samples. The samples show sleight weight loss from 300-500K. This is probably due to loss of adsorbed H_2O. An increase in the oxidation period promotes greater weight loss in this temperature range from 300-500K. This phenomena can be explained by the presence of polar oxygen groups on the polymer surface of the more highly oxidised samples and hence, on heating in the TGA, these samples will subsequently show greater weight losses over the 300-500K temperature range. The onset of pyrolysis can be observed for the samples after 500K. Rapid weight loss can be observed for the fresh and more mildly oxidised samples probably due to depolymerisation, and scission of C-O and C-C bonds within the cellulose ring units, accompanied with evolution of more H_2O, CO and CO_2 [3]. The more highly oxidised samples loose weight less rapidly than the less oxidised cellulose. This is because an increase in oxidation period causes an increase in weight loss during the oxidation process due to the loss mainly of H and O and some C and associated with this is an increase in cross-linking of the polymeric structure. Therefore the more highly oxidised samples contain less volatile species and are in fact much strengthened by cross-linking and so will lose less weight during pyrolysis. Mass transfer through the more heavily crosslinked structure will also be slower, thus allowing more time for carbonisation.

Surface Areas of The Carbons

Table 2 shows the 77K N_2 BET surface areas of the cellulose carbons. A clear trend can be seen whereby the surface area of the carbon increases with an increase in oxidation of the polymer precursor. The increase is an exponential rise which levels off at 456 hours oxidation, with a surface area nearly 9 times that of the fresh cellulose carbon. The similar physical properties of methane and nitrogen result in there being a close relationship between 77K N_2 BET surface area per unit mass of adsorbent and methane uptake. Large N_2 adsorption capacities are indicative of high levels of microporosity.

Conclusions

The cellulose structure goes through radical changes on air oxidation at 473K until, after 456 hours the structure bears little or no resemblance to the original polymer. Initial oxidation promotes dehydration of the cellulose, resulting in some aromatic formation and crosslinking of the structure. Further oxidation encourages extensive aromatic production combined with increased crosslinking, resulting in a highly aromatic, highly crosslinked network with increased strength and resistance to weight loss. The extent of oxidation is linked to the surface area of the carbon produced from the cellulose precursors. Increased oxidation period produced carbons with higher N_2 BET surface areas. The fresh cellulose probably produces large pores with a generally open structure on carbonisation, with the more highly oxidised cellulose developing a narrower porosity. Although these surface areas are a good representation of probable methane uptake, it is a high priority to carry out methane adsorption isotherms on the carbons. It is also intended to develop the porosity of the carbons through CO_2 activation followed by characterisation of the carbons with Hg porosimetry and Small Angle X-Ray Scattering. The pre-oxidation procedure has been shown to be a good method for controlling the porosity of unactivated cellulose precursor carbons.

References

[1] F.Stodolsky, d.Santini, "The Efficient Use Of Natural Gas in Transportation", Chem.Soc.Annual Meeting (1992)

[2] T.P. Nevell and S.H. Zeronian, Cellulose Chemistry and Applications, Ellis Horwood (1985)

[3] Cellulose: A review of the literature., Forestry Branch Departmental Publication No.1201, Ottawa (1967)

[4] T.Hatakeyama *et al*, Polymer, **23**, 1801 (1982)

[5] F.Rodriguez-Reinoso and M.Molina-Sabio, Carbon, **30**, 7, 1111 (1992)

[6] M.Jagtoyen and F.Derbyshhire, Carbon, **31**, 7, 1185 (1993)

[7] J.A.Franz, R.Garcia, J.C.Linehan, G.D.Love and C.E.Snape, Energy and Fuels, **6**, 598 (1992)

[8] M.Bardet *et al* ,Holzforschung, **40**, pp17-24 (1986)

[9] F.Shafizadeh, "Pyrolysis and Combustion of Cellulosic Materials"

[10] P.H. Brunner and P.V. Roberts, Carbon **18**,217(1990)

Table 1 Ultimate Analysis of Fresh and Oxidized cellulose

Sample	wt %C	wt %H	wt %O	H/C (g/g)	O/C (g/g)	arom/aliph
Fresh	42.41	6.46	51.13	0.152	1.21	
(C 100)	100	188	90			
24 hr	43.30	6.64	50.34	0.154	1.17	0.152
(C 100)	100	184	87			
44 hr	50.01	5.16	44.83	0.103	0.90	0.143
(C 100)	100	124	67			
50.5 hr	51.27	4.64	44.09	0.090	0.86	0.106
(C 100)	100	108	64			
75 hr	58.39	2.96	39.65	0.051	0.69	1.694
(C 100)	100	61	51			
165 hr	53.64	2.86	43.50	0.053	0.81	4.341
(C 100)	100	60	61			
456 hr	52.99	2.48	44.53	0.047	0.84	7.099
(C 100)	100	56	63			

Table 2 Pyrolysis Yields and Carbon Surface Areas

Sample	Wt loss on Oxidation (%)	Wt loss on Carbonization (%)	Carbon Yield (%)	BET SA (m^2g^{-1})
Fresh	-	81.6	18.4	65
150°C, 24 hr	4.0	80.7	19.1	414
150°C, 168 hr	9.4	80.0	18.2	384
200°C, 24 hr	9.9	80.2	17.8	360
200°C, 44 hr	38.3	69.9	18.6	415
200°C, 50.5 hr	44.3	67.9	17.9	420
200°C, 75 hr	65.4	57.4	14.7	459
200°C, 165 hr	76.2	59.5	9.6	507
200°C, 456hr	72.7	59.4	11.1	541

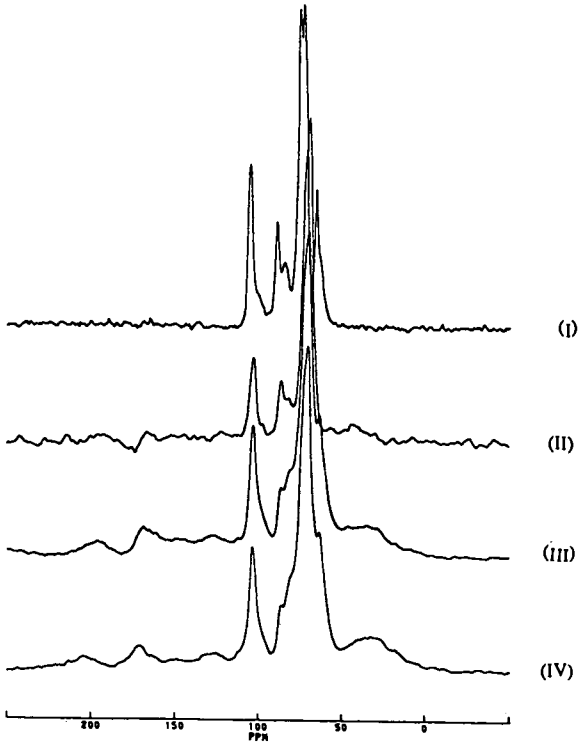

Figure 1(a) : ^{13}C NMR CP/MAS spectra of: Cellulose, (I) untreated, (II) oxidised at 473K for 24 hours, (III) oxidised at 473K for 44 hours, (IV) oxidised at 473K for 50.5 hours.

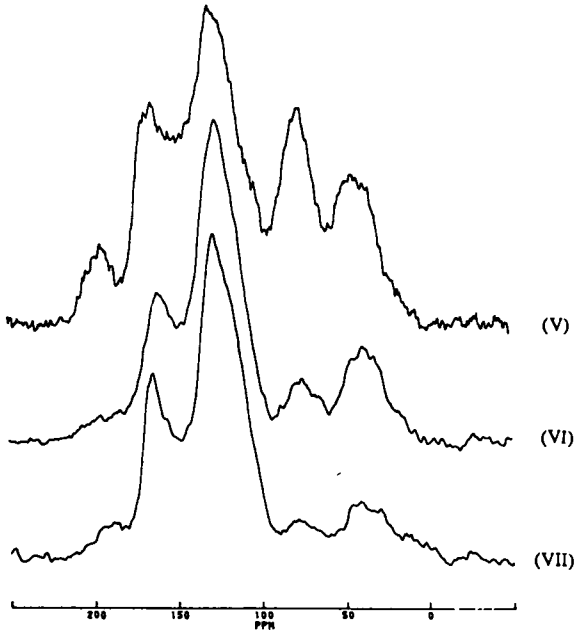

Figure 1(b) : ^{13}C NMR CP/MAS spectra of : Cellulose, (V) oxidised at 473Kfor 75 hours, (VI) oxidised at 473K for 165 hours, (VII) oxidised at 473K for 456 hours.

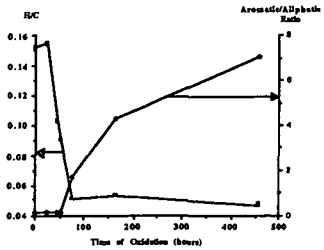

Figure 2 : Variation of H/C ratio and Aromatic/Aliphatic ratio with time of oxidation in air at 473K for cellulose powder. H/C values being derived from ultimate analysis and aromatic/aliphatic ratio from integration of the respective NMR peaks in Figure 1.

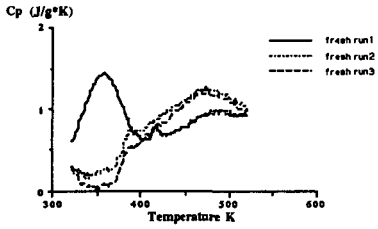

Figure 3 : DSC plot for untreated cellulose powder cycled from 323-523K in N_2 flow.

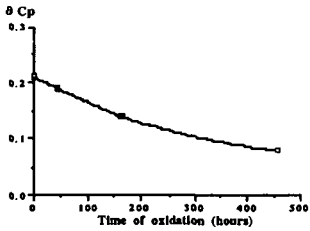

Figure 4 : Variation of δCp glass transitions of cellulose powder with time of oxidation in air at 473K.

MICROPOROUS CARBONS AS ADSORBENTS FOR METHANE STORAGE

D. F. Quinn, J. A. MacDonald and K. Sosin
Royal Military College of Canada, Kingston, Ontario

Keywords: Carbon Methane Storage

ABSTRACT

The volume available for gas storage is often limited. Because the density of the adsorbate is greater than the gas phase above it, gains in storage capacity at moderate pressures can be achieved through the use of adsorbents. Adsorbent storage systems can be used for various gases such as natural gas, hydrogen, ammonia or HFC's.

Optimal storage capacity will occur when that fraction of the storage volume that is micropore is maximized with no void or macropore volume. The average micropore diameter should be that most suited to the adsorbate molecule. In practice, this is difficult to achieve.

Carbons with high methane uptake per unit mass but with low bulk density may not be as suitable as carbons with lesser methane uptake but which have higher bulk density. The method of preparation of the adsorbent carbon is therefore very important. Conditions must be such that macropore formation is controlled and micropore enhanced.

INTRODUCTION

The acceptance of natural gas as a vehicular fuel has been slow, mainly due to a limited driving range. This range is restricted because of a much lower fuel or energy density than gasoline in the available storage volume. Initially an upper pressure of 2400 psi (16.3 MPa), equivalent to about 180 volumes of gas at STP per unit volume of storage, was used. This has been increased to 3000 psi (20 MPa), and even higher pressures have been called for.

The storage capacity of natural gas (methane) can be increased over that of compression alone through the use of an adsorbent. Methane density in a storage vessel at 3.4 MPa (500 psi) can be increased by a factor of four or more over that of compressed gas by using adsorbents, (1)(2). Thus through the use of carbons, methane storage densities of 180 V/V, equal to that of CNG at 2400 psi can be achieved at only one quarter or one fifth of the pressure, making adsorbed natural gas (ANG) an alternative to CNG. It should be noted here that storage is considered taking place at ambient temperature and cooling is not considered practical.

This increase in methane storage density in the storage vessel over CNG is due to adsorption of methane molecules in the micropore of the carbon. Therefore a carbon with a large micropore volume will adsorb more than one with a lesser micropore volume. However, these micropore volumes must be related to the storage vessel volume and not simply to a unit mass of carbon. The bulk or packing density of the carbon adsorbent therefore becomes very important.

When a vessel is packed with carbon, the volume occupied by the carbon atomic matrix is not available to methane. The fraction of the vessel volume which is void space or macropore volume will only store methane as compressed gas and that fraction which is micropore is the only one where there will be an increase in methane density. It follows, therefore, that a vessel packed without void space with a totally microporous carbon, maximized for microporosity, would be ideal.

Some carbons are closer to this ideal than others. The objective of this paper is to examine the characteristic properties of several carbons and relate these to methane storage. In doing this, it should be possible to consider different approaches to the preparation of adsorbent carbons in order to optimize them for methane storage.

Recent theoretical studies by Gubbins (3) and Myers (4) have shown that an optimal micropore would have a wall separation of about three to four methane diameters. The conclusion by Myers was that a highly idealized carbon composed of single graphitic layers 0.114 nm apart would store 209 V/V at 3.4 MPa.

Brookhaven National Laboratory have measured deliveries of methane from 3.4 MPa in excess of 150 V/V from carbon filled vessels at ambient temperature suggesting that storages of about 180 V/V have been achieved (5). Chaffee has prepared a carbon from Australian lignite which stored 202 V/V at 4.0 MPa (6).

EXPERIMENTAL

BET surface areas (7) and Dubinin-Radushkevich (8) micropore volumes for all the carbons were obtained using the Micromeretics ASAP 2000 to measure the nitrogen isotherm at 77K.

Mercury porosimetry measurements were carried out using the Quantachrome Autoscan 60 to obtain macropore volumes, and densities (9).

Methane isotherms were measured at 298K with the Sartorius M-25 high pressure balance. Buoyancy corrections were made by using equal weights of aluminum and magnesium as the counterweight. The deviation from ideality by methane was corrected using the data of Douslin et al. (10). For single stage compression, the practical benchmark pressure of 3.4 MPa (500 psi) was used in the comparison of the performance of each carbon.

TABLE 1

Carbons		BET Surface Area m^2/g	D-R Micropore Volume mL/g	Packing Density g/mL	Hg 1 atmos Particle Density g/mL	Mercury 60K psi Density g/mL	Macropore Volume mL/g	Methane Uptake 298K 500psia mgs/g
Norit	EX6	445	0.23	0.71	1.15	1.40	0.16	48
Calgon	SGL	900	0.4	0.49	0.78	1.33	0.53	65
Calgon	BPL	1030	0.47	0.44	0.75	1.11	0.43	75
Darco	Vapure 184-01	1095	0.51	0.58	0.81	1.19	0.39	84
ACCarbone	CNS 196	1190	0.49	0.44	0.85	1.22	0.36	80
Norit	R3	1270	0.58	0.42	0.65	1.06	0.80	92
Kureha	BAC	1350	0.60	0.59	0.90	1.08	0.19	99
California	GMS-70	1502	0.64	0.41	0.68	1.11	0.57	108
Barnebey	MI	1730	0.71	0.46	0.71	1.05	0.46	109
Sutcliffe	GS/60	1860	0.82	0.34	0.60	0.91	0.57	129
Osaka	M-30	2415	1.11	0.34	0.35	0.88	1.72	144
Kansai	Maxsorb	2671	1.29	0.27	0.29	0.90	2.34	164
Electrosynthesis	EL	2798	1.58	0.24	0.30	0.92	2.25	170

Table 1 lists the commercial carbons studied. These carbons come from a variety of precursors and have been made using different preparative methods. They cover a range of surface area and are listed on this basis. The Dubinin-Radushkevich micropore volume relates in a linear manner to the surface area. Methane uptakes at 3.4 MPa (500 psi) have been taken from the 298K isotherms, some of which are shown in Figure 1.

Figure 1

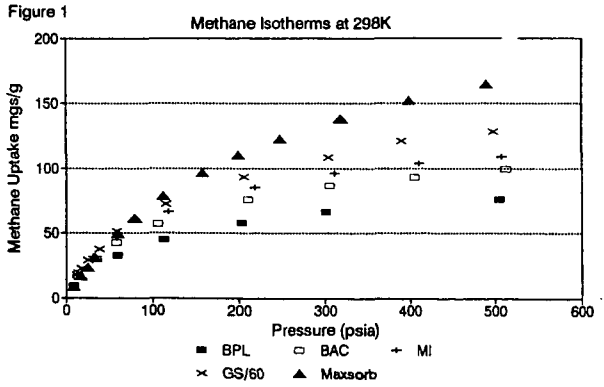

DISCUSSION

Many workers do not have the equipment to measure high pressure isotherms, but nearly every laboratory is able to measure surface areas and micropore volumes. Figure 2 shows the relationship between the 77K nitrogen surface area and the methane uptake at 3.4 MPa and 298K for these carbons. A more recent metbod, the alpba-s method, (11), distinguishes between micropore and surface area due to mesopore. This may be a better way of relating the extremely high surface area carbons to methane adsorption but has not been used in this paper. This relationship in Figure 2 is based on mass of adsorbent. The problem of gas storage is one of limited volume, and so the amount of methane which is stored in a vessel will be the product of the mass adsorption and the packed density of the carbon, plus methane stored as gas phase in the void and macropore volume.

Figure 2

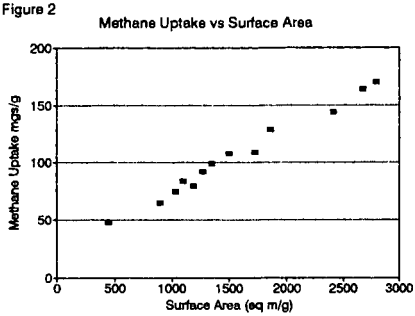

Figure 3

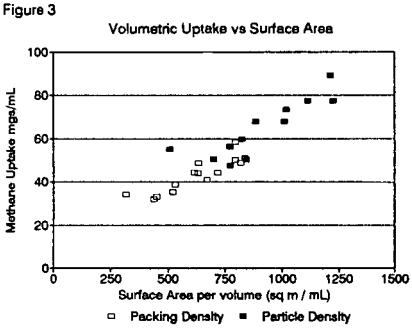

Because high surface area carbons often have low packing densities, they are often superseded in the amount of methane adsorbed per unit volume by carbons with greater packing densities. Figure 3 shows the surface area per mL with the methane adsorbed per mL of vessel using the normal packing density, (open squares). Additionally, Figure 3 illustrates the increase in adsorbed methane in the storage vessel if it could be packed to the particle density of the carbon. This latter situation is unrealistic but does serve to show the great gains to be made if packing density can be increased and voids reduced. The carbon which is most suited for methane storage is the Kureha BAC carbon, one of modest surface area per gram but which has both a high packing and particle density and low macropore volume. Figure 4 clearly shows that the high surface area per gram carbons are less suited for methane storage. Their large macropore volumes are mainly responsible for this.

Since storage of methane is taking place some hundred degrees above its critical temperature, adsorption will occur principally in the micropore. The methane density at 3.4 MPa and 298K in the micropore can be estimated. This has been plotted against the micropore volume per gram of carbon in Figure 5. Those carbons with large micropore volume (and high surface area) have low methane densities suggesting that the pore dimensions may be too large for efficient methane storage at temperatures well above its critical temperature.

Figure 4

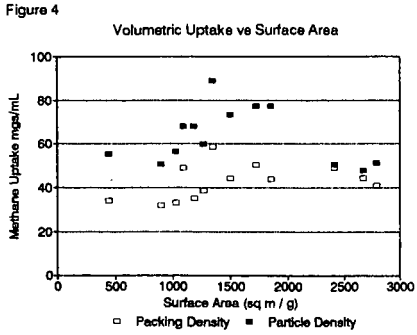

Dignum (12) has shown that the theoretical maximum density for methane at 298K is about 270 mgs/mL of pore. The low surface area Norit EX6 has a high methane density approaching this theoretical value. Takeda MSC-5A (13), a low surface area carbon, 445 m^2/g, has a methane

density in excess of 200 mgs/mL at 3.4 MPa and 298K. We have also found that unactivated coconut shell and peach pit chars of similar surface area to the Takeda carbon also have similar methane densities. This has also been shown for 5A and 13X molecular sieves (14).

Unfortunately all these materials have low micropore volumes per unit mass or volume and so are unattractive as candidates for methane storage. One carbon, made by the slow pyrolysis of PVDC polymer, has a methane micropore density of 219 mgs/mL at 3.4 MPa and 298K (15), suggesting that the pore dimensions are close to ideal. Additionally, about fifty percent of its particle volume is micropore with little or no macropore. It stores in excess of 150 V/V at 3.4 MPa and 298K.

Figure 5

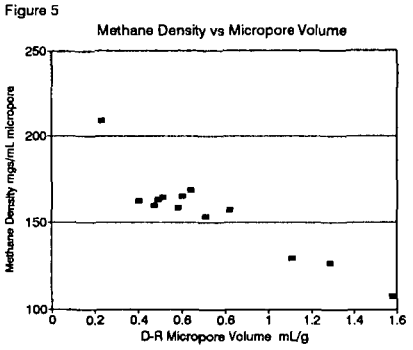

Traditionally carbons have been "activated" by heating them with air, steam or carbon dioxide at elevated temperatures. This results in carbons with higher surface areas per unit mass of carbon but with reduced packing and particle density. The reduction in density, however, is due not only to the creation of micropore but also to macropore formation. This macropore does not contribute to improved methane storage. The three high surface area carbons in Table 1 all have macropore volumes in excess of fifty percent of their particle volume.

The above shows that carbons can be made which have suitable micropore dimensions for methane storage, the problem is that these are not present in sufficient quantities to provide storage in excess of 180 V/V at 3.4 MPa and 298K. Methods of preparation which enhance micropore formation or reduce the production of macropore are desirable for gas storage carbons.

Figure 6

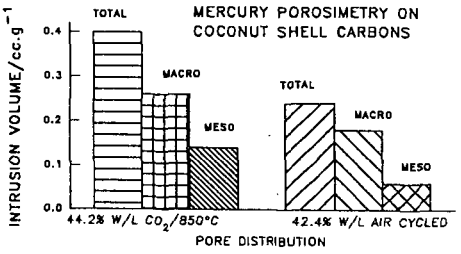

Figure 6 shows the meso and macropore volume for two CNS carbons. Both have been activated to about the same weight loss or burn off. One has been reacted with carbon dioxide at 850°C, a more conventional activation method. The other has been produced by cycling at low temperature with air followed by higher heat treatment under nitrogen (16). The latter method gave a carbon which had reduced macropore and mesopore volume, illustrated in Figure 6. It also had increased particle and packing density and showed an 18% increase in methane storage over the more conventionally prepared carbon.

Although storage has been emphasized in this paper, delivery from the storage vessel is perhaps more important. Delivery is considered as the amount of gas which is obtained from the vessel when the pressure is reduced to atmospheric. Carbons which have very narrow pore dimensions show high methane densities in these pores. They also have very steep Type 1 isotherms (17) and retain large amounts of methane at atmospheric pressure. PVDC carbon is a typical example of this type of carbon and retains at one atmosphere about thirty percent of the methane stored at 3.4 MPa. Treatment of this carbon with the air cycling technique improves the methane delivery.

Figure 7 relates carbon packing density and methane adsorption at 3.4 Mpa and 298K to delivery. The two curves for 100 and 150 V/V have been generated taking into account both the methane

desorbed isothermally and additionally the methane which would be stored as gas phase in void and macropore volume. The carbons from Table 1 are plotted using the normal packing density (open squares). They fall considerably short of the desirable 150 V/V delivered, however, if they were packed to their particle density (closed squares) then they come much closer to the goal.

Figure 7

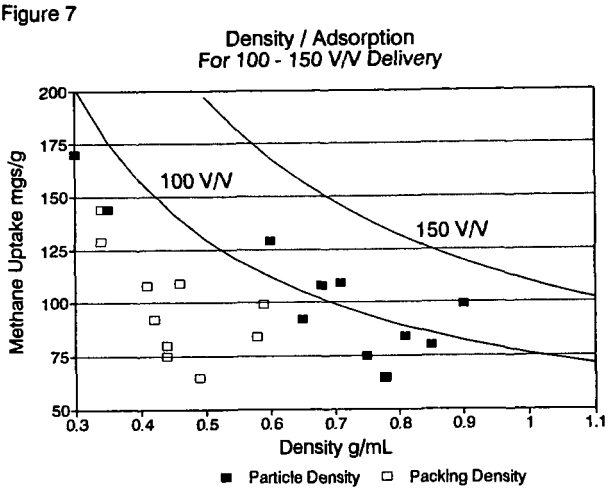

CONCLUSION

High surface area, low density carbons with high methane uptake per unit mass store and deliver less methane than some carbons with lower surface area but higher density. Carbons which have been optimized for micropore volume per unit volume will be most suited for ANG or other gas storage.

ACKNOWLEDGMENT

The authors wish to thank AGLARG, the Atlanta Gas Light Adsorbent Research Group, for their support for this study.

REFERENCES

1. J. Wegrzyn, H. Wisemann and T. Lee, SAE Proc. of Annual Automotive Technology Development, Nov 1992
2. C. Komodromos, S. Pearson & A. Grint, International Gas Research Confernce Proc. 1992, p588
3. Z. Tan and K.E. Gubbins, J Phys. Chem. 94 6061 (1994)
4. K.R. Matranga, A.L. Myers & E.D. Glandt, Chem. Eng. Sc. 47 1569 (1992)
5. J. Wegrzyn, Private communication, 1993
6. A.L. Chaffee, Proc. of Carbon 90, Paris, 1990
7. S. Brunauer, P.H. Emmett & E. Teller, J Amer. Chem. Soc. 60 309 (1938)
8. M.M Dubinin, E.D. Zaverina & L.V. Radushkevich, Zh. Fiz. Khim. 21 1351 (1947)
9. H.M. Rootare & C.F. Prenslow, J Phys. Chem. 71 2733 (1967)
10. D.R. Douslin, R.H. Harrison, R.T. Moore & J.P. McCullough,J Chem. Eng. Data 9 358 (1964)
11. P.J.M. Carrott & K.S.W. Sing in "Characterization of Porous Solids" p77 ed K.K. Unger et al, Elsevier (1988)
12. M.J. Dignum, Report 33259, Ontario Ministry of Transportation (1982)
13. S. Ozawa, S. Kusumi & Y. Ogino, J Coll. & Int. Sc. 56 83 (1976)
14. Y. Wakasugi, S. Ozawa & Y. Ogino, J Coll. & Int. Sc. 79 399 (1981)
15. D.F. Quinn & J.A. MacDonald, Carbon 30 1097 (1992)
16. U.S. Patent 5,071,820 (1991)
17. S. Brunauer, "Physical Adsorption of Gases and Vapours" Oxford University Press (1943)

MODELING THE FAST FILL PROCESS IN NATURAL GAS VEHICLE STORAGE CYLINDERS

Kenneth J. Kountz
Institute of Gas Technology
Chicago, IL 60632

Keywords: Natural Gas Vehicles, Gas Storage, Dynamic Gas Processes

INTRODUCTION

The on-board storage capacity of natural gas vehicles (NGVs) is a critical issue to the wide spread marketing of these alternate fueled vehicles. Underfilling of NGV cylinders, during fast fill (<5 min.) charging operations, can occur at fueling stations, at ambient temperatures greater than 50°F or 60°F. The resulting reduced driving range of the vehicle is a serious obstacle which the gas industry is striving to overcome, without resorting to unnecessarily high fueling station pressures, or by applying extensive overpressurization of the cylinder during the fueling operation. Undercharged storage cylinders are a result of the elevated temperature which occurs in the NGV storage cylinder, due to compression and other processes which have not, to the author's knowledge, been analyzed and documented to date.

This paper presents a model and solution methodology which quantifies the cylinder undercharging phenomena which occurs during rapid (<5 min.) fueling. The effects of heat transfer from the cylinder gas to its constraining walls and ambient are considered in the model analysis. The ramifications of the results on fueling station and cylinder designs are discussed. Suggestions are made for controlled experimental programs to verify the theoretical results, and for fueling station design studies which could minimize or eliminate cylinder underfilling.

ANALYSIS

MODEL ASSUMPTIONS

The following assumptions are made in the development of a mathematical model for fast charging natural gas cylinders.

1. The NGV cylinder is constant volume; there is negligible change in potential energy of the gas from the supply to the cylinder, and the kinetic energy of the cylinder gas is negligible. The pressure and temperature of the cylinder gas are not spatially dependent, i.e. quasi-steady perfect mixing occurs in the cylinder.
2. The mass flow, into the cylinder volume, is considered to be an isenthalpic expansion through an orifice.
3. The gas supply volume is infinite, with supply pressure and temperature remaining constant.
4. Heat transfer, from the cylinder control volume, is described by convective type heat flow to a lumped mass, cylinder wall. The cylinder wall temperature is not spatially dependent. Heat loss from the cylinder wall to the ambient is considered to be natural convection.

MODEL EQUATIONS

In applying the above assumptions to the natural gas storage cylinder charging model, shown in Fig. 1, one notes there are four basic dependent dynamic variables; the cylinder gas pressure, gas temperature, and mass of gas, and the lumped cylinder wall temperature. Four independent physical concepts are therefore needed for a dynamic solution.

The first physical concept applied is the dynamic energy equation for the NGV cylinder control volume, given in Equation (1). Note that each unit of supply gas, which enters the cylinder, has enthalpy, i.e. not only the internal energy of the gas in the supply, but also the supply "pv" work, associated with its flow. Note also that the gas in the cylinder volume contains only internal energy. One of the reasons behind the temperature rise of the gas in the cylinder, during a fast fill operation, lies in this conversion of enthalpy into internal energy.

The conservation of mass is the second physical concept utilized and is given in Equation (2). The supporting equations describing the assumed single orifice type flow rate are given in Equations (4) through (8). For adiabatic cylinder charging solutions of the set of modeled equations, the characteristics of the orifice, i.e. its area, rate of fill, or pressure ratio dependency will not affect the end temperature state in the cylinder, after a fill process to a given pressure. With heat transfer considered during cylinder charging, the flow rate characteristics of the orifice do influence the dynamic rates of heat exchange between the cylinder gas and cylinder wall, which in turn affects the end state cylinder gas temperature.

In this analysis, real natural gas properties are utilized to determine the property variables needed in the dynamic solution, i.e. enthalpy, internal energy, density, etc. These properties are obtained from subroutines which operate on pressure and temperature dependent tabulated results from the NIST computer program "STRAPP". The applicable equation of state, which provides a third physical concept, is given in Equation (3), or in its differential form, Equation (3a).

In deriving the basic differential equation set, reductions of Equations (1), (2), and (3) were used to solve for the NGV cylinder temperature, mass, and pressure respectively. The fourth dependent variable, the cylinder lumped mass wall temperature, is determined by the differential equation (10), after applying the supporting equations for the heat transfer into and out of the lumped mass wall, given in Equations (9) and (10) respectively. Fig. 2 shows a schematic of the cylinder wall heat transfer model.

SOLUTION PROCEDURE

The above described set of differential equations were numerically solved using the Runge-Kutta fourth order method, in a FORTRAN based computer program. Dynamic solutions for the cylinder gas pressure, temperature, and mass, and for the lumped cylinder wall temperature are output in the program together with integrated values for total heat transferred to and from the cylinder walls. Solutions end when the NGV cylinder pressure reaches a user-input pressure level.

MODEL RESULTS

TRANSIENT SOLUTIONS

Numerical solutions were developed using a mean U.S. natural gas composition whose components, by molar percentages are: Methane-92.87%, Ethane-3.34%, Nitrogen-2.07%, Carbon Dioxide-0.78%, Propane-0.63%, and less than 0.1% of I-Butane, N-Butane, I-Pentane, N-Pentane, and N-Hexane.

Examples of the dynamic pressure and temperature profiles in a 10" diameter, 50" long, NGV cylinder, during an adiabatic fill, are shown in Figures 3 and 4 respectively. In these results, the infinite supply gas conditions were 3000 psia and 70°F, while the initial cylinder pressure utilized was varied between 100 psia, simulating a nearly empty NGV cylinder, to 2500 psia, which could describe the topping off of a vehicle storage tank. The orifice size for the charging process was chosen so that the cylinder would fill to within 10 psi of the 3000 psia supply level in about 4 minutes, when starting from a nearly empty, 100 psia cylinder. In actual fueling operations, from 50 to 100 psi minimum pressure difference may be necessary between the fueling station cascade supply and the cylinder, to accommodate the station metering requirements or other piping or filtration flow impedances.

Note, from Fig. 4, that the cylinder gas temperature dips significantly during the early stages of charging a nearly empty cylinder, before rising to a final level of about 145°F. Note also that when charging a nearly full cylinder, the gas temperature profile is monotonic, reaching successively lower final values, as the initial pressure of the cylinder gas increases. The reason for the dip in temperature, in the early part of the filling of a nearly empty cylinder, lies in the

Joule-Thompson cooling effect, which the gas undergoes in the isenthalpic expansion through the orifice, from the 3000 psia supply pressure to the initially low 100 psia cylinder pressure. This cold gas mixes with and compresses the gas originally in the tank, with the result that the combined mixed gas temperature initially reduces. When the compression and conversion of supply enthalpy energy to cylinder internal energy overcomes the Joule-Thompson cooling effect, which becomes smaller as the cylinder pressure rises, the mixed gas temperature in the cylinder begins to rise. If the initial gas pressure in the cylinder is relatively high, the Joule-Thompson cooling effect is smaller, and does not, at any time, overcome the supply enthalpy conversion to cylinder internal energy. In this case, the cylinder gas temperature is seen to rise monotonically.

CYLINDER MASS FILL RATIOS

The charge parameter, which is directly related to the range of the NGV, is the cylinder "fill ratio", defined as the charged cylinder mass divided by the mass which the cylinder could hold at the rating condition of 70°F ambient and a pressure of 3000 psia. Fig. 5 shows how the mass fill ratio varies with initial cylinder pressure and supply pressure, for two values of the cylinder inside heat transfer coefficient. The adiabatic charge case corresponds to $H_{cyl}=0$, while the $H_{cyl}=5$ Btu/(hr-sqft-F) results apply to a heat transfer coefficient which is 10 times the assumed ambient side natural convection transfer coefficient of $H_{amb}=0.5$ Btu/(hr-sqft-F).

The inside cylinder heat transfer coefficient is difficult to estimate, since the gas flow into the cylinder is highly dynamic, and depends on numerous fluid, orifice, and cylinder parameters which are themselves rapidly changing in the charging process. Experiments are suggested which might lead to the measurement of average values which could then be used for this coefficient.

As seen in Fig. 5, the consideration of the heat transfer to the cylinder wall, with the assumed $H_{cyl}=5$ Btu/(hr-sqft-F) value, provides little change in the mass fill ratio. With initial cylinder pressures up to about 1000 psia, the model results show that a NGV fast fill operation will only load the cylinder to about 80% of the rated mass level. Thus, unless H_{cyl} is found experimentally to average much larger than 5 Btu/(hr-sqft-F), little help can be expected from the heat transfer to the cylinder wall in alleviating the cylinder underfilling situation.

CYLINDER CHARGING REQUIREMENTS

NGV fueling stations must take into account at least ambient conditions when recharging cylinders to maximize the range of the vehicle, while at the same time avoid overcharging, with its possible safety problems.

Fig. 6 plots, for the adiabatic charge case, how the charged pressure in the NGV cylinder would vary with ambient temperature, to achieve a fully charged mass condition, defined as the rated mass in the cylinder at 3000 psia and 70°F. Note the influence of the supply pressure is small in determining the required charged cylinder pressure. The cooled pressure curve reflects the effect of ambient temperature on the rated cylinder mass.

As an example, if the ambient were 70°F, to achieve a cooled cylinder pressure of 3000 psia, the cylinder would need to be fast charged to about 4000 psia, if the supply gas were at 5000 psia. If the ambient were 100°F, the cylinder would need to be charged to about 4600 psia, to achieve the rated mass level.

This dynamic overpressurization is a source of design difficulty for not only the NGV cylinder manufacturer, but also for the fueling station manufacturer and operator, since the fueling station compressor discharge and ground storage would need to be at least 5000 psia, to insure a fully charged cylinder at high ambients.

NOMENCLATURE

Parameters and Variables		Units
A	= area	in^2
C_d	= orifice discharge Coefficient	--
C_p	= specific heat at constant pressure	$Btu/(lb_m\text{-}^oR)$
C_v	= specific heat at constant volume	$Btu/(lb_m\text{-}^oR)$
d	= differential	--
f	= functional	--
g_c	= dimensionalizing factor	$(lb_m\text{-}in)/(lb_f\text{-}sec^2)$
h	= specific enthalpy	Btu/lb_m
H	= convective heat transfer coefficient	$Btu/(in^2\text{-}sec\text{-}^oR)$
k	= ratio of specific heats, C_p/C_v	--
M	= mass	lb_m
P	= pressure	$(lb_f/in^2)_{abs}$
Q	= heat transfer	Btu
R	= gas constant	$(in\text{-}lb_f)/lb_m\text{-}^oR)$
t	= time	sec
T	= temperature	^oR
u	= specific internal energy	Btu/lb_m
V	= volume	in^3
W	= orifice flow rate	lb_m/sec
Z	= compressibility factor	--

Subscripts

amb = ambient

cyl = cylinder

r = receiver cylinder

s = gas supply

w = cylinder wall

1 = orifice

EFFECTS OF COOLING THE SUPPLY GAS

One opportunity, to alleviate the need for creating and storing such high pressures in the fueling station, lies in the cooling of the supply gas, if a practical and cost effective way could be developed.

Fig. 7 shows the effects of cooling the supply gas, assumed to be at 4000 psia, to various temperature levels. As in Fig. 6, these results were created from the model for the adiabatic charge scenario. Note that by cooling the supply gas to 60°F, the required charged pressure, even at 100°F ambient, is reduced to about 3950 psia, to achieve a fully charged cylinder status.

RECOMMENDATIONS FOR FUTURE RESEARCH

Future research is recommended in three areas associated with the fast fill NGV problem. First, additional model development is needed to consider finite supply reservoirs, in a commonly used cascade group of three, which might be designed and controlled during the fast fill operation to reduce the temperature rise in the NGV cylinder. Second, experiments are proposed to support the model development, on well instrumented cylinders. Dynamic measurement of the mass entering the cylinder is needed to assure a proper model of gas flow rate profile. Experiments with the supply reservoir ambient at lower temperatures, relative to a cylinder located in a lab environment, would simulate the theoretically large supply gas cooling effect. Lastly, research and design studies are recommended to determine practical ways of cooling and storing the gas supply in the fueling station.

LIST OF EQUATIONS

Energy Balance

$$\frac{dQ_r}{dt} + W_1 h_s = \frac{d}{dt}\left(M_r u_r\right) \tag{1}$$

Conservation of Mass

$$\frac{dM_r}{dt} = W_1 \tag{2}$$

Equation of State

$$P_r V_r = R Z_r M_r T_r \tag{3}$$

in differential equation form, with V_r = constant

$$v_r \frac{dP_r}{dt} = R \frac{d}{dt}\left(Z_r M_r T_r\right) \tag{3a}$$

Orifice Flow Equation

$$W_1 = C C_{d_1} A_1 \frac{P_s}{\sqrt{T_s}} f\left(\frac{P_r}{P_s}\right) \tag{4}$$

where

$$C = \sqrt{\frac{g_c k}{R\left(\frac{k+1}{2}\right)^{\left(\frac{k+1}{k-1}\right)}}} \tag{5}$$

$$f\left(\frac{P_r}{P_s}\right) = 1 \text{ for } \frac{P_r}{P_s} \le \left(\frac{P_r}{P_s}\right)_{crit} \tag{6}$$

$$f\left(\frac{P_r}{P_s}\right) = \sqrt{\left(\frac{2}{k-1}\right)\left(\frac{k+1}{2}\right)^{\left(\frac{k+1}{k-1}\right)}}\left(\frac{P_r}{P_s}\right)^{\left(\frac{1}{k}\right)}\sqrt{1-\left(\frac{P_r}{P_s}\right)^{\left(\frac{k-1}{k}\right)}} \tag{7}$$

$$\text{for } \frac{P_r}{P_s} > \left(\frac{P_r}{P_s}\right)_{crit}$$

$$\left(\frac{P_r}{P_s}\right)_{crit} = \left(\frac{2}{k+1}\right)^{\left(\frac{k}{k-1}\right)} \tag{8}$$

Heat Flow Into Cylinder Wall

$$\frac{dQ_r}{dt} = -H_{cyl}A_{cyl}(T_r - T_w) \tag{9}$$

Heat Flow From Cylinder Wall to Ambient

$$\frac{dQ_{amb}}{dt} = H_{amb}A_{cyl}(T_w - T_{amb}) \tag{10}$$

Cylinder Wall Temperature

$$\frac{dT_w}{dt} = \frac{1}{M_w C_{p_w}}\left(\frac{dQ_w}{dt}\right) \tag{11}$$

$$\frac{dT_w}{dt} = \frac{1}{M_w C_{p_w}}\left(-\frac{dQ_r}{dt} - \frac{dQ_{amb}}{dt}\right) \tag{11a}$$

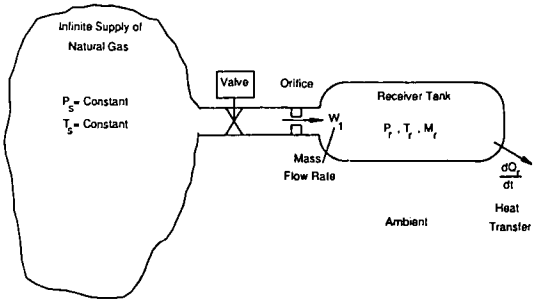

Fig. 1 Natural gas storage cylinder charging model

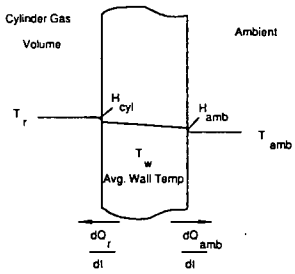

Fig. 2 Model of heat transfer through cylinder wall

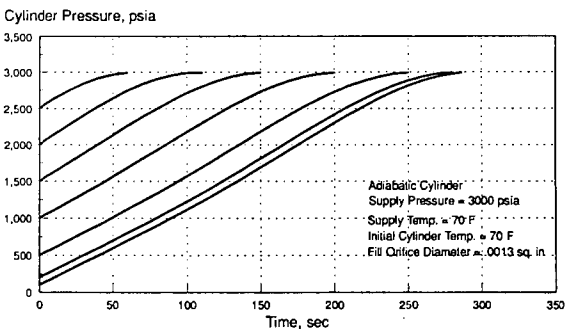

Fig. 3 Pressure in a 10"x50" Aluminum cylinder during a 3000 psia charge

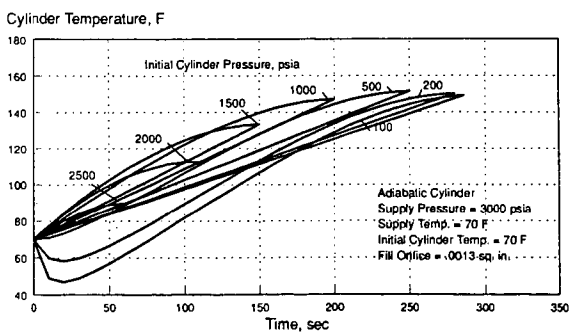

Fig. 4 Temperature in a 10"x50" Aluminum cylinder during a 3000 psia charge

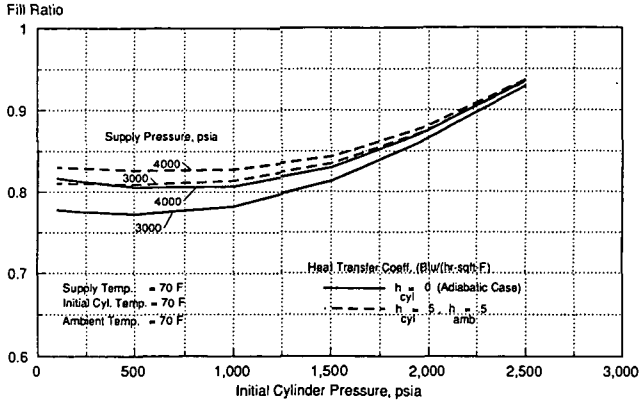

Fig. 5 Natural gas fill ratio in a 10"x50" Aluminum cylinder at the end of a 3000 psia charge

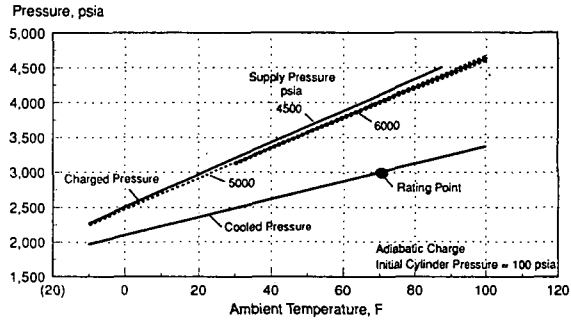

Fig. 6 Charged and cooled cylinder pressures for the rated charged mass, at 3000 psia and 70 F

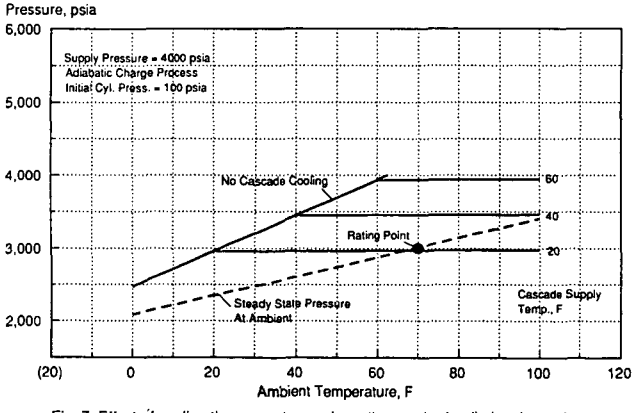

Fig. 7 Effect of cooling the cascade supply on the required cylinder charged pressure

AN INVESTIGATION OF THE USE OF ODORANTS IN LIQUEFIED NATURAL GAS USED AS A VEHICLE FUEL

Thomas Green, Ted Williams
Gas Research Institute, Chicago, Illinois 60631
Richard Bukacek, Prasan Chowdiah
Institute of Gas Technology, Chicago, Illinois 60632

Key Words: Liquefied Natural Gas, LNG Odorization, LNG Vehicles

ABSTRACT

Interest in liquefied natural gas (LNG) as an alternative vehicle fuel has increased significantly. Its greater storage density relative to compressed natural gas makes it an attractive option for both volume and weight constrained vehicle applications. The public transportation market, specifically transit bus properties, have been very aggressive in pursuing LNG as an alternative vehicle fuel. Naturally, when dealing with the general public and a new transportation fuel, the issue of safety must be addressed. With this in mind, the Gas Research Institute has initiated a number of safety related studies including an investigation of the use of odorants in LNG. This paper presents the preliminary results of an investigation performed by the Institute of Gas Technology to determine both the applicability and effectiveness of odorizing LNG. This includes an overview of the current state-of-the-art in LNG vehicle fueling and safety systems as well as a discussion of an LNG odorization program conducted by San Diego Gas & Electric in the mid 70s'. Finally, the paper discusses the results of the modeling effort to determine whether conventional odorants used in natural gas can be injected and remain soluble in LNG at temperatures and pressures encountered in LNG fueling and on-board storage systems.

INTRODUCTION

Interest in LNG vehicles and LNG refueling systems is growing due to the clean burning characteristics of natural gas and the abundant supply of natural gas in North America. As directed by many U. S. codes, natural gas distributed to customers is odorized to the extent that its presence in the atmosphere is readily detectable at gas concentrations of one-fifth of the lower explosive limit. Although LNG is currently not odorized, odorization may provide a significant increase in safety for over the road transportation of LNG and LNG vehicles. Unfortunately, the cryogenic temperature (-260°F) of LNG results in the immediate solidification of any known odorant. Therefore, special odorants and blending techniques must be developed to provide for the proper and effective odorization of LNG.

The objective of this paper is to present potential odorants (or odorant mixtures) and carriers for service in LNG. This includes an evaluation of the concentration of candidate odorants necessary to achieve an acceptable warning level and also the concentration level at which the candidate odorant reaches the solubility limit in LNG and the potential carrier.

SAFETY SPECIFICATIONS

In the United States, detection by odor is typically required before concentrations of natural gas in air reach 1/5th the lower combustible limit of the gas. That is, before natural gas concentration in air reaches 1%. It is implied that a large fraction of the adult population shall recognize the odor when the natural gas is diluted 100 to 1 in air.

Although human response to odors has long been studied, there has been to date little agreement on the theoretical basis for selecting odorants. A widely accepted measure of odorant effectiveness is the "median threshold" level: that concentration in air at which 50% of a test group can consistently detect the presence of the odor without necessarily being able to identify it. "Recognition" level, where 50% of a test group can characterize the odor, is said to be 2 to 5 times the threshold, Kniebes[3], but it is not often reported as measured.

More recently, Ripley et al.[6], introduced the concept of "Warning Level" at which an extrapolation of threshold data to 100% of a population experiencing threshold is the warning level. This definition of warning concentration has its foundation in theory and experiment, and it yields results that compare well with field practice and the data of Ripley. The factor 5 means that most of the population experiences this concentration as very much larger than 5 times their threshold. For t-butyl mercaptan, for example, 50% of the population should experience this odor at a concentration more than 120 times their threshold experience; for thiophane 44 times threshold. Note that the factor 5 is reasonable for odorizing LNG but not where odor fading is likely, i.e., odorizing gas for a transmission or distribution system.

SOLUBILITY

The presence of solids in the flow lines and fittings from an LNG storage tank to an engine can reduce or stop the flow of fuel. Thus, for potential odorants in LNG, it is important to know their solubility limits in LNG, that is, the concentration at which solid odorant begins to precipitate out of solution. A second solubility issue arises in consideration of procedures for introducing odorant into LNG. Because the triple point of candidate odorants are all above the temperatures at which LNG will be stored, the pure

odorants cannot be cooled to LNG temperature prior to placement in LNG. It is useful to consider dissolving the odorant into a carrier liquid and subsequently cooling the carrier/odorant mixture to LNG temperature. The candidate carrier liquids include only Propane and i-Butane.

It is always preferable to have experimental solubility data. In the event such data cannot be found then solubility can be estimated on the following thermodynamic basis. The solid at the triple point of pure material is used as a reference point. The solid is cooled to temperature at which the solubility limit is desired and its fugacity is calculated along this path. The pure liquid is cooled from the triple point to the temperature of interest, then mixed with the LNG: the fugacity of the odorant in solution is calculated along this path. At equilibrium the two fugacities thus calculated must be equal and the limiting concentration in the liquid phase can then be computed.

H = enthalpy	<u>subscripts</u>
F = Gibbs free energy	o - reference state
S = entropy	s - solid
f = fugacity	l - liquid
Hfusion = heat of fusion	i - component i
T = absolute temperature	t - temperature
v = volume	p - pressure
Cp = specific heat	
a = activity coefficient	

$$F = H - TS, \qquad (dF/dT)p = -S, \qquad (dF/dP)t = v;$$

For the solid at T

$$S_s = S_o + \int C_{ps}\, dT / T$$
$$F_i = F_s = F_o - \int (S_o + \int C_{ps}\, dT / T)\, dT$$

For the liquid at T

$$S_l = H_{fusion} / T_t + \int C_{ps}\, dT / T$$
$$F_l = F_o - \int (S_o + H_{fusion} / T_t + \int C_{ps}\, dT / T)\, dT$$

For the odorant in solution at T

$$F_i = RT\ln(a_i x_i) + F_l = F_s$$

The activity coefficient can be estimated from Scatchard's equation[2] as discussed by Preston and Prausnitz[5].

$$\ln(a_i) = v_i Vf_j((d_i - d_j)^2 + 2L_{ij} d_i d_j)/RT$$

Here:

- vi = the molar volume of the odorant at temperature T
- Vfj = the volume fraction of the solvent
- di and dj = the solubility parameters of odorant and solvent
- Lij = a parameter characterizing the interaction of i and j
- R = the gas constant in appropriate units.

The solubility parameters are effectively the internal energy change on vaporizing a unit volume of the liquid at 298.16°K and they characterize the cohesive energy density of a chemical. The activity coefficient calculated by this method is very sensitive to the term Lij: a value of 0 leads to maximum solubility, a value 0.08 to a very low solubility. In the absence of experimental data to guide the selection of Lij, it will be important to choose an extreme value, say 0.08, so that the limiting case solubility has been estimated.

Where the integrations cited above are over a relatively small temperature range and vapor/liquid equilibrium data can be used to calculate values for Lij, then it is not necessary to choose the limiting case value. Such data are available for thiophane, t-butyl mercaptan, isopropyl mercaptan, dimethyl sulfide and ethyl mercaptan in vapor/liquid equilibrium with propane.

There are data available for the solubility of t-butyl mercaptan in methane and LNG[4], but the temperature interval between t-butyl mercaptan's triple point, 274.26°K and LNG temperature, 112°K is such that a useful value of the integrals cited above cannot be adequately evaluated. For its solubility in propane the following limiting case approach was made: For several values of Lij for methane-t butyl mercaptan the integral was evaluated from the product xi*ai at 112°K with xi from Reference 4, then the solubility in propane was evaluated with Lij from vapor-liquid equilibrium data. On inspection of results a conservative value of the integral was selected to enable calculation of t-butyl mercaptan solubility in propane adequate for the screening process of this work.

Fortunately, AIChE's data compilation[1] provides up-to-date correlations for the heats of fusion, densities and specific heats of liquid and solid, and solubility parameters of the chemicals of interest here: various odorants, methane and the potential odorant carriers propane and i-butane. Table 1. lists the solubility limits for promising candidate odorants in methane with Lij = 0.08 (worst case) with their warning concentrations, both in ppm. It is clear that all are adequately soluble in methane and LNG.

TABLE 1. ODORANT SOLUBILITY AND REQUIRED CONCENTRATIONS IN METHANE

Odorant	Solubility, ppm	Warning Concentration, ppm
Ethyl Mercaptan	3785	0.4
i-Propyl Mercaptan	1746	0.6
n-Propyl Mercaptan	630	1.5
i-Butyl Mercaptan	941	1.0
t-Butyl Mercaptan	68	0.1
Thiophane	5	0.6
Dimethyl Sulfide	419	2.9

Values of Lij can be obtained from vapor-liquid equilibrium data. At the low vapor pressures of the odorants it is enough to have values of Ki = yi/xi in a given solvent to get ai = P*Ki/Pi. Here yi and xi are the mole fractions of odorant in the vapor and liquid phases, P is the total pressure and Pi is the vapor pressure of the odorant. The value of Lij thus evaluated at several temperatures should be temperature independent and applicable to estimating the solubilities in the solvent at LNG temperature. The data of Ng and Robinson[7] were used to evaluate Lij for ethyl, isopropyl and t-butyl mercaptans, and dimethyl sulfide dissolved in propane; Whisman et al. data[8] for Lij of thiophane in propane. The values of Lij and the solubilities of these compounds in propane are shown in the Table 2.

TABLE 2. ODORANT SOLUBILITY IN PROPANE

Odorant Name	Lij	Solubility limit ppm in Propane
Ethyl Mercaptan	0.032	83700
Isopropyl Mercaptan	0.042	27600
t-Butyl Mercaptan	0.044	736
Dimethyl Sulfide	0.031	7976
Thiophane	0.029	673

Note that the processes for evaluation require estimation of the properties of the subcooled liquid, but experimental data will be available only for saturated liquid. To test the validity of integration of the correlations of specific heat into the subcooled region an alternative extrapolation procedure was used and the two results compared. The alternative was a linear extrapolation from the triple point with the rate of change of Cp with temperature that at the triple point. Integrations from the triple points to 112° K for 9 potential odorants differed, on absolute average less than 0.2%, with the maximum deviation 0.5%. These results show that the extrapolations are justified, and they lend credence to the programming that implements the process of evaluation. Note also that pressures are low and the molar volume of solids and liquids are small. Thus neglecting the integral (vs-vl)dp will involve negligible error.

It will be observed that the activity coefficient is a function of odorant concentration so that the solubility limit can not be determined in a single step. In this work it was sufficient to start with the concentration estimated for ai=1 to calculate an initial value for solubility: the value for solubility was used to obtain a new value for ai which enabled calculation of a new solubility and the process was repeated until changes in solubility were less than 0.02% of the previous value.

In practice it is desirable to use relatively small amounts of carrier, in the range of 1 gallon carrier to 1000 gallons of LNG. These small amounts will not appreciably affect the composition of the liquid methane
(> 99.5% pure CH_4) being used by an increasing number of fleets. The concentration of odorant in carrier can be calculated

$$Co = Cw*(1+(Dl/Dc)*R)$$

Cw	=	the warning concentration of odorant in LNG at 1/5th LEL
Co	=	concentration of odorant in carrier required to achieve Cw warning concentration in LNG
Dl/Dc	=	the ratio of LNG to carrier densities in moles/volume
R	=	the ratio gallons LNG/gallon odorant

The symbol * in Table 3. indicates that the required concentration is greater than the solubility limit shown. At the level of 1 gallon per 1000 gallons of LNG n-propyl mercaptan is probably satisfactory because Lij is almost certainly smaller than 0.08, but n-butyl mercaptan and thiophane would require

experimental data to justify their use. The average value of Lij for thiophane reported above represents a wider scatter of individual values than the others and is therefore less adequate as a basis for estimating limiting solubility. Given the possibility of overdosing odorant under field conditions, the table above suggests that the ethyl, i-propyl and t-butyl mercaptans are best suited to odorization of LNG at the propane to LNG volume ratio of 1/1000.

Table 3. ODORANT REQUIREMENTS WITH PROPANE AS CARRIER

Odorant	Cw, ppm	R=1000 Co	Solubility limit, ppm	Lij
Ethyl Mercaptan	0.4	941	83700	0.032
i-Propyl Mercaptan	0.6	1294	27500	0.042
n-propyl Mercaptan	1.5	3528*	1766	0.08
i-Butyl Mercaptan	1.0	2234	2697	0.08
n-Butyl Mercaptan	1.0	2234*	185	0.08
t-Butyl Mercaptan	0.1	235	746	0.044
Dimethyl Sulfide	2.9	6821	7976	0.031
Thiophane	0.6	1411*	673	0.029

To produce a carrier with the desired concentration of odorant, we can assume the mixing process to take place at 25°C (77°F).

$$Vo = (Co/1000000)*(Dc/Do)*28316/7.48$$

Vo = volume of odorant needed, cc odorant/gallon carrier
Co = concentration of odorant desired, ppm
Dc/Do = ratio of densities in moles/volume, carrier/odorant at 77°F, 28316/7.48 = cc/gallon

Note that, on substitution from the previous relationship between Co and Cw and taking 1 << (Dl/Do)*R, we have

$$Vo = Cw*((Dl/Do)*R)*28316/7.48e6$$

We see that Vo is for practical purposes independent of the density of the carrier, and is thus as applicable for carriers other than propane. As shown in Table 4., 10 gallons of propane containing 11 cc of t-butyl mercaptan would odorize an LNG trailer load of 10,000 gallons.

Table 4. CUBIC CENTIMETERS OF ODORANT PER GALLON OF CARRIER; (PROPANE)

Odorant	Vo, cc/gal. R=1000
Ethyl Mercaptan	3.0
i-Propyl Mercaptan	5.2
n-propyl Mercaptan	13.6
i-Butyl Mercaptan	10.3
n-Butyl Mercaptan	10.2
t-Butyl Mercaptan	1.1
Dimethyl Sulfide	21.2
Thiophane	5.3

ODORANT CONCENTRATION IN EQUILIBRIUM LNG VAPOR

It is clear that all the odorant in LNG will be released to the surroundings if the liquid is totally evaporated. But the odorant concentration of the vapor in equilibrium with LNG liquid or of the vapors leaving an LNG spill are not going to be that of the original LNG. To establish the concentration of odorant in the vapor over LNG liquid the following process was used: Taking the reference states of pure component odorant and methane as 112°K and the vapor pressure of the odorant at 112°K, the equality of fugacities in the liquid and vapor phases can be expressed in terms of mole fractions

$$yi = ai*xi*Pi/P$$

Here:

ai = the activity coefficient of the odorant
yi, xi = the mole fractions of odorant in the vapor and liquid respectively
Pi = the vapor pressure of the odorant at T temperature
P = the pressure of the equilibrium mixture at T

The activity coefficient can be estimated from Scatchard's equation[2] as discussed by Preston and Prausnitz[5], and described above. The activity coefficient calculated by this method is very sensitive to the term Lij: a value of 0 leads to the minimum values for ai and yi; a value of 0.08 is extreme, and leads to very high values for ai and yi. Use of the value Lij = 0.08 therefore leads to an optimistic value for the concentration of odorant in the vapors in equilibrium with LNG. The values of 0.0 and 0.08 were used to screen potentially useful odorants. If, with Lij = 0.08, the concentration of odorant if far below the threshold level, then certainly the vapor will not be detected by its odor.

Daubert[1] and Danner's data compilation provides data for the vapor pressures, densities and solubility parameters of methane, ethane, propane and i-butane, and a variety of candidate odorants. Because LNG temperature is well below the triple point of the liquid where the pure odorant exits only as a solid, it is necessary to estimate the vapor pressure of the liquid by extrapolation. Two methods suggest themselves: 1) use the correlation of vapor pressure presented by Daubert and Danner at temperatures below the triple point and 2) assume the form ln(Pi) = A/T+B, and calculate the vapor pressure by evaluating dln(Pi)/dT and Pio at the triple point, so that Pi = Pio*exp((T-Tio)*(dln(pi)/dt)). To estimate yi, both values of Pi were calculated and the larger one used in the calculation. Because it is likely that the true values lie between the two, the larger value gives a conservative estimate given that the results are far below the warning level.

With odorant concentration of 5 ppm in methane, Lij = 0.08, T = 112°K, and p=16 psig, values of yi were calculated for 8 odorant candidates with the results shown in Table 6. For all odorants values of yi are far below that needed to obtain threshold concentrations when mixed with air at 1/5th the lower flammable limit for methane.

TABLE 6. ODORANT CONCENTRATION IN METHANE VAPOR

Odorant	yi, ppb	Pi, psia	ai	Ki=yi/xi
Ethyl Mercaptan	0.000200	3.9e-9	166	4e-8
i-Propyl Mercaptan	0.000043	8.6e-10	158	8.6e-9
n-Propyl Mercaptan	0.000129	8.9e-10	459	2.6e-8
n-Butyl Mercaptan	0.000004	1.0e-11	1203	8.0e-10
i-Butyl Mercaptan	0.000000	1.5e-12	598	-
t-Butyl Mercaptan	8.5	2.6e-4	103	1.7e-3
Dimethyl Sulfide	0.0234	4.0e-7	187	4.7e-6
Thiophane	0.000139	2.2e-11	20000	2.8e-8

All are far below the parts per million levels required for detection by odor. T-butyl mercaptan seems an anomaly in this list, but that is probably because the extrapolation from the triple point, 264.26°K, down to 112°K is so far that the estimate of Pi is much lower than the true value.

Vapor in equilibrium with LNG that is released into the atmosphere will not be detected by its odor: the concentration of odorant is just too small. However, the issue is not closed because the plausible occurrences and magnitude of such releases has not yet been established. Furthermore, LNG droplets or aerosols may emanate from the boiling liquid and become entrained in the escaping gas. To the extent that this may occur, additional odorant may be present in the released vapor.

CONCLUSION & RECOMMENDATIONS FOR ODORANTS & CARRIER

The elimination of some candidate carriers is quite easy: n-butane and the heavier hydrocarbons can be immediately eliminated as carriers because their freezing points are too high. Ethane is not a desirable carrier because its critical temperature, 90.1°F, is within the range of ambient temperatures so that phase densities can radically change with small temperature or pressure changes while mixtures are being make or transferred. Only propane and i-butane are sensible candidates, commercially available and typical components of LNG. Propane is clearly preferable to i-Butane because it is more universally available, and its phase equilibrium with odorants has received more experimental attention.

Although 10 mercaptans, hydrogen sulfide, dimethyl sulfide and thiophane were examined during this work, only 3 were found to satisfy the following criteria:

1. There exist adequate experimental data on its odor detection to define the warning concentration of odorant required in LNG. This rules out sec-butyl mercaptan.

2. Concentration of odorant in propane carrier, with Carrier/LNG ratio 1/1000, is well below the solubility limit with the warning concentration delivered to the LNG. Note that the warning concentration for most odorants is well below their solubility in LNG. This rules out thiophane.

3. At the propane/LNG ratio of 1/1000, any plausible overdose of odorant during mixing of odorant with propane will not lead to formation of solids when the result is cooled to LNG temperatures. This rules out all but the ethyl, i-propyl and t-butyl mercaptans on the basis of the experimental data available at present.

4. The odorant is not identified as acutely toxic by EPA - this rules out methyl mercaptan and dimethyl sulfide.

5. The odor in air is perceived as "gassy". This rules out dimethyl sulfide.

The acceptable candidate odorants are:

Ethyl Mercaptan
i-Propyl Mercaptan
t-Butyl Mercaptan

REFERENCES

1. Daubert, T.E. and Danner, R.P., "Physical and Thermodynamic Properties of Pure Chemicals", Design Institute for Physical Property Data, AIChE, Hemisphere Publishing Corporation, New york, 1991

2. Hildebrand, J.H. and Scott, R.L., "Solubility of Nonelectrolytes", Dover, New York, 1964

3. Kniebes, D.V.,"The nose as a Natural Gas Odorant Detector" p.24, IGT Odorization Symposium , Aug. 1980)

4. Kuebler, G.P. and McKinley, C., "Solubility of Solid tert-Butyl Mercaptan in Liquid Methane and an LNG Mixture", Advances in Cryogenic Engineering, V0l 25, 616-619, Plenum Press, N.Y., 1979

5. Preston, G.T. and Prausnitz, J.M., Thermodynamics of Solid Solubility in Cryogenic Solvents, Ind. Eng. Chem. Process Des. Develop., Vol 9, No 2, 1970

6. Ripley D.L. and Goetzinger, J.W. "LP-Gas Odorants", Proceedings of the IGT Odorization Symposium, Sept 1992

7. Robinson, D.B. and Ng,H.J., "VLE Data and Correlations for Odorants in Propane." Symposium on LP-Gas Odorization Technology Proceedings, Dallas, TX, April 1990

8. Whisman, M.L.; Goetzinger, J.W.; Cotton, F.O.; Brinkman, D.W.; and Thompson, C.J., "A New Look at Odorization Levels for Propane Gas," BERC/RI/77/1, 1977

FUEL COMPOSITION EFFECTS ON NATURAL GAS VEHICLE EMISSIONS

Christopher F. Blazek, John Grimes, and Patricia Freeman
Institute of Gas Technology, Chicago, Illinois 60632
Brent K. Bailey and Christopher Colucci
National Renewable Energy Laboratory

Keywords: Natural Gas Vehicles, Natural Gas Composition, NGV Emissions

ABSTRACT

Under a contract from DOE's National Renewable Energy Laboratory (NREL) and support from Brooklyn Union Gas Company (BUG), Northern Illinois Gas Co., the Institute of Gas Technology (IGT) evaluated four state-of-the-art, electronic, closed-loop natural gas vehicle (NGV) conversion systems. The systems included an Impco electronic closed-loop system, Mogas electronic closed-loop system, Stewart & Stevenson's GFI system, and an Automotive Natural Gas Inc. (ANGI) Level I electronic closed-loop conversion system. Conversion system evaluation included emission testing per 40 CFR Part 86, and driveability. All testing was performed with a 1993 Chevy Lumina equipped with a 3.1 L MPFI V6 engine. Each system was emission tested using three different certified compositions of natural gas, representing the 10th, mean and 90th percentile gas compositions distributed in the United States. Emission testing on indolene was performed prior to conversion kit testing to establish a base emission value. Indolene testing was also performed at the end of the project when the vehicle was converted to its OEM configuration to ensure that the vehicle's emissions were not altered during testing. The results of these tests will be presented.

INTRODUCTION

A number of conversion systems are commercially available to convert gasoline fueled vehicles to either dedicated or bi-fueled natural gas vehicles (NGVs). This paper presents the research results to date of four NGV conversion systems tested on the 1993 3.1L MPFI Chevrolet Lumina passenger car. This study included fuel emission testing based on the Federal Test Procedure (FTP) per 40 CFR Part 86 and fuel economy measurements using three different compositions of natural gas. Emission testing on indolene was performed prior to conversion system testing to establish gasoline base emission values. Any variations in emissions or fuel economy related to fuel quality will be better understood as a result of the FTP emission testing program. In addition to fuel quality, this investigation also evaluated conversion system performance, both in terms installation and driveability. All procedures required to convert the gasoline fueled vehicle to compressed natural gas (CNG) were fully documented including hardware installation, electronic hookups, and system calibration.

SPECIFICATION OF NATURAL GAS COMPOSITION

Natural gas is not pure methane or a homogeneous mixture, but varies in composition by location and seasonally. Variations occur between the originating fields and may be further modified due to processing prior to transmission. Additional mixing of different gases also occurs during pipeline transmission. As a result, natural gas does not describe a single type of fuel or a narrow range of characteristics, unlike gasoline or diesel fuel which is manufactured within certain specifications.

Fuel composition can affect vehicle emissions. The most recent work on natural gas composition was completed in 1991 by the American Gas Association Laboratories with the Institute of Gas Technology as a subcontractor, under Gas Research Institute funding.[1] The research focused on the mean average, minimum, maximum, 10th percentile, and 90th percentile gas fractions. However, information reported in the GRI sponsored study for the mean, 10th percentile, and 90th percentile values for each of the component gases allowed for only a pseudo-composition to be developed. For example, the 10 percentile value of methane could be combined with the 90th percentile values of the other constituents for a minimum-methane concentration natural gas. The rationale for this approach is that, when methane dominates the composition, the other gases would be expected to be at their lower values. However, this does not take into account that natural gas compositions are not manufactured but occur normally with certain relationships between each of the components. As a result, IGT concluded that a more detailed review was necessary to determine representative natural gas compositions.

Two primary factors that impact emissions and directly describe the general characteristics of natural gas include the concentration of methane and the Wobbe number. The methane concentration is a good measure because it is the dominant component in natural gas. The Wobbe number is a measure of the fuel energy flow rate through a fixed orifice under given inlet conditions. It is calculated as the ratio of the higher heating value divided by the square root of the specific gravity. Variations in Wobbe number of the gas will produce similar variations in the air-fuel ratio for gas metering systems used on vehicles. Variability of this parameter will most significantly affect engines equipped with open-loop controls, where the exhaust oxygen cannot be sensed and adjusted. In general, the Wobbe number is a good criteria for natural gas because it correlates well with the ability of an internal combustion engine to use a particular gas. It also takes into account many of the gas components because it is a bulk property.

The first step was to determine the minimum, maximum, mean average, median, 10th percentile, and 90th percentile values for the methane mole fraction, as shown in Table 1. This data represents over

6,000 gas samples taken from various locations throughout the continental U.S. It should be noted that the minimum value represents propane/air peakshaving gas. This gas is generated by many local utilities during severe periods of high demand which typically occur during the coldest periods of the year. During mild winters these plants may not even be used and during normal winters plants may only operate 1 to 2 days per year. The equivalent values for the Wobbe number are shown in Table 2.

TABLE 1. METHANE FRACTION ANALYSIS

Minimum:	55.8%
Maximum:	98.1%
Mean (avg):	93.0%
Std Deviation:	4.5%
Median:	94.9%
10th Percentile:	84.1%
90th Percentile:	96.3%

TABLE 2. WOBBE NUMBER ANALYSIS

Minimum:	1202.6
Maximum:	1418.7
Mean (avg):	1329.4
Std Deviation:	42.6
Median:	1347.0
10th Percentile:	1233.0
90th Percentile:	1358.5

Having identified the methane fraction and Wobbe number values to be used, the next step was to define a suitable method of calculating the mole fractions of each of the other components. Because of the inherent variability of an individual natural gas sample, it was unlikely that a representative composition could be formulated from just the few values that fit exactly on the selected Wobbe number values. To select a slightly wider, more representative range of natural gas compositions at a given value, the average of each of the components was calculated considering only those samples within 2 Wobbe number counts of the identified Wobbe number. These results are shown in Table 3 (values presented are mole %). The near equivalency between methane fraction and Wobbe number for the natural gas composition can be seen in comparing the resulting averages for each of the components in each of the desired ranges. For example, the methane and Wobbe number for the two 10th percentile compositions are fairly close, 83.84 mole % vs. 83.96 mole % and 1229.76 vs. 1232.97. This holds true for the other components. Although there is more variability within the mean and 90th percentile compositions, the differences are within the variations that may be seen throughout the year.

TABLE 3. COMPOSITION BASED ON WOBBE NUMBER

	10%-ile	Mean	90%-ile
METHANE	83.96	92.87	94.80
ETHANE	5.72	3.34	3.03
PROPANE	1.07	0.63	0.58
I-BUTANE	0.09	0.07	0.10
N-BUTANE	0.11	0.12	0.13
I-PENTANE	0.03	0.04	0.05
N-PENTANE	0.01	0.03	0.03
C6+	0.03	0.05	0.07
NITROGEN	6.05	2.07	0.56
CO_2	1.40	0.78	0.65
O_2	1.53	0.00	0.00
WOBBE	1232.97	1329.15	1358.61

Because fuel metering is a critical factor in all NGV conversion systems, both IGT and NREL agreed that the gas compositions based on the Wobbe number, as presented in Table 3, should be used for the test fuels. High pressure gas cylinders were then prepared for each of the three compositions and certified by IGT for use in this test program.

BASELINE EMISSION TEST

IGT leased a new 1993 Chevy Lumina 3.1 liter MPFI V6 (VIN# 2G1WN54T7P9146384) for the testing program. During December of 1992 and January of 1993 the vehicle was driven 5,000 mostly highway miles on gasoline to ensure proper engine break-in and catalyst aging. An inspection was performed on the Lumina at 4,803 to establish baseline parameters prior to emission testing and conversion.

FTP emission testing on indolene were initiated in March, 1993 per 40 CFR Part 86 on the Chevy Lumina. Two baseline indolene tests were performed with the dynamometer set for a 3,500 pound inertia and 6.0 ahp. The vehicle odometer read 6,410 miles. The test results are presented in Table 4. As can be seen from the test results, the vehicle passed the exhaust emissions and shed test. Weighted total hydrocarbon values were 0.23 and 0.27, carbon monoxide 2.74 and 2.84, nitrous oxides 0.48 and 0.49, carbon dioxide 489 and 491, respectively reported in grams per mile, with fuel economy for both tests at 18.0 mpg. The shed test results were 0.34 and 0.39 grams respectively.

CNG EMISSION TEST RESULTS

All systems were installed and setup according to the manufacturer's instruction. Following the installation, a test drive and dynamometer set-up were performed using a snap-on analyzer for ECM parameters. Power valve and idle adjustment were performed to minimize tailpipe emissions (through the converter) without sacrificing driveability. Following these adjustments, IGT conducted driveability tests following the CRC Report No. 577 "1990 CRC Driveability Workshop" recommendations

published in October 1990.[2] All four systems passed the driveability tests with no faults and did not experience engine stalling or hesitation, nor any problems with starting.

TABLE 4. EXHAUST AND EVAPORATIVE INDOLENE EMISSIONS DATA

Test Fuel Indolene		
Test Date	3/12/93	3/15/93
Vehicle Odometer, miles	6410	6429
Exhaust Emission Results		
Cold Transient, grams		
THC (C_3H_8 calibration)	2.65	3.15
CH_4 (a)	0.22	0.26
NMHC (a)	2.40	2.85
CO	23.24	26.97
NO_x	4.25	3.95
CO_2	1741	1767
Fuel Economy, MPG	17.9	17.6
Cold Stabilized, grams		
THC (C_3H_8 calibration)	0.34	0.25
CH_4 (a)	0.12	0.12
NMHC (a)	0.20	0.11
CO	4.70	4.32
NO_x	1.14	1.21
CO_2	1992	2004
Fuel Economy, MPG	17.9	17.0
Hot Transient, grams		
THC (C_3H_8 calibration)	0.45	0.74
CH_4 (a)	0.13	0.14
NMHC (a)	0.29	0.57
CO	9.82	8.99
NO_x	1.02	1.22
CO_2	1533	1536
Fuel Economy, MPG	20.5	20.5
Weighted Total, grams / mile		
THC (C_3H_8 calibration)	0.23	0.27
CH_4 (a)	0.04	0.04
NMHC (a)	0.19	0.22
CO	2.74	2.84
NO_x	0.48	0.49
CO_2	489	491
Fuel Economy, MPG	18.0	18.0
Shed, grams		
Diurnal 0.12	0.20	
Hot Soak	0.22	0.19
Total 0.34	0.39	

All emission tests were performed at the AutoResearch Laboratories per 40 CFR Part 86. The dynamometer was set for a 3,500 pound inertia and 6.0 ahp. The preliminary test results for the MOGAS system as tested in April, 1993 are presented in Table 5 for the three different gas compositions. From the weighted total results, it became clear that the vehicle was set-up lean following Mogas's set-up instructions. IGT did not attempt to optimize the emission results during set-up. However, the results do indicate that NO_x emissions could be reduced running richer, and thereby increasing carbon monoxide emissions which are currently significantly below the limit. It should be noted that for the 10th percentile gas the system did not pass the 1993 EPA NOx limit of 1.0 gr./mile.

The preliminary test results for the Impco system as tested in May, 1993 are presented in Table 6. As was the case with the MOGAS system, the weighted total test results indicate that the vehicle was set-up lean following Impco's set-up instructions. IGT did not attempt to optimize the emission results during set-up. Again, the results indicate that NO_x emissions could be reduced running richer, and thereby increasing carbon monoxide emissions which are currently significantly below the limit. However, the system met all applicable 1993 EPA emission standards for the entire range of natural gas compositions tested.

The preliminary test results for the GFI system as tested in July, 1993 are presented in Table 7. From weighted total results for the mean gas composition, it became clear that the vehicle was set-up rich by the GFI provided software. The carbon monoxide average (4.04 g/mile) was above the 3.4 g./mile EPA limit. However, the results do indicate that CO emissions could be reduced running leaner, and thereby increasing NOx emissions which are currently significantly below the limit. Since the software version supplied by GFI is specific to the 1993 Lumina tested, software changes may be required to "re-calibrate" the vehicle.

The weighted total results for the 90th and 10th percentile gas compositions further confirmed that the vehicle was set-up rich by the GFI provided set-up software. However, a closer analysis of the test results by IGT indicated that the 90th and the 10th percentile gas composition tests did not concur with

the repeatability guidelines set forth in the publication "Statistical Design and Analysis Methods for the Auto/Oil Air Quality Research Program" as published by Painter and Rutherford in SAE paper 920319.[3] Of the tests reported, the HC, CO, and NO_X cold stabilized test pairs and the HC weighted total values from the 90th percentile gas composition did not meet this criteria. Likewise for the tests conducted on 10th percentile gas composition, the NO_X and HC cold transient test pairs and the HC, CO, and NO_X hot transient pairs also were above the limiting ratios. Further investigation indicated that an "air leak" in the testing equipment may have been a contributing cause to these differences.

As a result of this discrepancy noted above, a third test was performed for just the 90th and 10th percentile gas compositions to verify that the "air leak" was corrected and to provide further correlation of the test results. The data for these additional tests are summarized in Table 7 along with the previous test data. As can be seen, the 90th and 10th percentile "third" test data agree more closely to the "first" tests performed on each composition. However, based on the Auto/Oil reference sited above, IGT took the recommended approach of averaging the three tests for the average values reported for the 90th and 10th percentile gas composition tests.

Based on the average values for each of the gas compositions, the GFI system failed the CO emissions test based on the 1993 CO standard of 3.4 g/mi. However, two factors must be taken into consideration when assessing the GFI system. Both the related NOx emission values and the system setup requirements and system sophistication. Unlike the previous two systems tested, the GFI system requires information about the gas composition during vehicle setup and calibration. For this test IGT used the system default values and did not attempt to "dial in" the gas composition for each of the three gas compositions tested. Since the other two systems were not "tuned" on each composition, it was decided that this would give the GFI system an advantage. Second, and even more important, unlike the other systems, the GFI system incorporates a built in learning algorithm in the electronic controls which gradually adjusts the fuel/gas mixture in response to operating parameters such as exhaust oxygen sensor output relative to load. This learning adjustment occurs gradually during normal driving. However, due to the nature of the emission testing, the vehicle was not driven between tests to allow the system to adjust to the new fuel composition. Because of the cost of the certified test fuel, driving between tests was not deemed practical. Since the GFI system incorporates an adaptive learning electronic control system, given enough time on a given gas composition, this system may have passed all of the emission standards. The very low and consistent NOx levels of the GFI system also suggest that this system may have the capability of meeting 1994 standards, even on the 1993 test vehicle

The preliminary test results for the ANGI system as tested in October, 1993 are presented in Table 8. From weighted total results for the mean gas composition, the average levels of CO and NO_X emissions are well below the current EPA limits. The weighted totals for the 10th percentile composition indicate that the ANGI system failed the current NO_X standard of 1.0 g/mile. This indicates that the system produced very low emission levels with the mean composition gas, but the 10th percentile composition caused the system to run too lean.

The test results for the 90th percentile gas composition for the levels of CO did not concur with the repeatability guidelines set forth in the Auto/Oil reference. Again, based on Auto/Oil recommendations, a third test was performed. The results of the second and third tests were within recommended limits. Since there was a possibility of high background levels of CO during the first test and since the second and third test results were in close agreement, the first test was treated as an outlier and the average results were taken from tests 2 and 3. Thus, the weighted total test results for the 90th percentile were well within the EPA limits for CO and NO_X. This indicates that the ANGI system operates well on the mean and 90th percentile compositions which have a higher methane content, but the system fails current EPA limits on NO_X emission levels when operating with 10th percentile gas composition fuel.

CONCLUSIONS

As can be seen from these results, the Mogas system produced the lowest carbon monoxide test results followed by the Impco, ANGI and GFI systems. The GFI system actually failed the CO emissions test based on the 1993 CO standard of 3.4 g/mi. However, two factors must be taken into consideration when assessing the GFI system. Unlike the other 2 systems, the GFI system requires information about the gas composition during vehicle setup and calibration. For this test IGT used the system default values and did not attempt to "dial in" the gas composition for each of the three gas compositions tested. Since the other two systems were not "tuned" on each composition, it was decided that this would give the GFI system an advantage. Second, and even more important, unlike the other systems, the GFI system incorporates a built in learning algorithm in the electronic controls which gradually adjusts the fuel/gas mixture in response to operating parameters such as exhaust oxygen sensor output relative to load. This learning adjustment occurs gradually during normal driving. However, due to the nature of the emission testing, the vehicle was not driven between tests to allow the system to adjust to the new fuel composition. Because of the cost of the certified test fuel, driving between tests was not deemed practical.

TABLE 5. MOGAS SYSTEM EMISSIONS SUMMARY

Fuel Type Mean CNG		
Vehicle Odometer, miles	6821	6832
Exhaust Emission Results		
Weighted Total, grams / mile		
THC (CH_4 calibration)	1.41	1.40
CH_4 (a)	1.40	1.42
NMHC (a)	0.16	0.11
CO	0.39	0.19
NO_x	0.85	0.90
CO_2	363	357
Fuel Economy, MPG	18.9	19.1
Fuel Type 90th Percentile CNG		
Vehicle Odometer, miles	6858	6869
Exhaust Emission Results		
Weighted Total, grams / mile		
THC (CH_4 calibration)	1.28	1.37
CH_4 (a)	1.22	1.34
NMHC (a)	0.16	0.09
CO	0.59	0.28
NO_x	0.79	0.83
CO_2	351	355
Fuel Economy, MPG	19.2	19.0
Fuel Type 10th Percentile CNG		
Vehicle Odometer, miles	6898	6910
Exhaust Emission Results		
Weighted Total, grams / mile		
THC (CH_4 calibration)	1.72	1.98
CH_4 (a)	1.66	2.00
NMHC (a)	0.17	0.18
CO	0.12	0.13
NO_x	1.03	1.01
CO_2	355	359
Fuel Economy, MPG	20.7	20.4

TABLE 6. IMPCO SYSTEM EMISSIONS SUMMARY

Mean CNG		
Vehicle Odometer, miles	7309	7320
Exhaust Emission Results		
Weighted Total, grams / mile		
THC (CH_4 calibration)	1.01	1.03
CH_4 (a)	1.11	1.01
NMHC (a)	0.04	0.05
CO	0.80	0.54
NO_x	0.82	0.83
CO_2	379	376
Fuel Economy, MPG	18.1	18.2
Fuel Type 90th Percentile CNG		
Vehicle Odometer, miles	7280	7291
Exhaust Emission Results		
Weighted Total, grams / mile		
THC (CH_4 calibration)	1.04	0.97
CH_4 (a)	1.03	1.10
NMHC (a)	0.05	0.04
CO	1.74	1.31
NO_x	0.57	0.63
CO_2	378	373
Fuel Economy, MPG	17.8	18.0
Fuel Type 10th Percentile CNG		
Vehicle Odometer, miles	7251	7262
Exhaust Emission Results		
Weighted Total, grams / mile		
THC (CH_4 calibration)	1.65	1.79
CH_4 (a)	1.63	1.82
NMHC (a)	0.14	0.14
CO	0.02	

TABLE 7. GFI SYSTEM EMISSIONS SUMMARY

Fuel Type Mean CNG			
Vehicle Odometer, miles	7620	7630	
Exhaust Emission Results			
Weighted Total, grams / mile			
THC (CH_4 calibration)	1.31	1.21	
CH_4 (a)	1.30	1.26	
NMHC (a)	0.08	0.07	
CO	4.16	3.92	
NO_x	0.18	0.22	
CO_2	389	394	
Fuel Economy, MPG	17.3	17.1	
Fuel Type 90th Percentile CNG			
Vehicle Odometer, miles	7650	7661	7854
Exhaust Emission Results			
Weighted Total, gr. / mile			
THC (CH_4 calibration)	1.27	0.77	1.18
CH_4 (a)	1.20	0.79	1.36
NMHC (a)	0.07	0.05	0.05
CO	4.27	2.56	4.05
NO_x	0.22	0.19	0.27
CO_2	373	378	382
Fuel Economy, MPG	17.8	17.7	17.4
Fuel Type 10th Percentile CNG			
Vehicle Odometer, miles	7691	7710	7873
Exhaust Emission Results			
Weighted Total, gr. / mile			
THC (CH_4 calibration)	1.05	1.04	1.00
CH_4 (a)	1.07	1.01	1.02
NMHC (a)	0.08	0.07	0.07
CO	3.40	3.16	3.36
NO_x	0.23	0.19	0.26
CO_2	395	377	386
Fuel Economy, MPG	18.5	19.4	18.9

TABLE 8. ANGI SYSTEM EMISSIONS SUMMARY

Fuel Type Mean CNG			
Vehicle Odometer, miles	8610	8621	
Exhaust Emission Results			
Weighted Total, grams / mile			
THC (CH_4 calibration)	0.52	0.50	
CH_4 (a)	0.49	0.52	
NMHC (a)	0.04	0.03	
CO	1.40	1.29	
NO_x	0.11	0.12	
CO_2	384	385	
Fuel Economy, MPG	17.9	17.8	
Fuel Type 90th Percentile CNG			
Vehicle Odometer, miles	8670	8681	8808
Exhaust Emission Results			
Weighted Total, g / mile			
THC (CH_4 calibration)	0.78	0.54	0.56
CH_4 (a)	0.82	0.53	0.58
NMHC (a)	0.04	0.03	0.05
CO	5.05	1.95	1.60
NO_x	0.09	0.18	0.10
CO_2	397	392	394
Fuel Economy, MPG	16.7	17.2	17.1
Fuel Type 10th Percentile CNG			
Vehicle Odometer, miles	8632	8651	
Exhaust Emission Results			
Weighted Total, g / mile			
THC (CH_4 calibration)	0.92	0.92	
CH_4 (a)	0.94	1.06	
NMHC (a)	0.06	0.06	
CO	0.23	0.24	
NO_x	1.09	1.46	
CO_2	387	428	
Fuel Economy, MPG	19.1	17.2	

(a) CNG Tests: Methane concentration is based on independent GC analysis. NMHC calculation from GC speciation analysis.

With respect to the average NOx emission level , the GFI system produced the lowest NOx test results for all compositions followed by the Impco and Mogas systems. The ANGI system produced even lower levels of NOx emissions with the mean and 90th percentile gas compositions, but did not pass the 1993 NOx standard of 1.0 g/mi with the 10th percentile gas composition fuel. The Impco and GFI systems passed the NOx standard while the Mogas system was slightly over the limit. In assessing these results one must take into consideration the system setup procedure. Both the Impco, and Mogas systems involved subjective tuning of the system to achieve low tailpipe emissions based on the use of a 4 gas analyzer. The subjective nature of the setup as well as the system sensitivity resulted in a lean mixture for all three of these conversion systems. This produced a combination of relatively low CO and high NOx, as would be expected. On the other hand, the GFI and ANGI systems calibrate themselves automatically, producing the opposite effect. This automatic rich setup produced surprisingly consistent low NOx values for each of the gas compositions tested, resulting in NOx emissions below both the 1993 and 1994 emission limits, except where noted above.

ACKNOWLEDGMENT

IGT would like to thank Mr. Brent Bailey and Mr. Chris Colucci at the U.S. Department of Energy, National Renewable Energy Laboratory for both their patience and support during this program. Special thanks goes to Ms. Heide Swanson and Mr. Wilson Tomala at Brooklyn Union Gas for supporting the testing of a fourth conversion system. Other organizations that contributed to the success of this program include the Northern Illinois Gas Company, Amoco, the Gas Research Institute and AutoResearch Laboratory as well as the cooperation of the equipment suppliers.

REFERENCES

1. W.L. Liss, W.H. Thrasher, G.F. Steinmetz, P. Chowdiah, and A. Attari, "Variability of Natural Gas Composition in Select Metropolitan Areas of the United States" Gas Research Institute Report No. GRI-92/0123; March 1992.

2. "1990 CRC Driveability Workshop", CRC Report No. 577 October, 1990.

3. Painter, Rutherford, "Statistical Design and Analysis Methods for the Auto/Oil Air Quality Research Program", SAE paper 920319.

SOME ASPECTS OF BASIC GEOCHEMISTRY IN COAL SCIENCE

Dalway J. Swaine
CSIRO Division of Coal and Energy Technology
P.O. Box 136, North Ryde NSW, 2113
Australia

Keywords: coal, geochemistry, trace elements

ABSTRACT

Several instances of the use of basic geochemistry in coal science are given, using Australian bituminous coals as examples. The mode of occurrence of manganese is related to associations with siderite and calcite, the reason being cation replacement. High concentrations of boron, arsenic, phosphorus and other elements in deposits found in some boilers were due to the presence of boron phosphate and boron arsenate, two compounds that have not been found in nature. The proportions of soil/rock and flyash particles in atmospheric particulates deposited near a power station have been estimated by using the marked differences in germanium concentrations.

INTRODUCTION

In his pioneering geochemical research, V.M. Goldschmidt studied trace elements in coal. Several elements were discovered and determined in coal by Goldschmidt and coworkers in Gottingen during the 1930s (1). The basic principles enunciated by Goldschmidt are applicable to coal geochemistry. Much of the early trace-element studies depended on the development of sensitive analytical methods, mainly in optical emission spectroscopy. Some examples of the applications of Goldschmidt's work will be outlined based on experimental work on Australian coal carried out at the CSIRO, North Ryde.

MANGANESE IN BITUMINOUS COAL

As with other trace elements in coal, manganese can be found associated with the organic and with the inorganic matter. In most bituminous coals manganese occurs predominantly in the mineral matter fraction. In Australian bituminous coals from the Sydney Basin, New South Wales and from the Bowen Basin, Queensland, it was found that there was a marked concentration of manganese in siderite and in calcite (Table 1). On the basis of ionic radii (1) Mn^{2+} is expected to be able to substitute for some of the Fe^{2+} in siderite. Although the difference in ionic radius between Mn^{2+} and Ca^{2+} is greater than that for Mn^{2+} and Fe^{2+}, substitution can still occur in calcite. These results were used initially to propose that manganese occurs in Australian bituminous coals mainly in siderite and calcite components of the mineral matter. Direct evidence for the replacement of some Ca^{2+} ions by Mn^{2+} ions in calcite from a Pittsburgh coal was found by an electron paramagnetic resonance method (2). There is indirect evidence for the close association of manganese and 'carbonate' iron (that is, total iron less pyritic iron) from data for 56 samples of coal from the Lithgow seam, New South Wales (Figure 1, correlation coefficient r = 0.89). Samples of coal containing dolomite had relatively low concentrations of manganese, namely 10-150 ppm Mn (3).

TRACE ELEMENTS IN PHOSPHATIC BOILER DEPOSITS

When bituminous coal is fired in boilers using spreader stokers or chain grates, deposits were found in some parts of the boiler system. These deposits often had very high concentrations of phosphorus and many trace elements, including arsenic, boron, germanium, lead and zinc (Table 2). Indeed, bismuth, indium and thallium were found in some boiler deposits before they had been detected in Australian coals (4). Results in Table 2 show some of the concentrations in deposits from the burning of Australian bituminous coals which are relatively low in trace elements. The highest concentrations were found in specific locations in the boiler system, for example in the vertical riser tubes of the spreader stoker-fired boiler. The deposit on the superheater tubes of the chain grate stoker-fired boiler was in two distinct layers, namely a 2 mm thick inner layer with an outer layer superimposed on it. The high elemental concentrations were confined to the inner layer. On the basis of laboratory work by Schulze (5) who prepared boron phosphate (BPO_4) and boron arsenate ($BAsO_4$) and determined their crystal structures, Goldschmidt (1) stated that these two compounds are isostructural with β-cristobalite. Since these compounds have never been found in nature they were sought in the two deposits highest in arsenic, boron and phosphorus, and boron phosphate was identified. Later a further study established that $BAsO_4$ was present in solid solution in BPO_4 (6).

A possible mechanism for the formation of BPO_4 involves a reaction between calcium phosphate and silica to give phosphorus pentoxide, which could then react with boron trioxide formed from the decomposition of organically-combined boron in coal, to give boron phosphate (4). A similar mechanism has been proposed for the formation of boron arsenate (6). It is interesting to note that there are some high concentrations of germanium in the boiler deposits, probably the highest found in coal-derived material. Such deposits have not been used for the production of germanium, but other coal-derived materials have been processed in several countries to yield small quantities of germanium for the manufacture of semi-conductors.

GERMANIUM AS AN INDICATOR OF FLYASH IN ATMOSPHERIC PARTICULATES

Power stations emit trace elements to the atmosphere, mostly associated with fine flyash particles. There is an on-going interest in the composition of atmospheric particulates, especially in the concentrations of trace elements of environmental significance. Samples of material deposited in areas near power stations, say up to about 20 km away, contain predominantly soil/rock and flyash particles in proportions that are not easily measured. A study of the trace-element contents of flyash from an Australian power station showed that there was a distinct enrichment of some elements in the fine particles (less than about 3 μm diamteter) which predominate in the stack emissions. Comparisons of the compositions of flyash with those for rocks and soils, using available geochemical data show that germanium has the highest ratio for flyash to soil/rock material (Table 3). The mean values for germanium in fine flyash and soils in the area around the Australian power station were 75 and 1.5 ppm respectively. Applying this to samples of deposition enabled the proportions of flyash to be calculated from results for 12 three-monthly samples (Table 4). As expected the proportions of flyash decreased with distance from the power station. The variations in the ranges of values at any location are caused by changes in meteorological conditions, especially wind direction. It is surprising to find some very low proportions, for example 4 and 7%, in samples collected near the power station, but this was in keeping with seasonal changes in wind direction. Another geochemical interpretation of these results was carried out by comparing them with the amounts of trace elements released by rock weathering (7).

CONCLUSIONS

The examples discussed here indicate how basic geochemistry, mostly emanating from Goldschmidt's work, can be used to elucidate some aspects of the trace-element geochemistry of coal and coal usage.

REFERENCES

1. Goldschmidt, V.M. 'Geochemistry', Clarendon Press: Oxford, 1954, 730 pp.
2. Malhotra, V.M.; Graham, W.R.M. 'Origin of the Mn^{2+} e.p.r. spectrum in Pittsburgh No.8 bituminous coal', Fuel 1985, 64, 270-272.
3. Brown, H.R.; Swaine, D.J. 'Inorganic constituents of Australian coals', J. Inst. Fuel 1964, 37, 422-440.
5. Schulze, G.E.R. 'The crystal structure of BPO_4 and $BAsO_4$', Z. Physik. Chem. 1934, B24, 215-240.
6. Swaine, D.J.; Taylor, G.F. 'Arsenic in phosphatic boiler deposits'. J. Inst. Fuel 1970, 43, 261.
7. Swaine, D.J.; Goodbeer, W.C.; Morgan, N.C. 'The deposition of trace elements from the atmosphere', In Trace Elements in New Zealand : Environmental, Human and Animal (Eds. R.G. McLaren, R.J. Haynes, G.P. Savage) 1989 pp. 1-10.

Table 1. Manganese in carbonate minerals found in Australian bituminous coals

Mineral and location	Mn (ppm)
Siderite, Tongarra seam, Sydney Basin	3000
Siderite, Benley seam, Queensland	10000
Calcite, Wallarah seam, Sydney Basin	10000
Calcite, Blackwater, Queensland	19000
Calcite from fissure in seam, Queensland	2240

Table 2. Contents of trace elements in boiler deposits; based on (4)

Type of boiler and coal	Content of trace element (as%)					
	As	B	Ge	P	Pb	Zn
Spreader stoker:						
superheater tubes	0.08	0.05	0.1	11.0	1.0	1.0
vertical riser tubes	0.8	3.0	0.1	15.0	0.3	0.6
economiser outlet dust	0.1	0.15	0.01	1.5	0.04	0.2
coal (ppm)	1	6	8	400	10	50
Chain grate stoker:						
superheater tubes						
inner layer	1.0	5.0	1.0	25	1.0	1.0
outer layer	0.0001	0.015	0.002	1.2	0.004	<0.03
coal (ppm)	1	15	9	580	10	50

Table 3. Contents of germanium

Earth's crust	1.5 ppm Ge	Soil	
Sandstone	0.8	- range	1-2.5 ppm Ge
Limestone	0.2	- mean	1.5
Shale	1.6	Fine flyash	
		- range	50-100
		- mean	75

Table 4. Flyash in deposition at different locations

Distance of location from power station (km)	Flyash range (%)	Flyash mean (%)
1.8	7-80	40
1.5	4-33	11
3.9	0.5-10	5
5.3	<1-5	2.5
27.4	0.1-2.5	0.7

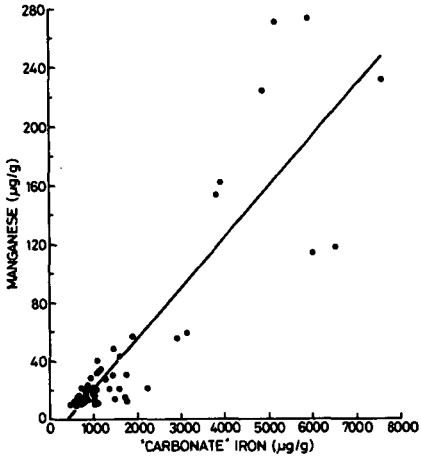

Figure 1. Plot of concentrations of manganese against 'carbonate' iron

A COMPARATIVE STUDY OF THE TRACE ELEMENT GEOCHEMISTRY IN COALS FROM ALBERTA, CANADA

Thomas Gentzis
Alberta Research Council
Devon, Alberta T0C 1E0 CANADA

Fariborz Goodarzi
Geological Survey of Canada
Calgary, Alberta T2L 2A7 CANADA

Keywords: Trace Elements, Geochemistry, Coal

INTRODUCTION

Alberta contains vast reserves (approximately 2185 megatonnes) of subbituminous and high-volatile bituminous coals, with an additional 1345 Mt considered as "indicated" and 3890 Mt as "inferred" (Smith, 1989). Virtually all of Canada's subbituminous coal resources, which are suitable for mine-mouth power generation, are found in the Interior Plains of Alberta. In addition, low sulphur (< 1.0%), high-volatile bituminous, exportable thermal coals occur in the Outer Foothills region of the province. Almost 90% of Alberta's power originates from six coal-fired generating stations. These are: (1) the 1987 MW Sundance station; (2) the 766 MW Keephills station; (3) the 570 MW Wabamun Lake station; (4) the 400 MW Genesee station; (5) the 735 MW Battle River station; and (6) the 760 MW Sheerness station (Figure 1a). The first four stations are located approximately 70-100 kms to the west and southwest of Edmonton, the fifth 180 kms east of Edmonton and the sixth 160 kms northeast of Calgary.

Coal contains almost every element in the periodic table and many of the elements are released, on particles or in vapour phase, to the environment, during coal combustion. In 1991, the Alberta Research Council, along with the Geological Survey of Canada, initiated a major program, financed by the power utility companies and the Alberta Government, on the "impact of coal quality on the utilization potential of Alberta subbituminous coals". Before examining the mobilization of elements during coal combustion and their emissions to the atmosphere, it is very important to study the concentration, mode of occurrence, lateral, and vertical variation of elements in the coal seams currently mined or those to be mined, within the boundaries of the minesite. As a result, this study deals with the elemental concentration and variation in coals from the Highvale mine (feedstock for the Sundance and Keephills plants), Whitewood mine (Wabamun plant), Vesta mine (Battle River plant) and Obed Mountain coal deposit (exported to Ontario as thermal coal) (Figure 1b).

The main focus of the paper is on the concentration of selected trace elements with known toxic responses to humans and the biological system, when emitted by coal-fired power stations, such as As, Hg, Mn, Se, and V, to name but a few. The elements in coals from the above mines will be classified according to the mode of their occurrence, with particular emphasis on the geological and geochemical factors influencing their distribution in the coal-bearing succession. Elemental concentrations will be compared and contrasted on a mine-by-mine basis rather than a seam-by-seam basis.

RESULTS AND DISCUSSION

Highvale Mine

Some of the elements of great concern because of their environmental effects are mercury (Hg) and cadmium (Cd). Mercury is volatile and is found either in gaseous form or enriched on the surfaces of fine particles following coal combustion (Clarke and Sloss, 1992). It is readily available for plant uptake and could be responsible for neural, renal and cardiovascular diseases in humans (US DOE, 1989). The Highvale coals contain Hg in the 100 to 400 ppb range (Gentzis, 1993, unpublished data), values which are slightly higher than Australian coals (100 ppb; Swaine, 1990) and lower than US coals (180 ppb; Finkelman, 1980). Low-sulphur coals, such as the Highvale coals (total S <0.5%), are generally low in Hg and the element is believed to have an inorganic association. Cadmium tends to bioaccumulate in the food chain (Neme, 1991) and is a possible carcinogen to humans and animals (US DOE, 1989). The Highvale coals have Cd content less than 0.2 ppm, values similar to Australian coals (0.01-0.02 ppm) (Swaine, 1990) and lower than US coals (1.3 ppm) (Finkelman, 1980).

Mean elemental concentrations in the Highvale coals are: As (3.82 ppm), Br (286.4 ppm), Cl (72.3 ppm), Cr (11.5 ppm), Cu (20.6 ppm), Se (1.65 ppm), U (2.57 ppm), Th (5.6 ppm), and V (17.1 ppm) (Gentzis *et al.*, 1993). The high concentration of Br in some coal samples is attributed to drilling mud contamination, a phenomenon also observed by Finkelman (*pers. commun.*, 1993) in coals from Pakistan. Sodium content averages 2500 ppm, approximately three times higher than the nearby (12 Kms) Whitewood mine coals. This element has an inorganic association in the Highvale coals, and any detrimental effect of Na may be compensated by Ca in the coals. Other elements with an inorganic association include As, Ba, Cs, Fe, K, Mg, Mo, U, and V; Sr and Ce show an intermediate association, while Br, Cl, B, Co, Dy, and Mn show an organic association. The elements Al, As, Sc, Th and all rare earth elements (REEs) tend to decrease from roof to floor of the coal seams and their concentration often shows a cyclical pattern within the coal-bearing strata, indicative of periods of inundation of the coal-forming environment by clastic sediments.

Crowley *et al.*,(1989) have explained a mobilization pattern when a volcanoclastic layer (tonstein) is located above coal beds using cluster analysis. According to Van der Flier-Keller (1993), the light rare earth elements (LREEs) are associated with clay minerals and the heavy rare earth elements (HREEs) with detrital heavy minerals. All REEs in the Highvale mine subbituminous coal closely follow the Al trend, a behaviour which is expected since the REEs are associated with the inorganic constituents in coals. The high concentration of REEs in the thin coal seam 3 in drillhole HV84-901, which is located underneath a Sr and Ba-rich tonstein band (Figure 2), is believed to be due to migration of the elements by groundwater and subsequent concentration in the coal. The coal seam contains more HREEs than the volcanoclastic layer above because the HREEs were preferentially hydrolyzed or bound to organic complexes and allowed to migrate from the tonstein. The LREEs, being mobile, when liberated during the breakdown of the parent volcanic ash caused by weathering, were preferentially accommodated in clay minerals. The REE pattern in the Highvale coal is thought to be controlled by source lithology (volcanic versus sedimentary partings), by weathering, and other geochemical patterns during and after coal formation.

Ashing of two suites of samples of Highvale coal at 120°C resulted in an enrichment of all elements by a factor of x1.5 to x6.5 in one suite and by x5 to x11 in the other. In the 400°C ashed sample, enrichment factors ranged from x1.5 to x6.5 in the first suite and by x1.5 to 9.5 in the second. The elements Br, Cl, and Se were, surprisingly, enriched by x2 to x6, pointing to the formation of salts (i.e. bromide salts), which occurs as a result of reactions of anions with cations during ashing. At 800°C, Br and Cl were completely volatilized, as expected. Relative enrichment factors (REF), calculated using two methods of the ratio of elemental concentration versus Al concentration in air/crust (method A) and in ash/coal (method B) show method B to give higher and more consistent values.

Generally, there is little information on the variation of elements in coal seams laterally over a long distance, mainly due to variations in basement conditions and other geological factors (folding and faulting). The concept of "variance ratio" (the ratio of maximum to minimum value of an element) was first introduced by Headlee and Hunter in 1953 and subsequently used by Zubovic (1960) and Swaine *et al.*,(1984). The lateral variation of selected elements in pits 3 and 5 of the mine for seams 1 and 2 (the thickest) and corresponding variance ratios show that elements with inorganic association in the Highvale coal (ie. As, Na, U, Se and Th) have narrow lateral variations in the pits and low variance ratios, whereas elements with organic association (ie. Br, Cl) have wider lateral variation and higher variance ratio.

Whitewood Mine

The following seams are present in this mine: 1U, 1L, 2, 3, 4, 5, and 6, of which seam 1U is not presently mined and seam 1L is stratigraphically correlatable to seam 1 in the nearby Highvale mine. The mean concentrations of elements are: As (4.7 ppm), Br (15.1 ppm), Cl (21.5 ppm), Co (3.3 ppm), Cr (7.0 ppm), Mo (4.8 ppm), Na (710 ppm), Mn (110 ppm), U (2.5 ppm), Th (6.0 ppm), and V (19.3 ppm) (Gentzis, 1993, unpublished data). Compared to the Highvale coals, these coals are slightly enriched in As and V, depleted in the halides Br and Cl, also in Ba, Cr, Na, Se, and have similar concentration of Co, Mn and U. By world standards (see Clarke and Sloss, 1992, Table 8, p. 26), the Whitewood mine coals are "clean" and suitable for utilization. The ash analysis shows the mean SiO_2 value for all seams to be between 50 and 70 wt.%, Al_2O_3 ranges from 12-27 wt.%, Fe_2O_3 ranges from 1.5-6 wt.%, TiO_2 ranges from 0.4-0.75 wt.%, and CaO is in the 6-15 wt.% range. In addition, MgO varies from 0.6-2.1 wt.%, K_2O from 0.15-0.55 wt.%, Na_2O from 0.4-0.8 wt.% (except for seams 3 and 6) and

SO_3 from 2-6 wt.% (TransAlta Utilities, 1993, unpublished data). The coal ash is depleted in Na_2O and enriched in SO_3 and CaO (lime) compared to the coal ash quality requirements for power generation, outlined by Skorupska (1993). The ash content of the coal is 12-25%, with the exception of seam 1U (37%). A coal containing 20% ash provides an uncontrolled dust loading of 30 g/m^2, therefore, a collection efficiency of 99.7% is required to meet acceptable emission standards (Skorupska, 1993). In the Wabamun Lake power station, electrostatic precipitators (ESPs) are used to achieve this objective. One problem related to ESP performance in the Wabamun plant is opacity, which results in a decrease in precipitator efficiency. Because the Na_2O content in the ash is lower than the standard requirements dictate, the fly ash resistivity increases resulting in a decrease of the corona current flow.

Vesta Mine

One of the most obvious differences in trace elements between coal from this mine and coal from the other three mines is its high boron (B) content (> 200 ppm) (Gentzis, 1993, unpublished data). Boron in coal is interesting from a geochemical point of view because it can differentiate whether freshwater, mildly brackish, or brackish water conditions prevailed during the early stages of coal formation (Swaine, 1971; Goodarzi and Van der Flier-Keller, 1989; Banerjee and Goodarzi, 1990). Boron is very sensitive to changes in water salinity and remains constant laterally within a minesite. Furthermore, B values usually fall nicely within the limits designated for each generalized depositional setting (< 50 ppm for freshwater, 50-110 ppm for mildly brackish and >110 ppm for brackish) unless there is a secondary B enrichment (Goodarzi and Swaine, 1992). The B content of the Vesta mine coal indicates that the peat interacted with brackish waters, which may have invaded the fluvio-deltaic depositional setting during a marine transgression. Boron in the Vesta mine coal is associated with the organic matter and is depleted (25 ppm) only in one, inertinite-rich sample. The petrological composition of the sample indicates exposure of the peat surface to fire or oxidation and higher temperatures. Depletion of B has been observed in oxidation and combustion zones of naturally heat-affected coal seams (Goodarzi and Swaine, 1993) and is attributed to possible volatilization of the element. During combustion of this coal, B will most likely be redistributed in the bottom ash, the flyash retained by ESPs and fine flyash, which will eventually reach the atmosphere with the stack gases. However, B is not considered to be toxic and may have little detrimental effect in the close environs of the Battle River power station. The Vesta coals are very low in As (<1.0 ppm), Br (<2.3 ppm), V (<3 ppm), U (<1.4 ppm), Mn (<30 ppm), Mo(< 2.5 ppm), but are extremely high in Na (range is 4200-4900 ppm) (Gentzis, 1993, unpublished data).

Obed Mountain Mine

The B content of the coal ranges from 27 to 100 ppm, but generally it is < 50 ppm, indicating freshwater to possibly slightly brackish water depositional environment. The element is depleted in the sedimentary partings (12-27 ppm) and enriched in the coal intervals immediately underneath. This behaviour points to downward mobilization of B from parting to coal of soluble to groundwater B, a phenomenon believed to be enhanced by increased oxidation leading to formation of leachates containing enough soluble B to affect groundwater (Goodarzi and Swaine, 1993). The range in elemental concentration in the two thickest seams are as follows: As 2-7.6 ppm; Br 5.9-10.1 ppm; Cl 76.4-87.2 ppm; Cr 3.4-11.2 ppm; Co 1.2-2.9 ppm; Mn 21.5-39.3 ppm; Mo 2.1-5.5 ppm; Se 1-1.2 ppm; U 1-2 ppm; Th 1.2-2.8 ppm (Gentzis, 1993, unpublished data); the lack of Na (mean is 117 ppm) could lead to potential problems in ESP performance.

Most elements increase in concentration with ash content, thus are inorganically associated in the coal. The vertical variation of certain elements is very similar, such as Th and U; also Zn, Rb, Cs, and K; Br and Cl; Na, Mg, Ti, As, and Fe. It was observed that U, Se, Sb, and Mo were concentrated preferentially in the upper part of the seams, while Br and Cl were enriched in the middle part. The elemental pairs: Mn and Sc, Co and Co, Se and U, Rd and Cs, and the HREE are concentrated in coal intervals immediately underneath roof sediments or major partings. The Obed Mountain coals are depleted in most elements compared to coals formed under freshwater conditions, such as Highvale and Whitewood, except for Cl.

CONCLUSION

The elemental concentrations in the subbituminous coals from Alberta are related to the environment of coal deposition, the presence of volcanoclastic layers (tonsteins), the action of groundwater, the degree of weathering, and the nature of country rocks. The coal seams studied contain low concentrations of environmentally or industrially-sensitive elements, such as As, B (except for the Vesta coal), Cl, Mo, Se, Na, Ca, U,

and S, both vertically and laterally. The coals are "clean" and suitable for utilization. Elements associated with the mineral matter in coal are concentrated in the 800°C ashed coal, when compared to the fresh coal. There is also a progressive concentration of Br from the fresh to the 120°C and the 400°C ashed samples, pointing to the formation of salts.

REFERENCES

1) Banerjee, I. and Goodarzi, F., 1990 Paleoenvironmental and sulphur-boron contents of the Mannville (Lower Cretaceous) coals of southern Alberta, Canada, Sedimentary Geology, vol. 67, p. 297-310.
2) Clarke, L.B. and Sloss, L.L., 1992 Trace Elements-emissions from coal combustion and gasification, International Energy Agency Report CR/49, London, 111 pp.
3) Crowley, S.S., Stanton, R.W. and Ryer, T.A., 1989 The effect of volcanic ash on maceral and chemical composition of the C coal bed, Emery coalfield, Utah, Organic Geochemistry, vol. 14, p. 315-331.
4) Finkelman, R.B., 1980 Mode of occurrence of trace elements in coal, Ph.D. thesis, University of Maryland, College Park, MD, 301 pp.
5) Gentzis, T., Goodarzi, F. and Hickinbotham, A., 1993 Impact of coal quality on the utilization potential of coals from the Highvale Mine, Alberta, Conference Proceedings, 7th International Conference on Coal Science, Banff, Alberta, September 12-17, vol. I, p. 93-97.
6) Goodarzi, F. and Van der Flier-Keller, E., 1989 Organic petrology and geochemistry of intermontane coals from British Columbia 3. The Blakeburn open cast mine near Tulameen, British Columbia, Canada, Chemical Geology, vol. 75, p. 227-247.
7) Goodarzi, F. and Swaine, D.J., 1992 Geochemistry of Boron in Australian and Canadian coals, Proceedings of the Canadian Coal and Coalbed Methane Geoscience Forum, Parksville, British Columbia, p. 319-332.
8) Goodarzi, F. and Swaine, D.J., 1993 Behaviour of Boron in coal during natural and industrial combustion processes, Energy Sources, vol. 15, p. 609-622.
9) Headlee, A.J.W. and Hunter, R.G., 1953 Elements in coal ash and their industrial significance, Industrial Engineering Chemistry, vol. 45, p. 548-551.
10) Neme, C., 1991 *Electric Utilities and Long-Range Transport of Mercury and Other Toxic Air Pollutants*, Centre for Clean Air Policy, Washington, DC, USA, 125 pp.
11) Skorupska, N.M., 1993 Coal specifications-impact on power station performance, International Energy Agency Report CR/52, London, 120 pp.
12) Smith, G.G., 1989 *Coal Resources of Canada*, Geological Survey of Canada Paper 89-4, 146 pp.
13) Swaine, D.J., 1971 Boron in coals of the Bowen Basin as an environmental indicator, Proceedings of the Second Bowen Basin Symposium, Geological Survey of Queensland, Report No. 62, p. 41-48.
14) Swaine, D.J., Godbeer, W.C and Morgan, N.C., 1984 Variations in contents of trace elements in coal from one seam, Report NERDDP, No. EG84/339, 103 pp.
15) Swaine, D.J., 1990 *Trace Elements in Coal*, Butterworths, London, 278 pp.
16) US DOE-United States Department of Energy, 1989 *Clean coal technology demonstration program, final programmatic environmental impact statement*, DOE/EIS-0146, US Department of Energy, Washington, DC, USA.
17) Van der Flier-Keller, E., 1993 Rare earth elements in Western Canadian coals, Energy Sources, vol. 15, p. 623-638.
18) Zubovic, P., 1960 Minor element content of coal from Illinois Beds 5 and 6 and their correlatives in Indiana and Western Kentucky, United States Geological Survey Open File Report, No. 537, 79 pp.

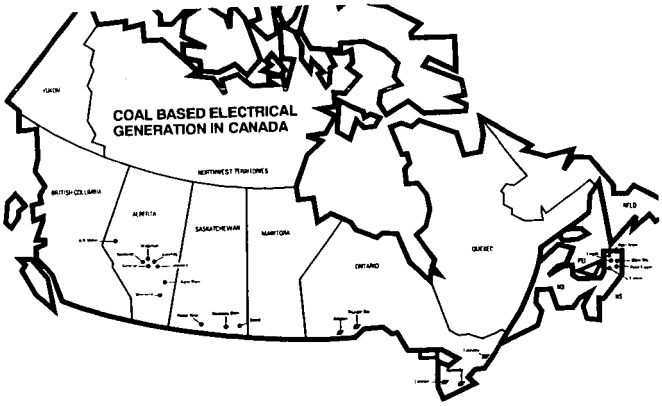

Figure 1a. Map of Canada showing location of power stations in Alberta (after Canadian Coal Association Directory, 1993).

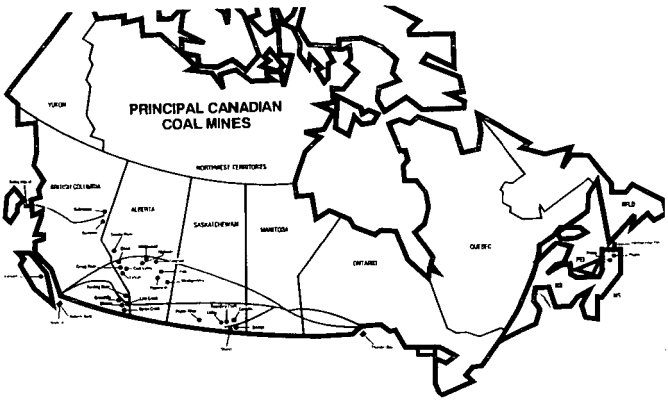

Figure 1b. Map of Canada showing location of coal mines in Alberta (after Canadian Coal Association Directory, 1993).

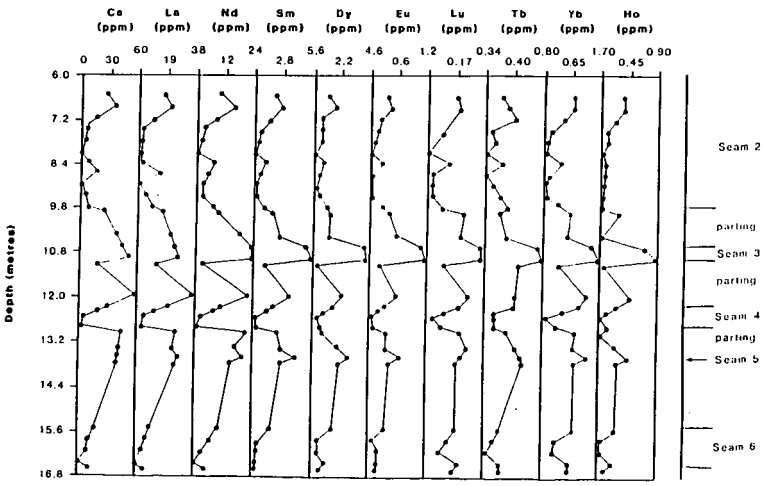

Figure 2 Vertical variation of REEs in drillhole HV84-901, Highvale mine.

PETROGRAPHIC AND GEOCHEMICAL ANATOMY OF LITHOTYPES FROM THE BLUE GEM COAL BED, SOUTHEASTERN KENTUCKY

James C. Hower[1], Darrell N. Taulbee[1], Susan M. Rimmer[2], and Liria G. Morrell[1]
[1]University of Kentucky Center for Applied Energy Research, Lexington, KY 40511
[2]University of Kentucky, Department of Geological Sciences, Lexington, KY 40506

Keywords: coal geochemistry, macerals, Kentucky

INTRODUCTION

The nature of the association of major, minor, and trace elements with coal has been the subject of intensive research by coal scientists (Swaine[1]; and references cited therein). Density gradient centrifugation (DGC) offers a technique with which ultrafine coal particles can be partitioned into a density spectrum, portions of which represent nearly pure monomaceral concentrates. DGC has been typically conducted on demineralized coals[2] assuring, particularly at lower specific gravities, that the resulting DGC fractions would have very low ash contents.

In order to determine trends in elemental composition, particularly with a view towards maceral vs. mineral association, it is necessary to avoid demineralization. To this end the low-ash, low-sulfur Blue Gem coal bed (Middle Pennsylvanian Breathitt Formation) from Knox County, Kentucky, was selected for study. The objective of this study was to determine the petrography and chemistry, with particular emphasis on the ash geochemistry, of DGC separates of lithotypes of the Blue Gem coal bed.

EXPERIMENTAL

Sample Preparation and Characterization

Samples were obtained from the Blue Gem coal bed from a mine site in the Barbourville 7½ minute quadrangle, Knox County, Kentucky. The coal bed, 70 cm thick, was sampled in a series of five benches. Sample KCER-5447 represents the 10.0 cm basal bench of the coal bed. KCER-5445 represents an 11.6 cm lithotype from the middle of the coal bed.

Bench samples were crushed and split following procedures recommended by ASTM standard D2013.[3]

Proximate, ultimate, and sulfur analyses were determined for each bench sample according to standard ASTM techniques.[3]

Subsplits of the -20 mesh coals were mixed with epoxy resin and prepared into pellets for petrographic analysis and polished according to standard procedures.[4]

Density Gradient Centrifugation Separation

Maceral separation was based on the DGC method developed by Dyrkacz and co-workers[5-6] with certain modifications.[2] Additional modifications included omission of the demineralization step, crushing the feed coal to -325 mesh, and adding Brij-35 surfactant to the separation media (due to the smaller particle size) to suppress particle agglomeration.

PIXE Ash Geochemistry

The major and minor element geochemistry of the high temperature ashes of all of the lithotypes, the whole coal samples of the three lithotypes subjected to DGC separation, and the "whole coal" DGC density fractions was determined using Proton Induced X-ray Emission (PIXE). Procedures for PIXE analysis can be found in Savage.[7]

X-ray fluorescence analysis of the lithotype high temperature ashes was conducted at the CAER using techniques described by Hower and Bland.[8]

RESULTS

Petrographic Analysis of Bench and DGC Samples

Petrographically, the bench samples have relatively high vitrinite contents, with samples containing between 77.6 and 87.3% vitrinite (Table 1). Coal rank is high volatile A bituminous (0.88% R_{max}). Petrography of the KCER-5445 DGC separates is given on Figure 1.

In the DGC fractions recovered between 1.25-1.30 g/mL, vitrinite content is over 90%. The partitioning of macerals into relatively pure fractions with little association of

mineral matter was therefore encouraging for the interpretations to be made in the accompanying geochemical studies.

In each study sample, there is an abrupt transition from vitrinite-dominated to semifusinite-dominated DGC fractions at about 1.30-1.31 g/mL and a similar, though less abrupt, transition from semifusinite- to fusinite-dominated fractions at about 1.33-1.34 g/mL. Mixed maceral fractions dominate the lower density range.

GEOCHEMICAL CHARACTERIZATION OF BENCH SAMPLES

Aside from the top bench of the coal bed, KCER-5443, which has an ash content of 9.15% and a total sulfur content of 2.32%, the coal is very low in ash (0.40 - 1.47%) and sulfur (less than 0.8%). Elemental analyses suggest the presence of clays (Si and Al), carbonates (Fe and Ca), and, in the upper bench, possibly pyrite (Fe and S). This is supported by previous observations on the mineralogy of this coal bed.[9] Several trace elements are enriched in the center of the coal bed (Ba, Cu, Mo, and Sr); other elements (Cr, Co, Mn, V, Ti, and Zr) increase towards the base of the coal.

GEOCHEMISTRY OF DGC SAMPLES

Based on analysis of the whole-coal and lithotype (non-DGC) ashes, Cs in the DGC-derived samples appears to be solely from the CsCl salt solutions used to prepare the DGC gradient. The PIXE geochemistry on the whole-coal basis was calculated on a Cs-free basis. The Cl content on the whole-coal basis was also adjusted stoichiometrically for Cs remaining from the DGC processing.

Cl and Br, both of which are best evaluated on the whole-coal basis, maximize in the vitrinite-rich separates.

In very-low ash samples such as these, organic sulfur is the most prevalent element other than C, H, N, and O. S and Cl trends for KCER-5445 are shown on Figure 2. On the whole-coal basis (pre-DGC), the sulfur content of KCER-5445 exceeds the ash content.

Ash-basis geochemistry is based on several assumptions: 1/ the "ash" percentage is 100% minus the "carbon" reported in the PIXE analysis ("carbon" includes all elements lighter than Na); 2/ most of the sulfur is organic and not part of the ash although organic sulfur can be fixed as sulfate in the low-temperature ashing process; and 3/ Cl and Br are volatilized, perhaps as HCl and HBr, in the ashing process.

Among the major elements, only P and Mg exhibit 10^2 order-of-magnitude ranges in concentration. In the case of Mg, the concentration peaks in the KCER-5445 >1.40 g/mL fractions. Ca and Mn are also relatively concentrated through this range, suggesting that the fusinite may be associated with a dolomite or magnesite with Mn substitution. Ca is also high in 5445 and 5447 1.22-1.30 g/mL fractions, but drops in the semifusinite-rich fractions. Fe is higher in 5445, peaking in the fractions above 1.31 g/mL. Siderite ($FeCO_3$), generally dispersed in vitrinite, is an important mineral phase in the Blue Gem.[10] The Ca-Fe-Mg trends could be indicative of a shift in the dominant carbonate phase.

Si has a high concentration in the 5445 <1.12 g/mL fraction, perhaps representing biogenic silica, and in the pellets (material that exceeds the range of the density gradient) from the DGC runs. The Al variation is high in 5445 but somewhat muted in 5447 where DGC fraction 1 was not analyzed. K and the K/Al ratio minimizes in the vitrinite-rich fractions. K is also higher in 5447 than in 5445. Rb, which can substitute for K, only appears in the high-ash pellets.

P is exceptionally high in the 5445 1.18-1.22 g/mL fractions. The 1.20-1.22 g/mL fraction was analyzed for the other two coals but P was not significantly higher than in the other fractions.

On the ash basis, Ti maximizes in the high vitrinite fractions with 5447 having higher Ti concentration than 5445. Zr generally follows the Ti trends, peaking in the 5447 1.29-1.30 g/mL fraction at 6.5% (ash basis).

V maximizes in the high-vitrinite fractions, with 5447 having much higher concentrations, up to 14% in the 5447 1.29-1.30 g/mL fraction. In part, Cr follows the V trend, maximizing in the same fraction. Cr also has a high concentration in the 5445 1.12-1.15 g/mL fraction, corresponding to high concentrations of Ni, Cu, Mn, Zn, and Pb.

Ga, Ge, and Y peak in the lighter fractions and in the vitrinite-rich fractions and are higher in 5447 than in 5445. As and Se have greater concentrations in 5445 and peak in the lighter fractions and in the vitrinite-rich fractions. The highest concentration of As was found in the whole-lithotype ash of KCER-5443, a lithotype not processed by DGC. The As may be associated with pyrite in that high-sulfur lithotype.

Sr peaks in the vitrinite-rich fractions with similar trends and concentrations in each lithotype.

The elemental associations, or at least coincidences, noted are: Mg-Ca, Fe-Ca, and Mn-Ca; Ti-Zr; V-Cr; Cr-Ni-Cu-Mn-Zn-Pb (in a low-density split), Co-Ni, and Cu-Zn; Ga-Ge-Y; and As-Se. Of additional interest is the consistency of association of an element with a particular density split. Fraction 21, the high density "pellet" recovered from the rotor outer wall should contain minerals and associated elements not otherwise associated with macerals. Not surprisingly, elements clearly associated with mineral phases, such as Si and Al in clays, exhibit much higher concentrations in the pellet than in the lighter fractions. Many elements have somewhat mixed trends but Cl and Br are clearly higher in the organic-rich fractions than in the pellet. As, with Se showing an indeterminate trend, and Ga, with Ge showing an indeterminate trend, are higher in the organic-rich fractions. As noted above, Sr is one element which is consistently higher in the highest vitrinite fractions. Ca is also high through the vitrinite range although its peak is broader than the Sr peak. It is possible that Sr is closely associated with the carbonate phase of the vitrinite-rich fractions. Ga and Ge also tend to peak in the vitrinite-rich fractions.

REFERENCES

1. Swaine, D.J., 1990, Trace elements in coal. London, Butterworths, 278 p.
2. Taulbee, D.N., Poe, S.H., Robl, T.L., and Keogh, R., 1989, Density gradient centrifugation separation and characterization of macerals groups from a mixed maceral bituminous coal. Energy & Fuels, 3, 662-670.
3. American Society for Testing Materials (ASTM), 1989, Annual book of ASTM Standards: Coal and Coke. ASTM, Philadelphia.
4. Stach E., Mackowsky, M-Th., Teichmüller, M., Taylor, G.H., Chandra, D, and Teichmüller, R., 1982, Stach's Textbook of Coal Petrology, Third Edition, Gebrüder Borntraeger, Berlin, 535 pp.
5. Dyrkacz, G.R., Bloomquist, C.A.A., and Horwitz, E.P., 1981, Laboratory scale separation of coal macerals. Separation Science and Technology, 16, 1571-1588.
6. Dyrkacz, G. R., and Horwitz, E.P., 1982, Separation of coal macerals. Fuel, 61, 3-12.
7. Savage, J.M., Wong, A.S., and Robertson, J.D., 1992, Thick-target PIXE/PIGE analysis of complex matrices. Jour. Trace and Microprobe Techniques, 10, 151-168.
8. Hower, J.C., and Bland, A.E., 1989, Geochemistry of the Pond Creek coal bed, Eastern Kentucky coalfield. International Journal of Coal Geology, 11, 205-226.
9. Rimmer, S.M., Hower, J.C., Esterle, J.S., and Moore, T.A., in preparation, Petrology of the Blue Gem coal bed. To be submitted to the International Journal of Coal Geology.
10. Hower, J.C., Rimmer, S.M., and Bland, A.E., 1991, Ash geochemistry of the Blue Gem coal bed. International Journal of Coal Geology.

Table 1. Proximate analysis and maceral content of samples used in study.

KCER #	Ash (dry)	S_T (dry)	VM (dry)	Vit	Fus	Sfus	Mic	Ex	Res
5445	0.40	0.63	39.13	78.5	6.0	2.8	2.5	10.1	0.1
5447	1.47	0.61	37.03	77.6	7.2	3.6	2.7	8.7	0.2

Figure 1. Group maceral content of KCER-5445 vs. DGC fraction.

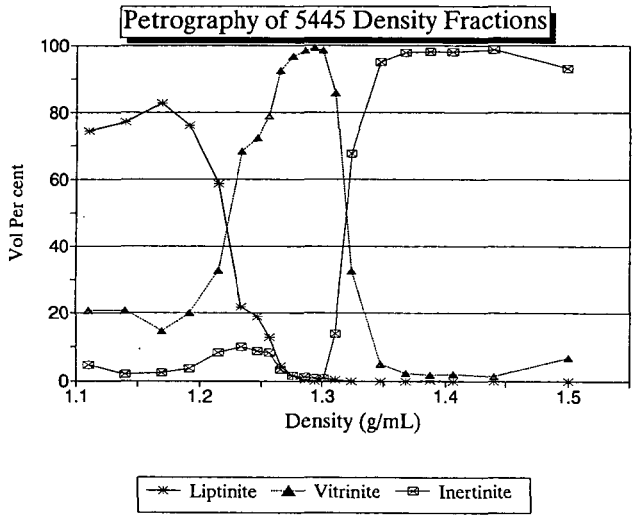

Figure 2. S_T and Cl of KCER-5445 vs. DGC fraction.

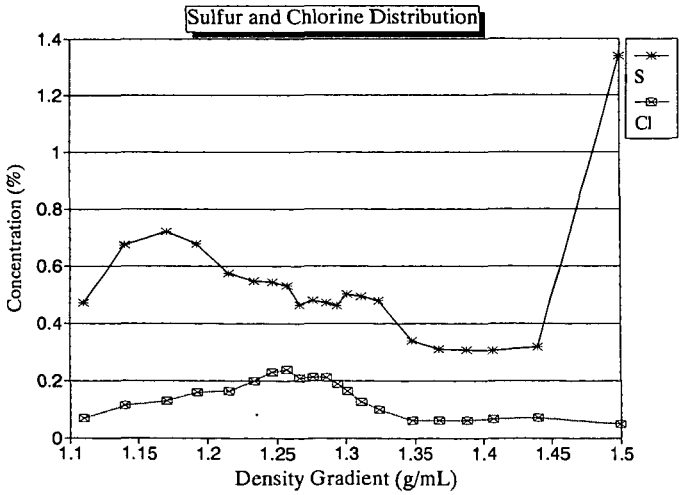

THE DISTRIBUTION OF TEN TRACE ELEMENTS AND MINERALS IN THREE LIGNITE SEAMS FROM THE MAE MOH MINE, THAILAND

Hart, Brian, Powell M.P., Fyfe, W.S. Department of Earth Sciences University of Western Ontario, London, Canada; Ratanasthien, B. Department of Geology, University of Chiang Mai, Chiang Mai, Thailand.

Keywords: Lignite, mineralogy, trace elements.

Introduction

Understanding the association of major, minor and trace elements in lignites and their accompanying strata is important from a number of perspectives (1) which include: potential health problems from environmental pollutants, rehabilitation after mining, combustion for power etc. The material which follows represents some preliminary observations on the mineralogy and distribution of 10 trace elements in lignites and accompanying sediments from the Mae Moh mine, Thailand.

Samples collected from freshly exposed mine faces were air dried and analyzed for moisture and ash. Trace element concentrations were determined on "whole" coals and sediments by NAA and XRF. All chemical analyses are expressed as a fraction of the total dry sediment. Mineralogy of both LTA and sediments was determined by XRD. The chemistry and morphology of individual particles were examined by the Electron microprobe. The analyses are used to make some conclusions about the spatial occurrence of these elements within the seam and their partitioning between organic and inorganic phases.

Mineralogy: XRD Analysis

In samples with >50% ash the mineralogy was determined on untreated material. In samples with <50% ash the mineralogy was determined on oxygen plasma low temperature ash. The minerals identified by XRD analysis include quartz, kaolinite , pyrite/marcasite, calcite, gypsum, illite, smectite (mixed-layer clay), jarosite, bassanite, spinel, anhydrite and ferrohexahydrite.

Mineralogy Discussion

For the most part, the greater than 50% ash samples represent the mineralogy of the sediments (overburden, underclays and interseam partings) associated with the coals. In both the Q and K seams as well as the lower portion of J seam calcite dominates the mineralogy. In a previous study (2) a similar distribution for calcite was identified where it was suggested that the calcite might be both biogenic and derived from weathered limestone bedrock. Both origins are possible as the underlying Triassic sequence is marine and fresh water gastropods have been identified in many interseam sediments (3). Pyrite was identified in all but 4 sediment samples. While preliminary SEM work has indicated that much of the pyrite within the sediment and coal samples is framboidal, it also occurs as nodules and fracture fillings. The occurrences suggest both a syngenetic and epigenetic formation for the sulphide. Based on SEM analysis the quartz identified in all but 2 samples appears to be mostly detritial. Siliceous zones in which some of the quartz is extremely fine grained, may be due in part to an authigenic or biogenic origin. Preliminary SEM work has shown the clay minerals to be very fine grained. Detailed clay mineralogy on selected samples indicates that the proportion of kaolinite is slightly higher than illite and the occurrence of expandable clays increases down the section. The illite is likely detritial, and the poor crystallinity of the kaolinite suggests a similar origin.

Within samples of LTA calcite, as in the sediments, appears to be more common in the Q and K seams while quartz is identified throughout the section. Pyrite is present, mostly a major constituent, in all but the upper 2 LTA samples from J seam. As in the sediments, the proportion of kaolinite is greater than illite in the LTA samples. Minerals not identified in the sediments; bassanite (except in 2 samples), anhydrite and ferrohexahydrite, are artifacts created during the ashing procedure. Anhydrite and bassanite are both dehydration products from gypsum. Bassanite can also form by the combination of organically associated Ca and sulphur released during the ashing procedure. Ferrohexahydrite forms from similar mobile components in the coal as they are released during the ashing (4).

Vertical element variations

The NAA and XRF analysis for 10 elements in samples collected from the three seams is given in table 1.

J seam. For the elements reported, except U, the concentration decreases from the top to the bottom of the seam (Fig 1a;Cr as an example). The consistently high concentration of ash in samples from the upper portion of the seam is coupled with higher concentrations of trace elements. The elements Mo and Sb (Fig 1a;Sb) also showed increased concentrations in samples from the lower portion of the seam, while the concentration of U (Fig 1b;U) is variable.

K seam. The elements As, Co, Cr, Mo and U show higher concentrations in the samples closer to the seam margins (Fig 1b;U). Antimony, and to some degree Pb, are concentrated in the upper portion of the seam only (Fig1b:Pb). The distribution of Se down the seam is variable. The lowest concentration of all elements is found in the mid portion of the seam where the ash content of the samples is also low.

Q seam. Within the Q seam all elements except As and Se show a marked overall concentration increase from top to the bottom of the seam (Fig 1c;Co). Selenium is concentrated in the middle of the seam (Fig 1c;Se) while As is enriched in the upper 2 samples as well as the lower portion of the seam (Fig 1c;As).

Interpretation of element distribution

The relationship between ash content and element concentration in a coal can be used as a guide to determine whether an element is preferentially associated with the organic or inorganic fraction of the coal (5). Pearson correlation coefficients were calculated for 10 elements versus ash in each of the 3 seams. Based on these correlations only 2 types of element associations were recognized; those elements which are inorganically associated and those elements which show a mixed inorganic-organic association.

Correlation coefficients in the J seam reveal that only Pb and Th are inorganically associated. The remainder of the elements had correlation coefficients indicative of mixed organic-inorganic associations. In a more restricted group of samples, representing only mine designated lignite seams, an inorganic affinity was indicated for all elements except Mo, Sb and U. Correlation coefficients for the latter 3 elements indicates a mixed organic-inorganic association. Correlation coefficients for elements in K seam indicate that Mo, Ni, Pb, Sb, and U are most likely to be inorganically associated, whereas As, Co, Cr, Se, and Th show a mixed organic-inorganic

association. In the Q seam Cr, Mo, Pb, Th and U show a strong inorganic affinity while a mixed association is indicated for As, Co, Ni, Sb and Se.

Except for those elements which are consistently inorganically associated, for example Pb, there appears to be no reasonable agreement between correlation coefficients of elements with ash and their vertical distribution. The concentration for most elements in this study group, expressed as a fraction of the total dry sediment , appears to be linked to the inorganic content of the lignite seam. For example the upper samples in J seam are both high in ash and high in trace elements. Furthermore the samples from K seam which are low in ash are consistently low in trace elements. These observations are not necessarily indicated by the correlation coefficients.

Inconsistencies in correlation coefficients exhibited by many of the trace elements can be related to their wide range in concentration. A single sample can easily skew the distribution thereby changing the elements apparent association from one group to another. A good example of this is Co in Q seam where, apart from one, sample Q4A (Fig1c), the concentration clearly parallels the ash content.

The interpretation therefore is that most of the elements are associated with inorganic grains and occur either bound within minerals, as oxide films surrounding mineral particles or as ions adsorbed onto the surface of a mineral such as kaolinite. This interpretation works well for those elements which show distinct enrichment in sediment samples; for example, Q seam where Cr and Th are concentrated in both the mid-seam parting and the underclay.

Since the ash content of lignites reflects both the actual mineral particles and exchangeable ions held in the organic material, the possibility exists that a number of trace elements could held in organic combination. Fractionation experiments (6) have shown that Cr, V and Ni were at least partially, or in the case of Cu and Zn wholly, complexed with the organic matter. Although no fractionation studies were performed on these coals an organic association is indicated for at least some of the Se, particularly in samples where high concentrations are not coupled with high ash content. The element As shows a similar relationship to ash in some samples and may also be partially organically complexed. However isomorphic substitution of As for Fe in pyrite may give rise to high As concentrations even in those low ash lignite samples which contain pyrite.

References

1. Swaine, D.J. "Trace Elements in Coal"; Butterworths and Co.: London, 1990; p.278
2. Ward, C.R., International Journal of Coal Geology, 1991, 17, 96-93.
3. Watanasak, M. "Proc. Int. Symp. on Intermontane Basins: Geology and Resources" T.Thanasuthipitak and P. Ounchanum, Eds. ; Chaing Mai University 1989, 327-335.
4. Morgan, M., E.; Jenkins, R.G.; Walker, P. L. Fuel 1981, 60, 189-193.
5. Karner, F.R.; Benson, S.A.; Schobert, H.H.; Roaldson, R.G. "The Chemistry of Low Rank Coals" ,H.H. Schobert Eds.; Amer. Chem. Symp. Series 264; Amer. Chem. Soc. Washington, DC, 1984, 175-193.
6. Miller, R.N.; Given, P. H. Geochem. Cosmochem. Acta. , 51, 1311-1322.

TABLE 1 TRACE ELEMENT CONCENTRATION FOR 10 ELEMENTS IN 3 SEAMS FROM THE MAE MOH MINE

SAMPLE #	% Ash	As	Co	Cr	Mo	Ni	Pb	Sb	Se	Th	U
J1-1,2	91.62	28.80	6.95	122.95	6.63	57.97	30.67	3.28	0.88	25.12	2.31
J1-3	76.07	71.11	13.19	127.68	5.35	60.19	21.35	2.09	2.07	17.03	1.83
J1-4	85.65	269.43	37.38	114.91	28.60	249.86	18.84	9.58	1.18	18.33	4.74
J1-5	48.31	160.29	16.23	60.52	16.30	32.53	10.56	11.22	1.46	6.62	4.45
J2	54.40	65.94	10.33	56.94	6.86	30.56	14.35	5.90	1.60	9.18	2.86
J3A/J2	93.27	350.74	11.18	97.11	4.80	46.17	17.07	4.05	1.09	21.82	1.98
J3A	71.00	93.91	21.61	85.75	9.74	57.31	9.57	6.60	1.12	12.94	4.80
J3A/J3B1	92.75	15.92	11.20	98.70	1.94	39.51	23.68	0.78		19.03	0.22
J3B1	28.78	28.86	6.18	14.27	5.62		5.7	1.49	0.36	1.87	
J3/J4	90.59	71.32	7.04	32.54	8.74		7.07	3.01		5.58	2.01
J4U	31.48	117.35	16.98	28.88	12.02	44.42	4.62	8.21	1.19	2.54	3.26
J4U/J4L	82.41	68.58	9.46	68.86	2.82	21.91	15.65	2.69		14.98	1.48
J4L	32.42	79.18	14.47	14.62	4.01	22.52	4.72	1.92	1.26	2.16	0.44
J4/J5	98.07	41.52	6.76	25.39	8.07	18.62	7.13	3.60		4.98	4.01
J5A	22.93	95.11	3.98	29.31	5.14	22.09	4.81	2.28	0.79	0.85	2.10
J5A/J5B	85.68	68.14	7.90	28.73	2.82		10.05	2.63		4.95	1.70
J5BU	28.36	37.85	7.86	15.78	3.34	23.72	4.04	0.59	0.84	1.71	0.37
J5BU/J5BL	89.48	23.69	3.08	8.64		8.39		0.83	0.42	2.01	0.45
J5BL	24.21	54.62	5.78	7.38	2.40	7.82	3.8	1.23	0.49	0.92	0.55
J5B/J5C	87.00	109.47	8.40	29.17	8.50		9.8	3.43	0.89	8.69	1.80
J5C	34.07	105.04	7.57	12.78	24.38	13.89	8.83	8.54		9.78	5.83
J5/J6	94.41	3.07	8.23	32.30	3.89	22.84	8.93	0.48	0.82	7.22	2.33
J6A	13.40	61.41	1.95	7.15	4.55	0.00	4.73	1.56	0.48	0.15	0.31
J6A/J6B	85.20	8.49	5.73	19.13	1.78	12.61	7.38	0.98	0.82	4.81	0.58
J6B	7.07	35.10	2.03	3.80	13.08		3.49	11.08	0.39	0.71	7.70
J6B-1	86.74	85.30	2.93	5.47	4.15	10.09		2.47	0.50	1.08	0.60

Sample #	% Ash	As	Co	Cr	Mo	Ni	Pb	Sb	Se	Th	U
K1-1	88.32	31.57	8.59	25.46	8.17		12.43	8.38	0.42	4.96	3.18
K1-2	24.34	40.95	3.38	14.58	3.31		7.34	1.15	0.38	3.07	1.00
K1-3	64.35	ND	8.96	32.44	ND	27.87	13.85	ND	0.90	8.85	ND
K1/K2	91.08	38.94	0.39	4.18	3.71			2.12		0.15	1.33
K2-1	41.98	21.79	8.76	29.11	5.31	14.67	12.26	2.90	0.82	8.26	2.02
K2-2	35.61	11.68	3.46	11.48			8.32	1.65		2.80	0.98
K2-3	15.42	13.08	2.05	7.58	1.77	13.35	8.48	1.28	0.69	2.00	0.64
K3-1	9.13	9.41	1.83	3.78	1.68	10.95	5.27	1.05	0.23	0.59	0.34
K3-2	38.78	58.28	9.86	18.32	3.55	19.17	9.69	2.00	1.08	3.11	0.73
K3/K4	88.70	28.02	7.88	15.04	8.83		8.68	2.50	0.38	2.68	2.50
K4	47.45	75.02	14.58	26.64	4.98	19.75	7.55	1.98	1.43	4.60	1.48

Sample #	% Ash	As	Co	Cr	Mo	Ni	Pb	Sb	Se	Th	U
Q1-1	15.38	40.17	1.76	2.66			4.32	0.21	0.34	0.21	
Q1-2	22.50	32.16	3.57	2.21	1.48	10.61	3.12	0.38	0.57	0.23	0.22
Q1-3	38.30	8.72	2.00	2.50			4.7	0.48	0.18	0.27	
Q1-4	11.33	6.84	1.39	2.98		5.44	4.22	0.33	0.22	0.28	
Q1/Q2	27.90	10.39	1.50	1.77			5.97	0.38	0.39	0.23	
Q2-1	18.55	31.42	3.08	9.56	2.97			0.95	1.20	2.08	0.58
Q2-2	87.68	4.58	10.82	35.31		28.78	11.88	0.40	1.35	8.70	
Q2-3	17.62	18.61	3.55	12.50	3.46	15.97	4.4	1.08	0.77	2.60	0.56
Q2/Q3	27.50	21.24	3.98	8.22	3.00	11.94	4	0.74	0.21	1.02	
Q3-1	17.44	27.05	8.73	17.75	6.60	24.07	9.13	1.64		4.33	1.85
Q3-2	32.87	21.24	8.73	23.88	3.46	22.95	11.17	0.72	0.63	5.98	0.49
Q4A	27.89	52.44	18.78	24.31	7.92	45.73	11.25	2.74	0.50	5.11	2.37
Q4B	18.30	19.65	3.22	9.18	2.70	14.90	4.87	1.01	0.27	0.46	
Q4	98.64	14.80	11.71	38.82	8.68	30.34	11.03	2.08		9.55	4.49

All trace element data reported as ppm.

Blank spaces in the table indicate the concentration was below detection limits

ND = no data

FIGURE 1. VERTICAL DISTRIBUTION OF10 ELEMENTS IN THE 3 LIGNITE SEAMS FROM MAE MOH, THAILAND FOR J SEAM, ONLY THOSE SEAMS DESIGNATED AS LIGNITE ARE INCLUDED

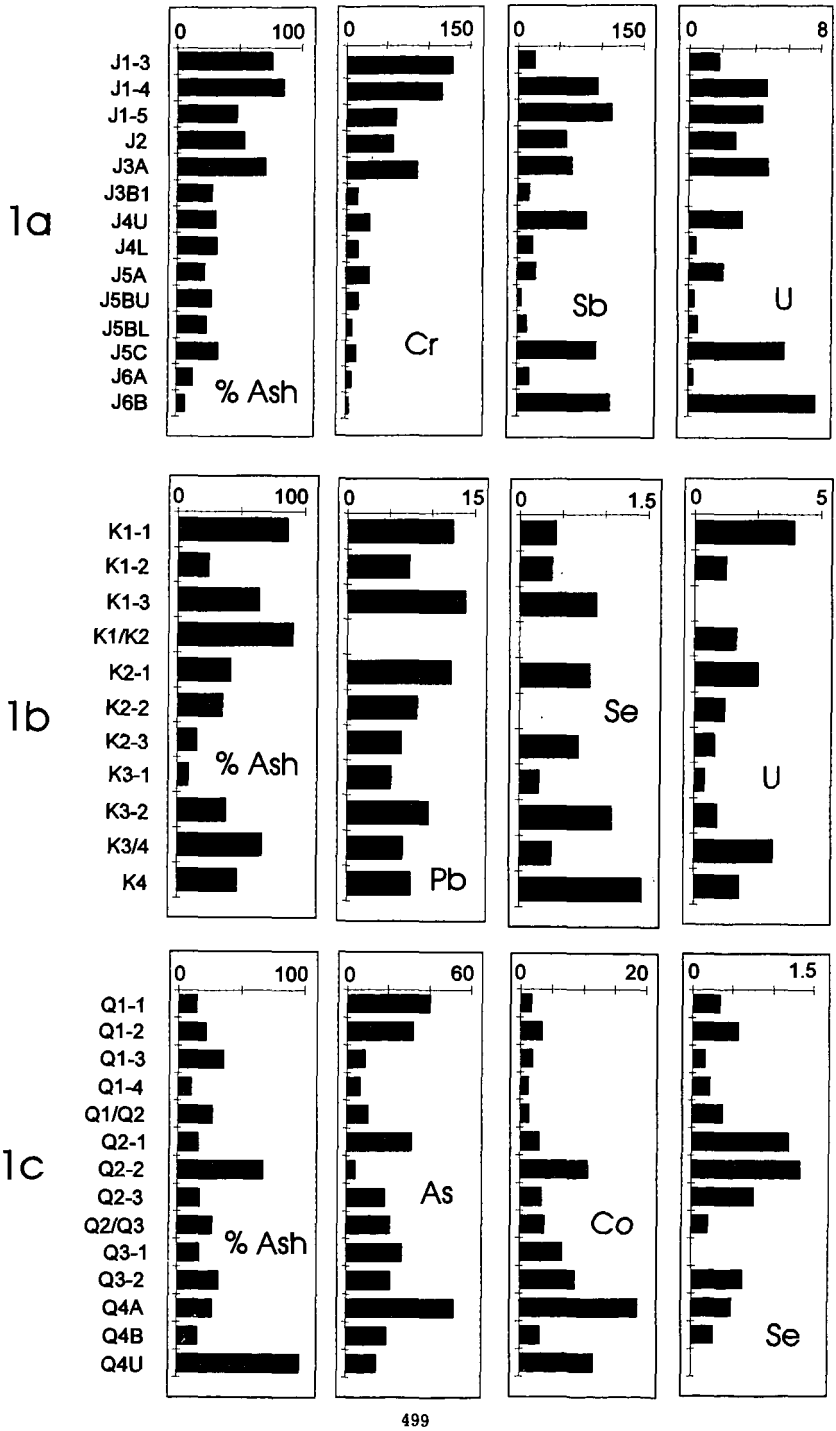

FLUORINE IN COAL AND COAL BY-PRODUCTS

J.D. Robertson,[1,2] A.S. Wong[1,2] and J.C. Hower[2]
Department of Chemistry[1] and Center for Applied Energy Research[2]
University of Kentucky
Lexington, KY 40506-0055

Keywords: Fluorine, PIGE, Coal

INTRODUCTION

Fluorine occurs in trace amounts in most coals. It is typically associated with minerals of the apatite group, principally fluorapatite and clays, and with fluorite, tourmaline, topaz, amphiboles and micas[1] The average fluorine content of US coal is, according to the tabulation of Swanson *et al.*[2], 74 μg/g. In the United States, the lowest average fluorine concentration of 30 μg/g is found in coals from Eastern Kentucky and the highest average value of 160 μg/g is found in coals from Wyoming and New Mexico.[3] The concentration range of fluorine in European coals is similar to that found in the US while the average fluorine content of Australian coals ranges from 15 to 500 μg/g.[4]

Fluorine is released into the atmosphere during the combustion of coal. According to a National Academy of Sciences report, coal combustion accounts for a significant fraction (10%) of the total atmospheric emissions of fluorine in the United States.[5] Because of its effect upon environmental quality and health, fluorine has been classified as an element of moderate concern in the development of the coal resource.[6] With the increased utilization of this energy resource, it is important to be able to reliably determine the fluorine content of coals and coal by-products.

The amount of fluorine in coals and geological materials is generally determined using an ion selective electrode or, more recently, ion chromatography to measure the concentration of fluoride ions in a solution prepared from the sample. The most common chemical pretreatment techniques include alkali fusion,[7,8] oxygen bomb digestion,[1,7] and pyrohydrolysis.[1,7,9,10,11] The ASTM standard method (D3761-79) is based on the oxygen bomb procedure; a simple and convenient sample preparation technique. The validity of the oxygen bomb and alkali fusion methods has, however, been called into question as these two procedures consistently yield lower results than those obtained by pyrohydrolysis.[7,9,12] This is most likely due to the incomplete dissolution of fluorine from the sample by these two procedures. The end result of this discrepancy is a wide range of fluorine values in the literature and the lack of certified fluorine values for coal and fly ash standards.

In order to aid the certification process, we have determined the fluorine content of several coal and fly ash standards by an alternate method; proton-induced gamma-ray emission (PIGE) analysis. PIGE is a rapid, non-destructive analysis technique that is based upon the detection of the prompt gamma rays that are emitted following a charged-particle-induced nuclear reaction. The energy of the gamma ray is indicative of the isotope present, and the intensity of the gamma ray is a measure of the concentration of the isotope. This ion beam technique is mainly used in the analysis of light elements. It has been used to determine the fluorine content of various geological materials[13,14] and of the NIST 1632a and 1633a coal and fly ash standards.[10,15] We have, using the method of standard additions, determined the fluorine content in NIST bituminous coal SRM 1632b, subbituminous coal SRM 1635, coal fly ash SRM 1633a, USGS Lower Bakerstown coal CLB-1, CANMET BCR 40 and SARM 20.

EXPERIMENTAL PROCEDURE

The PIGE measurements were performed at the University of Kentucky 7.5 MV Van de Graaff accelerator.[16] The nuclear reactions utilized in these PIGE measurements are $^{19}F(p,p_1)^{19}F$, $E\gamma$ = 110 keV and $^{19}F(p,p_2)^{19}F$, $E\gamma$ = 197 keV. The samples were irradiated with an external 2.5 MeV proton beam in 1 atm. of He. The γ rays were detected with an ORTEC HPGe detector, 20% relative efficiency, with a FWHM resolution of 2.40 keV at 1274 keV. The beam, normal to the target surface, was rastered over the sample at 1 Hz irradiating a spot of 5 mm by 7 mm. The proton beam current, on the extraction foil, ranged from 100 to 150 nA, and the collected charge ranged from 90 to 140 μC. The irradiation times were adjusted to obtain an uncertainty in the counting statistics of less than 5% (except for SRM 1635, where the uncertainty was less than 10% after 20 minutes of counting time) in the areas of the 110- and 197-kev γ-ray peaks. The irradiation time per sample ranged from 15 to 20 minutes. Rather than adjust the beam current to maintain a constant count rate, a pulser was used to correct for the dead time in the γ-ray spectra. Typically, the dead time in the measurements was less than 3%.

For the standard addition measurements, one blank and four spiked samples were prepared for each coal standard. The spiked samples were prepared by adding appropriate amounts (from 5 to 25 μL) of the NIST SRM 3183 fluoride ion chromatographic solution ([F^-] = 1000 μg/g) to

approximately 250 mg of coal. The concentration of fluorine spikes ranged from 25 to 90 μg/g. After addition of the fluorine solution, the spiked samples were oven dried for 24 hours at 50°C. The dried samples were then mixed in a polystyrene vial with a methacrylate ball for 30 minutes. The blank and spiked samples were then pelletized in a 13-mm stainless steel die at 90 Mpa. High purity graphite powder (Johnson Mathey, Ultra 'F' spectroscopic grade) was mixed with the NIST 1633a fly ash SRM in order to obtain a stable pellet. The blank and spiked samples of NIST 1633a were prepared from this mixture. Two sets of standard addition samples were prepared and analyzed for each standard. Figures I and II show the typical fluorine standard addition curves obtained.

RESULTS AND DISCUSSION:

The results obtained from the standard addition method for each standard are listed in Table I. The fluorine values, which are reported on a dry weight basis, are the weighted average of the concentratin values obtained from the 110- and 197-keV standard addition curves on two series of standard addition samples. The limits of detection (LOD) for the measurements (Table I) are based on a minimum observable peak area of $3\sqrt{bkg}$ where bkg is the background over 1 FWHM about the gamma-ray (197 keV) peak's centroid. The LOD for fluorine in coal ranged from 2 to 8 μg/g, depending upon the ash content in the coal. The relative standard deviation for a single measurement, based upon counting statistics, ranged from 0.9 % to 10 %.

In order to determine if the concentration of the fluorine changed during the proton irradiation, a single pellet of NIST SRM 1632a sample was subjected to four consecutive 15-minute irradiations at 150 nA. No significant variations were observed in the normalized 110- and 197-keV gamma-ray yields in the multiple bombardments. The average normalized yield was 133 ± 2 γ's/μC for the 110-keV gamma-ray peak, and 145 ± 1 γ's/μC for the 197-keV gamma-ray peak. The overall average of the normalized yield for SRM 1632a during four days of consecutive measurements (10 irradiations) was 126 ± 6 γ's/μC for the 110-keV gamma-ray peak, and 141 ± 6 γ's/μC for the 197-keV gamma-ray peak.

As can be seen from the comparison presented in Table II, the fluorine concentration values obtained in this work for the NIST, SARM and BCR standards agree well with the values obtained by pyrohydrolysis. The fluorine values obtained by oxygen bomb digestion are, on the other hand, consistently lower than the PIGE and pyrohydrolysis values. As noted above, this is most likely due to the incomplete dissolution of fluorine from the sample by this sample preparation procedure.

We are currently using PIGE as a rapid, instrumental technique to investigate how fluorine partitions in wet and dry FGD equipped coal combustion systems. Results from this study will be presented.

ACKNOWLEDGEMENTS

This work was supported in part by the Department of Energy and the Kentucky EPSCoR program. We are indebted to Ms. Jean Kane and Mr. Robert Dureau for the standards used in this work.

REFERENCES

1. W.G. Godbeer and D.J. Swaine, *Fuel 66*, 794 (1987).
2. V.E. Swanson, J.H. Medlin, J.R. Hatch, S.L. Colemen, G.H. Wood, S.D. Woodruff and R.T. Hilderbrand, *Collection, chemical analysis and evaluation of coal samples in 1975*, US Dept. of Interior, Geological Survey, Report No. 76-468, 1976.
3. A.J. Dvorak, US Nuclear Regulatory Commission Report No. NUREG-0252, 1977.
4. D.J. Swaine in *Combustion of Pulverized Coal-The Effect of Mineral Matter*, I.M. Stewart and T.F. Wall, Eds., University of Newcastle, NSW, 1979, pp 14-18.
5. M. Fleischer, R.M. Forbes, R.C. Harriss, L. Krook and J. Kubota in *Geochemistry and the Environment Vol. 1*, Nat. Acad. Sci., 1974.
6. U.S. National Research Council, *Trace Element Geochemistry of Coal Resource Development Related to Environmental Quality and Health*, National Academy Press, Washington, D.C., 1980.
7. K.J. Doolan, *Anal. Chim. Acta 202*, 61 (1987).
8. M.W. Doughten and J.R. Gillison, *Energy and Fuels 4*, 426 (1990).
9. T.D. Rice, *Talanta 35(3)*, 173 (1988).
10. V.B. Conrad and W.D. Brownlee, *Anal. Chem. 60*, 365 (1988).

11. E.L. Obermiller, Consolidation Coal Co., Library, PA, Personal Communication (1991).

12. A. Savidou and T. Paradellis, *J. of Coal Quality* 9 (2), 44 (1990).

13. I. Roelandts, G. Robaye, G. Weber and J.M. Delbrouck-Habaru, *Chem. Geol. 54*, 35 (1986).

14. J.R. Bird and E. Clayton, *Nucl. Instr. Meth. 218*, 525 (1983).

15. E. Clayton and L.S. Dale, *Anal. Lett. 18(A12)*, 1533 (1985).

16. J. M. Savage, A. S. Wong, and J. D. Robertson, Thick-Target PIXE/PIGE Analysis of Complex Matrices, J. of Trace and Microprobe Tech., 10 (2-3) (1992) 151-168.

TABLE I

Fluorine Concentrations* (μg/g) of NIST, SARM, CLB and BCR Coal and Fly Ash Standards Determined by Standard Addition PIGE Measurements.

Sample ID	Fluorine (μg/g)	Ash (wt%)	LOD (μg/g)
NIST 1635	28 ± 1	4.7	6.2
NIST 1632b	48 ± 2	6.8	3.9
SRM 1633a	93 ± 10	100	15
CLB-1	68 ± 7	-	2.0
BCR 40	114 ± 6	-	5.9
SARM 20	148 ± 13	35.3	4.6

* Dry weight.

TABLE II

Fluorine Concentrations for NIST, SARM and BCR Standards Obtained by PIGE, Pyrohydrolysis, and Oxygen Bomb Digestion.

Sample ID	PIGE	Pyrohydrolysis	Oxygen Bomb
NIST 1635	28 ± 1	39[7], 42[10], 34, 35[11]	18, 12[11]
NIST 1632b	48 ± 2	46[7], 58[10]	
NIST 1633a	93 ± 10	82[7], 73[9], 81[10], 89[11]	25, 22[11]
BCR 40	114 ± 6	128[10],122,119[11]	107[11]
SARM 20	148 ± 13	148[1], 152[7], 141[10], 130[11]	86[1], 107, 110[11]

FIGURE I

Fluorine Standard Addition Curve of NIST 1635 Coal Standard

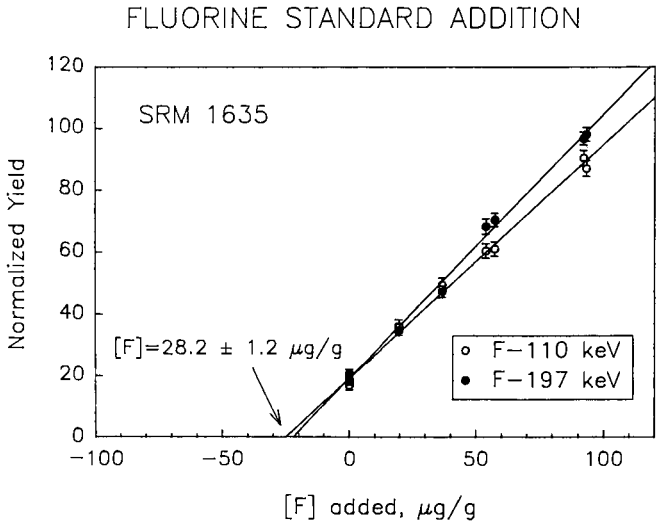

FIGURE II

Fluorine Standard Addition Curve of NIST 1632b Coal Standard

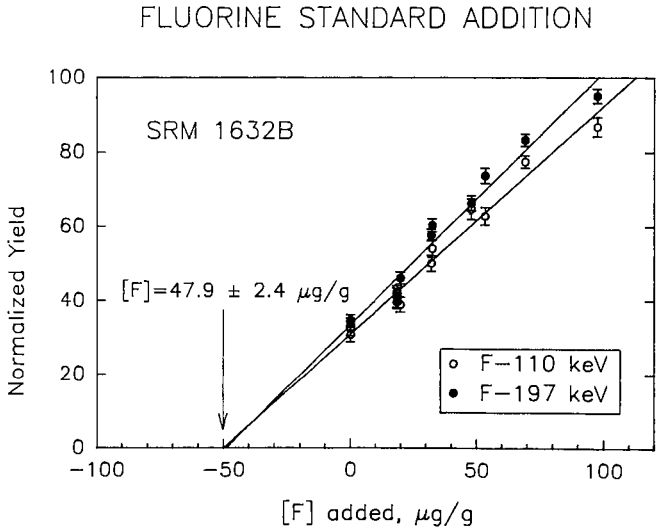

MODES OF OCCURRENCE OF TRACE ELEMENTS IN COAL FROM XAFS SPECTROSCOPY

Frank E. Huggins, J. Zhao, N. Shah, G.P. Huffman
233 Mining and Mineral Resources Building
University of Kentucky
Lexington, KY 40506

Keywords: XAFS spectroscopy, mode of occurrence, trace elements.

INTRODUCTION

It is well known that elements exist in coal in a variety of different modes of occurrence [1,2]. Such modes can vary from the element being totally dispersed in the macerals (e.g. organic sulfur, carboxyl-bound Ca in lignite) to discrete mineral occurrences (e.g. pyrite, FeS_2, quartz, SiO_2, etc.). Recently, we showed that X-ray absorption fine structure (XAFS) spectroscopy is capable of recording spectra from elements present in coal at concentration levels as low as 5 ppm [3]. Such information, obtained directly with a minimum of sample preparation, is proving to be invaluable for the elucidation of a trace element's mode of occurrence. In the previous work, we used XAFS spectroscopy to identify the principal modes of occurrence of arsenic and chromium in various coals. Here, we present more recent XAFS spectroscopic observations on these and other trace elements in coal and take the opportunity to discuss the ramifications of such XAFS studies for geochemical investigation of trace elements in coal.

EXPERIMENTAL

XAFS spectra of trace elements in coal were obtained at one or other of the two major U.S. synchrotron sources: the Stanford Synchrotron Research Laboratory (SSRL), at Stanford University, CA, and the National Synchrotron Light Source (NSLS), at Brookhaven National Laboratory, NY. Procedures for obtaining XAFS spectra of trace elements are described in detail elsewhere [3]. Spectra were recorded, usually in multiple scans, by means of a 13-element germanium detector specifically designed for trace element studies [4]. Coal samples were suspended in the X-ray beam in thin (6 μm) polypropylene bags. Analysis of the XAFS spectra was performed at the University of Kentucky on a MicroVAX II computer. As is usually done, the XAFS spectrum was subdivided into the X-ray absorption near-edge structure (XANES) and the extended X-ray absorption fine structure (EXAFS) regions. All XANES spectra shown here are calibrated with respect to a reference material containing the element of interest. The zero energy points in the Cr, Mn, As, and Br XANES spectra are defined as the first maximum in the derivative of the spectrum of Cr in stainless steel (5.989 keV), the spectrum of metallic Mn (6.539 keV), the spectrum of As_2O_3 (11.867 keV), and the spectrum of KBr (13.474 keV), respectively.

XAFS RESULTS

(a) Chromium:

The XANES spectra of chromium in most U.S. bituminous coals vary little from coal to coal, indicating that there is probably just one major chromium mode of occurrence [3]. Furthermore, the XANES spectra clearly demonstrate that chromium is present in coal exclusively in the trivalent state, Cr^{3+}. Previously, chromium has been postulated to occur in coals in association with clay minerals, or as chromite ($FeCr_2O_4$) [1,2], and possibly as an organic complex in low-rank coals [5,6]. However, comparison of the XANES spectra of a wide variety of Cr^{3+} compounds and minerals with the common XANES spectrum of Cr in coal eliminated all of the previously postulated chromium-bearing mineral forms as the Cr XANES spectra of coals showed little resemblance to either Cr^{3+}-bearing silicates or to chromium oxide minerals, including chromite. Finally, based on some published spectra of other Cr^{3+} phases [7], it was decided to investigate the chromium hydroxides and oxyhydroxides, although based on the rarity of such phases in nature [8,9], it appeared to be unlikely. $Cr(OH)_3$ was prepared by precipitation from a solution of chromium nitrate at 25°C using ammonium hydroxide. The blue-green precipitate was filtered, washed, and then dried in air. The XANES spectrum of Cr hydroxide closely resembled that published elsewhere [7], but, although there were superficial similarities to the Cr XANES of coal, it was not a compelling match. The chromium hydroxide was then heated overnight (18 hours) at 140°C. A weight loss of about 19% was recorded that corresponded well to the elimination of one water molecule from the unit formula of chromium hydroxide and the formation of CrOOH:

$$Cr(OH)_3 \quad \text{--->} \quad CrOOH + H_2O$$

X-ray diffraction of the CrOOH phase formed this way showed that it was an amorphous phase, closely related to ferrihydrite [10], rather than one of the very rare crystalline chromium oxyhydroxide minerals that have been found only in unique localities in Guyana and Finland [8]. More importantly, the Cr XANES of this material did closely resemble (Figure 1) the Cr XANES of coal and it now appears that the Cr XANES of coal arises from Cr in an oxyhydroxide form. However, it still remains to be demonstrated whether Cr exists as CrOOH in one of its own mineral forms, or whether it is in a complex oxyhydroxide solid solution with other trivalent ions. As has been demonstrated synthetically [10], substitution of Cr in goethite, FeOOH, can occur up to at least 10% of the Fe, and hence, Cr-substituted goethite might be considered a possible mode of occurrence for Cr. However, such an occurrence would only be possible if goethite were a primary occurrence of iron in coal. There is little or no evidence for such a supposition, and much against.

Once the primary occurrence of Cr in coal was established, some Cr XANES spectra that were not fully compatible with just CrOOH as the only Cr-bearing phase were re-examined. To assess the presence of a second Cr phase in addition to CrOOH in these spectra, spectral addition and subtraction procedures were attempted. Figure 2 shows the simulation of the Cr XANES spectrum of a lignite from Indonesia, in which personnel at the U.S. Geological Survey had observed chromite microscopically (R. B. Finkelman and L. F. Ruppert, pers. comm. 1992). A reasonably good simulation of this spectrum can be made from the weighted addition of the spectra of CrOOH (60%) and $FeCr_2O_4$ (40%). The sensitivity of this spectral simulation method of XANES analysis is about ±10%.

(b) Arsenic:
As demonstrated elsewhere [3], it is possible to use As XANES spectroscopy to discriminate between arsenical pyrite, in which arsenic substitutes for sulfur in the pyrite structure, and arsenopyrite (FeAsS), in which it is an essential element. Of the coals examined to date, only one, a Pittsburgh seam coal, has been found to contain significant arsenopyrite. More recently, we have examined coals of relatively low As content (<5 ppm) from low-rank coals from western U.S. coal-fields. Despite the poor signal-noise ratio of these spectra (Figure 3), it is possible to conclude that the As XANES spectra of such coals are similar to each other and different from those of the bituminous coals of higher arsenic content (>10 ppm) reported earlier. From the position of the main peak, it would appear that the oxidation state of the arsenic is As^{3+}; however, better quality data are needed to identify whether arsenic is enclosed in a sulfur or oxygen nearest neighbor environment.

(c) Manganese
As reviewed by Swaine [1], manganese has been postulated to occur in a variety of geochemical environments in coal, including carbonates, clays, pyrite, porphyrins, and, in lower-rank coals, in organic association. Owing to a similar ionic size and electronic structure, the geochemistry of Mn^{2+} tends to be similar to that of calcium, except that Mn has much a higher chalocophilic nature and can form sulfide minerals more readily.

Some preliminary XAFS data have been obtained on manganese in U.S. coals. A progression of Mn XANES spectra with rank are shown in Figure 4. The lowest rank coal (Beulah) exhibits a Mn XANES spectrum that is closely similar to that exhibited by calcium in carboxyl form in low-rank coals, whereas the Mn XANES spectrum of the Pocahontas #3 coal of highest rank, exhibits an asymmetric split main peak similar to that found for Mn in carbonates. The intermediate spectra, with the exception of the Wyodak coal, can <u>not</u> be simulated by additions of the two extreme spectra. Hence, there is at least one more Mn form of occurrence that contributes significantly to the Mn XANES spectra of the Pittsburgh and Upper Freeport coals. This form has yet to be identified.

(d) Bromine
XAFS spectroscopy has proven very useful for investigating the mode of occurrence of chlorine in coal [11]. XAFS spectroscopy clearly shows that chlorine is neither present as an organochlorine functionality nor as an inorganic chloride; rather, chlorine exists in coal as chloride anions in the moisture associated with the macerals, most probably held at the maceral surface by ionic attraction to polar organic functional groups. On geochemical grounds, it would be expected that the trace halogens (bromine and iodine) should have a similar mode of occurrence to that of chlorine. Some preliminary XAFS experiments on bromine in coal confirm this expectation. Bromine K-edge XANES spectra of KBr, KBr in aqueous solution, and of two coals are shown in Figure 5. The profiles of all four of these spectra are very

similar to the corresponding chlorine K-edge XANES spectra [11], indicating that the bromine mode of occurrence in coal is similar to that of chlorine.

DISCUSSION:
The unanticipated observation of Cr in oxyhydroxide form in coal by XAFS spectroscopy begs the question of whether other elements might also be present in coal in similar oxyhydroxide form or even hydroxide form. Presumably, such species would have to be sufficiently lithophilic not to react with sulfur, but incompatible with aluminosilicate (clay) structures. A number of elements that are typically trivalent in geochemical behavior would appear to fit such requirements; these include Sc, V, Y, and the rare-earth elements. All of these species have been reported to form an oxyhydroxide or hydroxide phase with stability fields compatible with geological conditions of coal formation [12]. Hence, it is possible, by analogy to chromium, that these elements may be found in coal as oxyhydroxide or hydroxide minerals. However, the larger trivalent cations (Y, REE) are also candidates for reaction with phosphate anions that may also be present during coal formation.

For two of the elements discussed here, arsenic and manganese, the mode of occurrence has been demonstrated to be quite different between low-rank coals (lignites and subbituminous coals) from the western U.S. and higher-rank coals (bituminous) from the eastern U.S. In previous work [13], the occurrence of calcium has also been shown to be distinctly different between such groups of coals. Many more elements are postulated [1,5] to be in organic association in low-rank coals than in higher-rank coals because of carboxyl groups present in the former. Clearly, this "decarboxylation" transition from low-rank coal to high rank coal is a key factor in the mobilization and mineralization of many elements during coalification and needs to be investigated in detail.

The terminology applied to elemental modes of occurrence is currently relatively imprecise because previous methods used to infer such information have not been sufficiently discriminating. For example, float/sink testing can be used to categorize elements by their "organic affinity", but such a concept does not impart any information as to how the element is actually bound to the coal macerals. Similarly, X-ray mapping in the electron microscope or microprobe can demonstrate that certain elements are associated with the organic matter, but do not provide information as to how the element is bound. However, in principle, such information can now be obtained from XAFS spectroscopy and a more expanded classification for elemental forms-of-occurrence is required. Such a proposed classification scheme with precise definitions for modes of occurrence is shown below. This scheme would appear to be sufficient for all the methods, both direct and indirect, that are currently used to infer elemental modes of occurrence in coal.

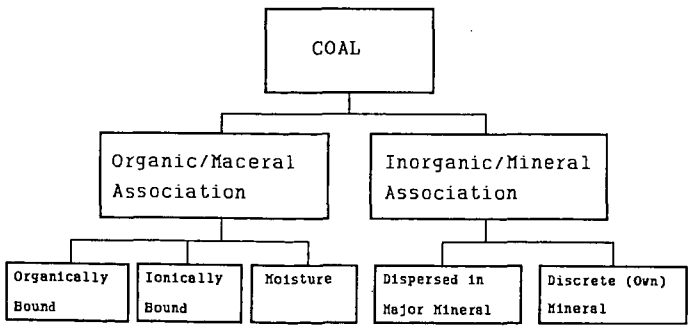

Organic/Maceral Association:
- Organically bound: Involves direct covalent -M-C- or similar bond
- Ionically bound: Involves an ionic bond with polar organic group
- Moisture: Soluble anionic or cationic species in maceral pore moisture

Inorganic/Mineral Association:
- Dispersed mineral: substitution of minor element for major element
- Discrete mineral: element is essential to mineral's existence.

CONCLUSIONS:
The potpourri of data on trace element modes of occurrence in coal presented in this paper demonstrate the value of XAFS spectroscopy in trace element geochemistry. All measurements are made directly on the coal with a minimum of preparation and,

hence, with minimal chance of alteration or contamination of the mode of occurrence. Furthermore, XAFS is equally capable of determining dispersed elements (e.g. carboxyl bound Mn in Beulah lignite; Br in moisture), as well as the discrete mineralogical occurrences (Mn in carbonates, CrOOH, etc.). Such direct measurements afford the opportunity to provide much new information about trace elements in coal and put to rest various misconceptions about trace element occurrences in coal that have accumulated over the years.

ACKNOWLEDGEMENTS
We are grateful to Feng Zhen (University of Kentucky) for assistance with the preparation of $Cr(OH)_3$, and to R. B. Finkelman and L. F. Ruppert (U.S. Geological Survey, Reston, VA) for donation of coal samples for this study. This work was supported by the Office of Exploratory Research, Electric Power Research Institute, Palo Alto, CA, and by the U.S. Department of Energy, Pittsburgh, PA. We also acknowledge the U.S. DOE for its support of the synchrotron facilities in the U.S.

REFERENCES

1. Swaine, D.J., Trace Elements in Coal, Butterworths, London, 1990.
2. Finkelman, R.B., In: Atomic and Nuclear Methods in Fossil Energy Research, (Eds. Filby, R.H., et al.); Plenum Press, New York, 1982, pp. 141-149.
3. Huggins, F.E., Shah, N., Zhao, J., Lu, F., and Huffman, G.P., Energy & Fuels, 7, 482-489, 1993.
4. Cramer, S.P., Tench, O., Yocum, N., and George, G.N., Nucl. Instrum. Meth., A266, 586-591, 1988.
5. Miller, R.N., and Given, P.H., Geochim. Cosmochim. Acta, 50, 2033-2043, 1986.
6. Miller, R.N., and Given, P.H., Geochim. Cosmochim. Acta, 51, 1311-1322, 1987.
7. Manceau, A., Charlet, L., J. Coll. Interf. Sci., 148, 425-435, 1992.
8. Milton, C., et. al., U.S. Geological Survey, Prof. Paper, 887, 1976, 29pp.
9. Burns, V.M., and Burns, R.G., Geochim. Cosmochim. Acta, 39, 903-910, 1975.
10. Schwertmann, U., and Cornell, R.M., Iron Oxides in the Laboratory, VCH, Weinham, 1991.
11. Huggins, F.E., and Huffman, G.P., submitted to Fuel, 1994.
12. Levin, E.M., Robbins, C.R., and McMurdie, H.F., Phase Diagrams for Ceramists, Vol. 1, American Ceramic Society, Columbus, OH, 1964.
13. Huffman, G.P., and Huggins, F.E., In: Chemistry of Low-Rank Coals, (Ed. Schobert, H.H.), ACS Symposium Series, Vol. 264, American Chemical Society, Washington, DC, 1984, pp. 159-174.

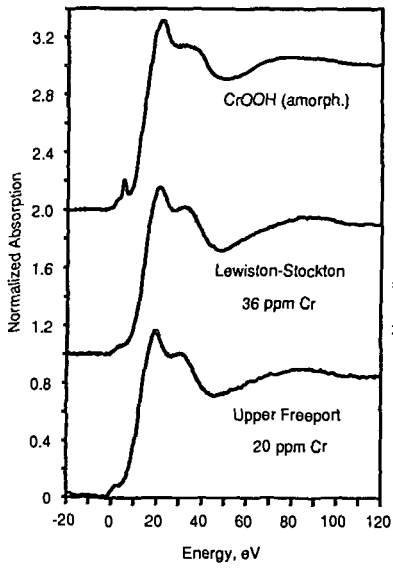

Figure 1: Comparison of Cr XANES spectrum of CrOOH with those for two bituminous coals.

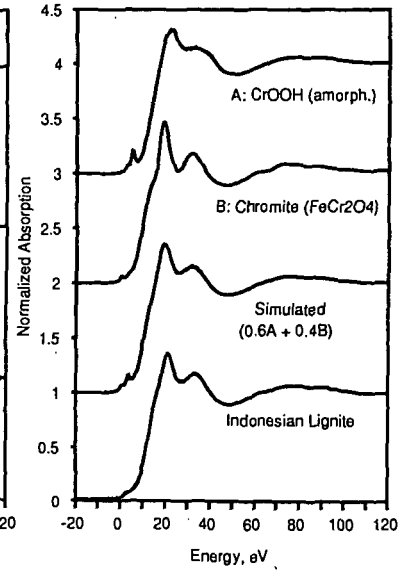

Figure 2: Simulation of Cr XANES for a coal by addition of Cr standard spectra.

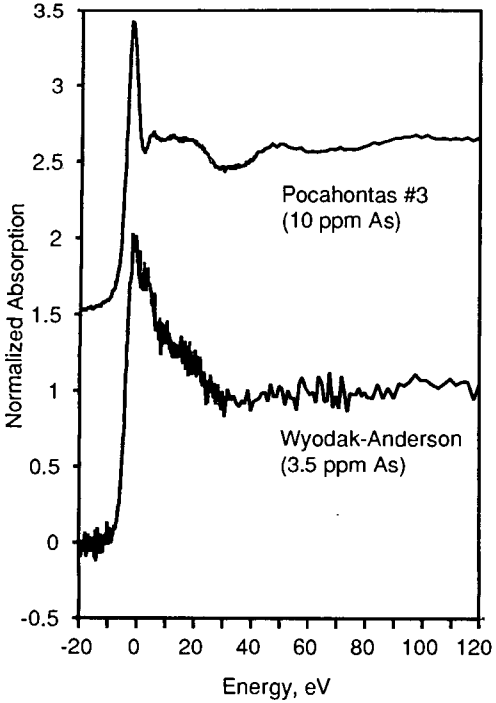

Figure 3: Comparison of As XANES spectra of bituminous and subbituminous coals.

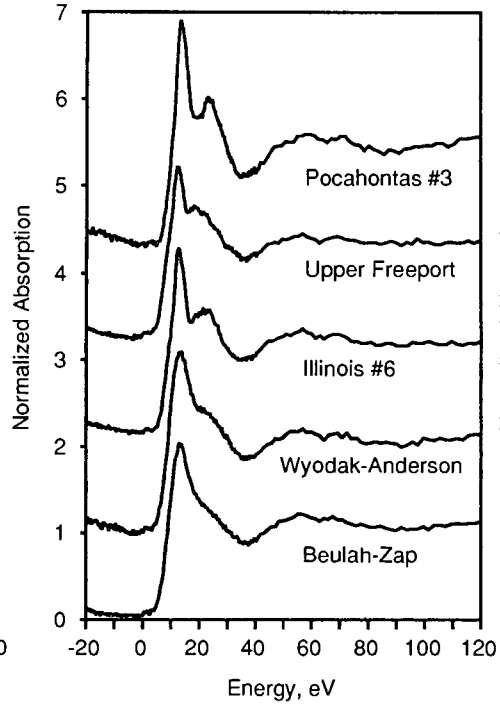

Figure 4: Mn XANES spectra of five Argonne premium sample coals

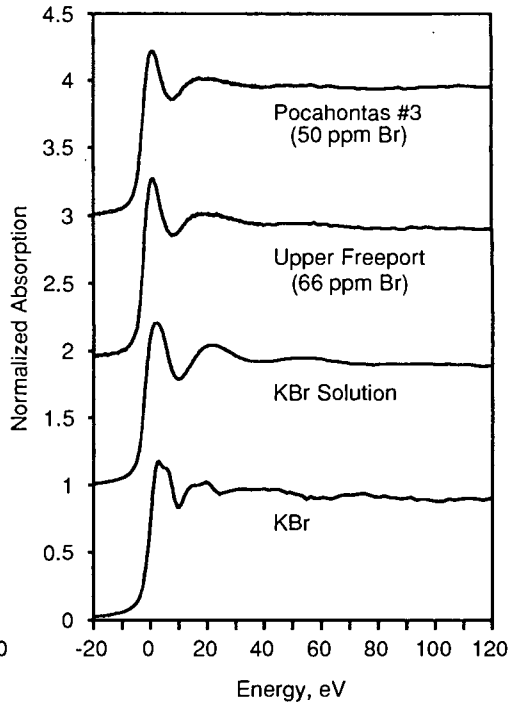

Figure 5: Br XANES spectra of two coals, KBr, and KBr in aqueous solution.

ELEMENTAL CHARACTERIZATION OF COAL ASH LEACHATES

by

John F. Cerbus
Department of Civil Engineering, University of Illinois,
205 North Mathews Ave., 3230 Newmark Laboratory

Sheldon Landsberger
Department of Nuclear Engineering, University of Illinois,
103 South Goodwin Ave., 214 Nuclear Engineering Laboratory

Susan Larson
Department of Civil Engineering, University of Illinois,
205 North Mathews Ave., 3230 Newmark Laboratory

Urbana, Illinois 61801

Keywords: Heavy metals in coal ash leachates, Use of multi-elemental techniques in coal ash analysis.

INTRODUCTION

Over 50 million tons of coal ash are produced annually in North America [Warren and Dudas, 1989] Technological improvements in air pollution control have decreased stack emissions but have also increased contaminant concentrations in the ash of coal-fired boiler applications. The leaching of heavy metals and other elements during regulatory tests may cause coal ash to be classified as hazardous waste, complicating land disposal. The hazardous nature of coal ash remains unclear because current toxicity tests fail to characterize effectively the elemental distribution and chemical solubility of trace metals in the landfill environment. Leaching characteristics of ash samples can be investigated with various laboratory extraction procedures in association with multi-elemental techniques (e.g. Neutron Activation Analysis and Inductively Coupled Plasma Atomic Emission Spectroscopy). Such methods provide a more thorough analysis of coal ash leaching dynamics than the regulatory assessments can demonstrate. Experimental results may assist operators of coal-fired boiler industries in selecting coal types and operating conditions to minimize the leaching of environmentally key elements.

RESEARCH OBJECTIVES

Recent state environmental agency concern about the classification of coal-fired boiler technology wastes may result in substantial cost increases for waste disposal. The objective of this research study is to investigate the hazardous potential of industrial coal-fired boiler technology wastes. A laboratory leaching procedure known as a water-batch extraction was performed on fly ash samples. Additionally, through the use of multi-elemental analytical techniques, the fly ash and corresponding coal samples were characterized. In this way, the elemental leaching dynamics and relationships of elemental levels between coal, ash, and leachates have been examined.

COAL ASH CHARACTERISTICS

Certain physical and chemical properties undoubtedly play key roles in ash-water interactions. Coal fly ash is the partially combusted solid waste particulates of small enough diameter to be entrained in flue gas. One study determined 63% of the examined fly ash particles were in the range of 2-50 μm in diameter [El-Mogazi et al., 1988]. Forms of potentially toxic metals are selectively deposited on the outer surface of coal ash particles [Hopke, 1983]. Such surface components are not bound to the internal silicate matrix and therefore are readily leachable [Hopke, 1983]. Three major matrices compose fly ash, silicate glass, mullite quartz, and magnetic spinel [El-Mogazi et al., 1988] Investigations have found the magnetic matrix to be particularly important in the release of toxic elements [El-Mogazi et al., 1988].

SAMPLE DESCRIPTION

The coal, and fly ash samples for this study were provided by the United States Army Construction Engineering Research Lab (USACERL). The samples originated from Abbott Power Plant (Champaign, Illinois), Chanute Air Force Base (Rantoul, Illinois), and the Rock Island Arsenal (Rock Island, Illinois).

REGULATORY CONSIDERATIONS

The current regulatory benchmark test designed to identify wastes likely to leach hazardous concentrations of toxins is the toxicity characteristic leaching procedure (TCLP). If extract concentrations of certain elements or organic compounds exceed regulatory limits the waste is classified as hazardous. The eight regulated elements are As, Ba, Cd, Cr, Hg, Pb, Se, and Ag. The TCLP replaced the existing extraction-procedure (EP) toxicity test standard in 1990, which was inadequate for organic compounds [Bishop, 1990]. With the implementation of the TCLP, the regulatory focus is now on

environmental impact, behavior, and leachability of contaminants instead of on contaminant levels in waste [Bishop, 1990]. The TCLP uses acetic acid as the extractant and is run for 18 hours in a closed vessel. Acetic acid is a common product of the anaerobic degradation processes found in municipal solid waste landfills. The test, however, fails to effectively characterize the elemental distribution and chemical solubility of coal ash in an ash monofill.

Waste stabilization may be used to reduce leaching in conjunction with land disposal. Such processes attempt to immobilize a waste within an inert matrix. Examples include using Portland Cement, specialized polymers, and plastics as binding agents but such processes are often cost prohibitive [Wentz, 1989]. The TCLP may be implemented following stabilization to gauge the success of the such processes [Biedry, 1990].

LEACHING TECHNIQUES

Previous workers have employed a variety of methods to examine coal ash leaching. Techniques have ranged from laboratory scale extractions to monitoring large outdoor test plots of ash. Some researchers used aggressive, 'worst-case' approaches trying to leach as much from the ash as possible. Such methods most likely involve leaching conditions which would never be encountered naturally.

The preferred strategy is to construct a leaching scheme which accelerates the natural behavior of ash buried in a landfill [Buchholz, 1993]. The EP and TCLP regulatory leaching tests were not specifically designed to measure the behavior and toxicity of coal ash in an ash monofill. The use of acetic acid as an extractant in the above tests may not be representative of the leaching conditions found in an ash monofill.

For this study, the long term washing of coal ash in an ash monofill was simulated in the laboratory using a water (deionized) batch extraction technique. The deionized water used was a simulated acid-rain solution with low levels of nitric and sulfuric acid added. The resulting pH was a mildly aggressive 5.2. The liquid-to-solid (LS) ratios were slowly increased, using short intervals initially to better characterize the first stages. Samples for each LS ratio were prepared over consecutive days with orbital agitation periods of approximately 24 hours in between.

ELEMENTAL ANALYSIS

Thorough analysis of trace elements present in coal, ash and leachate samples usually involves the use of atomic emission spectroscopy. Multi-elemental techniques in which many elements can be analyzed simultaneously are desirable. Elemental concentrations in the coal and ash samples were determined using Neutron Activation Analysis (NAA). Furthermore, the leachates produced by the laboratory extraction methods were characterized with Inductively Coupled Plasma Atomic Emission Spectroscopy (ICP-AES). Quality assurance and quality control were maintained through the use of standard reference materials, procedure blanks and appropriate trace metal laboratory procedures such selecting ultra-pure reagents.

ELEMENTAL COMPOSITION OF COAL AND FLY ASH SAMPLES

Figures 1 and 2 depict the levels of the TCLP elements in the coal and fly ash samples, respectfully. Cadmium and levels were not determined for the coal and ash samples but were examined in the leachate analysis. Levels of Hg and Ag are below detection limits for all three varieties of coal and ash. Ba and Cr are the most dominant TCLP elements in the coal and ash samples. Concentrations are elevated in the fly ash compared to the coal as expected, most likely due to the high surface area to volume ratio differences.

ELEMENTAL COMPOSITION OF LEACHATES

Levels of Ag (MDL = 8 ppb), As (MDL = 280 ppb), Cd (MDL = 24 ppb), Cr (MDL = 18 ppb), Hg (MDL = 40 ppb), Pb (MDL = 51 ppb) and Se (MDL = 490 ppb) were below method detection limits (MDL) for all LS ratios. Be, Cu, Fe, Sb, Sn, Ti, and Tl levels were also below detection limits for all samples. The MDL is defined as the minimum concentration of a substance that can be identified, measured, and reported with a 99% confidence of a greater-than-zero concentration. Therefore, of the TCLP elements, only Ba was found at significant levels. Figure 3 depicts the Barium leaching pattern. The detectable elements with the highest levels in the leachates included, in descending order, S, Ca, Na. K, B, Si, Mg, Al, Sr, Mo, Li, Ba, V, Cr, Zn, Mn, Co, Ni, and P. Figure 4, depicts the leaching pattern for boron which is somewhat common for elements susceptible to quick initial leaching with decreasing levels thereafter. In contrast, the Ba pattern for the Abbott ash (Figure 3) shows increasing levels after reaching an apparent minimum. This may be explained by the outer layers of the ash matrices having been washed off thereby exposing more barium to the leaching solution.

DISCUSSION AND CONCLUSIONS

Bowen (1966) reported average boron levels in soil to be approximately 10 ppm. Elevated levels of boron in leachates may be of environmental interest. El Mogazi et al. (1988) described a coal ash which leached boron levels toxic to plants. It should be stressed that slightly elevated levels of naturally occurring elements may not result in readily apparent effects, but such levels may be toxic to soil microbial communities and surface vegetation.

The coal fly ash varieties examined in this study apparently are not likely to leach high concentrations of TCLP elements when disposed of in an ash monofill. High levels of sulfur would be expected to leach quite readily. Space limitations in this preprint prohibit the discussion of other, possibly environmentally significant leaching patterns of elements such as Al, V, Co and Ni.

CONTINUING RESEARCH AND ACKNOWLEDGMENTS

The research presented above is a small part of a larger project involving 40-element characterizations of three coal varieties, 40-element characterizations of corresponding fly and bottom ash samples, and 32-element characterizations of water batch and selective-reagent sequential extractions of the fly and bottom ash. The sequential technique employed was developed by Tessier et al. (1979). Selective reagents were used to partition trace elements into chemical forms likely to be released under various environmental conditions. A rough idea of the chemical speciation of trace metals can be inferred from the analysis. The chemical partitions are readily exchangeable, bound to carbonates or surface oxides, bound to iron and manganese oxides, and bound to organic matter. [Tessier, et al., 1979]. The use of sequential techniques provides the researcher with a significant improvement in characterization over the regulatory extraction tests.

This work was funded by the United States Army Construction Engineering Research Laboratory (USACERL). The required inductively-coupled plasma analysis was performed at the Illinois State Water Survey located in Champaign, Illinois.

LITERATURE CITED

Biedry, J., Managing Waste to Meet Federal Land Ban Rules, *Pollution Engineering,* October, (1990).

Bishop, J., Range of Options Shrinks for Disposing RCRA Wastes; Enforcement Tightens, *Hazmat World,* November, (1990).

Bowen, H. J. M., *Trace Elements in Biochemistry,* Academic Press, New York, (1966).

Buchholz, Bruce Alan, Elemental Characterization of Municipal Solid Waste Incinerator Ash and its Leachates Using Neutron Activation Analysis and Inductively Coupled Plasma Atomic Emission Spectroscopy, Ph.D. Thesis, University of Illinois at Urbana-Champaign, Department of Nuclear Engineering, (1993).

El-Mogazi, D., D. J. Lisk and L. H. Weinstein, A Review of Physical, Chemical and Biological Properties of Fly Ash and Effects on Agricultural Ecosystems, *Science of the Total Environment,* 74 (1988) 1-37.

Hopke, Phillip K., *Analytical Aspects of Environmental Chemistry,* Chemical Analysis Series, Vol. 64, John Wiley and Sons, New York, (1983).

Tessier, A., P. G. C. Campbell and S. Bisson, Sequential Extraction Procedure for the Speciation of Particulate Trace Metals, *Analytical Chemistry,* 51 (1979) 844-850.

Warren, C. J. and M. J. Dudas, Leachability and Partitioning of Elements in Ferromagnetic Fly Ash Particles, *Science of the Total Environment,* 83 (1989) 99-111.

Wentz, Charles A., *Hazardous waste management,* Chemical Engineering Series, McGraw-Hill, New York, (1989).

Figure 1
TCLP ELEMENTS IN COAL SAMPLES

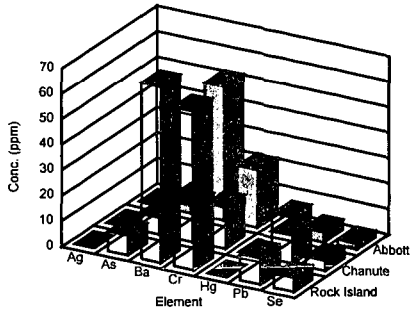

Figure 2
TCLP ELEMENTS IN FLY ASH SAMPLES

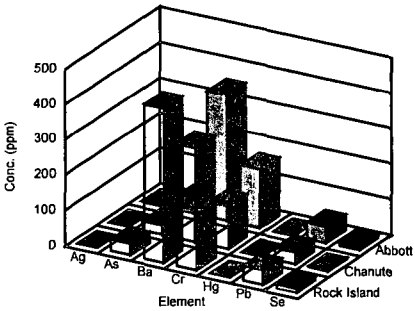

Figure 3 Barium (Ba) MDL = 0.002 ppm
Water Batch Extraction - Fly Ash

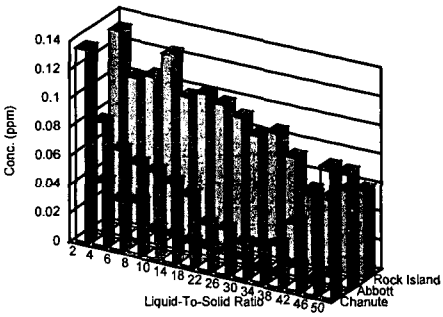

Figure 4 Boron (B) MDL = 0.030 ppm

Water Batch Extraction - Fly Ash

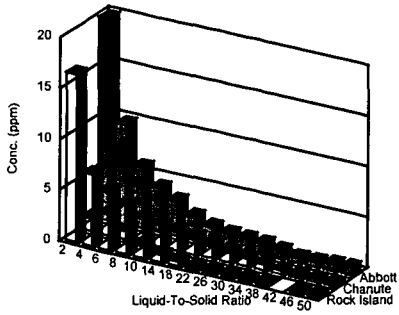

Figure 5 Sulfur (S) MDL = 0.090 ppm

Water Batch Extraction - Fly Ash

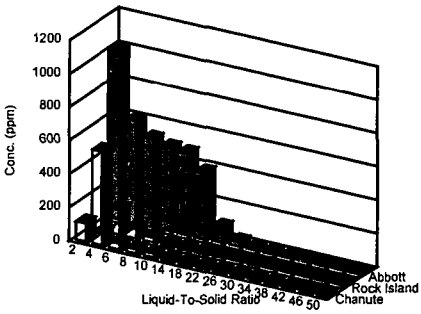

RELIABILITY AND REPRODUCIBILITY OF LEACHING PROCEDURES TO ESTIMATE THE MODES OF OCCURRENCE OF TRACE ELEMENTS IN COAL

Curtis A. Palmer, Marta R. Krasnow, Robert B. Finkelman and William M. d'Angelo;
U.S. Geological Survey, National Center, MS 956, Reston, VA 22092

Key words: Solvent leaching of coal, trace elements, reproducibility and reliability

INTRODUCTION

The 1990 amendments to the Clean Air Act have renewed interest in chemical forms or modes of occurrence of trace elements for potentially toxic trace elements in coal. Selective solvent leaching has been useful in estimating these modes of occurrence [1,2,3,4,5]. This technique is much faster than previous attempts to determine the modes of occurrence of trace elements in coal, such as scanning electron microscopy[6], analysis of density separates of coal[7,8] and low-temperature ash[9]. However, relatively little has been published about the reproducibility and reliability of the solvent leaching procedure. For this paper, three previously analyzed coal samples were leached individually and (or) sequentially with 1*N* CH_3COONH_4, 2*N* HCl, 48% HF, and 2*N* HNO_3 using procedures described previously[4,5]. The concentrations of 45 elements were determined by analyzing the leachate by inductively coupled argon plasma-atomic emission spectroscopy (ICAP-AES) and (or) the residue by instrumental neutron activation analysis (INAA).

RESULTS

The percent determined by both INAA and ICAP-AES of each element sequentially leached by each solvent in the Illinois #6 coal is given in Table 1. The method of determining the percent leached is different for each technique. The percent leached by ICAP-AES is calculated by:

$$(C_S V_S / W_S) / C_{WC} \times 100 \qquad (1)$$

where C_S is the concentration of the element in solution V_S is the volume of the solution, W_S is the weight of the fraction prior to leaching (starting weight) ; and C_{WC} is the concentration of the element in the original whole coal sample given in Table 2. The percent leached in each fraction determined by INAA was calculated by

$$P_L - (C_{WC}W_S - C_F W_F / C_{WC}W_S) \times 100 \qquad (2)$$

where P_L is the total percent leached by all fractions previously leached (P_L is zero for the CH_3COONH_4 fraction); C_F is the concentration of the element in the residue after leaching and W_F is the weight of the fraction after leaching (final weight). The errors calculated are based on counting statistics[10] and are propagated through the calculations for the elements determined by INAA. Although the errors of concentrations determined by INAA are generally relatively low (1-10%), errors in the final calculation are much greater due to the subtractions and division in equation 2. Errors on individual elemental concentretions were not available for ICAP-AES. The data indicates that errors in these concentrations are generally higher than INAA errors, because more elements are near the detection limits of the ICAP-AES technique[11]. Because equation 1 does not have subtraction terms, the overall errors may be comparable. In cases where the error was greater than the percent leached value, this value was converted to an upper limit and denoted by a * in the tables. In a few cases, equation 2 lead to a negative number. If that number was less than the calculated error, then the value was reported as an upper limit with a * as above; but when the value exceeded the error value, no value could be calculated and a ? was reported in a manner similar to Finkelman et al[4] in 1990.

Considering the errors, there is generally good agreement between INAA and ICAP-AES results. The INAA results can also be evaluated against the data reported in the 1990 study included in Table 1. The comparison to previous data is generally good, but there are some exceptions. The 1:7 HNO_3 solution used in this study was more effective than
1:9 HNO_3 . The differences in nitric acid leaching between this study and the 1990 study have been attributed to oxidation of the coal matrix by the stronger solution[5].

Results for the Buelah-Zap lignite sample and the Lower Bakerstown coal sample (Tables 3-6) are similar to the results found for the Illinois #6 coal sample. The leaching study on the Lower Bakerstown coal was done in duplicate to further assist in evaluate reproducibility. Results from individual leaching experiments some in duplicate or triplicate can be found on Table 7. Many of these experiments were done in duplicate or triplicate. Hot (80° C) and room temperature (RT) HCl and HNO_3 acid were used to determine if differences in temperature were important. Generally, differences in temperature were not as significant as were differences in concentration.

(1) Miller, R.N.; Given, P.H., A Geochemical Study of the Inorganic Constituents in Some Low Rank Coals, *DOE*, Final Report FE-2494-TR-1, 1986 314 pages.
(2) Hurley, J.P.; Steadman, E.N.; Kleesattel, D.R. Distribution of Inorganics, *DOE*, Final Report for Period Ending March 31, 1986.1986, 320 pages.
(3) Baxter, L.L.; Hardesty, D.R. Fate of Mineral Matter. In Hardesty, D.R. ed. Coal Combustion Science Quarterly Progress Report January-March 1992., *Sandia Report* SAND92-8210, 1992 p. 3-1-3-47.
(4) Finkelman, R.B.; Palmer, C.A.; Krasnow, M.R.; Aruscavage, P.J.; Sellers, G.A.; Dulong, F.T. *Energy and Fuels*, 1990, 4 (6) 755-766.
(5) Palmer, C.A.; Krasnow, M.R.; Finkelman, R.B.; d' Angelo, W.M. Submitted to J. Coal Quality.(4) (6) Finkelman, R.B., Modes of occurrence of trace elements in coal, *US Geol. Surv.* 1981, OFR 81-99. 301 pages.
(7) Zubovic, P.; Standnichenko, T.; Sheffey, B.The Association of Minor Elements with Organic and Inorganic Phases of Coal, *US Geol. Surv.* 1960, Professional Paper No.400-B, p B84-B87.
(8) Gluskoter, H.J.; Ruch, R.R.; Miller, W.G.;Cahill, R.A.; Dreher, G.B.; Kuhn, J.K., Trace elements in Coal: Occurrence and Distribution, *IL Geol. Surv.*1977, Circular 499. 154 pages.
(9) Palmer, C.A.; Filby, R.H. *Fuel* , 1984, 63, 318-326.
(10) Palmer, C.A. *Energy and Fuels*, 1990, 4(5), 436-439
(11) Doughten, M.W.; Gillison, J.R. *Energy and Fuels*,1990, 4(5), 426-430

Table 1. Percent of selected elements sequentially leached from the Illinois #6 coal by different solvents. The concentrations of elements used to calculate the percent leached were determined by instrumental neutron activation analysis (INAA) on residue of the leached coal. The concentrations of the elements used to calculate the percent leached were determined directly by inductively coupled argon plasma atomic emission spectrometry (ICAP-AES) on the leached solutions. *=number converted to an upper limit due to high errors in calculations; ND= not determined, ? No value could be determined from data, 1990 refers to data previously reported by Finkelman et al.[4]

	CH_3COONH_4		HCl		HF		HNO_3	
Element-method	Run1	1990	Run1	1990	Run1	1990	Run1	1990
B-ICAP-AES	1	ND	32	ND	45	ND	<18	ND
Na-INAA	73±4	65	10±5	0	15±6	0	6±0.4	15
Na-ICAP-AES	70	ND	12	ND	<2	ND	<3	ND
Mg-ICAP-AES	8	ND	7	ND	57	ND	142	ND
Al-ICAP-AES	17	ND	36	ND	42	ND	47	ND
Si-ICAP-AES	0	ND	1	ND	ND	ND	2	ND
P-ICAP-AES	<44	ND	<50	ND	<58	ND	<100	ND
K-INAA	9±7	13	<12*	0	<91	78	<10*	>7
K-ICAP-AES	<21	ND	<24	ND	81	ND	<57	ND
Ca-ICAP-AES	71	ND	21	ND	2	ND	3	ND
Sc-INAA	<10*	0	<23*	15	64±14	32	20±16	4
Ti-ICAP-AES	<2	ND	3	ND	81	ND	9	ND
V-ICAP-AES	<20	ND	30	ND	219	ND	124	ND
Cr-INAA	<1*	0	?	22	53±4	9	33±8	24
Cr-ICAP-AES	<3	ND	22	ND	71	ND	52	ND
Mn-ICAP-AES	71	ND	21	ND	8	ND	<8	ND
Fe-INAA	9±1	0	9±1	0	4±1	0	75±6	48
Fe-ICAP-AES	0.5	ND	4	ND	10	ND	122	ND
Co-INAA	10±1	19	47±2	39	15±3	0	23±4	7
Co-ICAP-AES	<24	ND	43	ND	<31	ND	<64	ND
Ni-INAA	27±16	35	<30*	32	39±20	0	41±23	0
Ni-ICAP-AES	17	ND	36	ND	42	ND	47	ND
Cu-ICAP-AES	<10	ND	<11	ND	<13	ND	78	ND
Zn-INAA	8±6	ND	21±9	ND	58±9	ND	12±10	ND
Zn-ICAP-AES	<1	ND	26	ND	58	ND	18	ND
As-INAA	10±7	0	19±10	17	<18*	0	60±11	0
Se-INAA	21±4	0	<7*	0	<7*	0	65±5	0
Br-INAA	40±9	53	?	?	?	?	?	?
Rb-INAA	<26*	ND	<27*	ND	67±21	ND	<38*	ND
Sr-INAA	<49*	30	<100*	0	<40*	5	<20*	ND
Sr-ICAP-AES	36	ND	10	ND	19	ND	22	ND
Y-ICAP-AES	<25	ND	<29	ND	<33	ND	<69	ND
Zr-ICAP-AES	<5	ND	<5	ND	46	ND	<12	ND
Ag-ICAP-AES	<100	ND	<100	ND	<100	ND	<100	ND
Sb-INAA	<16*	0	<16*	13	22±11	0	60±13	6
Cs-INAA	<2*	0	15±7	0	71±8	0	20±8	88
Ba-INAA	28±13	11	22±19	25	31±20	9	20±15	8
Ba-ICAP-AES	32	ND	18	ND	35	ND	28	ND
La-INAA	<3*	0	38±3	37	11±2	4	43±1	29
Ce-INAA	<10*	8	45±15	38	<25*	0	40±17	24
Ce-ICAP-AES	<17	ND	34	ND	<22	ND	<46	ND
Nd-INAA	20±12	ND	<100*	ND	?	ND	58±20	ND
Sm-INAA	13±10	0	40±15	44	<20*	0	37±17	13
Eu-INAA	17±10	0	29±14	40	<20*	0	38±16	7
Tb-INAA	21±16	0	<40*	28	<40*	0	39±26	12
Yb-INAA	<15*	0	<22*	0	25±16	18	53±16	0
Lu-INAA	<18*	ND	<38*	ND	<40*	ND	55±28	ND
Hf-INAA	?	0	<2*	8	62±11	23	<12	9
Ta-INAA	<16*	0	<18*	0	48±17	0	36±19	0
W-INAA	?	0	?	0	?	0	?	0
Pb-ICAP-AES	<24	ND	30	ND	12	ND	50	ND
Th-INAA	<2*	0	24±14	30	<28*	0	51±16	14
U-INAA	<19*	0	<22*	16	24±15	0	40±16	0

Table 2. Concentrations of trace elements in the original Illinois #6 coal sample in parts per million except as noted.

B	Na	Mg	Al (%)	Si(%)	P	K (%)	Ca (%)	Sc	Ti	V	Cr	Mn
160	1020	750	1.25	3.0	47	0.2	0.93	2.3	700	34.5	35.8	76

Fe (%)	Co	Ni	Cu	Zn	As	Se	Br	Rb	Sr	Y	Zr	Ag
2.7	4.4	30	10.1	201	4.7	4.2	5.72	16	32.2	4.1	22.8	0.62

Sb	Cs	Ba	La	Ce	Nd	Sm	Eu	Tb	Yb	Lu	Hf	Ta
0.84	0.94	86	5.99	10.2	6.5	1.03	0.226	0.134	0.47	0.06	0.435	0.176

W	Pb	Th	U
1.51	8.6	1.65	4.27

Table 3. Percent of selected elements sequentially leached from the Buelah-Zap lignite by different solvents. The concentrations of elements used to calculate the percent leached were datermined by instrumental neutron activation analysis (INAA) on residue of the leached coal. The concentrations of the elements used to calculate the percent leached were determined directly by inductively coupled argon plasma atomic emission spectrometry (ICAP-AES) on the leached solutions. *=number converted to an upper limit due to high errors in calculations; ND= not determined, ? No value could be determined from data, 1990 refers to data previously reported by Finkelman et al.[4]

	CH_3COONH_4		HCl		HF		HNO_3	
Element-method	Run1	1990	Run1	1990	Run1	1990	Run1	1990
B-ICAP-AES	<17	ND	40	ND	<26	ND	<40	ND
Na-INAA	54±4	95	26±5	0	18±5	0	19±1	0
Na-ICAP-AES	<100	ND	<100	ND	<100	ND	<100	ND
Mg-ICAP-AES	101	ND	11	ND	17	ND	42	ND
Al-ICAP-AES	1	ND	28	ND	66	ND	1	ND
Si-ICAP-AES	<1	ND	10	ND	ND	ND	3	ND
P-ICAP-AES	<22	ND	100	ND	<34	ND	<66	ND
K-INAA	41±21	?	<32*	0	<100	>85	<100	ND
K-ICAP-AES	<100	ND	<100	ND	<100	ND	<100	ND
Ca-ICAP-AES	82	ND	23	ND	1	ND	0	ND
Sc-INAA	?	0	50±6	15	45±11	32	<13*	4
Ti-ICAP-AES	<7	ND	23	ND	66	ND	<21	ND
V-ICAP-AES	167	ND	<86	ND	<100	ND	<100	ND
Cr-INAA	?	14	?	70	?	0	22±6	0
Cr-ICAP-AES	371	ND	<66	ND	203	ND	<100	ND
Mn-ICAP-AES	46	ND	42	ND	<5	ND	<10	ND
Fe-INAA	<10*	15	37±14	0	<26*	0	50±22	0
Fe-ICAP-AES	<1	ND	34	ND	9	ND	30	ND
Co-INAA	?	5	75±5	58	13±7	0	<12*	0
Co-ICAP-AES	<100	ND	<100	ND	<100	ND	<100	ND
Ni-INAA	<17*	0	32±14	0	<44*	0	<30*	0
Ni-ICAP-AES	<27	ND	69	ND	<100	ND	<100	ND
Cu-ICAP-AES	76	ND	<32	ND	<41	ND	<79	ND
Zn-INAA	3±1	0	<73*	76	<23*	16	<1*	0
Zn-ICAP-AES	<27	ND	82	ND	67	ND	<79	ND
As-INAA	<6*	16	22±8	4	19±1	0	44±1	11
Se-INAA	<17*	0	9±6	0	?	0	58±12	0
Br-INAA	1±0.1	0	?	?	?	?	?	?
Rb-INAA	16±8	ND	<23*	ND	>23	ND	>34[a]	ND
Sr-INAA	64±1	45	>32*	54	?	0	?	0
Sr-ICAP-AES	76	ND	26	ND	1	ND	<1*	ND
Y-ICAP-AES	<67	ND	<100	ND	<100	ND	<100	ND
Zr-ICAP-AES	<11	ND	<13	ND	61	ND	<33	ND
Ag-ICAP-AES	<100	ND	<100	ND	<100	ND	<100	ND
Sb-INAA	<13*	0	<19*	0	68±30	14	<40*	30
Cs-INAA	<10*	0	<46*	0	>68	82	?	?
Ba-INAA	<13*	23	71±13	73	29±15	?	<1	?
Ba-ICAP-AES	18	ND	87	ND	16	ND	1	ND
La-INAA	?	0	75±9	83	13±10	0	<18*	7
Ce-INAA	?	14	69±13	70	18±13	0	14±8	7
Ce-ICAP-AES	<61	ND	92	ND	<91	ND	<100	ND
Nd-INAA	33±25	ND	>47	ND	0	ND	>16	ND
Sm-INAA	<5*	0	73±8	81	18±14	0	<21*	7
Eu-INAA	<19*	0	71±30	79	>50	0	<40*	7
Tb-INAA	<11*	0	70±15	84	17±15	0	<20*	3
Yb-INAA	<20*	0	67±31	72	<40*	0	<45*	7
Lu-INAA	<22*	ND	64±18	ND	<38*	ND	<28*	ND
Hf-INAA	?	0	<10*	0	81±10	55	<10*	0
Ta-INAA	?	0	<13*	0	94±13	37	14±11	0
W-INAA	?	0	?	0	?	0	?	0
Pb-ICAP-AES	<100	ND	172	ND	<100	ND	<100	ND
Th-INAA	?	0	39±8	60	60±8	0	21±9	29
U-INAA	<18*	0	54±27	60	34±31	27	<40*	0

[a]Includes amount leached by HF

Table 4. Concentrations of trace elements in the original Buelah-Zap lignite sample in parts per million except as noted.

B	Na	Mg	Al	Si	P	K	Ca (%)	Sc	Ti	V	Cr	Mn
79	4960	3740	4000	6700	120	250	1.48	0.76	190	3.7	2.4	81

Fe	Co	Ni	Cu	Zn	As	Se	Br	Rb	Sr	Y	Zr	Ag
4800	0.82	5	5	5.23	2.63	0.59	1	0.93	530	2	12	0.14

Sb	Cs	Ba	La	Ce	Nd	Sm	Eu	Tb	Yb	Lu	Hf	Ta
0.173	0.5	610	2.67	3.92	2.3	0.4	0.081	0.52	0.26	0.036	0.293	0.92

W	Pb	Th	U
0.38	1.5	0.9	0.41

Table 5. Percent of selected elements sequentially leached from the Lower Bakerstown coal by different solvents. The concentrations of elements used to calculate the percent leached were determined by instrumental neutron activation analysis (INAA) on residue of the leached coal. The concentrations of the elements used to calculate the percent leached were determined directly by inductively coupled argon plasma atomic emission spectrometry (ICAP-AES) on the leached solutions. *=number converted to an upper limit due to high errors in calculations; ND= not determined, ? No value could be determined from data, 1990 refers to data previously reported by Finkelman et al.[4]

	CH_3COONH_4			HCl			HF			HNO_3		
Element-method	Run1	Run2	1990	Run1	Run2	1990	Run1	Run2	1990	Run1	Run 2 80°C	1990
B-ICAP-AES	<100	<100	ND	<100	<100	ND	<100	<100	ND	<100	<100	ND
Na-INAA	10±4	10±4	0	<7*	<10*	0	75±5	75±5	65	<8*	<9*	0
Na-ICAP-AES	19	13	ND	8	<9	ND	61	72	ND	<13	<16	ND
Mg-ICAP-AES	10	12	ND	6	7	ND	41	48	ND	5	5	ND
Al-ICAP-AES	59	45	ND	11	16	ND	36	24	ND	38	<16	ND
Si-ICAP-AES	<0.2	<0.3	ND	0.3	0.5	ND	ND	ND	ND	4	<1	ND
P-ICAP-AES	12	<9	ND	54	78	ND	14	17	ND	<13	19	ND
K-INAA	<13*	<13*	0	<22*	<18*	0	>89	>85	>79	>2	>1	ND
K-ICAP-AES	<58	<88	ND	<64	<88	ND	84	<100	ND	<100	<100	ND
Ca-ICAP-AES	75	66	ND	21	22	ND	18	18	ND	9	8	ND
Sc-INAA	<3*	<3*	8	14±3	16±3	63	33±3	31±3	23	<3*	6±3	0
Ti-ICAP-AES	<4	<3	ND	<3	<4	ND	49	53	ND	21	11	ND
V-ICAP-AES	<20	<30	ND	<22	<30	ND	49	52	ND	<44	<53	ND
Cr-INAA	<4*	<4*	0	?	?	0	?	?	12	?	?	11
Cr-ICAP-AES	<12	<17	ND	<12	<18	ND	104	109	ND	77	73	ND
Mn-ICAP-AES	65	60	ND	<23	<32	ND	<26	<39	ND	<48	<57	ND
Fe-INAA	<12*	<11*	15	29±7	42±7	26	29±7	23±7	8	40±8	33±8	4
Fe-ICAP-AES	17	<0.2	ND	40	61	ND	8	8	ND	35	49	ND
Co-INAA	60±3	60±3	59	11±3	12±3	8	<7*	<6*	0	8±3	8±3	0
Co-ICAP-AES	79	67	ND	<17	<23	ND	<19	<28	ND	<33	<40	ND
Ni-INAA	39±14	39±14	55	<38*	<19*	0	<19*	<19*	0	22±18	34±18	0
Ni-ICAP-AES	59	45	ND	10	15	ND	36	24	ND	39	<16	ND
Cu-ICAP-AES	46	<15	ND	21	24	ND	21	30	ND	<22	<26	ND
Zn-INAA	53±6	53±6	64	31±8	19±8	21	<9*	<13*	0	<11*	<11*	0
Zn-ICAP-AES	72	64	ND	18	43	ND	9	9	ND	<5	39	ND
As-INAA	<5*	6±4	0	57±5	46±5	41	15±6	16±6	6	30±5	30±5	6
Se-INAA	<10*	<11*	0	<18*	<23*	0	<14*	<25*	0	74±14	70±14	0
Br-INAA	<4*	<4*	0	7±4	17±4	19	9±4	<4*	15	<40*	<40*	0
Rb-INAA	<24*	<24*	ND	<22*	<23*	ND	>91	>90	ND	>7	>3	0
Sr-INAA	<25*	<25*	16	<24*	<33*	0	58±24	63±24	9	<28*	<30*	11
Sr-ICAP-AES	19	17	ND	7	9	ND	41	44	ND	8	8	ND
Y-ICAP-AES	<31	<47	ND	<34	<47	ND	<39	<57	ND	<69	<83	ND
Zr-ICAP-AES	<6	<10	ND	<7	<10	ND	30	36	ND	14	<17	ND
Ag-ICAP-AES	<100	<100	ND	<100	<100	ND	<100	<100	ND	<100	<100	ND
Sb-INAA	<6*	<6*	10	37±4	38±5	33	20±4	21±4	21	22±4	30±4	0
Cs-INAA	<17*	<17*	12	<17*	<18*	?	84±19	85±20	37	>21*	<21*	14
Ba-INAA	<17*	<17*	23	<19*	<19*	?	75±19	79±18	?	17±15	23±18	>23
Ba-ICAP-AES	22	11	ND	67	12	ND	27	19	ND	10	<8	ND
La-INAA	<4*	<4*	0	10±5	11±5	0	13±5	16±5	5	25±4	34±4	22
Ce-INAA	<4*	<4*	0	14±4	14±4	3	12±5	14±4	0	22±5	34±3	22
Ce-ICAP-AES	<20	<30	ND	<22	<30	ND	<25	<37	ND	<44	<53	ND
Nd-INAA	<19*	<19*	ND	22±17	30±17	ND	17±1	16±3	ND	26±17	32±17	ND
Sm-INAA	<3*	<3*	0	22±5	19±4	9	10±4	12±4	0	15±4	24±4	17
Eu-INAA	<5*	<5*	0	28±7	23±6	14	<14*	9±7	7	12±7	22±7	16
Tb-INAA	<7*	<7*	0	23±10	20±10	15	<16*	<10*	0	12±10	23±10	16
Yb-INAA	<12*	<12*	20	<18*	16±9	?	13±8	<15*	?	<15*	17±8	9
Lu-INAA	<8*	<8*	ND	<16*	<23*	ND	<17*	11±8	ND	11±9	15±8	ND
Hf-INAA	<10*	<10*	0	<8*	<10*	0	41±8	40±8	21	<9*	10±8	7
Ta-INAA	<9*	<9*	0	<20*	<13*	0	19±13	17±12	0	19±12	34±12	0
W-INAA	?	?	0	<25*	<23*	0	42±24	40±21	15	<30*	26±19	0
Au-INAA	>31	>28	ND	?	?	ND	?	<32*	ND	?	<33*	ND
Pb-ICAP-AES	35	<53	ND	62	101	ND	5	<7	ND	<79	<94	ND
Th-INAA	<4*	<4*	0	9±5	13±4	0	9±4	9±4	6	15±4	16±4	10
U-INAA	15±13	<20*	0	<18*	<18*	0	37±17	24±17	22	<24*	19±17	9

Table 6. Concentrations of trace elements in the original Lower Bakerstown coal sample in parts per million except as noted.

B	Na	Mg	Al (%)	Si (%)	P	K	Ca (%)	Sc	Ti	V	Cr	Mn
2.86	170	330	0.74	1.07	360	700	1.4	2	430	10.4	9.1	9.7

Fe (%)	Co	Ni	Cu	Zn	As	Se	Br	Rb	Sr	Y	Zr	Ag
0.86	6.92	17.9	10.6	47.9	2.63	0.59	34.1	4.85	82	3.33	16	0.41

Sb	Cs	Ba	La	Ce	Nd	Sm	Eu	Tb	Yb	Lu	Hf	Ta
1.5	0.29	34	6.08	10.4	3.65	1.20	0.23	0.14	0.54	0.67	0.38	0.11

W	Au	Pb	Th	U
0.65	0.001	5.84	1.32	0.53

Table 7. Percent of selected elements leached from the Lower Bakerstown coal by different solvents. Individual experiments were conducted using room temperature solvents (RT) and 80°C solvents (hot). The numbers after RT and hot indicate run numbers. The concentrations of elements used to calculate the percent leached were determined by instrumental neutron activation analysis (INAA) on residue of the leached coal. The concentrations of the elements used to calculate the percent leached were determined directly by inductively coupled argon plasma atomic emission spectrometry (ICAP-AES) on the leached solutions. *=number converted to an upper limit due to high errors in calculations; ND= not determined, ? No value could be determined from data,

	CH_3COONH_4	HCl					HF	HNO_3				
Element- method	RT1	RT1	RT2	RT3	Hot1	Hot2	RT1	RT1	RT2	RT3	Hot1	Hot2
B-ICAP-AES	<100	<100	<100	<100	<100	<100	<100	<100	<100	<100	<100	<100
Na-INAA	9±4	17± 3	15±3	19±3	31±4	30±4	86±4	35±4	25±4	19±4	18±4	30±4
Na-ICAP-AES	15	16	<59	<59	<59	<65	124	31	<59	<65	<65	<65
Mg-ICAP-AES	47	57	28	29	57	60	67	30	30	31	40	51
Al-ICAP-AES	59	57	<56	<56	68	67	70	75	66	78	81	80
Si-ICAP-AES	<0.3	1	<2	<2	16	17	ND	3	<2	17	6	7
P-ICAP-AES	<9	69	72	72	88	92	83	73	71	99	80	92
K-INAA	<13*	12±10	13±11	12±11	37±11	39±11	<99*	31±10	15±11	13±11	16±11	22±11
K-ICAP-AES	<86	<9	<100	<100	<100	<100	99	<86	<100	<100	<100	<100
Ca-ICAP-AES	62	77	100	97	121	131	41	108	106	119	117	135
Sc-INAA	<3*	17±2	18±3	19±2	29±2	28±2	47±2	35±2	21±2	20±2	20±2	29±3
Ti-ICAP-AES	<4	<43	<23	<23	<23	<26	54	<4	<23	<25	<23	<26
V-ICAP-AES	<29	<29	<100	<100	<100	<100	57	<29	<100	<100	<100	<100
Cr-INAA	<6*	<4*	<6*	<4*	<4*	9±4	23±4	15±4	<7*	<5*	?	8±6
Cr-ICAP-AES	<17	<17	<100	<100	<100	<100	42	<17	<100	<100	<100	<100
Mn-ICAP-AES	56	43	<100	<100	<100	<100	68	40	<100	<100	<100	<100
Fe-INAA	<4*	49±4	48±4	53±3	54±4	53±4	59±4	97±5	96±5	96±5	96±5	96±5
Fe-ICAP-AES	<0.2	53	53	53	58	60	56	108	104	113	103	116
Co-INAA	60±2	70±2	70±2	72±3	73±3	73±2	72±3	85±2	79±2	80±3	79±3	83±2
Co-ICAP-AES	65	65	<100	<100	<100	<100	65	73	<100	<100	<100	<100
Ni-INAA	33±13	44±13	50±13	51±13	46±13	61±13	59±13	70±13	63±13	65±13	61±13	68±13
Ni-ICAP-AES	47	57	<56	<56	66	67	70	75	66	76	81	80
Cu-ICAP-AES	<14	31	<94	<94	<94	<100	57	87	<94	<100	<100	<100
Zn-INAA	57±8	84±5	84±5	85±5	86±5	85±5	85±5	93±5	87±5	86±5	83±5	90±5
Zn-ICAP-AES	88	100	220	124	128	116	138	150	103	144	125	116
As-INAA	<5*	60±4	59±4	62±4	61±4	60±4	65±4	96±4	94±4	96±4	96±4	95±4
Se-INAA	<10*	<10*	21±9	<15*	11±10	<15*	<15*	86±10	57±10	58±10	49±9	78±10
Br-INAA	<4*	11±3	16±3	16±3	73±3	73±3	29±3	57±3	36±3	23±3	23±3	44±3
Rb-INAA	<14*	<24*	<22*	18±14	48±14	45±14	81±16	38±14	<24*	15±14	<34*	26±14
Sr-INAA	<18*	23±17	<34*	<29*	64±18	73±18	52±17	61±17	40±20	30±17	22±17	49±17
Sr-ICAP-AES	17	22	28	29	83	90	48	48	35	38	68	75
Y-ICAP-AES	<45	<45	<100	<100	<100	<100	<45	<45	<100	<100	<100	<100
Zr-ICAP-AES	<10	<9	<62	<62	<62	<70	81	<10	<62	<69	<70	<69
Ag-ICAP-AES	<100	<100	<100	<100	<100	<100	<100	<100	<100	<100	<100	ND
Sb-INAA	<5*	36±3	44±3	32±3	28±3	25±3	34±3	56±3	21±4	48±3	47±3	54±3
Cs-INAA	<14*	<17*	18±12	22±12	56±13	56±13	78±14	42±12	15±12	27±12	23±12	36±14
Ba-INAA	<22*	<20*	<17*	<15*	45±11	53±12	70±12	47±12	<15*	23±18	>25	19±14
Ba-ICAP-AES	15	12	<30	<30	64	72	141	29	<29	<33	49	54
La-INAA	<5*	13±3	17±3	20±3	58±3	58±3	13±3	52±3	22±3	19±3	19±3	43±3
Ce-INAA	<3*	15±4	21±4	24±3	59±3	59±3	9±3	55±3	25±3	24±3	23±3	47±3
Ce-ICAP-AES	<29	<29	<100	<100	<100	<100	<29	29	<100	<100	<100	<100
Nd-INAA	<13*	14±12	<25*	17±12	40±12	61±12	<16*	57±12	24±11	<15*	31±12	46±12
Sm-INAA	<5*	25±3	29±3	30±3	59±3	58±3	11±3	59±3	36±3	32±3	32±3	50±3
Eu-INAA	<5*	24±5	30±5	32±5	56±5	54±5	10±5	56±5	34±5	35±5	35±5	51±5
Tb-INAA	<7*	17±7	29±7	28±7	40±7	39±7	8±7	43±7	27±7	27±7	24±7	42±7
Yb-INAA	<7*	8±6	<12*	9±6	25±5	21±6	<6*	35±5	14±6	12±6	12±6	18±6
Lu-INAA	<6*	11±6	<13*	13±7	23±5	24±5	6±5	34±5	16±5	13±6	9±6	24±6
Hf-INAA	<6*	<9*	?	<6*	<12*	8±6	40±6	12±6	<6*	<11*	<13*	7±6
Ta-INAA	?	?	?	?	?	?	<13*	<9*	?	?	?	?
W-INAA	?	?	?	?	<14*	?	23±13	<14*	?	?	?	?
Au-INAA	<60*	<44*	33±30	?	59±33	<31*	?	<32*	<42*	<56*	?	?
Pb-ICAP-AES	<52	93	<100	<100	<100	<100	32	98	<100	<100	<100	<100
Th-INAA	<3*	9±3	10±5	13±3	29±3	29±3	8±3	32±3	14±3	17±5	15±3	25±4
U-INAA	<24*	<19*	<24*	34±12	29±11	32±11	21±12	44±11	23±12	28±12	20±12	36±12

TRACE ELEMENTS IN COAL: A USGS PERSPECTIVE OF THE CLEAN AIR ACT

R. B. Finkelman
U.S. Geological Survey, MS 956
Reston, VA 22092

Keywords: coal quality, data base, modes of occurrence.

INTRODUCTION

The provisions of the 1990 Clean Air Act Amendments require the U.S. Environmental Protection Agency (EPA) to evaluate the hazards to public health resulting from emissions by electric utility steam-generating plants. Among the substances listed in the Act as hazardous air pollutants are about a dozen elements found in coal (As, Be, Cd, Co, Cr, Hg, Mn, Ni, Pb, Sb, Se, and U). Coal combustion can be a primary anthropogenic source for some of these elements (especially Be, Co, Hg, Sb, Se).

There is no publicly available data base that contains comprehensive information on the trace element content of coal beds that are used for combustion. Therefore, the EPA has chosen the U.S. Geological Survey (USGS) Coal Quality Data Base to use in their evaluation of the impact of coal switching and to estimate the trace element input load to electric utility steam generating plants.

THE USGS COAL QUALITY DATA BASE

The USGS Coal Quality Data Base is an interactive, computerbased data base. It contains comprehensive analyses of more than 13,000 samples of coal and associated rocks from every major coal-bearing basin and coal bed in the United States and about 1,000 analyses of coal samples from other countries. The data in the Coal Quality Data Base represent analyses of the coal **as it exists in the ground.** The data commonly are presented on an as-received whole-coal basis.

SAMPLE COLLECTION AND ANALYTICAL PROTOCOL

The recommended procedures for collecting samples for analyses that were included in the data base are described by Stanton (1). Detailed information on the geographic location (State, county, longitude and latitude, mine, etc.) and geologic and stratigraphic information (thickness, depth, geologic age, formation, member, bed, etc.) are recorded for each sample.

Coal and associated rock samples were analyzed for the concentrations of approximately 75 major, minor, and trace elements (2) by the USGS, and for the standard coal characteristics by the U.S. Bureau of Mines and commercial testing laboratories using American Society of Testing and Materials standards (3). The standard coal characteristics include proximate and ultimate analysis, calorific value, forms of sulfur, ash-fusion temperatures, free-swelling index, and air-drying loss. Equilibrium moisture, apparent specific gravity, and Hardgrove Grindability Index are determined on selected samples. A total of 136 parameters are determined for each sample.

NATURE OF THE COAL QUALITY DATA BASE

The samples collected and submitted for analysis and inclusion in the data base consist primarily of full bed core and channel samples. Some of the bed samples were collected in benches or in measured intervals of the bed. The bench or interval analyses can be weighted by thickness and composited to obtain a calculated analysis of the full coal bed. Where possible, clastic rocks (partings, overburden, underburden) associated with the coal bed also were collected and analyzed.

Finkelman and others (4) compiled a bibliography of publications containing element data from the Coal Quality Data Base. This report also contains the number of analyzed samples for each State and the number of those analyses that have been published. Approximately half of the data in the data base has been included in publications.

During the past 5 years an additional 500 analyses have been added to the data base. About 75 percent of the samples were collected and analyzed prior to 1982. In some basins, many of the coal samples were collected from active surface and underground mines. In some of these areas, mining is no longer active. Nevertheless, the data from these areas are still useful for regional projections of coal quality variation.

The addition of coal quality data from the Illinois Geological Survey (approximately 700 analyses) and from the New Mexico Bureau of Mines and Geology (approximately 550 analyses) will enhance the Coal Quality Data Base.

VERTICAL AND LATERAL VARIATIONS OF THE COAL QUALITY DATA

One of the more common uses of the USGS coal quality data is to evaluate vertical and lateral distribution of coal quality parameters. Table 1 contains arithmetic means for the potentially hazardous air pollutants in several coal basins (data for all tables are from reference 5). Several elements exhibit a wide range of concentrations among the coal basins; for example, cadmium ranges from 0.1 ppm in the Appalachian basin to 4.2 ppm in the Interior Coal Province. In contrast, mercury ranges from 0.12 ppm in the Powder River basin to only 0.22 ppm in the Gulf Coast Province.

Table 2 contains arithmetic means of the potentially hazardous air pollutants in six coal beds within the Appalachian basin. Mercury and antimony show a greater range within the coal basin than among coal basins. Table 3 contains arithmetic means for the potential air pollutants in six coal samples from the Pittsburgh coal bed from Ohio, Pennsylvania, and West Virginia. In this sample suite arsenic and beryllium have larger ranges than they do in tables 1 or 2. Finally, at bench scale, the smallest sampling scale in the data base, table 4 shows large trace element ranges, among bench samples from the Pittsburgh coal bed, for arsenic, beryllium, cobalt, chromium, and mercury. These data demonstrate that trace element ranges may be larger within a coal bed than between coal basins (for example see mercury).

STATISTICAL CORRELATIONS

One indirect method of deducing an element's mode of occurrence is to determine its correlation with ash yield, sulfur, or other coal quality parameters. This is often a useful, but potentially misleading, procedure. In a geologic data base, such as the USGS Coal Quality Data Base, correlation coefficients generally reflect a common source rather than a close chemical or physical affinity. For example, Cecil and others (6) found evidence of extensive mobilization of many trace elements in the Upper Freeport coal bed. Because this geochemical system was closed for many elements, the elements retained statistical correlations with ash yield and other parameters, despite these elements having changed chemical form and distribution patterns. Finkelman (7) came to a similar conclusion on the basis of research on the Gulf Coast lignites.

MODES OF OCCURRENCE AND TEXTURAL RELATIONS

The USGS Coal Quality Data Base provides information on the concentration and vertical and lateral distribution of many coal quality parameters including the major, minor, and trace elements. This information is useful, especially for seeking coals with particular coal quality characteristics or for determining regional trends. However, to anticipate the environmental impact, technological behavior, or byproduct potential of an element, information is needed on the modes of occurrence (chemical form) and textural relations of the element. Currently, this information is not included in the data base. The USGS has, however, conducted extensive investigations on the modes of occurrence and textural relations of the elements in coal (8-12).

CONCLUSION

The trace element information contained in the U.S. Geological Survey Coal Quality Data Base may aid EPA in addressing several provisions of the 1990 Clean Air Act Amendments. Information on the modes of occurrence and textural relations of potentially hazardous elements may lead to more efficient mitigation of the environmental impact of these elements found in coal.

LITERATURE CITED

1. Stanton, R. W., 1989, Sampling of coal beds for analysis. In Methods for sampling and inorganic analysis of coal, D. W. Golightly and F. O. Simon, editors. U.S. Geological Survey Bulletin 1823, p. 7-13.
2. ASTM (American Society for Testing and Materials), 1993, Annual book of ASTM standards, Volume 05.05 Gaseous fuels: Coal and coke. ASTM, Philadelphia, 526 p.
3. Golightly, D. W., and Simon, F. O., editors, 1989, Methods for sampling and inorganic analysis of coal: U.S. Geological Survey Bulletin 1823, 72 p.
4. Finkelman, A. C., Wong, C.-J. J., Cheng, A. C., and Finkelman, R. B., 1991, Bibliography of publications containing major, minor, and trace element data from the National Coal Resources Data System. U.S. Geological Survey Open-File Report 91-123, 19 p.
5. Finkelman, R. B., Oman, C. L., Bragg, L. J., and Tewalt, S. J., in press, The U.S. Geological Survey Coal Quality Data Base. U.S. Geological Survey Open-File Report.
6. Cecil, C. B., Stanton, R. W., Allshouse, S. D., and Finkelman, R. B., 1979, Interbed variation in and geologic controls on element concentrations in the Upper Freeport coal. American Chemical Society, Fuel Chemistry Division, Chemical Congress Abstract no. 48.
7. Finkelman, R. B, 1981, Modes of occurrence of trace elements in coal. U.S. Geological Survey Open-File Report 81-99, 312 p.
8. Zubovic, P., Stadnichenko, T., and Sheffey, N. B., 1960, The association of minor elements with organic and inorganic phases of coal. U.S. Geological Survey Professional Paper 400-B, p. B84-B87.
9. Finkelman, R. B., Palmer, C. A., Krasnow, M. R., Aruscavage, P. S., and Sellers, G. A., 1990, Heating and leaching behavior of elements in the eight Argonne Premium Coal Samples. Energy and Fuels, v. 4, no. 6, p. 755-767.
10. Finkelman, R. B., 1993, Trace and minor elements in coal. In Organic geochemistry: Principles and applications, M. H. Engel and S. A. Macko, editors. Plenum Publishing Corp., New York, p. 593-607.
11. Finkelman, R. B., in press, Modes of occurrence of hazardous elements in coal: Level of confidence. Fuel Processing Technology.
12. Palmer, C. A., and Filby, R. H., 1983, Determination of mode of occurrence of trace elements in the Upper Freeport coal bed using size and density separation procedures. Proceedings, 1983 International Conference on Coal Science, International Energy Agency, p. 365-368.

Table 1. Variation of potential air toxics among coal basins. (Values are arithmetic means in parts-per-million on a whole-coal basis; figures in parantheses are number of samples.)

Element	Appalachian basin (4,700)	Interior Province (800)	Gulf Coast lignites (200)	Fort Union lignites (350)	Powder River basin (800)
Antimony	1.4	1.5	1.0	0.69	0.57
Arsenic	35.0	20.0	10.0	11.0	5.6
Beryllium	2.5	2.4	2.4	1.0	0.84
Cadmium	0.1	4.2	0.55	0.16	0.16
Chromium	17.0	19.0	24.0	6.4	8.5
Cobalt	7.2	10.0	7.2	2.4	2.3
Lead	8.4	40.0	21.0	4.8	5.5
Manganese	29.0	78.0	150.0	83.0	63.0
Mercury	0.21	0.15	0.22	0.14	0.12
Nickel	17.0	27.0	13.0	4.1	6.4
Selenium	3.5	3.2	5.7	0.82	1.1
Uranium	1.7	3.1	23.0	1.8	1.6

Table 2. Variation of potential air toxics among coal beds in the Appalachian basin. (Values are arithmetic means in parts-per-million on a whole-coal basis; figures in parentheses are number of samples.)

Element	Meigs Creek coal bed (54)	Redstone coal bed (80)	Pittsburgh coal bed (194)	Lower Freeport coal bed (119)	Lower Kittanning coal bed (219)	Sewell coal bed (73)
Antimony	0.3	0.7	0.6	1.2	0.9	1.1
Arsenic	6.7	29.1	20.4	37.3	25.2	11.1
Beryllium	1.4	1.6	1.4	2.7	2.6	2.2
Cadmium	0.08	0.07	0.11	0.11	0.14	0.10
Chromium	16.4	13.8	14.7	17.4	16.8	11.8
Cobalt	3.2	3.5	4.6	7.6	6.7	8.0
Lead	5.3	4.0	4.9	10.4	10.6	5.5
Manganese	30.8	46.3	31.9	42.8	27.2	18.5
Mercury	0.12	0.22	0.18	0.34	0.24	0.16
Nickel	9.5	9.5	10.7	20.4	20.5	18.9
Selenium	2.9	2.4	1.9	5.0	4.3	2.4
Uranium	1.8	1.7	1.1	1.7	1.8	1.4

Table 3. Lateral distribution of potential air toxics within the Pittsburgh coal bed from Ohio, Pennsylvania, and West Virginia. (Values are arithmetic means in parts-per-million on a whole-coal basis.)

	Sample					
	1	2	3	4	5	6
Element						
Antimony	0.4	1.4	0.4	0.4	1.4	0.3
Arsenic	13.3	75.1	15.0	9.6	79.8	10.0
Beryllium	1.1	1.2	1.6	1.4	1.0	0.3
Cadmium	0.10	0.07	0.14	0.06	0.09	0.04
Chromium	14.4	9.3	10.1	10.3	9.2	10.2
Cobalt	2.8	3.1	11.8	2.7	4.9	1.7
Lead	3.6	3.7	1.5	3.8	6.9	1.0
Manganese	17.8	19.1	55.1	19.7	25.6	25.3
Mercury	0.10	0.22	0.60	0.16	0.28	0.22
Nickel	7.1	6.3	20.9	9.0	9.5	4.3
Selenium	1.5	3.4	3.0	0.9	1.7	1.0
Uranium	0.8	0.3	2.0	0.9	1.4	2.4

Table 4. Variations of potential air toxics from the top to the bottom of a set of bench samples from the Pittsburgh coal bed in Ohio. (Values are in parts-per-million on a whole coal basis. Total thickness of the bed is 52.5 inches.)

	Sample						
	top 1	2	3	4	5	6	bottom 7
Element							
Antimony	0.6	0.2	0.2	0.2	0.3	0.3	0.4
Arsenic	10.4	12.6	4.9	6.3	8.2	31.9	12.8
Beryllium	3.0	1.5	0.8	0.7	1.6	1.3	3.4
Cadmium	0.10	0.09	0.03	0.05	0.08	0.08	0.09
Chromium	30.4	7.4	6.9	9.8	32.7	11.8	12.5
Cobalt	9.2	2.2	1.6	2.1	6.6	1.3	3.3
Lead	8.7	1.6	1.3	1.4	5.5	1.5	5.1
Manganese	12.6	10.3	8.8	7.34	24.8	8.4	13.7
Mercury	0.24	0.29	0.10	0.14	0.20	0.19	0.05
Nickel	16.6	5.8	2.9	4.7	21.3	5.9	13.7
Selenium	8.5	3.3	1.1	1.5	2.2	0.9	0.9
Uranium	2.0	0.3	0.3	0.4	1.3	0.3	0.6

COAL CLEANING: A PRE-COMBUSTION AIR TOXICS CONTROL OPTION

David J. Akers, Robert L. Dospoy, and Clifford E. Raleigh, Jr.
CQ Inc.
One Quality Center
Homer City, PA 15748

Barbara Toole-O'Neil
Electric Power Research Institute
Palo Alto, CA 94303

Keywords: Coal Cleaning; Air Toxics Control; Trace Element Reduction

INTRODUCTION

A number of elements and their compounds commonly found in coal are identified by the Clean Air Act (CAA) of 1990 as among 189 hazardous air pollutants (HAPs). These elements include: antimony, arsenic, beryllium, cadmium, chromium, cobalt, lead, manganese, mercury, nickel, and selenium. In addition to these specific elements, radionuclides are also listed as HAPs; these too are known to occur naturally in some coals. Finally, fluorine, in the form of hydrofluoric acid, is listed. The CAA mandates a study of utility air emissions. This study, to be performed by the United States Environmental Protection Agency (EPA), is expected to be presented to Congress by November 1995. In addition, EPA is required by law to perform a health risk assessment and to recommend new air toxic regulations, if necessary, to protect human health. Furthermore, the legislation requires separate studies of mercury emissions, deposition, and health effects. In order to make estimates of power plant HAP emissions, EPA requires information on the HAP concentrations in as-fired coal (i.e., as burned by utilities).

PUBLIC SOURCES OF COAL TRACE ELEMENT DATA

Starting in 1973 and continuing through the present, the United States Geological Survey (USGS) has collected and analyzed thousands of channel and core samples of coal for various quality parameters. The measurement of trace element content was part of this geochemical study. Channel and core samples are sometimes taken of the entire height of a coal seam, including interbedded rock and minerals (partings). In such cases, they represent in-place coal, which is similar to as-mined coal without the roof or floor rock sometimes extracted along with the coal during mining (out-of-seam dilution). USGS sampling protocol is to treat partings under ten centimeters thick as part of the coal seam, while those greater than ten centimeters thick are sampled separately unless they are normally extracted with the coal during mining. Partings are sometimes removed separately in surface mining, but in underground mining, they are always extracted with the coal. Therefore, USGS samples taken in underground mines normally represent in-place coal, while those taken from surface mines may or may not represent in-place coal.

Currently, no comprehensive trace element database is available to government and industry other than the database developed by the USGS. EPA is constrained by the absence of other comprehensive data sources and may use the USGS database for the emissions estimates necessary to perform the health risk assessments required by the Clean Air Act Amendments even though the available analyses are for in-place coal and not as-fired coal. This is a concern because, as shown in Table 1, about 77 percent of eastern and midwestern as-mined coal is cleaned before it is burned. In some cases, the primary effect of coal cleaning is to remove out-of-seam dilution; however, partings may also be removed during cleaning along with fracture filling mineral matter. Recent studies have demonstrated that coal cleaning can also reduce the concentration of most trace elements (Akers and Dospoy, 1993 and DeVito et al., 1993). Since the coal samples in the USGS represent as-mined or in-place coal, the trace element data in the USGS database on many of the eastern and midwestern coals will be higher than as-fired data because most of these coals are cleaned before combustion. Health risk assessments based on the existing USGS coal database will, therefore, tend to overestimate the risk of burning eastern and midwestern coal.

THE CURRENT PROJECT

CQ Inc., under funding by the Electric Power Research Institute, developed an approach that can be used to make coal samples in the USGS database more representative of as-fired rather than in-place coal. This paper presents a description of this approach, which involved the development of regression equations and algorithms for each of 11 trace elements. These equations and algorithms are used to predict the amount of a trace element in as-fired coal given the trace element analyses of channel and core samples in the USGS database. The

paper also presents discussion of the accuracy of the projections and provides an example of how the algorithms are being used.

The final part of this project, currently in progress, is to select those coals in the USGS database that exceed the typical as-fired ash content for the seam and county in which they were mined. For each USGS sample that exceeds the typical ash content, the appropriate algorithm will be applied to predict the trace element concentration of the core or channel sample assuming the coal had been cleaned to the typical ash content. At the conclusion of the project, a modified version of the USGS database will be available for estimating power plant emissions of HAPs.

MATHEMATICAL MODELING AND REGRESSION ANALYSES

Mathematical equations can often be developed to describe the relationships between input and output parameters of a system. In some cases, equations that are derived from theoretical or generally accepted cause-and-effect relationships can be used for modeling reactions to changes in measurable parameters. This is sometimes referred to as mechanistic or fundamental modeling. However, when theoretical knowledge about the relationships between inputs and outputs of a system is lacking, empirically-derived equations may still be developed to describe variable relations in a system.

A common method of empirical modeling is statistical correlation. Correlation, which involves the development of equations to relate results to system effects, can be used to analyze process data, describe its tendencies, and evaluate the intensity of associations among process parameters. A disadvantage with this modeling method is that the existence of a correlation does not mean that the system outputs are necessarily causally related to the input variables used to build the model. A measure of high correlation indicates only that the random variation of the data can be mathematically explained and that a specific tendency or behavior within the data is identified. However, when used correctly, statistical correlation can be an effective and reliable modeling method.

The primary operation involved in statistical correlation is regression analysis. Regression involves fitting linear or nonlinear mathematical equations to data sets in order to describe changes in dependent variables resulting from changes in independent parameters. In the case of linear regression, this is typically referred to as "least-squares" line fitting. In addition, regression is sometimes completed in stages to eliminate variables that are found to be mathematically and statistically unimportant; this is known as step-wise regression.

In order to develop equations that can predict the content of selected trace elements in clean coal after commercial-scale conventional coal cleaning, regression analyses were performed to relate various raw coal quality parameters and cleaning performance data to the trace element reduction. The data used for this work was collected from several sources: CQ Inc. has a database that includes ten commercial-scale coal cleaning tests; Consolidation Coal Company (CONSOL) has published information on trace element reductions in eight commercial cleaning plants (DeVito et al., 1993); and Bituminous Coal Research (BCR) has published trace element data for six commercial plants (Ford and Price, 1982). Finally, Southern Company Services, Inc. (SCS) gathered data on two commercial-scale cleaning tests during a project funded by DOE and EPRI. The final report for the SCS work has been prepared and supplied to EPA by DOE. Altogether, trace element removal data from 26 commercial-scale cleaning tests using coal mined east of the Mississippi River were located. Sufficient information was located to allow development of equations for the following elements: arsenic, beryllium, cadmium, chromium, cobalt, fluorine, lead, manganese, mercury, nickel, and selenium.

Multi-parameter, backward elimination regression analyses and statistical analysis of variance were conducted to develop equation models for each of 11 trace elements. For each system, trace element reductions from the commercial-scale coal cleaning tests and their respective raw coal quality parameters and coal cleaning performance results were gathered and stored into a database file. Various mathematical transformations (square root, logarithmic, and negative inverse) of the original data were also generated and included within this file. Regression of data transformations provided a means to ensure that both linear and non-linear correlation possibilities were examined. These data sets were then input to Minitab™, a computer software statistics package, for backward elimination regression. Information and output from Minitab includes statistics on summary of fit (the applicability and hardiness of the equation to describe the variances in the data), analysis of variance, and parameter estimates. All of the equations developed contained ash reduction as a major predictive parameter. Three of the equations also included a total sulfur reduction predictor, while several equations included one or more raw coal analyses in addition to ash reduction.

DATA SCATTER AND MODELING ACCURACY

The primary method used to evaluate regression equation accuracy was to evaluate the comparative fit of measured trace element reductions versus calculated trace element reductions. An example of this method of accuracy check is shown in the figure. In these types of graphs, the dotted line represents an exact correlation between the measured and predicted reductions. That is, if data appear on this line, the equation produced exactly the same value that was measured for a particular coal cleaning test. Similarly, values that plot away from this line indicate that the equation predicted trace element values greater than or less than the actual measured values. Therefore, equation accuracy can be determined by the distance individual values are away from this line. In this example, the graphic suggests that the equation developed for fluorine is accurate, though some points are a significant distance from the line. Some portion of this data scatter is likely caused by sampling or analytical error, but other explanations must also be considered.

Lack of fit may also be caused by differences in the mode of occurrence of these trace elements in raw coal and differences of response to a variety of coal cleaning operations. The mode of occurrence of an element is the physical form and location in which the element is found within a raw coal. In general, trace elements can be found within either the organic portion of a coal or within the mineral matter that is associated with a raw coal. When trace elements are associated with mineral matter or exist as discrete mineral particles, physical coal cleaning methods can be used to remove much of the mineral matter and trace elements from a raw coal. For example, mercury has been reported to occur in coal in a variety of modes: it can be found in pyrite, in epigenetic pyrite, and in sulfides other than pyrite as well as organically bound within coal (Finkelman, 1980). Any organically-bound mercury that may occur in coal cannot be removed by physical coal cleaning technologies, while epigenetic pyrite is often coarse grained and readily removable. Thus, if mercury is organically-bound, concentrations will increase with cleaning; if it is contained in coarse-grained mineral matter, it will be reduced by cleaning with quantities dependent upon the cleaning devices employed, method of operation, and coal characteristics.

Local geologic environment during and after coal formation can also affect the mode of occurrence of a trace element. As a result, mode of occurrence may vary between coal basins or even within a single basin. Because trace element mode of occurrence may vary with location, it is reasonable to expect such a change to be reflected in the geographic location of the coal samples used. An indication of possible impacts based on geographic location is shown in the fluorine data. The figure shows that for the Pennsylvania coals, measured fluorine reductions are always equal to or lower than their corresponding predicted values. For the Alabama coal samples, this situation is reversed--measured fluorine reductions are always equal to or higher than the predicted values. This indicates that the mode of occurrence of fluorine in Pennsylvania coals may inhibit the effectiveness of coal cleaning to remove this trace element. Conversely, the mode of occurrence of fluorine in Alabama coals may help make its removal easier. Unfortunately, when the data used in this study were grouped by state of origin or by coal basin, the number of commercial-scale tests became too small to allow a statistical assessment of the impact of geographic location.

The level of trace element reduction obtained during coal cleaning can also be affected by the different techniques and technologies utilized to remove ash-forming and sulfur-bearing minerals. However, as with location differences, this could not be adequately addressed in this study because of insufficient data. To illustrate this point, consider that most of the known mineral forms of mercury in coal are sulfides, which are typically dense, finely-sized minerals. When liberated from raw coal by crushing or grinding, sulfides can be easily removed by cleaning devices that depend on the differences in density between coal and mineral matter--this is the most common method of coal cleaning. Examples of density-based cleaning devices, which have a wide range of applicability and varying degrees of coal-mineral matter separation performance, include heavy-media cyclones and baths, jigs, and concentrating spirals. Other devices such as froth flotation or agglomeration units clean coal based on the differences in surface properties between the coal and mineral matter. The surface characteristics of many sulfides and coal are sometimes very similar, though, which makes sulfide removal using surface-based methods difficult at times.

AS-FIRED COAL QUALITY DATA

In order to use the regression equations to adjust the USGS channel or core sample data to an as-fired basis, it is first necessary to estimate the ash and sulfur content of a target clean coal. The quality of clean coal produced from coal cleaning plants is primarily driven by raw coal characteristics and market price and specifications. Because raw coal characteristics vary by region and seam and because utility fuel quality demands can vary from region to region, a wide spectrum of clean coal qualities are produced for the utility market. In order to

develop clean coal quality targets that are applicable to specific samples in the USGS database, both raw coal characteristics and local market specifications must be examined.

Within a very limited geographical area (e.g., a county), the characteristics of an individual coal seam are reasonably uniform. In addition, most of the clean coal that is produced from a particular seam in this limited region is of similar quality, especially if much of the coal produced in the localized region is competing for fuel sales to the same electrical generating station. Thus, clean coal quality targets used in algorithms that adjust USGS as-mined or in-place coal quality data to typical as-fired quality levels must be developed for each individual seam in a given county where active mining is occurring. Several public databases and other published sources can be used in gathering the specific information needed to relate regional coal production and individual coal seam information.

SAMPLE ALGORITHM CALCULATION

To apply the algorithms developed during this project, the following information is necessary:

- Initial sample data (raw coal quality data or USGS channel or core data).
- Target clean coal quality.
- The calculated ash, and in some cases sulfur, reduction between the initial sample and the target quality.
- The results of applying the regression equations.
- The results of the trace element concentration calculation.

The sample calculation presented below illustrates the procedures for determining the expected nickel concentration in the cleaned Sewickley Seam coal from Pennsylvania.

SAMPLE DATA

Raw Ash = 32.9%; Raw Heating Value = 9,804 Btu/lb; Raw Nickel = 23.5 ppm

TARGET CLEAN COAL QUALITY (Assumed)

Typical As-fired Sewickley Seam Coal, Greene County, PA
Ash = 12.0% and Heating Value = 13,300 Btu/lb

REDUCTION CALCULATION

Ash reduction is calculated by the following equation:

$$\text{Ash Reduction} = \frac{\dfrac{\text{Raw Coal Ash Content}}{\text{Raw Coal Heating Value}} - \dfrac{\text{Clean Coal Ash Content}}{\text{Clean Coal Heating Value}}}{\dfrac{\text{Raw Coal Ash Content}}{\text{Raw Coal Heating Value}}} \times 100$$

$$\text{Ash Reduction} = \frac{\dfrac{32.9}{9{,}804} - \dfrac{12.0}{13{,}300}}{\dfrac{32.9}{9{,}804}} \times 100 = 73.11\%$$

APPLICATION OF THE REGRESSION EQUATIONS

In this example, the equation for nickel reduction is used:

$$\text{Nickel Reduction} = -\frac{1}{[-0.0867 + (0.0368 \times \text{Log (Ash Reduction)})]} = -\frac{1}{[-0.0867 + (0.0368 \times \text{Log } (73.11))]} = 55.23\%$$

TRACE ELEMENT CONCENTRATION CALCULATION

Once the calculated nickel reduction is determined, the next step is to determine the clean coal nickel concentration using available raw coal data for heating value and nickel concentration and the target clean coal heating value.

$$\text{Nickel Reduction} = \frac{\dfrac{\text{Raw Coal Nickel Content}}{\text{Raw Coal Heating Value}} - \dfrac{\text{Clean Coal Nickel Content}}{\text{Clean Coal Heating Value}}}{\dfrac{\text{Raw Coal Nickel Content}}{\text{Raw Coal Heating Value}}} \times 100$$

$$55.23 = \frac{\dfrac{23.5}{9{,}804} - \dfrac{\text{Clean Coal Nickel Content}}{13{,}300}}{\dfrac{23.5}{9{,}804}} \times 100$$

$$\text{Clean Coal Nickel Content} = -\left[\left(\frac{55.23}{100} \times \frac{23.5}{9{,}804}\right) - \left(\frac{23.5}{9{,}804}\right)\right] \times 13{,}300 = 14.27 \text{ ppm}$$

Table 2 shows the results of applying this algorithm to adjust the trace element concentration of raw Sewickley Seam coal to an as-fired quality using each of the equations developed for the 11 trace elements. The table also provides a measure of the accuracy of this approach, with differences in predicted versus actual concentrations averaging about 20 percent.

SUMMARY

In order to make more representative estimates of power plant HAP emissions and to perform the health risk assessments required by the Clean Air Act Amendments, EPA requires information on the HAP concentrations in as-fired coal (i.e., as burned by utilities). Currently, the USGS coal database is the only comprehensive source for information on the trace element concentration of coals that is openly available to EPA. Unfortunately, USGS samples taken from many eastern and midwestern underground and surface mines represent in-place or as-mined coal, but not as-fired coal, which is often cleaned before it is burned. To address this problem, equations and algorithms were developed to convert trace element analyses in the USGS database from an in-place to an as-fired basis. This work has provided one means for modifying the USGS database so that it can be used to estimate power plant emissions of HAPs. The study also provides a tool to estimate the impacts of using conventional or advanced coal cleaning techniques to reduce the concentration of trace elements in coals burned by utilities.

REFERENCES

Akers, D. and Dospoy, R., "An Overview of the Use of Coal Cleaning to Reduce Air Toxics," Minerals and Metallurgical Processing, Published by The Society for Mining, Metallurgy, and Exploration, Littleton, CO, Vol. 10, No. 3, pp 124-127, August 1993.

DeVito, M., L. Rosendale, and V. Conrad, "Comparison of Trace Element Contents of Raw and Clean Commercial Coals," Presented at the DOE Workshop on Trace Elements in Coal-Fired Power Systems," Scottsdale, AZ, April 1993.

Finkelman, R., Modes of Occurrence of Trace Elements in Coal, PhD Dissertation, University of Maryland, Published by University Microfilms International, Ann Arbor, MI, 1980.

Ford, C. and A. Price, "Evaluation of the Effects of Coal Cleaning on Fugitive Elements: Final Report, Phase III," DOE/EV/04427-62, July 1982.

Table 1. Extent of Coal Cleaning by State. *Includes metallurgical, steam, and industrial coal.*

State	Estimated Raw Coal Mined (Million Tons/Year)	Estimated Tonnage Cleaned (Wt %)
Alabama	37.7	77
Illinois	83.7	93
Indiana	49.5	93
Kentucky	215.6	65
Maryland	4.9	92
Ohio	46.7	81
Pennsylvania	90.2	73
Tennessee	7.0	38
Virginia	62.0	81
West Virginia	223.6	81
Total/Average	821.0	77

Source: Coal Preparation and Solids Division, U.S. Department of Energy, Pittsburgh Energy Technology Center, Pittsburgh, PA 15236.

Table 2. Results of an Application of Algorithms on Raw Sewickley Seam Coal

Trace Element	Actual Raw Coal Conc. (ppm)	Actual Clean Coal Conc. (ppm)	Predicted Clean Coal Conc. (ppm)	Absolute % Difference Predicted vs. Actual
As	14.40	9.20	8.43	9.1
Be	1.07	0.98	1.21	19.0
Cd	0.21	0.10	0.12	16.7
Cr	44.00	23.60	29.49	20.0
Co	8.74	4.11	5.66	27.4
F	226.0	97.90	114.42	14.4
Pb	88.80	5.15	45.54	88.7
Mn	206.00	73.00	73.19	0.3
Hg	0.18	0.18	0.16	12.5
Ni	23.50	11.20	15.26	26.6
Se	3.61	2.85	2.81	1.4

Estimation of Algorithm Accuracy. *Fluorine.*

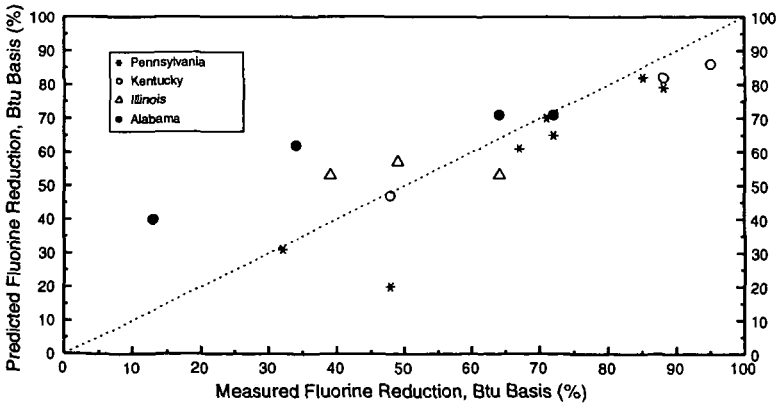

TRACE ELEMENTS IN ILLINOIS COALS BEFORE AND AFTER CONVENTIONAL COAL PREPARATION

I. Demir[1], R. D. Harvey[1], R. R. Ruch[1], J. D. Steele[1], and K. K. Ho[2]
[1]Illinois State Geological Survey, 615 E. Peabody Drive, Champaign, IL 61820,
[2]Illinois Clean Coal Institute, Coal Development Park, PO Box 8, Carterville, IL 62918

Keywords: trace elements, Illinois coals, cleaned coal

INTRODUCTION AND BACKGROUND

Responding to recent technological advances and renewed environmental concerns requires improved characterization of Illinois and other US coals. Much of the existing trace element data on Illinois coals are on channel samples; these data need to be supplemented with data on as-shipped coals. Such data will provide a factual basis for the assessment of noxious emissions at coal-fired electric power plants.

The Clean Air Act of 1990 [Public Law 101-549, 1990] identified many trace elements as "Hazardous Air Pollutants" (HAP) (Table 1). A parallel regulation is also underway in Illinois [Illinois Pollution Control Board, 1990]. All of these HAP elements are present in Illinois and other coals [Gluskoter et al., 1977; Harvey et al., 1983] in widely varying amounts. Utilities are presently exempt from having to consider emissions of trace elements; however, this may eventually change after the U.S. EPA completes its risk analyses and establishes emission standards. A database of trace element concentrations in the coals used by utilities is a prerequisite to defining the problem and establishing workable regulations.

Human sources constitute significant portions of the total global input of most trace elements into the atmosphere (Fig. 1). Emissions of trace elements from coal-fired power plants vary widely among countries and regions, reflecting varying trace element concentrations in coals from different sources. Among human sources, energy production (electrical utilities and industrial/domestic sector) is estimated to account for major portions of atmospheric emissions of Hg, Ni, Se, Sn, and V and lesser, but still significant, portions of As, Cd, Cr, Cu, Mn, and Sb. Oil combustion contributes larger portions of Ni, Sn, and V emissions than does coal combustion [Nriagu and Pacyna, 1988; Clarke and Sloss, 1992].

During combustion, trace elements in feed coals are partitioned among gas (flue gas), light particulate (fly ash), and slag/ash phases (Fig. 2). Typically, Hg, Br, Cl, F, and Rn end up in the flue gas; As, Cd, Ga, Ge, Pb, Sb, Sn, Te, Tl, and Zn in fly ash; and Eu, Hf, La, Mn, Rb, Sc, Sm, Th, and Zr in slag/ash deposits. Others show mixed affinities.

Swaine [1989] reviewed the environmental aspects of trace elements in coal. With respect to combustion, modern electrostatic precipitators can trap up to 99% of the fly ash. Swaine concluded that, in general, no trace element posed a significant environmental problem. This assumes that state-of-the-art electrostatic precipitators are used at the power plants and that the coals burned do not have exceptionally high concentrations of noxious elements that would be emitted in a gas phase. Deep physical cleaning of raw coal would reduce the levels of those elements that are associated with minerals [Capes et al., 1974; Gluskoter et al., 1977; Cavallaro et al., 1978; Norton and Markuszewski, 1989].

The purpose of this study was to determine trace element concentrations in as-shipped coals from Illinois mines, and compare the results with data on channel samples that represent coal in place prior to mining. Samples of 34 as-shipped samples were collected and analyzed for trace, minor and major elements, including the 18 HAP elements and others identified to be of greatest environmental concern by the U.S. National Committee for Geochemistry [1980]. Results on 20 of these elements of environmental concern are reported and discussed here. Radioactivity of the as-shipped coal samples was calculated from concentrations of U, Th, and K in the samples. Future work will concentrate on evaluating the further beneficiation of the as-shipped coal samples by fine coal cleaning.

EXPERIMENTAL

Samples and Sample Regions

Cleaned (as-shipped) samples of Illinois coals were collected from each of 33 preparation plants and from a mine that sells its coal after crushing. In most cases, the samples were splits from automatic samplers. Multiple cuts were taken across the coarse output belt over a period of 4 or more hours (commonly 8 to 24 hours) to obtain a representative sample. In some cases, the sample was collected from a stock pile, taking 15 to 20 widely spaced increments with a sampling shovel. All samples were sealed in 5 mil plastic bags or in 5 gallon plastic buckets and transported or mailed to our laboratory within two days. Within a week, the samples were homogenized riffled, crushed, and packaged at our sample preparation laboratory, according to the procedure described in Figure 3.

To maintain confidentiality of the results with respect to individual mines, the Illinois coal field was divided into five multi-county regions (Fig. 4); only the regions from which the samples came from were identified.

Analyses for Trace Elements

Each of the 34 samples was analyzed for trace, minor, and major elements. These elements, their method of analysis, and the precision and accuracy of the methods are shown in Table 2.

RESULTS AND DISCUSSION

Trace Element Database

Our computerized database contains trace element information on 900 samples (Table 3). Figure 5 identifies the 60 elements for which concentrations are

available on many samples in the database. The most useful records are from the 222 channel or equivalent samples which represent coal in-place prior to mining and cleaning. Table 4 and Figure 6 give the averages and variabilities for 20 critical environmental elements for channel samples from Illinois.

Trace Elements and Radioactivity in 34 As-shipped Samples

The concentrations of most of the environmentally critical trace elements in the 34 as-shipped coals (Table 4) vary less widely than those in the channel samples (compare Figs. 6 and 7). Comparison of the data from channel samples and from cleaned coals indicates that conventional coal cleaning can reduce the state-wide mean concentrations of trace elements in channel samples up to 67% (Fig. 8), except for U (12% enrichment). The reduction in elemental concentrations results from the reduction of mineral matter and some leaching by the process water. The enrichment of U in the as-shipped samples relative to channel samples suggests that this element is primarily associated with the organic material. Harvey et. al [1983], who calculated organic affinities from washability tests for Illinois coals, also concluded that U had organic affinity. However, even if U were largely associated with the organic matter, it would likely be located in very fine mineral grains disseminated within the organic matter [Finkelman, 1981; Clarke and Sloss, 1992].

It should be pointed out that, for a given mine, channel samples do not necessarily represent those portions of the seam where feed coals for as-shipped samples were mined. Therefore, the average trends of trace element reductions observed in Figure 8 may not hold for individual mines, as Figure 9 indicates. Zinc enrichment shown in Figure 9 suggests that the channel samples had been preferentially taken from low-Zn parts of the seam in a mine from the NW coal region. Zinc is concentrated in structurally disturbed zones of the seam which are mined but were not channel-sampled.

Because the channel samples were analyzed for fluorine (F) by an old technique, which tends to underestimate F in many coal samples [Wong et al, 1992], the F data from the channel samples and from as-shipped coals cannot be compared to evaluate the fate of F during coal preparation. At present, F analysis is carried out according to Australian hydropyrolytic procedure standard AS1038.10.4-1989.

The natural radioactivity of coal, which is derived from the decay of Th-232, U-238 and U-235, and K-40, can be calculated from the observed masses (weights) of U, Th, and K [Cahill, ISGS, personal communication]. The calculated radioactivity data for coals agres with observed radioactive measurements [Coles et al., 1978]. Table 5 shows that for cleaned Illinois coals, the contribution to radioactivity from U and Th is relatively small compared to that from K, which contributes to background radioactivity not only in coal but in all natural environments.

SUMMARY AND CONCLUSIONS

A database on trace elements in channel samples of Illinois coals was used to show the degree of reduction of key environmental elements in 34 as-shipped coals from Illinois mines collected and analyzed for this study. The results indicate that the state-wide mean concentrations of all tested trace elements, except U, are reduced in the cleaned coals relative to those in the channel samples that represent coal in place prior to mining. Because elemental concentrations in coal vary widely from place to place and coal to coal, only mean concentrations from a large number of channel and as-ehipped samplee should be compared. Better yet, washability studies on individual samples should be done to assess the degree and limit of the removal of trace elements from coal during coal preparation.

ACKNOWLEDGEMENTS

We thank Illinois coal companies for their cooperation in obtaining samples of their as-shipped coals. We also thank H. H. Damberger and W. T. Frankie for their help in the collection of the samples. This research was funded in part by the Illinois Department of Energy and Natural Resources through its Coal Development Board and Illinois Clean Coal Institute and by the U.S. Department of Energy. However, any opinions, findings, conclusions, or recommendations expressed herein are those of the authors and do not necessarily reflect the views of IDENR, ICCI, and US DOE.

REFERENCES

Capes, C.E., McElhinney, A.E., Russell, D.S., and Sirianni, A.F, Environmental Science & Technology, 8 (1), 35 (1974).

Cavallaro, J.A., Deurbrouck, A.W, Schultz, H., Gibbon, G.A., and Hattman, E.A., A Washability and Analytical Evaluation of Potential Pollution From Trace Elements in Coal. US EPA, EPA-600/7-78-038, Washington, D.C (1978).

Clarke, L.B. and Sloss, L.L., Trace Elements- emission from coal combustion and and gasification. IEA Coal Research, IEACR/49, London (1992).

Coles, D.G., Ragaini, R.C., and Ondov, J.M., Environmental Science and Technology, 12, 442 (1978).

Finkelman, R.B., Modes of Occurrence of Trace Elements in Coal. US Geological Survey, Open File Report, OFR-81-99 (1981).

Gluskoter, H.J., Ruch, R.R., Miller, W.G., Cahill, R.A., Dreher, G.B., and Kuhn, J.K., Illinois State Geological Survey, Circular 499 (1977).

Harvey, R.D., Cahill, R.A., Chou, C.-L., and Steele, J.D., Mineral Matter and Trace Elements in the Herrin and Springfield Coals, Illinois Basin Coal Field: Illinois State Geological Survey Contract/Grant Report: 1983-4 (1983).

Illinois Pollution Control Board, Toxic Air Contaminants List, Title 35 Illinois Administrative Code, Part 232 (1990).

Norton, G.A. and Markuszewski, R., Coal Preparation, 7, 55 (1989).

Nriagu, J.O., Environment, 32, 7 (1990).

Nriagu, J.O. and Pacyna, J.M., Nature, 333, 134 (1988).

Public Law 101-549, Clean Air Act Amendments, Title 3, 104 Stat 2531-2535 (1990).

Swaine, D.J., J. Coal Quality, 8, 67 (1989).

U.S. National Committee for Geochemistry, Trace Element Geochemistry of Coal Resource Development Related to Environmental Quality and Health: National

Academy Press (1980).
Wong, A. S., Robertson, J.D., and Francis, H.A., J. Trace and Microprobe Techniques, vol. 10 (2,3), p. 169-181 (1992).

Table 1. Elements analyzed in project samples

Elements regulated* and analyzed	Other elements analyzed
Antimony	Aluminum
Arsenic	Boron
Beryllium	Calcium
Cadmium	Carbon
Chlorine	Copper
Chromium	Hydrogen
Cobalt	Iron
Fluorine	Lithium
Lead	Molybdenum
Manganese	Nitrogen
Mercury	Oxygen
Nickel	Phosphorus
Polonium #	Potassium
Radium #	Silicon
Radon #	Sodium
Selenium	Sulfur
Thorium	Titanium
Uranium	Vanadium
	Zinc

* Regulated by Public Law 101-549, 1990
\# Radioactive isotopes of these elements were calculated from the analytical concentrations of Th and U.

Table 2. Relative precision and methods for minor and trace elements

Element	Relative Precision	%	Average detection limit		Method* WDXRF	AAS	INAA	OEP	EDX	PyroIC
MINOR oxides										
Al_2O_3	ash	3	0.1	%	X					
CaO	ash	3	0.02	%	X					
Fe_2O_3	ash	3	0.01	%	X					
MgO	ash	5	0.1	%	X					
MnO	ash	5	0.01	%	X					
MnO	coal	7	3	ppm			X			
P_2O_5	ash	5	0.02	%	X					
K_2O	ash	2	0.01	%	X					
SiO_2	ash	1	0.1	%	X					
Na_2O	ash	5	0.05	%	X					
TiO_2	ash	3	0.01	%	X					
TRACE elements										
As	coal	7	1	ppm			X			
B	ash	15	10	ppm				X		
Be	ash	5	0.5	ppm				X		
Cd	ash	10	2.5	ppm		X				
Co	coal	5	0.3	ppm			X			
Cr	coal	10	7	ppm			X			
Cu	ash	5	2.5	ppm		X				
F	coal	10	20	ppm						X
Hg	coal	15	0.01	ppm		X**				
Li	ash	12	5	ppm		X				
Mo	ash	25	10	ppm					X	
Mo	ash	25	10	ppm				X		
Mo	coal	20	10	ppm			X			
Ni	ash	10	15	ppm		X				
Pb	ash	20	25	ppm		X				
Pb	ash	20	10	ppm				X		
Sb	coal	10	0.2	ppm			X			
Se	coal	10	2	ppm			X			
Th	coal	5	0.4	ppm			X			
U	coal	15	3	ppm			X			
V	ash	3	8	ppm				X		
Zn	ash	7	1.5	ppm		X				

* WDXRF - wave length-dispersive x-ray fluorescence spectrometry
AAS - atomic absorption spectrometry
INAA - instrumental neutron activation analysis
OEP - optical emission (photographic) spectrometry
PyroIC- pyrohydrolysis and ion chromotography
** Hg by cold vapor atomic absorption spectrometry

Table 3. Summary of sample types and seams in the ISGS database on trace elements in coal

	Samples from Illinois	Other states	Total no. samples
SAMPLE TYPES			
Channel & equivalent	222	67	289
Bench (partial seam)	158	11	169
Float-sink fractions	77	20	97
Run-of-mine	20	17	37
As-shipped	47	8	55
Shales & coal associated rock	240	13	253
All types	764	136	900
SEAMS			
Herrin seam (Ill. no. 6)	473	4	477
Springfield seam (Ill. no. 5)	166	20	186
Colchester seam (Ill. no. 2)	50	5	55
Other seams & rocks	75	107	182

Table 4. Ash content (dry, wt%), heating value (dry, BTU/lb), and trace element concentrations (dry, milligram per million BTU (mg/MBTU)) in channel samples and in as-shipped coals from Illinois

Sample type	Region		ash	BTU/lb	As	B	Be	Cd	Co	Cr	Cu	F	Hg	Li	Mn	Mo	Ni	Pb	Sb	Se	Th	U	V	Zn
Channel	all	mean	12.4	12532	506	3778	63	132	227	651	481	2320	6	565	2419	389	702	1426	44	90	78	71	1037	9094
		stddev	3.4	646	814	1810	37	339	147	365	338	1458	5	610	2014	301	422	1561	45	49	40	54	707	21753
		cases	186	195	201	190	199	90	198	198	200	167	161	112	193	170	196	191	201	197	142	111	200	204
	all (excluding NE)	mean	12.4	12535	497	3777	63	115	229	658	484	2420	6	518	2150	410	678	1464	43	90	78	73	1097	9292
		stddev	3.4	660	732	1900	39	330	148	377	344	1541	4	560	1715	313	337	1591	44	48	39	56	728	23145
		cases	159	167	175	166	171	81	172	172	172	141	136	92	166	148	168	167	175	171	121	99	172	176
	NE	mean	12.8	12511	562	3781	66	286	211	605	464	1779	8	781	4075	252	848	1167	51	92	79	54	670	7849
		stddev	3.5	566	1254	1010	19	393	143	271	303	675	6	783	2824	134	745	1336	54	52	50	35	401	9148
	NW	mean	12.8	12278	605	5167	86	334	254	693	612	1978	7	480	2670	395	818	2178	62	94	75	75	1117	21346
		stddev	3.0	590	1021	1515	54	621	216	413	397	794	4	372	1606	274	435	2530	67	58	48	42	633	44374
	SC	mean	12.0	12706	450	3237	52	42	247	608	473	2079	6	744	2061	289	664	1115	35	76	76	47	945	4478
		stdev	4.4	722	514	1050	27	45	111	408	492	620	4	1019	1365	294	277	758	22	33	48	33	546	4759
	SE	mean	11.8	12838	605	2260	63	55	224	610	445	2870	6	439	1891	515	623	1761	43	92	75	85	1247	6529
		stdev	3.3	627	721	1181	35	55	129	331	217	2455	5	224	2039	384	294	1402	34	55	30	79	998	9586
	SW	mean	13.3	12210	214	5653	46	29	185	757	408	2699	5	434	2159	382	182	512	27	96	89	73	993	5465
		stdev	2.5	412	376	1494	13	22	95	360	132	892	3	297	1518	182	274	383	32	35	29	40	363	4882
As-shipped	all (excluding NE)	mean	10.1	12952	263	3222	50	39	124	494	325	3325	3	334	1336	387	500	996	31	69	52	81	1088	3026
		stddev	2.4	476	292	1649	21	48	49	240	96	1435	2	263	1198	125	197	915	25	34	16	66	569	3122
		cases	34	34	34	34	26	12	34	34	34	34	34	34	34	19	34	30	34	34	34	32	34	34
	NW	mean	9.7	12860	209	4918	64	53	94	404	338	3005	3	147	1964	390	491	1427	32	63	41	77	722	3935
		stddev	2.5	435	203	1378	33	67	33	136	106	726	2	89	2116	106	270	1633	26	30	11	77	224	4755
	SC	mean	9.8	13069	330	2283	41	32	159	437	334	3169	2	579	1031	173	527	969	41	52	59	33	944	3116
		stdev	3.3	523	220	372	11	0	77	133	128	1092	1	445	662	0	192	704	41	12	24	8	347	4097
	SE	mean	9.6	13193	354	1788	46	26	135	440	290	2981	5	366	936	422	458	1127	30	63	52	106	1281	2012
		stddev	2.0	402	408	635	8	13	34	72	64	834	2	143	354	103	142	817	15	22	10	81	692	1061
	SW	mean	11.9	12473	83	4639	46	24	105	805	368	4675	2	265	1545	377	567	406	16	109	60	100	1423	3587
		stddev	1.8	254	17	302	9	16	21	419	92	2664	0	73	487	154	200	109	6	50	12	26	600	1087

Table 5. Natural radioactivity in as-shipped Illinois coals

Region		Th (ppm)	Th-232 series * (Bq/kg)	U (ppm)	U-238 series ** (Bq/kg)	U-235 series*** (Bq/kg)	K (ppm)	K-40 (Bq/kg)
All	mean	1.5	6.0	2.2	27.8	0.68	2039	63.2
	stddev	0.4	1.6	1.9	24.0	0.59	792	24.6
NW	mean	1.2	4.7	2.1	25.6	0.6	1676	51.9
	stddev	0.3	1.2	2.3	28.0	0.7	427	13.2
SW	mean	1.6	6.6	2.7	33.7	0.82	2122	65.8
	stddev	0.3	1.1	0.7	8.5	0.21	1559	48.3
SC	mean	1.7	6.8	0.9	11.7	0.29	2225	69.0
	stddev	0.6	2.4	0.2	2.7	0.07	650	20.2
SE	mean	1.5	6.1	2.9	40.0	0.90	2163	67.0
	stddev	0.2	1.0	2.4	29.2	0.72	515	16.0

* Th232, Ra228, Ac228, Th228, Ta224, Rn220, Po216, Pb212, Bi212, Po212, Tl208
** U238, Th234, U234, Th230, Ta226, Rn222, Po218, Pb214, Bi214, Po214, Pb210, Bi210, Po210
*** U235, Th231, Pa231, Ac227, Th227, Ra223, Pb211, Bi211

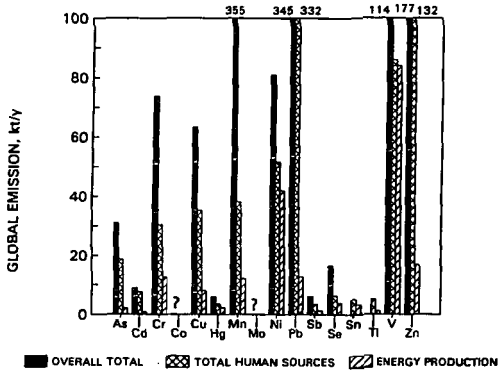

Figure 1. Global emissions of trace elements into atmosphere(after Nriagu, 1990).

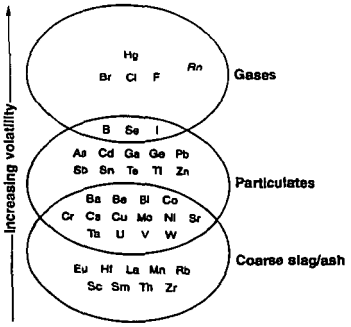

Figure 2. Behavior of trace elements during coal combustion and gasification (after Clarke and Sloss,1992).

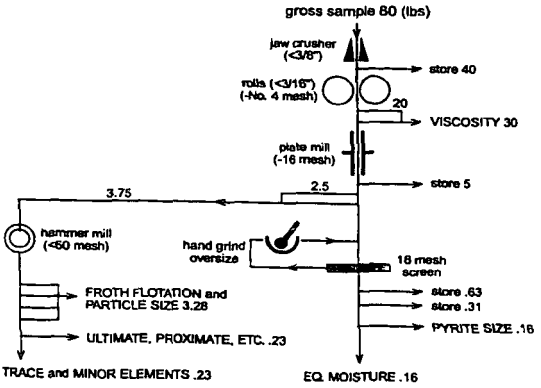

Figure 3. Flow chart for sample preparation. The weight (lbs) of the laboratory sample is given after the indicated test.

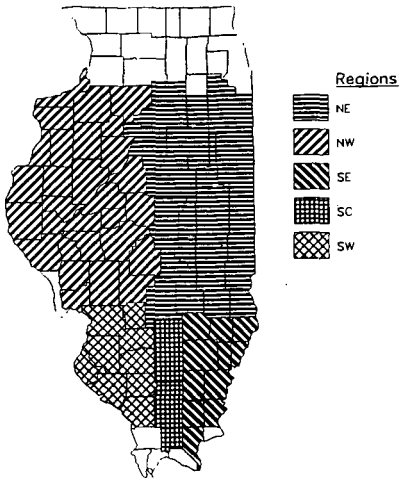

Figure 4. Sample regions of Illinois coal field.

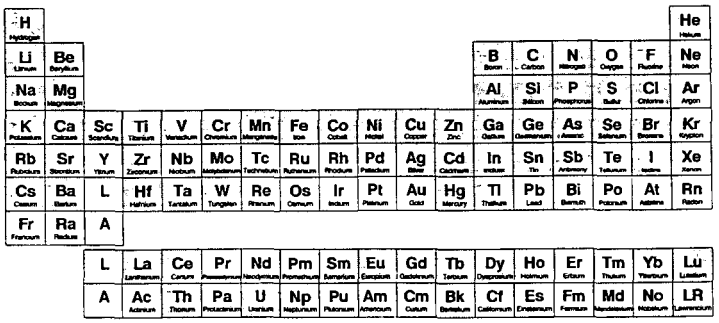

Figure 5. Analytical results on these 60 elements (shaded) are available for many sample-records in the ISGS database of trace elements in coal.

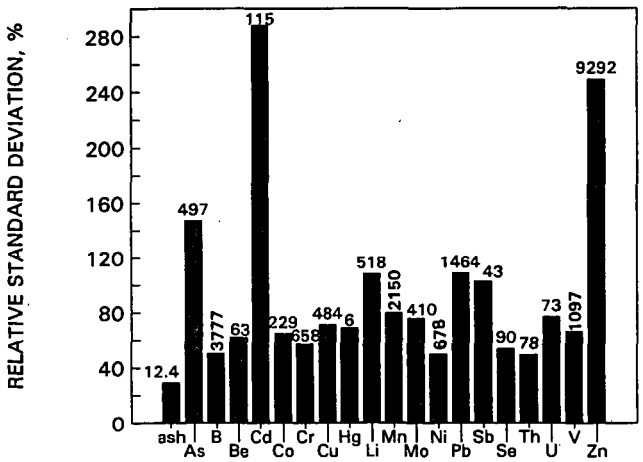

Figure 6. Variability of trace element concentrations in channel samples of Illinois coals, all regions (excluding NE region). Relative standard deviation was obtained by dividing standard deviation by mean and multiplying the result by 100. Numbers over bar indicate average concentrations of ash (wt%) or trace elements (mg/MBTU).

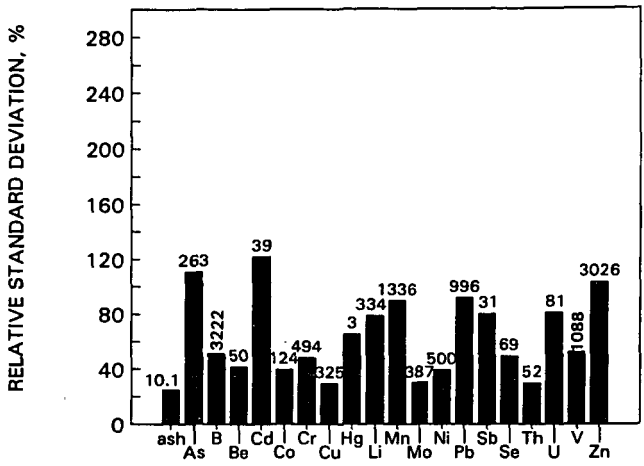

Figure 7. Variability of trace element concentrations in the 34 as-shipped coals, all regions (excluding NE region). Relative standard deviation was obtainsd by dividing standard deviation by mean and multiplying the result by 100. Numbers over bar indicate average concentrations of ash (wt%) or trace elements (mg/MBTU).

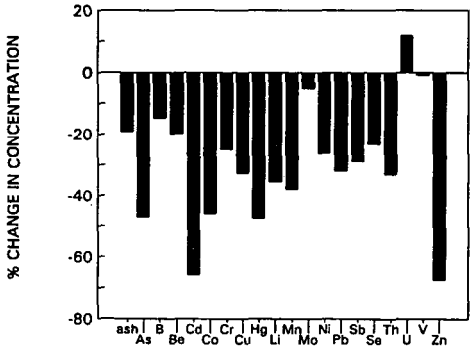

Figure 8. Reduction of trace element concentrations in as-shipped coals relative to those in the database channel samples, mean of state, excluding samples from NE region.

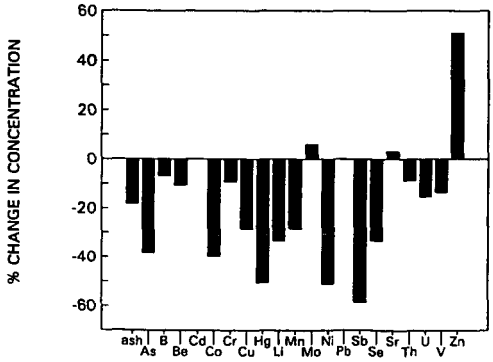

Figure 9. Reduction of trace element concentrations in the as-shipped coal relative to those in channel samples from a mine in the NW region. Data for Cd and Pb was not sufficient to compute the reduction for these two elements.

Surface Composition and Chemical State of Fe and Mo Impregnated Subbituminous Coal

Hengfei Ni, Richard K. Anderson, Edwin N. Givens, John M. Stencel
University of Kentucky Center for Applied Energy Research
3572 Iron Works Pike, Lexington, KY 40511-8433

Keywords: X-ray Photoelectron Spectroscopy, Coal Liquefaction, Catalyst, Iron, Molybdenum

ABSTRACT

The surface composition and chemical states of elements in samples of Wyodak subbituminous coal impregnated with Fe and Mo were investigated. The concentrations of Fe, Mo, S, Al, Si, Ca, C, O, and N were determined by x-ray photoelectron spectroscopy (XPS) in samples impregnated with 0.7-2.0 wt% Fe and 500-1000 ppm Mo. The metals were deposited on the samples by an incipient wetness technique using solutions of ferric nitrate, ferric sulfate, ferrous sulfate and ammonium molybdate. The effect of the metal precursor, the relative amounts of Fe and Mo loading, the effect of base-treatment with NH_4OH and the chemical states of the elements are discussed. Deconvolution of the overlapped S_{2s} and Mo_{3d} peaks is described along with a brief overview of the liquefaction performance of these coals.

INTRODUCTION

Highly dispersed iron-based catalysts have been extensively studied for direct coal liquefaction during the last several years. Cugini and his workers[1,2] found that finely divided and highly dispersed FeOOH-impregnated coals prepared by an incipient wetness technique have high activity in direct liquefaction. These coals were prepared by impregnating the surface of the coal with a solution of ferric nitrate followed by precipitation of FeOOH using an excess of NH_4OH. The influence of several parameters in the preparation procedure on the surface chemistry and performance of the impregnated coals was previously reported.[3]

Considerable research has been directed toward exploiting the improved liquefaction performance of mixed Fe and Mo catalyst.[4,5] Garg, et al., found higher conversion and oil yields by simultaneously impregnating coal with 1% Fe and 0.02% Mo using solutions of 10% ferrous sulfate and 0.5% ammonium molybdate.[6] The iron sulfates are among the least expensive form of iron compounds that are available because of their abundance as a by-product from the iron and steel industry. Andres, et. al.,[7] prepared Mo-free impregnated coals using aqueous solutions of $FeSO_4$ and reported poor reproducibility of the impregnation technique and relatively low catalytic activity in liquefaction. Pradhan, et al.,[8] reported increased activity for direct liquefaction of subbituminous coal with sulfated α-hematites containing small amounts of added Mo.

Since Mo is expensive, its application in liquefaction will depend on maximizing activity at low concentrations while simplifying the preparation in order to minimize catalyst processing costs. In order to optimize the metal function, it is necessary to understand the surface chemistry of the catalytic components. The present study extends the investigation to coals impregnated with both ferric and ferrous sulfate and compares them with results previously reported using ferric nitrate. The effect of base precipitation and method of drying, whether in air or N_2 at atmospheric pressure or under vacuum, were determined for coals impregnated with 0.7-2.0 wt % Fe and 0.05-0.1 wt % Mo. The surface composition and chemical state of several surface elements were studied using XPS. The technique for measuring low concentrations of Mo by XPS is discussed.

EXPERIMENTAL

Materials - Reagent grade $Fe(NO_3)_3 \bullet 9H_2O$, $FeSO_4 \bullet 7H_20$ and $Fe_2(SO_4)_3 \bullet 5H_2O$ were purchased from Aldrich Chemical Co. and Wyodak coal from the Black Thunder Mine in Wright, Wyoming was provided by CONSOL, Inc. The ultimate analysis of the coal on a dry basis was as follows: carbon, 72.2%; hydrogen, 4.3%; nitrogen, 1.2%; sulfur, 0.5%; oxygen (by difference), 16.0%; ash, 5.8%.

Preparation of Impregnated Coals - Metal impregnated coal samples were prepared as described previously[3]. To as-received coal, which contained 21 wt% moisture, was added dropwise, while stirring, 0.25 ml per gram dry coal of ammonium molybdate solution followed by 0.5 ml per gram dry coal of aqueous Fe salt solution. For those samples treated with base, 1.54 M NH_4OH solution was added at an NH_4OH/Fe mole ratio of 139 and filtered. In some cases samples were further washed with water. All were dried to a final moisture content of 3-10%.

XPS Analysis - XPS analyses were performed on a LHS-10 Leybold-Heraeus spectroscope

as described previously[3]. The quantification of elemental concentrations was performed using background subtraction and element sensitivity factors. Mo measurements were complicated by the overlap of the S_{2s} peak with the Mo_{3d} peaks. Reference samples containing sulfated iron oxides were used to determine the correct position and the area under the S_{2s} peak. Knowing the area of the S_{2p} peak and the S_{2s}/S_{2p} ratio, the S_{2s} peak area was calculated. Subtraction of the S_{2s} peak area from the Mo_{3d} peak area provided a measurement of the Mo concentration.

RESULTS AND DISCUSSION

The surface composition of coals impregnated with the Fe^{++} or Fe^{+++} sulfates are shown in Table 1 and compared with coal impregnated with $Fe(NO_3)_3$ and precipitated as FeOOH by addition of NH_4OH (CH-31). The surface iron concentrations of the 0.77 wt% Fe-impregnated coals prepared from either Fe^{++} or Fe^{+++} sulfates were less than for the $Fe(NO_3)_3$ impregnated coal. For these same coals the sulfur concentrations on the surface are significantly less when base was used to precipitate the iron. Sulfate analysis of the NH_4OH filtrate from the base treatment of CH-51 indicated that all of the $SO_4^=$ ion had dissolved in the filtrate making the surface free of any sulfur and oxygen associated with the $SO_4^=$ ion. Although several of the NH_4OH preparations were further washed with water with the intention of removing sulfate, including CH-51, it was not necessary. The surface concentrations of Si and Al, and Ca for the 0.77 wt% Fe-impregnated coals, except for CH-502, decreased on the surface when base was used. There was no consistent bias from drying in air, nitrogen or under vacuum.

Surface concentrations of Fe-Mo impregnated coals are shown in Table 1. For those coals subjected to base precipitation (CH-6,CH-61), the Mo concentration is lower (CH-601,CH-604), presumably because part of the molybdate had partially dissolved in the NH_4OH solution. Coals impregnated with Mo at 500 (CH-61) and 1000 ppm (CH-6) had Mo concentrations on the surface of 1100 and 1400 ppm, respectively. For the non-base washed coals, to which 1000 ppm Mo was added, the final Mo levels were 3000 and 5100 ppm. The Fe concentrations of 2.3-3.0 wt% on Mo-impregnated coals were higher than for the Mo-free coals, but still tended to be lower than for the base-treated coals, of which CH-6 is at the lower end. The oxygen levels were slightly higher while the sulfur levels were significantly higher for the non-base treated samples indicating significant deposition of $SO_4^=$ on the surface relative to the $SO_4^=$-free ferric nitrate impregnated coals. The rather narrow range of oxygen concentrations on the surface for these 0.77 wt% Fe-impregnated coals (23.1-26.6) suggest that oxygen concentration is related to the iron surface concentration. Like the Mo-free coals, the surface concentrations of Si and Al decreased for the NH_4OH treated coals. No difference in Ca concentration was observed. There didn't appear to be any significant differences in the surface compositions of the Fe^{+++} and Fe^{++}-impregnated coals, even though in the preparations the instability of the ferrous salt solution was obvious. The original blue-green color of the $FeSO_4$ solution rapidly changed to yellow upon exposure to air during the application step. A slight deposit of particles was found in the beaker.

Surface Chemistry - The binding energies of the various elements are shown in Table 2. For both the Fe- and Fe-Mo-impregnated coals treated with base, binding energies for $Fe_{2p\,3/2}$ and Fe_{3p} were $\geq$711.1 eV and 56.0-56.6 eV, respectively. The O_{1s} binding energies for all the samples prepared with iron sulfates were $\geq$532.0 eV, except for the base-treated sample containing 2 wt% added Fe, CH-51. The $Fe(NO_3)_3$ impregnated coal had a lower O_{1s} binding energy (CH-31), which is consistent with the FeOOH structure. The higher binding energies, reported previously for the raw coal and low Fe concentrations[3], indicate the dominance of the Si and Al oxide structures. The $Fe_{2p\,3/2}$ peak for the non-base treated samples was broadened toward lower energy suggesting either more contribution from FeO, Fe_3O_4, or Fe_2O_3 type structure. Low-intensity peaks were observed in the sulfur region at 169.0-169.7 eV, specifically for the base-treated samples, and much more intense peaks were observed between 170.9-171.5 eV for the non-base treated samples. The latter are related to the abundance of $SO_4^=$ species present in the samples while the lower energy peaks are related to the background mineral sulfur content of the coal.

The $Ca_{2p\,3/2}$ and $Ca_{2p\,1/2}$ binding energies for the base-treated samples (347.2-347.5 eV) were lower than for the non-treated samples (349.8-350.1 eV). The lower binding energy observed for the treated coals is consistent with CaO while the higher energy of the non-treated coals is related to $CaSO_4$.

Molybdenum Analysis - The dual Mo_{3d} peaks were uniform for the Mo containing coals indicating that base-treatment had little effect on the bonding of the metal. The concentration of the metal was so small that no perturbation of the oxygen binding energy was observable. Quantification and characterization of Mo in the 500-1000 ppm range is difficult because it is close to the detection limit of XPS, even though the surface concentration is typically higher than the

bulk concentration. The S_{2s} peak overlaps with the Mo_{3d} peak measurement and is especially troublesome in samples having low concentrations of Mo and high concentrations of S. Pradhan, et al.,[8] employed a peak subtraction method to resolve this problem. Although the Mo_{3d} peak in the Fe-Mo-impregnated coals is broadened, peak deconvolution was performed based upon external standards and knowing the S_{2s} and Mo_{3d} peak positions and the relative intensities of the S_{2p} peak (169-171 eV), which is quite intense, and the S_{2s} peak. Standards were provided by Mo, Ni and W impregnated sulfated iron oxide samples. The S_{2s} and S_{2p} peak positions for $SO_4^{=}$ were at 169.5 eV and 232.6 eV, respectively. The relative intensity ratio of S_{2s}/S_{2p} was 0.45-0.52. The $Mo_{3d\,5/2}$ peak at 232.0 and $Mo_{3d\,3/2}$ at 235.1 agree with those observed for the Fe-Mo-impregnated coals. Subtraction of the half-height S_{2p} peak area from the measured Mo_{3d} peak area provided a reliable method for determining Mo concentration.

Liquefaction Performance - The Fe- and Fe-Mo-impregnated coals gave significantly higher THF conversion and oil yields than raw coal when reacted in tetralin at 415°C, 1 hour, and 1000 psi H_2 cold. As-received coal gave 85 wt% THF conversion and 43 wt% oil yield; Fe-impregnated coals gave THF conversions of 88-90 wt% and oil yields of 45-50 wt%; Fe-Mo-impregnated coals gave THF conversions from 88-93 wt% and oil yields from 51-52 wt%. The use of iron sulfate salts without base-treatment appears to provide increased THF conversion and oil yield compared to metal impregnation with either sulfate or nitrate salts followed by base-treatment.

Conclusions - 1. Fe concentrations on the surface of Mo-free coals, impregnated with either Fe^{++} of Fe^{+++} sulfates, were lower than obtained with Fe^{+++} nitrates.
2. Fe concentrations on the surface of Mo-Fe-impregnated coals, whether prepared from sulfate or nitrate salts, were intermediate between the Mo-free sulfate and nitrate preparations.
3. Fe on the surface of all of the sulfate-impregnated coals was not present as FeOOH, which was the dominant form for the nitrate-impregnated, base-treated coals.
4. Mo was present on the surface of the coal as MoO_3.
5. Sulfate is removed from sulfate-treated coals during the base-treatment step.
6. Sulfur, on the surface of the non-base-treated coals that were treated with sulfates, was present as $SO_4^{=}$.
7. Oxygen concentrations on the surface of all the 0.77 wt% Fe-impregnated coals fall within a narrow range.
8. Si, Al and Ca concentrations on the surface of the base-treated coals tend to be lower than for the non-base-treated samples.

ACKNOWLEDGEMENT

The authors gratefully acknowledge financial support provided by the Commonwealth of Kentucky and the U. S. Department of Energy under contract number DE-AC22-91PC91040. They also thank G. Thomas, M. Moore and W. Schram for the analysis of the coals and filtrates and T. Hager for supplying the sulfated iron oxides.

REFERENCES

[1]. Cugini, A. V.; Utz, B. R.; Krastman, D.; Hickey, R. F. *Prep. Pap. - Amer. Chem. Soc., Div. Fuel Chem.* **1991**, *36 (1)*, 91.
[2]. Utz, B. R.; Cugini, A. V. U. S. Patent 5,096,570, Mar. 17, 1992.
[3]. Ni, H. F.; Anderson, R. K.; Givens, E. N.; Stencel, J. M. *Prep. Pap. - Amer. Chem. Soc., Div. Fuel Chem.* **1993**, *38 (3)*, 1107
[4]. P. Courty and C. Marcilly, Preparation of Catalysts, edited by B. Delmon, P. A. Jacobs and G. Poncelet, 1976, Elsevier Scientific; New York; p 191.
[5]. Scaroni, A. W.; Derbyshire, F. K.; Abotsi, G. M. K.; Solar, J. M. Final Technical Report, DOE/PC/60050, June, 1987.
[6]. Garg, D.; Givens, E. N. *Fuel Processing Technology*, **1984**, 8, 123.
[7]. Andres, M.; Charcosset, H.; Chiche, P.; Djega-Mariadassou, G.; Joly, J. P.; Pregermain, S. *Preparation of Catalysts III*; Elsevier Science; New York, 1983, p 675.
[8]. Pradhan, V. R.; Tierney, J. W.; Wender, I. *Prep. Pap. - Amer. Chem. Soc., Div. Fuel Chem.* **1992**, *37 (1)*, 254.

Table 1. Surface Composition of Fe-Impregnated Coals[a], wt%

Number		CH-31	CH-51	CH-53	CH-503	CH-504	CH-52	CH-502	CH-501	CH-6	CH-61	CH-604	CH-601
Impregnating Salt[b]	none	FN	Fe^{+3}	Fe^{+3}	Fe^{+3}	Fe^{+3}	Fe^{+2}	Fe^{+2}	Fe^{+2}	FN-AM	FN-AM	Fe^{+3}-AM	Fe^{+2}-AM
Added Fe, wt% dry coal	none	0.77	2.0	0.77	0.77	0.77	0.77	0.77	0.77	0.77	0.71	0.77	0.77
Precipitated[c]	-	Y	Y	Y	N	N	Y	N	N	Y	Y	N	N
Washing	-	N	Y	Y	N	N	Y	N	N	N	N	N	N
Drying @ 40°C	-	Vac	Vac	Vac	N_2	Air	Vac	N_2	Air	Vac	Vac	Air	Air
Fe	0.33	4.2	7.9	1.5	1.6	1.9	1.2	1.9	0.8	2.5	3.0	2.3	2.5
Mo, ppm wt	-	-	-	-	-	-	-	-	-	0.14	0.11	0.51	0.30
Carbon	71.1	62.4	50.9	67.9	63.3	57.1	66.3	57.1	60.9	62.8	63.9	56.3	58.7
Oxygen	20.6	24.8	30.6	23.1	23.2	26.6	23.2	26.6	25.6	24.4	24.4	25.5	25.3
Nitrogen	1.3	1.2	1.0	1.1	1.0	1.0	1.3	1.0	1.0	1.5	1.4	1.5	1.2
Silicon	4.0	3.3	4.2	2.5	4.3	5.0	4.1	5.0	5.7	3.8	2.8	5.9	5.3
Aluminum	2.0	2.5	4.3	2.6	3.4	4.6	2.6	4.6	4.1	3.5	3.4	5.5	4.9
Calcium	0.5	1.0	0.9	0.8	1.2	1.5	0.8	1.5	0.8	1.3	0.9	1.0	0.8
Sulfur	0.2	0.6	0.2	0.4	1.9	2.4	0.4	2.4	1.2	0.03	0.03	1.4	1.1

a. Starting coal as "as-received" coal b. $FN = Fe(NO_3)_3 \bullet 9H_2O$; $F^{+3} = Fe_2(SO_4)_3 \bullet 5H_2O$; $Fe^{+2} = FeSO_4 \bullet 7H_20$; AM = Ammonium Molybdate
c. Precipitated with NH_4OH solution; Y = yes, N = no.

Table 2. Binding Energies of Elements in Fe and Fe-Mo Impregnated Coals

	Salt[1]	Base	Fe eV			O_{1s} eV	N_{1s} eV	Si_{2p} eV	Al_{2p} eV	Ca_{2p} eV		S_{2p} eV	Mo_{3d} eV	
			$Fe_{2p\ 3/2}$	$Fe_{2p\ 1/2}$	Fe_{3p}					$Ca_{2p\ 3/2}$	$Ca_{2p\ 1/2}$		$Mo_{3d\ 5/2}$	$Mo_{3d\ 3/2}$
CH-31	FN	Y	711.1	725.1	56.6	531.7	399.1	103.8	75.0	346.2	351.0	162.1 168.4	N.D.	N.D.
CH-51	Fe^{+3}	Y	711.3	725.1	56.6	531.7	399.5	N.D.	N.D.	N.D.	N.D.	163.3 167.0	N.D.	N.D.
CH-52	Fe^{+2}	Y	711.7	725.4	56.3	532.5	399.1	N.D.	N.D.	347.4	350.6	164.0 169.7	N.D.	N.D.
CH-53	Fe^{+3}	Y	711.5	725.6	56.2	532.4	400.0	103.6	N.D.	347.2	351.0	163.6 169.6 168.4	N.D.	N.D.
CH-501[2]	Fe^{+2}	N	710.5 711.8	727.5 725.9	54.1	532.9	400.2 396.6	104.5	76.1 74.2	349.9	353.1	163.2 171.2	N.D.	N.D.
CH-502	Fe^{+2}	N	710.0 711.4		55.6	532.6	399.8	104.1	75.6	349.8	353.3	163.3 171.1	N.D.	N.D.
CH-504	Fe^{+3}	N	710.9 711.4 711.9	726.6	56.4	532.7	400.7	104.1	75.4	350.1	353.9	163.6 171.5	N.D.	N.D.
CH-6	FN-AM	Y	711.3	724.8	56.1	532.2	399.6	103.0	74.8	N.D.	N.D.	164.8 169.2	232.4	235.9
CH-61	FN-AM	Y	711.3	725.1	56.0	532.0	399.8	N.D.	74.8	347.5	351.0	163 169	232.5	235.6
CH-601	Fe^{+2}-AM	N	709.8	727.4	53.5	532.6	400.1 392.3	104.0	73.3	349.9	354.0	164.3 171.2	232.5	235.4
CH-604	Fe^{+3}-AM	N	710.5	727.6	55.4	532.6	399.5 394.1	104.1	73.7	N.D.	N.D.	163.0 170.9	232.3	235.4

N.D. = not detected

1. FN=$Fe(NO_3)_3 \bullet 9H_2O$; F^{+3}=$Fe_2(SO_4)_3 \bullet 5H_2O$; Fe^{+2}=$FeSO_4 \bullet 7H_2O$; AM=Ammonium Molybdate 2. CH-501 Fe_{3s}=93.8 and 96.0 eV.

AN *IN SITU* EXAMINATION OF THE FE SPECIES IN THE ARGONNE PREMIUM COAL SAMPLES USING X-RAY ABSORPTION SPECTROSCOPY

Stephen R. Wasserman, Randall E. Winans, and Kathleen A. Carrado
Chemistry Division
Argonne National Laboratory
9700 S. Cass Ave.
Argonne, IL 60439

Keywords: XAS, XANES, EXAFS, iron, coals, neural networks

Introduction

The elucidation of the inorganic materials within coals is particularly important for coal processing, since these compounds may function as *in situ* catalysts for coal liquefaction. In addition, these species will have to be separated from the organic compounds prior to the use of coal as a fuel or chemical feedstock, a process that will be facilitated by detailed knowledge of the materials to be removed. In recent years, X-ray absorption spectroscopy (XAS) has been used to probe the trace transition metals which are contained within the matrix of coals,[1,2] as well as the nitrogen[3] and sulfur[4] functionality within organic coal constituents. Here we present the results of XAS studies, both near edge (XANES) and extended fine structure (EXAFS), on the iron species present within the eight Argonne Premium Coal Samples (APCS). Our aim is to provide at least a semi-qualitative analysis of the composition of the iron moieties in these particular coals. Previously the determination of Fe species in coals has been the province of Mössbauer spectroscopy[5,6] although the surface iron species of the Argonne coals have also been examined by XPS.[7] Because of the availability of these alternative methods for analyzing iron, XAS has not been applied, in general, for this element. Here we compare the results from XAS with those previously found by Mössbauer spectroscopy for the Argonne premium coals.[6]

Experimental

X-ray absorption spectra were taken on fresh Argonne Premium Coals, which were removed from their containers and mounted in holders two days prior to acquisition of the spectra. The absorption spectra were acquired at beamlines X23-A2 and X19A of the National Synchrotron Light Source. The beamlines were equipped with Si[311] (X23) and Si[220] (X19) double crystal monochromators. Harmonics were rejected on X19 by detuning of the monochromator. Transmission spectra were collected using ion chambers with nitrogen fill gas. A Lytle detector with argon fill gas was utilized for the fluorescence data. The energy calibration was maintained by monitoring the maximum at 7112 eV in the derivative spectrum of Fe foil. The reported data are the average of 2 scans.

Results

For convenience we have divided the eight Argonne Premium Coals into two groups of four. The first set consists of those coals that contain significant amounts of pyrite, FeS_2. The Upper Freeport, Illinois, Pittsburgh, and Blind Canyon coals fall into this category. The absorption edges and radial structure functions for these samples are shown in Figure 1. The radial functions indicate the presence of long-range order about the iron, at least out to 8 Å.

The second set consists of the Wyodak-Anderson, Pocahontas, Lewiston-Stockton, and Beulah-Zap coals. Figure 2 presents the absorption edges and radial functions for these materials. In some of these samples, in particular the Beulah-Zap, the presence of pyrite is detected. But within this subset, both the absorption edges and the radial distributions indicate that the iron species are present in a variety of different structures. The Wyodak-Anderson and the Beulah-Zap apparently contain similar mixtures of iron species, since the absorption edges are nearly identical. The EXAFS spectra suggest that, at least qualitatively, the other iron compounds in these four coals are not as well ordered as pyrite.

The analysis of mixtures of materials by XAS is somewhat problematical. We have used a new approach based on neural networks to separate the individual iron components.[8] The advantage of this method is that spectra of standard compounds which exactly match the components of the system are not required. There is, however, an accompanying loss in numerical precision. The network was trained with authentic spectra of FeO, Fe_2O_3, and FeS_2, as well as simulated mixtures of these materials. These standards effectively provide a method for distinguishing between ferrous, ferric, and pyritic species in the coals. The resulting network was then verified using ferrous ammonium sulfate, magnetite (Fe_3O_4), and a pyrite whose spectrum differed markedly in intensity from that which was used in the training process. Finally the network was used to analyze the near edge (XANES) spectra for each of the Argonne coals. The results of this analysis are shown in Table I. The numbers in parenthesis, when present, indicate the actual results from the neural network. Comparisons on duplicate samples indicate that these numbers are accurate to ± 10 % absolute.

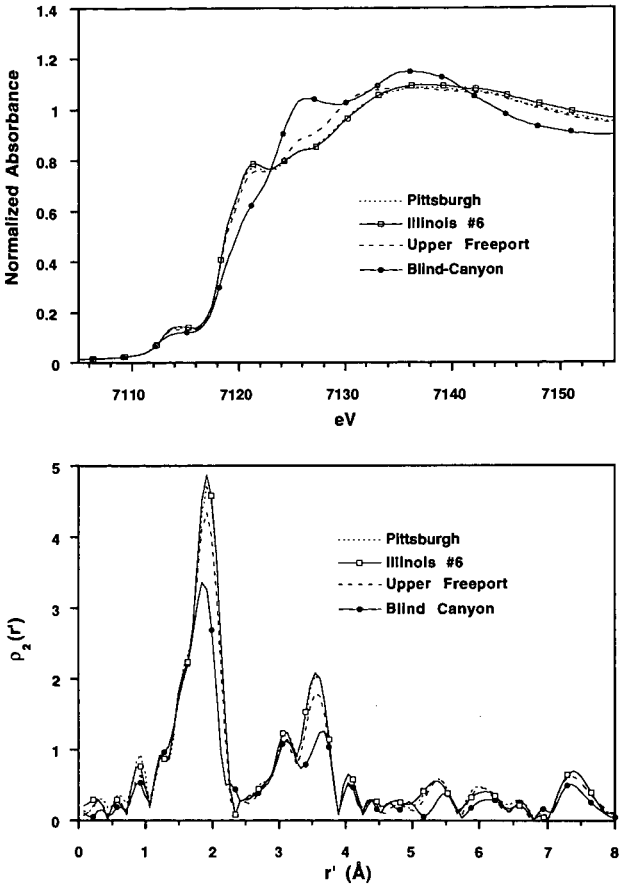

Figure 1. **(top) X-ray absorption near edge spectra (XANES) and (bottom) radial structure functions for iron in Upper Freeport, Illinois #6, Pittsburgh #8, and Blind Canyon Coals**

Table 1

Iron Composition of Argonne Premium Coals

Coal	Ferrous (%)	Ferric (%)	Pyritic (%)
Upper Freeport	10	2	88
Wyodak-Anderson	7	59	32
Illinois #6	0 (-2)	0	100 (104)
Pittsburgh #8	0	0	100 (101)
Pocahontas #3	90 (111)	10 (12)	0 (-20)
Blind Canyon	28	8	62
Lewiston-Stockton	51	43	5
Beulah-Zap	0 (-3)	52	48

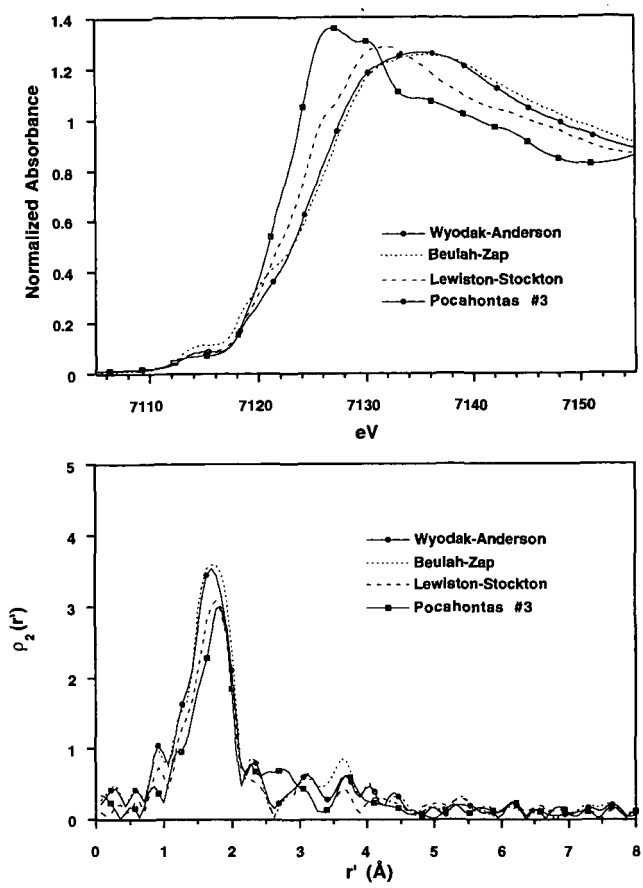

Figure 2. **(top) X-ray absorption near edge spectra (XANES) and (bottom) radial structure functions for iron in Wyodak-Anderson, Beulah-Zap, Lewiston-Stockton, and Pocahontas #3 Coals**

For seven of the eight coal samples, the results appear reasonable. However, in the case of Pocahontas, our analysis yields a significant negative percentage of pyrite, while the ferrous composition is over 100 %. We deduce that the Pocahontas coal consists primarily of ferrous species, but that the compounds present are not well represented by FeO. The XANES and EXAFS spectra for this coal support this supposition. The edge spectrum of Pocahontas does not coincide with those of the other coals. In addition, there is an extra peak in the radial structure function at 2.6 Å which is not found in the other premium samples. Both these observations indicate that the iron species in Pocahontas is unique among the APCS.

The iron compositions presented here are in approximate agreement with those from Mössbauer spectroscopy[6] for the Upper Freeport, Illinois #6, Pittsburgh #8 and Blind Canyon coals. Significant discrepancies exist between the Mössbauer and XAS analyses for the remaining four samples. The question remains as to which technique results in the more reliable analysis. Fortunately, the radial structure functions provide an independent check on the pyrite content deduced from the analysis of the XANES spectra. The peak in the radial distribution at 3.6 Å primarily results from an Fe-Fe interaction in pyrite.[9] Figure 3 plots this feature for six of the APCS. (Pocahontas is omitted for the reasons discussed above, while the iron content of Illinois #6 is virtually identical to that in Pittsburgh #8). The intensity of this feature clearly correlates with the pyrite content as deduced from the near edge spectra.

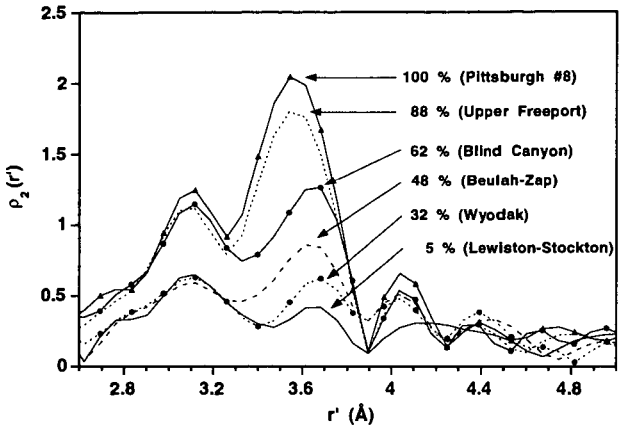

Figure 3. **Intensity of Fe-Fe scattering in pyrite from EXAFS. The percentages of pyrite are those determined from XANES.**

Summary

We believe that XAS can reliably assign the various iron species present in coal in terms of Fe(II), Fe(III), and pyritic constituents. A search for the best representation of the iron species in Pocahontas is underway, since it does not appear to be well represented by the standards used in this investigation.

In addition, the application of neural networks to the analysis of XANES spectra has been demonstrated for the first time. This approach appears to be a viable method for the analysis of complex mixtures.

Acknowledgment

We would like to thank F. W. Lytle for providing several of the spectral standards for the neural network and K. Pandya for aid in obtaining some of the preliminary spectra for this study. This work was performed under the auspices of the Office of Basic Energy Sciences, Division of Chemical Sciences, U. S. Department of Energy, under contract number W-31-109-ENG-38.

References

1. Huggins, F. E.; Shah, N.; Zhao, J.; Lu, F.; Huffman, G. P. *Energy Fuels* **1993**, *7*, 482-489.

2. Huggins, F. E.; Helble, J. J. ; Shah, N.; Zhao, J.; Srinivasachar, S.; Morency, J. R.; Lu, F.; Huffman, G. P. *Prepr. Div. Fuel Chem. Am. Chem. Soc.* **1993**, *38*, 265-271.

3. Mitra-Kirtley, S.; Mullins, O. C.; Branthaver, J.; van Elp, J.; Cramer, S. P. *Prepr. Div. Fuel Chem. Am. Chem. Soc.* **1993**, *38*, 762-768.

4. George, G. N.; Gorbaty, M. L.; Kelemen, S. R.; Sansone, M. *Energy Fuels*, **1991**, *5*, 93-97.

5. Montano, P. A. *Coal Structure, Advances in Chemistry Series, Vol. 192*; Gorbaty, M. L. and Ouchi, K., Eds., American Chemical Society: Washington, D. C., 1981, pp. 337-361.

6. Shah, N.; Keogh, R. A.; Huggins, F. E.; Huffman, G. P., Shah, A.; Ganguly, B.; Mitra, S. *Prepr. Div. Fuel Chem. Am. Chem. Soc.* **1990**, *35*, 784-792.

7. Kelemen, S. R.; Gorbaty, M. L.; George, G. N.; Kwiatek, P. J. *Energy Fuels*, **1991**, *5*, 720-723.

8. Freeman, J. A. *Simulating Neural Networks with Mathematica*, Addison-Wesley Publishing Company: Reading, Massachusetts, 1994.

9. Brostigen, G.; Kjekshus, A. *Acta Chem. Scan.* **1969**, *23*, 2186-2188.

PATHWAYS AND MECHANISMS FOR THERMOLYSES OF METHYLATED ACENES

P.S. Virk and V.J. Vlastnik
Department of Chemical Engineering
M. I. T., Cambridge, MA 02139

KEYWORDS: Thermolysis, Reaction Paths, Kinetics, Demethylation, Hydrogen Transfer.

ABSTRACT: Thermolyses of three methylated aromatic acenes, 9,10-Dimethyl-Anthracene (910DMA), 9-Methyl-Anthracene (9MA), and 1,4-Dimethyl-Naphthalene (14DMN), were studied to mimic the thermal decomposition of methyl-substituted aromatic moieties in coal and coal liquids. Experiments were conducted at temperatures from 315-550 C, initial substrate concentrations from 0.08-2.5 mol/l, and fractional substrate conversions, X, from 0.05-0.99. The observed thermolysis kinetics ranged from ~3/2 to 2 order wrt substrate, with activation energies ~45 kcal/mol. At fixed T = 370 C and [C]o ~0.85 mol/l, decomposition half-lives for (910DMA, 9MA, 14DMN) were respectively (9900, 23000, 530000) s. In general, three primary pathways operated during thermolysis of these methylated acenes. For 910DMA these were: (P1) Hydrogenation, to 9,10-Dihydro-9,10-Dimethyl-Anthracene, (P2) Demethylation, to 9-Methyl-Anthracene, and (P3) Methylation, to 1,9,10-Trimethyl-Anthracene (and isomers). These pathways further operate upon the primary products themselves, forming 9,10-Dihydro-9-Methyl-Anthracene, a host of Dimethyl-Anthracenes (1,9-, 1,10-, 2,9-, and 3,9-isomers), and Anthracene, as well as 1- and 2-Methyl-Anthraeenes. Observed initial selectivities to the primary hydrogenation, demethylation, and methylation products were respectively about 0.1, 0.3 and 0.1, while the selectivities to methane gas and to heavy products were respectively 0.2 and 0.2. A radical mechanism comprizing 10 elementary steps was proposed for 910DMA thermolysis at low conversions, and shown to aecount for the experimental observations.

INTRODUCTION

Motivation. The present work on thermolysis of methylated aromatic acenes is part of a continuing study [1,2] of simple substrates that mimic the chemical moieties found in complex fossil materials of engineering interest. The 910DMA, 9MA and 14DMN substrates were chosen becausc their acene rings are prototypical of the aromatic ring systems found in fossil materials, while their methyl groups model the electron-donating substituents commonly pendant thereon.

Previous Work. Neither 910DMA nor 14DMN thermolyses appear to have been studied previously. The literature contains two earlier references to 9MA thermolysis [3, 4].

Outline. We first describe the experiments and present results for the concentration histories, product selectivities, and kinetics observed during 910DMA thermolysis. These results are combined with data from 9MA and 14DMN thermolyses to provide general reaction pathways for the decomposition of multiply-methylated acenes. Finally, a radical mechanism comprizing 10 elementary steps is proposed for 910DMA thermolysis at low conversions, and shown to accommodate many of the experimental observations.

EXPERIMENTAL

Conditions. The upper portion of Table 1 summarizes conditions for the experiments, listing the model substrates, their structures and the ranges of temperatures, holding times and initial concentrations studied, as well as the temperatures at which light gases were analysed. Thermolyses were conducted in batch reactors, volume 0.6 ml, made from 1/4" stainless steel Swagelok parts. The reactors were charged with weighed amounts of biphenyl (internal standard) and substrate (say, 910DMA) totalling 0.30 g, sealed and placed in an isothermal, fluidized-sand bath for the appropriate holding times, after which they were quenched in ice-water, and their contents extracted into methylene chloride. Reactor contents were in the liquid phase during all experiments.

Assays. Gaseous and liquid thermolysis products were identified and analyzed by GC, augmented by GC/MS. All gas peaks were identified by injections of standards. Most liquid products were identified by injections of standards with some minor liquid products identified by determining their masses by GC/MS and relating their retention times to those of known molecules. Heavy thermolysis products, mostly dehydrogenated dimers of the substrates, were identified by GC/MS. For example, in 910DMA thermolyses, the MS of a prominent late GC peak showed a molecular ion at mass 410 and a fragment at mass 205, suggestive of a bibenzylic, dehydrogenated dimer of 910DMA. Product assay trains developed for each substrate using the preceding GC and GC/MS techniques typically identified ~15 reaction products. Identified products accounted for > 90% of the reacted mass at low substrate conversion, X < 0.4, and > 65% of the reacted mass at the highest conversions, X > 0.8. Experimental details are available [5].

RESULTS and DISCUSSION

Histories. Fig. 1 chronicles the concentration histories of substrate and products during thermolysis of 910DMA at T = 370 C and [C]o = 0.82 mol/l, using arithmetic coordinates of absolute mols J of either substrate or product present in the reactor versus reaction holding time t in seconds. Part (a), left panel, shows that the substrate 910DMA decayed monotonically, with half-life t* ~ 9000 s. The major products formed, in order of initial abundance, were 9MA, methane, abbr CH4, various trimethyl-anthracenes, abbr TMA, dihydro-dimethyl-anthracenes, abbr DHDMA, and anthracene, abbr ANT. The main product 9MA exhibited a maximum, characteristic of an intermediate in the demethylation sequence 910DMA → 9MA →

ANT. The formation of TMA and DHDMA products concurrent with 9MA shows that during 910DMA thermolysis, methylation and hydrogenation always occur in parallel with demethylation. Part (b), right panel, shows minor product histories, including those of the dimethyl-anthracene isomers, 1,9-, 1,10-, 2,9-, and 3,9-DMA, all of which arose subsequent to 9MA, the methyl-anthracene isomers, 1MA and 2MA, both of which arose subsequent to ANT, and the 9,10 dihydro- hydrogenated species, DHMA and DHA, both formed subsequent to their parent aromatic. The foregoing suggest that the minor 1,9-, 1,10-, 2,9-, and 3,9-DMA products originated by methylation of 9MA rather than the isomerization of 910 DMA substrate and also that 1MA and 2MA likely arose from methylation of ANT rather than isomerization of 9MA.

Selectivities. Fig. 2 depicts the preceding product history data as selectivity diagrams, with ordinate of product selectivity S = mols J produced/mol of substrate 910DMA decomposed, and abscissa of substrate fractional conversion X. Part (a), left panel, shows that the products formed at the lowest conversions were 9MA, TMA, and CH4 with selectivities respectively S = 0.35, 0.20 and 0.20, as well as DHDMA and ANT, with respective S ~ 0.06 and 0.03. With increasing conversion, 9MA selectivity remained roughly constant at S ~ 0.4 for X < 0.80, while TMA and CH4 exhibited mirror image selectivity decreases and increases, likely reflecting demethylation of the TMA; the selectivity of DHDMA decreased monotonically, to near zero at the highest conversions, while ANT selectivity increased monotonically, reflecting its position as demethylation terminus. The sum of the selectivities of all identified liquid products (circles) was ~0.75 over the major range of conversions, 0.2 < X < 0.8, from which the selectivity of unidentified, mostly heavy, product formation is inferred to be ~0.25.

Product Ratios. The importance of each of the observed hydrogenation, methylation, and methane formation pathways relative to the dominant demethylation pathway can be assessed from the respective primary product ratios R, namely R[DHDMA/9MA], R[TMA/9MA] and R[CH4/9MA]. Of these, the ratio of hydrogenation to demethylation, R[DHDMA/9MA] → 0.4 at the lowest conversions, X → 0, and then decreased rapidly to 0.04 ± 0.02 for X > 0.20. This variation of R[DHDMA/9MA] versus X was essentially independent of initial concentration and temperature, implying that the hydrogenation and demethylation pathways were of similar overall order wrt substrate and possessed similar activation energies. Fig. 3(a), left panel, shows that the ratio of methylation to demethylation, R[TMA/9MA] = 0.24 for X > 0.20 at all temperatures while Fig. 3(b), right panel, shows that the ratio of methane formation to demethylation, R[CH4/9MA] = 0.63 for X > 0.20 at T = 355 and 370 C. The sum R[TMA/9MA] + R[CH4/9MA] ~ 0.87 was close to unity, accounting for the methyl radicals implicitly associated with the demethylation pathway. It is interesting that ~3/4 of all methyl radicals formed were quenched by hydrogen abstraction, forming methane gas, while ~1/4 were trapped by addition to the 910DMA substrate, eventually appearing as TMAs.

Kinetics. Observed decomposition kinetics are illustrated in Fig. 4. Part (a), left panel, is a log-log plot of decay half-life t* versus initial concentration [C]o at fixed temperature. The data for 910DMA substrate (circles), spanning two decades of [C]o, describe a line of slope -1/2, which implies that the decomposition was of 3/2 order wrt substrate. Part (b), right panel, is an Arrhenius type of semi-log plot, showing decay half-life t* versus the reciprocal of a scaled absolute temperature $\Theta = 0.004573*(T\ C + 273.2)$. Data for 910DMA substrate (circles), spanning two decades of t*, define a line of slope ~43; on these coordinates, the slope is directly the activation energy of decomposition E*, in kcal/mol. Decay half-lives obtained for thermolyses of the other substrates, 9MA (squares) and 14DMN (triangles) are also shown in Fig. 4. Kinetics are summarized in Table 1, in the form of decay half-lives at T = 370 C, orders wrt substrate, and Arrhenius parameters (log A, E*). The relative decomposition rates of 910DMA, 9MA, and 14DMN were roughly in the ratio 1 : ~1/2 : ~1/50. All decompositions were of high order, between 3/2 and 2, wrt substrate, and exhibited activation energies ~45 kcal/mol.

Pathways. The concentration history, selectivity and product ratio observations detailed for 910DMA substrate were broadly echoed in thermolyses of the other two substrates, 9MA and 14DMN, as well. From these results, general decomposition pathways for multiply-methylated acenes containing, say, X total methyl substituents were deduced. Fig. 5 shows that three primary pathways operate in parallel upon the original X-Methyl Acene, namely: (P1) Hydrogenation, to the Dihydro-X-Methyl Acene, (P2) Demethylation, to the (X-1)-Methyl-Acene, and (P3) Methylation, to the (X+1)-Methyl-Acene. Too, the demethylated acene product is associated with formation of methane gas CH4, and the scheme also includes formation of a heavy bibenzylic dimer of the X-Methyl Acene. Further, the primary demethylation and methylation products in the above scheme can be secondarily operated upon by a pathway triad analogous to the one from which they arose, leading respectively to the formation of (X-2)- and (X+2)-Methyl Acenes, and thence, recursively, to all levels of methylation from the denuded parent to the fully methylated acene nucleus. In 910DMA thermolysis the primary pathway triad is (P1) Hydrogenation, to DHDMA, (P2) Demethylation, to 9MA, and (P3) Methylation, to TMA. Continued operation of this general pathway triad upon the primary products is evidenced by the appearance, at high conversions, of DHMA, a host of DMAs (1,9-, 1,10-, 2,9-, and 3,9-isomers), ANT, and 1MA and 2MA. Pathway results for all substrates are summarized in the bottom sections of Table 2, which show, in generalized form, major product selectivities and ratios at T = 370 C and conversions X = 0.05 and 0.4. Results for 9MA were qualitatively similar to those obtained for 910DMA, but showed a two-fold greater selectivity to the methylated product, and also roughly two-fold greater ratios of hydrogenated/demethylated and of methylated/demethylated products at low conversions. Results for 14DMN were noteworthy in that the hydrogenation pathway (P2) was essentially absent, with other product selectivities and ratios akin to those for 910DMA.

Mechanism. A possible mechanism for 910DMA thermolysis is presented in Fig. 6. This elementary step "graph" is constructed with substrate and all stable molecular products arrayed in the bottom row and unstable radical intermediates arrayed in the top row. Reaction "nodes", arrayed in the middle row, connect the individual species in the bottom and top rows with arrows indicating the initial direction of reaction (all reactions are, of course, reversible). Arrow thicknesses are set roughly proportional to elementary reaction traffic, as inferred from the observed product selectivities. Initiation reactions are denoted by solid interconnecting lines, propagation reactions by various kinds of dashed lines and termination reactions by dotted lines. The 910DMA substrate is in the middle of the bottom row, with light (propagation) products to its right and heavy (termination) products, to its left. The free-radical cycle is initiated by the bimolecular disproportionation of substrate (R1), an intermolecular hydrogen transfer reaction, to form the respectively dehydrogenated and hydrogenated radical species 910DMA* and HDMA*. Of these, the latter can either abstract hydrogen from 910DMA by (R2), to form DHDMA products, or undergo a β-scission type of radical decomposition by (R3), forming 9MA product and a methyl radical CH_3*. The CH_3* can either abstract H from 910DMA by (R4), to form methane product, or add to 910DMA by (R5), to form the trimethyl radical HTMA1*. The latter can then abstract H from 910DMA via (R6) to form the observed TMA product. The radical cycle is terminated by the species 910DMA* and HDMA* engaging in both pure- and cross-combinations, (R7-R9), to form various dimeric products. HDMA* radical can also terminate by disproportionation, (R10), to form 910DMA and DHDMA.

The proposed mechanism evidently accounts for most of the major products, 9MA, TMA, DHDMA, CH4 and heavies, observed during the initial stages of 910DMA thermolysis. Each of the observed triad of primary pathways, namely, P1 hydrogenation, P2 demethylation and P3 methylation, also arise naturally as limiting cases of the elementary step graph, with P1 comprising the set [R1, R2, R7], P2 the set [R1, R3, R4, R7] and P3 the set [R1, R3, R5, R6, R8]. The stoichiometry of these sets restricts the maximum selectivity of each major product to 1/3, which is of the magnitude of the highest selectivities actually observed. The mechanism also offers some theoretical insights. It suggests that the relative kinetics of the observed hydrogenation and demethylation pathways, (P1)/(P2), are essentially controlled by the HDMA* radical, through the ratio of its H-abstraction to β-scission reactions (R2)/(R3). Further, the observed methylation to demethylation pathway ratio, (P3)/(P2), is essentially governed by competition between methyl radical reactions (R4) and (R5), in which CH3* either abstracts H from or adds to the 910DMA substrate.

In future work it is hoped that the mechanism presented above will provide a basis for both the further quantitative modelling and numerical simulation of 910DMA thermolysis and also for the construction of new, analogous, mechanisms for 9MA and 14DMN thermolyses.

ACKNOWLEDGEMENT: This work was supported by Cabot Corporation, Boston, MA.

REFERENCES

[1] Virk, P.S.; Vlastnik, V.J.: PREPRINTS, Div. of Petrol. Chem., ACS, 38(2), 422 (1993).
[2] Virk, P.S.; Vlastnik, V.J.: PREPRINTS, Div. of Fuel Chem., ACS, 37(2), 947 (1992).
[3] Pomerantz, M.; Combs Jr., G.L.; Fink, R.: J. Org. Chem., 45, 143 (1980).
[4] Smith, C.M.; Savage, P.E.: A.I.Ch.E. J., 39, 1355 (1993).
[5] Vlastnik, V.J.: Sc.D. Thesis, Dept. of Chem. Eng., MIT, Cambridge, MA (1993).

Table 1. Experimental Grid, Kinetics, and Major Product Selectivities and Ratios for Thermolyses of Methylated Acenes.

Substrate		**910DMA**	**9MA**	**14DMN**
Structure		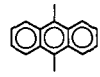	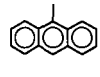	
Experimental Grid				
Temperature, T C		315-409	315-409	370-550
Holding Time, t s		450-57600	450-57600	150-115200
Initial Concentration, [C]o, mol/l		0.082-2.47	0.082-2.06	0.081-2.07
Gas Analyses at T C		335, 370	370	450
Kinetics				
Decay Half-Life, t* s at T = 370 C		9900	23000	530000
Order wrt substrate		1.53	1.50	2.05
Arrhenius Parameters (log A, E*)		(10.6, 43.1)	(11.4, 46.4)	(8.5, 42.0)
Product Selectivities at T = 370 C	**X**			
Demethylated	0.4	0.42	0.37	0.32
Methylated	0.4	0.10	0.22	0.10
Hydrogenated	0.05	0.06	0.03	0
Heavies	0.4	0.15	0.13	0.06
Product Ratios at T = 370 C	**X**			
[Hydrogenated/Demethylated]	0.05	0.21	0.43	0
	0.4	0.04	0.05	0
[Methylated/Demethylated]	0.05	0.35	0.69	0.54
	0.4	0.28	0.36	na

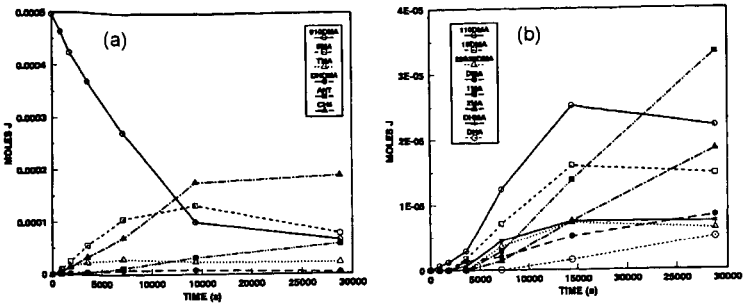

Fig. 1. Concentration Histories in 910DMA Thermolysis at T = 370 C and [910DMA]o = 0.82 mol/l. (a) Major and (b) Minor Products.

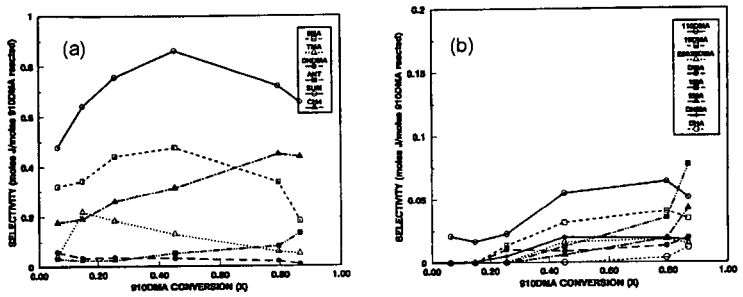

Fig. 2. Product Selectivities in 910DMA Thermolysis at T = 370 C and [910DMA]o = 0.82 mol/l. (a) Major and (b) Minor Products.

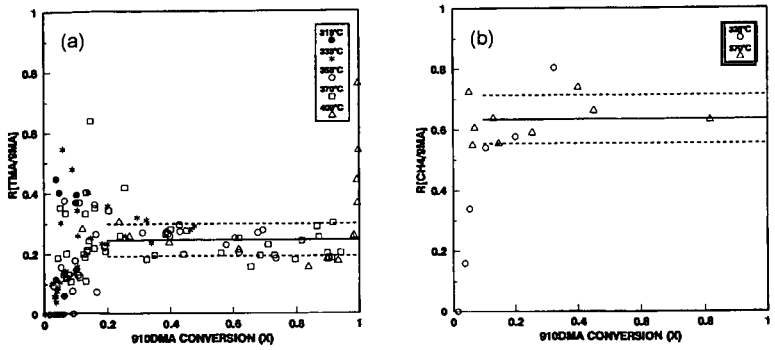

Fig. 3. Major Product Ratios in 910DMA Thermolyses at T = 315 to 409 C and [910DMA]o = 0.82 mol/l. (a) R[TMA/9MA] and (b) R[CH4/9MA].

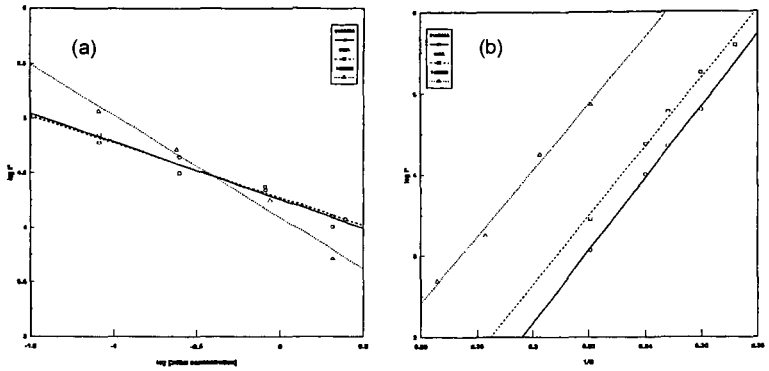

Fig. 4. Decay Half-Lives in Methylated Acene Thermolyses. (a) Effect of Initial Concentration at Fixed T = 355 C (910DMA), 370 C (9MA), and 450 C (14DMN), and (b) Effect of Temperature at Fixed [C]o ~ 0.85 mol/l (all).

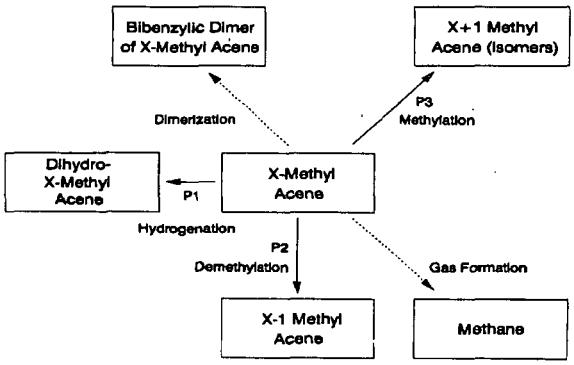

Fig. 5. General Decomposition Pathways for an X-Methyl Acene.

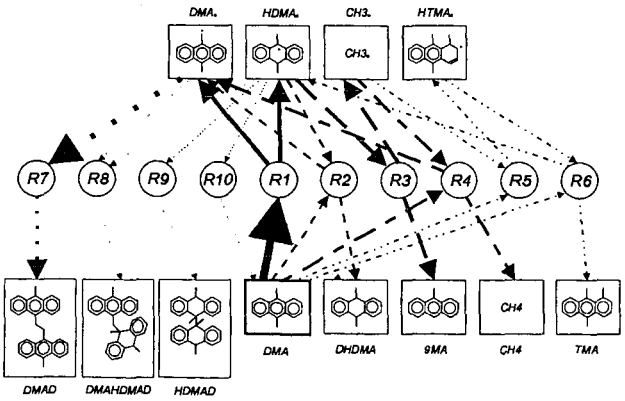

Fig. 6. Elementary Step Graph of 910DMA Thermolysis Mechanism Showing Relative Reaction Traffic at Low Substrate Conversions.

SULPHUR-CONTAINING PHENOL-FORMALDEHYDE RESINS TO MODEL THE THERMAL CHEMISTRY OF ORGANIC SULPHUR FORMS IN COALS

Khudzir Ismail, Gordon D. Love, Stuart C. Mitchell, Stephen D. Brown and Colin E. Snape

University of Strathclyde, Dept. of Pure and Applied Chemistry, Glasgow, G1 1XL, UK.

Keywords: Temperature programmed reduction, calibration, hydropyrolysis, retrogressive chemistry.

ABSTRACT

Non-melting silica immobilised substrates have previously been used to investigate pyrolysis behaviour and were shown to be ideal calibrants for temperature programmed reduction (TPR), with the SiO-C linkage stable at temperatures above 500°C. An alternative class of materials that should prove equally suitable are phenol-formaldehyde resins which enable model moieties to be incorporated into a highly cross-linked matrix. A series of sulphur containing co-resites have been prepared using phenol with, as the second component, dibenzothiophene, diphenylsulphide, phenylbenzylsulphide and thioanisole. A mole ratio of 3:1 (phenol to sulphur-containing component) was adopted to ensure that a reasonably high degree of cross-linking was achieved in the initial preparation of the resoles. The formation of the resites by curing the resoles at 200°C was monitored by solid state ^{13}C NMR. A resole has also been prepared from diphenyldisulphide but due to the comparable bond strengths of the S-S and C-O linkages, the curing temperature was reduced to 120°C to avoid cleavage of the disulphide bond. As well as being used as calibrants for TPR, the resites offer considerable potential for probing the influence of catalysts in hydropyrolysis and for investigating the effect of pyrolysis conditions on the interconversion of sulphides into thiophenes.

INTRODUCTION

In order to obtain insights into the complex reactions which occur during the pyrolysis and liquefaction of solid fuels, detailed structural information about the starting material and an understanding of how the different functionalities present behave under processing conditions are required. To achieve the latter aim, model compound studies performed in both the vapour and liquid phases have been used extensively [1]. However, a major drawback with such studies is the fact that the radicals generated via bond homolysis are mobile and free to diffuse independently prior to further reaction. In contrast, for solids such as coals and oil shales, many of the reactive intermediates remain covalently attached to the cross-linked macromolecular framework and thus their reactivity is subject to diffusional restraints.

In order to explore the effects of restricted mobility in multipathway free-radical reactions, Buchanan and coworkers pioneered work on model compounds immobilised on silica [2-4]. Recently, a series of silica immobilised diphenylalkanes and sulphur-containing substrates have been used at Strathclyde to study solid fuel pyrolysis phenomena. In addition, the sulphur-containing substrates have been used as calibrants for temperature programmed reduction (TPR) [5,6]; a technique based on the principle that different organic sulphur forms present in solid fuels have different characteristic reduction temperatures at which hydrogen sulphide (H_2S) evolves. Previously, the technique had met with only limited success, primarily because only

labile non-thiophenic forms were observed. Poor overall sulphur balances resulted, with virtually all the thiophenic sulphur remaining in the char due to the low pressures and the low boiling reducing agents used [7-10]. Further, little account has been taken of the reduction of pyrite to pyrrhotite and retrogressive reactions, particularly the conversion of sulphides into thiophenes. These drawbacks have been overcome by the use of a well-swept fixed-bed reactor operating at relatively high hydrogen pressures (up to 150 bar) [11,12]. Typically, over 70% of the organic sulphur is reduced to H_2S with the remainder being released in the tars. The use of effective catalysts, such as sulphided molybdenum can further improve the extent of desulphurisation [13].

In contrast to the reflux-type reactors used in low (atmospheric) pressure TPR studies [7-10] where liquids have been used for calibration, solids which do not soften prior to the onset of thermal decomposition are essential due to the nature of the well-swept high presure reactor [5,6]. In this respect, non-melting silica immobilised substrates are ideal, as demonstrated by immobilised benzene where the SiO-C linkage was found to be stable to *ca* 500°C, even in reducing atmospheres [14]. Immobilised samples of dibenzothiophene, diphenylsulphide, benzylphenylsulphide and thioanisole were subsequently prepared and used as calibrants [5,6] for both the well-swept high pressure and a reflux-type low pressure TPR reactor. Further, the substrates were found to be suitable for probing coal and oil shale pyrolysis mechanisms at temperatures in the range 400-600°C, generally used to maximise tar yields in both fluidised and well-swept bed reactors.

An alternative class of materials that should prove equally suitable are phenol-formaldehyde resins which offer the option of incorporating a wide variety of sulphur-containing moieties. A series of co-resites have been prepared using phenol together with a series of sulphur-containing precursors; 2-hydroxydibenzothiophene, *p*-hydroxydiphenylsulphide, 4-hydroxyphenylbenzylsulphide and 4-hydroxythioanisole, the same precursors used previously for the preparation of silica-immobilised substrates [5,6]. A resole has also been prepared using dihydroxydiphenyldisulphide (DHDPDS). This paper details the monitoring of the curing treatment by ^{13}C solid state NMR and the desulphurisation behaviour, of the formed resites, by high pressure temperature programmed reduction (TPR).

EXPERIMENTAL

Synthesis Thioanisole was the only commercially-available precursor used. 2-Hydroxydibenzothiophene was prepared via the base hydrolysis of the corresponding bromo derivative [15]. Benzene sulphinic acid was reacted with phenol using a modification of Hinsberg's method [16] to prepare 4-hydroxydiphenylsulphide. 4-hydroxyphenylbenzylsulphide was prepared by reacting 4-hydroxythiophenol with benzylbromide [17]. 4-hydroxythiophenol was oxidised with dimethyldithiobis(thioformate) to yield 4,4'-dihydroxydiphenyldisulphide [18].

The co-resites were prepared using the procedure described by Bar and Aizenshtat [19] with a phenol to formaldehyde mole ratio of 1:2.5. The mole ratio of phenol to the sulphur-containing component was 3:1 to ensure that a reasonably high degree of crosslinking was achieved in the intial resoles and *ca* 6 weight % sulphur was present in the final cured resites. Sodium hydroxide was used as catalyst in the condensation reaction with mole ratio of 0.1 with respect to phenol. The resites were cured in an oven purged with nitrogen gas at a temperature of 200°C. The resin containing DHDPDS was prepared without addition of phenol and was partially cured at the much lower temperature of 130°C to avoid cleaving the disulphide bonds.

^{13}C-NMR Analysis Solid state ^{13}C NMR was used to follow the removal of the ether/alcohol functional groups which occurred during curing. Cross polarisation/magic-angle spinning (CP/MAS) spectra were obtained using a Bruker MSL100 instrument operating at 25MHz for carbon. A contact time of 1 ms and a recycle delay of 1.5s were employed.

High pressure TPR Details on the high pressure system are described elsewhere [5,6,12,13]. As previously, a hydrogen pressure of 150 bar was used with a heating rate of 5°C/min over the range 100-600°C. Typically, between 0.2 and 0.3 g of the resite (particle size range of *ca* 0.1-1.0 mm) was mixed with 2-3 g sand. Hydrogen sulphide and other volatiles evolved were detected on-line using a quadrupole mass spectrometer (VG Sensorlab, 0-300 a.m.u).

RESULTS AND DISCUSSION

Characterisation of the co-resites The elemental compositions of the cured co-resites and the disulphide resole, together with their chloroform solubilities are listed in Table 1. These results indicate that the desired level of sulphur incorporation (*ca* 6% w/w) has been achieved and that the resites are macromolecular in character with chloroform solubilities below 1% w/w. The DHDPDS resole obviously contains a much higher sulphur content than the resites because of the disulphide linkage and the fact that phenol was not employed in the preparation.

Figure 1 shows the CP/MAS ^{13}C NMR spectra for the partially-cured (130°C) phenylbenzylsulphide and dibenzothiophene co-resites and Figure 2 compares the spectra for the partially cured dibenzothiophene resole and the corresponding resite cured at 200°C. The spectra of all four fully cured co-resites are shown in Figure 3. Table 2 summarises the assignments for the peaks observed. In the inital resoles, the peaks at *ca* 60 ppm and 73 ppm attributable to methylol carbon directly attached to the ortho or para position of the phenol ring and dimethylene ether carbons, respectively, dominate over the methylene bridge carbon peaks. In addition, the resoles display another intense C-O peak at *ca* 93 ppm due to hemiacetal carbons (OCH_2O). For the resites cured at 200°C, the spectra only contain aliphatic carbon peaks centred at 35 and 18 ppm with no major discernible peaks at 70 ppm from ether linkages.

Figure 1 indicates that the spectra of the partially-cured resites still contain major aliphatic C-O peaks which necessitated the use of a significantly higher curing temperature to eliminate all of the ether linkages. The peak at 18 ppm observed in all the spectra of the co-resites in Figure 3 is attributable to arylmethyl and, for dibenzothiophene and diphenylsulphide, its intensity is approximately one-quarter of that for the methylene peak at 35 ppm. The intensity of the 18 ppm peak in the case of the thioanisole resite is somewhat greater due to the contribution from S-CH_3.

High pressure TPR Figures 4-8 show the high pressure TPR evolution profiles of H_2S (m/z=34), and, where appropriate, CH_3SH (m/z=48), benzene (m/z=78), toluene (m/z=91) and methane (m/z=16), obtained for the four co-resites investigated. Figure 5 also shows the H_2S evolution profile for the DHDPDS resole. In addition, the desulphurisation behaviour of the dibenzothiophene co-resite was also investigated with a sulphided molybdenum catalyst (nominal loading of 0.4%w/w Mo) [13,14]; the H_2S evolution profile is shown in Figure 4.

For dibenzothiophene (Figure 4), the H_2S profile is remarkably similar to that for the corresponding immobilised substrate with the temperature of maximum evolution (T_{MAX}) being close to 500°C [6]. The use of the sulphided Mo catalyst does not significantly affect the T_{MAX}

although the H_2S profile is suprisingly sharper. The continuation of the H_2S evolution profiles above 500°C in both cases suggests that some condensation might be occurring to form larger thiophenic structures. The sulphur balance for the dibenzothiophene resite without catalyst, indicated that virtually 100% desulphurisation was achieved with *ca* 50% of the sulphur being released as H_2S with the remainder being in the tar collected.

The primary scission of the C-S bonds in the diphenylsulphide co-resite occurs at 330°C (Figure 5), similar to the characteristic reduction temperature found for the immobilised substrate [6]. The further release of H_2S at temperatures up to 600°C indicates that much of the sulphidic sulphur has been converted into complex thiophenes. The initial reduction is accompanied by the evolution of CH_3SH and the onset of toluene evolution (Figure 5) possibly via reactions with the methylene bridges. It is interesting to note that no benzene evolves below 400°C suggesting that the non-hydroxy substituted ring in the diphenylsulphide moieties may have been cross-linked by the curing process. The partially cured resole of DHDPDS gave a characteristic H_2S T_{MAX} below 300°C (Figure 5) which is similar to that found previously for cysteine [6]. However, the occurrence of secondary reactions leading to the formation of sulphides and complex thiophenes was indicated by over 70% of the H_2S evolving above 320°C.

For the phenylbenzylsulphide co-resite, initial H_2S evolution occurs at *ca* 280°C (Figure 6) from the primary scission of the C-S bond. The extent of secondary chemistry is again considerably greater than found with the corresponding immobilised substrate [6]. A significant amount of CH_3SH also evolves at 280°C from the C-S scission, together with some methane and toluene (Figure 6). As with diphenylsulphide no benzene was observed at low temperature presumably because it is still bound via the methylene linkages to the remainder of the resite.
Figure 7 indicates that, like its phenylbenzylsulphide counterpart, the thioanisole co-resite displays complex behaviour with the bulk of the H_2S evolving after the primary reduction of the C-S bond at *ca* 300°C. The initial H_2S release is accompanied by a considerable proportion of the sulphur evolving as methyl mercaptan.

General discussion Characteristic H_2S T_{MAX}s for the primary C-S bond scissions for the co-resites were very similar to their immobilised counterparts [6]. However, the nature and extent of secondary reactions clearly differ in each case with the co-resites generally displaying a much greater extent of retrogressive chemistry. This may be due to the much larger particle size used (0.1-1 mm, cf. <0.05 mm) and possibly the generation of many more diverse radical species during pyrolysis. The co-resites are, by nature, much more convenient to use than the immobilised substrates and the focus of future research will beto investigate the effects of dispersed catalysts in vehicle-solvent liquefaction, hydropyrolysis and batchwise hydrogenation.

ACKNOWLEDGEMENTS

The authors thank the Science & Engineering Research Council for financial support (Grant No. GR/J/08997).

REFERENCES

1. M.L. Poutsma, *Energy & Fuels* , 1990, **4(2)**, 113 and references therein.
2. A.C. Buchanan III and C.A. Biggs, *J. Org. Chem.*, 1989, **54**, 517.
3. A.C. Buchanan III, P.F. Britt and M.L. Poustma, *Prepr. Am. Chem. Soc. Div. Fuel Chem.*, 1990, **35(1)**, 217.

4. P.F. Britt and A.C. Buchanan III, *J. Org. Chem.*, 1991, **56**, 6132.
5. S.C. Mitchell, C.J. Lafferty, R. Garcia, K. Ismail, C.E. Snape, A.C. Buchanan III, P.F. Britt and E. Klavetter, *Prepr. Amer. Chem. Soc. Div. Fuel Chem.*, 1992, **37(4)**, 1691.
6. K. Ismail, R. Garcia, S.C. Mitchell, C.E. Snape, A.C. Buchanan III, P.F. Britt, D. Franco and J. Yperman, *Proc.1993 Int.Conf. on Coal Science*, Banff, September 1993.
7. A. Attar in *"Analytical Methods for Coal and Coal Products"*, Vol III, Academic, 1979, Ch.56 and DOE/PC/30145TI Technical Report.
8. B.B. Majchrowicz, J. Yperman, G. Reggers, J.M. Gelan, H.J. Martens, J. Mullens and L.C. van Poucke, *Fuel Process. Technol.*, 1987, **15**, 363.
9. B.B. Majchrowicz, J. Yperman, H.J. Martens, J.M. Gelan, S. Wallace, C.J. Jones, M. Baxby, N. Taylor and K.D. Bartle, *Fuel Process. Technol.*, 1990, **24**, 195.
10. B.T. Dunstan and L.V. Walker, *Final Report to Australian Nat. Energy Res. Dev. and Dem. Council* (1988).
11. C.J. Lafferty, S.C. Mitchell, R. Garcia and C.E. Snape, *Fuel*, 1993, **72**, 367.
12. S.C. Mitchell, C.E. Snape, R. Garcia, K. Ismail and K.D. Bartle, *Fuel*, accepted. Paper presented at Conference on "Coal and the Environment", Orlando, May, 1993.
13. R. Garcia, S.R. Moinelo, C.J. Lafferty and C.E. Snape, *Energy & Fuels*, 1991, **5**, 582.
14. S.C. Mitchell, C.J. Lafferty, R. Garcia, K. Ismail, C.E. Snape, A.C. Buchanan III, P.F. Britt and E. Klavetter, Energy & Fuels, 1993, **7**, 331.
15. N.M. Cullinane, C.G. Davies and G.I. Davies, *J. Chem. Soc.*, 1936, 1435.
16. G.E. Hilbert and T.B. Johnson, *J. Am. Chem. Soc.*, 1929, 51, 1526.
17. E. Miller and R.R. Read, *J. Am. Chem. Soc.*, 1933, **55**, 1224.
18. E.I. Stout, B.S. Shasha and W.M. Doane, *J. Org. Chem.*, 1974, **39(4)**, 562.
19. H. Bar and Z. Aizenshtat, *J. Anal. Appl. Pyrolysis*, 1991, 265.

Table 1 Elemental compositions and chloroform solubilities of the resites and the disulphide resole

Co-Resites/Resole	%C	%H	%S	% Solubility
Dibenzothiophene	72.3	4.2	5.4	< 1%
Diphenylsulphide	72.4	4.9	5.2	< 1%
Phenylbenzylsulphide	72.7	5.0	5.5	< 1%
Thioanisole	69.3	5.1	6.2	< 1%
Diphenyldisulphide	54.0	4.4	19.5	n.d

n.d = not determined

Table 2 ^{13}C NMR peak assignments the resoles and resites

Chemical Shifts (ppm)	Functional Groups Assignment
18	Arylmethyl, ortho position relative to the OH group
30, 35 and 40	2,2', 2,4 and 4,4'-methylene carbon, respectively
58-65	Methylol carbon, ortho or para position relative to the phenol ring, $ArCH_2OH$
68-73	Dimethylene ether linkages; $Ar\text{-}CH_2\text{-}O\text{-}CH_2\text{-}$
95	Hemiacetals, OCH_2O
110-135	Phenolic ring carbons other than C-OH
152, 160	Phenolic, C-OH; C-O, aromatic ethers

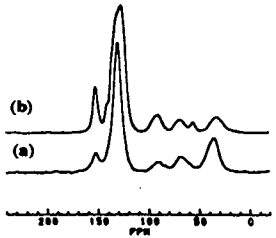

Figure 1 : ^{13}C NMR CP/MAS spectra of partially cured (130 °C) (a) phenylbenzylsulphide and (b) dibenzothiophene co-resites

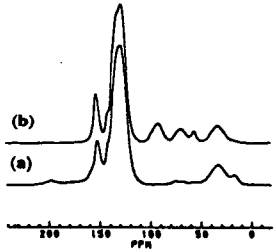

Figure 2 : ^{13}C NMR CP/MAS spectra of (a) fully cured (200 °C) and (b) partially cured (130 °C) dibenzothiophene co-resite

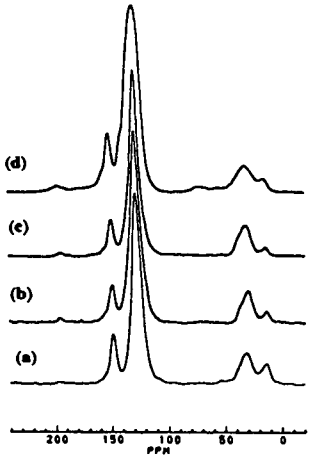

Figure 3 : ^{13}C NMR CP/MAS spectra of fully cured (200 °C) (a) thioanisole , (b) diphenylsulphide , (c) phenylbenzylsulphide , (d) dibenzothiophene co-resites

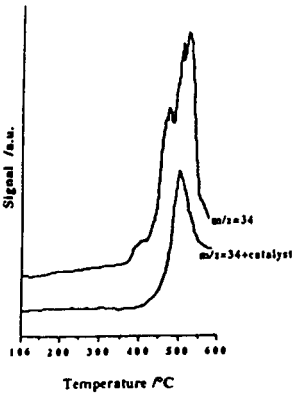

Figure 4: Hydrogen sulphide (m/z=34) evolution profiles for dibenzothiophene co-resite with and without catalyst

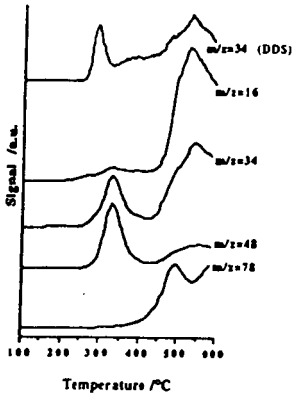

Figure 5: Evolution profiles for diphenylsulphide (m/z=16, 34, 48 and 78) and m/z = 34 for diphenyldisulphide (DDS)

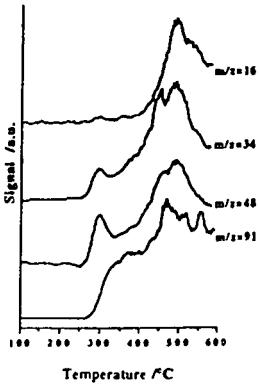

Figure 6: Evolution profiles for phenylbenzylsulphide (m/z=16, 34, 48 and 91)

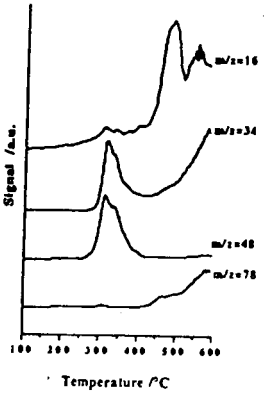

Figure 7 : Evolution profiles for thioanisole (m/z = 16, 34, 48 and 78)

INVESTIGATION OF PHYSICAL CONTROL MECHANISMS IN THE THERMAL DECOMPOSITION OF COAL BY MEANS OF ON-LINE MASS SPECTROMETRIC TECHNIQUES

Xiansheng Nie, Kui Lui, Waleed Maswadeh, Ashish Tripathi and Henk L.C. Meuzelaar

Center for Micro Analysis & Reaction Chemistry
University of Utah, Salt Lake City, UT 84112

KEYWORDS: novel TG/MS techniques; coal devolatilization mechanisms; heat and mass transport resistance

INTRODUCTION

During the past decade marked progress has been made with regard to our understanding of the chemical processes occurring during the thermal degradation ("devolatilization", "desorption + pyrolysis") of coal and several advanced mechanistic models offering a qualitative and quantitative description of these processes, e.g., FG-DVC [1] and CPD [2] models, are now available. By contrast, there appears to be a comparative lack of progress in the description and understanding of the physical processes involved. It is becoming increasingly clear that the frequent lack of interlaboratory reproducibility almost invariably originates within the physical parameters of the experiment. Although heating rate, particle size and reactor pressure have long been recognized as the dominant physical parameters influencing the rates and product yields of coal devolatilization processes [3,4], current models pay little or no attention to heat and mass transport limitations. In fact, particle size is not an input parameter in these models. Furthermore, although most industrial scale coal devolatilization processes occur at near ambient pressures, current renewed interest in high pressure coal conversion processes would seem to dictate a more detailed look at the effects of pressure.

The objective of the research reported here is to exploit the capabilities of two novel experimental techniques, based on the on-line coupling of microscale, TG-type reactors to mass spectrometry and combined gas chromatography/mass spectrometry systems. The TG/GC/MS techniques has high pressure TG capabilities [5] and will be described separately at this meeting [6]. The direct TG/MS instrument is characterized by a heated, all quartz interface and will be discussed here. The complementary nature of both systems enables us to investigate the nature and extent of physical control mechanisms over a broad range of experimental conditions.

EXPERIMENTAL

Materials - Two different particle sizes (-100 mesh and +65 -20 mesh) of all 8 ANL-PCSP coal samples (Beulah Zap, Wyodak, Illinois #6, Blind Canyon, Lewiston-Stockton, Pittsburgh #8, Upper Freeport and Pocahontas) and of a Blind Canyon DECS 6 sample were used. Only Beulah Zap and Blind Canyon DECS 6 were analyzed by high pressure TG/GC/MS. All sample ampoules were opened just before the experiment and stored under nitrogen at -26 C for max. 2 weeks.

Methods - The TG/MS system shown in Figure 1, consisting of a Perkin-Elmer TFS-2 microbalance (sensitivity 0.1 μg, accuracy 0.1%) and a Perkin Elmer 7 series high temperature furnace was operated at heating rates between 1 and 75 K/min up to temperatures of 750 C. An Extrel EL 1000 quadruple mass filter operating at 12 eV electron energy and a Teknivent Vector 2.2 interface combined with a PC based data system operating at scanning rates of 2.5 spectra/scan covering the 10-600 amu range.

Five to fifty mg aliquots of samples of coal were loaded into a regular platinum or specially-made "deep" gold crucible (Figure 1), and placed in the TG furnace where pyrolysis was performed in helium at atmospheric pressure. A 100 ml/min flow of helium was introduced through the top (95%) and bottom (15%) of the TG furnace. Between TG and mass spectrometer a special interface similar to an arrangement first described by Emminger and Kaisersberger [7], and consisting of concentric outer (15 mm i.d.) and inner (3 mm i.d.) quartz tubes reduces the pressure and transfers the vapor products. A countercurrent helium flow acts to direct the evolved gas and descending flows towards 80 μm dia orifices on the upper tips of the quartz tubes. All of the sample vapors are drawn through the outer orifice and about 5% of sample vapor is drawn through the inner orifice into the MS ion source region (10^{-6} torr). The short distances between sample holder and vapor sampling inlet (< 2 cm) and between inlet and MS ion source (< 15 cm) ensure vapor product response times <2 seconds, which minimizes secondary reactions. High pressure TG experiments were performed in a TG/GC/MS system consisting of a CAHN TG-151 high pressure TG, a capillary pressure reduction line, an automated vapor sampling inlet [8], a short column transfer line GC and a HP 5871 mass selective detector (MSD). A detailed description of the system is given elsewhere [5,6].

RESULTS AND DISCUSSION

Typical examples of the type of data produced by the TG/MS system are shown in Figure 2. Note how the total ion current profile clearly matches the DTG curve, due to the special direct interface which causes little or no condensation losses. In fact, the quartz nozzle directly below the crucible (see Figure 1) remains remarkably clean even when using relatively large (e.g., 40 mg) coal samples. It should be noted that the selected ion profiles at m/z 108, 122, 110 and 142 are prominent mass signals believed to represent primarily cresols, C2 phenols, dihydroxybenzenes and methylnaphthalenes, respectively. Note that the alkylphenol profiles virtually overlap, confirming their closely similar chemical nature and origin, whereas the dihydroxybenzenes (known to consist primarily of the *ortho*-form) start evolving at a somewhat lower temperature. Finally, the methylnaphthalenes profile at m/z 142 reveals a marked contribution from low MW, bitumen-like components evolving at lower temperatures. Detailed analyses and discussions of time-resolved pyrolysis MS and TG/MS profiles from various ANL-PCSP coals can be found in earlier publications [9,10].

Effects of Pressure - DTG profiles from Beulah Zap lignite (selected because of its high moisture content), obtained at 3 different pressures are shown in Figure 3 and reveal a marked shift (approx. 100 K) in the Tmax of the moisture loss peaks, whereas the Tmax of the relatively small volatile matter loss peaks, known to represent primarily pyrolytic bond scission phenomena [9,10], does not shift noticeably between ambient pressure and 900 psi. This is in obvious agreement with present insight into the underlying phenomena. Moisture desorption, primarily a transport process, is sensitive to pressure changes affecting transport parameters such as viscosity and diffusivity, whereas the primarily unimolecular (first order) decomposition reactions should be more or less insensitive to pressure as long as the reactions are under chemical control, i.e., relatively free of transport limitations. The bitumen desorption component of the methylnaphthalenes signal also shifts approx. 100 K towards higher temperatures at 900 psi (not shown here). However, it would be erroneous to conclude that transfer resistances do not play a measurable role during the pyrolysis step of TG experiments at higher pressures. As shown in Figure 4, a small but definite increase in char yield (66% vs 62%) is found at 900 psi. Char formation reactions in coal obviously involve two or more reactants, and thus cannot be regarded as first order.

Effects of Heating Rate - Figure 5 demonstrates the effect of heating rate on transport resistance in Pittsburgh #8 coal. The pseudo-Arrhenius plot shown in Figure 5 is produced simply by dividing the observed evolution rates of the cresol (m/z 108) ion signal by the corresponding percent of unreacted material (assuming 100% conversion of the m/z 108 precursor moieties). The resulting "rate at constant driving force" is then plotted in the well-known natural logarithm vs. inverse temperature format without attempting to extract any Arrhenius parameters. The resulting plot provides a sensitive test for the presence of transport control. This can be understood when assuming that in an ideal instrumental set-up with "zero" response time and under experimental conditions free of transport resistances the relationship between temperature and normalized reaction rate should be independent of heating rate for first order reactions. Between 9 and 15 K/min a relatively minor shift is observed, whereas between 15 and 25 K/min, a marked shift towards higher temperatures and lower (normalized) rates signals the rapidly increasing effect of transport control. At 25 K/min, also a clear increase in char yield is observed, especially when using larger samples (with regard to particle diameter and/or bed size). This is illustrated in Figure 6 for TG weight loss profiles of Illinois #6 coal samples. However, up to 9 K/min heat and mass transport resistances appear to be minor, even when using larger coal particles (+65, -20 mesh).

Finally, a highly sensitive probe of heat and mass transport resistances can be designed when using some of the most reactive tar components, namely the *ortho*-dihydroxybenzene signals at m/z 110, as markers for secondary tar reactions. In order to compensate for variations in sample size and experimental conditions, the abundance of the signal at m/z 110 is measured against the abundance of the cresol signal at m/z 108, thus effectively using the more stable cresols as an internal standard. A similar dihydroxyaromatic/monohydroxyaromatic ratio as a measure of tar stability has been proposed by McMillen et al. [11]. Although it might have been preferable to use even more stable tar components such as the methylnaphthalenes as internal standards, the substantial contribution of bitumen-like compounds to the methylnaphthalene signals at m/z 142 (see Figure 2) poses a problem. Since secondary tar reactions tend to increase with temperature and Tmax values increase at higher heating rates more secondary reactions are observed, as shown in Figure 7, which also illustrates the rapidly decreasing abundance of dihydroxybenzenes with increasing coal rank. This well known fact [12] may well limit the applicability of the m/z 110/108 ratio measurements to high volatile bituminous and lower rank coals. Figure 8 shows the combined effects of heating rate, particle size and bed depth on the m/z 110/108 ratio. At first approximation, the effects of each of these three parameters appear to be additive.

Particle and Bed Size Effects - More experiments need to be done at different bed depths since the only two depths (0.5 mm vs. 12.5 mm) investigated at this point represent rather extreme cases. It should be noted here that Figure 8 includes two control experiments. In order to eliminate the possibility that the difference in m/z 110/108 ratio's between the -100 mesh and +65 (-20) mesh samples could be due to chemical heterogeneities, a small aliquot of the 65 mesh coal sample was further ground to -100 mesh and found to exhibit the m/z 110/108 ratio typical of -100 mesh samples. Also, since the "deep" crucible required a larger amount of sample (40 mg) than the regular crucible (10 mg), a single run of a 40 mg sample was performed in the regular crucible (increasing the bed depth approximately 4-fold) and found to produce an m/z 110/108 ratio close to that of the regular 10 mg sample. In other words, bed depth, rather than total sample weight, appears to be the controlling factor. Closer examination of Figure 6 shows that mesh size and bed depth also do have a marked effect on char yield. These observations are echoed by the m/z 110 (dihydroxybenzene) evolution profiles in Figure 9, demonstrating the expected reduction in absolute yield as heat and mass transport resistances increase. All observations indicate that the dihydroxybenzene moieties play a significant role in the increase in char formation under transport controlled conditions. Dihydroxybenzenes are known to be prone to secondary reactions [11]. Nonetheless, all tar components appear to be involved to a varying degree with total tar yields decreasing by almost 50% when heating a 40 mg, +65 mesh sample of Illinois #6 coal at 25 K/min in a deep crucible (as compared to a 10 mg, -100 mesh sample at $\leq$ 10 K/min).

CONCLUSIONS

- Marked transport resistance effects on the evolution rates, yields and temperatures of key coal devolatilization products (moisture, bitumen, pyrolytic tar components) are observable under commonly used thermogravimetry conditions.
- Elevating reactor pressures to 900 psi increases the moisture as well as "bitumen" desorption Tmax values by approximately 100 K without causing a readily measurable shift in the bulk pyrolysis Tmax. However, at 900 psi, a small but consistent increase (3-5%) is seen in the amount of char formed.
- Char yield increases up to 10% are observed in ambient pressure TG experiments at higher heating rates, larger particle sizes and greater bed depth. Strong indications of increased physical control over cresol and dihydroxybenzene evolution rates are observed at heating rates above 10 K/min, particle sizes above 100 mesh and bed depths above 1 mm.
- The m/z 110/108 (primarily dihydroxybenzene/cresol) ratio is a highly sensitive indicator of increased heat and mass transport resistances as a function of heating rate, particle size and bed depth. Effects of particle size variation and bed depth appear to be additive.

ACKNOWLEDGEMENTS

This work was sponsored by the Advanced Combustion Engineering Research Center (funds for this Center are received from the National Science Foundation, the State of Utah, 23 industrial participants and the U.S. Department of Energy) and by the Consortium for Fossil Fuel Liquefaction Science (DOE grant no. UKRF-4-23576-90-10).

REFERENCES

1. Serio, M.A., Hamblen, D.G., Markham, J.R., Solomon, P.R., Energy & Fuels, 1987, 1, 138-152.
2. Fletcher, T.H., Kerstein, A.R., Pugmire, R.J., Solum, M.S., Grant, D.M., Energy & Fuels, 1992, 6, 414-431.
3. Howard, J.B., Peters, W.A., Serio, M.A. EPRI Report AP1803, EPRI, Palo Alto, CA, 1981.
4. Van Heek, K.H., Juntgen, H., Prepr. Pap. Am. Chem. Soc., Div. Fuel Chem., 1984, 29,2, 2-11.
5. Nie, X.; McClennen, W.H.; Liu, K.; Meuzelaar, H.L.C. Prepr. Pap. Am. Chem. Soc., Div. Fuel Chem., 1993, 38(4), 1147-1154.
6. Kui, L., Jakab, E., Meuzelaar, H.L.C., Prepr. Pap. Am. Chem., Div. Fuel Chem., 1994, in press.
7. Emminger, W.D., Kaisersberger, E., J. Thermal Anal., 1979, 17, 197-212.
8. Arnold, N.S., McClennen, W.H., Meuzelaar, H.L.C., Anal. Chem., 1991, 63, 289-304.
9. Yun, Y., Meuzelaar, H.L.C., Simmleit, N., Schulten, H.-R., Energy & Fuels, 1991, 5, 22-29.
10. Simmleit, N., Schulten, H.-R., Yun, Y., Meuzelaar, H.L.C., in "Advances in Coal Spectroscopy", Plenum Press, New York, 1992, 295-338.
11. McMillen, D.F., Malholtra, R., Chang, S., Nigenda, S.E., St. John, G., EPRI Report AP-4253-SR, EPRI, Palo Alto, CA, 1985.
12. Meuzelaar, H.L.C., Harper, A.M., Given, P.H., Proc. 5th ROMOCO Symp. 1982, 118, 192-202.

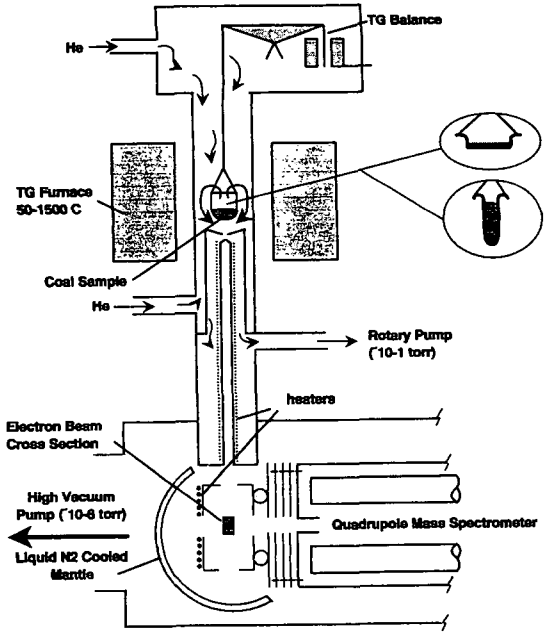

Figure 1. TG/MS system configuration. Note special flow arrangements and close proximity of crucible to concentric, heated quartz nozzles.

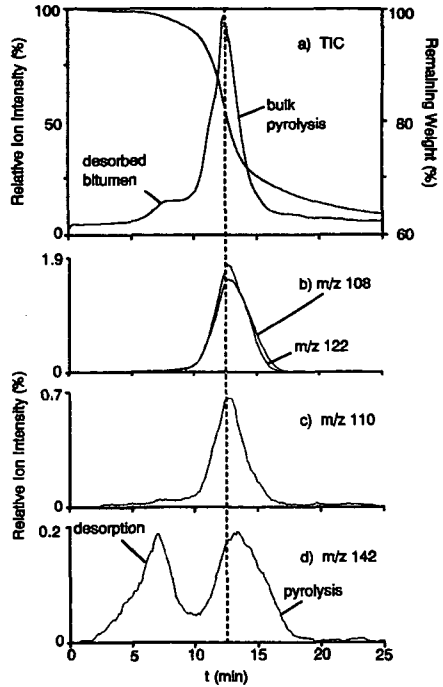

Figure 2. Example of time- and temperature-resolved TG and MS profiles from Pittsburgh #8 coal, as described in text.

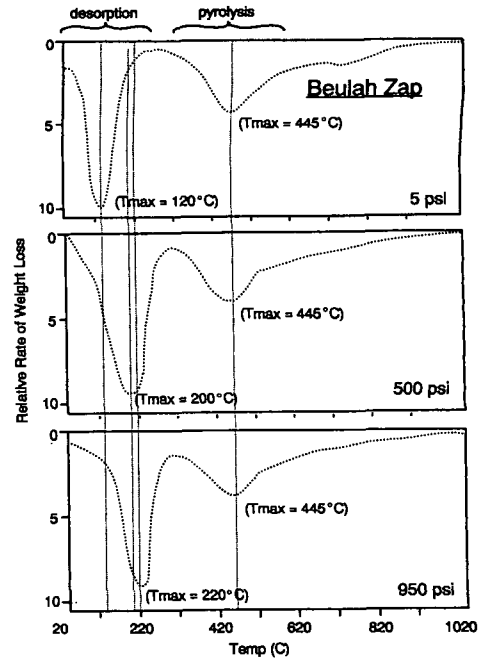

Figure 3. Comparison of DTG profiles of Beulah Zap lignite showing effect of pressure on moisture desorption Tmax.

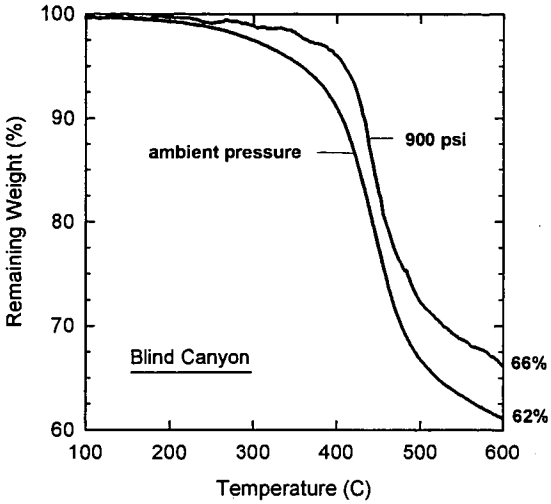

Figure 4. Effect of pressure on TG weight loss profiles for Blind Canyon Coal showing increased char residue at 600 C.

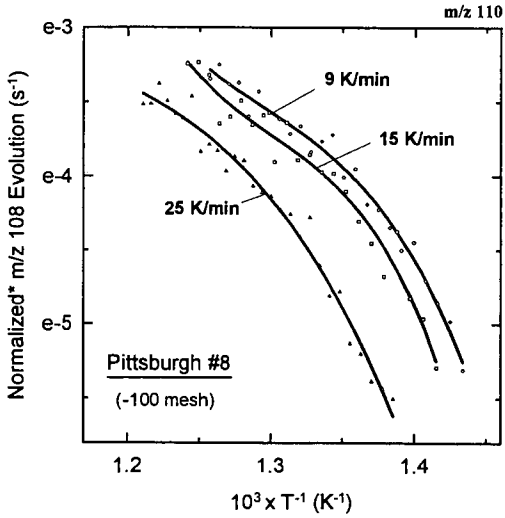

Figure 5. Pseudo-Arrhenius plot demonstrating effect of heating rate on apparent tar evolution rates (represented by cresols at m/z 108).

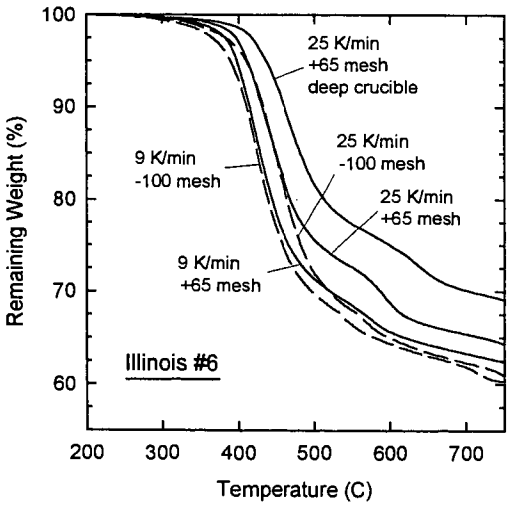

Figure 6. Effect of heating rate, particle size and bed depth on TG weight loss profiles for Illinois #6 coal (see text).

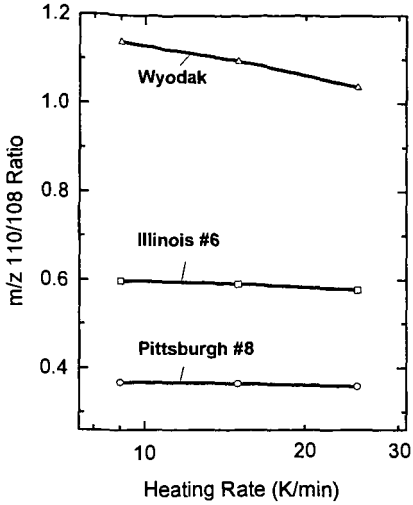

Figure 7. Effect of heating rate and coal rank on dihydroxy-benzene/cresol (m/z 110/108) ratios (see text).

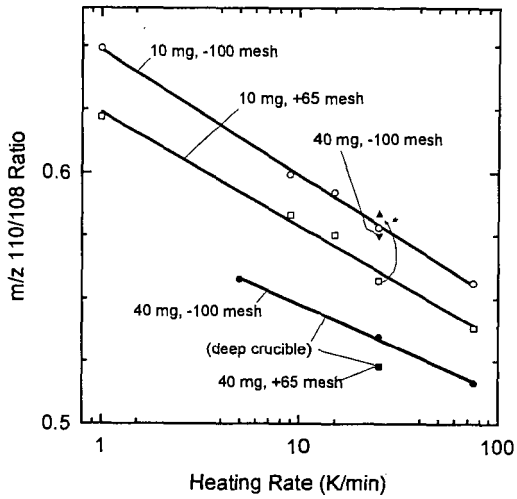

Figure 8. Effect of heating rate, particle size and bed depths on m/z 110/108 ratios for Illinois #6 coal. Note m/z 110/108 ratios of 2 control samples at 25 K/min, as discussed in text.
* = +65 mesh sample reground to -100 mesh.

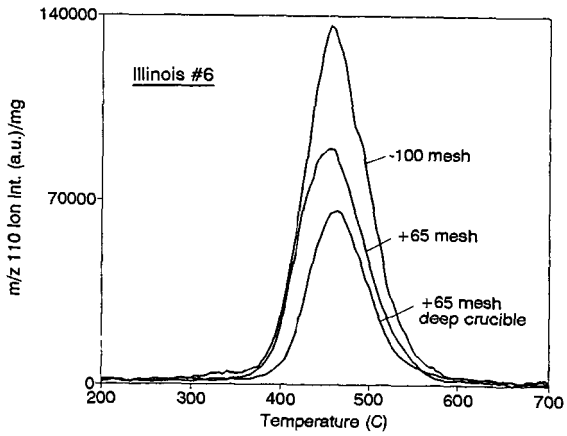

Figure 9. Effect of particle size and bed depth on dihydroxybenzene yields (corrected for sample weight) from Illinois #6 coal at 25 K/min. Note marked decrease at larger particle size and bed depth. Estimated variability between duplicate runs ±5% (1 day) and ± 10% (1 week).

HIGH TEMPERATURE DEACTIVATION OF COAL CHARS

T. J. Beeley, J. R. Gibbins, R. Hurt+, C. K. Man, K. J. Pendlebury
& J. Williamson*
Department of Mechanical Engineering,
*Department of Materials, Imperial College, London SW7 2BX
+Sandia National Laboratory, Livermore, CA 94551-0969

Keywords: coal char combustion, reactivity

INTRODUCTION

High levels of char burnout, typically to less than 5% by weight of residual carbon in the fly ash, are desirable in large, multi-burner utility boilers fired with pulverised coal in order to optimise plant efficiency and allow the ash to be incorporated in building materials. Achieving high levels of char burnout can be a particular problem with air-staged low-NOx combustors, where air/fuel ratios (and flame temperatures) have to be constrained to give satisfactory emission levels. Switching to imported low-sulphur coals can also be associated with a need to at least assess the potential for burnout problems.

In general the levels of carbon in ash required represent very high overall fuel conversion. For example, a coal with 10%w/w ash dry basis giving 5% carbon in ash will still achieve 99.4% conversion. The difference between satisfactory and unsatisfactory burnout thus depends on whether a very small fraction of the coal does or does not burn. Due to the heterogeneous nature of pulverised coal the properties of this 'least likely to burn' (LLB) fraction could well differ from the bulk properties of the whole coal. Consideration of heat and mass transfer would suggest that larger particles make up the bulk of the LLB fraction, and particularly those larger particles which form less reactive chars. In contrast to this material, which might be classed as being unlikely to burn because it is inherently 'bad', there is also a strong likelihood that some coal particles do not burn because they are 'unlucky'. Particles which enter through burners which, because of poor fuel distribution, have a lower than average air/fuel ratio fall into this latter category, especially if they also enter in an upper row of burners or adjacent to a wall.

Previous work by one of the authors has confirmed the heterogeneous nature of pulverised coals by showing that combusting coal particles exhibit a range of reactivities, and that average reactivities decrease with increasing conversion[1]. A band of reactivities has also been observed in chars collected from utility boiler fly ash, with a general trend for char reactivity to reduce with increasing particle size[2]. Even at relatively high levels of conversion (~ 50%) chars produced in a laboratory entrained flow reactor (EFR) still had significantly higher reactivity than utility fly ash chars from the same coal[3].

The deactivation of coal chars obviously has considerable implications for interpreting char burnout behaviour in itself, but why it occurs is not clear. One explanation is that, with a heterogeneous coal and hence char, the components which are inherently more reactive are burnt preferentially leaving a residue of less-reactive material. Another mechanism, which may either dominate or operate in parallel, is that even at the short particle residence times occurring in utility boilers (~2 seconds) thermally-induced heteroatom loss and/or structural reordering in the chars have occurred, with a consequent reduction in the number of active sites. High resolution transmission electron microscopy in fringe image mode has confirmed that chars from utility boilers are indeed more ordered than chars from the EFR[3], but this may reflect either heterogeneity in the parent coal plus differences in degree of conversion, or differences in peak particle temperature and residence time (>1800°C vs. ~1570°C, ~1s vs. ~100 ms respectively).

In order to promote an understanding of the relative importance of the two mechanisms, this study examines the effect of time/temperature history on char reactivity. A recently-developed wire mesh (WM) apparatus was used to achieve char temperatures up to 1800°C with, unlike entrained flow apparatus, essentially no constraint on particle heating times. Since heating takes place under inert gas (helium) any effects due to selective oxidation are avoided. The work formed a preliminary stage in a larger project which will also examine the effect of coal heterogeneity in more detail.

EXPERIMENTAL METHODS

Fly ash samples containing char for analysis were obtained from plant trials. Pulverised coal samples were either sampled on plant or prepared from corresponding lump coal. All coal samples were dry sieved to give a 125-150μm size cut for WM analysis. This was dried overnight in a nitrogen-purged oven at 105°C and stored under nitrogen until required. Char samples were obtained from fly ash either by sieving to give a carbon-enriched size cut >150μm, or by particle density segregation in a sub-fluidised bed.

Coal samples were charred using a high-temperature WM reactor developed at Imperial College. The sample (~10mg) is held between layers of folded molybdenum wire mesh which also act as an electrical resistance heater. Heating currents of up to 2000 A are provided under computer control from a 24 V DC source, with a two-colour pyrometer for temperature measurements. A helium gas sweep flows across the mesh (at atmospheric pressure) to remove volatile products. A more detailed description of the apparatus will be published elsewhere[4]. Char samples for two of the coals were also prepared in an entrained flow reactor at Sandia National Laboratory in 12% oxygen at a gas temperature of 1327°C, peak particle temperatures of 1570°C, and residence times from 47 to 234 ms.

Char reactivities were compared using thermogravimetric analysis (TGA). Samples were heated in a PL Thermal Sciences TG760 series TGA to 900°C at 15 K/min in 7% oxygen in nitrogen. This reduced oxygen concentration eliminates 'ignition peaks' (uncontrolled autothermal combustion within the char sample) that can occur if the sample is heated in air. Char samples were ground to <10μm to eliminate any effects due to particle size. Although this technique utilises standard commercial equipment some development work was required to achieve consistent, repeatable results with small samples (2-3mg).

TGA data logging and analysis were carried out using in-house software. The instantaneous sample mass was monitored as the sample was heated. Sample temperature was measured using a thermocouple positioned 0.7 mm under the crucible. Results were expressed as burning profiles (rate of weight loss versus sample temperature), or as Arrhenius plots (logarithmic reaction rate against inverse temperature). This non-isothermal characterisation technique has several advantages over isothermal methods (e.g. time for 50% burnoff). In isothermal char reactivity tests the char must be first heated to the desired temperature in inert gas, before switching to the desired oxygen concentration. Data for the intermediate oxygen levels during switchover periods, which can represent a considerable portion of the total burnoff at elevated temperatures, cannot then be used. Analysis times will also vary significantly at a given temperature with the range of char reactivities encountered in char combustion studies (e.g. low reactivity chars may require a number of hours for 50% conversion at 500°C in 7% O_2). Errors in sample temperature measurements may, however, be worse in non-isothermal analysis due to differential heating, particularly if (as in this case) the thermocouple is not placed in direct contact with the sample.

RESULTS AND DISCUSSION

The variation in reactivity for chars prepared from Illinois #6 coal by different methods is shown as an Arrhenius plot in Fig. 1. As noted already, chars from the EFR have significantly higher chemical reactivities than the utility boiler fly ash chars. Chars obtained after heating in the WM reactor at 1600°C are also significantly more reactive. The reactivity of the WM chars decreases with increased hold time at peak temperature, but even at 10 s hold the 1600°C WM char is more reactive than the fly ash char. The Arrhenius plot line for a WM char obtained with a peak temperature of 1800°C and a residence time of 2 s, however, intersects the Arrhenius plot line for the utility char, being apparently less reactive at low conversions in the TGA but more reactive at higher conversions. Similar trends for the WM chars as compared with the fly ash chars were also observed for a South American coal (Fig. 2) and US Daltex coal (Fig. 3), although this last coal appears to be particularly susceptible to thermal deactivation.

An interesting feature of Figs 1 to 3 is the difference between apparent activation energies for WM and fly ash chars. Both exhibit reasonably straight lines on the Arrhenius plots over the range 5% to 95% conversion (signal/noise ratio makes interpretation difficult at higher conversions), suggesting modelling by a familiar first order reaction rate expression for loss of sample weight, W, of the form:

$$dW/dt = -a.W.e^{-E/RT}$$

For the WM chars, increased heating severity changes the pre-exponential factor, *a*, but not the activation energy, *E*, suggesting that the number, but not the type, of active sites is being affected. The lower apparent activation energy for the fly ash chars might then be taken as an indication of the presence of a significantly different type of char, perhaps due to selective oxidation.

If, however, the WM and fly ash chars are in fact different types, it might be considered an unusual coincidence that overall reactivities are still comparable for the similar peak temperatures. This observation is explored in more detail in Fig. 4, which shows the TGA burning profile that would be obtained for a hypothetical heterogeneous char with a single activation energy, but a normal distribution of pre-exponential factors (the WM char data show that this could, for example, be obtained by subjecting a batch of coal particles to a range of different time/temperature histories during devolatilisation). The Arrhenius plot line for 5% to 95% conversion for the modelled TGA burning profile is still extremely linear (correlation coefficient of 0.997), but the heterogeneity has the effect of reducing the apparent activation energy from an assumed 175 kJ/kmole to 145 kJ/kmole.

Since particles in a utility boiler will have experienced a range of time/temperature histories it appears plausible that this, at least partly, accounts for the apparently lower activation energies for fly ash chars shown in Figs 1 to 3. If temperature alone is responsible, then it can further be concluded that the fly ash chars have experienced temperatures both above and below 1800°C. This scenario corresponds with the LLB fraction being made up of particles that are simply 'unlucky'.

The very low reactivities of fly ash chars at higher conversion levels in the TGA compared to 1800°C WM chars suggest, however, that extremely high particle temperatures would have to have occurred to account for all of the differences observed. Some additional char heterogeneity due to differences between the parent coal particles therefore seems likely. This pulverised coal heterogeneity may be in the organic fraction or in the catalytic properties of the mineral matter for graphitisation and/or oxidation. In either case, the LLB fraction would then consist, at least in part, of particles that were inherently 'bad'.

It is also worth considering to what extent the original WM coal samples are themselves heterogeneous in this way. In this case even the higher apparent activation energies observed for the WM chars could still be an underestimate, with considerable implications for extrapolating low-temperature TGA data to boiler combustion temperatures.

CONCLUSIONS

Char oxidation reactivity reduces progressively with increased temperature and hold time under conditions encountered in pulverised coal combustion. At elevated temperatures (1800°C) char reactivities obtained by heating alone approach fly ash residual char reactivities.

Fly ash residual char from utility boilers is probably heterogeneous in its reactivity. If some of the char particles have experienced temperatures well in excess of 1800°C then temperature alone could explain this heterogeneity, otherwise heterogeneity in the original coal plus loss of more reactive material, or catalysis of oxidation or char graphitisation by mineral matter, must also be occurring.

Char reactivities measured by non-isothermal TGA methods are likely to give correct relative trends, but apparent activation energies may not be reliable due to char heterogeneity (and possibly also temperature offsets).

ACKNOWLEDGEMENTS

The authors would like to acknowledge financial support for this work from the UK Science and Engineering Research Council, the British Coal Utilisation Research Association, the UK Department of Trade and Industry through ETSU, National Power PLC, and the US Department of Energy.

REFERENCES

1. Hurt, R.H., Energy & Fuels 7, 1993, 721-733.
2. Gibbins, J.R. & Williamson, J., Proc. 7th ICCS, Banff, Sep. 1993, paper PS1.9.
3. Hurt, R.H., Yang, N.Y.C., Headley, T.J. & Gibbins, J.R., Proc. 7th ICCS, Banff, Sep. 1993, paper OS12.2.
4. Pendlebury, K.J., Man, C.K. & Gibbins, J.R., Rev. Sci. Instrum., (in preparation).

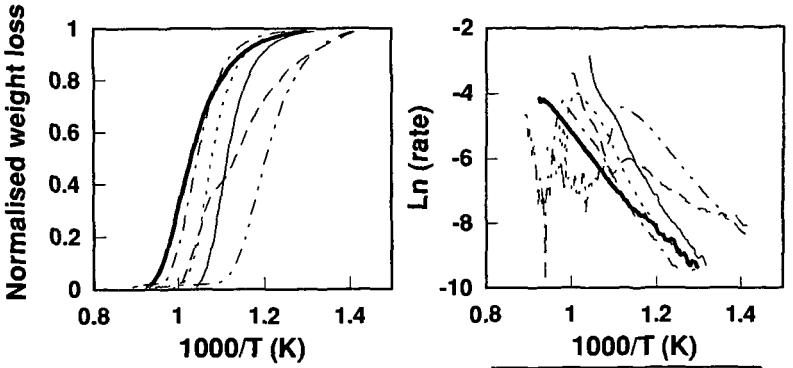

Figure1 TGA sample weight and reaction rate as a function of inverse temperature for Illinois #6 chars

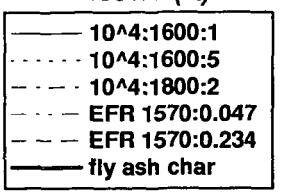

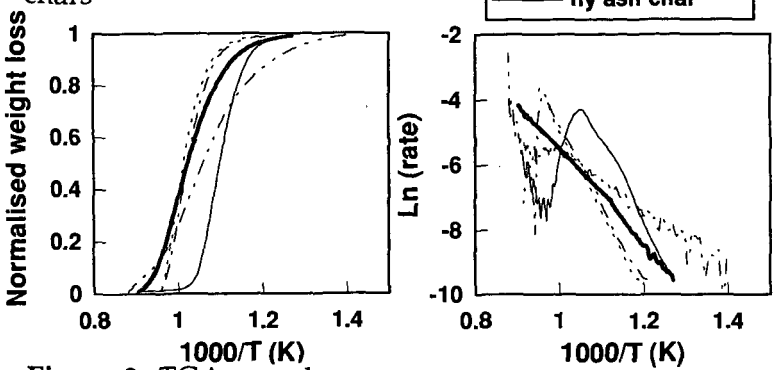

Figure 2 TGA sample weight and reaction rate as a function of inverse temperature for South American coal chars

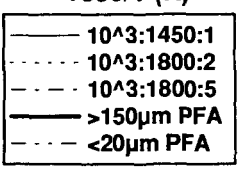

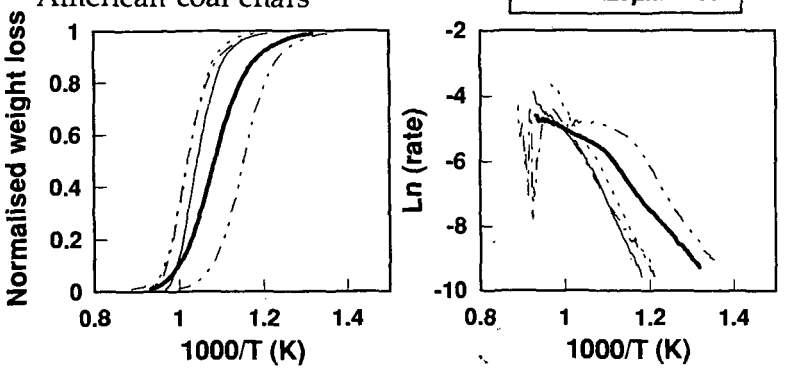

Figure 3 TGA sample weight and reaction rate as a function of inverse temperature for Daltex chars

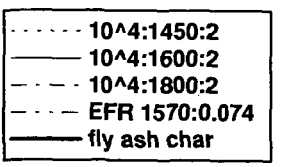

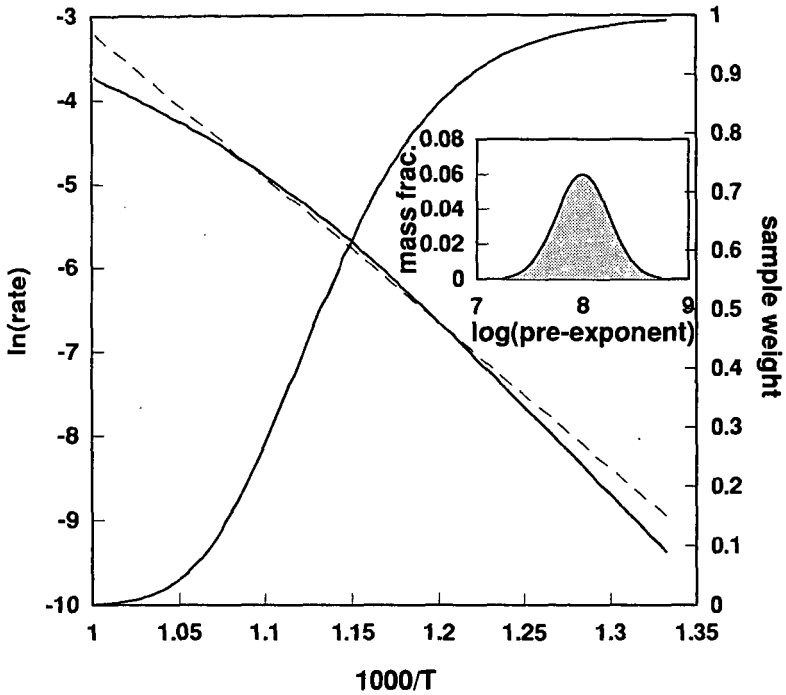

Figure 4 Effect of char heterogeneity on apparent activation energy

A PRIORI SIMULATION OF COAL PYROLYSIS EXPERIMENTS BASED ON COAL ELEMENTAL COMPOSITIONS

Yuxin Zhao, Michael A. Serio, and Peter R. Solomon
Advanced Fuel Research, Inc.
87 Church Street, East Hartford, CT 06108, U. S. A.

Keywords: Coal Pyrolysis, Modeling, Tar Yields.

INTRODUCTION

Coals come in various ranks and from different geological origins. Substantially different characteristics are commonly observed for coals of different ranks. Coal samples from the same seam can exhibit large variations in their devolatilization and related thermal and combustion behavior. Such variations have large impacts to the design and operating conditions of coal combustion systems. It is imperative that coals are well characterized before their utilization. This normally requires sophisticated instrumentation and special expertise, which are not likely available in a single laboratory. Robust methods of predicting coal devolatilization behavior before invoking expensive experiments can be of practical importance.

Recently, there have been developments of several coal devolatilization models [1-6], which have various capabilities of predicting coal thermal decomposition under practical conditions. A common shortcoming of these models is that they require a large set of data input, including kinetic parameters, gas precursor compositions and additional parameters describing the coal polymeric structure. These input data must be generated based on a series of experimental measurements for each coal of interest. Predictions are limited to coals that have been studied. This limitation has long been criticized although it originates from the complicated nature of the coal structure. On the other hand, some investigators have tried to correlate the devolatilization properties to the coal types. For instance, Ko et al. [7] and Neavel et al. [8] have developed methods of predicting the upper bound of tar yields, X_{tar}, from coal elemental compositions. The predicted X_{tar} can be used as an input parameter of general tar kinetic models such as those developed by Serio et al. [9] and Suuberg et al. [10]. Niksa and Kerstein [11,12] have also proposed a correlation method for the FLASHCHAIN coal devolatilization model which predicts tar and the total volatile yields in pyrolysis based on ultimate analysis.

This paper presents a general method that provides a direct correlation between coal elemental compositions and the input parameters of a general coal devolatilization model, FG-DVC [1-3], which can predict, in addition to the tar and total volatile yields, the yields of individual gas species, the tar molecular weight distribution, and the char fluidity. This model was validated for the eight Argonne Premium coals based on measurements of pyrolysis kinetics from TG-FTIR analysis, solvent extraction and solvent swelling to measure extractables and initial crosslink density, respectively, Gieselar plastometer experiments to measure fluidity, pyrolysis-FIMS to measure the tar molecular weight distribution and ultimate analysis to determine the elemental compositions (C, H, N, S, O) [3]. The large number of experimental inputs allowed the development of a model which can make detailed predictions of coal devolatilization, as indicated above. However, this feature presented a difficulty when applying the model to unknown coals. The correlation method presented in this paper enables us to apply the FG-DVC model to coals of a wide range of types without prior knowledge of them except the elemental analysis, and supports our contention that the FG-DVC model is a general model that can perform expeditious evaluations of coal thermal decomposition under many heating and pressure conditions. This correlation approach in its preliminary form has been implemented into a 2-dimensional coal combustion model, PCGC-2 [13]. After a description of the method, the model predictions are compared with tar yield data collected at fast heating rates and various pressures from the literature [7, 14-21], and with tar yields at slow heating rates measured with TG-FTIR analysis in our laboratory.

BACKGROUND

FG-DVC [1-3] is a general coal devolatilization model that predicts coal thermal decomposition into light gases, tar and char. It also predicts other related property changes, i.e., coal viscosity and swelling, during pyrolysis. Recent improvements of this model have given it the ability to predict gaseous sulfur and nitrogen species evolved during pyrolysis [22]. The following is just brief description of this model, as the details have been published elsewhere [1-3, 22,23].

Coal has a very complicated structure, which is essentially a mixture of an aromatic matrix, side chain components and some loose fragments. The thermal decomposition of the coal structure involves many parallel and competitive processes. In modeling these

processes, FG-DVC uses two submodels. The FG model simulates the thermal evolution of various functional groups and the DVC model predicts the depolymerization, vaporization and crosslinking processes occuring in the coal polymer network. In the FG submodel, the gas evolution from functional group precursors is modeled with parallel first order differential equations and a distributed activation energy formulation is used to reflect the diversity of coal structures. The thermal evolution of the coal polymer matrix is modeled with a network model [2], which consists of nodes and the connections between them. The nodes represent the polymer clusters and there are two types of connections between them, i.e., bonds and crosslinks. At elevated temperatures, there is a competition between bond breaking and crosslinking. The properties of the network are fully determined by these two competing processes through percolation theory [24]. The most important property of the network is the molecular weight distribution of the clusters. The heavy molecules remain in the condensed phase to become char, while the light ones evaporate to become tar. The vaporization is calculated based on a mechanism given by Fletcher [25]. The tar rate is further limited by internal transport, which is assumed to be controlled by the total rate of gas species evolution plus the light tar [1]. This mechanism enables the model to predict the pressure variation of tar yields.

Input parameters are required to describe the coal structure and its evolution kinetics. Sets of parameters have been developed for the eight coals provided by the Argonne Premium Coal Sample Program [26], employing various analytical methods, including TG-FTIR, solvent swelling and extraction, fluidity, NMR, and FIMS.

CORRELATION APPROACH

The behavior of coal when subjected to a physical and chemical analysis or treatment exhibits rank dependence in most instances. For example, Solomon et al. [3] have shown a consistent variation of coal functional group compositions with rank. The basis of the correlation formulation presented here relies on the well-known van Krevelen diagram [27], which indicates that the progress of coalification in terms of the coal's atomic hydrogen to carbon (H/C) and oxygen to carbon (O/C) ratios forms a distinctive band in the H/C and O/C two dimensional plane. Each coal has a coordinate (O/C, H/C) in the van Krevelen diagram. Fig. 1 illustrates the variation of the vitrinite reflectance index (v.r.i.) as a function of H/C and O/C, for 45 PSOC coals sponsored by the U. S. Department of Energy. As v.r.i. is commonly accepted as a rank indicator, it is reasonable to assume that there exists a correlation between rank and elemental composition. Therefore, a parameter for an unknown coal can be interpolated from those for a set of coals that are well-studied. These well-defined coals are called library coals, a term used by Williams [28].

We propose to use a two dimensional linear interpolation method commonly used in finite element analyses, with O/C and H/C as two rank indicators. Let x be a parameter of an unknown coal and $x0(i)$ (i=1,N) are the corresponding parameters of the N library coals. The N library coals form a 2 dimensional triangular element mesh in the van Krevelen diagram as displayed in Fig. 2, where N is 9 with each node representing a coal. The mesh nodes are plotted as filled circles and other symbols in the plot are the coals to be interpolated. Each triangle element contains three nodes (coals). If an unknown coal is inside the element J, whose three nodal numbers are $i^{(1)}_J$, $i^{(2)}_J$, and $i^{(3)}_J$, the unknown parameter, x, is interpolated as

$$x=(1-r-s)\cdot x0(i_J^{(1)})+r\cdot x0(i_J^{(2)})+s\cdot x0(i_J^{(3)}) \tag{1}$$

where r and s ($0\le r$, $s\le 1$) are the local coordinates of the unknown coal in element J and are determined from the positions of the unknown coal and the three interpolating coals in the van Krevelen diagram. Let U denote the point of the unknown coal in the van Krevelen diagram. Δ ($i^{(1)}_J$, $i^{(2)}_J$, $i^{(3)}_J$), Δ ($i^{(1)}_J$, U, $i^{(3)}_J$), and Δ ($i^{(1)}_J$, $i^{(2)}_J$, U) are the areas of the triangles formed by nodes ($i^{(1)}_J$, $i^{(2)}_J$, $i^{(3)}_J$), ($i^{(1)}_J$, U, $i^{(3)}_J$), and ($i^{(1)}_J$, $i^{(2)}_J$, U), respectively. r and s are calculated as follows

$$\begin{aligned} r &= \frac{\Delta(i_J^{(1)},U,i_J^{(3)})}{\Delta(i_J^{(1)},i_J(2),i_J^{(3)})} \\ s &= \frac{\Delta(i_J^{(1)},i_J^{(2)},U)}{\Delta(i_J^{(1)},i_J(2),i_J^{(3)})} \end{aligned} \tag{2}$$

The interpolation mesh is composed of nine coals, six of which come from the Argonne Premium Coal Sample Program and three of which are PSOC coals (PSOC 1474, PSOC 1448, and PSOC 1521). Extensive experimental studies have been carried out on the Argonne Premium Coals and the model input parameters are well established [3].

Predictions of the pyrolysis yields of these coals under various conditions are in very good agreement with the data collected in many types of reactors [29]. The Lewston-Stockton coal was not used because it has a very similar elemental composition to the Pittsburgh Seam Coal. The Pocahontas #3 coal was not selected since it is of substantially high rank and is far away from the rest of the coals. Three PSOC coals were added to this mesh recently, so that a larger area is covered. The functional group compositions and the pyrolysis evolution kinetic parameters of these three coals were obtained based on data from TG-FTIR analysis and solvent extraction experiments performed recently in our laboratory and fluidity data from the PSOC coal data base.

With this scheme, any of the model parameters for the FG-DVC model can be interpolated for an unknown coal when its elemental composition is identified. Special caution must be used in interpolating the functional group compositions of the oxygen, sulfur and nitrogen gases in order to maintain a proper mass closure. For example, the total amount of the oxygen containing functional groups is limited by the oxygen content. Therefore, instead of interpolating the amounts of oxygen gas precursors directly, only the fraction of oxygen in a functional group is calculated and is used to compute the amount of this functional group from the oxygen content. The same procedure is followed for the sulfur and nitrogen gases.

TAR YIELD PREDICTIONS

Tar composes up to about 50% of the total volatiles during coal combustion for most coals. The secondary reaction of tar in the system produces soot, PAH, and light gases that affect ignition, flame stability and the radiative property of the flame. Tar yields vary with coal type and are affected by reactor conditions such as pressure and heating rate. The interpolation scheme presented above enables the FG-DVC model to predict the tar yield of a coal from its elemental analysis under various pressure and heating rate conditions. To verify this capability, tar yield data were assembled from literature and were compared with the model predictions. These data were measured with heated grid systems under fast devolatilization (heating rates from 100 °C/s to 1000 °C/s) for various coals and pressures (10^{-4} to 7 MPa). In addition to these data, tar yields from eight PSOC coals were measured with a TG-FTIR system at heating rate of 30 °C/min and atmospheric pressure. The details of the TG-FTIR system have been presented elsewhere [30]. The data used for model verification were selected to span a wide range of coal types, from lignite to low volatile bituminous, and pyrolysis conditions. Part of the data set was taken from the tabulation given by Ko et al [7].

For each of these coals, the FG-DVC input parameters were interpolated with the scheme proposed above and the tar yields from these coals were predicted with the pressures and the heating rates specified in these references. Eleven coals from the references and the eight PSOC coals are inside the mesh and the standard interpolations were performed. The Pocahontas, Illinois #6 and North Dakota lignite studied by Suuberg et al. [17] are outside the mesh and were predicted with the input parameters of the corresponding Argonne coals. The Alabama bituminous coal studied by Freihaut and Seery [15] and the Beulah Zap coal studied by Ko et al. [7] were predicted based on input files used for the Argonne Upper Freeport coal and Zap lignite, respectively. The Colstrip lignite by Reitzen [21] is close to the edge of the triangle formed by Zap lignite, Wyodak, and Illinois #6 coals, and was modeled with an elemental composition inside this triangle and closest to Colstrip.

The predictions and the data are compared in Fig 3. The standard errors of the estimates are 3.84%, 3.12%, and 3.38% for data collected at vacuum, atmospheric and high pressures, respectively. The total standard error of the estimate is 3.35%. This is in the same range of experimental scatter commonly encountered in tar measurements. The standard error the of estimate, σ, is calculated as follows:

$$\sigma = \sum_{i}^{N} \frac{(y_i^m - Y_i^p)^2}{N}^{1/2} \qquad (3)$$

where Y_i^m and Y_i^p are the measured and predicted tar yields, and N is the number of data points compared.

Fig. 4 compares the predicted and the measured variations of tar and total volatile yields as a function of heating rate for a Linby coal studied by Gibbins and Kandiyoti [20]. For a Illinois #6 coal studied by Cai et al. [19], the variations of tar and total volatile yields as a function of heating rate and pressure were predicted and are compared with the data [19] in Fig. 5. These plots show that the predictions are in a reasonably good agreement with the data. It should be noticed that this is achieved based only on the elemental compositions

without further prior knowledge of these coals.

DISCUSSION

The success of this interpolation scheme depends on a thorough understanding of the library coals. Selection of these library coals must be performed with care so that none of these coals has peculiar behavior and deviates from coals in its rank. Although the current mesh contains only nine coals, it is one advantage of this method that it can be easily extended to include more coals. Adding more coals in the interpolation mesh will certainly increase the reliability of the predictions and will allow coverage of a wider range of coal types.

A few large discrepancies were observed for some coals, indicating needs for further improvements. Under-predictions of tar yields in vacuum were seen for a group of Pittsburgh seam coals, for which the measured tar yields are 39.0% [15], 37.0% [10] and 37.7% [18] and the predicted vacuum tar yields are 33.0%, 29.2% and 32.6%, respectively. However, good agreement was obtained at atmospheric pressure for these coals (26.5% [10] vs. 24.5% and 26.5% [17] vs. 26.9). Since the pressure variations are correctly predicted for other coals, the high vacuum tar yields for the Pittsburgh seam coals appear to be caused by a mechanism particular to these coals. The model also under-predicts tar yields for PSOC 1519 and 1492 coals. The Sesser sub-bituminous coal studied by Ko et al. [14] is the only coal that has a large over-predicted atmospheric tar yields (21.5% [14] vs. 27.0%). This coal seems to be an unusual coal as a relatively low tar yield was also reported by Reitzen [21] (11%). For most of the coals the predictions are within 3% of the data and the standard error of estimation calculated without the above large discrepancies is 2.54 wt%.

The basis of this interpolation method is the assumption that coals within the same rank behave similarly. Predictions based on this method are targeted at the normal or mean behavior of coals within the same rank. Deviations from normal, however, should be expected. If the deviation is large and can not be identified with an existing mechanism, the behavior of coals becomes unpredictable with the current method. The comparisons presented in Figs. 3 to 5 indicate that, for most coals, the deviations are small enough that the tar yields are well predicted. Some improvement may be achieved by including one additional parameter, such as the volatile matter content, in the correlation.

The yields and the compositions of the volatile gases are also important. The capability of FG-DVC in predicting the total volatile yields has been demonstrated in Figs. 4 and 5. The amounts of individual gas species are also predicted by FG-DVC along with the tar yields and this is one of the chief advantages of this model. However, comparisons are more difficult because of the relatively small amount of available data. This will be the subject of further studies.

CONCLUSIONS

An interpolation method was proposed to correlate the input parameters of a coal devolatilization model, FG-DVC, for untested coals, and is conceptually applicable to other devolatilization models. This method uses a set of well defined coals (library coals) to form a triangular mesh in the van Krevelen diagram. If an unknown coal is within a triangle formed by three library coals, the model input parameters for this unknown coal can be interpolated from those of the three library coals based solely on a knowledge of the elemental composition. This method allows the FG-DVC model to be used for any coal that can be interpolated. It is also easy to accommodate more library coals, so that a wider range of coal types can be covered.

The validity of this method was demonstrated by comparing the tar yields measurements and predictions for 27 coals under a wide range of pressures and heating rates. For most of the coals, the predictions compare very well with the data.

ACKNOWLEDGMENTS

This work was supported by the Morgantown Energy Technology Center of the US Department of Energy, through contract DE-AC21-86MC23075. The authors also wish to acknowledge helpful comments from Professor Eric M. Suuberg of Brown University.

REFERENCES

1. Solomon, P. R., Hamblen, D. G., Carangelo, R. M., Serio, M. A., and Deshpande, G. V., Energy & Fuels, 2, 405 (1988).
2. Solomon, P. R., Hamblen, D. G., Yu, Z. -Z. and Serio, M. A. Fuel, 69, 754 (1990).
3. Solomon, P. R., Hamblen, D. G., Serio, M., A., Yu, Z. -Z. and Charpenay, S. C., Fuel, 72, 469 (1993).
4. Grant, D. M., Pugmire, R. J., Fletcher, T. H., and Kerstein, A. R., Energy & Fuels, 3,

175 (1989)
5. Reynolds, J. G., and Burnham, A. K., submitted to Energy and Fuels, 1992.
6. Niksa, S., AIChE J., 34, 790 (1988).
7 Ko, G. H., Sanchez, D. M., Peters, W. A. and Howard, J. B., Twenty-Second Symp. (Intl) on Comb., p. 115, The Combustion Institute, Pittsburgh, 1988.
8 Neavel, R. C., Smith, S. E., Hippo, E. J., and Miller, R. N., Proc. of Intl. Conf. on Coal Sci., p.1, Dusseldorf, Sept. 1981.
9. Serio, M. A., Peters, W. A., and Howard, J. B., I & EC Res., 26, 1831 (1987).
10. Suuburg, E. M., Peters, W. A., and Howard, J.B., 17th Symposium (Int.) on Combustion, The Combustion Institute, Pittsburgh, PA pp. 117-130 (1979).
11. Niksa, S. and Kerstein, A. R., Am. Chem. Soc. Div. Fuel Chem. Preprints, 38(4), 1346 (1993).
12. Niksa, S. and Kerstein, A. R., proceedings of the Intl Conf. on Coal Sci., pp. 397-400, (1993).
13. 93-PCGC-2, Users Manual, Brigham Young University and Advanced Fuel Research, Inc., 1993.
14. Ko, G. H., Peters, W. A. and Howard, J. B., Fuel, 66, 1118 (1987).
15. Freihaut, J. D. and Seery, D. J., Am. Chem. Soc. Div. Fuel Chem. Preprints, 26(2), 133 (1981).
16. Arendt, P. and van Heek, K-H., Fuel, 60, 779 (1980).
17. Suuberg, E. M., Unger, P. E., and Larsen, P. E., Energy & Fuels, 1, 305 (1987).
18. Suuberg, E. M., Lee, D. and Larsen, J. W., Fuel, 64, 1668 (1985).
19. Cai, H. -Y., Güell, A. J., Dugwell, D. R. and Kandiyoti, R., Fuel, 72, 322 (1993).
20. Gibbins, J. R. and Kandiyoti, R., Fuel, 68, 895 (1989).
21. Reitzen, T. R., Effects of Pyrolysis Conditions on Products of Interests in Formed Coke Production, M. S. thesis, Massachusetts Institute of Technology, 1978.
22. Bassilakis, R., Zhao, Y., Solomon, P. R., and Serio, M. A., Energy & Fuels, 7, 710 (1993).
23. Hamblen, D. G., Yu, Z. Z., Charpenay, S., Serio, M. A., Proc. of Intl. Conf. on Coal Sci., pp. 401-404, (1993).
24. Stauffer, D., and Aharony, A., Introduction to Percolation Theory, 2nd Edition, Taylor & Francis, London, UK, 1991.
25. Fletcher, T. H., Kerstein, A. R., Pugmire, R. J., Solum, M. S., and Grant, D. M., Energy & Fuels, 6, 414 (1992).
26. Vorres, K. S., Energy & Fuels, 4(5), 420 (1990).
27. van Krevelen, D. W., Coal, 3rd Edition, Elsevier Publishing Company, Amsterdam, 1993.
28. Williams, A., Pourkashanian, M., Bysh, P. and Norman, J., Keynote address to the Coal Utilization and the Environment Conf., May 18-20, 1993, Orlando, U. S. A.
29. Serio, M. A., Solomon, P. R., Yu, Z. -Z., Deshpande, G. V., and Hamblen, D. G., Am. Chem. Soc. Div. Fuel Chem. Preprints, 33(3), 91, 1988.
30. Solomon, P. R., Serio, M. A., Carangelo, R. M., Bassilakis, R., Gravel, D., Baillargeon, M., Baudais, F., Vail, G., Energy & Fuels, 4, 319 (1990).

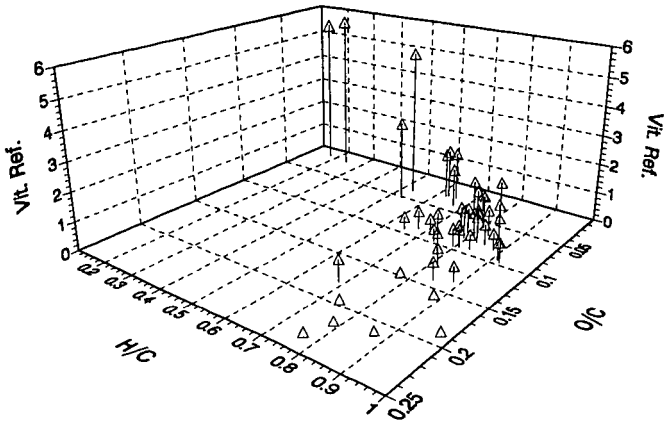

Figure 1. Variation of Vitrinite Reflectance of Coals from the PSOC DOE Sample Bank as a Function of H/C and O/C Ratios in the van Krevelen Diagram.

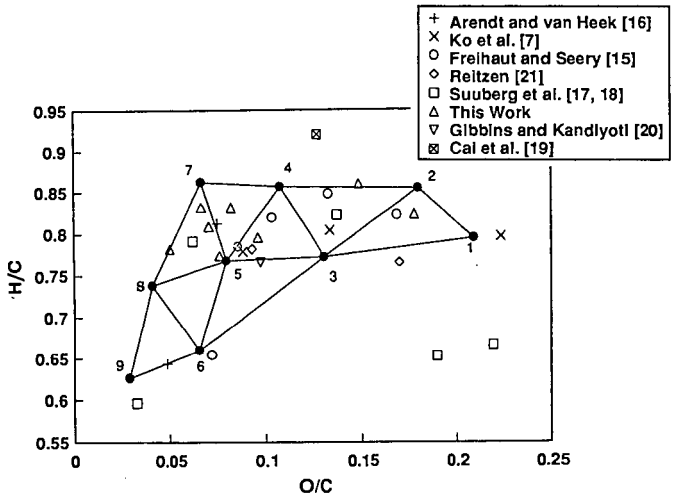

Figure 2. The Interpolation Mesh in the van Krevelen Diagram and Coals Used for Tar Yield Comparison. Argonne Coals: (1) Beulah Zap; (2) Wyodak; (3) Illinois #6; (4) Blind Canyon; (5) Pittsburgh #8; (6) Upper Freeport. PSOC Coals: (7) PSOC 1448; (8) PSOC 1474; (9) PSOC 1521.

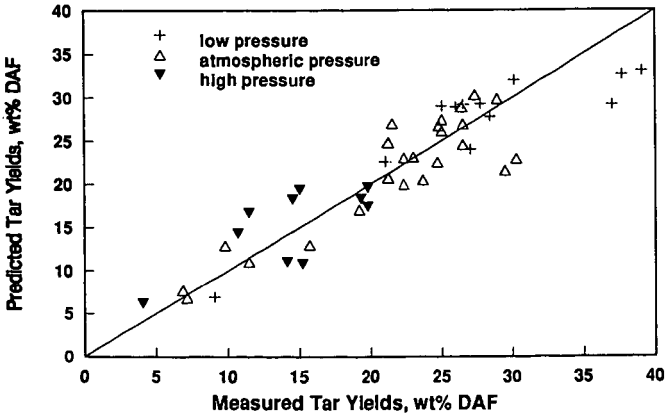

Figure 3. Comparison of the Measured and the Predicted Tar Yields for Coals Given in Fig. 2.

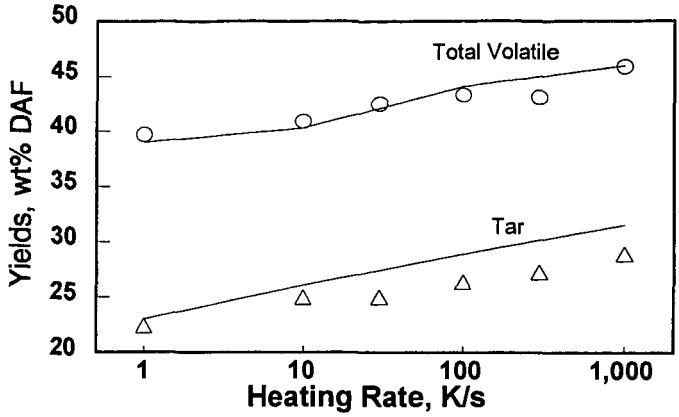

Figure 4. Variations of Tar and Total Volatile Yields as a Function of Heating Rate for a Linby Coal Studied by Cai et al. [19]. The Lines are Predictions and the Symbols are the Data.

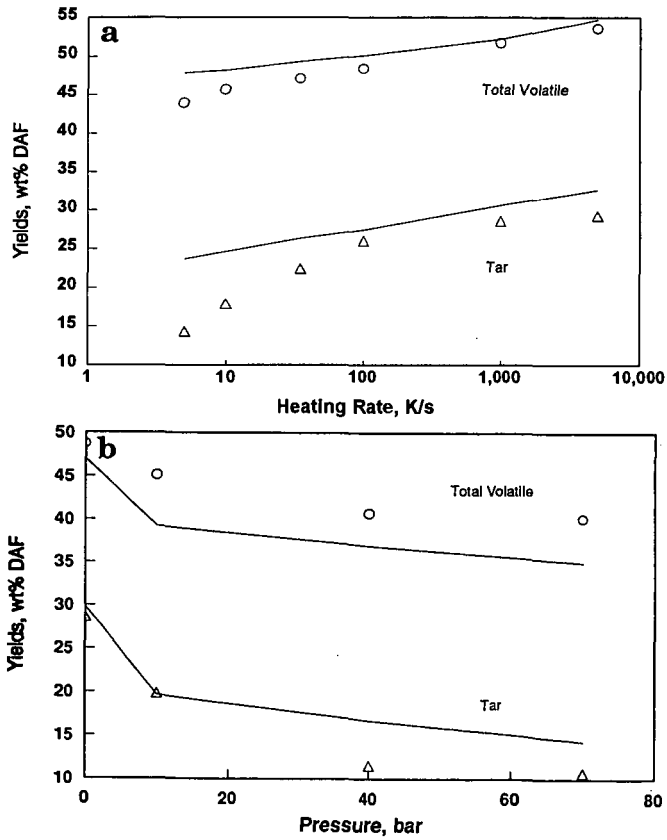

Figure 5. Variations of Tar and Total Volatile Yields as a Function of a) Heating Rate and b) Pressure for a Linby Coal Studied by Cai et al. [19]. The Lines are the Predictions and the Symbols are the Data.

STUDIES OF THERMAL AND CATALYTIC HYDROLIQUEFACTION OF MODEL COMPOUNDS, WASTE POLYMERS AND COAL BY HIGH PRESSURE TG/GC/MS

Kui Liu, Emma Jakab, Wlodzmierz Zmierczak*, Joseph Shabtai* and Henk L.C. Meuzelaar
Center for Micro Analysis & Reaction Chemistry
*Department of Chemical and Fuels Engineering
University of Utah, Salt Lake City, UT, 84112

KEYWORDS: high pressure TG/GC/MS techniques; catalytic hydropyrolysis mechanisms; coal/waste polymer co-processing

INTRODUCTION

A recently developed on-line high pressure thermogravimetry (TG)/gas chromatography (GC)/mass spectrometry (MS) system [1] provides certain advantages over other on-line analysis techniques for high pressure reactors reported previously [2,3]. The high pressure TG/GC/MS system enables the simulation of solvent-free thermal and catalytic reactions for polymers and coal. During the reactions the total weight change is monitored and the volatile intermediate products are identified. It requires only very small amounts (10-100 mg) of sample and can be operated at high pressure under different atmospheres (N_2, He, H_2, etc.). Current efforts to recycle lower grade postconsumer polymers such as colored polyethylene and polystyrene or used rubber tires, are concentrated on co-processing with coal [4-6]. Purely thermal degradation processes involve both decomposition and condensation (recombination) reactions and the resulting product is highly olefinic and often aromatic. In order to improve the yield and selectivity of the process, a great deal of effort has been spent on finding the proper catalysts. Catalysts selected for the present studies include $ZrO_2/SO_4^=$, $(NH_4)_2MoS_4$ and carbon black. Carbon black present in waste rubber tires has been reported to be very selective for the cleavage of specific alkylaryl bonds [7]. $(NH_4)_2MoS_4$ has been shown to improve the liquid yields in coal liquefaction [8]. The superacid catalyst $Zr_2O_2/SO_4^=$ possesses markedly higher hydrogenolytic activity compared to that of conventional SiO_2-supported soluble Fe salts [9].

EXPERIMENTAL

Experiments with a styrene-butadiene rubber (SBR; nonvuleanized) sample in the presence of various catalysts (carbon black, $(NH_4)_2MoS_4$ and $ZrO_2/SO_4^=$) and coprocessing runs of coal and polymers (polyethylene, polystyrene, waste rubber tire, commingled plastic mixture) were conducted in a high pressure TG/GC/MS system at a hydrogen pressure of 900 psi. The experimental procedure and schematic of the equipment were described in detail in a previous paper [1]. The styrene-butadiene rubber (SBR) (30% polystyrene, 20 mesh), polystyrene (MW 45000, -100 mesh), polyethylene, carbon black (Black Pearl 2000) and $(NH_4)_2MoS_4$ were obtained from Aldrich Chemical Company. The superacid catalyst $ZrO_2/SO_4^=$ was prepared as reported by Shabtai et al. [9]. In the case of commingled postconsumer plastic, the plastic bottles and containers were washed to remove contaminants and labels before sizing and shaving. Final size reduction was done by grinding in a K-TEC kitchen mill. A high volatile bituminous coal (DECS-6, Blind Canyon, Utah, obtained from the Penn State Coal Sample Bank) was used in a 1:1 mixture ratio with both model and waste polymers.

RESULTS AND DISCUSSION

The thermal and catalytic reactions of a styrene-butadiene rubber (SBR) polymer as a model compound of rubber tire were studied in a high pressure thermobalance at a hydrogen pressure of 900 psig. As shown by the weight loss profiles in Figure 1, the 10% superacid ZrO_2/SO_4 catalyst added has little influence upon the rate of decomposition of SBR polymer at a constant heating rate of 10 C/min. However, when the same sample is subjected to a different temperature program using a heating rate of 10 C/min up to 370 C and then kept under isothermal conditions for one hour before being heated up to 500 C at 10 C/min, the effect of the catalyst on the rate of decomposition of SBR polymer is clearly observed (Figure 2). The catalyst greatly increases the rate of degradation of the polymer at 370 C. The results suggest that at a constant heating rate the reactions are dominated by thermal processes so the catalyst effect is not observed. However, the difference between catalytic and thermal processes is brought out effectively at a relatively low isothermal temperature level (e.g., 370 C) chosen to minimize the contribution of thermal reactions.

In addition, the catalytic reactions of SBR with other catalyst types, viz. carbon black and $(NH_4)_2MoS_4$ were studied. In order to compensate for the poor contact between the powdered catalyst and SBR, 10% of catalyst was added to the polymer samples. Comparison of the thermogravimetric curves (Figure 2) shows that the $ZrO_2/SO_4^=$ catalyst increases the weight loss by about 17% at 370 C whereas carbon black and $(NH_4)_2MoS_4$ have no measurable effect on the overall rate of SBR decomposition. As discussed in the literature [9], the $ZrO_2/SO_4^=$ catalyst

causes primarily hydrogenolytic bond cleavage resulting in more weight loss whereas the mild bifunctional catalyst, $(NH_4)_2MoS_4$ appears to be ineffective in bond-cleavage reactions. Indeed at the relatively low temperature of 300 C, this catalyst has been found to have little effect on liquids production [8]. The temperature applied in our isothermal experiments is somewhat higher, but the reaction severity is mild due to the very short residence time of the reactants (estimated to be about 15 sec).

Several main product evolution profiles of SBR with various catalysts are shown in Figure 3. The production of benzene is significantly promoted by the $ZrO_2/SO_4^=$ catalyst indicating that the solid superacid catalyst has very strong hydrogenolysis activity for α-alkyl-arene bond cleavage. The catalyst contains both the Bronsted acid and the Lewis acid sites [10]. The Bronsted acid sites protonate the aromatic ring and the subsequent α-cleavage results in the formation of benzene and aliphatic compounds. These findings are in agreement with the observation of Shabtai et al. [9] that the $ZrO_2/SO_4^=$ catalyst is very effective in the hydrogenolytic α-cleavage of 1,2-dinaphthylethane. The presence of Bronsted acid sites also promotes trans-alkylation reactions between alkylbenzenes and styrene as evidenced by the increased evolution of isomeric methylstyrenes (Figure 3b), ethylstyrene and benzene. The increased yield of styrene (Figure 3c) and α-methylstyrene can be explained by the parallel Lewis acid functionality character of the catalyst. When the Lewis acid sites abstract hydride ions from the benzylic carbons, benzylic carbonium ions are formed. Subsequently, styrene and α-methylstyrene are formed by β-scission of the benzylic carbonium ion. Mild hydrogenation activity of the $ZrO_2/SO_4^=$ catalyst was indicated by the increased yield of saturated products such as ethyl benzene (Figure 3d) and isopropylbenzene.

Although, the $(NH_4)_2MoS_4$ catalyst does not affect the overall rate of decomposition significantly, some changes in the product composition are observed. The $(NH_4)_2MoS_4$ catalyst behaves as a bifunctional catalyst, showing both ring hydrogenation (more ethylbenzene (Figure 3d) and isopropyl benzene) and hydrogenolysis (more styrene (Figure 3c) and α-methylstyrene (Figure 3b)) activity. Carbon black does not produce a measurable effect at 370 C, but at temperatures above 400 C it has some ring hydrogenation activity as indicated by the higher yield of saturated products (ethylbenzene (Figure 3d) and isopropylbenzene).

Experiments on the thermal (non-catalytic) decomposition of Blind Canyon DECS-6 coal, waste rubber tire, commingled plastic, polyethylene and polystyrene samples were performed at a hydrogen pressure of 900 psi with a linear heating rate of 10 C/min. The weight loss profiles are shown in Figure 4. The TG curves indicate the different course of decomposition the various samples. Coal continues to lose weight due to pyrolysis and char gasification at temperatures up to 600 C. The high (33%) rubber residue must be mainly due to the presence of carbon black. The post-consumer plastic and polyethylene samples follow a similar weight loss course except for a slightly higher decomposition temperature and residue yield of the waste plastic. This is in agreement with the fact that polyethylene represents the main constituent of the commingled plastic. Polystyrene, on the other hand, decomposes at relatively low temperatures.

Co-processing runs of coal with waste rubber tire, commingled waste plastic, polyethylene and polystyrene (ratio 1:1) were carried out at a constant heating rate of 10 C/min under 900 psi hydrogen pressure. Figure 5 shows the TG curves of coal and polystyrene as an example of non-catalytic co-processing. The dotted line is the predicted weight loss curve of the mixture, which is the linear sum of their individual components. The mixtures of coal with the various polymers studied all show approximately additive rate and yield behavior when applying a 10 C/min heating rate. Because of the continuous temperature rise unimolecular decomposition reactions prevail and the total weight loss is primarily controlled by the thermal behavior of the individual components. However, when using a suitable isothermal procedure, as described previously for studying the catalytic effect, both the TG and GC/MS profiles indicate a strong interaction between the coal and the polystyrene (Figure 6). The weight loss of the mixture is increased compared to the predicted value at 370 C (Figure 6a). The results are confirmed by the total product evolution profiles. The coal has lost about 18% weight at the end of the 370 C period but volatile products are not detectable by MS due to their low intensity. Therefore, the total ion chromatogram is not shown in Figure 6. The yield of the volatile polystyrene products detectable at 370 C can be seen in the total ion chromatogram (TIC) in Figure 6b. Since the polystyrene is not yet completely degraded after 60 mins at 370 C, the remaining polystyrene reacts further when the temperature is increased, resulting in additional product evolution at temperatures above 400 C. The total ion chromatogram of the mixture (Figure 6c) shows that the products are formed mostly during the isothermal period. The strong interaction between coal and polystyrene may be due to some extent to the mineral matter in the coal acting as a catalyst and accelerating the decomposition of the polystyrene. Seehra et al. [11] studied mixtures of coal with polymers such as polystyrene, polyethylene and rubber tire by ESR techniques and reported that free radical concentrations are increased when mixing coal with polystyrene and polyethylene. This may well be due to the occurrence of interactions between

the feed components (or their intermediate products). The possible occurrence of these reactions can be another explanation for the increased weight loss of the mixture.

CONCLUSIONS

Isothermal runs at relatively low temperature (370 C) are found to be effective in bringing out differences between catalytic and thermal processes, whereas at linear heating rates of 10 C - 20 C/min thermal reactions overwhelm the catalytic effect.

The $ZrO_2/SO_4^=$ superacid catalyst possesses high hydrogenolytic activity and causes a strongly increased rate of decomposition of SBR polymer at 370 C. The $(NH_4)_2MoS_4$ catalyst exhibits some ring hydrogenation activity at 370 C. Carbon black, on the other hand, has no measurable effect at 370 C, but shows some hydrogenation activity above 400 C.

Under thermally controlled (non-catalytic) conditions, mixtures of coal and polymers behave at first approximation in an additive manner. However, at lower temperatures, a synergistic effect is observed for polystyrene/coal mixtures.

High pressure TG/GC/MS is demonstrated to be a viable and useful technique for studying at a molecular level the effects of catalysts and blending under simulated process conditions, thus providing insight into the underlying reaction mechanisms.

ACKNOWLEDGEMENTS

The authors would like to thank Professor Larry L. Anderson and W. Tuntawiroon (University of Utah) for providing some of the samples. This work was sponsored by the Consortium for Fossil Fuel Liquefaction Science (DOE grant no. UKRF-4-23576-90-10).

REFERENCES

1. Liu, K., Jakab, E., McClennen, W.H., Meuzelaar, H.L.C., Prepr. Pap. Am. Chem. Soc., Div. Fuel Chem., 38 (1993), 823.
2. Huai, H., Tsai, C.H., Shabtai, J.S., Meuzelaar, H.L.C., Prepr. Pap. Am. Chem. Soc., Div. Fuel Chem., 37 (1992), 925.
3. Dworzanski, J.P., Chapman, J.N., Meuzelaar, H.L.C., Prepr. Pap. Am. Chem. Soc., Div. Fuel Chem., 37 (1992), 424.
4. Anderson, L.L., Tuntawiroon, W., Prepr. Pap. Am. Chem. Soc., Div. Fuel Chem., 38 (1993), 816.
5. Farcasiu, M., Chem Tech, January (1993), 22.
6. Taghiei, M.M., Huggins, F.E., Huffman, G.P., Prepr. Pap. Am. Chem. Soc., Div. Fuel Chem., 38 (1993), 810.
7. Farcasiu, M., Smith, C., J. Energy Fuels, 1991, 5, 83.
8. Derbyshire, F.J., Terrer, M.-T., Davis, A., Lin, R., Fuel, 1988, 67, 1029.
9. Zmierczak, W., Xiao, X., Shabtai, J., J. Energy Fuels 1994, in press.
10. Arata, K., Advances in Catalysis, 37, 1990, 165.
11. Ibrahim, M.M., Seehra, M.S., Prepr. Pap. Am. Chem. Soc., Div. Fuel Chem., 38 (1993), 841.

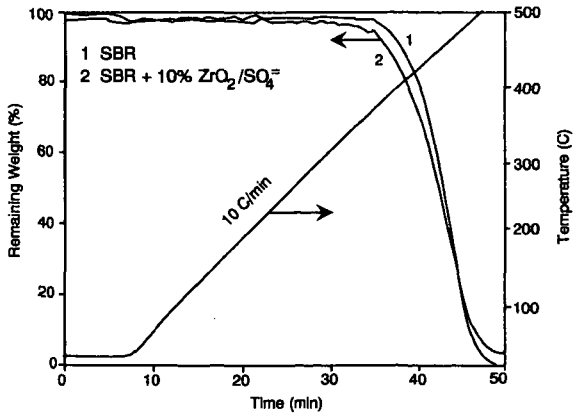

Figure 1. TG curves of SBR polymer at 900 psig (H_2).

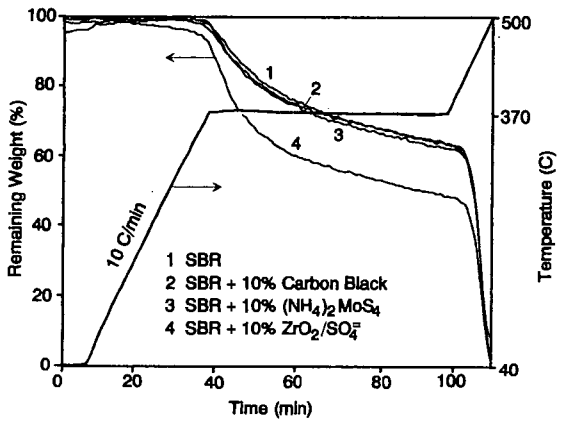

Figure 2. TG curves of SBR polymer with various catalysts at 900 psig (H_2).

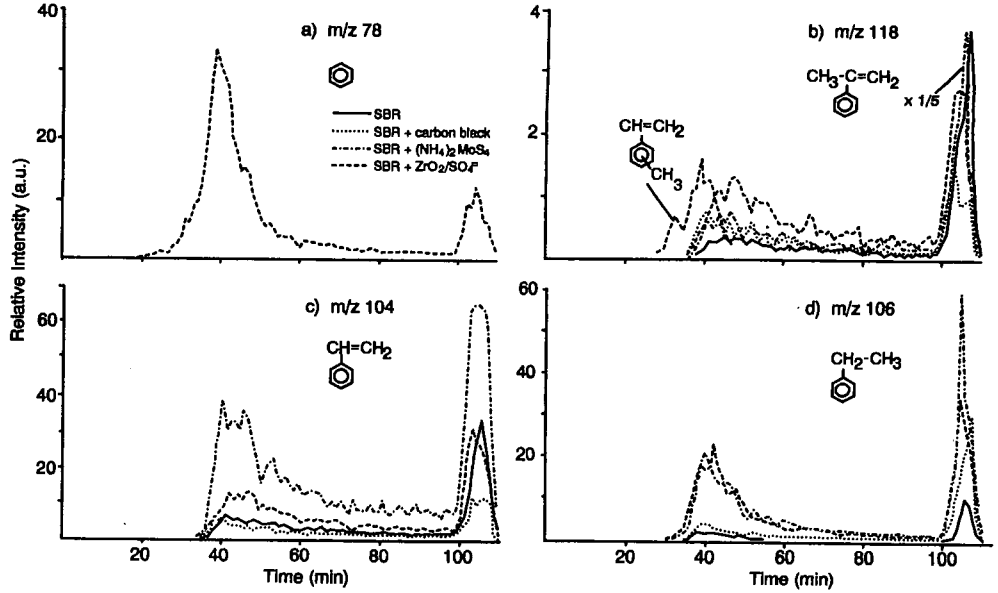

Figure 3. Effect of catalysts on evolution profiles of SBR polymer decomposition products. a) m/z 78, benzene; b) m/z 118, methylstyrene; c) m/z 104, styrene; and d) m/z 106 ethylbenzene.

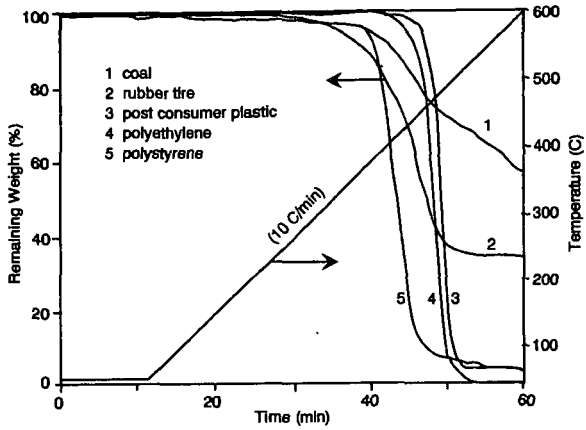

Figure 4. TG curves of various polymers at 900 psig (H_2).

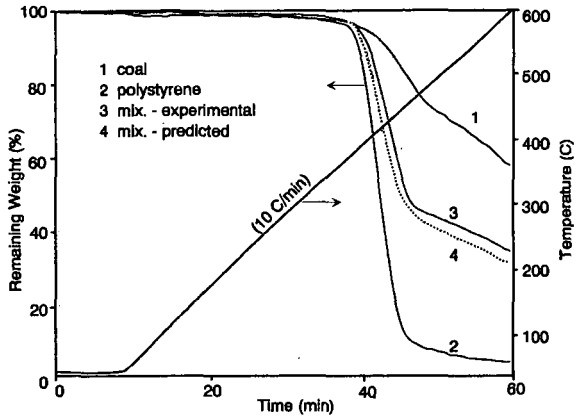

Figure 5. TG curves of coal and polystyrene at 900 psig (H_2).

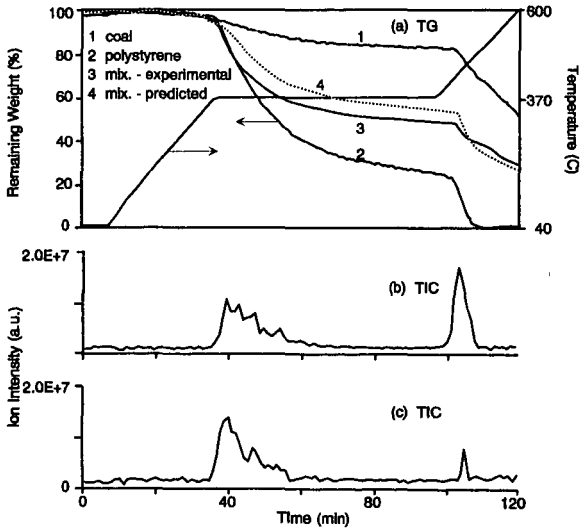

Figure 6. Effect of blending on coprocessing of coal and polystyrene at 900 psig (H_2). a) TG curves; b) total ion intensity profile of polystyrene; c) total ion intensity profile of coal and polystyrene.

THE USE OF THERMOGRAVIMETRIC ANALYSIS TO FOLLOW THE CONVERSION OF COAL DERIVED RESIDS IN THE RESID RECYCLING PROCESS

He Huang, W. H. Calkins* and M. T. Klein
Dept of Chemical Engineering, University of Delaware, Newark, DE 19716

Keywords: TGA, coal derived resid, resid conversion

INTRODUCTION

Direct Coal Liquefaction produces a substantial amount of high boiling non-distillable product (resid). The amount and character of this material depends upon the coal used and the conditions and reaction times in the liquefaction process. Because of its high boiling point and potential thermal instability, this material is not suitable for processing in a conventional petroleum refinery. In a commercial liquefaction process as it is visualized today, therefore, this material would be recycled to the process. Indeed, it has also been shown to actually have a beneficial effect in the liquefaction process(1).

Since these resids are complex and high boiling materials, their performance in the recycling process is not well understood or currently predictable. To this end, considerable analytical work has been accomplished for characterization purposes(2-5). These analyses have not really provided information about the reactivity of these resids under recycle conditions. Some measure of the ability to convert these resids to lower boiling, fuel-grade products is critically needed for design and scale up purposes. For example, it is important to know whether all resids are alike in their convertability, what conditions were optimum for their conversion, and what catalyst if any is needed for the conversion.

This has motivated the development of a coal-derived resid reactivity research program at the University of Delaware. A critical part of this program has been the development of a laboratory scale batch reactor(6) (Short Time Batch Reactor, STBR) capable of running liquefactions up to 450°C and 2500 psi at well defined reaction times from a few seconds to 30 minutes or longer. This reactor is simple in design and can be conveniently operated in the laboratory. In this STBR equipment, we have made a preliminary study of the actual conversion of coal liquefaction non-distillable resids to lower boiling, lower molecular weight material under conditions closely approximating the direct coal liquefaction process.

These resid conversion studies required a reasonably convenient means of determining the conversion of the resid from any particular experiment. For this purpose, we have relied heavily upon Thermogravimetric Analysis (TGA) augmented with Gas Chromatography and to a lesser extent GC/MS.

EXPERIMENTAL

Apparatus

The design and operation of the STBR reactor system were described at the 1993 national American Chemical Society meeting in Chicago (6).

The thermogravimetric analyzer (TGA) used is a Model 51 TGA (TA Instruments, New Castle Delaware). The gas chromatography was done on a Hewlett-Packard HP 5970 series II GC using a flame ionization detector. The gas chromatography/mass spectrometry was also performed on a Hewlett-Packard HP5970 series II using HP Series mass selective detector.

Materials Studied

The two coal derived 850 °F distillation resids were obtained from the Wilsonville Pilot Plant Runs 259 and 260, and prepared and composited by CONSOL Research. They are solids which were ground by CONSOL to about fourteen mesh. Ultimate analyses for these two resids are shown in Table 1.

The catalyst used was a presulfided Ni/Mo on alumina catalyst (Shell 324) (10.5 wt% Mo and 2.08 wt % Ni). The catalyst was presulfided in a distillate oil at the Wilsonville Plant. The oil was removed and the catalyst dried and ground under nitrogen by CONSOL.

Resid Conversion Reactions

All reactions were run as mixtures of tetralin (T, the donor solvent) and resid (R) over a range of T/R ratios and temperatures with and without catalyst.

Reaction Product Workup Procedure

The reaction product work up procedure is given in Figure 1. This resulted in the production of a liquid filtrate which consisted mainly of tetralin with dissolved resid and a solid filter cake which consisted of unconverted or partially converted resid. These two fractions were analyzed separately to determine the amount of resid that was converted.

TGA analysis on the liquid filtrate, which contained most of the tetralin, confirmed

that there was no mineral matter in the liquid sample (see Figure 2). This is critical, as our conversion measurements were based on comparison of the ash content of the converted product with that of the unreacted resid. As shown in Figure 2, the tetralin content of the liquid filtrate as well as the amount of higher boiling materials which were soluble in the liquid could be determined by TGA in nitrogen. The liquid filtrate was also analyzed by GC/MS and GC to determine the number of compounds dissolved in the tetralin from the resid conversion and to determine, if possible, their identities. However, much of the resid material which dissolved in the tetralin, even after the liquefaction reaction under the conditions used, was still too low in volatility to be detected with GC or GC/MS. The soluble material in the liquid consisted of some low boiling conversion products of the tetralin, some material in the original resid that was tetralin soluble, and also material formed by breakdown of the resid into tetralin soluble substances.

The tetralin soluble resid plus that solubilized in the liquefaction process was estimated by comparison of the ash content of the solid filter cake with that of the unreacted resid. The filtered solid resid was dried in a vacuum oven at 100 °C for 48 hr, then ground in a mortar and pestle and dried again to remove any residual tetralin. This is important, as change of the resid by the tetralin occurs during the TGA analysis itself (see Figure 3). A TGA run on the filtered solid resid is shown in Figure 4. TGA runs on the filtered solid resids give several characteristic parameters, such as VM (volatile matter), FC (fixed carbon), and Ash for an un-catalyzed sample(7). By running in nitrogen at a ramp of 10°C/min to 600 °C, the amount of volatile matter (VM) can be determined. Then, by introducing oxygen at 600°C, the loss in weight was observed. It is due to the oxidation of the combustible materials in the resid, so called "fixed carbon (FC)", leaving the residue as mineral matter or ash. Thereafter, it is run at a ramp of 100 °C/min to 900 °C in oxygen to determine any further oxidation of the ash residue at higher temperatures. As shown in Figure 4, there is no further loss in weight for un-catalyzed samples.

Determination of Catalyst Concentration

For a catalyzed sample, the 600 °C-oxidized residue includes the ash from the resid and partially oxidized catalyst. Since the mineral matter (ash) from the resid was used as a reference for determination of conversion, the amount of the residue must be corrected for the catalyst added. A TGA run on a solid resid with catalyzed sample is shown in Figure 5. For this catalyzed sample, VM determined by TGA consists of VM from resid and weight loss of the catalyst; FC determined by TGA represents FC from resid and the first stage of catalyst oxidation; Ash_1 determined by TGA contains ash from the resid and partially oxidized catalyst; and Ash_2 determined by TGA includes ash from the resid and ash from the catalyst. During the second oxidation period, i.e., the interval of the temperature ramped at 100 °C/min to 1000 °C in oxygen and kept at 1000 °C for 120 min, an additional loss in weight was obtained. It is due presumably to the oxidation of the sulfided catalyst to the oxides. This can be translated into catalyst concentration by comparison of the weight loss at 1000 °C with the weight losses obtained on catalyst alone and a calibration sample. A TGA run on the pure sulfided catalyst is demonstrated in Figure 6. Running in nitrogen at 10 °C/min to 600 °C, the first drop in weight loss was detected. As oxygen was added at 600 °C, the second drop in weight loss was obtained. This loss in weight is due to the partial oxidation of the catalyst, designated as the first stage of catalyst oxidation. When finally running in oxygen from 600 °C at 100 °C/min to 1000 °C and holding at 1000 °C for 120 min, the third drop in weight loss was observed. This loss in weight was due to the complete oxidation of the catalyst, designated as the second stage of catalyst oxidation, leaving the residue (so called "Ash_2") as the ash from the catalyst, i.e., metal oxides. As mentioned above, this third drop in weight loss is solely caused by the second stage of catalyst oxidation, because there is no such drop for the un-catalyzed resid sample alone (see Figure 4). Therefore, the amount of catalyst present in the resid-catalyst mixture is proportional to the third drop obtained by TGA, i.e.,

$$Catalyst\ (wt\%) = \alpha\,(Ash_1(wt\%) - Ash_2(wt\%)) \qquad (1)$$

where α is a scale constant which can be determined by a calibration sample, Ash_1 a 600 °C residue (wt%), and Ash_2 a 1000 °C residue (wt%). The amount of ash from the resid can be estimated by the mass balance of the ash in the resid and that from the catalyst. Since the ash from the catalyst ($Ash_{catalyst}$) and the ash from the resid (Ash_{resid}) are unchanged throughout the reactor runs, their ratio should be a constant, i.e.,

$$k = \frac{Ash_{catalyst}(wt\%)}{Ash_{resid}(wt\%)}. \qquad (2)$$

The constant k can be determined by running a calibration sample. For a catalyst-resid mixture, the final residue (Ash_2) by TGA includes ash from the resid and ash from the

catalyst. Therefore, we have another equation which can be used to solve simultaneously with Equation 2 for the amount of the ash from the resid:

$$Ash_{catalyst}(wt\%) + Ash_{resid}(wt\%) = Ash_2(wt\%) . \quad (3)$$

Determination of Resid Conversion

Significant proportions of the resids are soluble in tetralin at room temperature (48 to 55 % for resid 1 and 37 to 42 % for resid 2 , depending on the tetralin to resid ratio). During the liquefaction process, particularly in the presence of a catalyst, further solid resid becomes soluble in the tetralin. To the extent that this solubilization represents conversion of the resid, it can be estimated by comparing the amount of ash present in the solid filter cake (X) with that of the unreacted resid (X_0). The total amount of resid dissolved in the tetralin, D, can be calculated using the equation:

$$D\ (wt\%) = (1 - \frac{X_0}{X}) \times 100\ (wt\%) . \quad (4)$$

D of course is the sum of the soluble resid and the resid which has become solubilized in the conversion process. Conversion can be estimated by subtracting the soluble portion of the resid D at time zero, from the D at time t. Equation 4 is valid because no inorganic matter (ash) goes into the liquid (see Figure 2). When catalyst is used, the ash determined by TGA must be corrected for the ash from the catalyst added.

RESULTS AND DISCUSSION

The experimental error for determination of the TGA characteristic variables (VM, FC, and Ash) is less than ±0.5% of the measured values. A TGA run on a liquid filtrate shown in Figure 2 gives two fractions: a fraction boiling in the tetralin range and a higher-boiling tetralin soluble fraction. TGA measurements can not discriminate among the converted components whose boiling points are close to tetralin. Therefore, GC and GC/MS were used to detect them. Tests on both un-catalyzed and catalyzed samples by GC and GC/MS have shown that there is some (up to 0.5 wt% for un-catalyzed runs, and 2 wt% for catalyzed runs) of material in the liquid filtrate boiling close to tetralin, which is formed by breakdown of resid. This represents about 5% to 20% conversion of the resid which has been converted to low boiling material. These low boiling substances consist of more than 50 individual compounds detected by GC, each too low in concentration to be identified. The GC/MS used in this work is not sensitive enough to detect these many low boiling materials in the very low concentrations involved.

The percent resid dissolved in tetralin (D) was calculated using Equation 4. A portion of the resid is tetralin soluble even at room temperature. To visualize the source of the dissolution portion in the resids under various conditions, resid-normalized VM, FC and D are plotted with various conditions for Resid 1 in Figure 7. It is obvious that the majority of the dissolution portion (about 80 wt%) comes from the VM in the resid.

For un-catalyzed 30 min reactor runs of Resid 1, the percent resid dissolved in tetralin (D) increases only about 1 wt% at 412 °C, and only about 6 wt% at 435 °C for T/R = 3.0 samples. For un-catalyzed 30 min reactor runs of Resid 2, the percent resid dissolved in tetralin (D) increases about 2 wt% at 410 °C, and about 13 wt% at 434 °C for T/R = 3.0 samples, which shows about twice the reactivity as resid 1.

Evolution rate versus temperature (DTG vs. T curve) of these uncatalyzed liquid samples were determined on the liquid filtrate from the calibration sample (treated with tetralin at room temperature), and resid 1 reacted for 5 min at 434 °C, and for 30 min at 435 °C. The results as plotted in Figure 8 indicate a bimodal distribution in the evolution pattern. There is no observable change in the evolution pattern through the reactor runs under the experimental conditions we have used in this project, although the material went into solution. A similar evolution rate vs. temperature of the liquid samples for the resid 2 conversion at 435 °C is obtained. There is also no significant change in the molecular weight distribution (evolution temperature pattern) in the liquid filtrate.

Plots of the D vs. reaction times for resid 1 at different temperatures and at T:R:Cat. (Tetralin:Resid:Catalyst) = 3:1:1 are shown in Figure 9. For reaction temperature around 415 °C, the percent resid dissolved in tetralin (D) increases with reaction time up to about 10% for 30 min (ten times higher than the un-catalyzed run). For a reaction temperature around 434 °C, the percent resid dissolved in tetralin (D) increases with reaction time up to 20 min, then it levels off. In 20 min, it increases to about 17% (four times higher than un-catalyzed runs). Plots of the D vs. reaction times for resid 2 at different temperatures and at T:R:Cat. = 3:1:1 are similar to the plots in Figure 9. For a reaction temperature around 415 °C, the percent resid dissolved in tetralin (D) increases with reaction time up to about 31.6% for 30 min (fifteen times higher than un-catalyzed runs). For a reaction temperature around 440 °C, it increases with reaction time up to 10 min, then it levels off. In 10 min, it

increases to about 33.2% (eight times higher than un-catalyzed runs). It is interesting to point out that:

1. in the lower temperature runs, they approached the same value of D in high temperature runs at longer reaction time (Figure 9);
2. at reaction time 30 min, the percent resid dissolved in tetralin (D) on an ash-free basis for 421 °C approaches about 87% and that for 442 °C to about 91%;
3. the reactivity of the resid 2 in catalyzed conversion is higher than that of the resid 1, the similar order which is observed in un-catalyzed conversion.

To examine the evolution pattern (a function of the molecular weight distribution) of the converted materials in the liquid filtrate, slow ramp TGA (1 °C/min) was run on selected liquid samples. Evolution rate vs. temperature of the liquid samples from the catalyzed resid 1 conversion: 0 min (the liquid filtrate from calibration sample, which is treated with tetralin at room temperature), 5 min at 434 °C, and 30 min at 435 °C for resid 1 was plotted in Figure 10. This shows that the evolution rate for reactor runs significantly shifted to lower temperature. In other words, there is a notable reduction in the average molecular weight by the catalyst. This can be quantitatively described by two characteristic variables: peak evolution temperature (T_{peak}) and mean evolution temperature (T_{mean}). T_{peak} is defined as the evolution temperature at maximum evolution rate. T_{mean} is defined as the mean evolution temperature weighted by the evolution rate. Mathematically,

$$T_{mean} = \frac{\sum_i (Evolution\ Rate)_i T_i}{\sum_i (Evolution\ Rate)_i}. \qquad (5)$$

The calculated T_{peak} and T_{mean} for the catalyzed runs and reference sample (at 0 min) are listed in Table 2. For longer reaction time, not only T_{mean} decreases by about 60 °C, but also T_{peak} shifted to lower temperature direction by about 50 °C. The same behavior was observed in the resid 2 catalyzed conversion. It is interesting to note from Figures 8 and 10 that the soluble fraction of the resids shows a bimodal distribution of differential evolution peaks in the TGA. The higher temperature peak disappears after catalytic reactions, but is unchanged in reactions without catalyst.

SUMMARY AND CONCLUSIONS

1. The combination of reaction in the STBR (Short Time Batch Reactor) with TGA analysis of the liquid filtrates and the "un-converted" filtered solid resids provides a direct and reproducible means of indicating the breakdown of coal-derived liquefaction resids under liquefaction conditions.
2. The conversion of resid to tetralin soluble material is determined by relating the inorganic matter (ash) in the reacted resid with that of the un-reacted resid. Conversion of un-catalyzed tetralin-insoluble resids to tetralin soluble products in this study was very low (< 10 wt%) under coal liquefaction conditions, however, up to 50 wt% of the resid is tetralin-soluble at room temperature.
3. Up to 80% (ash-free basis) of the room temperature tetralin insoluble resid is solubilized in tetralin using sulfided Ni/Mo on alumina catalyst at 434 °C for 10 min.
4. A method has been devised for determining the catalyst concentration and the ash from the resid by TGA.
5. The two resids examined showed somewhat different reactivities.
6. In the catalyzed experiments, a progressive decrease in the temperature evolution range (as measured by TGA) of the solubilized materials with time under liquefaction conditions is observed by TGA. In the un-catalyzed experiments, no change in the evolution range of the solubilized materials with time up to 30 min is observed by TGA.
7. The majority of tetralin soluble or solubilized materials come from the volatile matter in the resids.
8. While liquefaction conditions, particularly in the presence of Ni/Mo on alumina catalyst are effective in converting tetralin insoluble to tetralin soluble material and in reducing the average molecular weight (as shown by TGA), only a small fraction (perhaps 20 percent) of this material is converted to the boiling range of gasoline or diesel fuel under the liquefactions conditions studied (30 minutes at 434°C) as shown by GC.

ACKNOWLEDGEMENTS

The Assistance and advice of F.P. Burke, R.A. Winschel and S.D. Brandes of CONSOL Inc in preparation and analysis of the resid and catalyst samples used in this project is gratefully acknowledged. This work was supported by subcontract from CONSOL Inc. under U. S. DOE Contract No. DE-AC22-89PC89883.

REFERENCES

1 Whitehurst, D.D., Mitchell, T.O., and Farcasiu, M. *Coal Liquefaction* Academic Press, Chapter 7, p.192 (1980)

2 Ibrahim, M.M. and Seehra, M.S. *DOE/PC 89883-57* Oct 1992

3 Malhotra, R. and McMillan,D. *DOE/PC 89883-39* Jan 1992

4 Solum, M.S. and Pugmire, R.J. *DOE/PC 89883-65* Nov. 1992

5 Stock, L.M. and Cheng, C. *DOE/PC 89883-64* Nov 1992

6 Huang, H.; Calkins, W.H.; and Klein, M.T. *ACS Fuel Division Preprints* **38** (3), 1080 (1993)

7 Ottaway, M. *Fuel*, **61** (8), 713 (1982)

Table 1 Ultimate Analyses of the Two Resids

Sample	Ultimate (wt% MAF):	
Resid 1	C	90.24
Plant: Wilsonville	H	6.39
Run Number: 259	N	1.05
Sample Designator: V1067	S	1.49
Sampling Point: 2nd Stage Product	O (dif)	0.83
Feed Coal: Pittsburgh Seam, Ireland Mine	Ash, wt% as det.	10.21
Resid 2	C	91.03
Plant: Wilsonville	H	6.56
Run Number: 260	N	1.15
Sample Designator: V1067	S	0.09
Sampling Point: 2nd Stage Product	O (dif)	1.17
Feed Coal: Wyodak & Anderson Seam, Black Thunder Mine	Ash, wt% as det.	18.30

Table 2 Peak Evolution Temperatures (T_{peak}) and Mean Evolution Temperatures (T_{mean}) of the Liquid Filtrates from the Catalyzed Resid Conversion

Sample	T_{peak}, °C	T_{mean}, °C
Resid 1 + Catalyst		
0 min	320	349
5 min at 434 °C	318	322
30 min at 435 °C	273	291
Resid 2 + Catalyst		
0 min	307	321
30 min at 442 °C	274	282

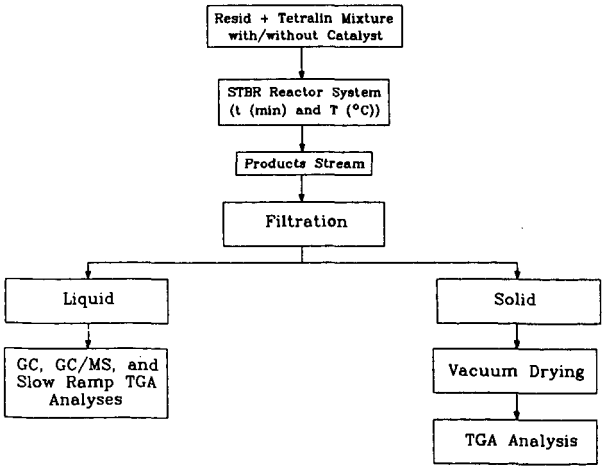

Figure 1 Schematic Diagram of the Experimental Procedure

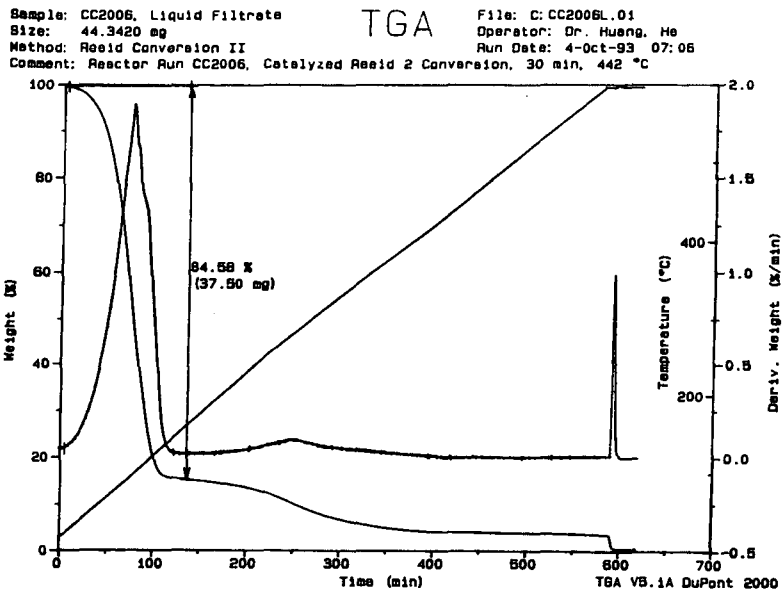

Figure 2 A TGA Run on a Liquid Filtrate of Catalyzed Reactor Run

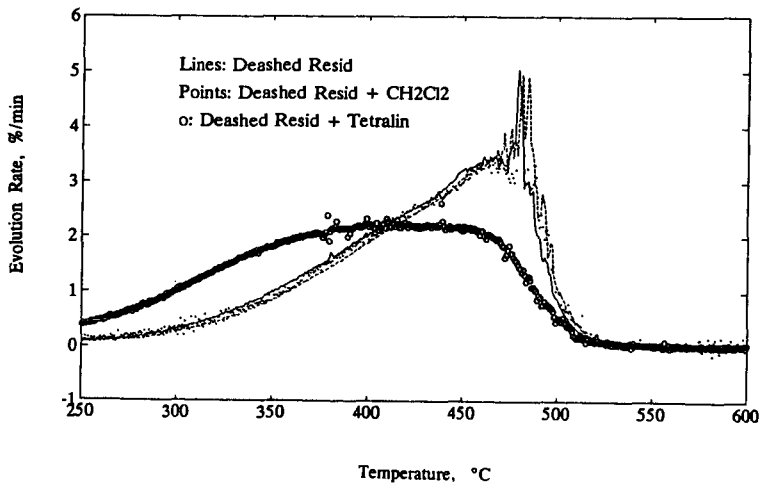

Figure 3 Effect of tetralin on TGA Analysis

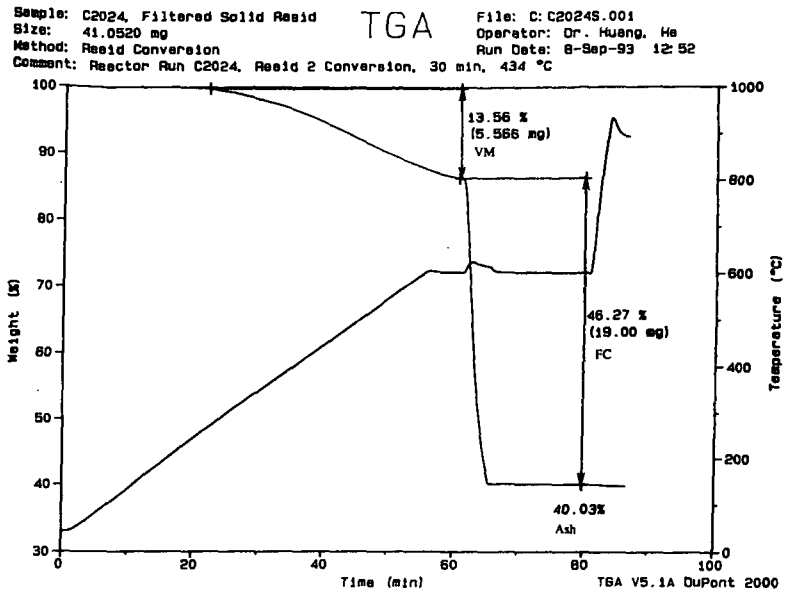

Figure 4 A TGA Run on a Filtered Solid Resid of Un-catalyzed Reactor Run

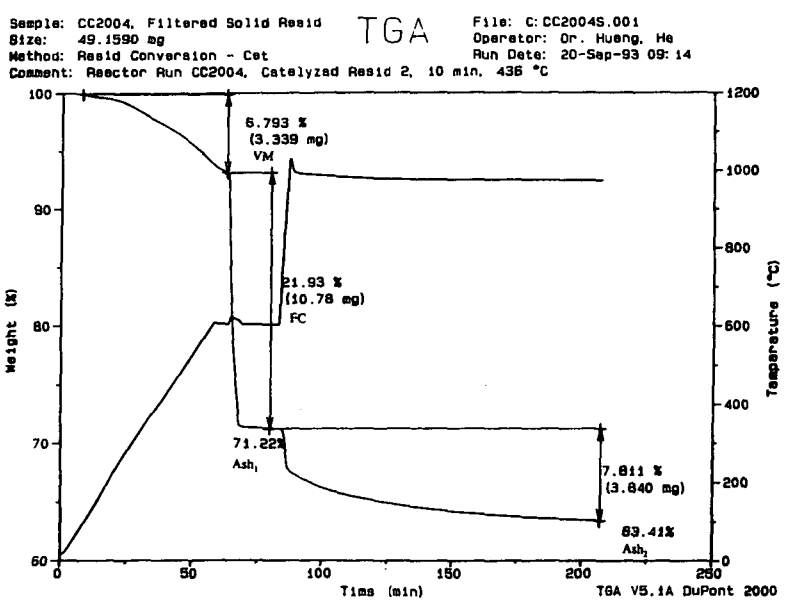

Figure 5 A TGA Run on a Filtered Solid Resid of Catalyzed Reactor Run

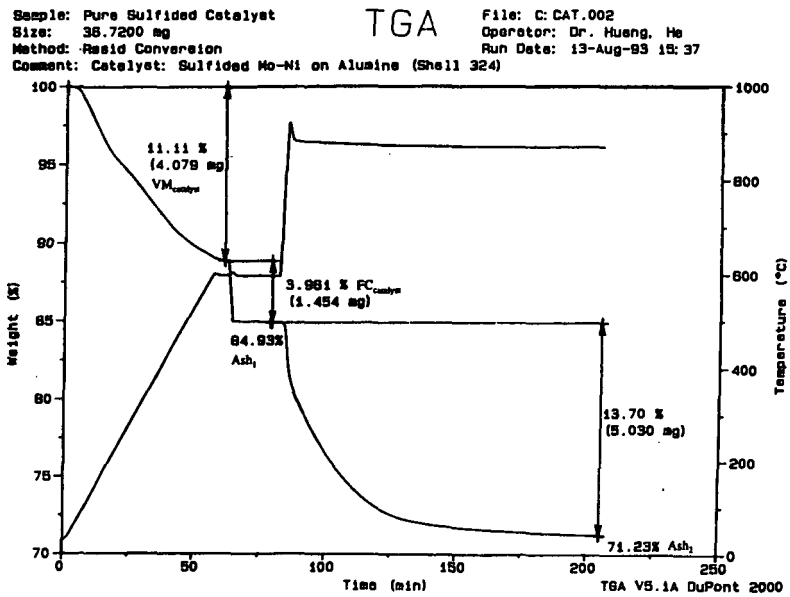

Figure 6 TGA Curves of the Pure Sulfided Catalyst of Mo-Ni on Alumina

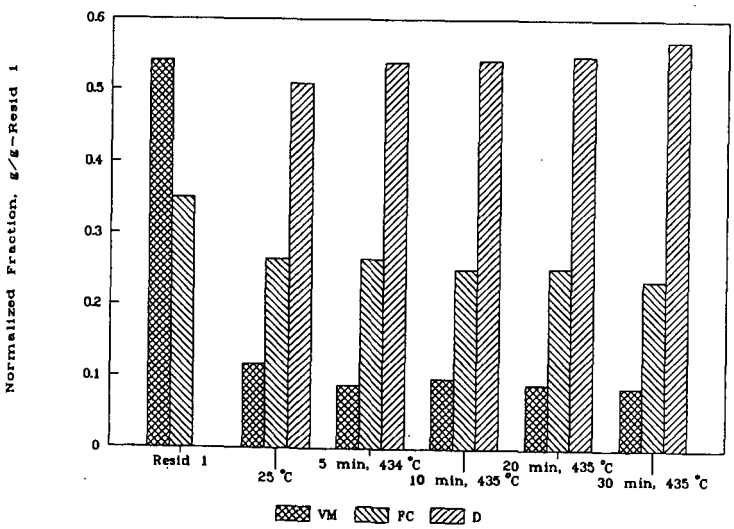

Figure 7 Resid-normalized VM, FC and D in the Resid 1 Treated or Reacted with Tetralin under Various Conditions (T/R = 3.0)

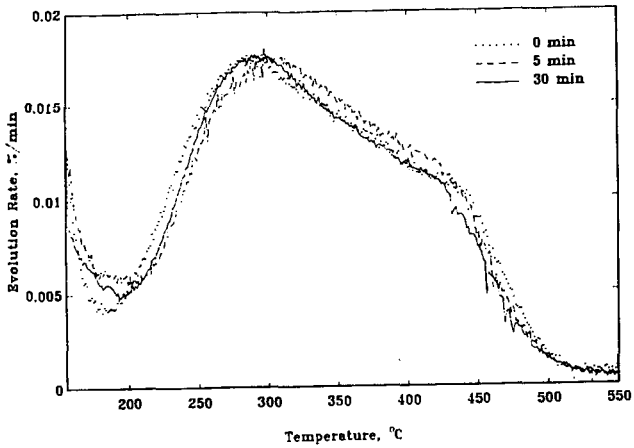

Figure 8 Evolution Rate (DTG) Versus Temperature Determined by Slow Ramp TGA (5 °C/min) for the Liquid Filtrates of Un-catalyzed Resid 1 Conversion (T/R = 3.0): 0 min, 5 min at 434 °C, and 30 min at 435 °C

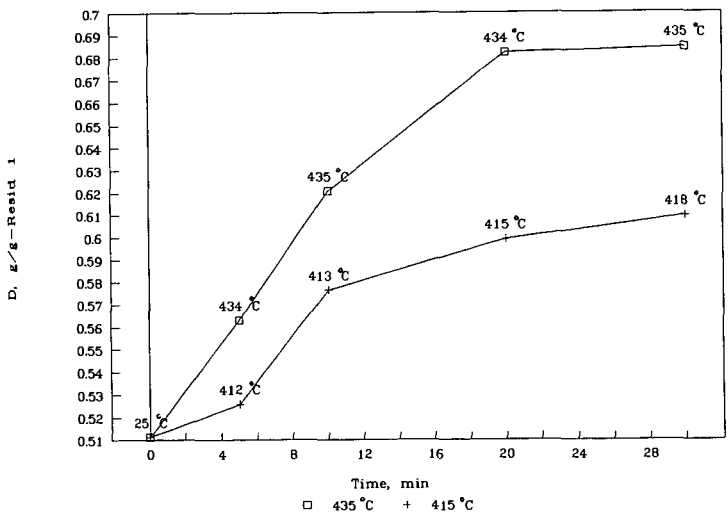

Figure 9 Percent Resid Dissolved in Tetralin (D) Versus Reaction Time of Catalyzed Resid 1 Conversion at Two Temperatures (T:R:Catalyst = 3:1:1)

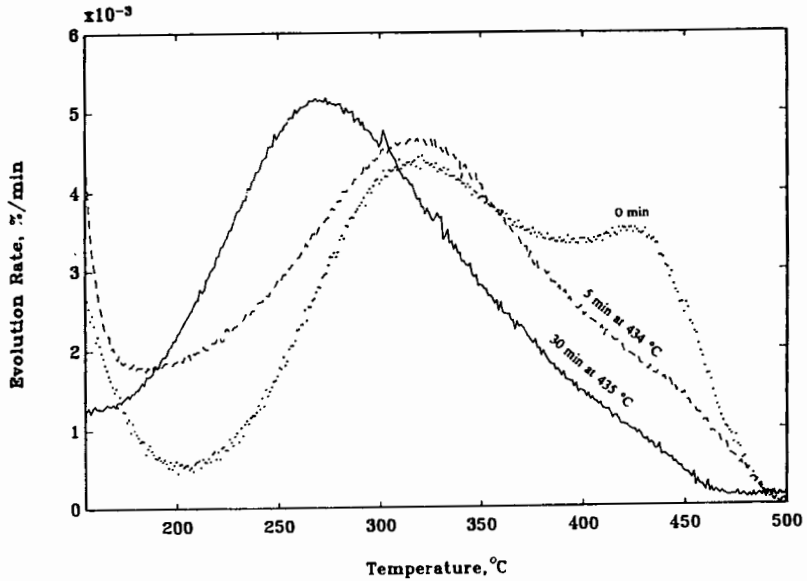

Figure 10 Evolution Rate (DTG) Versus Temperature Determined by Slow Ramp TGA (1 °C/min) for the Liquid Filtrates of Catalyzed Resid 1 Conversion (T/R = 3.0): 0 min, 5 min at 434 °C, and 30 min at 435 °C

polarization magic angle spinning (CPMAS) technique. All CPMAS spectra were obtained on a Chemagnetics NMR Model M100s. The ^{13}C frequency was 25.15 MHz. The pulse delay was 1 second and the contact time was 1 ms.

RESULTS AND DISCUSSION

Conversions of Liquefaction

The structures of low-rank coals are characterized by smaller aromatic ring clusters joined by a higher proportion of weak crosslinks than coals of higher rank. This kind of structural feature results in their thermally sensitive natures. The bond cleavages of those weak crosslinks may occur at low temperatures to yield free radicals. If the radicals are not stabilized, retrogressive reactions producing materials difficult to liquefy will take place. Therefore, it is important to determine the optimum temperatures for each coal at which thermal cleavages readily occur while retrogressive reactions are unlikely to occur. Liquefaction experiments were carried out at 250°C, 300°C, 350°C, 400°C and 450°C with the presence of H_2 and the absence of a catalyst and a solvent. The conversion data are shown in Figure 1. At 350°C and below, reactions of all three coals are very limited, with conversions below 20%. As temperature increases to 400°C and 450°C, conversions significantly and continuously increase. However, our earlier study [8] has shown that although a temperature of 450°C seems to be more beneficial in obtaining high conversions, it causes severe retrogressive reactions which are indicated by very high aromaticities of the reaction residues. Therefore 400°C is considered to be the best temperature for liquefaction of these coals.

However, even at the optimum temperature, 400°C, no more than 50% of the coals can be converted to THF solubles when neither a catalyst nor a solvent is involved. In an effort to enhance the conversions, ATTM was added as a catalyst precursor; tetralin and 1-methylnaphthalene were used as a hydrogen donor and a non-donor solvent respectively. The effects of the catalyst and solvents are presented in Figure 2. By using the catalyst, the conversions were increased from 45% to 95.5% for the DECS-1 coal, from 24.2% to 78.5% for the DECS-9 coal, and from 30.6% to 63.5% for the DECS-11 coal. These increases are contributed by significant gains in oils and asphaltenes. The gas yields in the catalytic and non-catalytic reactions are very similar for each coal, which is in an agreement with our earlier observation that the gas yield is a function of temperature, and the use of the catalyst or the donor solvent has no significant effect on it [8]. To maximize the conversion, tetralin and 1-MN were applied in addition to the catalyst. As a donor solvent, tetralin further causes more coal converted to THF solubles for DECS-9 and DECS-11. For DECS-1, there is no increase in conversion, although that is because even with only the catalyst, the conversion reaches 95%. It is reasonable to say that this may already be the practical maximum conversion limit. As a non-donor solvent, 1-MN has a very insignificant effect on the conversions of all the three coals. Comparing conversions at different reaction conditions, it is found that adding the catalyst is sufficient to achieve the highest conversion for the DECS-1 coal; while it is necessary to add both the catalyst and the donor solvent for the DECS-9 and the DECS-11 coals. Among these coals, the DECS-11 is relatively unreactive, its conversion can reach only about 80% at the best reaction condition applied in this study.

Product Characterization

To produce materials from a coal for making the special chemicals, a high conversion has to be achieved and, more importantly, those desirable structural units in the coal macromolecular network have to be converted to individual molecules. In this work, one- to four-ring aromatic or alkylaromatic compounds were desired. In other words, more aromatic carbons have to be converted to THF solubles. To determine the amounts of aromatic carbons converted, the reaction residues as well as the vacuum-dried coal samples were analyzed by CPMAS ^{13}C NMR. The spectra were curve-fitted and integrated, and the aromaticities (f_a) were calculated based on the areas covered by the spectra in aromatic and aliphatic regions. Since the weights of both coals and residues are known, and data of overall conversions from coals to THF solubles are available, the percentages of the reacted aliphatic and aromatic carbons can be determined, as shown in Figure 3 and 4. In these figures, it is apparent that converting aliphatic carbons from the coal networks to THF solubles is much easier than converting aromatic carbons. At 400°C, even without catalyst or solvent, over 50% of aliphatic carbons are converted for all three coals. Adding the catalyst can increase the aliphatic conversions to greater extents. Furthermore, if tetralin is used in addition to the catalyst, slight increases in the aliphatic carbon conversions of DECS-9 and DECS-11 are observed, while that of DECS-1 shows almost no change, which is expected because even only with the catalyst, the conversion approaches 100%. Comparing these three coals, the aliphatic carbons in DECS-1 are the easiest to be converted; those in DECS-11 are the least. In Figure 4, the aromatic carbons appear to be more difficult to be removed from the coal networks, and they are affected more strongly by the catalyst or the donor solvent than the aliphatic carbons. Without the presence of the catalyst or the donor solvent, less than 20% can be converted. For the DECS-9 coal, the conversion is negative, meaning that there are more aromatic carbons than we start with. This indicates the occurrence of retrogressive reactions. Therefore, to convert the aromatic carbons, it is crucial to use the catalyst, the donor solvent or both. For the

polarization magic angle spinning (CPMAS) technique. All CPMAS spectra were obtained on a Chemagnetics NMR Model M100s. The ^{13}C frequency was 25.15 MHz. The pulse delay was 1 second and the contact time was 1 ms.

RESULTS AND DISCUSSION

Conversions of Liquefaction

The structures of low-rank coals are characterized by smaller aromatic ring clusters joined by a higher proportion of weak crosslinks than coals of higher rank. This kind of structural feature results in their thermally sensitive natures. The bond cleavages of those weak crosslinks may occur at low temperatures to yield free radicals. If the radicals are not stabilized, retrogressive reactions producing materials difficult to liquefy will take place. Therefore, it is important to determine the optimum temperatures for each coal at which thermal cleavages readily occur while retrogressive reactions are unlikely to occur. Liquefaction experiments were carried out at 250°C, 300°C, 350°C, 400°C and 450°C with the presence of H_2 and the absence of a catalyst and a solvent. The conversion data are shown in Figure 1. At 350°C and below, reactions of all three coals are very limited, with conversions below 20%. As temperature increases to 400°C and 450°C, conversions significantly and continuously increase. However, our earlier study [8] has shown that although a temperature of 450°C seems to be more beneficial in obtaining high conversions, it causes severe retrogressive reactions which are indicated by very high aromaticities of the reaction residues. Therefore 400°C is considered to be the best temperature for liquefaction of these coals.

However, even at the optimum temperature, 400°C, no more than 50% of the coals can be converted to THF solubles when neither a catalyst nor a solvent is involved. In an effort to enhance the conversions, ATTM was added as a catalyst precursor; tetralin and 1-methylnaphthalene were used as a hydrogen donor and a non-donor solvent respectively. The effects of the catalyst and solvents are presented in Figure 2. By using the catalyst, the conversions were increased from 45% to 95.5% for the DECS-1 coal, from 24.2% to 78.5% for the DECS-9 coal, and from 30.6% to 63.5% for the DECS-11 coal. These increases are contributed by significant gains in oils and asphaltenes. The gas yields in the catalytic and non-catalytic reactions are very similar for each coal, which is in an agreement with our earlier observation that the gas yield is a function of temperature, and the use of the catalyst or the donor solvent has no significant effect on it [8]. To maximize the conversion, tetralin and 1-MN were applied in addition to the catalyst. As a donor solvent, tetralin further causes more coal converted to THF solubles for DECS-9 and DECS-11. For DECS-1, there is no increase in conversion, although that is because even with only the catalyst, the conversion reaches 95%. It is reasonable to say that this may already be the practical maximum conversion limit. As a non-donor solvent, 1-MN has a very insignificant effect on the conversions of all the three coals. Comparing conversions at different reaction conditions, it is found that adding the catalyst is sufficient to achieve the highest conversion for the DECS-1 coal; while it is necessary to add both the catalyst and the donor solvent for the DECS-9 and the DECS-11 coals. Among these coals, the DECS-11 is relatively unreactive, its conversion can reach only about 80% at the best reaction condition applied in this study.

Product Characterization

To produce materials from a coal for making the special chemicals, a high conversion has to be achieved and, more importantly, those desirable structural units in the coal macromolecular network have to be converted to individual molecules. In this work, one- to four-ring aromatic or alkylaromatic compounds were desired. In other words, more aromatic carbons have to be converted to THF solubles. To determine the amounts of aromatic carbons converted, the reaction residues as well as the vacuum-dried coal samples were analyzed by CPMAS ^{13}C NMR. The spectra were curve-fitted and integrated, and the aromaticities (f_a) were calculated based on the areas covered by the spectra in aromatic and aliphatic regions. Since the weights of both coals and residues are known, and data of overall conversions from coals to THF solubles are available, the percentages of the reacted aliphatic and aromatic carbons can be determined, as shown in Figure 3 and 4. In these figures, it is apparent that converting aliphatic carbons from the coal networks to THF solubles is much easier than converting aromatic carbons. At 400°C, even without catalyst or solvent, over 50% of aliphatic carbons are converted for all three coals. Adding the catalyst can increase the aliphatic conversions to greater extents. Furthermore, if tetralin is used in addition to the catalyst, slight increases in the aliphatic carbon conversions of DECS-9 and DECS-11 are observed, while that of DECS-1 shows almost no change, which is expected because even only with the catalyst, the conversion approaches 100%. Comparing these three coals, the aliphatic carbons in DECS-1 are the easiest to be converted; those in DECS-11 are the least. In Figure 4, the aromatic carbons appear to be more difficult to be removed from the coal networks, and they are affected more strongly by the catalyst or the donor solvent than the aliphatic carbons. Without the presence of the catalyst or the donor solvent, less than 20% can be converted. For the DECS-9 coal, the conversion is negative, meaning that there are more aromatic carbons than we start with. This indicates the occurrence of retrogressive reactions. Therefore, to convert the aromatic carbons, it is crucial to use the catalyst, the donor solvent or both. For the

DECS-1 coal, the catalyst is sufficient to achieve over 95% aromatic conversion; for the DECS-9 coal, with both the catalyst and the donor solvent, 98% can be obtained; while for the DECS-11 coal, the least convertible coal in terms of conversion, even with both the catalyst and the donor solvent, only about 70% aromatic conversion can be achieved.

The asphaltenes and the preasphaltenes were also studied by CPMAS ^{13}C NMR. Unfortunately, their spectra look so much like the vacuum-dried coals that they can not be characterized without other analytical techniques. The hexane solubles, defined as oils, were analyzed by gas chromatography, identified by gas chromatography/mass spectrometry. Figure 5 represents the oils from the DECS-9 coal without the catalyst or the donor solvent, *a*; with the catalyst but not the donor solvent, *b*; and with both the catalyst and the donor solvent, *c*. In Figure 5-*a*, the oil contains a high proportion of long-chain alkanes, i. e. from n-C_{12} to n-C_{33}. At retention time of about 6.0 minutes, there is a very strong peak identified as toluene. In low-rank coals such as DECS-9, small aromatic clusters dominate [4, 5], and they are connected by aliphatic crosslinks. Once the crosslinks break, these small aromatic clusters will be released. In the DECS-9, as shown in our recent work [4], one-ring structural units are abundant and thus when liquefying the coal, toluene (instead of benzene) will be a major product, because the benzylic C-C bond has a much lower dissociation energy than the phenyl C-C bond [9]. Relative to those of aliphatics, the amounts of aromatic compounds in the oil (with relation times from 15 minutes to 30 minutes) are much smaller (Figure 5*a*), indicating that this reaction condition suppresses the production of aromatic compounds in the oil. Comparing with the case without the catalyst or the donor solvent, adding ATTM into the reaction system appears to favor the yields of aromatic compounds. As shown in Figure 5*b*, the alkylbenzenes, phenol and alkylphenols are the major components in the oil. This observation agrees with our earlier finding that the catalyst is particularly beneficial in converting the aromatic carbons from the coal to THF solubles rather than converting the aliphatic carbons [8]. Furthermore, when we use tetralin in addition to the catalyst, the yields of phenolic compounds remain very high, Figure 5*c*; the one-ring aromatics seem to be in a lower proportion; and the yields of two-ring aromatics, such as indane, alkylindanes and alkylnaphthalenes have increased. The large peaks at retention times about 24.5 minutes and 27.0 minutes are due to tetralin and naphthalene, the solvent and the dehydrogenated solvent. It is likely that the increased yields of alkylindanes and alkylnaphthalenes are due, at least in part, to the use of tetralin. In the GC study, three- or four-ring compounds appear to be in small amounts and not affected by either the catalyst nor the solvent. This may be because they are less abundant than the one- or two-rings in the coal, or because their solubilities in hexane are smaller and therefore it is hard to detect the differences at different cases.

CONCLUSIONS

In liquefaction of the three low-rank coals, temperature is found to be optimum at 400°C. Reactions without the catalyst or the donor solvent provide very low conversion, i. e. less than 50%, for all three coals. As for the DECS-1 coal, the ATTM-derived catalyst is sufficient in terms of a high conversion. As for the DECS-9 coal, only when both the catalyst and the donor solvent are used can conversion as high as 98% be achieved. For the DECS-11 coal, even under the best reaction condition, which is at 400°C with the catalyst and the solvent, the conversion only reaches 78%. Therefore, the DECS-11 coal is the least convertible coal among the three.

The investigation on reaction residues by solid-state NMR shows that it is relatively easier to convert aliphatic carbons from coals to THF solubles, and that the catalyst and the donor solvent can both be beneficial but the effects are moderate. The amounts of aromatic carbons being converted from the coals appear to be small when the catalyst or the donor solvent is not present, and they can even be negative, indicating that retrogressive reactions have occurred. Adding the catalyst and the solvent significantly enhances the reactions of aromatic carbons.

The study of the oils agrees with what has been observed on the residues. Without the presence of the catalyst or the solvent, the oils contain large amounts of long-chain alkanes; while with the catalyst and the donor solvent, more aromatic materials, such as phenolic compounds, alkylbenzenes and some two-ring compounds, can be produced. With further extraction and purification, these compounds might be used as for making specialty chemicals for some advanced materials.

ACKNOWLEDGEMENT

The authors gratefully thank the United States Department of Energy for the financial support. We also want to thank Dr. M. Baird and Dr. M. A. Nowak for helpful discussions.

REFERENCES

1. Song, C., and Schobert, H. H., *ACS Div. of Fuel Chem. Prepr.* **1992**, 37(2), 524-532
2. Song, C., and Schobert, H. H., *Fuel Proc. Tech.*, **1993**, 34, 157-196

3. Schlosberg, R. H., Chemicals from coal, in *Fuel Science and Technology Handbook*, Ed. by J. G. Speight., **1990**, Chap 24, Marcel Dekker
4. Song, C., Hou, L., Saini, A. K., Hatcher, P. G., and Schobert, H. H., *Fuel Proc. Tech.*, **1993**, 34, 249-276
5. Schobert, H. H., *Resources, Conservation and Recycling*, **1990**, 3, 111-123
6. Schobert, H. H., *The Chemistry of Hydrocarbon Fuels*, **1990**, Butterworth
7. Huang, L., Song, C., and Schobert, H. H., *ACS Div. of Fuel Chem. Prepr.* **1992**, 37(1), 223-227
8. Huang, L., Song, C., Schobert, H. H., *ACS Div. of Fuel Chem. Prepr.* **1993**, 38(3), 1093-1099
9. McMurry, J. *Organic Chemistry*, **1984**, Brooks/Cole

Table 1. Analysis of the coal samples

	DECS-1	DECS-11	DECS-9
Sources & Rank			
state	Texas	North Dakota	Montana
county	Freestone	Mercer	Bighorn
city	Fairfield		Decker
seam	Bottom	Beulah	Dietz
ASTM rank	subbit C	lignite	subbit B
sampling date	12/11/89	6/15/93	6/12/90
Proximate (wt%, ar)			
moisture	30.0	33.4	24.7
ash	11.1	6.4	4.8
volatile	33.2	37.4	33.5
fixed carbon	25.8	22.9	37.1
Elemental (wt%, dmmf)			
carbon	76.1	74.2	76.1
hydrogen	5.5	4.4	5.1
nitrogen	1.5	1.0	0.9
organic sulfur	1.1	0.4	0.3
oxygen	15.8	20.0	17.5

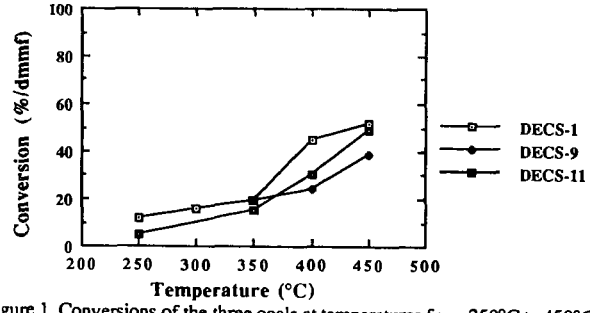

Figure 1. Conversions of the three coals at temperatures from 250°C to 450°C without a catalyst or a solvent

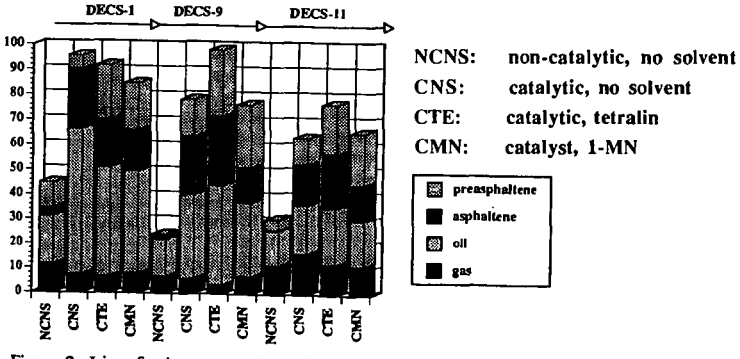

Figure 2. Liquefaction conversions of the three coals at 400°C under four different reaction conditions

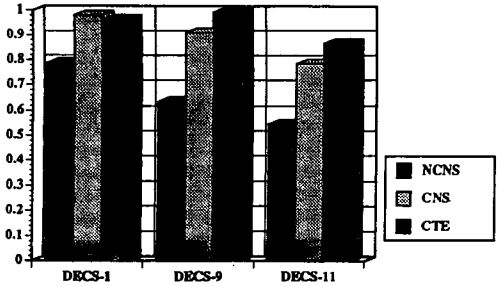

Figure 3. The amounts of aliphatic carbons being converted from the three coals to THF solubles at 400°C under three different conditions

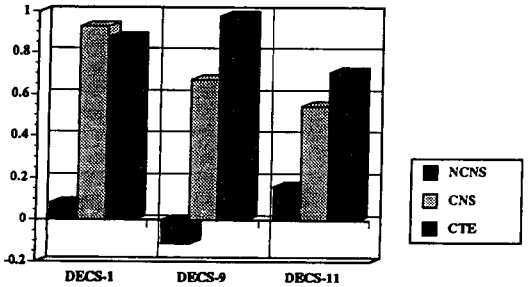

Figure 4. The amounts of aromatic carbons being converted from the three coals to THF solubles at 400°C under three different conditions

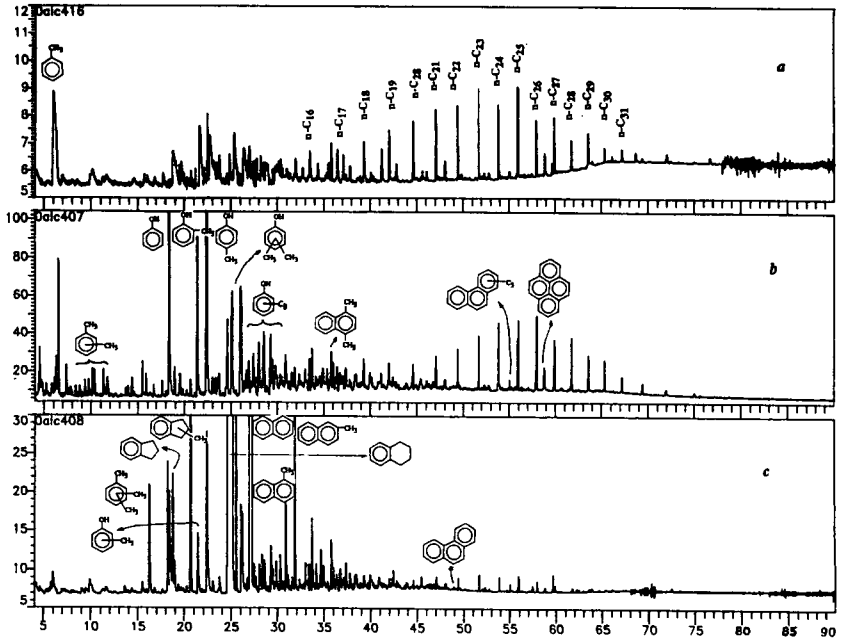

Figure 5. Analysis of the oil samples from the DECS-9 coal using gas chromatograph. a) the sample from the reaction without a catalyst or a solvent; b) the sample from the reaction with the ATTM-derived catalyst but without a solvent; c) the sample from the reaction with both the catalyst and tetralin.

PRODUCTION OF ACTIVATED CARBONS FROM A VITRAIN CONCENTRATE FROM THE STOCKTON COAL.

Chris Toles, Susan M. Rimmer (Department of Geosciences, University of Kentucky, Lexington, KY 40506-0053)
Frank Derbyshire, and Marit Jagtoyen (Center for Applied Energy Research, University of Kentucky, 3572 Iron Works Pike, Lexington, KY 40511)

Keywords: Activated carbon, chemical activation, phosphoric acid

Introduction

Earlier, related studies have shown that porous carbons can be produced by phosphoric acid activation of coals and hardwood [1-4]. One of the findings was that the development of surface area appears to be rank-dependant. It is also supposed that maceral composition will affect the response to phosphoric acid activation, although there is no available information on this subject.

In this context, a study has been initiated of the phosphoric acid activation of coal macerals. The objectives are to examine the effects of maceral composition and rank on porosity development, and to understand the individual and collective contributions of maceral groups to the activation of coals by phosphoric acid.

In this study, a vitrinite concentrate from an hvA bituminous coal (Stockton) was used as starting material for the production of activated carbons by H_3PO_4 activation. The chemical, morphological, and surface area changes were followed as a function of reaction temperatures and are compared to the results of previous studies.

Experimental

Maceral Separation

Bench samples of Stockton coal (hvA bituminous) were collected from fresh highwall exposures in the field in eastern Kentucky. Samples were chosen for their high vitrain content. In the laboratory, vitrain-rich benches were chosen to facilitate hand picking of vitrains. The samples were coarsely ground in a mortar and pestle to about 4 mesh and then split into approximately 10g samples for later experiments.

Petrographic pellets were made from a representative split of the vitrain concentrate to ascertain maceral content and purity. Standard preparation and polishing techniques were used. The Stockton sample was found to have a mineral matter-free vitrinite content of 93.5%. Table 1 shows maceral composition for this sample as determined by point-count analysis.

Carbon Synthesis

Activated carbons were produced according to procedures described in earlier carbon studies [1-4]. A split of the vitrinite concentrate was placed in a quartz crucible with a known volume and concentration of phosphoric acid to give an acid/dry coal ratio of approximately 0.96. The quartz boat was placed in a stainless steel oven tube, which was then flushed with nitrogen gas. It was then reacted at a low temperature (170°C) for 0.5h after which it was heated to a final heat treatment-temperature (HTT) ranging from 350°C to 550°C, and allowed to react for 1h at temperature. After the sample had cooled to room temperature it was leached with hot distilled water until the pH of the leachate was at or near neutral. Leached samples were then dried in a convection oven at about 100°C for 1.5 to 2h. Prior to nitrogen BET analysis, these samples were further dried in a vacuum oven at 110°C to insure complete outgassing. For comparison thermal counterparts were also run. These splits were treated as already described except that no acid was added prior to heat treatment.

Characterization

Proximate and ultimate analyses were performed following standard procedures. Fourier-transform infrared spectroscopy (FTIR) data were collected on a Nicolet 20SX spectrometer at 4 cm^{-1} resolution using pressed KBr pellets which contained approximately 0.5wt % sample. Spectra were normalized to a 1/200 concentration of sample/KBr to allow direct comparison between spectra.

Epoxy impregnated pellets of each activated carbon were prepared for petrographic and vitrinite reflectance analysis. Optical characterization was performed on a Zeiss microscope equipped with a 40x oil immersion lens. Modal maximum vitrinite reflectance ($\%R_{max}$) measurements were collected from 25 samples/pellet. Measurements were taken at 546nm wavelength and standardized against a set of glass standards. Photographs were taken of several of the fields of view using the same microscope equipped with a 40x Antiflex lens. In several instances, the polars were crossed to determine the extent of anisotropy in the carbons.

Surface area measurements were obtained from nitrogen adsorption isotherms at 77K using a Quantachrome Autosorb 6. Macro and meso-pore volumes and surface areas were measured using a Quantachrome Autoscan-60 mercury porosimeter.

Results and Discussion

Optical Characteristics

The maximum vitrinite reflectance of the vitrinite-rich samples heat treated in the presence and absence of acid increases with increasing HTT (Fig.1). As found in earlier studies, up to HTT of 450°C the acid-treated carbons exhibit higher vitrinite reflectances than their thermal analogs, while above 450°C this relationship is reversed. Vitrain rich samples follow the same trends that were observed for whole coals [1-4].

In most of the carbons, it was noted that the desmocollinite reflectance was slightly lower than that of telocollinite, throughout the range of activation temperatures. Reflectance data reported here were measured on telocollinite. The apparent difference in reflectance between the two submacerals lessened with increasing HTT. At HTTs above 350°C it became more difficult to differentiate between desmocollinite and telocollinite, and this, as well as misidentification of semifusinite, may account for the spread in vitrinite reflectance values that were found in taking measurements. Resinite occurs in the desmocollinite of the vitrinite-rich samples up to HTTs of 350°C, after which it was no longer evident, having been either transformed or removed.

Some degree of anisotropy was observed in the vitrinites at higher HTTs, changes in reflectance of up to 0.1% were noted upon rotation of the stage. This anisotropy was clearly visible when the antiflex lens was used. The anisotropy did not develop to a great extent even at 450°C or 550°C, rather it occurred around vacuoles in the vitrinites.

These vacuoles (approximately 50 μm in diameter) were formed in both the thermal and acid-treated samples and become far more prevalent with increasing HTT. In the acid-treated samples at HTT of 350°C, some of the larger pieces of vitrinite showed evidence of a reaction front, usually associated with some of the vacuoles as well as with cracked edges. There was a visible difference in reflectance of the vitrinite by as much as 0.3% across these aureoles, with the higher reflectances being in the outer region. Examination of these aureoles with the antiflex objective suggested that they were reaction fronts rather than anisotropic zones. At the maximum HTT (550°C) the acid treated samples appeared much more macerated and friable, exhibiting many small pits between the larger vacuoles.

Chemical composition

Both the acid-treated and thermal suites of samples show a loss of hydrogen with increased HTT (Fig. 2); however, the loss of hydrogen with HTT is more extensive upon reaction with H_3PO_4. This result supports the FTIR observation that the acid treated samples lost aliphatic hydrogen more quickly than the thermal samples as found in previous studies with whole coals [1-4]. A negative relationship is found to exist between $\%R_{max}$ and H/C ratio. As the samples in both suites lose hydrogen there is a corresponding increase in $\%R_{max}$ (Fig.1).

FTIR analyses show good correspondence with the elemental data with respect to loss of hydrogen. As can be seen in Figure 3, the overall trend of decreasing aliphatic content with increased HTT can be seen by the disappearance of peaks in the 2900 cm^{-1} wavenumber range. The existence of various inorganic phases present in these samples obscures many of the peaks in the lower wavenumber range.

In the acid-treated samples there is a very strong peak around 1200cm^{-1} that in previous studies has been assigned to phosphate esters [3-4]. In these samples it appears that there is significant overlap in this region with inorganics that appear in the thermal control samples as a peak only slightly shifted up from the 1200 cm^{-1} peak.

The carbonyl peak at 1700cm^{-1} decreases in intensity and shifts to lower wavenumbers with increasing HTT in both the thermal and acid-treated samples. It disappears completely above 350°C. This shift is greater in the thermal blanks, between the parent and 350°C, than in the acid-treated samples. This may indicate that the carbonyl functions in the acid-treated samples are more strongly bound, perhaps by resonance with nearby double bonds.

Aliphatic peaks at about 2900cm^{-1} decrease in both of the sample suites and are virtually eliminated above 350°C. These peaks decrease more quickly for the acid-treated samples than for the thermal samples, and the aromatic C-H peak at 3000cm^{-1} appears more well developed in the acid runs. This latter effect may be more a function of greater intensity of the -OH broad peak which may be overlapping this peak in the thermal runs.

Surface Area Measurements

Table 2 shows that the thermally treated vitrain samples develop virtually no porosity or surface area. Upon acid treatment, porosity starts to develop after 350°C, with most of the porosity residing in the microporous range.

The data on the development of surface areas of acid treated samples with HTT are shown in figure (4) which also shows results obtained by Jagtoyen et al. [6] for different starting materials. In each case there is a maximum in the surface area with HTT which decreases with rank and shifts to higher temperatures.

The extent of surface area development decreases in the order: hardwood > subbituminous coal > hvC bituminous coal > hvA vitrain, which tends to confirm the supposition that the extent of metamorphism reduces the response to phosphoric acid activation [6].

Conclusions

A study has been made of the chemical activation of a vitrain concentrate, hand-picked from the Stockton hvA bituminous coal. Reactions were conducted at HTT from 350°C to 550°C. Thermal blanks were generated under similar conditions for comparison.

Changes in chemical compositon were followed by elemental analysis and FTIR. With increasing HTT, acid-treatment promotes more extensive loss of hydrogen. The infrared spectra show the early loss of aliphatic groups and increasing aromaticity for samples reacted with H_3PO_4. Shifting behaviour of the carbonyl peak at 1700cm^{-1} in the spectra suggests greater resonance stabilization of carbonyl functions in the acid-treated samples than in the thermal control samples.

Corresponding to these chemical changes, there is an increasing maximum vitrinite reflectance with HTT: this is higher for acid-treated than thermal carbons up to about 450°C, above which temperature the reverse is the case. These changes are in keeping with the findings of earlier studies.

Surface area development with HTT is less than found for lower rank materials, which is also in keeping with the suggestion that metamorphic changes reduce the response to H_3PO_4 activation. Hence, at this stage of the research, it is not yet possible to distinguish maceral from rank effects on pore structure development.

Acknowledgments

This study was made possible with the assistance of the DOE EPSCoR traineeship. Thanks go to the University of Kentucky Department of Geological Sciences and the University of Kentucky Center for Applied Energy Research for significant contributions of funds and access to equipment.

References

1. Derbyshire, F.J., Jagtoyen, M., McEnaney, B., Rimmer, S.M., Stencel, J.M., Thwaites, M.W., Proceedings 1991 ICCS Conference, 480-483, Newcastle, England, 16-20 September, 1991, Butterworth-Heinemann Ltd, 1991.

2. Derbyshire, F.J., Jagtoyen, M., McEnaney, B., Sethuraman, A.R., Stencel, J.M., Taulbee,D., and Thwaites, M.W., American Chemical Society, Fuel Division Preprints, **36** (3), 1072-1080, 1991.

3. Jagtoyen, M., McEnaney, B., Stencel, J.M., Thwaites, M.W., and Derbyshire, F.J., American Chemical Society, Fuel Division Preprints, **37** (2), 505-511, 1992.

4. Jagtoyen, M., Thwaites, M.W., Stencel, J.M., McEnaney, B., and Derbyshire, F.J., Carbon., **30** (7) 1089-1096, 1992.

5. Jagtoyen, M., Toles, C., Derbyshire, F.J., Fuel Division Preprints, American Chemical Society **38**, 400, 1993

6. Jagtoyen, M., Derbyshire, F.J., Carbon, **31** (7) 1185-1192, 1993

Table 1. Maceral composition of hand-picked Stockton bench 2.

Maceral	% Composition (mineral matter free)
Telocollinite	70.5
Desmocollinite	23.0
Pyrofusinite	2.5
Semifusinite	2.0
Exinite	2.0

Table 2. Composition and porosity of samples in this study.

HTT/Treatment	%Rmax	Atomic H/C	BET S.A. (m^2/g)
Parent	0.8	0.06	000
350°C/Acid	1.4	0.05	000
350°C/Thermal	1.0	0.06	000
450°C/Acid	2.0	0.04	110
450°C/Thermal	1.5	0.04	000
550°C/Acid	2.5	0.02	361
550°C/Thermal	2.8	0.03	000

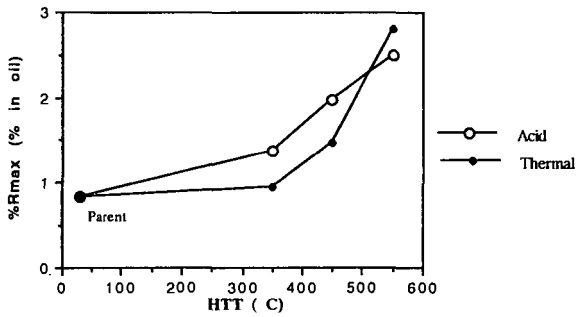

Figure 1: Relationship between reflectance and HTT for carbons produced from Stockton vitrinite-concentrate

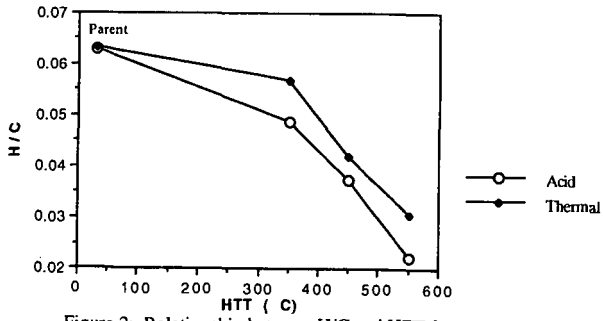

Figure 2: Relationship between H/C and HTT for Stockton vitrinite-concentrate

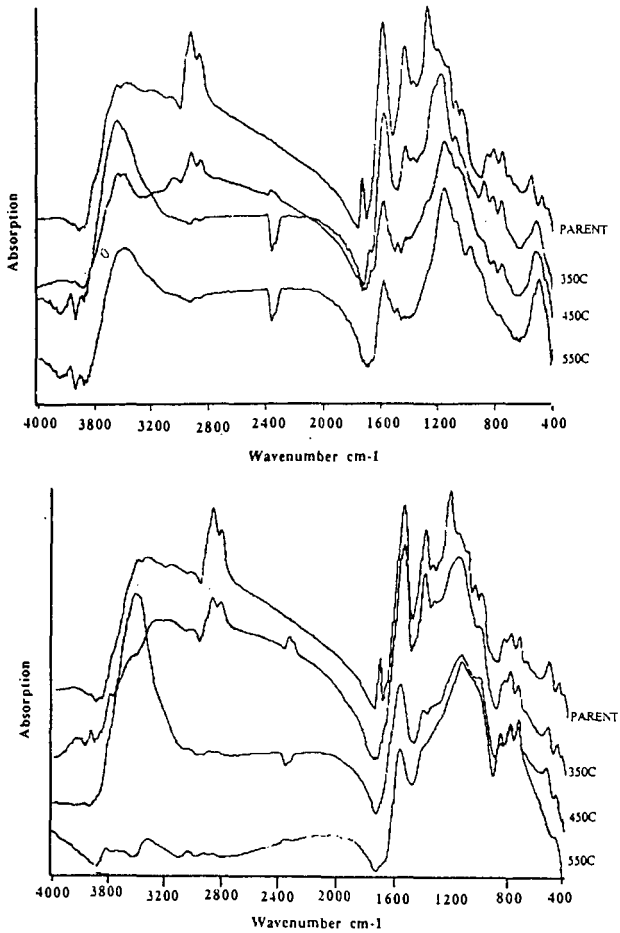

Figure 3: FTIR spectra for acid treated carbons (top) and thermal counterparts (bottom) from vitrain concentrates.

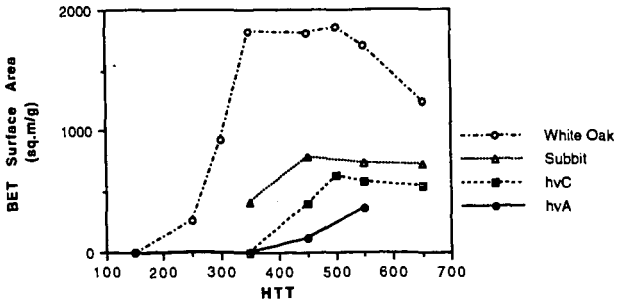

Figure 4: Surface area related to parent material [modified after ref. 6]

ADDING VALUE TO COAL CONVERSION'S CHAR: A STRATEGY FOR LOWER-PRICED FUELS

Carl W. Kruse
Illinois State Geological Survey
615 E. Peabody, Champaign, IL 61820

Mohammad Fatemi
Amoco Corporation
Amoco Research Center, P.O. Box 3011
Naperville, IL 60566

Cuneyt Feizoulof
Civil Engineering Department
University of Illinois
Urbana, Illinois 61801

Keywords: Char, activated carbon, adsorbent, catalyst

INTRODUCTION

Coal's low hydrogen to carbon ratio gives coal physical properties that are not the most desired in fuel markets. The problem is dealt with in conversion technologies designed to upgrade coal to more desirable fuels by either: 1) chemically adding hydrogen, as in liquefaction or high-BTU gasification, or 2) the production of char, as in mild gasification. The first option is neither cost-effective nor environmentally sound. Liquefaction results in the production of one mole of carbon dioxide for each mole of hydrogen needed. The result is that despite the preferred hydrogen to carbon ratio in the fuel, carbon dioxide is produced in greater quantities than it would be by simply burning the coal. The depressed market value of char is the primary drawback of coal utilization technologies exercising the second option. Making value-added, non-fuel products from char could significantly improve the economics of overall operations and result in competitively-priced premium hydrocarbon fuels. The research goal of a growing number of groups, including ours, is to produce and describe carbon products which will command higher prices than the carbon (coal) from which they were produced.

Opportunities for developing specialty chemicals and advanced materials from coals were recently reviewed (Song and Schobert, 1993). One- to four-ring aromatics from coal may be necessary to feed the rapidly growing engineering applications of aromatic polymer materials. Development of high-performance carbon materials, such as carbon fibers, graphites, and advanced adsorbents for environmental applications, is another approach for moving coal's carbon into non-fuel uses (Economy et al., 1992; Thwaites et al., 1993). Carbons suitable for methane storage are being produced (Quinn and MacDonald, 1992). Carbon molecular sieves manufactured for commercial pressure swing adsorption (PSA) systems are now competing with zeolites for air separation applications. Illinois Basin coals have been shown to be good feedstocks for making molecular sieves from coal (Lizzio and Rostam-Abadi, 1993). Europeans and Japanese are reportedly testing carbons for adsorption of radon (Kinner et al., 1993; Nakayama et al., 1993). There are biotechnology applications involving carbon as a support material (Rittmann, 1993). Commercial use of activated carbon to reduce SO_2, NO_x, and mercury in the flue gas from waste incineration plants is well-advanced in Germany (Brueggendick and Pohl, 1993) and Japan (Tsuji and Shiraishi, 1991). Oxidized activated char catalysts have not only the capacity to adsorb volatile organic chlorides but, when heated, they catalyze decomposition of the adsorbed chlorides (Fatemi et al., 1993).

This paper describes a portion of ongoing efforts to differentiate between types of oxidized carbon surfaces, especially those that have catalytic activity for elimination reactions, and those that have selective adsorptive properties for organics in the aqueous phase. It is motivated by the belief that identifying now the uses for high-quality carbon will stimulate future demands. Demands for non-fuel uses of coal will pull coal toward the market place rather than having to push products on reluctant buyers who may presently consider coal products inferior.

Oxidized carbon surfaces were discovered in the 1960s to be catalysts for elimination of hydrogen chloride from alkyl halides and alkylation of aromatics (Kruse and Ray, 1966; Mahan et al., 1967; Kruse, 1969). Brief exposure to air at 550-700°C was shown to activate a wide variety of carbon substrates. Heating to 950°C destroyed all catalytic activity. Amines and potassium salts modified the selectivity of these catalysts. Other workers reported later that inactive carbon surfaces could be made active for catalysis of oxidation reactions and hydrogen halide elimination

reactions by treatment with ammonia or HCN at elevated temperatures (Boehm et al., 1984). Substitution of carbon by nitrogen atoms at the edges of the carbon sheets was postulated to be responsible for the catalytic properties. Recent studies have revealed that nitrogen incorporated in activated carbons increases resistance to burn-off with CO_2 at 850°C (Mang et al., 1992). The rate of gasification did not correlate directly with the nitrogen content. Gasification rates with 5% O_2 in argon of four carbons at temperatures between 500°C and 650°C showed the rate was significantly reduced by nitrogen at 500°C. Curves describing burn-off rates became steeper for the nitrogen-enriched chars at higher temperatures. Above 570°C a carbon prepared from a mixture of sugar and glucosamine was oxidized more rapidly than the reference sample. Enrichment of nitrogen in the remaining carbon during the combustion of carbons has been seen previously (Spracklin et al., 1991).

We report our observations of differences in surface nitrogen, oxygen and sulfur for a series of carbons as determined by X-ray Photoelectron Spectroscopy (XPS). XPS has been widely applied to study the surfaces of organic materials. Surface chemistry, which is frequently determined by varying the types of functional groups, may be revealed by XPS. Different functionalities containing oxygen, nitrogen, and sulfur can be quantitatively identified by XPS. Moreover, changes in surface functionalities due to chemical modifications can also be studied.

EXPERIMENTAL

Seven samples were prepared from granular activated carbon (GAC), Filtrasorb-400 (F-400), designated herein as AR000, manufactured from a bituminous coal by the Calgon Corporation. Proximate and ultimate analyses were made with a LECO Mac-400 and a LECO CHN-600, respectively. Brunauer, Emmett, and Teller (BET) surface area, micropore volume and mesopore volume were all calculated for nitrogen adsorption isotherms obtained at 77K using a Micromeritics Nitrogen Surface Analyzer 2400 ASAP. See Table 1.

AR000 was placed in an acid washing column and washed with 10 bed volumes of 1.0 M hydrochloric acid followed by 10 bed volumes of 1.0 M nitric acid. The carbon was then rinsed with 20 bed volumes of deionized water followed by 5 bed volumes of a carbonate solution buffered at pH 6. The carbon was then rinsed with 5 bed volumes of distilled-deionized water. The acid-washed AR000 was fluidized in ultra-high-purity (UHP) N_2 at 950°C for 30 minutes to produce the sample designated FN950, from which six samples were prepared by the methods given in Table 2. Two additional samples, SA10-14 and OSA10-14, described previously (Kruse et al., 1992), were made from a mixture of Illinois No. 5 and No. 6 coals. The oxidized steam-activated char (OSA10-14) was active as a dehydrochlorination catalyst.

Table 1. Characterization of AR000

Proximate analysis[1]	
Moisture	1.1
Volatile Matter	5.4
Fixed Carbon	88.3
H-T Ash	6.2
Ultimate analysis[1]	
Hydrogen	0.25
Carbon	91.80
Nitrogen	0.72
Oxygen	0.40
Sulfur	0.59
BET Surface Area[2]	1035 m^2/g
Micropore Volume[2]	0.421 cc/g
Mesopore Volume[2]	0.231 cc/g

[1] moisture-free basis
[2] moisture ash-free basis

XPS involves irradiation of a sample with monoenergetic x-rays resulting in subsequent emission of photoelectrons. By determining the kinetic energies of the emitted electrons, the characteristic binding energies that are dependent on the local chemical environment can be calculated. Since the escape depth is 30-60 Å, XPS is a surface sensitive technique. Functional groups and the binding energies (eV) associated with them are: elemental and organic sulfur species at 164.2±0.2, sulfates and sulfonates at 168.3±0.3, amines and pyridines at 398±0.3, pyrolic nitrogen, amides and amino groups at 400.2±0.3, ammonium derivatives at 401.2±0.3, nitrates at 405.9±0.7, metal oxides at 529.5±0.2 and 531.5±0.2, numerous special carbon-oxygen species and superoxide (O_2^- ions) at 533.2±0.2. Surface compositions (% atomic) calculated from XPS analyses for atoms appearing in amounds greater than 0.1% are given in Table 2 and the binding energies of selected atoms in this same group in Table 3.

DISCUSSION OF RESULTS

The adsorption characteristics of the carbons described herein were reported earlier this year (Feizoulof et al., 1993). It was found that the adsorptive capacity for p-nitrophenol increased as oxygen-containing functional groups put onto the carbon by nitric acid oxidation were removed by temperature programmed desorption.

The variation in carbon's fraction of atoms on the surfaces of the samples (see Table 2) is related to coverage by oxygen for the first eight samples and to ash-forming constituents in the last two.

Ammong the distribution of C 1s binding energies, it appears that the sample OSA10-14, the catalyst, has the highest fraction of carbon-oxygen functional (C-O and C=O) groups. The oxygen pattern is that to be expected, except for DS950. Fluidization at 950°C with nitrogen (FN950) produced the lowest surface oxygen, stripping away some of the oxygen on the as-received carbon. Brief air oxidation at 300°C introduced some oxygen (AO305) and boiling nitric acid even more (HN100). Some of this oxygen on HN100 was in the form of nitrates. This sample's nitrogen value was higher than any other and it had a 405.9 eV XPS peak indicative of nitrates. This extra nitrogen was lost in desorption at 405 °C (DS405). Oxygen drops to the lowest values as the desorption is continued through two higher temperatures where carbon dioxide is known to be the primary gas evolved. The increase in oxygen for DS950 is believed to have occurred after the sample was cooled. The 168 eV sulfur binding peak, not seen in the DS525 or DS725, is associated with sulfates. This is additional evidence that DS950 underwent oxidation after preparation at 950°C and prior to XPS analyses. No conclusions are drawn from the distribution of O 1s binding energies; the lack of resolution of types for the last two samples, run at a different time by a different operator, are not considered significant.

The coverage by nitrogen is approximately constant (0.67±0.15%), within the accuracy of the determination at this low percentage, for nine samples (excluding HN100). Binding energies for N 1s are similar, except for HN100, which has a nitrate peak, and FN950, which shows some differentiation in the 398-400 eV range not observed elsewhere. The ratio of types of nitrogen functionalities remaining after nitrates have been removed by heating to 405°C is not what one would project by simple subtraction. There may be a transformation of material initially responsible for a part of the 400.5 eV peak to new material having a 401 eV binding energy. Decomposition of amides is a possibility. Sulfur coverage is constant for the first eight samples and much higher for the two chars from high sulfur coal, as expected. The absence of sulfate in the last two samples is surprising considering how easily sulfate appears to form in the first eight, but this too may be a difference in instrument calibration by different operators.

XPS binding energies at *ca.* 400 eV, usually associated with amino groups or amides, and at *ca* 398 eV, typically associated with nitrogen bound in aromatic rings in pyridine-like fashion, were reported for three carbons having differing nitrogen contents. The peak at 398 eV was much higher with NH_3-treated carbons but neither signal was reported to be associated with eatalytic activity of the carbons (Mang et al., 1992; Stohr et al., 1991). We too find no correlation between the dehydrochlorination activity of an oxidized-carbon catalyst, OSA10-14, and the surface functional groups as determined by XPS.

If nitrogen atoms contribute to the catalytic properties of oxidized carbons discovered in the 1960s, those nitrogen atoms are likely those already present in the materials. We are unaware of evidence that indicates the fixation of nitrogen in burning carbonaceous material in air at 500-700°C. If the nitrogen inhibition reported by Mang and others is spatially limited to areas adjacent to bound nitrogen atoms, the nitrogen-containing formations could be left in relief on surface areas. This effect would be most pronounced at temperatures for which the rates of gasification differ the most for nitrogen-containing structures compared to nitrogen-free zones. Depending on the dimensions of the volume affected by the nitrogen, the distribution of nitrogen atoms, and the degree of gasification, nitrogen-containing functional groups would be generated on pore wall surfaces.

It is postulated that the observed catalytic activity may be the result of specialized spatial arrangements of specific functional groups within the pores of the carbon. XPS would not reveal special spatial arrangements of two or more functional groups on pore walls which may be responsible for catalysis. Figure 1 diagrams one of many arrangements that could catalyze elimination in high yields without rearrangement of the carbon skeleton. This lack of rearrangement was of special importance to the industrial research goals in the 1960s because biodegradability of commercial detergents depended on preserving the linearity of the olefins.

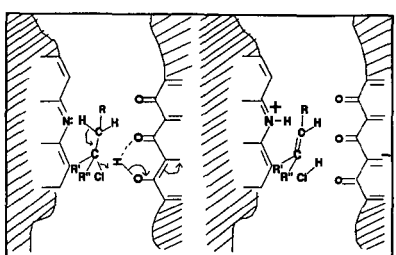

Figure 1. An E2 trans elimination

CONCLUSIONS

Failure to correlate surface functional groups, identified by XPS, with catalyst activity is not unexpected if activity is dependent on functional groups located on critically-spaced opposing surfaces of pores. If catalyst sites are internal,

determining adsorption differences and increased strengths of adsorption due to chelation between properly spaced groups may be more fruitful. The use of Mossbauer Spectroscopy to follow field effects of the type studied with tin is another possibility (Larsen et al., 1982). Future work should include monitoring the evolution of nitrogen oxides in TPD analyses in addition to CO_2 and CO to determine what combination of groups may be involved.

ACKNOWLEDGMENTS

This was supported in part by grants made possible by the Illinois Department of Energy and Natural Resources (ENR) through its Coal Development Board and the Illinois Clean Coal Institute (ICCI), and from the United States Department of Energy (Grant Number R 91-1/1.1B-4M). However, any opinions, findings, conclusions, or recommendations expressed herein are those of the authors and do not necessarily reflect the views of ENR, ICCI, and the DOE. The ICCI project managers were Frank Honea and Daniel Banerjee. In-kind contributions by the Alternative Feedstock Development (AFD) program of Amoco Corporation are gratefully acknowledged. Without this support and the encouragement of R. E. Lumkin (AFD), this work would not have been possible. The authors acknowledge contributions by ISGS staff members Massoud Rostam-Abadi, Anthony Lizzio, Ilham Demir and Steve Carlson.

REFERENCES

Boehm, H. P., G. Mair, T. Stoehr, A.R. De Rincon, B. Tereczki **1984** Carbon as a catalyst in oxidation reactions and hydrogen halide elimination reactions *Fuel* **63** (8) 1061-3.

Brueggendick, H., F.G. Pohl **1993** Operating experience with Steag's activated carbon processes-a/c/t™- in European waste incineration plants *Brochure published by Steag AG, Huyssenalle 88, D-45128 Essen, Germany.*

Economy, J., K. Foster, A. Andreopoulos, H. Jung **1992** Tailoring carbon fibers for adsorbing volatiles *Chemtech* **October** 597-603.

Fatemi, S.M., C.W. Kruse, R.T. Lagman **1993** Oxidized activated char as an adsorbent and catalyst *Abstracts of papers at 21st Biennial Conference on Carbon, State University of New York at Buffalo June 13-18* 505-506.

Feizoulof, C., V.L. Snoeyink, C.W. Kruse **1993** The effect of carbon surface chemistry on enhanced adsorption of a targeted compound from water *Abstracts of papers at 21st Biennial Conference on Carbon, State University of New York at Buffalo, June 13-18* 367-368.

Kinner, N.E., J.P. Malley, J.A. Cement, K.R. Fox **1993** Using POE techniques to remove radon *Journal-American-Water-Works-Association* **85** (6) 75-86.

Kruse, C.W., G.C. Ray **1966** Dehydrohalogenation of hydrocarbon halides *US Patent 3,240,834* Mar. 15.

Kruse, C.W. **1969** Polymerization *US Patent 3,437,695* April 8.

Kruse, C.W., M.I.M. Chou, C. Feizoulof, M. Fatemi, P. Beaulieu **1992** Oxidized coal char as a catalyst: characterization *Preprints of Papers Presented at San Francisco, CA ACS Div. of Fuel Chemistry, April 5-10* **37** (2) 556-563.

Larsen, J.W., P.A. Nadar, M. Mohammidi, P.A. Montano, P.A. **1989** Spatial distribution of oxygen in coals. Development of a tin labelling reaction and Mossbauer studies *Fuel* **61** (10) 889-893.

Lizzio, A.A., M. Rostam-Abadi **1993** Production of carbon molecular sieves from Illinois coal *Fuel Processing Technology* **34** 97-122.

Mahan J.E., R.E. Reusser, C.W. Kruse **1967** Dehydrohalogenation process *US 3,352,935*, November 14.

Mang, D., H.P. Boehm, K. Stanczyk and H. Marsh **1992** Inhibiting effect of incorporated nitrogen on the oxidation of microcrystalline carbons *Carbon* **30** (3) 391-398.

Nakayama, Y., H. Nagao, M. Mimura, H. Yamasita, E. Tanaka, K. Hosokawa **1993** Radon adsorption in activated carbon related to specific surface area and water absorbing *Abstracts of papers at 21st Biennial Conference on Carbon, State University of New York at Buffalo, June 13-18* 402-403.

Quinn, D.F., J.A. MacDonald **1992** Natural gas storage *Carbon* **30** 1097-1103.

Rittmann, B.E. **1993** The significance of biofilms in porous media *Water Resources Research* **29** 2195-2202.

Song, C., H.H. Schobert **1993** Opportunities for developing specialty chemicals and advanced materials from coals *Fuel Processing Technology* **34** 157-196.

Spracklin, C.J., K.M. Thomas, H. Marsh, I.A.S. Edwards **1991** Nitrogen functionality in carbons and its release as NO_x during gasification *Abstracts of papers at 20th Biennial Conference on Carbon, Santa Barbara, California* 212-213.

Stohr, B., H.P. Boehm, R. Schlogl **1991** Enhancement of the catalytic activity of activated carbons in oxidation reactions by thermal treatment with ammonia or hydrogen cyanide and observation of a superoxide species as a possible intermediate *Carbon* **29** 707.

Thwaites, M.W., M.L. Stewart, B.E. McNeese, M.B. Summer **1993** Synthesis and characterization of activated pitch-based carbon fibers *Fuel Processing Technology* **34** 137-145.

Tsuji, K., I. Shiraishi **1991** Mitsui-BF dry desulfurization and denitrification process using activated coke *in Proceedings of the EPRI SO_2 Control Symposium, Washington D.C.* 307-324.

Table 2 Surface composition (% atomic) by XPS

ID #	Description	C	O	N	S	Si
AR000	Calgon F400 commercial activated carbon	88.8	9.7	0.6	0.2	0.5
FN950	Acid-washed AR000 fluidized in high purity N_2 at 1223 K for 30 min.	90.8	7.2	0.8	0.2	0.4
AO305	FN950 oxidized, 573 K, 10% O_2/90% N_2, 5 min	90.5	8.1	0.7	0.2	0.4
HN100	FN950 oxidized with 1.0 M HNO_3	87.7	10.1	1.1	0.2	0.5
DS405	HN100 outgassed at 678 K in high purity N_2	88.1	10.3	0.7	0.2	0.4
DS525	HN100 outgassed at 798 K in high purity N_2	91.1	7.4	0.5	0.2	0.5
DS725	HN100 outgassed at 998 K in high purity N_2	90.6	7.7	0.7	0.2	0.5
DS950	HN100 outgassed at 1223 K in high purity N_2	87.8	10.4	0.7	0.3	0.5
SA10-14[1]	Steam-activated, Illinois coal char[2], 1123 F 50% steam/50% nitrogen	80.0	10.4	0.5	3.7	2.6
OSA10-14[1]	SA10-14 Oxidized at 723 K, 10% O_2/90% N_2, 15 min	80.0	10.2	0.8	3.9	2.3

[1] Al 1.6%, Fe 0.8%, Ca 0.3%.
[2] A mixture of Illinois No 6 and No 5 coals charred at 500 °C

Table 3. Binding Energies (eV) from XPS Analyses of the Original and Treated Calgon F-400 Activated Carbon Samples

Sample ID	C 1s	%	O 1s	%	N 1s	%	S 2p	%
AR000	284.6	62	531.5	52	399.4	27	164.4	71
	286.0	21	533.3	48	401.4	73	168.6	29
	288.9	17						
FN950	284.6	62	531.5	32	397.9	11	164.2	61
	286.0	22	533.2	68	399.8	51	168.6	39
	288.9	16			401.3	38		
AO305	284.6	66	531.5	32	399.3	35	164.2	77
	286.1	19	533.2	68	401.2	65	168.6	23
	289.2	15						
HN100	284.6	68	531.5	53	400.5	85	164.2	63
	286.2	18	533.2	47	405.9	15	168.4	37
	289.1	14						
DS405	284.6	58	531.6	32	399.3	31	164.1	84
	286.0	25	533.1	68	400.9	69	168.2	16
	288.7	17						
DS525	284.6	66	529.5	22	398.8	35	164.1	100
	286.1	22	531.5	35	401.1	65		
	289.6	12	533.2	43				
DS725	284.6	63	531.4	54	398.8	33	164.2	100
	286.0	21	533.3	46	401.2	67		
	289.2	16						
DS950	284.6	65	531.5	55	400.8	31	164.3	83
	286.0	21	533.3	45	401.2	69	168.3	17
	289.3	14						
SA10-14	284.6	64	533.2	100	398.6	22	163.9	100
	286.3	23			401.2	78		
	289.7	12						
OSA10-14	284.6	60	533.2	100	398.7	22	163.9	100
	286.0	30			402.3	78		
	290.0	10						

COAL/OIL COPROCESSING USING SYNGAS: EFFECTS OF D_2O DURING HYDRODESULFURIZATION

Yuan C. Fu, Katsuya Ishikuro, Makoto Akiyoshi
Department of Applied Chemistry
Muroran Institute of Technology
Muroran 050, Japan

Mitsuyoshi Yamamoto, Takeshi Kotanigawa
Government Industrial Development Laboratory, Hokkaido
Sapporo 061, Japan

Keywords: Hydrodesulfurization, Syngas, Deuterium Oxide

INTRODUCTION

It has been shown that coal liquefaction[1] and coprocessing[2,3] of coal with petroleum solvents could be carried out using syngas (H_2+CO) and steam instead of hydrogen. High coal conversion could be obtained with considerable saving in hydrogen consumption. Earlier studies have also shown that model compounds could be hydrogenated and desulfurized in the presence of petroleum solvents and catalyst using syngas with steam. It was considered that the CO in the syngas reacts with steam to form hydrogen via water-gas shift reaction, and that the hydrogen formed could also participate in the hydrogenation of coal, but the fate of hydrogen formed from the water-gas shift reaction was not known. It is known that deuterium is incorporated into reaction products during coal liquefaction under D_2 gas[4], and that hydrogen/deuterium transfer occurs among solvent, reaction products and gas when deuterium-labled solvents are used in coal liquefaction experiments[5].

This study deals with hydrodesulfurization of a sulfur-containing model compound using syngas and steam. In order to understand the roles of molecular hydrogen and water in the syngas system during the hydrodesulfurization, experiments were carried out to treat dibenzothiophene in the presence of solvent and catalyst under pressure using H_2-CO-D_2O, D_2-CO-H_2O and N_2-D_2O systems. Deuterium gas and D_2O were used in an effort to study the incorporation of hydrogen from the gas and water by tracing the migration of deuterium through the system.

EXPERIMENTAL

The hydrodesulfurization of dibenzothiophene was conducted in a shaking 25-ml microreactor in the presence of decalin solvent and a commercial NiMo/Al_2O_3 catalyst(Nippon Mining Co.) using syngas and water at an initial pressure of about 70 kg/cm^2 in most cases. The reactor was quickly heated up in a fluidizing sand bath and maintained at 400℃ for 45 minutes, and then rapidly quenched in a cold water bath. Various H_2:CO:H_2O mole ratios with H_2/CO mole ratios varying from 1 to 3 and H_2O/CO mole ratios varying from 0.3 to 1.0 were used. For the experiments, a mixture of 30 parts of dibenzothiophene and 70 parts of solvent was placed in the microreactor, 10 weight %(based on the mixture) of ground presulfided catalyst was charged, and calculated amount of water was added before the reactor was pressured with syngas. After the reaction, the liquid products were analyzed by a Shimadzu GC-14A gas chromatograph using OV-1 fused silica capillary column(60m× 0.25mmϕ), and gasous products were analyzed by a Shimadzu GC-14A gas chromatograph.

In experiments using D_2 gas and D_2O, an initial pressure of about 40 kg/cm^2 was used because of low pressure available for the D_2 bomb. The liquid products were analyzed by a Shimadzu QP-1000 gas chromatograph-mass spectrometer. Spectral analysis was performed using the known split patterns of various undeuterated compounds. For these runs, samples of the gaseous products were obtained by passing through a dry ice and acetone trap to remove moisture prior to analysis using gas chromatograph and a ULVAC MSQ-150A quadrapole mass analyzer. For hydrogen analysis, relative intensities of peaks of molecular ions were used to estimate the relative portions of H_2, HD, and D_2.

RESULTS AND DISCUSSION

Hydrodesulfurization of Dibenzothiophene in Various Solvents. During coal liquefaction, large coal molecules fragment thermally and are hydrogenated via hydrogen transfer from a donor solvent. Coprocessing of coal with petroleum solvents using either hydrogen or syngas with steam was also aided by the presence of tetralin[3]. Dibenzothiophene was initially hydrodesulfurized in the presence of various solvents including decalin, tetralin, and a mixture of decalin and an aromatic compound. The results of hydrodesulfurization carried out under hydrogen and syngas pressures are shown in Table 1. Dibenzothiophene was easily hydrogenated and desulfurized by hydrogen to form mainly biphenyl, cyclohexylbenzene, bicyclohexyl, and decomposed products. Tetralin donated some hydrogen to form naphthalene, but was also hydrogenated to form decalin. Decalin converted to small amounts of tetralin and naphthalene. An aromatic compound was added with an intention of finding out the effects of aromatic compounds on hydrogen transfer between decalin and dibenzothiophene. The hydrogenated products from 1-methylnaphthalene was not included in the table. When an aromatic compound was added to decalin as the solvent, the effect on the product distribution was not conclusive, but high dibenzothiophene conversions were obtained with all solvents. It appears that catalytic hydrogenation by hydrogen gas plays the dominant role with respect to the hydrodesulfurization.

When dibenzothiophene was treated with syngas and steam (H_2:CO:H_2O=1:1:0.3), the hydrogenation and desulfurization activeties were lower. The yields of hydrogenated products, cyclohexylbenzene and bicyclohexyl, were lower. These results indicate that the performance of syngas in hydrodesulfurization did not come up to the satisfactory level that was observed in coal liquefaction. In coal liquefaction, the performances with syngas and H_2 compare rather closely except that asphalten levels of the syngas products were somewhat higher[1].

Table 2 shows the results of hydrodesulfurizing dibenzothiophene using decalin solvent and syngas with steam at various H_2:CO:H_2O ratios. The dibenzothiophene conversion increased with H_2/CO mole ratio, while H_2O/CO mole ratio was maintained at 0.6. The data indicate that the H_2O level at the H_2O/CO mole ratio of about 0.6 is appropriate or about optimum to give better results yielding more hydrogenated products. The extent of water-gas shift reaction was rather extensive as can been seen from high CO conversions obtained in all runs. The CO conversions were calculated on the basis of the amounts of CO_2 formed. As was observed in coal liquefaction and coprocessing using syngas, H_2 formation via water-gas shift reaction resulted in reduction of hydrogen consumption and increase of H_2/CO mole ratio after the reaction.

Hydrodesulfurization Using Syngas Containing D_2O and D_2. Experiments with syngas containing D_2O and D_2 were carried out to observe how the hydrogen transfer reactions occured from H_2O and gas-phase hydrogen. Dibenzothiophene was hydrodesulfurized in the presence of decalin solvent using H_2-CO-D_2O(1:1:1) and D_2-CO-H_2O(1:1:1) gas systems as shown in Table 3. Another experiment using N_2-D_2O(2:1) system was also carried out. Initial pressures of syngas and N_2 used were lower(about 40 kg/cm^2) in this series of experiments because only a limited pressure of D_2 gas was available. Similar to the results shown in Table 2, both the hydrodesulfurization and water-gas shift reaction progressed moderately. In the experiment using N_2-D_2O system, some dibenzothiophene decomposed to form biphenyl, and the formation of naphthalene from decalin increased.

The reaction products and remaining solvents were analyzed using GC-MS, and deuterium distributions in the products and solvents are shown in Figure 1. In the H_2-CO-D_2O system, the cyclohexylbenzene product was deuterated extensively to form d_2, d_3, d_4, d_5, and d_6 species, but no d_0 or d_1 species was present. Deuterium was also distributed widely to the biphenyl product, and all species from d_0 to d_6 were present. Large parts of cis-decalin was isomerized to trans-form, but both forms similarly contained about 30% of d_1-decalin. Only trans-decalin was shown in Figure 1. The H/D exchange of D_2O with the decalin solvent

was not as extensive as that with the products. In the D_2-CO-H_2O system, it was noted that deuterium was incorporated only moderately into cyclohexylbenzene and biphenyl, both forming d_1, d_2, and d_3 species. Only about 20% of d_1 species was present in either trans- or cis-decalin. It is of interest to observe that, under N_2 pressure, H/D exchange occured extensively between D_2O and dibenzothiophene. Even though the amounts of cyclohexyl and biphenyl formed were smaller, deuterium was incorporated into these products more extensively than was observed in the D_2-CO-H_2O system. Although not shown in the figure, the spectra of the unreacted dibenzothiophene obtained from the experiments carried out in the H_2-CO-D_2O and N_2-D_2O systems indicated that they were all D-substituted species containing d_1, d_2, d_3, and d_4 species. However, it was observed that the unreacted dibenzothiophene obtained in the D_2-CO-H_2O system was nothing but the d_1 species.

The extensive H/D exchange observed between dibenzothiophene and D_2O under N_2 pressure is consistent with the results reported by Kabe et al[6] dealing with hydrogen exchange of H_2O with coal or phenolic model compounds. In the case dealing with hydrogen exchange between syngas-H_2O and dibenzothiophene, the situation is not the same. Water participates in the water-gas shift reaction as evidenced by the formation of CO_2. It is expected that the D_2O in the syngas-D_2O system reacts with CO to form active deuterium which leads to the formation of D_2, and in the process, some active deuterium may be incorporated into dibenzothiophene and the substrates.

To observe the extent of D atoms from D_2O transfer back to form dihydrogen such as HD and D_2 in gaseous products, the gases were analyzed by gas chromatograph and quadrapole mass spectrometer. The analytical results are given in Table 4. It is noted that some deuterium in D_2O is present in HD and D_2 in the syngas-D_2O system, while no deuterium is present in the "hydrogen gases" of the gaseous products in the N_2-D_2O system. A small amount of H_2 formed in the N_2-D_2O system may have come from the dehydrogenation or decomposion of the solvent and reactant. In contrast to the experiment in the H_2-CO-D_2O system where HD and D_2 were formed , the experiment in the D_2-CO-H_2O system yielded gasous products containing HD and H_2 in the "hydrogen gases". These results indicate that, unlike D_2O in the N_2-D_2O system, D_2O in the syngas-D_2O system or H_2O in the D_2-CO-H_2O system forms active deuterium or hydrogen, respectively, which in turn is incorporated into the reactant and substrates or leads to the formation of HD and D_2 or HD and H_2, respectively. In the N_2-D_2O system, most deuterium is probably incorporated into the reactant by exchange reactions. It may then be concluded that both gas-phase hydrogen and hydrogen formed via the water-gas shift reaction in the syngas-H_2O system contribute to hydrodesulfurization, and the accompanying water-gas shift reaction is benefitial in reducing H_2 consumption.

ACKNOWLEDGEMENTS

We thank the support of Grant-in Aid of Scientific Research provided by the Ministry of Education, Japan.

REFERENCES

1. Batchelder, R.F., Fu, Y.C., Ind.Eng.Chem. Process Des. Dev. Vol.18, No.4, 594(1979)
2. Fu, Y.C., Akiyoshi, M., Tanaka, F., Fujiya, K., Preprints, Div. Fuel Chem., Am.Chem.Soc. Vol.36, No.4, 1887(1991)
3. Fu, Y.C., Tanabe, K., Akiyoshi, M., Preprints, Div. Fuel Chem., Am.Chem.Soc. Vol 37, No 4, 1776(1992)
4. Skowronski, R.P., Ratto, J.J., Goldberg, I.B., Heredy, L.A., Fuel, Vol 63, 440(1984)
5. Cronauer, D.C., McNeil, R.I., Young, D.C., Ruberto, R.G., Fuel, Vol 61, 610(1982)
6. Ishihara, A., Takaoka, H., Nakajima, E., Imai, Y., Kabe, T., Energy & Fuels, Vol 7, 362(1993)

Table 1. Hydrodesulfurization of Dibenzothiophene
(Catalyst:$NiMo/Al_2O_3$, Initial Press:70 kg/cm^2, Temp:400 ℃, Time:45 min)

Gas system	H_2			H_2-CO-H_2O(1:1:0.3)		
Solvent	Decalin	Tetralin	Decalin + 1-methyl-naphthalene	Decalin	Tetralin	Decalin + 1-methyl-naphthalene
Dibenzothiophene conv., %	94.2	94.1	94.8	74.8	77.1	80.4
Bicyclohexyl formed, %	7.4	3.8	3.8	0.3	1.2	1.0
Cyclohexylbenzene formed, %	24.8	32.6	30.8	21.2	21.1	16.6
Biphenyl formed, %	33.6	39.5	43.8	42.0	44.0	54.5
Decalin remained, %	84.2	16.9[a]	83.8	91.2	4.3[a]	89.4
trans/cis ratio	4.8	4.0	4.5	4.0	3.7	4.1
Tetralin formed, %	2.9	67.2[b]	5.0	3.8	75.3[b]	4.8
Naphthalene formed, %	0.2	7.0	1.6	1.1	18.4	2.0
1-Methylnaphthalene remained, %	-	-	22.9	-	-	51.5
CO conv., %	-	-	-	32.5	40.3	39.8
H_2 consump., wt% of dibenzothiophene	5.2	6.0	7.3	2.0	2.0	3.4

[a]Decalin formed
[b]Tetralin remained

Table 2. Hydrodesulfurization Using Syngas at Various $H_2/CO/H_2O$ Mole Ratios
(Catalyst:$NiMo/Al_2O_3$, Solvent : Decalin, Temp:400 ℃, Time:45 min)

Syngas-H_2O	H_2-CO-H_2O (1:1:0.3)	H_2-CO-H_2O (1:1:0.6)	H_2-CO-H_2O (1:1:1)	H_2-CO-H_2O (2:1:0.6)	H_2-CO-H_2O (3:1:0.6)
Initial syngas press., kg/cm^2	70	63	55	70	70
Dibenzothiophene conv., %	74.8	72.0	63.7	78.7	81.0
Bicyclohexyl formed, %	0.3	1.5	0.6	2.5	2.8
Cyclohexylbenzene formed, %	21.2	20.6	14.6	24.1	26.1
Biphenyl formed, %	42.0	41.5	44.5	36.7	36.8
Decalin remained, %	91.2	92.2	92.2	91.4	92.8
trans/cis ratio	4.0	4.0	3.8	4.3	4.3
Tetralin formed, %	3.8	4.1	4.6	3.0	3.2
Naphthalene formed, %	1.1	1.1	1.9	0.4	0.5
CO conv., %	32.5	34.7	26.6	25.8	35.3
H_2 consump., wt% of dibenzothiophene	2.0	0.9	0.1	1.6	2.7
H_2/CO ratio after the reaction	1.5	1.6	1.4	2.7	5.2

Table 3. Hydrodesulfurization Using Syngas-D_2O or Deuterium Containing Gases
(Catalyst:$NiMo/Al_2O_3$, Solvent:Decalin, Temp:400 ℃, Time:45 min)

Gas system	H_2-CO-D_2O (1:1:1)	D_2-CO-H_2O (1:1:1)	N_2-D_2O (2:1)
Initial press., kg/cm^2	40	40	40
Dibenzothiophene conv., %	74.5	69.5	35.0
Bicyclohexyl formed, %	0.6	0.3	trace
Cyclohexylbenzene formed, %	14.1	11.4	0.2
Biphenyl formed, %	43.9	45.4	27.2
Decalin remained, %	84.0	87.0	82.6
trans/cis ratio	3.8	4.0	2.2
Tetralin formed, %	5.5	5.3	3.7
Naphthalene formed, %	2.5	2.9	7.1
CO conv., %	30.1	23.3	-

Table 4. G.C. and M.S. Analysis of Gaseous Products

Gas system	H_2-CO-D_2O	D_2-CO-H_2O	N_2-D_2O
Gaseous Products*, mol %			
CO	40.1	35.2	-
CO_2	15.0	12.7	-
N_2	-	-	94.9
Hydrogen	41.3	48.7	3.6
(H_2)	(63)	(13)	(100)
(HD)	(31)	(11)	0
(D_2)	(6)	(76)	0

* The remainders are CH_4, C_2H_6, and H_2S.

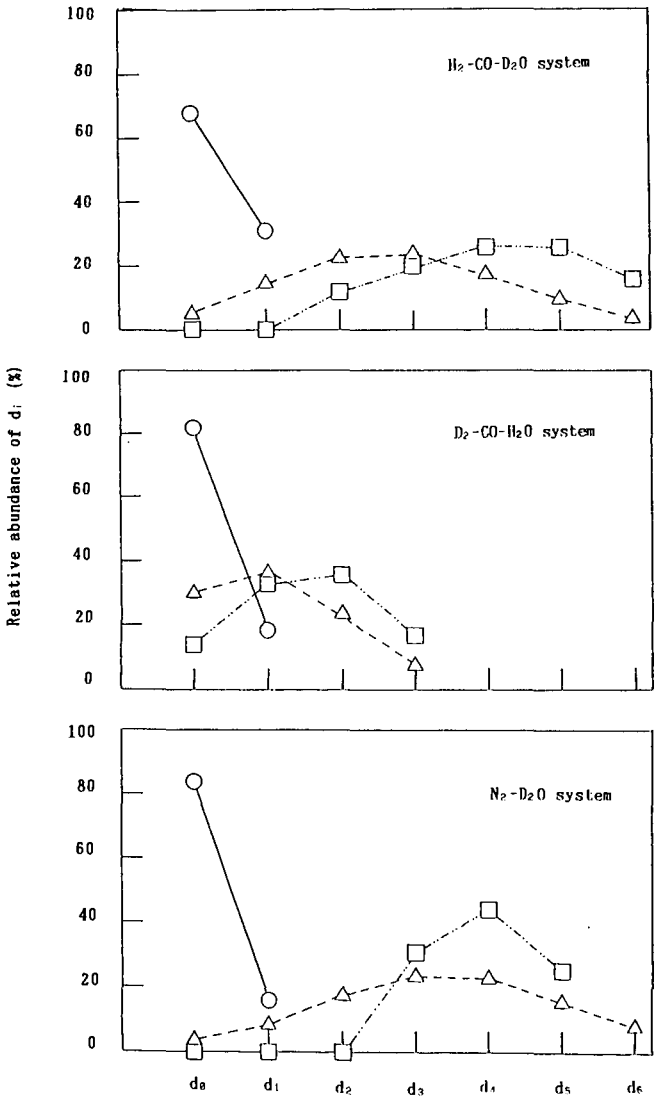

Figure 1 Distribution of deuterium in solvent and products
○ t-Decalin △ Biphenyl □ Cyclohexylbenzene

HDS ACTIVITY AND SURFACE PROPERTY OF ALUMINA-SUPPORTED RUTHENIUM CATALYST

Masatoshi Nagai and Kenji Koizumi
Department of Chemical Engineering,
Tokyo University of Agriculture and Technology,
Koganei, Tokyo 184, Japan

Keywords: HDS, Ru/Al_2O_3, NH_3-TPD

INTRODUCTION

Ruthenium and its compounds have wide ranging application in both heterogeneous and homogeneous catalysis. Recent environmental and economic problems offer a challenge for developing new catalysts capable of deep hydrodesulfurization (HDS) and hydrogenation of aromatics in the presence of sulfur and nitrogen compounds. Unsupported ruthenium sulfides were reported to show a high activity for HDS and hydrogenation (1,2). The catalytic activity for HDS reaction is likely to depend upon greatly the preparation and pretreatment of the ruthenium catalysts, such as surface composition, surface acidity, and electronic property of ruthenium (3,4). The objective of this study was to report the effects of catalyst pretreatment on the catalytic activity of an alumina-supported ruthenium catalyst for thiophene HDS.

EXPERIMENTAL

0.49% Ru/Al_2O_3 (JRC-A4-0.5Ru2) was prepared by impregnation of alumina powder with aqueous solution of ruthenium trichloride. 0.2 g of catalyst was charged to the reactor for a typical series of experiments. The Ru/Al_2O_3 catalyst was pretreated with three ways prior to catalyst characterization and activity measurement; reduced in H_2 for 4 h (Ru-R catalyst), oxidized in air at 400 °C for 3 h, following reduction in H_2 for 4 h (Ru-OR catalyst), or sulfided in a 10 % H_2S/H_2 stream (Ru-S catalyst). The HDS activity measurement for thiophene HDS was carried out in a continuous-flow microreactor.

The surface property of the catalyst was measured by NH_3-TPD, H_2 adsorption, XPS, and in-situ DRIFT FT-IR spectroscopy. For the NH_3-TPD experiment, the catalyst was heated to 500 °C at a rate of 10 °C/min under He flow. It was maintained under these conditions for 1 h and then slowly cooled to room temperature. The He flow was switched to a 5.1% NH_3/He flow to adsorb NH_3 to the catalyst. The catalyst was heated at a rate of 10 °C/min to 500 °C (or 600 °C) under He flow. The outlet gas was analyzed by either a gas chromatograph or a quadrupole mass spectrometer with a valunarable-leak valve. Hydrogen adsorption was analyzed by a thermal conductive detector of a gas chromatograph after the pretreatment. The H_2 uptake was measured using pulses of 10 % H_2/He to the reactor at room temperature. The surface composition of the catalyst was measured by X-ray photoelectron spectroscopy.

RESULTS AND DISCUSSION

The physical properties and HDS activity of the catalyst are shown in Table 1. The Ru-S300 catalyst was the most active of the all catalysts for thiophene HDS, but the Ru-S400 catalyst had lowest activity. The Ru-OR300 catalyst was more active than the Ru-R200 and Ru-R400 catalysts.

Three kinds of peaks (low-, middle-, and high-temperature) were observed in NH_3-TPD profile. The Ru-S300 and Ru-OR300 catalysts have a predominant high-temperature peak with a small low-temperature peak. However, the Ru-S400, Ru-R200 and Ru-R400 catalysts have no high-temperature peaks, but middle-temperature peaks together with a small low-temperature peak. Alumina support has only middle-temperature peaks in the NH_3-TPD profile. Mass spectroscopy and XPS analyses showed that the low-, middle- and high-temperature peaks were assigned to RuO_2 (280.7-281.1 eV), acid sites on alumina, and Ru metal (280.2 eV),

respectively (5,6). The spectra at 280.2 eV was not observed for the fresh catalyst but for the reduced and sulfided catalysts.

The HDS activity was not concerned with low-temperature peak of NH_3-TPD, but high-temperature peak. The high-temperature peak of NH_3-TPD was related to H_2 adsorption and the intensity of XPS Ru3d spectra at 280.3 eV (Ru metal).

The particle size was determined by H_2 chemisorption at room temperature. The Ru-R300 catalyst had smaller particles than the Ru-R400 catalyst. The selectivity of the Ru/Al_2O_3 catalyst for hydrogenation of butenes to butane in thiophene HDS was calculated. The ratio of butane/butenes indicated the hydrogenation activity. The ratio for the Ru-R400 catalyst was higher than that for the Ru-R300 catalyst. The ratio of butane/butenes in the products was increased with increasing particle size for the catalyst. The selectivity of the Ru-R400 catalyst was more than the Ru-R300 catalyst for the hydrogenation of butenes to butane. Since the particle size of the Ru-R400 catalyst was larger than that of the Ru-R300, the large Ru particle of the catalyst appeared to facilitate the hydrogenation of butenes to butane. The particle size was concerned with the selectivity of butane/butanes (hydrogenation) in the reaction.

LITERATURE CITED

(1) Pecoraro, T. A., and Chianelli, R. R., J. Catal. **67** 430 (1981).
(2) Lacroix, M., Boutarfa, N., Guillard, C., Vrinat, M., and Breysse, M., J. Catal. **120**, 473 (1989).
(3) Cocco, A., and Tatarchuk, B. J., Langmuir **2**, 1309 (1989).
(4) Lu, K., and Tatarchuk, B. J., J. Catal. **106**, 166 (1987).
(5) De los Reyes, J. A., Gobilos, S., Vrinat, M., and Breysse, M., Grimblot, J., J. Catal. **142**, 455 (1993).
(6) Mitchell, P. C. H., Scott, C. E., Bonnelle, J.-P., Grimblot, J. G., J. Catal. 107, **482** (1987).

Table 1. Surface property and HDS activity of Ru/Al_2O_3 Catalyst

Catalyst	Pretreatment Temp.			Conversion	Amount of adsorbed H_2	Ru particle size	NH_3-TPD[4]		
	Oxi[1]	Red[2]	Sul[3]	[%]	[10^{-2}ml/g]	[nm]	LTP	MTP [°C]	HTP
Ru-OR300	400	300	-	37.5	6.8	2.6	167s	327m	427s
Ru-OR400	400	400	-	14.6	2.2	7.6	192s	321m	
Ru-R300	-	300	-	51.5	1.2	4.5	200w	300m	
Ru-R400	-	400	-	8.8	1.0	22.9	200w	300m	
Ru-S300	-	-	300	13.9	8.9	2.0	178s	364m	418s
Ru-S400	-	-	400	4.9	0.8	26.6	186w	330w	

1)Oxidation, 2)Reduction, 3)Sulfidation, 4)LTP, MTP, HTP, and w, m and s represent low-, middle-, and high-temperature peak, and weak, middle and strong intensity, respectively.

EVIDENCE FOR THE TRIBOCHEMICAL GENERATION OF HYDROGEN FROM HIGHER RANK COALS

Karl S. Vorres
Chemistry Division, Bldg. 211
Argonne National Laboratory
Argonne, IL 60439

ABSTRACT:

Analysis of gases in sealed ampoules of higher rank Argonne Premium Coal Samples over a period of years has revealed the presence of significant (up to about 18%) constant amounts of hydrogen and increasing amounts of carbon dioxide. Comparison with the gas contents of sealed 55 gallon drums which have not been pulverized indicates that these gases came from activity following the collection of the samples. Several hypotheses are examined. The evidence indicates a possible tribochemical reaction involving fresh surface generated during pulverizing in the nitrogen atmosphere. It is probable that water reacts with the coal surface to release hydrogen. The oxygen from the water appears to bound to active sites, and later diffusion leads to formation and release of carbon dioxide.

INTRODUCTION:

The Argonne Premium Coal Sample Program (1) has produced a set of coal samples which have been sealed in glass for periods of up to 9 years. As part of a study of the stability of these samples, analyses of the gas in the ampules have been made at varying intervals. The original objective of studying the oxygen concentration was readily met, and the analytical data provided additional insights into interesting changes during the storage period and also in the processing of the coal itself.

It has been observed (2) that a number of gases have accumulated. Not surprisingly, the lower rank coals release carbon dioxide and the higher rank coals evolve methane. It has also been observed that substantial amounts of hydrogen have been found in the samples of some of the higher rank coals. In addition increasing amounts of carbon dioxide were observed in some of the higher rank coals.

A number of hypotheses were formulated and tested to account for these observations. This paper describes the hypotheses and efforts to understand these observations.

EXPERIMENTAL

The collection of the Premium Coal Samples was done with very fresh samples which were transferred to 55 gallon stainless steel drums. These drums were taken to the surface of the underground mines, and purged with argon gas within .5-5 hours of the collection. Purging continued to give about 100 ppm or less of oxygen in the drums, with an overpressure of a few psi. After 1-2 days of travel to the Argonne National Laboratory, the drums were processed in a large (2000 ft^3) glove box containing a crusher, pulverizer, mixer-blender and packaging equipment. This glove box was filled with nitrogen and kept at or below 100 ppm oxygen during the processing.

For a typical processing, the coal was initially crushed to pass between bars spaced at .5", pulverized to -20 mesh, and blended in a one ton batch. Half a ton of -20 mesh coal was packed in 5 gallon leverlock pails, moved through air locks and repulverized to -100 mesh. About 80% of the coal was placed in 5 gallon glass carboys, while the balance was sealed in ampules containing either 5 grams of -100 mesh or 10 grams of -20 mesh material. The sealing was done with a torch using stoichiometric hydrogen and oxygen, controlled with a mass flow controller.

At all processing times, the gas contents in the glove box were monitored by an oxygen analyzer, hydrogen analyzer and total hydrocarbon analyzer (Beckman model 108A). Sample lines led from central points in the box, air locks, and other critical locations in the system to the analyzing system.

The oxygen concentration in the box was controlled during the operation by circulating the atmosphere through ductwork connecting the boxes to a catalytic reactor containing palladium-on-alumina catalyst. The reactor was connected to a supply of hydrogen which permitted the impurity oxygen to combine to produce steam. Upstream from the catalytic reactor were a high efficiency particulate filter with pressure differential measuring equipment and a cyclone separator for larger particulate material.

In operation the hydrogen concentration in the box was to be kept below 1.0%. The gauge had a single range with a maximum reading of 5%.

A typical sample consisted of one ton of coal held in six drums. A seventh drum was collected and retained for archival purposes. The gas pressure in the drums increased substantially for some samples and periodically required release of some gas for safety.

RESULTS AND DISCUSSION

Gas analyses were run by the Analytical Chemistry Laboratory at ANL and reported in volume percent. A set of ampules was provided which were opened in an evacuable chamber in a CEC mass spectrometer, and more recently in a VG 3001 mass spectrometer.

The data were reported for the species which were observed by the analyst. These species were: nitrogen, argon, water vapor, methane, carbon dioxide, ethane and higher hydrocarbons and hydrogen. The use of the VG spectrometer permitted resolution of the nitrogen and carbon monoxide in more recent measurements. Recently ammonia was also observed and other samples were checked for this gas.

In general the concentrations of a gas are higher in the -20 mesh ampules than the -100 mesh containers. The gas volume per gram of coal is comparable for most samples. The exception to this generalization is hydrogen. For hydrogen, the concentrations are higher in the -100 mesh ampules. This observation is consistent with a process-related origin for the majority of this gas.

The results obtained for the carbon dioxide analyses (six highest concentrations) are indicated in Figure 1.

The results for the hydrogen analyses are shown in Figure 2.

The operating records for the processing were checked for appearance of hydrogen in the process gas analysis system. In all cases with substantial release of hydrogen, the monitor indicated a rapid increase at the time the pulverizing started. The hydrogen supply to the catalytic reactor was checked, found to be normal, and shut off to prevent additional hydrogen entering the system from the gas cylinder.

Several hypotheses to explain the rapid appearance of the hydrogen and the slower appearance of the carbon dioxide were developed. Discussions with a number of individuals led to more. A summary of them follows, together with comments in support and against them.

Hypothesis 1: "The hydrogen and carbon dioxide were in the higher rank coal. The hydrogen was released more quickly because of its lower molecular weight."

Comments on hypothesis 1: The gases in the archival drums were sampled and analyzed. Hydrogen was below the limits of detection (.015%) while the hydrogen from the initial analysis of a -100 mesh Pocahontas ampule was 17.6%. Further, the carbon dioxide content of the gas in the drum of Pocahontas coal was 0.82%, while the methane was 52.9 and the ratio of the two was 0.016. The recent measurement of carbon dioxide in the -20 mesh sample gave 4.7% and the methane was 6.5% for a ratio of 0.72. Evidently much more carbon dioxide is evolved in the ampule than the drum.

Hypothesis 2: "The gases were produced by microbial action."

Comments on Hypothesis 2: Different workers have cultured samples. Some find no growth, while others find growth but only on low rank samples.

Hypothesis 3: "Coal dust found it way to the palladium catalyst, and lost hydrogen there."

Comments on hypothesis 3: The volume of the box is 2000 ft^3. The hydrogen content from the Pocahontas sample was up to 14.7%. That represents almost one pound mole or about 2 pounds of hydrogen. Since the coal is about 4% hydrogen, the observed concentration would require the equivalent of about 40 pounds of coal accumulating on the catalyst bed and losing all of the hydrogen. Such a substantial deposition would require a major break in the filter and would have been observed in a notable drop in the pressure differential across the filter. That drop was not observed.

Hypothesis 4: "The methane gas coked on the palladium catalyst, releasing hydrogen". That may have been possible, however the catalyst activity did not decrease as might have been expected. The carbon dioxide generation is not explained by this hypothesis.

Hypothesis 5: "Low temperature oxidation produced the hydrogen as a byproduct."

Comments on hypothesis 5: Low temperature oxidation has been shown to produce hydrogen as a byproduct gas (5,6). The reported hydrogen gas concentrations range up to 1121 ppm for reaction with oxygen over 65 hours. The experiments showed about 11 ppm per 1% of oxygen consumed at 95°C. The hydrogen concentrations observed in the ampules from the processing facility ranged up to 17.6% (176,000 ppm) or two orders of magnitude greater than the maximum observed for the low temperature oxidation studies. The hydrogen production in the facility is a moderately rapid reaction during and after pulverizing. The oxygen consumption reported is much greater than the hydrogen production. In the processing facility the oxygen available was less than 100 ppm, while the hydrogen production was four orders of magnitude greater. The relative humidity in the processing facility was indicated to vary from 42 to 91%. A significant amount of moisture was available for reaction.

Hypothesis 6: "Tribochemical reactions are responsible for both of the gases."

Comments on hypothesis 6: Tribochemistry deals with the chemical reactions that are due to adding mechanical energy to a system (3). Pulverizing is an example. The surface of a solid is disturbed to a depth of about 10 atom layers in many solids during pulverizing. The disrupted zone is called the Beilby layer. The imperfections caused by grinding permit gases to readily diffuse through the damaged surface into the Beilby layer. During pulverizing fractures cleave bedding planes for the coal, but also break through the large macromolecular structure, rupturing carbon-carbon and other bonds. Radicals are created in this process. Water molecules are present from water contained in the coal and in the gas atmosphere. Through a succession of reactions, the water molecules could react with active sites on the fresh surface, and hydrogen could be removed while oxygen remained bound to the surface. The hydrogen could escape quickly, giving the rapid observed increase in hydrogen concentration. The slower increase of carbon dioxide could be attributed to a slow diffusion of oxygen around the surface until two oxygen atoms joined a removable carbon to form carbon dioxide.

CONCLUSIONS

The observation of an increasing hydrogen evolution with some higher rank coals during the processing of the large chunks into pulverized material has been made. Carbon dioxide has also been observed, but in smaller amounts. A number of hypotheses have been examined to explain this behavior. The most plausible at this time seems to be the tribochemical generation of hydrogen due to the creation of chemically active sites as a result of the

pulverizing. Reaction of moisture with the coal results in relatively rapid release of hydrogen and bonding of oxygen to the surface. A slow diffusion of oxygen around the surface coupled with release of gaseous carbon dioxide then follows. Additional work with isotope ratios for the carbon, hydrogen and oxygen species should help confirm the nature of the reactions and is planned.

ACKNOWLEDGMENTS

The author expresses appreciation to the Office of Basic Energy Science, Chemical Sciences Division, U. S. Department of Energy for support for this work.

REFERENCES

1. Vorres, K. S. Energy Fuels **1990** 4 420-

2. Vorres, K. S., Proc. 7th Int. Conf. Coal Sci. **1993** II 367-370; K. H. Michaelian, Ed. See also: Vorres, K. S., Preprints, Fuel Chem. Div., Am. Chem. Soc., **1992** 37 (4) 1945-1950

3. Heinicke, G. "Tribochemistry" Carl Hanser, Berlin, 1984

4. Polman, J. Kevin; Breckenridge, Cynthia R.; Delezene-Briggs, Karen M., Energy Fuels **1993** 7 (3) 380-383

5. Grossman, S. L., Davidi, S., Cohen, H. Fuel **1991** 70:7 897-8

6. Grossman, S. L., Davidi, S., Cohen, H. Fuel **1993** 72:2 193-7

Fig. 1, Six Highest −20 Mesh Carbon Dioxide Concentrations

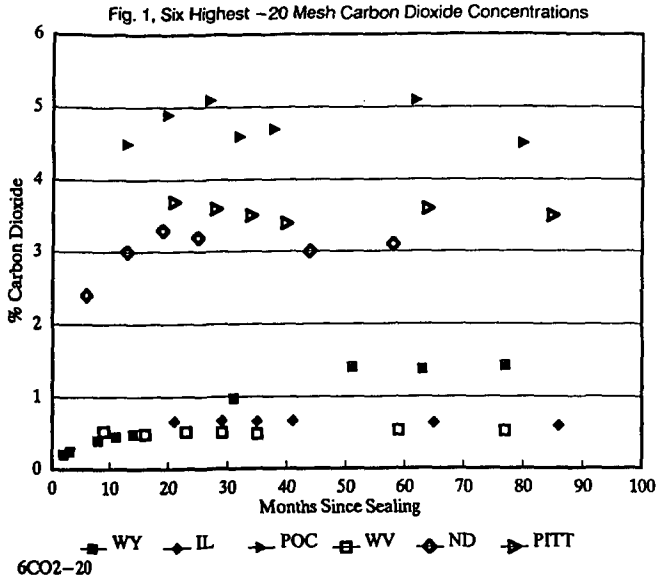

Fig. 2, Six Highest −100 Mesh Hydrogen Concentrations

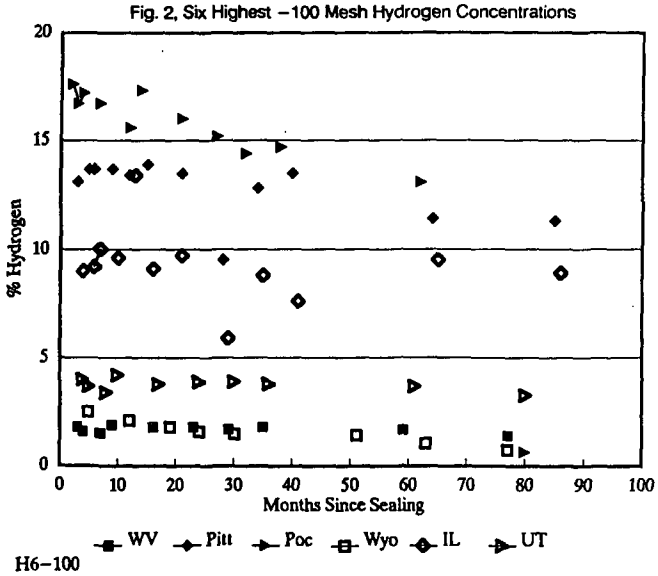

BIOMIMETIC SOLUBILIZATION OF BROWN COAL BY OXYGENASE MODEL WITH HYDROGEN PEROXIDE

Keiji Miki and Yoshiki Sato
Energy Resources Department
National Institute for Resources and Environment
16-3, Onogawa, Tsukuba, Ibaraki 305
Japan

Keywords: Brown coal, Solubilization, Oxygenase model

INTRODUCTION

As an alternative processing of coal conversion, biosolubilization has been intensively studied[1-4]. Most of the studies in 1980's involve the oxidative solubilization of preoxidized coal or lignite to render the coal water soluble. The products contain primarily polycarboxylic compounds and are suggested to be of lower quality than the materials derived from conventional thermochemical conversion[5]. Thus there has been arguments about the biological processes for the production of alternate fuels or chemicals from coal[6]. Current reductive solubilization of coal under anaerobic conditions could provide more desirable products[7,8]. On the other hand, these biological processes imply a potential route to liquefy coal catalytically under considerably mild conditions. The elucidation of mechanisms involved in the biosolubilization and the application of the catalyst systems in analogous to enzymes or microorganisms may offer an attractive processing for coal conversion.

During the past decade, numerous studies on oxidation reaction catalyzed by synthetic metalloporphyrin have been reported[9]. These catalysts have been synthesized as the models for cytochrome p450 and peroxidase, and some of them exhibit extremely high turn over number in the oxidations of alkenes and alkanes[10,11]. To date the mechanisms of oxidation reactions catalyzed by synthetic metalloporphyrins are fairly well understood and the utilization of the catalyst for the oxidations of various stable compounds is of great interest. Preliminary attempt using a simple iron porphyrin complex for coal conversion, however, did not show a significant effect on the solubilization. In addition, the contamination of catalyst and residual oxidant affected the evaluation of the products. Therefore as the first step, we developed a new supported biomimetic catalyst capable of using hydrogen peroxide as an oxidant. In this paper we describe the solubilization of coal by the oxygenase model, immobilized iron porphyrin catalyst.

EXPERIMENTAL

Preparation of catalyst

A biomimetic model for monooxygenase enzyme was synthesized on a silica surface as the following 5 steps (Fig. 1), based on the detailed design considering the structures of bulky porphyrin and the silica surface[12]. 1) Amorphous silica powder, Aerosil 200, was dispersed in toluene to which 3-mercaptopropyltrimethoxysilane was added. Refluxing overnight and removal of solvent under vacuum yielded the support-anchored silica (**a**). 2) **A** was dispersed in pyridine, to which phthalocyaninatoiron (II) was added. The mixture was stirred overnight and the solid collected by filtration. Drying under vacuum gave phthalocyaninatoiron-loaded silica (**b**). 3) **B** was dispersed in CH_2Cl_2, to which excess dodecyltriethoxysilane was added. After removing solvent, the container was evacuated, sealed and heated for 24 h at 150-160℃. It was cooled, opened and washed with CH_2Cl_2 and acetone resulting hydrophobic silica (**c**). 4) **C** was subjected to Soxhlet extraction with pyridine for 72 h and yielded iron-free silica (**d**). 5) **D** was dispersed in benzene, to which iron tetraphenylporphyrin acetate was added under argon. After refluxing 48 h with stirring, the solid was collected by filtration and washed with CH_2Cl_2 until the filtrate turn to colorless. The dark green solid obtained (**E**) had a loading of iron tetraphenylporphyrin complex of 1.34×10^{-2} mmolg^{-1}.

Solubilization of brown coal

A brown coal (Australian Yallourn coal), ground to <149 μm, dried and stored in a glass ampoule, was used.

The catalyst (1.0-1.5 μmol) and the coal (300 mg) were dispersed in 10 ml of deionized water or acetate buffer (pH 5.0) to which imidazole (1 mmol) and H_2O_2 (2 mmol) were added. The container was sealed with a septum and shaken at 150 stroke/min at 40℃ using a Bio-shaker for 24 h. For anaerobic assays, manipulations were done in a glove box.

After reaction, the mixture was filtrated and extracted with tetrahydrofuran/H_2O (v/v=4:1) until the filtrate turn to colorless. The filtrate and extract were combined, evaporated and dried at 110℃ under vacuum.

RESULTS AND DISCUSSION

Catalytic activity of oxygenase model

As mentioned above, from the point of product quality, it is most desirable to mimic enzymes functioning reductive reactions under anaerobic conditions. But the studies on such enzymes involving electron transfer seem to be at an early stage. For that reason we attempted the synthesis of the model for cytochrome P450 monooxygenase.

The active sites, iron tetraphenylporphyrin units, were immobilized by coordinative ligation to anchored mercaptopropyl groups in hydrophobic cavities formed by alkyl chains attached to silica surface. This is the characteristic structure distinguished from other efficient iron porphyrin catalysts (Table 1). When the oxidation reaction is performed in aqueous solution, lipophilic substrates are assumed to condense on the catalyst surface by hydrophobic interactions. Further it inhibits contact between the active center and H_2O_2. As the result, the catalytic reaction takes place even with a small amount of substrate without the decomposition of fragile porphyrin structure by H_2O_2 attack.

The catalytic activity of the synthetic catalyst was clarified by the epoxidation of alkenes. In the presence of externally added imidazole, the substrates were efficiently epoxidized (Table 2). Although the iron center have an axial sulfur ligand in the same manner as native enzyme, the promotion of heterolytic cleavage of H_2O_2 by general catalyst seems to be required. Thus the following coal solubilization reactions were carried out in the presence of imidazole.

Solubilization of brown coal

It has been reported that coal reacts rapidly with H_2O_2 in the study on the coal solubilizing activity of horseradish peroxidase[13]. H_2O_2 is known to decompose at a higher pH, but a lower pH may favor hydrolysis reaction of coal. Further the aqueous buffers contaminate the residue in the concentrated solubles. Hence controls were always run and deionized water was mainly used in the coal solubilization experiments. As shown in Table 3, a considerable amount of soluble fraction was obtained after the treatment with H_2O_2 or H_2O_2/imidazole in the absence of the catalyst. The yields seem to be strongly affected by the presence of oxygen and imidazole.

The results indicate clearly the effect of catalyst addition in every series of experiments. The presence of 1 μmol catalyst increased in conversion by 10-15% under aerobic conditions. Anaerobic assay required a slightly larger amount of catalyst to obtain the similar conversion. No appreciable effect on the solubilization was found in the absence of imidazole.

Elemental analyses showed high nitrogen contents in the products derived from imidazole-added runs. There was a difficulty in removing it completely even by prolonged vacuum drying at 110℃. Therefore the correction of elemental compositions was made for the evaluation of oxygen incorporation. The amount of imidazole in the product was calculated from the excess of nitrogen, assuming that the nitrogen content equals that in imidazole-free control. The results showed the remains corresponding to about a half of initially added imidazole. Recalculated elemental compositions from the data were shown in Table 4. The catalytic treatment caused a decrease in carbon content and an increase in oxygen content. The change is not so drastic as seen in the oxidative microbial conversion. As the result, the solubilization reaction does not involve the introduction of a high concentration of carboxylic acid. The assumption is also supported by FT-IR analysis which reveals the decrease in the relative intensity of carbonyl band to aromatic band by the catalyst addition compared with that from control. Further no aromatic acid derivative is detected in the catalytic oxidations of various model compounds.

At present further detailed studies are in progress to explore the function of biomimetic model in connection with the solubilization reaction of coal, including the capability of catalytic carbon-carbon bond scission.

CONCLUSION

A biomimetic model for monooxygenase enzyme was synthesized and utilized for the solubilization of brown coal. In the presence of imidazole as a general catalyst and H_2O_2 as an oxidant, it was suggested that the model catalyzed the solubilization reaction of coal. This is partly due to the characteristic nature of the model in addition to the catalytic activity.

REFERENCES

1. Cohen, M.S., and Gabriele, P.D., *Appl. Environ. Microbiol.*, **1982**, 44, 23-27
2. Couch, G.R., "*Biotechnology and Coal*", **1987**, IEA Coal Research, London
3. Cohen, M.S., Bowers, W.C., Aronson, H., and Gray, Jr.,E.T., *Appl. Environ. Microbiol.*, **1987**, 53, 2840-2843
4. Pyne,Jr., J.W., Stewart, D.L., Fredrickson, J., and Wilson, B.W., *Appl. Environ. Microbiol.*,**1987**, 53, 2844-2848
5. Wilson, B.W., Bean, R.M., Franz, J.A., and Thomas, B.L., *Energy & Fuels*, **1987**, 1, 80-84
6. Narayan, R., and Ho, N.Y., *Am. Chem. Soc., Div. Fuel Chem. Prepr.*, **1988**, 33, 487-495
7. Jain, M. K., Burgdorf, D., and Narayan, R., *Fuel*, **1991**, 70, 573-576
8. Scott, C.D., Faison, B.D., Woodward, C.A., and Brunson, R.R., *1991 Second International Symposium on the Biological Processing of coal*, **1991**, EPRI, Palo Alto, CA, 4-5-4-22
9. Meunier, B., *Chem. Rev.*, **1992**, 92, 1411-1456
10. Traylor, P.S., Dolphin, D., and Traylor, T.G., *J. Chem. Soc., Chem. Commun.*, **1984**, 279-280
11. Traylor, T.G., Tsuchiya, S., Byun, Y-S., and Kim, C., *J. Am. Chem. Soc.*, **1993**, 115, 2775-2781
12. Miki, K., and Sato, Y., *Bull. Chem. Soc. Jpn.*, **1993**, 66, 2385-2390
13. Quigley, D.R., Breckenridge, C.R., Polman, J.K., and Dugan, P.R., *Fuel*, **1991**, 70, 581-583

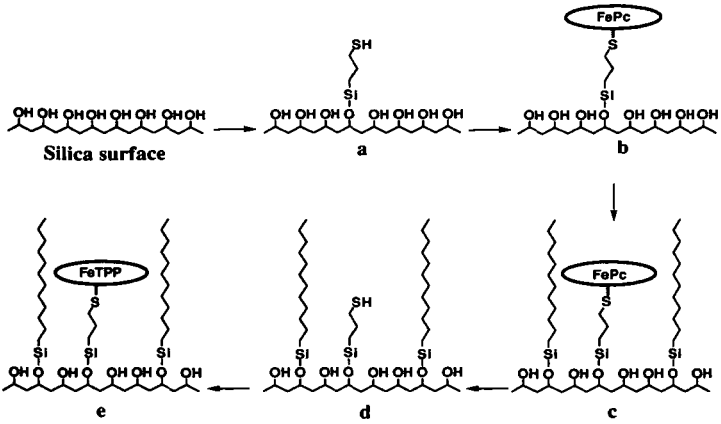

Fig. 1 Synthetic pathway of oxygenase model

Table 1. Structure and reaction system of oxygenase model and efficient iron porphyrin catalyst

active center	reaction site	axial ligand	oxidant	medium	reference
oxygenase model					
FeTPPOAc[a)]	highly hydrophobic	immobilized alkyl thiol	H_2O_2	H_2O	this work
efficient iron porphyrin catalyst					
FeTDCPPCl[b)]	—	imidazole	H_2O_2	CH_2Cl_2/CH_3CN	9
FeTDCPPCl	—	—	C_6H_5IO C_6F_5IO	CH_2Cl_2/MeOH	10
FeTPFPPCl[c)]	—	—	H_2O_2	CH_2Cl_2/MeOH	11

a) Iron tetraphenylporphyrin acetate. b) Iron tetrakis(2,6-dichlorophenyl)porphyrin chloride.
c) Iron tetrakis(pentafluorophenyl)porphyrin chloride.

Table 2. Oxidation of alkene with immobilized iron porphyrin and hydrogen peroxide[a)]

			product[b)]	
run	atmosphere	substrate	oxide	aldehyde
1	aerobic	*trans*-ß-methylstyrene	125	154
2	anaerobic	*trans*-ß-methylstyrene	98	45
3	aerobic	*cis* -stilbene	30	7
4	anaerobic	*cis* -stilbene	31	5
5	aerobic	*cis*-cyclooctene	49	-
6	anaerobic	*cis*-cyclooctene	42	-

a) Alkene / H_2O_2 / imidazole / catalyst = 0.4 mmol / 0.4 mmol / 0.2 mmol / 4mmol in 2ml H_2O at 40°C for 17h. b) Yield based on equivalents of catalyst used.

Table 3. Solubilization of Yallourn coal with immobilized iron porphyrin and hydrogen peroxide[a)]

run	catalyst (μmol)	imidazole (mmol)	H_2O_2 (mmol)	conversion (%)
1-1	0	0	2	51
1-2	0	1	2	23
1-3	1.0	1	2	66
2[b)]-1	0	0	2	26
2-2	0	1	2	41
2-3	1.0	1	2	44
2-4	1.5	1	2	53
3[c)]-1	0	0	2	44
3-2	0	1	2	46
3-3	1.0	1	2	56

a) Yallourn coal (300mg) was treated in deionized water (10ml) at 40℃ for 24 h. b) Under argon. c) In 200 mM acetate buffer at pH 5.0.

Table 4. Elemental analysis of solubilizeation product[a)]

run	elemental analysis C	H	N	O+S	H/C	O/C
	(%)					
original coal	64.2	4.9	0.7	30.2	0.91	0.35
1-1[b)]	59.7	4.9	1.1	34.4	0.97	0.43
1-2	59.4	4.6	1.1	35.0	0.93	0.44
1-3	60.0	4.5	1.1	34.4	0.90	0.43
2-1	59.9	5.0	1.2	34.0	1.00	0.43
2-2	60.0	4.7	1.2	34.2	0.93	0.43
2-3	60.2	4.6	1.2	34.2	0.91	0.43
2-4	60.3	4.6	1.2	34.0	0.92	0.42

a) Corrected data (Refer to text). b) Run number is the same in Table 2.

OXIDATIVE DESULFURIZATION OF LIQUID FUELS

Tetsuo Aida*, Daichi Yamamoto
Department of Industrial Chemistry, Faculty of Engineering in Kyushu
Kinki University
11-6 Kayanomori, Iizuka, Fukuoka 820, JAPAN

Keywards: Desulfurization, Liquid fuels, Oxidation reaction

INTRODUCTION

Among the alternatives of petroleum oil, coal is considered to be one of the most practical energy resouces in the next generation, because of its unlocalized abundance. Under such circumstances, the consumption of the fossile fuel such as petroleum oil or coal-derived liquid fuels could be drastically increased in the next decade, and it will take place fatal environmental ploblems like an acid rain and a grobal warming. Particulary, the increase of the emission of sulfur oxides due to a combastion of those fuels is secirously concerned in the developing countries. Although it has long been anticipated the development of efficient desulfurization technologies for fossile fuels, except the flue-gas desulfurization processes, most of the research projects seem to be in trouble. In particular, the desulfurization of diesel fuels such as light or heavy oils is going to be critically important to sustaine our modernized life.

we had initiated research projects for developing efficient chemical desulfurization processes of coal, and revealed that the oxidation reaction significantly enhanced the chemical reactivity of the organic sulfur fuctionalities in coal, and it made them easy to remove from a solid coal. For instance, the alkaline fusion under oxygen gas, "Oxy-Alkalinolysis", achieved the sulfur removal upto 95-98% for most of the coals(1). To use such drastic change of the chemical and phisical properties of organic sulfur compounds by oxidation is our strategy for developing an efficient desulfurization process for liquid fuels.

This paper present the results of the study on the desulfurization process using oxidation reactions for liquid fuels.

PROPOSED PRINCIPLE OF OXY-DESULFIRIZATION FOR LIQUID FUELS

In general, there are many types of organic sulfur compounds in the fossile fuels. In particular, arylic sulfide-type sulfur and thiophene-type sulfur such as , benzothiophene or dibenzothipophene are believed to be major components(2) These types of organic sulfur atom are known to be chemically so stable that the carbon-sulfur bond-fission does not occur easily. Traditionaly, the catalytic hydrogenetaion reaction has been used for such bond cleavage, which has several advantages for industrial purposes, but also some disadvantages. Particularly, the use of hydrogen gas and catalyst forced to take more and more drastic reaction conditions(higher pressure and higher temperature) in order to get the higher degree of the sulfur removal. In Japan, it is assumed that the cost of the capital investment to decrease the sulfur content in a commercial light upto 0.05%-level will be over five hundred billion yen(3). The recent researchs revealed that one of the reason of the difficulty of sulfur removal from a light oil will be the steric hindrance due to the alkyl functions surrounding the sulfur atom in the sulfur compounds. This means that the developement of highly active catalysts may be vital to achieve the long term target , but there seems to be a fatal limitation.

In the meantime, the principle of the proposed oxydative desulfurization process is as follows: It may be very fortunate for us that the most of the organic sulfur atoms in the fossile fuel are thought to be divalent, like a sulfide or thiophene. In general, oxidized sulfur compounds such as sulfoxide or sulfone have

significantly defferent chemical and physical properties, particularly boiling point and solubility towards various solvents based on a molecular polarity, compared to the corresponding divalent compounds.

Now, an simple idea comes in our mind, that is, a large degree of differences of the boiling point and polarlity before and after oxidation should make easy to separate them from other hydrocarbon components through ordinarly purification procedures like a distillation, an solvent extraction or/and a chromatographic adsorption.

It can be also enphasized that this process could provide the organic sulfur components in the fuels as a potential low materials to the industrial uses. Namely, our understanding is that the sulfur components in fossile fuels is not a waste. It is a valuable natural resourse.

EXPERIMENTAL

Solvents and Reagents: Gold rabel grade reagents were used without further purification.

Sulfur Analyses: High sensitivity sulfur analyzer(Model TS-03, Mitsubishi Kasei Co.) is used for the determination of sulfur content in the liquid fuels.

Oxidation of Liquid Fuels: A typical run as follows. In the three necked flask(300ml) equiped by a mechanical stirrer and reflux condencer, 100ml of liquid fuel lwas plased, and a mixture of formic acid(10ml) and aqueous hydrogen peroxide (30%, 10ml) was added with vigorous stiring keepin temperature below 60oC for 2 hours. After the reaction the reaction mixture was cooled down at ice-water temperature, and separated the oil layer, and washed by distilled water.

Solvent Extarction: Extraction of sulfur components was carried out by using same mount s of liquid fuel and extarction solvent (1/1 vol/col).

Adsorption: Adsorption of sulfur component in liquid fuel was carried out by using a column chromatography paked by absorbent(silica gel or alumina) The ratio of the liquid fuel and absorbebt was 100/10(wt). The sulfur content was determined to the combined liquid passed through the column.

RESULTS AND DISCUSSION

Obviously, the key step of this desulfurization process is the oxidation reaction, which has to selectively oxidize the sulfur atom in the contamination. We have examined many type of oxidants, and found that the peroxyacid, like a performic acid or a pertrifluoro acetic acid, was one of the positive candidate for that. These oxidants are known to oxidize not only sulfur compounds but also olefinic hydrocarbons affording the corresponding epoxy compounds. However, we do not think that this type of the side reaction causes critical damages to the total fuel efficiency.

The reaction mechanism of the oxidation of organic sulfur compound, i.e., dibenzotiophene, by performic acid(a mixture of formic acid and hydrogen peroxide) is illustrated as shown in Figure 1. Namely, formic acid reacts with hydrogen peroxide and gives performic acid and water. Then, the performic acid reacts with dibenzothiophene and gives dibenzothiophene sulfoxide, and a further oxidation gives the corresponding sulfone. Thus overall oxidation reaction consumes only hydrogen peroxide recycling formic acid.

We have initiated this reserch project from a modeling experiments as follows: A model liquid fuel was prepared by using dibenzothiophene as organic sulfur and cyclohexane as hydrocarbon component. The sulfur content in the model fuel was controled in 0.30% and it was treated by the mixture of formic acid And aqueous hydrogen peroxide(30%) below 60°C temperature.for 2 hours. After the reaction, the mixture was cooled down at 0°C, and resulted white

crystal was filtrated which was determined as dibenzothiophene sulfone. The sulfur content of the fitrate was 0.002%. Then the filtrate was extracted by aqueous dimethylformamide(water content, 3%). The cyclohexane layer was separates an washed with distilled water. After dried over anhydrous magnesium sulfate, the sulfur content was determined as 0.0007%. Also, the filtrate was passed through a silica gel column(oil/silica gel = 100/10 wt/wt). The sulfur content of the eluted solution was 0.0000%(exceeded the detectable limit of the sulfur analyzer Model TS-03, Mitubisikasei Co.)

Based on the results described above, the working principl seems to be correct. It will be also true that the sulfur comonents in liquid fuel such as light oil is not simple like in this.model. So that we have applied these procedures to the actual commercial light oil. Figure 2 shows the gas-chromatogram(OV-1, packed glass-column; FPD-detector) of the reaction mixture of dibenzothiophene by this oxidation system. The shift of the retention time of the reaction product(sulfone) clearly suggests the increased boiling point and polarity by oxidation.

Figure 3 shows the gas-chromatogram(OV-1, packed glass-column; FPD-detector) of the reaction mixture of a commercial light oil(sulfur content, 0.56%) before and after oxidation. The wide range of distribution of peaks is observed due to a mixture of alkylderivatives of mainly benzothiophene and dibenzothiophene. Interestingly, there is a significant deference between the retention time in both peak distributions before and after oxidation, which is considered to be resulted by the oxidation as well as shown in Figuure 2

Table 1 and 2 show the part of the results examined the sulfur removals of the commarcial light oil and its oxidized one, which were achieved by the solvent extraction and the adsorption by silicagel and alumina column-chromatography.

Table 1 Sulfur Removal of Light Oil by Solvent Extraction[a)]

Solvent	sulfur content(%)	
	commercial light oil[b)]	oxidized light oil
Acetonitrile	0.52	0.057 (0.012)*
OMF[c)]	0.49	0.018 (0.003)*

* *Trifluoroacetic acid / hydrogen peroxide*
a) Ratio of oil and solvent was 1 / 1(vol) and a single extraction
b) Original sulfur content was 0.56%
c) *N,N'-Dimethylformamide*

Table 2 Sulfur Removal of Light Oil by Adsorption [a)]

Adsorbent	sulfur content(%)	
	commercial light oil[b)]	oxidized & extracted(DMF) light oil[c)]
Silicagel	0.54	0.0046 (0.0009)*
Alumina	0.53	0.0038 (0.0005)*

*Trifluoroacetic acid / hydrogen peroxide
a) Ratio of oil and adsorbent was 100 / 5(wt), glass column(ϕ=0.5mm)
b) Original sulfur content was 0.56%
c) After extracted by N,N'-Dimethylformamide

CONCLUSION

The proposed "Oxy-desulfurization Process" has exibited a powerful ability to remove sulfur from diesel fuels like a light oil. The characteristc features of this efficient new process can be summarized as follows.

1. High degree of sulfur removal: Possible to down to a ppm-order sulfur-content
2. Mild reaction conditions: Ambient pressure and temperature
3. Useful by-product: Organic sulfur compounds
4. Applicable to havier oil desulfurization
5. Economical ?

REFERENCE

* Author to whom correspondence should be addressed.

(1) T. Aida, K. Ofuji, M. Fujii, M. Yoshihara, T. Yonezawa, T.Maeshima, Proc. Fukuoka Intetnational Sympo. Grobal Environment & Energy Issues, Fukuoka, JAPAN p.255(1990)

(2) G. N. Georg and M. L. Gorbaty, J. Am. Che. Soc., 111, 3182(1977)

(3) A. Inoue, Abstract Japanese Chemical Society National Meeting,Osaka, JAPAN p.2237(1992)

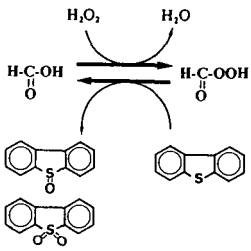

Figure 1 Oxidation reaction mechanism

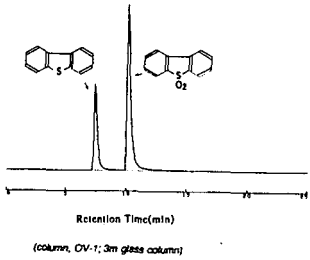

Figure 2. FPD-Gas chromatogram of Model-fuel oxidized by Formic acid/Hydrogen peroxide

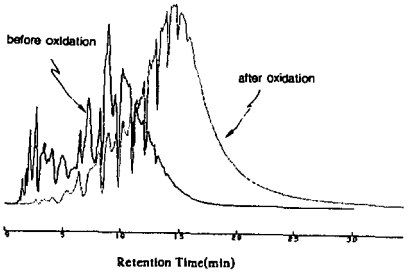

Figure 3 FPD-Chromatogram of Light Oil oxidized by Formic acid/Hydrogen peroxide